Faculty of Engineering and Science

Rainfall Analysis and Hydrochemical Characterisation of the Limbang River Basin, Northern Borneo

Ninu Krishnan Modon Valappil

This thesis is presented for the Degree of
Doctor of Philosophy
of
Curtin University

March 2019

Declaration

To the best of my knowledge and belief this thesis contains no material previously published by any other person except where due acknowledgment has been made. This thesis contains no material which has been accepted for the award of any other degree or diploma in any university.

Signature: 

Ninu Krishnan Modon Valappil

Date: 20.03.2019

Acknowledgements

First of all, I express my sincere gratitude to Curtin University for providing an opportunity to pursue doctoral research with a full scholarship.

I express my paramount gratitude to the thesis committee, A/Prof. Perumal Kumar, A/Prof. Prasanna MV and Dr. Hamza V for their support, guidance and encouragement throughout the research.

Thanks to Prof. Clem K, (Dean), A/Prof. Goi Chai Lee (Deputy Dean) and Prof. Nagarajan R (Associate Dean), R&D and all administrative staffs of Graduate Research School for their support during the period of research. I also express my sincere gratitude to Prof. Marcus, former Dean, Graduate Research School for his encouragement and support during the initial period of research.

Thanks to Dr. Anand Kumar A and Dr. Prabhakaran K for their kind help and support during the initial period of research. Special thanks to Dr. Eswaramoorthy SG for providing technical support in analytical processes. Extended thanks to all HDR colleagues.

Thanks to State Planning Unit (Sarawak) and DID, Sarawak (Malaysia) for granting permission to conduct research in Sarawak and also for providing long term hydrological data.

Heartfelt thanks to the people of Limbang especially, Mrs. Mardiana, Mr. Clarence Ranggat, Mrs. Indiana, Mrs. Helen Chin and Mr. Sainet Sentunitas for their kind help during the entire period of rainwater sample collection. Without their help, one year sample collection was not possible.

Thanks to Mr. Stephan Ongetta and Mr. Renald for providing transportation in the inaccessible areas of Limbang and other supports during field work.

Sincere thanks to Ms. Helda Puyang Jau, (Lab Manager) and also to all other lab technicians especially Ms. Rassti Binti Serati, FoES. Thanks to all administrative staffs of FoES and Finance. I also extend thanks to all members of Library, Campus Service and Security Department. Special thanks to all staff members of Department of Applied Geology.

I extend my sincere thanks to Dr. Jobin Thomas, Ms. Cicily Kurian (Environment and Water Resources Engineering Lab, Department of Civil Engineering, IIT Madras, India) and Mr. Anil Kumar (Project Scientist, High Altitude Cloud Physics Laboratory, Indian Institute of Tropical Meteorology, India) for their kind help in rainfall-runoff modelling.

Thanks to late Dr. Unnikrishnan Warrier C (Head Scientist), Dr. Resmi TR (Scientist) and Mr. Sudheesh M (Technical Officer), Isotope Hydrology Division, Centre for Water

Resources Development and Management, India for help in analysing stable isotopes in rainwater samples.

Thanks to Dr. Anita Jimmie, Department of Culture and Language Studies, Curtin University for spending her valuable time for proofreading and correcting the thesis.

Thanks to my parents for their understanding, constant support and motivation, which helped me complete the research on time.

List of Abbreviations

AAS – Atomic Absorption Spectrometer

ACF – Autocorrelation Function

ANN – Artificial Neural Network

ANOVA – Analysis of Variance

APHA – American Public Health Association

CAI – Chloro - Alkaline Indices

CCF – Cross Correlation Function

cm – Centimeter

CR – Corrosivity Ratio

CV – Coefficient of Variation

CWRDM – Centre for Water Resource Development and Management

d-excess – Deuterium excess

DID – Department of Irrigation and Drainage

DO – Dissolved Oxygen

DoA – Department of Agriculture

EC – Electrical Conductivity

ENSO – El Niño-Southern Oscillation

EV – Volumetric Error

GNIP – Global Network of Isotopes in Precipitation

GWML – Global Meteoric Water Line

HDPE – High density Polyethylene

HEP – Hydro-electric project

IAEA – International Atomic Energy Agency

IM – Inter-monsoon

IOD – Indian Ocean Dipole

ITCZ – Inter Tropical Convergent Zone

JUPEM – Department of Survey and Mapping

L - Liter

LnR – Larson Ratio

LRB – Limbang River Basin

LWML – Local Meteoric Water Line

m – Meter

m^3/s – cubic meter per second

MAE – Mean Absolute Error

MAPE - Mean Absolute Percentage Error

MDL – Minimum Description Length

Meq/L – Micro equivalent /Liter

mg/L – milligram/ Liter

MGDM – Minerals and Geoscience Department Malaysia

MJO – Madden Julian Oscillation

MK – Mann Kendall

mm - millimeter

mm/year – millimeter/ year

MNN – Multilayer Neural Network

MR – Magnesium Ratio

MSL – Mean Sea Level

MW – Mega Watt

MWQS – Malaysian Water Quality Standards

NE – North East

NEM – Northeast Monsoon

NNW – North-North-West

NRM – Normal Ratio Method

NSE – Nash Sutcliff Efficiency

NTU – Nephelometric Turbidity Unit

NW – North West

^oC – Degree Celsius

PACF – Partial Autocorrelation Function

pCO_2 – Partial Pressure of Carbon dioxide

PI – Permeability Index

RF - Rainfall

RMSE – Root Mean Square Error

RPE – Relative Peak Error

RRMSE – Relative Root Mean Square Error

RSC – Residual Sodium Carbonate

RW - Rainwater

SAR – Sodium Absorption Ratio

SCS – South China Sea

SE – South East

SEB – Sarawak Energy Berhad

SI – Saturation Index

SR – Spearman's Rho

SRTM – Shuttle Radar Topographic Mission

SSE – South-South-Eastern

SSW – South-South-West

SW – South West

SW – Surface water

SWM – Southwest Monsoon

T - Temperature

TDS – Total Dissolved Solids

VWA – Volume Weighted Average

WHO – World Health Organisation

$\delta^{18}O$ - Composition of Oxygen

δD – Composition of Deuterium

% – Percentage

µm – micrometer

µS/cm – micro Siemens per centimeter

‰ – per mil

List of Publications

Krishnan, M. N., Prasanna, M. V., & Vijith, H. (2017). Optimisation of morphometric parameters of Limbang river basin, Borneo in the equatorial tropics for terrain characterisation. *Modeling Earth Systems and Environment*, *3*(4), 1477-1490. DOI: 10.1007/s40808-017-0394-9.

Krishnan, M. N., Prasanna, M. V., & Vijith, H. (2018). Statistical analysis of trends in monthly precipitation at the Limbang River Basin, Sarawak (NW Borneo), Malaysia. *Meteorology and Atmospheric Physics*, 1-14. DOI: 10.1007/s00703-018-0611-8.

Krishnan, N., Prasanna, M. V., & Vijith, H. (2018). Fluctuations in monthly and annual rainfall trend in the Limbang River Basin, Malaysia: A statistical assessment to detect the influence of climate Change. *Journal of Climate Change*, *4*(2), 15-29. DOI: 10.3233/JCC-1800010.

Krishnan, M. N., Prasanna, M. V., & Vijith, H. (2019). Annual and seasonal rainfall trends in an equatorial tropical River Basin in Malaysian Borneo. *Environmental Modeling & Assessment*, 1-16. DOI: 10.1007/s10666-018-9649-8.

Abstract

The present research aims to understand and characterise the hydroclimatology of the Limbang River Basin (LRB) through hydrometeorological modelling and hydrochemical analysis. Rainfall trend analysis and runoff modelling contributes to the hydrometeorological part, whereas chemical characteristics of precipitation (rainwater) and surface water along with stable isotope signatures define the hydrochemical aspects of the river basin. Rainfall trends in the LRB was determined by analysing 69 years (1948-2016) of rainfall data from 13 rain gauges collected from the Department of Irrigation and Drainage (DID) Sarawak, and by applying statistical non-parametric Mann Kendall and Spearman's Rho tests. Minimum Description Length (MDL) algorithm based Multilayer Neural Network (MNN) model was used to simulate the runoff in the river using rating curve equation based runoff (10-year data, 1991-2000) calculated from water level data of Insungai Nanga station. In order to assess the chemical characteristics of rainwater and isotopic composition, monthly cumulative rainwater from five locations in the LRB for a period of one year (October-2016 to September-2017) was collected. The surface water chemistry was characterised by collecting samples from 24 locations during three sampling periods (November-2016, March-2017 and September-2017). Standard analytical methods were applied to detect the physico-chemical characteristics (physical characteristics (pH, electrical conductivity (EC), total dissolved solids (TDS), dissolved oxygen (DO), temperature and turbidity), major ions (Carbonate (CO_3^{2-}), Bicarbonate (HCO_3^-), Chloride (Cl^-), Calcium (Ca^{2+}), Magnesium (Mg^{2+}), Sodium (Na^+) and Potassium (K^+)), nutrients (Nitrate, Phosphate, Ammonia and Sulfate) and trace metals (Cu, Pb, Fe, Mn, Zn, Cd, Ni and Co). In addition, continuous-flow Isotope Ratio Mass Spectrometer (IRMS) was used to determine the composition of stable isotopes, oxygen-18 ($\delta^{18}O$) and deuterium (δD) in rainwater. Furthermore, different techniques such as Piper diagram, Gibbs plot, water quality indices, partial pressure of carbon dioxide (pCO_2) and the saturation index (SI) of carbonate minerals were applied to identify the major geochemical processes in the LRB. Later, the results were statistically processed by applying two-way ANOVA, Pearson's correlation and Factor analysis to identify the significant characteristics, inter-relationship and also to detect the processes responsible for (geo)chemical characteristics of rainwater and surface water.

The LRB experienced a prolonged period of monsoon (10 months) with two inter-monsoon months. The dominant monsoon seasons are the southwest monsoon (May to

September) and the northeast monsoon season (November to March). The months April and October are the inter-monsoon periods. The study area receives an annual average rainfall of 3851mm with monthly average rainfalls exceeding 250mm. Basic statistical characteristics show comparatively accurate rainfall data with less dispersion. Lag-1 autocorrelation of rainfall data indicates the homogeneous and non-correlated nature of rainfall data by accepting the null hypothesis through r_1 coefficients in the limit of 95% confidence level. Rainfall data show very less missing percentage indicates comparatively high accuracy in data collection. The missing rainfall values were filled by applying normal ratio method. Trend analysis of rainfall measured at each individual rain gauge station revealed varying trend (significant or non-significant increasing and decreasing) characteristics in monthly, seasonal and annual rainfall. Among the thirteen rain gauging stations, rainfalls recorded at Long Napir shows consistent increasing trends in monthly, seasonal and annual rainfall. However, considering the LRB as whole, monthly (nine months), seasonal (southwest, northeast and inter-monsoon) and annual rainfalls showed increasing trends. Among this, statistically significant increase in trend was noted in the northeast monsoon (2.24mm/year) and annual rainfall (1.90mm/year). The spatial pattern of rainfall trend shows two clusters of dominant increasing trends in the lower and the upper catchment, separated by a prominent decreasing trend in middle catchment. The rainfall-runoff modelling performed with MNN MDL model shows comparatively higher accuracy while comparing the measured (calculated) and predicted values. In training and testing, the observed and predicted runoff shows an average value of 197 and 198m^3/S and 190 and 195m^3/S respectively. In addition, correlation coefficients of simulated runoff in training and testing showed a higher positive correlation with coefficients ≥ 0.80 (r = 0.84 and 0.85 for training and testing respectively). Evaluation of the results through different statistical methods also support the findings and suggests the applicability of the MNN MDL model in forested catchments which lack detailed and up to date discharge measurements.

Findings also reveal that the composition of stable isotopes ($\delta^{18}O$ and δD) in rainwater indicates the equilibrium condition of rain formation and increased convective activity. The local meteoric water line (LMWL) shows comparatively near value of global meteoric water line (GWML). Further, the characteristic depletion of vwδD and vw$\delta^{18}O$ with 'V' shaped pattern indicates the dominance of two rainy seasons and amount effects over the composition of stable isotopes in rainwater. Re-evaporation, inland moisture source and high humidity in the region also influences the composition of stable isotope. The water chemistry (both rainwater and surface water) assessed shows spatial and temporal variation in the

concentration of physico-chemical parameters. Rainwater was slightly alkaline with mean pH higher than 5.8, whereas the surface water showed slightly acidic characters with a mean pH of around 6.8. Bicarbonate (HCO_3^-) and chloride (Cl^-) are the dominant major ions and Fe and Ni are the dominant trace metals found in rainwater and surface water in all locations and sampling periods. The mean concentration of major ions and trace metals in rainwater follows the decreasing order of $HCO_3^- > Cl^- > Na^+ > Ca^{2+} > Mg^{2+} > K^+$ and Fe > Ni > Pb > Mn > Co > Zn > Cu > Cd. At the same time, in surface water the mean concentration was in the decreasing order of $HCO_3^- > Cl^- > Na^+ > Mg^{2+} > Ca^{2+} > K^+$ and Fe > Ni > Pb > Mn > Zn > Co > Cu > Cd. It was also discovered that the rainwater shows a slightly polluted nature compared with findings of other studies around the world. Surface water was found to be good in quality (except turbidity) when compared with Malaysian Water Quality Standards (MWQS) and World Health Organization (WHO) standards. The intense logging in the river basin contributes to high turbidity in surface water. Further, the water quality indices recommended the use of surface water for various purposes. Furthermore, Pearson's correlation and two-way ANOVA revealed statistically significant relationships and variation in the concentration of physico-chemical characteristics. Factor analysis provided information about the major processes controlling the chemistry of rainwater, such as contributions from the sea and barren land, monsoon winds originating from long distances, the presence of petro-chemical industries, transportation based pollution (both land and sea) and regional forest fires (biomass burning) in South East Asia.

Geochemical processes control the chemistry of surface water showing a general enrichment in most of the parameters considered. The piper diagram identified two distinct chemical facies such as mixed Ca^{2+}- Mg^{2+}- Cl^- and Ca^{2+}- Mg^{2+}- HCO_3^- irrespective of seasons in surface water samples. Gibbs plots indicate dominant control of precipitation (rainfall) with an influence of mineral dissolution over the surface water chemistry. An increasing trend of Log pCO_2 values from upstream to downstream shows the direct recharge of rainwater with lower Log pCO_2 values in the upstream side and mixed water with higher Log pCO_2 in the downstream side. The saturation index indicates the under-saturated state of the carbonate minerals in the order of $SI_{Magnesite} > SI_{Calcite} > SI_{Aragonite} > SI_{Dolomite}$ and suggesting the effect of dilution through monsoon rainfall. Normalisation of surface water chemistry with rainwater chemistry also supports the findings. Significant relationships observed in the statistical analysis guided the interpretation of the processes which controls the geochemistry of surface water. Though factor analysis showed different factor components in samples collected during three different seasons, the dominance of high sediment load in response

to severe rainfall, weathering, leaching and dissolution of bed rocks, hydrolysis of organic nitrogen through decomposition of microorganisms and the aerobic decomposition of organic nitrogenous matter and atmospheric fallout are identified as the major contributors of surface water geochemistry. Overall, the hydroclimatic characterisation of the Limbang River Basin indicates that rainfall is the major factor controlling the runoff and geochemistry of surface water whereas natural and anthropogenic processes influence the chemical characteristics of rainwater. However, rainfall shows an increasing trend, indicating the influence of climate change, which is well reflected as seasonal variation in the composition of stable isotopes.

Key words: Hydroclimatics; Rainfall trend; Rainfall-runoff; Hydrochemistry; Stable isotopes; Climate change; Limbang; Borneo.

Contents

List of Figures

List of Tables

Chapter 1 Introduction

1.1 General

Hydrometeorology and hydrogeologic processes, which include the atmosphere, surface and groundwater processes are the most important processes in the hydrosphere and this domain is also undergoing the impacts of climate change at regional as well as a local scale. Effects of climate change over hydrometeorology will reflect as variations in precipitation pattern and amount, frequent as well as uncommon occurrence of extreme weather phenomena such as severe rainfalls, thunder storms, droughts and cyclones (Peterson et al., 1998; Barnett et al., 2004; Maurer et al., 2007; Boé & Terray, 2008; Vrochidou et al., 2013; Madsen et al., 2014; Knapp et al., 2015; Baltas, 2016; Walsh et al., 2016; Milly & Dunne, 2017; Vozinaki et al., 2018). At the same time, variability in quality as well as quantity of water resources (surface and groundwater) also showed the strong influence of climate change (Delpla et al., 2009; Whitehead et al., 2009; Park et al., 2010; Le et al., 2018). Overall, climate change will affect the equilibrium of the hydrological cycle, the never ending process, which circulates the water in the earth and makes life sustainable. This will have a negative effect on the geological, environmental and ecological processes too (Lavee et al., 1998; Lioubimtseva & Henebry, 2009; Robins et al., 2016).

In an effort to understand the influence of climate change due to increased atmospheric pollution and related global warming over the hydrological processes, scientists around the world are putting more priority on studying the water balance cycle. This includes the natural processes such as the transformation of water starting from evaporation, transpiration, condensation, precipitation, infiltration and runoff and discharge to lakes or oceans (Chahine, 1992; Trenberth, 2011; Tang et al., 2018). Result of these research reveal that though the processes involved in the hydrological or water cycle depends each other, it shows spatial and temporal variation. Due to the involvement of various hydrometeorological and geo-environmental variables and ecological processes, the branch of hydroclimatology has evolved (Sankarasubramanian & Vogel, 2002; Shelton, 2009; Molina-Carpio et al., 2017; Engström & Waylen, 2017; Petersen et al., 2018). Hydroclimatological studies of river basins or regions will provide a comprehensive idea about the impacts of climate change over water resources by integrating the analysis of hydrometeorology and the surface as well as near-surface water processes such as evaporation, runoff, groundwater recharge and interception (Tardy et al., 2005; Oguntunde et al., 2006; Burford et al., 2009; Oguntunde & Abiodun, 2013; Oguntunde et al., 2016; Wise et al., 2018).

Research on pattern variability and trend analysis of rainfall (wet precipitation) over a region has gained rapid development in recent decades. This is because precipitation is considered as the principal component and main input source of the hydrological cycle which is the first and best variable that reflects the influence of climate change (Bhutiyani et al., 2010; Trenberth, 2011; Ngah et al., 2012; Loo et al., 2015; O'Gorman, 2015). Numerous attempts have been reported from different parts of the world, to identify and quantify the influence of climate change over precipitation characteristics at regional scale (country or river basin) by applying various statistical techniques (De Luis et al., 2000; Hidalgo et al., 2003; Ghosh et al., 2009; Longobardi & Villani, 2010; Rana et al., 2012; Caloiero, 2015; Frazier & Giambelluca, 2017; Caloiero et al., 2018). However, it was noted that, in most cases rainfall showed more localised character and the effect of climate change also varies locally. Furthermore, few studies have reported that the precipitation acts as the scavenger of atmospheric pollutants and the chemical characterisation of rainwater will help to identify the contribution of natural and anthropogenic activities which deliver pollutants to atmosphere and induce the effect of climate change (Zunckel et al., 2003; de Mello & de Almeida, 2004; Al-Khashman, 2009; Huang et al., 2010; Al-Khashman et al., 2013; Niu et al., 2014; Szép et al., 2019). Chemical characteristics of rainwater shows variation in close spatial proximity and was controlled by regional and site specific meteorological characteristics such as humidity, temperature, wind direction and speed and contribution from local sources through evaporation (Kulshrestha et al., 2003; André et al., 2007; Chetelat et al., 2008; Akoto et al., 2011; Chughtai et al., 2014; Akpan et al., 2018). Source contribution of chemical constituents in rainfall over a region can be defined through the air mass back trajectory analysis and also by determining the composition and temporal variation in stable isotopes such as $\delta^{18}O$ (oxygen-18) and δD (deuterium) (Bergamaschi et al., 1998; Wang et al., 2005; Sjostrom & Welker, 2009; Uygur et al., 2010; Zhang et al., 2012; Salamalikis et al., 2015; Crawford et al., 2017; Gautam et al., 2018; Naimabadi et al., 2018; Zhou et al., 2019).

The amount of rainfall controls the runoff characteristics. In addition to that, runoff is also influenced by topography, land cover, land use, soil property, geology and other human induced activities (Kimaro et al., 2005). In order to understand the runoff characteristics, detailed data about the spatial and temporal characteristics of precipitation and river cross section are essential (Wang, 1994). Information about decreasing or increasing trends in rainfall and the rainfall-runoff characteristics will help in the development of specific strategies for flood hazard reduction and mitigation, in areas frequently affected. Precipitation dynamics along with the parameters described above and

its spatial variability, together influences the surface water (especially the river water) chemistry (Morgan & Good, 1988; Simeonov et al., 2003; Yidana et al., 2008). Proper understanding of the spatial and temporal variation in river (surface) water chemistry and the factors that control the chemical characteristics are essential for the development of water supply schemes such as irrigation, domestic use and human consumption. Overall, in order to get a comprehensive understanding about the hydroclimatological characteristics of the river basin, it is essential to investigate the rainfall trend patterns, runoff characteristics and chemical composition of rainwater and surface water.

In view of this, the present research was initiated to understand the impact of climate change over water resources, especially in rainfall (both quantity and quality), runoff process and surface water (quality) for regional as well as on a local scale. This study attempts to characterise the hydroclimatology of an equatorial tropical river basin, by examining trend analysis of long term rainfall along with runoff modelling. This is because as explained earlier, any change in the quantity of rainfall directly or indirectly influences runoff. Further chemical characteristics of rainfall (including stable isotopes) reaching the river basin and surface water collected from different locations were assessed through hydrochemical and statistical techniques. The study area, research purpose and scope, problem statement and research questions are discussed in the following sections.

1.2 Study Area

The Limbang River Basin (LRB) is the sixth largest river basin in the Sarawak state of East Malaysia, northern Borneo, located in the equatorial tropical region, where the environmental systems are very dynamic. The LRB extends from the northern Kalimantan in the south-south-eastern (SSE) part to the South China Sea in the northern part and covers a total area of 3950km^2. The LRB borders Brunei Darussalam on both its banks, in the lower catchment region and falls between the latitudes N 03^0 47’ 7” to 04^0 54’ and longitudes E 114^0 46’ 7” to 115^0 31’ 30” (Figure 1.1). The Limbang River flows 196km in the northwest ward direction, before finally discharging into the Brunei Bay. The river shows varying shape from linear to highly sinuous in its total flow. The LRB is an eight order river basin, and shows an elongated shape with maximum width in the central part and high drainage density in middle and upper parts. The Limbang River originates from Gunung Murud and Batu Lawi mountains summits, which is the highest elevated points in the LRB. Elevation of the river basin varies from 1m above mean sea level (MSL) near to the Brunei Bay to the higher than 2400m above MSL in the southern part. Though the basin is covered with tropical forests of

various densities and types, oil palm cultivation and small scale agricultural activities by the local people are also present. More details about the study area are presented in the following sections and a general nature of the study area is shown in Figure 1.2.

1.2.1 Accessibility

Limbang, one of the farthest administrative division of Sarawak in northern Borneo is connected with major other cities in Sarawak by air (domestic) and also by road network which passes through Brunei Darussalam. Limbang has very short distance of road networks that are well maintained (a maximum distance of 35km around Limbang City). However, numerous kampongs are located in the interior mountain ranges and river banks, which are not well connected with road networks and access is very limited. In order to access the middle and upper catchment region of the LRB, logging roads need to be accessed, and depending on the condition of the day i.e. if heavy rain persists, one cannot travel through the road due to its muddy and slippery nature.

1.2.2 Geological setup

1.2.2.1 Regional tectonic settings

Borneo, the third largest island in the world is located in South East Asia, a tectonically complex region, composed of smaller micro-continental and oceanic fragments between the Indo-Australian plate and the Philippine-Pacific plate and form part of Sundaland (Wilson & Moss, 1999; Hall, 2013). Three deep basins such as the South China Sea (SCS), Sulu and Celebes Seas are present in the north and northeast of Borneo and the narrow Makassar Strait form the boundary in the east, whereas the shallow Sunda Shelf in the west and south connect Borneo with Indochina, Peninsular Malaysia, Thailand, Sumatra and Java (Hall & Nichols, 2002). Mesozoic accretion of ophiolitic, island arc crust and micro-continental fragments of South China and Gondwana origin, along with the sedimentary cover on to the Palaeozoic continental core of the Schwaner Mountains in the SW of the island resulted the origin of Borneo (Hamilton, 1979; Hutchison, 1989). Borneo formed a promontory of Sundaland at the eastern margin of Eurasia at the beginning of Cenozoic period, partly separated from Asia by oceanic crust of a proto-South China Sea (Hall, 1996). During Early Miocene period, Borneo has rotated counter clockwise (approximately 45^0) and the rotation was well evident in the geological and palaeomagnetic records (Fuller et al., 1999). This oriented most of the northwest Borneo margin to NW-SE in most of the Oligocene and Early

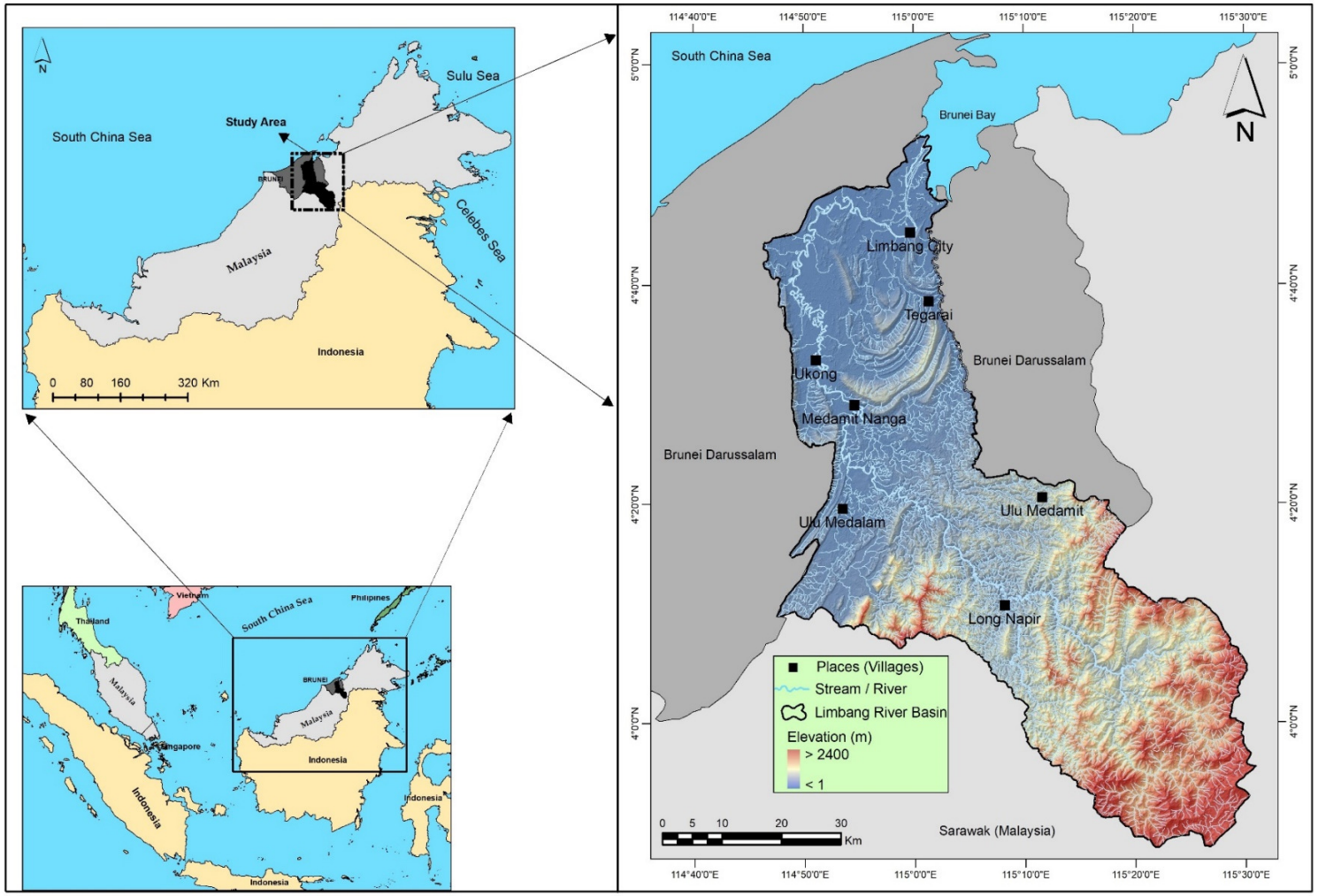

Figure 1.1: Location map of the study area (LRB) with river networks and terrain elevation.

Figure 1.2: General view of the LRB.

Miocene era, suggesting that most of the Palaeogene sediment in north Borneo was fed southwards across the Sunda Shelf from Indochina (Hall, 1996; Hutchison et al., 2000; Milsom et al., 2001). During the latest Oligocene and Early Miocene era, there was mountain building, erosion and change in character of sedimentation throughout much of Borneo (Rangin et al., 1990; van de Weerd & Armin, 1992; Hutchison, 1996; Moss & Chambers, 1999; Hutchison et al., 2000).

In northern Borneo, from Late Cretaceous to Early Tertiary (though Paleocene and Eocene) sandstone-shale turbidites were deposited in deep water forming the Rajang Group flysch (Hutchison, 2005). The sediments were derived from SW Borneo (Hall et al., 2008). These deposits now form the mountainous backbone of Borneo (Central Borneo Mountains and Crocker Ranges) which have been uplifted during the Sarawak Orogeny (Hutchison, 2005). The Sarawak Orogeny was the result of comprehensive deformation under a subduction related regime during Late Eocene (Hutchison, 2005) as the Proto-South China Sea subducted beneath north Borneo (Hall et al., 2008). The orogeny led to intense folding of the Rajang Group sediments and low grade metamorphism. A regional unconformity separates the steeply dipping and complexly folded Rajang Group from the overlying post-Eocene sediments deposited under shallower conditions (Hutchison, 2005). During the post-Eocene period, there was migration of the Sundaland shoreline in a NNW direction, from an Eocene position in the central Borneo to its current position with sediments continually accumulating offshore (Wilson & Moss, 1999). Many authors have commented on the size and considerable sediment thickness accumulated in sedimentary basins in and around Borneo since Cenozoic (Hall et al., 2008; Van Hattum et al., 2013) and in particular the extent and thickness of Eocene-Lower Miocene Crocker Fan of north Borneo (Hall et al., 2008). The Crocker Fan sediments are derived from nearby local sources in Borneo and SE Asia, (Van Hattum et al., 2013) i.e. from elevated and sediment-shedding Sundaland source area in the SSW (Hall et al., 2008). The Miocene witnessed the collision of South China microcontinent blocks with the western edge of Borneo and the cessation of deep water sedimentation (Van Hattum et al., 2013) with ongoing uplift in central Borneo. There was a change from deep water sediments and mélanges to shallow marine and fluvio-deltaic sediments (Hall et al., 2008; Van Hattum et al., 2013). The thick Neogene sediments were deposited in marginal basins on and around Borneo. Between 18Ma and 15Ma (Early to Mid-Miocene), the coastline shifted from a NNW direction to its present NE direction (Hutchison, 2005). Besides the sedimentary formations, there are few numbers of Quaternary volcanoes (basaltic formations) also present in Borneo (Hall et al., 2008). It was considered that, the Borneo region does not possess any continental or plate boundaries and active faults and is considered comparatively stable land but the recent occurrence of earthquakes in the northern Borneo (Sabah) indicate the ongoing tectonic processes in the region (Sapin et al., 2011; Wang et al., 2017; Shah et al., 2018).

Moreover, considering the region specific geology, the LRB was part of the Sarawak region in northern Borneo, which was divided into four zones such as Miri zone (north), Sibu

zone (central), Kuching zone (southwest) and West Borneo basement (most southerly zone) based on the geologic history (Haile, 1974). The Miri zone is dominated by shallow marine shelf sediments deposited upon older continental crust whereas the Sibu zone consists of thick shale-sandstone turbidite formations over oceanic crust (Williams & Harahap, 1987; Hutchison, 1989, 2005). Rock formations in the Kuching zone consist of Jurassic–Cretaceous shelf deposits, molasses and related non-marine deposits on the edge of the West Borneo Basement Complex (Haile, 1974; Hutchison, 2005). However, rock formations in West Borneo Basement Complex include the intruded volcanic and plutonic rocks of Cretaceous over the Carboniferous-Permian basement rocks (Haile, 1974; Williams et al., 1988). The boundary between different geological zones in Sarawak was marked by Tatau-Mersing Line (divides Miri and Sibu zones) and Lupar Line (divides Sibu and Kuching zones) (Tan, 1979; Hutchison, 1989).

1.2.2.2 Geological set up of the Limbang River Basin

As discussed in the regional geological setting section, most parts of Borneo is composed of sedimentary formations with varying geological age consisting of varying assemblage of rock types. The LRB in the northern part of Borneo, is completely (more than 90%) made up of Tertiary sedimentary formations followed by coastal and riverine alluvium of Quaternary period. Major rock formations present in the LRB are given in Table 1.1 and in Figure 1.3. Though different formations are present in the LRB, most dominant rock types are sandstone, shale, slate, phyllite and limestone.

The Mulu and Kelalan formations consist of shale, slate, phyllite, sandstone with marlstone, calcareous sandstone, conglomerate and limestone lenses spatially located at the western part of the river basin. These formations also underwent weak regional metamorphism. The Melinau limestone formation is found to be localised in the southwestern side of the river basin and is occasionally present in the downstream reach. These formations consist of thick biohermal limestone, mainly composed of calcarenite, some calcilutite and rare marlstones. The greater Mulu Caves are located in this area. The Setap shale followed by Meligan formations in the region consist of sandstone, shale, mudstone, limestone, lignite with some marlstone, siltstone and calcareous sandstone in which the Setap shale formations covers a major part of the river basin. The Belait formations which is comparatively young compared to other formations in the LRB consists of sandstone, siltstone, shale, sand, clay with some conglomerate and lignite which are poorly consolidated. However, low elevated areas and flood plains are covered by recent riverine

and coastal alluvium. Due to strong structural disturbances during the recent geological past, a multitude of regional structural features such as faults, folds and structural trend lines are present in the region. Numerous anticlines and synclines are present in the LRB, which is reflected as undulations in terrain characteristics. It is also noted that the influence of structural features can be well identified from the drainage characteristics.

Table 1.1: Geological formations in the LRB with stratigraphic age and major rock types in each formations (MGDM, 2013).

Period	Formation/Age	Rock types
Quaternary	Coastal and Riverine Alluvium (Pleistocene – Holocene)	Coastal riverine alluvium, and terraces of clay, silt, sand and gravel with layers of peat.
Tertiary	Belait (N_2Be) (Miocene – Pliocene)	Sandstone, Siltstone, shale, sand, clay with some conglomerate and lignite: poorly consolidated in general.
	Maligan (N_1Me) Miocene	Sandstone, shale, mudstone, limestone, lignite with some marlstone, siltstone and calcareous sandstone.
	Setap shale (P_7S) (Oligocene - Miocene)	Sandstone, shale, mudstone, limestone, lignite with some marlstone, siltstone and calcareous sandstone.
	Melinau limestone (P_5MI) (Eocene – Miocene)	Thick biohermal limestone, mainly calcarenite, some calcilutite and rare marlstone.
	Kelalan (P_2Ke) (Paleocene – Eocene)	Shale, slate, phyllite, sandstone with marlstone, calcareous sandstone, conglomerate and limestone lenses. Weak regional metamorphism.
	Mulu (P_2Mu) (Paleocene – Eocene)	Shale, slate, phyllite, sandstone with marlstone, calcareous sandstone, conglomerate and limestone lenses. Weak regional metamorphism.

1.2.3 Soil

Soil cover present in the LRB varies widely in its textural type and characteristics. Variation in soil type is more in the lower river basin than the upper catchment areas. Overall, most of the river basin are covered with three dominant types of soil such as Kapit, Merit and Meluan (DoA, 1972; Liong, 1982). Among this, Kapit soil covers more area. Kapit soils are classified as residual skeletal soil, formed from shale and sandstone parent material having

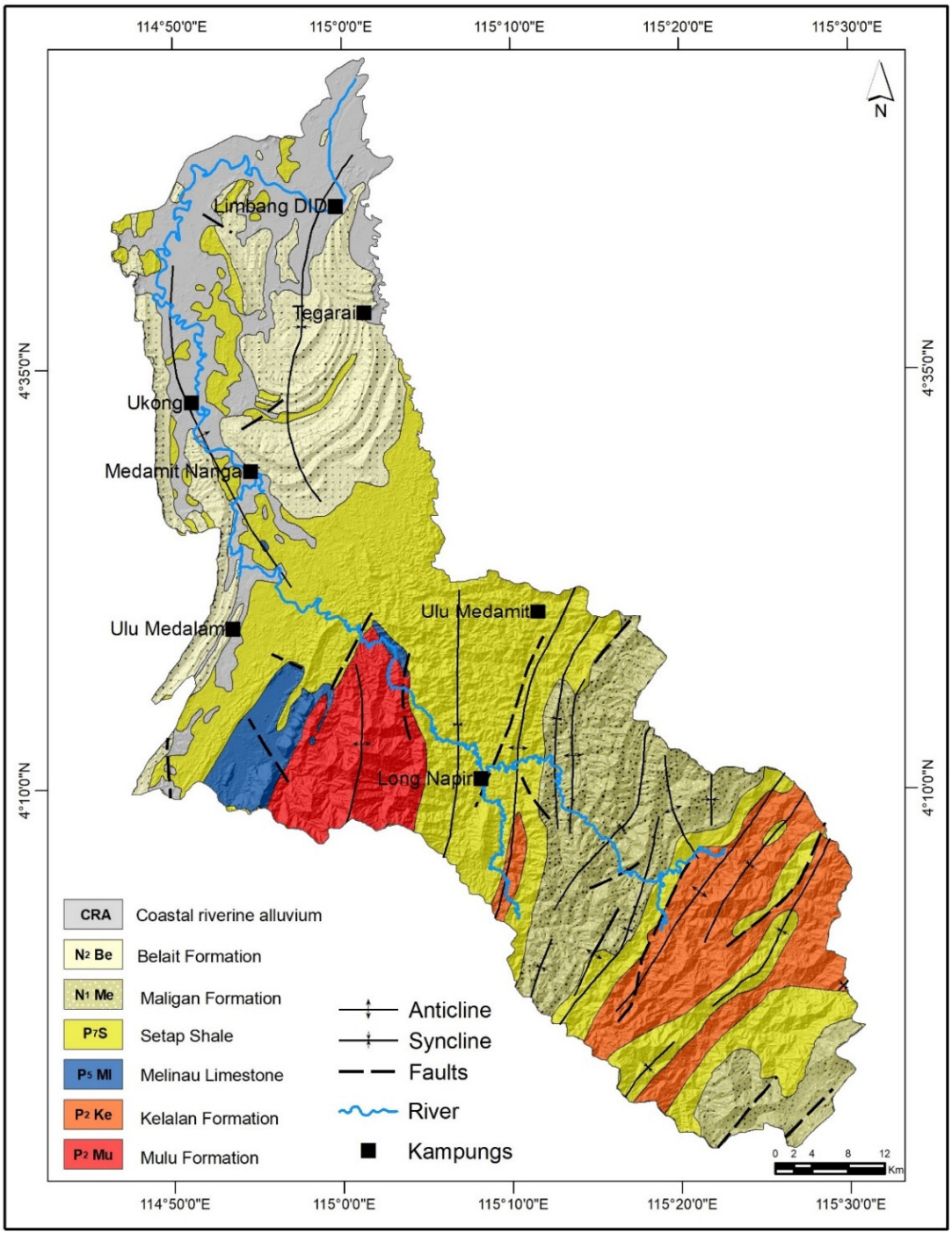

Figure 1.3: Geological set up with major rock formations present in the LRB (Source: MGDM, 2013).

clay or sandy clay texture. Areas covered by Merit and Meluan follows that of Kapit and are mainly concentrated in the upper river basin as well as in the lower reach. Merit soil shows fine clay textures whereas the Meluan soil shows lithic or paralithic textures. All the soil characteristics in this region were highly influenced by the composition of parent rock. However, the soil present in the lower river basin shows the influence of marine and riverine

deposition environment in its characteristics. Most of the lower river basin was covered with a vast stretch of peat soil, flood plain riverine clay (non-calcareous) and marine calcareous sediments.

1.2.4 Land use / land cover

As an equatorial tropical rainforest region, a major portion of the LRB was covered with secondary, primary and montane forests. Secondary forest covers lower elevation reaches and was the product of intense logging activity in the region. Meanwhile, primary forests exist in the inaccessible areas and protected regions. Montane forests are located at higher elevation mountains. Besides the forest cover, the major land use in the river basin is oil palm plantations, which are seen up to the middle reach of the basin. Other land uses present in the region are paddy fields (both wet and hill paddy) and mixed fruit land. These are associated with kampongs in the river basin. Overall, the LRB can be considered as a forested river basin.

1.2.5 Climate and rainfall characteristics

One of the biggest equatorial tropical island, Borneo experiences tropical hot, humid climate with abundant rainfall throughout the year. Based on the climatic classification proposed by Köppen (1900), Borneo is considered in the class Af, which specifies the climate as tropical rain without a dry season and a long-term mean precipitation in the driest month higher than 60mm (Ritzema & Wösten, 2002). Borneo as a whole receives an average annual rainfall exceeding 3000mm and shows high variations in daily mean temperature in the range of 20^0C to 34^0C (Hamada et al., 2002). As an equatorial tropical rainfall region, relative humidity exceeds 90% in most time. Borneo's climate is highly influenced by large scale weather phenomena such as El Niño-Southern Oscillation (ENSO), Indian Ocean Dipole (IOD) and Madden-Julian oscillation (MJO), which leads to torrential rainfall, flash floods, and severe storms (Aldrian & Djamil, 2008; Tangang et al., 2008; Hidayat & Kizu, 2010; Moron et al., 2010; Salahuddin & Curtis, 2011; Robertson et al., 2011). Along with this, Inter Tropical Convergence Zone (ITCZ), also has higher influence on the long term and monsoon rainfall characteristics of Borneo which enables the region to receive two periods of heavy rainfall in a year (Zhang, 2005; Maloney & Shaman, 2008). Though the region receives a higher amount of rainfall in most months, its spatial distribution in the region will vary widely. The mountain ranges in the central and northwest Borneo receive higher rainfall than any other places. At the same time, the south and east coastal low land receives the lowest precipitation (Tapper, 1999; Kirono, 2004; Wooster et al., 2012).

The present study area, the LRB, which is located in the Sarawak state of Malaysia in northern Borneo, is marked as the region that receives an average annual rainfall higher than 3500mm, which shows high influence of the South China Sea in precipitation characteristics. It was also noted that, the region recorded a higher rate of rainfall than the country's average annual rainfall i.e. 3851mm against the national average of 2000mm. In addition, it was recorded that the rain gauging station Tegarai in the LRB received an annual rainfall of 6926mm in the year 1996. Though the LRB receives a higher amount of annual average rainfall, it shows high spatial variability in distribution. Coastal regions and higher elevated regions receive lower amount of rainfall than moderate elevation regions and areas encircled by higher elevated mountains. Rain gauging stations in the LRB recorded monthly rainfalls in the range of 180mm to 800mm and it has been observed that in this region, no clear discrimination exist between the seasons because almost every month receives an average rainfall of more than 250mm. However, due to the effect of oscillation of the Inter Tropical Convergence Zone (ITCZ) between north and south, the whole region experiences two dominant monsoon seasons, which were well evidenced in the study area (Asnani, 1993). Rainfall distribution in a year in the region is divided into two, i.e. monsoon seasons and inter-monsoon periods (Langner et al., 2007; DID, 2015). The south west monsoon (SWM) which covers five months from May to September, marked a comparatively dry season (lower rainfall) in the study area. At the same time north east monsoon (NEM) season which covers a period of five months from November to March recorded the wettest period (higher rainfall) in the region. These two monsoon seasons were separated by a short inter-monsoon period of one month each, i.e. April and October also recorded comparatively higher amounts of rainfall. During the SWM, the LRB receives an average rainfall of 1412mm whereas in NEM, average rainfall recorded in LRB shows comparatively higher value of 1672mm. Considering the inter-monsoon periods, the LRB received an average rainfall of 341mm and 335mm in April and October respectively. As a hot humid equatorial river basin, the average daily temperature in the LRB ranges from 16˚C to 34˚C with a high average relative humidity level of 90%.

1.3 Purpose and Scope

The LRB possesses highly dynamic climatic and terrain conditions along with intense logging activities which control the overall hydrologic characteristics of the basin. Unlike other countries and regions, isolated villages inside the tropical forest regions in the East Malaysia (including the study area) are located in the river banks and peoples in the villages predominantly depend on the river (Sungai in Malay) water for livelihood, agricultural

practices and daily needs. Recent time (last three decades), the study area and neighbouring regions has undergone rapid change in the terrain and vegetation characteristics due to deforestation as timber logging and plantations (oil palms) activities, which increased the runoff, erosion and sedimentation, ultimately altered the hydrological characteristics of the basin. Consequently, this has increased the terrain instability, caused reduction in water infiltration which leads to the increased delivery of sediment to the river leading to siltation and increases turbidity and frequent flooding with high sediment load in the lower segments of the river. Furthermore, the Sarawak Energy Berhad's (SEB), plan to implement two hydro-electric projects (HEP's) to produce 245MW power from the Limbang River and initial feasibility studies have been completed (SEB Annual Report, 2010). Under this circumstance, the present research can be considered as the first attempt which has been formulated to address and characterise the hydrologic characteristics of the LRB in terms of hydrometeorology and hydrochemistry. The findings of the present study will provide a clear cut idea about the river basin hydrology and insight into the hydrological process and its interrelationships. Further the findings of the present research will serve as basic information about hydrologic characteristics of the LRB during the pre-Dam scenario.

1.4 Problem Statement

Equatorial tropical rainforest river basins (especially the LRB) in Borneo were highly exploited during the last few decades in connection with industrial development, agricultural development and logging activities. These processes highly alter the hydrological characteristics of the river basins due to extensive alteration of terrain conditions in connection with intense timber logging, log recovery, skidder trail, logging road development and oil palm plantation development. Intensification of logging and plantation activity related to terrain alteration has increased the sediment load in rivers and influences the water quality. Along with this, severe weather phenomena such as El Nino, Tropical cyclones and typhoons will effect climate changes and induce variation in meteorological characteristics of this region, which requires detailed understanding for framing better management strategies in agriculture and hydrological development processes. Moreover, understanding the water quality in the river basin is an important requirement because people living in the Limbang administrative region of Sarawak, Malaysia are highly dependent on the Limbang River for their livelihood and daily use. Though the study area has a network of rainfall, water level and sedimentation observation stations, no studies have been conducted to address the spatial and temporal variability in catchment scale hydrological processes in the LRB (Muhammad Noor Hisyam, 2010; Tie, 2010). Thus, understanding the

existing research gap and lack of detailed information about the hydrometeorological and hydrochemical characteristics of the LRB, the present study is initiated. The present research uses available secondary data (rainfall and discharge) and field based analysis of chemical and isotopic characteristics of precipitation (rainwater) and surface water samples. The result of rainfall trend and rainfall-runoff model serves as a valuable guide for making reliable decision for better developmental planning in the low laying flooded areas by reducing the social impacts of flooding through framing proper management strategies. Further, the result of physico-chemical analysis and isotopic study provides important information about the natural and anthropogenic activities in the region and its impact on water resources. Tropical regions are experiencing environmental degradation due to natural (climatic changes) and anthropogenic causes and the present study will help to generate a baseline data for the LRB in terms of catchment hydrologic characteristics.

1.5 Research Questions

The present research attempts to address the following questions:

1. What will be the trend characteristics of rainfall over the LRB and how is the rainfall-runoff linked?
2. What is the chemical characteristics of rainfall and surface water in the present period and how do they vary spatially and temporally at catchment scale?
3. How are the stable isotopes ($\delta^{18}O$ (oxygen-18) and δD (deuterium)) temporally distributed in rainfall over different locations in the LRB?
4. What are the dominant factors that control the (geo)chemistry of rainwater and surface water and how do the rainfall and runoff influence the overall hydrologic characteristics of the catchment?

1.6 Aim and Objectives

The present research was formulated with a specific aim of understanding the catchment scale hydrological characteristics of the Limbang River Basin in northern Borneo through the (a) assessment of hydrometeorological and (b) hydrochemical as well as the hydrostatistical characteristics of the LRB.

The declared aim of the present research is achieved through five well defined objectives as given below:

1. Analysis of historical rainfall data to understand the characteristics of rainfall (spatial and temporal changes) in the study area using statistical methods.
2. Rainfall-runoff modelling using ANN model with the support of rainfall data and comparison of the observed and predicted runoff values.
3. Analysis of stable isotopes in precipitation (rainwater) to identify the moisture source and its temporal variation.
4. Analysis of physico-chemical parameters in rainwater and surface water to determine the (geo)chemical characteristics.
5. Cross validation of the finding of rainfall trend and runoff model using hydrochemistry and stable isotopes.

1.7 Structure of the Thesis

This thesis has five chapters. Chapter 1 deals with the background of the research, purpose and scope, aim and objectives of the research, along with a basic description of the study area. An extensive review of literature related to the research carried out on hydrometeorology and hydrochemistry is presented in chapter 2. Next, appropriate methodology for the successful completion of present research and in achieving the declared objectives and details of primary and secondary data used in the research is described in chapter 3. In chapter 4, interpretation of the analysis results and its discussions were given. Rainfall trend analysis, rainfall-runoff modelling, hydrochemistry and hydrostatistics of rain and surface water, stable isotopes in rainwater and the interrelationship between the parameters considered are discussed in detail in this chapter. Finally, the summary and conclusions drawn from the research along with its applicability in hydrological development projects and scope for future studies are examined in chapter 5.

1.8 Summary

This chapter explained the overview of the research carried out. It also briefly stated the research problem along with research questions and the defined objectives to achieve the aim of the research. The scope and purpose of the research argues the necessity of carrying out the present research, and is the first time attempt done in the region to study the hydrologic characteristics of the forested river basin which will be altered by the implementation of hydroelectric projects. The research took a comprehensive approach, i.e.

through the analysis of spatial and temporal characteristics of hydrometeorology and hydrochemistry of forested river basin in northern Borneo to examine how these factors come into play in influencing the overall hydroclimatological characteristics of the basin.

Chapter 2 Literature Review

2.1 General

Catchment is the area from which water drains into the river and catchment hydrology mainly deals with the hydrological process taking place at the catchment scale. Understanding about the availability of water resources in the current and future situation is important for better management of water resources. Spatial and temporal changes of water resources have significantly affected agricultural, industrial and urban developmental activities. Climate change has a major impact on the natural system which significantly controls the water resources. In addition, further changes in the spatial and temporal pattern of precipitation are the direct indications of climate change. Rainfall is the primary source of runoff. In addition to rainfall, runoff is also influenced by many factors such as soil characteristics, the area of catchment, slope, wind, temperature, evaporation, humidity and land use / land cover (Baig et al., 2008). Therefore, identification of local impacts of climate change in catchment level is important for the development and management of water resources. Catchment hydrology and hydroclimatology are growing research areas in water resource management with an enormous number of researches undertaken (Uhlenbrook, 2006).

The present research focuses on rainfall trend analysis, rainfall-runoff modelling and water chemistry (rainwater and surface water) including stable isotope composition in rainwater to generate a comprehensive idea about the catchment hydrology of the Limbang River Basin (LRB). In order to understand the progress and current status of each objective of the present research, an extensive and detailed literature survey was carried out. Importance is given to studies which used well established, tested and replicable methodologies in rainfall trend analysis, rainfall-runoff modelling, water chemistry and isotope analysis. In view of the objectives declared and the methodology to be undertaken to achieve the declared objectives, the review of literature is categorized into four sections.

2.2 Rainfall Trend Analysis

Trend analysis is a method to assess past rainfall pattern and also to predict the future rainfall pattern and characteristics using historic rainfall data. It will provide an early warning for the impending problem of climate change. Different statistical methods are available for the rainfall trend analysis and are classified into two, such as parametric and

non-parametric methods. Numerous studies were carried out using these two methods. Parametric tests need highly accurate, independent, continuous data with homogeneity (normally distributed) which is very rarely possible in hydrological measurements while the non-parametric tests which also use independent data sets but the method are capable of accommodating errors in datasets (Mann, 1945; Kendall, 1948; Lehmann & D'Abrera, 2006).

Monthly and annual precipitation trends in the Iberian Peninsula were analysed by Serrano et al. (1999) through the Mann Kendall test by considering 75 years (1921-1995) of data from 40 meteorological stations. Results indicate a significant decreasing trend in monthly rainfall especially in the month of March but annual rainfall does not show any significant trends. Partal and Kahya (2006) studied the trend in Turkish precipitation using 64 years (1929-1993) of daily rainfall data through the Mann Kendall and Sen's T tests. Their analysis revealed a strong decreasing trend in the month of January, February and September and in annual mean precipitation in western, southern Turkey and the coasts of the Black Sea. Time series analysis of precipitation at Uccle, Belgium was carried out by De Jongh et al. (2006) using 105 years (1898 - 2002) of data by applying the Mann Kendall, Adaptive Kolmogorov - Zurbenko filter (KZA) and Wavelet techniques. The Mann Kendall trend results of Uccle precipitation shows a statistically significant positive trend in the month of March along with annual and winter season precipitation. KZA analysis of drought estimation indicated a drier condition than normal. Meanwhile, the Wavelet analysis of monthly precipitation revealed a statistically significant yearly cycle in the region. Considering 30 years (1961-2006) precipitation data of 81 meteorological stations in the Yellow River Basin, China, Liu et al. (2008) studied the spatial and temporal change in the annual precipitation trend using the Shannon entropy, Mann Kendall and linear fitted model. Overall, the results showed a decreasing trend in 33 stations and an increasing trend in 2 stations. Similarly, Fatichi and Caporali (2009) carried out a study to understand the change in precipitation pattern in Tuscany, Central Italy, using 40 indexes and precipitation trend using four statistical tests (Pearson linear correlation and F-Fisher test, Mann Kendall test, Cox and Stuart test and Daniels test which uses Spearman test to verify if the variables shows monotonous changes). A total of 87 years of data (1916-2003) was collected from 785 rain gauges and 40 indexes were applied to detect the change in precipitation patterns. An absence of a trend was noted in the average precipitation regime and in the intensity of extreme events of 3-6 and 12h in almost all stations. A similar result was also noted in the four methods considered.

Using 23 years (1871-1994) of monthly rainfall data, Krishnakumar et al. (2009) studied trends in rainfall over entire Kerala, India by applying the Mann Kendall rank statistics and linear trend analysis method. They identified an insignificant increasing trend in the winter and summer season's rainfall in Kerala. Abaje et al. (2010) carried out a rainfall trend analysis study through Cramer's test using 35 years (1974-2008) of data in Kafanchan in the Kaduna State of Nigeria. They sub-divided the entire data into 10 years overlapping periods. The results showed a decreasing trend in the sub-period (1999-2008) in annual rainfall series. Similarly, the trend analysis (Mann Kendall, Spearman's Rho, Linear regression test) and step change (Distribution free CUSUM, Cumulative deviation and Worsley likelihood ratio test) of annual rainfall and runoff in the Murray-Darling Basin (MDB), south eastern Australia was carried out by Potter et al. (2010) using long term daily data for a period of 112 years (1895-2006). The results indicate that only a small area of MDB shows a statistically significant decreasing trend for rainfall and runoff and a large step change was observed in the mid 1940's in most of the region. It was also noted that the results of trend analysis and step change for a statistically significant levels are almost similar in the case of rainfall data and runoff data. Using 12 years of data from 4 meteorological and 1 hydrometric stations in the Jhikhu Khola watershed, Nepal, Gautam et al. (2010) carried out the trend analysis of annual and seasonal rainfall, stream flow and temperature through Mann Kendall, Spearman's Rho and Modified Mann Kendall test. Results show an increasing trend in the case of annual precipitation and annual average stream flow. At the same time, statistically significant increasing trend was observed in the monsoon and pre-monsoon period rainfall and monthly rainfall. But in the case of post monsoon rainfall and temperature, the trend is insignificant.

Annual and seasonal rainfall trends at Calabria, Southern Italy was studied by Caloiero et al. (2011) through Mann Kendall and linear regression methods by considering 85 years (1916-2000) of rainfall data from 296 stations. Both tests gave similar results for trend analysis such as decreasing trend for annual and winter-autumn rainfall and increase in rainfall for summer seasons. The extreme rainfall trend during the monsoon rainfall in 30 meteorological subdivisions in India was investigated by Subash et al. (2011) through Mann Kendall, Spearman's Rho and Sen's slope methods by considering the data during the period of 1871-2008. They observed that both trend tests gave similar results for all subdivisions and half of the subdivision showed a positive trend during the monsoon, and among that 4 are statistically significant. Another study was carried out by Raj and Azeez (2012) in the Bharathapuzha River Basin, Kerala, India to detect monthly, seasonal and annual rainfall trends by considering 34 years (1968-2002) of monthly rainfall data using Mann Kendall's

rank correlation statistics and wavelet analysis methods. The analysis revealed a significant decrement in annual rainfall towards the later years in the Bharathapuzha River Basin. Shanmugasundram (2012) conducted a study in the Yarra Water Catchment in Melbourne, Australia to understand the climate change and its impact on water resources through step change detection (Median change point, rank sum, likelihood ratio, student t and CUSUM test) and trend detection (Mann Kendell, Spearman's Rho and linear regression test) methods using an average 80 years (1856-2007) data from 11 rain gauges and 3 temperature stations. Statistically significant decreasing trend was observed in the annual rainfall and statistically significant increasing trend was observed in the case of annual minimum temperature. Step change analysis showed two major climatic shifts in rainfall during the middle of the century and in the last decade whereas in temperature, major change occurred between the period of 1950s and 1960s.

By considering 92 years (1917-2008) of precipitation and rainy days' data from 400 stations in the United States, Martino et al. (2012) carried out a trend detection study through Mann Kendall, Spearman's Rho and Sen's slope tests. The result shows a statistically significant increasing trend in annual precipitation and rainy days in less than half of the stations. Considering seasonal precipitation (summer, winter, spring and fall seasons), more number of stations showed positive trends than annual precipitation. Gocic and Trajkovic (2013) carried out a study to understand the monthly, seasonal and annual precipitation trend and behavior of drought in Serbia, the central part of Balkan Peninsula, through Mann Kendall, Spearman's Rho and linear regression tests by considering 30 years of data (1980-2010) from 12 synoptic stations. They found that in February all stations showed a decreasing trend whereas in all other months, both decreasing and increasing trends were observed. An increasing trend was observed in the autumn and winter season and no significant trend was observed in the case of annual rainfall. In addition to that, two main drought periods (1987-1994 and 2000-2003) was also detected in which the year 2000 was the driest. In similar vein, Li et al. (2013) conducted a study on precipitation trends and periodic traits in the Beijing area in China, using 286 years (1724-2009) of data through Mann Kendall test and wavelet transformation and found a significant (5%) increase in precipitation. In addition, statistical analysis of precipitation and regionalisation of significant geographic regions based on hydroclimatic changes in Western Algeria was carried out by Hamlaoui-Moulai et al. (2013) through principal component analysis, Spearman's Rho and Mann Kendall tests by considering annual rainfall data from 21 metrological stations during the period of 1914-2004. They found a decreasing trend of annual rainfall in most of the stations. Taxak et al.

(2014) conducted a rainfall trend analysis and homogeneity study in Wainganga Basin, Central India through Homogeneity, Mann Kendall test, Sen's slope estimator and Pettitt-Mann-Whitney test using 111 years (1901-2012) of data. They observed a non-significant increasing trend in the post monsoon season, a significant decreasing trend in the monsoon and a non-significant decreasing trend in pre-monsoon and winter season respectively.

Annual, seasonal and monthly rainfall trends of seven rain gauge stations in the west Iran was studied by Talaee (2014) by considering 40 years (1969-2009) of data through non-parametric tests (Kendall, Spearman and Mann Kendall) at 95% confidence level. The magnitude of the trend was evaluated through Theil Sen estimator. Based on the study, the annual and seasonal rainfall shows an insignificant trend in almost all the stations whereas monthly rainfall showed a significant trend during the months of February, March and November. By considering more than 30 years (1970- 2007) of data from 95 hydroclimatic stations in the Urmai Basin, Iran, Fathian et al. (2015) conducted a study to understand the trend in annual and seasonal temperature (25 stations), precipitation (35 stations) and stream flow (35 stations) through Mann Kendall, Spearman's Rho and Sen's T test. They found a significant increasing trend in temperature throughout the basin. In the case of precipitation, 75% of the stations shows no trend and the remaining stations shown increasing and decreasing trend. 80% of the station show a decreasing trend in stream flow. Huang et al. (2015) also carried out monthly and seasonal rainfall trend at the Langat River Basin, Malaysia by selecting 10 stations using 25 years (1970 to 2012) of data through Holt's, Kendall Tau, Spearman's Rho test. They observed a positive trend in March, July and November and a negative trend in May and September in monthly rainfall. Among the 10 stations, 7 stations showed an increasing trend for seasonal rainfall. The annual rainfall trend of Turkey (Anatolian Peninsula) was analysed by Asikoglu and Ciftlik (2015) using an average of 40 years of (1961-2005) data from 47 rain gauges through parametric (Student's T test) and non-parametric (Mann Kendall, Spearman's Rho and Sneyers test) tests. Statistically significant decreasing trend in annual rainfall was observed in the northern half of the Aegean region of Turkey and the results of parametric and non-parametric tests are complementing.

Trends of extreme rainfall event of different durations (10min, 30min, 1h, 3h, 6h, 12h, 24h and 48h) from 23 stations in Victoria, Australia for an average of 50 years were analysed by Yilmaz and Perera (2015) through Mann Kendall and Spearman's Rho tests. Increasing trends were observed in the case of short storm duration whereas long storm duration showed decreasing trends, and most trends are statistically significant. Che Ros et

al. (2016) conducted a homogeneity test (Pettit test, standard normal homogeneity test, Buishand range test, and von Neumann ratio test) and trend analysis (Mann Kendall test) of long and short term characteristics of annual rainfall variability in the Kelantan River Basin, Malaysia using 63 years (1948-2011) of rainfall data. Three sampling methods were considered to understand the long term and short term characteristics; in which a 30 year sampling showed decreasing trends during 1957-1987 and an increasing trend during the years of 1981-2011. They also observed a significant rainfall variability in 10 years moving segment sampling. In the case of sequentially increased sampling, no significant increasing or decreasing trend was observed. Trend analysis (Mann Kendall and Spearman's test) of precipitation along with correlation coefficient relationships between time and precipitation was calculated through non-parametric tests (Spearman's Rho and Kendall's tau) in the State of Florida by Metellus (2016) using 173 years (1843-2010) of data from different short and long duration rain gauges. Among 73 short duration stations, 15% stations show statistically significant increasing trends, 8% out of 112 stations showed increasing trends in hourly duration and for the daily duration, while 5% stations (out of 242 stations) show an increase in precipitation. Monthly, seasonal and annual rainfall trend of Logone catchment, Chad Basin in Africa was carried by Nkiaka et al. (2017) using 50 years (1951-2000) of rainfall data from unevenly distributed 17 rain gauges, through Mann Kendall, Spearman's Rho test and Sen's slope methods. A negative trend was observed in the case of annual and seasonal (monsoon and pre-monsoon) rainfall, but monthly rainfall shown insignificant positive trends in 32% of the stations. Rahman et al. (2017) studied the trend of annual, monthly and dry seasonal rainfall over 14 rain gauges in Bangladesh through Mann Kendall and Spearman's Rho tests and ARIMA modelling using 60 years (1954 -2013) of data. No significant trend was observed in the case of annual and dry season except few (2 or 3 stations) but monthly rainfall shown a mixed trend.

Zhao et al. (2017) analysed precipitation data and standard precipitation index for a period of 1958-2015 by considering 14 rain gauges on Loess Plateau, China, where precipitation has major role in erosion, using trend free pre-whitening, linear trend estimation, Spearman's Rho test, Mann Kendall trend test, Mann Kendall abrupt change test and rescaled range analysis. They observed a decreasing trend in the rainy seasons (July, August and September) and annual rainfall but other months show increasing and decreasing trends. The trend analysis of annual maximum rainfall intensity data at 60 pluviograph stations in New South Wales, Australia was carried out by Hajani et al. (2017) by means of considering rainfall data during the period of 1955-2010 through Mann Kendall and

Spearman's Rho test at 0.10, 0.05 and 0.01 confidence levels. Result showed a statistically significant positive trend rather than negative trend for rainfall with short duration intensity. In another study, a combination of non-parametric method such as Mann Kendall and Spearman's Rho tests were considered by Al Mamoon and Rahman (2017) to understand the spatial and temporal variation of rainfall in Qatar by analysing 49 years (1962-2010) of data from 29 rain gauges. They observed a mixed trend (increasing and decreasing trends), in annual total and maximum daily rainfall. The result also indicates that the seasonal rainfall in Qatar is changing. Besides that, the trend analysis of annual and seasonal rainfall, along with hourly extreme rainfall event recorded at 31 rainfall stations in Sarawak, Malaysia for a period of 1980-2014 were analysed by Sa'adi et al. (2017) through Mann Kendall and Modified Mann Kendall tests. Five stations showed a significant increasing trend in annual rainfall and regionalised significant trend were observed in the case of extreme rainfall. At the same time, increase in rainfall were observed during the northeast monsoon and decrease in rainfall was observed in the southwest monsoon season. In addition to that, 15 different rainfall indices of the trend were recorded and Sen's slope to estimate the rate of change in trend was carried out, which identified a mixed trend.

Parametric and non-parametric methods such as linear regression, conventional Mann Kendall, Spearman's Rho and Sen's slope estimator were used to understand the precipitation trends in Chhattisgarh state, India by Meshram et al. (2017) considering 102 years (1901-2002) data from 16 stations. The result show a decreasing trend (95% significant level) in annual precipitation at 14 stations. Meanwhile, Yu et al. (2017) carried out a study in Hexi Corridor, northwest China, through Mann Kendall, Spearman's Rho test and linear regression to understand the precipitation trends and also considered standard precipitation index to identify the effectiveness of drought. They considered data from 9 meteorological stations during the period of 1970-2012. Results of monthly rainfall showed a significant increasing trend in three stations, while seasonal rainfall showed significant increasing and decreasing trends in five stations whereas annual rainfalls showed a significant increasing trend in one station. Drought estimation revealed three drought intervals in the period of analysis, among which 1986 was the driest year. In another study, Kamruzzaman et al. (2018) studied annual, cropping seasonal rainfall and temperature trend through Mann Kendall, Spearman's Rho and Modified Mann Kendall test using 51 years (1961-2011) of data from 12 stations in the western part of the Bangladesh to understand the spatial and temporal variations in climate. Almost 71% of the stations shown insignificant trends in annual rainfall for both tests whereas 83% of the stations shown a significant positive trend in annual

temperature. Annual and seasonal trends in precipitation and evaporation in the Narmada River Basin, India was carried by Pandey and Khare (2018) through Mann Kendall and Spearman's Rho tests. They considered 102 years (1901-2002) of data from 12 precipitation and 28 evaporation stations. Most of the stations showed no trend in annual, seasonal precipitation and monthly evaporation whereas all stations showed a positive trend in the annual evaporation. Sen's slope estimator was used to understand the rate of change in precipitation at basin scale. The result revealed a reduction of 9% in precipitation in the upper part of the basin and an increase of 5% in the lower part of the basin whereas the evaporation rate shows a 4-12% increase.

The trend of daily precipitation frequency in Urmia Lake Basin, Iran was carried out by Bavil et al. (2018) using 30 years (1981-2011) of data from 60 stations through Mann Kendall, Spearman's Rho and linear regression methods. The result showed 1% significant increasing trend in the daily precipitation frequency (<5mm), no trend in 5-10mm frequency, 10% decreasing trend in 10-15mm frequency and insignificant decreasing trend in 15-20mm and above. Raja and Aydin (2018) conducted a study on annual precipitation trend in Mauritius through Mann Kendall and Spearman's Rho test by considering 30 years (1981-2010) of data from 53 meteorological stations. They divided the whole data into 5 year intervals. The 5-year interval data showed a mixture of positive and negative trends whereas an increasing trend in precipitation was observed while considering the data as whole during the study period. Recently, the monthly, seasonal and annual precipitation trends in Dongting Lake, China was assessed by Tayyab et al. (2019) using 52 years (1961-2012) data to understand the precipitation inconsistency by selecting data from 23 stations through non-parametric methods Mann Kendall and Spearman's Rho tests. Results showed a fusion of a significant and non-significant decreasing and increasing trends at different stations in monthly and seasonal data but annual rainfall shows no significant trend. They also found a good agreement between the results of Mann Kendall and Spearman's Rho test.

Based on the literature review, it can be summarized that most of the trend analysis studies were done using the statistical, non-parametric Mann Kendall and Spearman's Rho tests which showed comparatively high accuracy. So, considering the wide acceptance of these two methods and it's compatibility with the results of analysis, Mann Kendall and Spearman's Rho tests were applied in the present research to determine the rainfall trends in the LRB.

2.3 Rainfall-Runoff Modelling

Rainfall-Runoff (RR) model is a mathematical model which is capable of describing the complex nonlinear relationship where the physical equation fails to identify. The relationship between rainfall and runoff can be described with the help of the RR model. Different methods and models are available for the predication and modelling of rainfall-runoff. The present literature review mainly concentrates on the application of artificial neural networks (ANN) in RR modelling. The ANN model possesses different methods and its application depends on catchment characteristics as well as the size and quality of the data.

Considering two different river basins in two different regions such as the Lee River in UK and the Thuthapuzha River in India, and using 9 years (1984-1992) of rainfall and runoff data, Sajikumar and Thandaveswara (1999) developed a monthly rainfall-runoff model using Artificial neural network (Temporal back propagation Neural network - TBP-NN). The result of TBP-NN was compared with Fictional series model and found that TBP-NN gave better results. Tokar and Markus (2000) also selected three different drainage basins in the USA (Fraser River in Colorado, Raccoon Creek in Iowa and Little Patuxent River in Maryland) which experiences different climatic and physiographic condition and compared the conceptual model based rainfall-runoff with ANN model. The results show that the ANN model based rainfall-runoff modelling creates higher accuracy than the conceptual models. Sudheer et al. (2000) conducted a forecast study of daily runoff calculation for the Baitarani River Basin, Orissa, India using daily precipitation and previous runoff values through two different ANN models (Back error propagation network and Radial Basis Function). They compared the results of the two models using statistical tests and found that the RBF models gave better result than the BEPN model. In a separate study, forecasting of river flow in the Apure River Basin, southwest part of Venezuela was carried out by Dibike and Solomatine (2001) using rainfall and runoff for a period of 5 years (1981-1985) through two different ANN models (Multilayer perceptron and Radial Basis Function). The results of ANN models were compared to each other and also compared with conceptual rainfall-runoff model. The comparison suggests better result in rainfall-runoff in multilayer perceptron model with back propagation algorithm. The daily rainfall-runoff model of the Narmada River, India during monsoon period was modelled by Rajurkar et al. (2002) using 10 years (1981-1990) of data. They introduced varying input layers in the ANN model i.e. single input, two input and three input layers and found that three layered input model performed better and provided higher accuracy in rainfall-runoff modelling.

A comparative study of performance of the rainfall-runoff modelling (1h, 3h, and 6h lead time prediction) using ANN model and Model Trees (MTs) was conducted by Solomatine and Dulal (2003) for a European catchment in the Sieve River Basin. They found similar results for 1h lead time prediction using the two methods but the ANN model gives a better result for higher lead time. Agarwal and Singh (2004) developed a rainfall-runoff model using multilayer back propagation artificial neural network (MBPANN) for the two sub basins of the Narmada River and compared the results with linear transfer function. The comparison reveals that the MBPANN showed higher prediction accuracy than the linear transfer function. Similarly, Riad et al. (2004) conducted a comparative study of the rainfall-runoff relationship using the multilayer perception model and classical regression model in the Ourika River Basin, Morocco. Their results revealed ANN model is better than classical regression to predict the runoff. In addition to this, rainfall-runoff modelling of Sungai Bekok, Sungai Ketil, Sungai Klang and Sungai Slim River Basins in Malaysia were conducted by Ahmat Nor (2005). In their research, multilayer perceptron (MLP) and radial basis function (RBF) networks of ANN were considered and the results were compared with the HEC-HMS, XP-SWMM and multiple linear regression (MLR) model based runoff. The results indicated comparatively good correlation of runoff values predicted through ANN methods with the observed values compared to the other three methods. Meanwhile, Senthil Kumar et al. (2005) carried out a study to determine the best and suitable ANN model for rainfall-runoff modelling using multilayer perceptron and radial basis function in the Malapranka River Basin, India by considering 5 years (1987 to 1991) of data. However, they could not determine a superior method which produced better prediction due to the limitations and merits of each methods. Comparison of various training methods for multilayer perceptron in modelling rainfall-runoff process was carried out by Srinivasulu and Jain (2006) using 26 years of daily rainfall and stream flow data from the Kentucky River Basin in the United States. They considered different training methods such as back propagation algorithm, real-coded genetic algorithms and self-organizing map and achieved better results by utilising real coded genetic algorithm based MLP model for nonlinear and complex rainfall-runoff process.

Antar et al. (2006) carried out rainfall-runoff modelling in the Blue Nile catchment area using daily data during 1992-1999, through an artificial neural network model. Results of the analysis were compared with physically based distributed model and it was found that the ANN model is suitable for the simulation of rainfall-runoff. In order to compare the performance of different ANN models (Single neural network, Radial Basis Function and Multilayer perceptron) eight catchments located in different parts of the world (Nepal, China,

Ireland, Vietnam, Malaysia and Thailand) having different climatic and hydrologic conditions were considered by Shamseldin et al. (2007). They recommended the multilayer perceptron neural network model for rainfall-runoff modelling based on the higher prediction accuracy. In the local context, Kuok and Bessaih (2007) developed a rainfall-runoff model of the Sungai Bedup Basin, Sarawak using daily rainfall and mean runoff data calculated from rating curve equation and water level data. Results show that the ANN model is able to generate the daily runoff with higher accuracy and the method recurrent (REC) network model is better than multilayer perceptron (MLP) model. Rainfall-runoff modelling using two different neural network models (Multilayer perceptron and Radial Basis Function) and the comparison of the results of these models were carried out by Mutlu et al. (2008). They used data from 4 different stations in the Eucha watershed, USA, for a period of 4 years (2002-2004) and found that MLP gave better results in rainfall-runoff modelling. Meanwhile, Cigizoglu (2008) conducted a study to forecast the stream flow and sediment delivery by considering two stations such as Derecikviran station (35 years of data) in Filuos River and Uzunkopru station (25 years of data) in Ergene River in Turkey through three different ANN models (Feed forward back propagation, Generalised regression neural network and Radial basis function). The ANN modelling results were compared with conventional and stochastic method based predictions. They found that the ANN models are superior in forecasting the hydrologic data than other conventional and stochastic methods. Among ANN models, RBF shows more accurate performance. In Tinjar catchment, Sarawak, Malaysia, Suhaimi and Bustami (2009) carried out rainfall-runoff modelling by applying radial basis function (RBF) network and the result was compared with the runoff modelled through multilayer perceptron (MLP) model. The results show that the RBF neural network model given highly accurate results and they suggest the suitability of the RBF model in predicting runoff from Malaysian catchments.

In order to understand and predict the river flow of an ungauged basin in USA (Winooski River Basin), Besaw et al. (2010) considered two recurrent neural network models (Generalised Regression Neural Network and Counter Propagation Network). Two recurrent ANN models were trained using climate-flow data from a gauged basin and used to predict the climate data of nearby ungauged station. They obtained a successful result for the prediction of data using an ANN model. Monthly rainfall-runoff in the Jangada River Basin, Brazil was carried out by Machado et al. (2011) using ANN methods and the result was compared with the conceptual model IPHMEN. They found that the ANN models established a better relationship between rainfall and runoff than conceptual model. Daily outflow from the Khosrow Shirin watershed, Iran was analysed by Rezaeianzadeh et al. (2013) using

different modelling methods (HEC-HMS, Soil moisture accounting and Multilayer Perceptron) by considering 5 years (2002-2007) of daily rainfall data from 4 rain gauge stations and one stream flow measuring station. Later, the results obtained from different models were compared to identify the best performing model. The result indicates that the ANN model (MLP) shows better results compared to other models. In another study, two distinct linear and nonlinear methods such as multilayer perceptron and Volterra model were considered by Kashani et al. (2014) to simulate the nonlinear rainfall-runoff process and forecasting flooding in the Navrood River Basin, Iran. The performance of these two models were evaluated and it was concluded that the multilayer perceptron provided better results compared to the other model because of the nonlinear nature of the rainfall-runoff process. Aichouri et al. (2015) also decided to model the rainfall-runoff process in the Seybous catchment, Algeria using 18 years (1986-2004) of rainfall-runoff data through ANN and compared the results with the multiple linear regression (MLR) model. The result indicates superiority of ANN model in predicting runoff process compared to the MLR model. Gökbulak et al. (2015) conducted a comparative study for the prediction of flow estimation and peak discharge from the Istanbul watershed in Turkey through statistical methods, feed forward back propagation (FFBP) ANN model and rational model. They found that FFBP model of ANN is superior than other models in estimating the flow whereas the rational model performed good in peak discharge estimation.

Comparisons of conceptual models (Sacramento Soil Moisture Model - SAC-SMA) and artificial neural network model (Input Delay Neural Network - IDNN) was carried out by Daliakopoulos and Tsanis (2016) using 20 years of monthly rainfall, stream flow and potential evaporation data from 15 ephemeral catchments in the Island of Crete, Southern Greece. The result shows that even if the conceptual models produced good results for a few catchments, overall the ANN model performed better than the conceptual model. Tayyab et al. (2016) compared three different ANN models (feedforward back propagation neural networks (FFBPNN), generalized regression neural networks (GRNN), and the radial basis function neural networks (RBFNN)) and an autoregression model to forecast the discharge and flood prediction in the Jinsha River Basin, China. They found that the ANN gives better results than the autoregression model. Among the different ANN models, the FFBPNN model offered best prediction and forecasting. Kharroubi et al. (2016) conducted a study in the Eure River Basin, France to predict the hourly runoff rate through the ANN model by considering 30 years of annual rainfall and runoff data. The model gave good forecasting and prediction of flood in the concerned region. In another study, prediction of river flow was carried out by

Ghorbani et al. (2016) using monthly river flow time series data during 1989-2011, from Safakhaneh, Sentah and Polanian station in the Zarrinehrud River, north western Iran. They compared the results of multilayer perceptron (MLP), radial basis function (RBF) and support vector machine (SVM) using RMSE and correlation coefficient. The result show that MLP and RBF models performed better than SVM in predicting monthly river flow time series. Nawaz et al. (2016) modelled the continuous and event based rainfall-runoff in Lui River, Malaysia through multilayer perceptron (MLPNN) and autoregression moving average with exogenous input (ARMAX). They considered five years (1999-2013) of rainfall and runoff data in the study. The results show that MLPNN provided better prediction, and recommended the use of MLPNN model in the rainfall-runoff modelling in the tropical catchments. Predictions of stream flow in Bear River, USA was carried out by Khatibi et al. (2017) through multilayer perceptron by considering data during the period of 1961-2012. They compared the results of MLP with learning algorithms Levenber-Marquardt backpropagation (LM) and Fire-fly algorithm (FFA). Results show that improved prediction is attributed through MLP-FFA to identify the global minimum.

Forecasting of 1, 3, 5, 7 and 14 ahead of daily flow discharges in the Hadizen River, Turkey was modelled by Nacar et al. (2018) through multilayer perceptron (MLPNN), principle component analysis neural network (PCA-NN) and time lagged recurrent neural network (TLR-NN) using the data in the period of 1998-2009. The result shows that 1, 3 and 5 days ahead stream flow forecast, PCA-NN and MLPNN yielded better performance whereas TLR-NN produced better performance for 7 and 14 days ahead predictions. Shoaib et al. (2018) conducted rainfall-runoff modelling of four different catchments in the world (Baihe and Yanbian watershed in China, Brosna watershed in Ireland and Nan watershed in Thailand) using hybrid wavelet feed forward neural network models (multilayer perceptron neural network - MLPNN, generalised feed forward neural network - GFFNN, radial basis function neural network - RBFNN, modular neural network - MNN, coactive neuro fuzzy interference system - CANFIS). Results show better prediction and modelling by MLPNN, GFFNN and MNN methods compared to other models. River flows in three gauges at the Ajichay watershed, East Azerbaijan was studied by Darbandi and Pourhosseini (2018) by considering data obtained from January 2004 to July 2016 through MLP-ANN and hybrid MLP (MLP-FFA). Results of these models were verified through RMSE and determination coefficients. The authors found a satisfactory result in monthly river flow estimation by MLP-FFA. Stimulation of daily runoff in the Ladra River Basin and the Segura River Basin in Peninsular Spain located in different climate zones were studied by Jimeno-Sáez et al. (2018)

using SWAT and feed forward neural network (FFNN) model. Comparison of the results of these methods were also carried out by considering very low, low, medium, high and very high flow duration curves. The findings indicates good results by both methods for daily stream flow modelling. While comparing the results, for lower flows, SWAT gave better result whereas for higher flow, FFNN provided better result. Prediction of monthly and ten-day stream flow in the Nile River at five key stations was carried out by Elganiny and Eldwar (2018) through deseasonalised autoregressive moving average model (DARMA) and multilayer perceptron neural network (MLPNN). The performance of the model was estimated through statistical methods and it was found that ANN has more potential for forecasting of river flow.

Most of the studies revealed that ANN models are more accurate in the predicting rainfall-runoff from a catchment, which depends heavily on availability of quality data and in-situ measurements to validate the accuracy of the model. In this research, for accurate modelling of rainfall-runoff, ANN methods were considered. However, the suitability of a particular method can be finalised only after collecting secondary hydrological data of the Limbang River Basin from the concerned departments.

2.4 Chemistry of Rainwater and Surface Water

Water chemistry helps to assess the quality of the water. The natural processes and anthropogenic changes which takes place in the environment can alter the quality of rainwater and surface water in a river basin. Spatial and temporal variation in chemical characteristics of rainwater and surface water can be achieved through regular monitoring (Boggs et al., 2007; Talabi et al., 2013).

2.4.1 Rainwater chemistry

Carroll (1962) carried out a review study to understand the influence of the geological process such as rock weathering and soil forming process on chemistry of rainwater and the results indicate a good correlation between the rainwater chemistry with rock weathering and soil formation. To understand the chemical composition in atmospheric precipitation and river water, Fisher (1967) analysed two years of atmospheric precipitation data from eastern North Carolina and southeastern Virginia, USA. Results indicate that the main source of the rainfall in the study area is from the sea water and local evaporation, whereas the chemistry of surface water results pointed towards the influence of agricultural, industrial and biological activities in the region. Khemani and Ramana Murty (1968) studied

chemical compositions and characterisation of the rainwater by collecting samples from different locations and seasons from Delhi, India. Chemical components such as chloride, sulphate, sodium, potassium and calcium were analysed from collected samples. They identified raindrop size and the variation in the characteristics of the formation of rainwater as the reason for the deviation of concentration of chemical components. Chemical composition of rainwater in eastern France was characterised by Sanusi et al. (1996) by collecting weekly samples at nine sites during October-1991 to March-1992. They analysed pH, conductivity and major ions such as Cl^- , NO_3^-, SO_3^{2-}, NH_4^+, Na^+, K^+, Mg^{2+} and Ca^{2+}. Results indicate higher concentration of major ions in the urban area where the amount of rainfall is low. They found that rainfall is acidic in urban areas and this may be due to the $CaCO_3$ presents in Loess, a major constituent of soil in the Upper Rhine valley indicating the supply of dust by wind. In another study, chemical composition of rainfall in the two Amazonian ecosystems (Serra do Navio District (SNV) and Tartarugalzinho District (TRT)) in northeast Brazilian Amazon was studied by Forti et al. (2000). They evaluated the composition of Na^+, K^+, Ca^{2+}, Mg^{2+}, Cl^-, NO_3^-, SO_4^{2-}, Fe, Al, Zn and Mn by collecting rainwater samples during the period July 1993 to June 1997 from SNV and January 1996 to June 1997 from TRT. Results indicate a significant difference in the chemical composition of rainwater between the sites and seasons due to the difference in the contribution of sea salt source, biogenic aerosols and soil dust.

The influence of anthropogenic process in the rainwater at the Piracicaba River Basin, southeast Brazil was studied by Lara et al. (2001) by analysing F^-, CH_3COO^-, $HCOO^-$, MSA, Cl^-, NO_2^-, Br^-, NO_3^-, SO_4^{2-}, $C_2O_4^{2-}$, PO_4^{3-}, Na^+, NH_4^+, K^+, Mg^{2+}, Ca^{2+}, dissolved organic carbon, dissolved inorganic carbon, pH and conductivity in 272 rainwater samples collected from August 1997 to July 1998. They found that rainwater was acidic in all sampling sites and the variation of acidity was correlated with different land use. They also discovered that the main sources which control the rainwater composition in the region was soil dust, sugar cane burning and industrial emission. Meanwhile, Topçu et al. (2002) conducted a study to understand the rainwater chemical composition and its seasonal variation in Cubuk, Ankara, Turkey by collecting rainwater samples from EMEP station during the period of September 1994 to December 1996. pH, conductivity, SO_4^{2-}, NO_3^-, Cl^-, NH_4^+, Na^+, K^+, Mg^{2+}, Ca^{2+} and H^+ was measured from the samples collected, and seasonal variation was observed in the concentration of parameters. They found that the average value of pH was greater than 5.6 due to the alkaline nature of the soil ($CaCO_3$) whereas low concentration of H^+ suggests the neutralisation of alkaline particle by H_2SO_4 and HNO_3. The chemical composition of

precipitation near Büyükçekmece Lake, Istanbul was studied by Başak and Alagha (2004) by collecting 79 bulk precipitation samples from October-2001 to July-2002 and the parameters pH, H^+, SO_4^{2-}, NO_3^-, Cl^-, NH_4^+, Na^+, K^+, Mg^{2+}, Ca^{2+}, Al, Ba, Fe, Cu and Mn were analysed. They observed high concentration of sulfate with H^+ ion through factor analysis and correlation analysis and identified that the acid neutralisation was mainly by calcium than ammonium. Báez et al. (2007) studied the chemical composition of rainwater at southwest of Mexico City, Mexico by collecting rainy season samples during 2001-2002. They analysed the trace metals Cd, Cr, Mn, Ni, Pb, V and Al in the soluble and insoluble fraction and SO_4^{2-}, NO_3^-, Cl^-, HCO_3^-, Na^+, K^+, Mg^{2+}, Ca^{2+}, NH_4^+ and H^+ in soluble fraction. Results show higher concentration of Al in the soluble and insoluble fraction, whereas ammonia showed higher concentration among major ions. It was also noted that during rainy days, the concentration of trace metals and SO_4^{2-}, Mg^{2+}, Ca^{2+}, NH_4^+ and H^+ were associated with the air mass back trajectories. Enrichment factor analysis revealed that the trace metal and major ions are anthropogenic in origin whereas the factor analysis indicates that the chemistry of rainwater was controlled by anthropogenic and crust origin.

To understand the chemical characteristics of precipitation in north and south China, Huo et al. (2010) collected rainwater samples from four locations along with the measurement of atmospheric particles and gases. They found that the rain in this region is acidic in nature, and they also discovered that the southern region rainwater was more acidic than north because of the presence of SO_4^{2-} in the rainwater whereas NH_4^+ and Ca^{2+} acts as the neutralising ions. Chemical composition and seasonal variations of the acid deposition in Chiang Mai, Thailand was studied by Sillapapiromsuk and Chantara (2010) by collecting 132 rainwater samples. They analysed the major anions ($HCOO^-$, CH_3COO^-, Cl^-, NO_3^-, and SO_4^{2-}) and cations (Na^+, NH_4^+, K^+, Ca^{2+}, and Mg^{2+}). Results show that the chemical composition of rainwater was influenced by agricultural activity, fuel combustion, marine source, soil re-suspension and biomass burning. A study on chemical composition of rainwater in acid rain control zone in Chengdu, southwest China was carried out by Wang and Han (2011) by collecting one year sample (January to December, 2008) and analysing parameters such as pH, F^-, NO_3^-, Cl^-, SO_4^{2-}, NH_4^+, Na^+, K^+, Mg^{2+} and Ca^{2+}. The results showed that Ca^{2+} was the most abundant element and the concentration of NO_3^- is higher than the most polluted cities. They concluded that the acid rain is due to fuel consumption from urbanisation and rapid increase of vehicles which contributed more SO_2 and NO_x in the atmosphere, whereas the high concentration of Ca^{2+} and NH_4^+ in atmosphere was neutralising the acidity of rainwater to a small extent. Olowoyo (2011) carried out a study to identify the rainwater quality of the Warri

axis of Delta state in western Niger using physico-chemical characteristics. Flaring of gas into the averment were noted, but the other chemical results were almost same as the value given by the WHO standard. Chemistry of rainwater at Kothi, north western Himalayas, India was studied by Tiwari et al. (2012) by collecting event to event rainwater samples during 2006-2007 and pH, conductivity and major ions (F^-, Cl^-, NO_3^-, SO_4^{2-}, NH_4^+, K^+, Na^+, Ca^{2+} and Mg^{2+}) were analysed. Results indicated non-marine origin of Ca^{2+}, SO_4^{2-}, K^+ and Mg^{2+} and Ca^{2+} acting as major acid neutralising agent. They concluded that the air born primary and secondary particles influenced the chemical composition of rainwater.

Major process and sources controlling the chemistry of cloud and rain were examined by Gioda et al. (2013) by collecting cloud and rainwater samples during 1984 to 2007 from three locations in Puerto Rico. The parameters considered in the study are: pH, conductivity, Cl^-, NO_3^-, SO_4^{2-}, Na^+, K^+, Ca^{2+}, Mg^{2+} and NH_4^+. The results show that the Puerto Rican cloud and rainwater chemistry were strongly influenced by the natural and marine sources compared to the local anthropogenic activities. Chemical compositions of rainwater in the Oleiros, A Coruña, Spain was studied by Moreda-Piñeiro et al. (2014) by assessing the soluble and insoluble fraction of major ions (Cl^-, NO_3^-, SO_4^{2-}, Na^+, K^+, Ca^{2+}, Mg^{2+} and NH_4^+) and trace metals (Al, As, Ba, Co, Cu, Cr, Fe, Mn, Ni, Pb, Sr, V and Zn) by collecting samples from March-2011 to August-2012. The results indicates that Ca^{2+} originated from non-sea salt and SO_4^{2-}, Al and Fe are of terrestrial origin whereas Mg^{2+}, Na^+, Cl^-, K^+, NH_4^+, NO_3^-, Fe, Mn, Pb, Sr, V and Zn are of marine origin. They attributed ubiquitous source of Ba, Co, Cu, Cr and Ni concentration in rainwater samples. Cerqueira et al. (2014) studied the chemical composition of rainwater by collecting 50 samples from Juiz de Fora City, Brazil during the period of 2010-2011. Parameters analysed include pH, conductivity, redox potential, major ions (H_3O^+, Na^+, NH_4^+, K^+, Mg^{2+}, Ca^{2+}, NO_3^-, SO_4^{2-}, Cl^- and HCO_3^-), hydrogen peroxide and trace metals (Cu^{2+}, Zn^{2+}, Cd^{2+} and Pb^{2+}). They concluded that the K^+, Mg^{2+}, Ca^{2+} and HCO_3^- originated from soil whereas Na^+ and Cl^- from the sea salt and NO_3^-, SO_4^{2-} and NH_4^+ are from anthropogenic activity. Chemical characteristics of the rainwater in Guilin, China was analysed by collecting 396 samples between January 2008 and November 2011 by Yu et al. (2015). pH of rainwater revealed the presence of acid rain in the area and this might be due to natural and human activities, whereas the presence of large amount of alkali ions neutralises the acidity. They suggested rainwater chemistry in the region was controlled by human activity, weathering of soil and rock, dust transported from the long distance and vehicle and festival emission. Besides that, physico-chemical parameters of rainwater in the urban west region of Zanzibar Island were studied by Mohamed et al. (2016) by collecting samples during December-2012.

Parameters analysed includes pH, EC and metals such as As, Be, Ca, Cd, Co, Cr III, Cu, Fe, Li, Mg, Mn, Mo, Ni, Pb, Sb, Se, Sr, Ti, Tl and Zn and the results were compared with WHO standards. The result shows that the pH is lesser than drinking water quality standards as proposed by the WHO guidelines, but all the other parameters were within the permissible limit.

To understand the impact of land use activity and temporal variation in rainwater Okoya et al. (2017) conducted a study in the residential and semi industrial region of Osun state of Nigeria from October 2012 to September 2013. They found a higher concentration of chemical parameter in rainwater collected during the dry season than the wet season. They concluded that the seasonal variation in the chemistry of rainwater was caused due to the dust supply from industry, agricultural activity, soil re-suspension and vehicular activities. Chemical compositions of rainwater and its transportation was investigated by Anil et al. (2017) by collecting 172 rainwater samples throughout the year 2009 from the Istanbul watershed area, Turkey. They considered soluble fractions of F^-, Cl^-, NO_3^-, SO_4^{2-}, and NH_4^+ and insoluble and soluble fractions of Al, As, Ca, Cd, Co, Cr, Cu, Fe, K, Mg, Mn, Na, Ni, Pb, V, and Zn. They concluded that the chemical composition of rainwater was influenced by anthropogenic pollutants from southwestern and eastern Europe, Saharan dust intrusion from northern Africa, cluster mineral re-suspension from the nearby region and Mediterranean and Black sea marine aerosol. Rainwater chemistry and source of ions in the Cius Basin, Romania was studied by Szép et al. (2017) by collecting 11 years (January 2006-December 2016) of samples. The result indicates a small number of samples having acidic nature and the neutralising agents are NH_4^+, Ca^{2+} and Mg^{2+}. They also found that the chemistry of the rainwater was influenced by the local natural and anthropogenic sources. Physico-chemical characteristics of dew and rain in Paris were studied by Beysens et al. (2017) by collecting 34 dew and 77 rain samples during the period between April-2011 and March-2012. They measured pH, EC, major anions (Cl^-, SO_4^{2-} and NO_3^-) and cations (Na^+, K^+, Ca^{2+} and Mg^{2+}) and minor ions (Fe^{2+}, Cu^{2+}, Cd^{2+}, Mn^{2+}, Pb^{2+}, Zn^{2+}, NO_2^-, Br^-, F^-). Comparison of the results of dew and rainwater indicate that the rainwater is slightly acidic compared to that of the dews, and the total ionic content in the dew is four times higher than the rainwater samples. Furthermore, compared with the WHO drinking water standards, both dew and rainwater fall within the desirable limit. They also identified that the concentration of Cl^- and Mg^{2+} is influenced by the sea and Ca^{2+}, SO_4^{2-}, NO_3^- and NO_2^- originated from anthropogenic sources.

The chemistry of rainwater in the Qua Iboe Estuary, Nigeria was studied by Akpan et al. (2018) by collecting 36 samples from six locations during the period of November-2007 to January-2008. Results of physico-chemical parameters (pH, CO_3^-, Cl^-, NO_3^-, SO_4^{2-}, S^{2-} and CN^-) and trace metals (Zn, Mn, Cu, Fe, Cr, Pb, Ni, Cd) were statistically processed and interpreted. The result indicates a seasonal (dry and wet season) variation in the rainwater chemistry and major factors influencing the chemistry of rainwater are soil dust, sea salt, biomass burning, flared gas and vehicle exhausted fumes. Sources of pollutants in rainwater in the city of Limeira, São Paulo, Brazil was investigated by Martins et al. (2018) by collecting 30 samples during September-2013 to March-2014. Parameters such as pH and major ions Na^+, K^+, Mg^{2+}, Ca^{2+}, NH_4^+, H^+, HCO_3^-, SO_4^{2-}, NO_3^- and Cl^- were analysed. They considered principal component analysis (PCA), air mass trajectory clustering and enrichment factors for the identification of chemical sources. PCA indicates agricultural emission of pollutants whereas the trajectory clustering explained contribution originate from a continental source. At the same time, the enrichment factor pointed out anthropogenic activities like agriculture, mining, industrial and heavy vehicle traffic as the source of SO_4^{2-}, NO_3^- , Cl^-, K^+, Mg^{2+} and HCO_3^- whereas Ca^{2+} and Na^+ was contributed from crustal and anthropogenic sources. Potential source effecting the precipitation composition in the Po Valley, Italy was studied by Tositti et al. (2018) by collecting precipitation during 2009-2013. The result indicates a slightly alkaline nature of precipitation due to the presence of ammonia and crustal elements. The back trajectory analysis suggests influence of local re-suspension over long range transport. The results of statistical analysis identified input from agricultural activity as the key source in the chemical composition of precipitation. Chemical compositions of rainwater and source of pollutants in the Ahvaz, Iran was studied by Naimabadi et al. (2018) by collecting 24 rainwater samples. They analysed pH, major ions (Na^+, NH_4^+, Ca^{2+}, Mg^{2+}, HCO_3^-, NO_3^-, Cl^- and SO_4^{2-}) and trace metals (Fe, Al, Pb, and Cd) and statistical methods were applied to identify the processes control the chemistry of rainwater. Results of the principal component analysis indicates that the rainwater chemistry in this region was strongly influenced by anthropogenic sources, middle eastern dust and biomass burning.

Khan et al. (2018) studied the physico-chemical interactions and potential source of pollutants by collecting rainwater samples from an urban site of Kuala Lumpur and highland rural area in the middle Peninsular Malaysia during January-2000 to December-2014. They found that anthropogenic and developmental activities influence the concentration of sulfate and nitrate in the urban area whereas agriculture and forestry influence the contribution of ammonia in the rural areas. To understand the influence of peat fire and

related atmospheric circulation, Szép et al. (2019) conducted a study by collecting daily rainwater samples from intra-mountain basins (Ciuc Basin and Giurgen Basin), Romania in the year 2012. Half of the samples from both locations show pH>7 and the major neutralising agents present in the rainwater is NH_4^+ and Ca^{2+}. Factor analysis suggests different sources of contributions such as anthropogenic (biomass burning, peat fire and fertilizer), marine and terrestrial. Toxic potential of rainwater was evaluated by Vlastos et al. (2019) by collecting rainwater samples from three cities in western Greece (Corfu, Agrinion and Patras) during May, October, November and December- 2014. pH, EC, TDS, major ions (PO_4^{3-}, SO_4^{2-}, Cl^-, NO_3^- and NH_4^+) and heavy metals (Al, Mn, Fe, Co, Ni, Cu, Zn, As, Sb, Pb and Cd) were analysed for the purpose. They found that, irrespective of sampling locations and sampling months, conductivity, SO_4^{2-}, NH_4^+ and total metal burden were related with both cytokinesis block micronucleus (CBMN) and Microtox assays and the rainwater physico-chemical profile significantly related with induction of adverse effect on biota.

2.4.2 Surface water chemistry

The spatial and temporal changes in the water quality parameters such as temperature, conductivity, pH, DO, turbidity, total alkalinity, hardness, Ca^{2+}, CO_2^{2-}, Cl^-, SO_4^{2-}, NO_3^--N, NO_2^--N, NH_4^+-N and PO_4^{3-}-P in the Alberche River, Spain was studied by Perona et al. (1999) by collecting seasonal river water samples from 10 locations for a period of 2 consecutive years (1991-1993). The result showed a gradual increase in alkalinity and the concentration of sulphate, calcium and chloride in downstream direction whereas nutrients show spatial and temporal variation. Variation in the nutrients was caused by the varying influence of anthropogenic sources. Water quality (50 parameters) analysis and modelling of the Elba River, Germany using autoregression component and ARIMA was conducted by Lehmann and Rode (2001) using weekly samples collected during 1984 to 1996. They found a significant difference in the water quality before and after 1990. Water quality of the Bangpakong River in eastern Thailand, was studied by Bordalo et al. (2001) by collecting samples from 11 locations during June 1998 to May 1999. Parameters such as temperature, DO, turbidity, suspended solids, pH, ammonia, fecal coliforms, BOD, COD, EC, phosphate, Hg, Cu, Fe, Zn and Cd were analysed. Scottish water quality index (WQI) indicated a seasonal variation in water quality and suggests a poor quality of environment in the region. Scarsbrook et al. (2003) analysed twelve water quality parameters from water samples collected from 77 rivers for a period of thirteen years (1989 to 2001) in New Zealand to understand the influence of water quality in relation to climate change. They found that climate variation has a strong influence on water quality characteristics.

Multivariate statistical analysis (cluster analysis, principle component analysis and multiple regression analysis on principle component) of surface water quality parameters of major river systems (Aliakmon, Axios, Gallikos, Loudias and Strymon) in northern Greece were carried out by Simeonov et al. (2003) by considering 27 parameters (pH, EC, DO, TSS, nitrate, nitrite, ammonium, orthophosphate, COD, BOD, organic nitrogen (TON), acid-hydrolysable (total) phosphorus (TP), Ag, As, B, Ba, Cd, Cr, Cu, Hg, Fe, Mn, Ni, Pb, Se and Zn) of 3 years (February 1997 to January 2000) monthly samples from 25 sampling locations. The results of cluster analysis identified 4 groups showing similarity between the sampling sites whereas the principle component analysis explained a 90% of the total variation with six factor components indicating processes responsible for the loading of parameters as organic, nutrient, physico-chemical, weathering, soil-leaching and toxic anthropogenic factors. Spatial and temporal variation in the chemistry of the Pearl River in Zhujiang, China was examined by Zhang et al. (2007) by collecting samples from 75 hydrological stations during 1958 -2002. They analysed pH, TDS, major ions such as Na^+, K^+, Ca^{2+}, Mg^{2+}, HCO_3^-, Cl^- and SO_4^{2-} and dissolved silica in river water. Based on the results, they concluded that river water chemistry is dominantly controlled by rock weathering but anthropogenic activities such as domestic and industrial wastewater discharge, acid deposition and basin water resource development also played a role in influencing the chemistry of river water. Total dissolved trace metal concentration (Fe, Zn, Mn, Ni, Cu, Cr, Co, Cd and Pb) in water samples collected at 5 sites during March to June, 2009 from the Sava River, Croatia was studied by Dragun et al. (2009). They found that, river water quality was dominantly controlled by anthropogenic activities in the basin and the concentration of trace metals is not significantly above natural levels based on the European regulation for water quality. Gandaseca et al. (2011) collected 72 water samples from 12 locations from major river and tributaries of the Sungai Sibuti, Sarawak, Malaysia during the year 2010 (June, August and October) to understand the physico-chemical characteristics of the river water. They found that the water quality was good and almost all the parameters considered fell under the class I and II of Malaysian classification of water based on the use.

Seasonal variation of saturation index (SI) of carbonate minerals and partial pressure of carbon dioxide (pCO_2) in the layered coastal aquifer of Pondicherry, India was assessed by Chidambaram et al. (2012) by collecting 98 samples during pre-monsoon (May, 2007) and post-monsoon (January, 2008) seasons. They found that the saturation index of carbonate minerals in the state of under saturation to saturation and follows the order of $SI_{Calcite} > SI_{Aragonite} > SI_{Dolomite(c)} > SI_{Magnesite} > SI_{Dolomite(d)}$. They also identified a higher

pCO_2 during the post-monsoon than the pre-monsoon and found that it was caused by the recharging of the aquifer during the post-monsoon. Analysis of physico-chemical parameters of river water (temperature, conductivity, pH, salinity, BOD, COD, dissolved solids, suspended solids, ammonia nitrogen, turbidity, chromium, cadmium and lead) in the Jakara River Bain, Nigeria was assessed by Mustapha et al. (2013) by considering 27 samples from the upper Jakara River Basin. Statistical tests were also carried out to understand the relationship between the parameters (Pearson's product–moment correlation and partial correlation analysis) and the source of origin (principal component analysis). Pearson's product moment correlation and partial correlation analysis revealed a significant correlation (relationship) between the quality parameters. Principal component analysis identified anthropogenic and natural process as the factors controlling the river water quality and spatial variation in the concentration of parameters. Water quality and trace metal concentration in the Awat-Awat, Sunder and the Trusan River, Sarawak, Malaysia was investigated by Gandaseca et al. (2014) by analysing 52 samples between the periods of November 2012 to May 2014. They categorised the river water samples into the class III status according to Malaysian water quality standards based on the concentration of physico-chemical parameters and suggested that the quality of water was controlled by high suspended solids and turbidity caused by anthropogenic activity in the region. Meanwhile, Mostafaei (2014) evaluated the water quality of the Kashkan River in Iran by applying multivariate statistical methods and water quality index by considering 36 years (1974-2009) of data from 10 sampling stations. The results of physical parameters (pH, electrical conductivity), cations (Na^+, K^+, Ca^{2+}, Mg^{2+}) and anions (HCO_3^-, Cl^- and SO_4^{2-}) indicate that the water was suitable for industries and irrigation without much treatment (on average) whereas the water quality index identified deteriorated quality of water in all sampling locations.

Physico-chemical parameters (pH, TDS, EC, TSS, Turbidity, NO_2^-, NO_3^-, S_2^-, SO_4^{2-}, CN^-, Na^+, Ca^{2+}, K^+ and Mg^{2+}) and heavy metals (As, Pb, Fe, Cd, Ni and Zn) in Jimi River and its tributaries at the Obuasi mining enclave in Ghana was assessed by Asare-Donkor et al. (2015) through the analysis of 67 samples. Along with the quality characterisation, health risk assessment of the heavy metals was also carried out. They found that most of the physico-chemical parameters are within the limit of WHO standards and the health hazard risk assessment indicated no cumulative potential of adverse health risk in the drinking water source. Characterisation of hydrochemical parameters (pH, EC, TDS, Ca^{2+}, Na^+, K^+, Cl^-, CO_3^{2-}, HCO_3^-, SO_4^{2-}) in eight different surface water and groundwater sources in Matahara plain, Ethiopia was carried out by Dinka et al. (2015) by analysing 64 samples collected during

November and May of 2008 and 2009. They found that the water quality was influenced by natural and different anthropogenic activities including sewage from factories, domestic and farming activities. To understand water quality and contamination source in the Oum Er Rbia River Basin, Morocco, Barakat et al. (2016) collected samples from 14 locations for a period of 2 years (2000-2012). They analysed physico-chemical parameters such as temperature, pH, electrical conductivity, turbidity, total suspended solids, dissolved oxygen, NH_4^+, NH_3^-, total phosphorus, biological oxygen demand, chemical oxygen demand and fecal coliforms. Multivariate statistical analysis of the results suggested that in some locations the quality of the water exceeds the Moroccan water quality standards. They suggested that due to the potentially hazardous nature of the water, the industrial and municipal waste water needed treatment before being discharged into the river, and sustainable agricultural practices had to be implemented to avoid health hazards and other adverse effects. Physico-chemical parameters (pH, DO, BOD, COD and TOC) of river water and heavy metals (Cu, Cd, Pb, Zn and As) in surface sediments collected from 14 locations in the in the Nakdong River Basin, Korea was studied by Chung et al. (2016). They concluded that, the water and sediment was contaminated by the mixing of industrial waste, irrigational effluents and domestic sewage. Also, Barzegar et al. (2016) investigated the hydrogeochemistry, water quality and trace metal contamination in the Aji-Chay River in Iran by collecting 12 samples. Multivariate statistical methods and piper plots were applied to interpret the results. Cluster analysis identified two distinct clusters and the piper diagram classified most samples as Na-Cl type. Cross-plot showed that rock weathering, dissolution of minerals (including salinization) and ion exchange are the natural geochemical process controlling hydrogeochemistry of the Aji-Chay River.

Cluster analysis, principal component analysis and time series analysis of quality parameters (pH, temperature, EC, TDS, Ca^{2+}, Mg^{2+}, Cl^-, HCO_3^-, Na^+, K^+, NO_3^-) of monthly surface water from October 2007 to April 2008 from 3 sampling stations (total 21 samples) in the Arab River at Babar dam, Algeria was carried out by Gaagai et al. (2017). Cluster analysis categorised samples into three groups and the principal component analysis explained 87% of the total variance with two factor components. The time series analysis showed that TDS was controlled by the concentration of Ca^{2+}, Mg^{2+}, Na^+, Cl^-, SO_4^- and K^+, $NO_3^-$was contributed by fertilizers and domestic sewage inputs from tributaries. Seasonal variation of water quality parameters (temperature, pH, EC, DO, spectral absorption coefficient, oxidation reduction potential, BOD, COD and TSS) in Atoyac River Basin, Central Mexico was investigated by Martinez-Tavera et al. (2017) by considering 66 samples through statistical techniques such

as correlation matrix, factor analysis and cluster analysis. High pH, conductivity and redox potential was observed in the dry season and the water was highly influenced by the input from adjacent industrial, agricultural and urban zones. Nienie et al. (2017) studied the quality of water in different seasons (wet and dry) of Kikwit area, Congo by considering 3 well and 2 river water samples through the measurement of physico-chemical parameters (pH, temperature, EC, DO, dissolved organic carbon and total organic carbon) and trace metal concentration (Cr, Mn, Co, Ni, Cu, Zn, As, Mo, Ag, Cd, Sn, Sb, Pb, Na^+, K^+, Mg^{2+}, NH_4^+, SO_4^{2-}, NO_3^- and Cl^-). The results showed that pH was lower in the wet periods than dry whereas the physico-chemical parameters and concentration of trace metals are high during the wet periods than the dry periods. It was also noted that, all parameters except Mg^{2+} (in both seasons) fell within the drinking water quality standard of WHO and the higher concentration of Mg^{2+} is due to natural weathering.

Water quality index based quality assessment of Poyang Lake, China was carried out by Wu et al. (2017) by considering 24 samples from 15 sites collected from January 2009 to October 2014. The results showed a moderate (water) quality according to the classification of surface water quality index, China and the water collected during summer shows good quality whereas in the winter, it was found to be of bad quality. Etteieb et al. (2017) collected water samples from 17 locations in the Medjerda River, Tunisia during May 2013, to understand the suitability of water for irrigation purposes. The result showed suitability of water collected from three locations for irrigation purposes and the reaming locations are classified as doubtful to unsuitable due to the salt tolerance. Chemical compositions of the Tireh River water, Iran was studied by Qishlaqi et al. (2017) by collecting samples from 14 locations and analysing the temperature, pH, conductivity, HCO_3^-, SO_4^{2-}, Cl^-, Na^+, Mg^{2+}, Ca^{2+}, NO_3^- and river discharge. They found that, the water collected from all locations are suitable for drinking purposes according to WHO standards and irrigation purposes, according to agricultural standard (FAO standards). Piper diagram classified water samples into bicarbonate and calcic facies and Wilcox diagram indicates that 78% of the samples comes in the C3-S1 and 21.5% in C2-S1 classes. They pointed out that the major source of river water pollution was the industrial seepage injection. Concentration of different ions in the water of the Seybouse River, north east Algeria was evaluated by Guettaf et al. (2017) through the analysis of 48 water samples collected during April and August in 2010 and from January and April in 2011. High water quality index (WQI) value was observed, owing to the higher concentration of elements and nutrients. They also found that the WQI value in the downstream is twice as that of upstream and came as result of the discharge of urban and

industrial waste. Natural and anthropogenic factors influencing the water quality of the Jialing and Yangtze River, SW China was studied by Qin et al. (2018) by collecting samples from 3 locations from January to December, 2016. Piper plot classified river water samples into HCO_3-SO_4-Ca hydrochemical facies and rock weathering, soil erosion, domestic sewage and agricultural activities are major processes controlling the hydrochemistry of the rivers.

Qaisar et al. (2018) investigated the spatial distribution of physico-chemical characteristics along with quality classification and source identification of the elements present in the Indus River, Pakistan by collecting 84 samples from different locations from June to August, 2016. They analysed pH, EC, TDS, major ions (Ca^{2+}, Mg^{2+}, K^{+}, Na^{+}, Cl^{-}, SO_4^{2-}, and NO_3^{-}) and Si in the collected samples. Carbonate weathering and evaporate dissolution are the major process controlling the geochemistry of river water in the basin. Considering the WHO standards, the water there is suitable for irrigation purposes. Water quality of the Gorgan River Basin, northern Iran was assessed by Khaledian et al. (2018) by collecting samples from 18 stations during the period of 1984 to 2008. Water quality parameters considered in the research are EC, TDS, total hardness, pH, HCO_3^{-}, Cl^{-}, CO^{3-}, Mg^{2+}, K^{+}, Na^{+}, Ca^{2+} and SO_4^{2-}. They found that land use is the major anthropogenic process that controls the water quality and water collected from some stations shown poor quality whereas stations located at pristine environment have good water quality. Marescaux et al. (2018) studied the spatial and temporal variation of pCO_2 in the Seine River network in France by measuring pCO_2 from the field during the period 2016 to 2017 and then comparing the result with calculated pCO_2. They identified supersaturated state of CO_2 in Seine River Basin with respect to atmospheric equilibrium due to the hydroclimatic condition and groundwater discharge, and the pCO_2 showed seasonal variations during the period between winter and summer. In order to understand the factors controlling the hydrogeochemistry of the Gandaki River Basin in the central Himalaya, Nepal and its spatial variation Pant et al. (2018) collected 165 water samples from 55 locations in the year 2016. Parameters such as pH, EC, TDS and major ions (Mg^{2+}, K^{+}, Na^{+}, Ca^{2+}, Cl^{-}, SO_4^{2-} and NO_3^{-}) were analysed. They found that the water was slightly alkaline and the hydrogeochemistry was controlled by geogenic weathering with carbonate dominant lithology. It was also noted that, hydrochemical facies identified through piper plots show varying characteristics with 83% of the samples falling under Ca-HCO_3 facies, followed 13% of samples in mixed Ca-Mg-Cl facies and 4% samples in Ca-Cl facies. In another study, Levshina (2018) examined the concentration of dissolved metals (Co, Cr, Cu, Fe, Mn, Ni, V, Zn, Ca, Mg, and Cd) and their compound in humic substances (Me-HS complex) in water samples collected during summer and autumn in 2011-2012,

from the Upper Amur River. Result showed that the concentration of Me-HS complexes increases from south-western steppe to the north-eastern taiga and the toxic metal such as Ni, Cu, Zn, Cr, Fe and V is dominant in Me-HS complexes.

In the present study, though the river basin selected is devoid of industries, physico-chemical characteristic of rainwater and surface water was analysed through standard methods to identify the spatio-temporal variation in the chemical characteristics of rainwater and surface water in the Limbang River Basin.

2.5 Stable Isotopes in Hydrological Studies

Isotope hydrology is the newly developed and well utilized technique to solve the hydrological problems using environmental isotopes such as stable, radioactive isotopes and artificial radioactive isotopes. Isotopes are used as tracers for identifying surface water-groundwater interrelation, origins of geothermal water, sources of groundwater, artificial recharge efficiency and sources of recharge (Gat 1995; Rodgers et al., 2005; Sánchez-Murillo et al., 2016). Stable isotope oxygen-18 ($\delta^{18}O$), deuterium ($\delta D/^{2}H$), chlorine (^{37}Cl), carbon (^{13}C) and sulphur (^{34}S) and radioactive isotope tritium (^{3}H) and carbon (^{14}C) are most often used environmental isotopes in hydrology. Factors such as altitude, latitude, amount of rainfall and continental effects influence the isotopes composition (Dansgaard, 1964; Rozanski et al., 1993).

The origins of river water and the effect of irrigation activity in the Lake Biwa Basin, Japan was evaluated by Taniguchi et al. (2000) by collecting 17 river water and 11 precipitation samples. They observed that the precipitation and river water in the basin was influenced by the regional difference and composition of stable isotopes showed altitude effect. In addition to that, the composition of $\delta^{18}O$ in river water in the eastern and southern area of the river basin was influenced by irrigation. Comparisons of isotope in precipitation at two continental stations and 6 Adriatic coastal stations in Slovenia and Croatia was carried out by Vreča et al. (2006) using samples collected during the years of 2001-2003. They identified that, the seasonal variation in $\delta^{18}O$ is lesser in maritime stations than in continental stations and was influenced by a slight variation in seasonal temperature. Good correlation was observed between the composition of $\delta^{2}H$ with $\delta^{18}O$ and $\delta^{18}O$ in monthly precipitation with air temperature in all stations and the local meteoric water line falls very close to the global meteoric water line. Temporal variation in O^{18} and deuterium isotopes in precipitation and soil water was studied by Lee et al. (2007) through monitoring monthly precipitation and

weekly soil water for a period of 1 year (2002-2003). The results showed inter-relationship between soil water and precipitation (recharge) where the influence of evaporation is negligible even during the hot summer. They also attempted two well mixed or exponential models (EM) and one exponential position flow model (EPM) using composition of $\delta^{18}O$, δD and deuterium excess value to estimate the mean residence time and found that the deuterium excess value is the better parameter for the estimation of mean residence time of subsurface water. Mayr et al. (2007) considered two lakes (Laguna Azul and Laguna Potrok Aik), in the semi-arid Patagonia (Argentina) to understand the origin of precipitation and evaporation. The result showed that in southeastern Patagonia, composition of isotopes in rainfall is controlled by precipitation amount and moisture source. They found that the surface and subsurface flow of water is the major source of water for the two lakes and the groundwater in the region was recharged by the lake water.

Variations in isotopic composition in Kenya and Ethiopia was studied by Levin et al. (2009) by collecting 349 samples from stream, river, spring, well, rain and tap water during 1975 to 2007. They concluded that the variation in isotope composition was controlled by wind and its flow direction. Pelig-Ba (2009) conducted a study on stable isotope analysis in the northern region of Ghana, by collecting 15 rainwater and 36 groundwater samples during 1997. They concluded that, local precipitation was the source of groundwater recharge and the recharging water undergoes evaporation during transportation. Chidambaram et al. (2009) investigated the factors affecting precipitation in Tamil Nadu, India by characterising the composition of stable isotopes. They suggested that South East Arabian Sea (SEAS) and the Indian Ocean (IO) are the major sources of rainfall in Tamil Nadu whereas evaporation from local water bodies also contribute a small extent. They identified that the composition of stable isotopes in samples collected from different locations show altitude and continental effects. Al Charideh and Abou Zakhem (2010) carried out a study to figure out the distribution of isotopes (Tritium, $\delta^{18}O$ and δD) in precipitation over Syria by monitoring 12 stations from 2000 to 2003. Analysis revealed a high seasonal variation in the eastern continental stations compared to the western stations whereas the deuterium excess showed higher values in western stations than the eastern stations. They also found that, Tritium showed similar variations in western and eastern stations. Composition of stable isotopes in precipitation over Debrecen, Eastern Hungary was studied by Vodila et al. (2011) by collecting event based samples during 2001 to 2009. They observed that, local meteoric water line (LMWL) of monthly precipitation falls very close to the global meteoric waterline (GMWL) but slope and

intercept showed lower values indicating the effect of secondary evaporation of falling rainfall.

Precipitation, groundwater and surface water transformation in the Sanjiang plain, northeast China was investigated by Xu et al. (2013) through the analysis of the composition of stable isotopes oxygen and deuterium in the samples collected from 2004-2005. Seasonal difference in the composition of stable isotopes was observed in precipitation. Low composition of $\delta^{18}O$ and δD was linked with minimum temperature in cold half year whereas samples collected during the rainy seasons showed higher composition of isotopes. Composition of isotopes in surface water indicated a higher evaporation rate in the month of August and September whereas the groundwater indicates rainfall as the major source of recharge. Temporal variation of isotopic composition in precipitation and its relationship with the meteorological, geographical parameters and long term process in the German precipitation was investigated by Stumpp et al. (2014) using long term data sets (36 years) from 28 stations. They found higher influence of latitude and altitude (the meteorological and geographical parameters) over the composition of isotopes and its variation. Trend analysis indicated a positive trend in the long term isotope composition in 20 stations. Composition of stable isotopes in rainfall and water vapour was studied by Munksgaard et al. (2015) by collecting rainfall, water vapour and discrete rainfall samples during the passage of tropical cyclone Ito through north eastern Australia in April 2014. They found a close relationship with the composition of isotopes and cyclonic features (spiral rainbands, periods of stratiform rainfall and the arrival of subtropical and tropical air masses). They identified a near equilibrium rainfall-vapour fractionation which indicates strong exchange of the isotopes between the rainfall and vapour. de Souza et al. (2015) carried out a study in the Urucu Oil Province, Brazil to understand the interrelationship between the groundwater and surface water using the composition of isotopes in rainfall, surface water and groundwater samples collected during the period of 2008-2009. They identified meteoric origins of surface water and groundwater, in which groundwater showed fractionation by evaporation.

Sánchez-Murillo et al. (2015) estimated the mean transit time (MTT) in natural and human altered watershed in the inland Pacific, northwest of the USA through stable isotope ratio. The regional meteoric water line showed a temperature dependent seasonality variation and low d excess value which indicates the incorporation of recycled local water in to the travelling air mass and secondary evaporation processes at basin scale. Furthermore, a significant regression between base flow MTT and damping ratio was observed in the

analysis. Kerr et al. (2015) studied the isotope concentration in the Southern Alps of New Zealand by analysing samples collected from 29 locations (in a west-east transect) during April, 2013. They observed an increase in the concentration of isotopes from west to east and this was attributed by the origin of precipitation from higher and/or colder condensation. Based on d excess value, transect was divided into three areas, such as increasing d excess region, low d excess region and high d excess region. Using 113 rainfall samples collected during pre-monsoon, northeast monsoon and southwest monsoon in 2010, Unnikrishnan Warrier et al. (2016) carried out a study in Kozhikode, India and found that the composition of isotopes in the daily rainfall between and within the monsoon season varies periodically. They also pointed out the role of secondary evaporation which controlled the composition of isotopes in pre-monsoon rainfall. Composition of isotopes in rainwater and flood water in the Brisbane River, Australia was investigated by Adame et al. (2016) by collecting samples during January 2013. Results show low composition of isotopes in flood water and was linked to the high concentration of suspended sediment in the flood water. Chakraborty et al. (2016) studied the isotopic variation in rainwater and atmospheric control over the variation of isotopes in the Andaman Island and the Bay of Bengal, India by analysing samples collected during the period of 2012-2013. They identified the role of dynamic moisture over the variation in the composition of isotopes in rainwater.

Brahim et al. (2016) attempted to identify the major factor control the composition of isotopes in precipitation and its variation over Morocco by analysing monthly precipitation and event based precipitation collected from 17 rain gauge stations of three different monitoring networks (IMPETUS-2002 to 2006, IAEA/GNIP-1994 to 2004 and LAGAGE-2004 to 2015). The analysis identified the influence of topography and distance from the sea as the major factors affecting the variation in the composition of stable isotopes in precipitation over Morocco. The influence was also confirmed by identifying the most depleted composition of stable isotopes in samples collected from higher regions of the Atlas Mountain. At the same time, samples collected from southwestern Morocco which show enriched composition of isotopes whereas while comparing the seasons, samples collected during dry season show enriched composition of isotopes compared to humid seasons. Ichiyanagi et al. (2016) analysed the spatial distribution of annual mean isotopes in precipitation across Japan by considering 56 sites in the year 2013. They identified a strong latitude effect in the composition of isotopes in southern part of the study area but the data does not show any influence of amount effect. To understand the effect of aridity in the composition of precipitation isotopes, Wang et al. (2016) collected 1052 event based

precipitation samples from 23 stations during the period of 2012-2013 from the Tianshan Mountain, Central Asia. They identified seasonal and spatial variations in the composition of δD and δ^{18}O and the samples collected during summer show more enriched composition, whereas the winter samples showed depleted composition. They also found an isotopic rain shadow effect in winter and a significant correlation between δ^{18}O and air temperature. Sources of monsoon precipitation and the amount of dew formed in the Western Jilin Province, China was studied by Wenguang et al. (2017) through the analysis of stable isotopes in precipitation collected during the period of July 2012 to October 2013. From the results, they found that the summer precipitation contributed by the East Asian monsoon and the middle and high latitude of Eurasia influences the atmospheric circulation in winter. They concluded that the amount of dew was controlled by the wind speed, relative humidity and low temperature.

Spatio-temporal variation in the composition of rainwater isotope and its effect on isotope hydrograph separation (HIS) in a small catchment in Switzerland was investigated by Fischer et al. (2017) by collecting event based, 13 rainfall samples during snow free period of 2010-2011. They summarized the results as this; the temporal variation is larger than the spatial variation of isotopic composition and the spatial variability of rainfall isotope composition is significant enough to consider the HIS studies even if the catchment is small. Burnik Šturm et al. (2017) conducted a field based study of stable oxygen and deuterium isotopes in the Dzungarian Gobi, southwest Mongolia by collecting 26 event based precipitation samples, 39 river water samples and 75 samples from other water bodies from June 2012 to September 2013. They found that the isotope composition in summer shows extreme range and high seasonal variation whereas samples collected during winter shows lower variation. They explained that the variation is not only caused by the different origin of the air mass but also by the combination of different process affecting the isotope composition. Analysis of stable isotopes in precipitation and stream water in southeastern part of the Tibetan plateau was carried out by Ren et al. (2017) to understand the moisture source and empirical relationship between isotopes and elevation. For that, they collected event based samples throughout the year 2011. They found seasonal variation in the composition of stable isotopes and discovered that this was linked with the wind. For example, southerlies dominates in summer and southerlies or a mix of southerlies and westerlies dominates in spring. They observed an inverse relationship between elevation and composition of isotope.

Feng et al. (2017) carried out a study on stable isotopes in precipitation and atmospheric moisture by considering samples collected from 3 sites in the Pailugon catchment in northwestern China between the period of 2012 to 2013. Seasonal variation in oxygen isotope was observed with enriched values in summer season and depleted values in winter season. They identified a positive correlation between the composition of $\delta^{18}O$ and $\delta^{2}H$ with air temperature. Spatial and temporal variation in stable isotopes in monthly rainfall samples (collected during 2013 to 2014) and its relationship to the regional water cycle and the controlling factors in Cameroon (Douala and Yaounde cities) were investigated by Wirmvem et al. (2017). Based on the slope value of LMWL, they explained that the equilibrium isotopic condition occurs during rain formation while negligible evaporation happens during precipitation. They suggested that, the Atlantic Ocean supply moisture and the isotopic variation were controlled by the amount effect and moisture cycle. Zhao et al. (2018) analysed the isotopic characteristics of precipitation and source of water vapour in two regions (Fengxiang and Ningwu) in northern China by collecting event based 49 samples and 52 precipitation samples for 1 year period (2016-2017) from each sites. The slope and intercept of LMWL indicated that the Tropical Ocean acts as the source of water vapour. They found that the temperature has a significant positive relation with the composition of isotopes in the dry season whereas the amount of rainfall and composition of $\delta^{18}O$ showed a significant negative relationship during the wet season. Hollins et al. (2018) studied the variation of rainfall isotope over the Australian continent and its implication in hydrology by considering GNIP data (1962-2002) from seven sites along with monthly data (2003-2014) from 15 sites. They considered isoscape to understand the process of groundwater recharge. They discovered that the amount of precipitation has a strong influence over the composition of isotopes, compared to temperature in most of the sites. They also suggested that spatial variation of isotope was due to the difference in latitude, elevation and distance from the coast rather than amount of rainfall and temperature.

To understand the influence of meteorological factors on isotopes in precipitation, Tian et al. (2018) carried out a study in the Zionsville, Indiana, USA by measuring stable isotopes $\delta^{2}H$, $\delta^{18}O$ and $\delta^{17}O$ from 235 event based precipitation samples (201 rainfall and 34 snowfall) for a period of two years (2014-2016). They pointed out that the variation in composition of isotopes in this region was controlled by daily temperature. They found that the precipitation experiences kinetic fractionation associated with evaporation whereas snowfall experiences equilibrium fractionation and they concluded that local meteorological factors are not affected by $\delta^{17}O$ excess in rainfall and snowfall during the period of study.

Characterising isotopes in precipitation, inflow and outflow of lake Toba, Indonesia, Sidauruk et al. (2018) conducted a lake balance study. They collected monthly rainfall from 4 rain collectors in 2014 and several samples from stream inflow, outflows, springs and lake water for 2-3 times during the same period. The result showed a low LMWL value indicating the transportation of water vapour from the warmer ocean. They found that, water samples collected from inflow streams experience evaporation before reaching the lake, based on the relationship between δD and $\delta^{18}O$. Composition of stable isotopes in precipitation at the Galápagos island was investigated by Martin el al. (2018) by considering 354 events and 14 intra-event precipitation data for 3.5 year (2012-2016) and 13 years (1995-2008) which was extracted from monthly record of the international atomic energy agency (IAEA). The results indicated a significant negative relation between the composition of $\delta^{18}O$ and daily and monthly precipitation and was attributed by evaporation, equilibrium with boundary layer vapour and rainout effects. Relationships between precipitation, surface water and groundwater in a large trans-boundary watershed (Seversky Donets River Basin), Ukraine/Russian federation was carried out by Vystavna et al. (2018) by considering precipitation samples from Kharkiv station collected from November-2013 to February-2015. Besides this, 29 surface and groundwater samples were also collected during high and low flow in 2014. The result was compared with the early measured composition of isotope in precipitation data to understand the isotope fractionation and regional scale process. They found that, enriched values of isotope from upstream to downstream in surface water occurred through progressive evaporation and the groundwater recharge occurs mainly during winter and spring.

In summary, analysis of stable isotopes like $\delta^{18}O$ and $\delta^{2}H$ is capable of revealing the origin (source) and movement of rainwater in a region. Hence, in the present research, the analysis of stable isotopes $\delta^{18}O$ and $\delta D/^{2}H$ is included to determine the sources and characterisation of precipitation in the Limbang River Basin (LRB).

2.6 Research reported from the Limbang River Basin

Review of literature regarding the different aspect of environmental geology and hydroclimatics indicates very few research attempts to study the Limbang River Basin. It was noted that, few studies also reported data related to rainfall trend, runoff modelling and water quality (Lim & Lye, 2003; Muhammad Noor Hisyam, 2010; Chen et al., 2012; Hua et al., 2013; Gandaseca et al., 2014; Sa'adi et al., 2017a,b; Tahir et al., 2018). Among these, rainfall trend characterisation and climate change studies considered the Limbang River Basin as a

part of regional characterisation of Sarawak by selecting representative rain gauge locations from the Limbang River Basin (Hua et al., 2013; Sa'adi et al., 2017a, b). However, studies conducted by Muhammad Noor Hisyam (2010) and Tahir et al. (2018) considered the Limbang River Basin as a whole in their research. Muhammad Noor Hisyam (2010), attempted to model and predict the water level in the Limbang River by considering the ANN model such as multilayer perceptron (MLP) and radial basis function (RBF). They found satisfactory performance by MLP rather than RBF. Tahir et al. (2018) attempted to characterise the effect of climate change over precipitation characteristics in the LRB by assessing the severity of rainfall under three Representative Concentration Pathways (RCPs) from Global Climate Model data of CanESM2. They also checked the capability of Statistical Downscaling Model (SDSM) in the tropical region by selecting 30 years (1976-2005) of data from nine rain gauges in the LRB. They concluded that rainfall in the LRB shows a constant increase in the amount due to the effect of climate change.

However, it was also noted that, there were no studies were carried out to create a comprehensive picture of hydroclimatics of the Limbang River Basin by integrating hydrometeorology and hydrochemistry to establish the present environmental status of the river basin. In order to fill the research gap, in the present research, statistical rainfall trend characteristics, runoff modelling, chemical characteristics of rainwater and surface water, along with stable isotopes composition in rainwater were taken in to account.

2.7 Summary

Based on the literature review, it is clear that comprehensive information about catchment hydrology or hydroclimatology can be obtained by the rainfall trend analysis, rainfall-runoff modelling and hydrochemical characterisation of rainwater and surface water. Moreover, vast literature survey was made to support the declared research gap in the study area (no studies were reported from the study area in terms of the proposed aim and objectives) and to justify the selection of the LRB for the present research. Besides this, the review of literature done also facilitated the selection of appropriate methodology to achieve the declared objectives.

Chapter 3 Data Collection and Methodological Background

3.1 General

The present research incorporates a comprehensive approach towards understanding the meteorological and hydrological characteristics of the Limbang River Basin through continuous monitoring, collection, analysis and statistical modelling of hydro-meteorological variables. In order to obtain detailed information regarding the study area and parameters considered in the research, different sources of information, materials and methods were used. Brief descriptions about different sources of information and methodology used to collect, store, analyse and interpret the results are also provided in this chapter.

3.2 Datasets Used

Data sets and sources of information used in the present research vary from field based primary data collection to secondary data collected from different sources such as Government Departments and space agencies. Primary data includes surface water and rainwater samples collected from various locations in the study area. In order to collect the field based water samples, guidelines proposed by APHA (American Public Health Association, 2012) and IAEA (International Atomic Energy Agency, 1997) were followed. Secondary data sets used are topographical maps, geological maps, satellite images and daily rainfall data and water level data of the LRB. A brief detail about different data sets and its collection methods can be found in the following sections.

3.2.1 Primary data

3.2.1.1 Field data collection

Primary data utilised in the present research was directly collected from the field and analysed either in the field itself or in the laboratory. Considering the drainage networks and constraints of accessibility in the LRB, a total of 24 sampling locations were identified from the main stream and tributaries. While fixing the surface water sampling locations, an accurate representation of the whole river basin was assured by using the distributed sampling method (Figure 3.1). Details of 24 surface water collection locations are given in Table 3.1. Surface water sampling from rivers started from upstream of the river (upper basin). Among the total sampling locations, 11 samples were collected from the major river (Limbang River) and 13 samples were collected from tributaries. Elevation of the sampling

locations vary in the range of 9 to 366m above mean sea level. The upper basin sampling locations have very clear water with exposed river beds consisting of bed rocks, huge boulders, cobbles and pebbles. At the same time, below the middle reach of the basin, most locations show turbid water with increased depth and fine sand / clay particles deposited on river banks. Water flow in different locations of river show varying characters with laminar flow in upstream locations, whereas highly turbulent flow dominated in downstream area. In order to determine the physico-chemical characteristics of surface water in the LRB, three distinct sampling periods (seasons) were fixed to collect the water samples by considering the rainfall characteristics in the region. The first sampling was carried out in November-2016 (starting of NE monsoon season), while the second samples were collected during March-2017 (end of NE monsoon) and the third sampling was carried out in the month of September-2017 (end of SW monsoon).

Surface water samples were collected using a water scooper from a depth of 5 to 10cm from the water surface. A few samples were collected from the river bank and some others were collected from the center part of the river (by using country boat). The physico-chemical parameters pH, Total dissolved solids (TDS), Electrical conductivity (EC), Turbidity and Temperature were measured in the field using portable meters. In order to analyse nutrients, major ions and trace metals, collected water samples were transferred to 1L polyethylene bottles and stored in the cool box (ice preserved as per the guideline of APHA, 1995). In order to avoid contamination, the bottles were rinsed with distilled water and at the sampling location the bottles were rinsed again with the water to be sampled. Figure 3.2 shows field photographs of different surface water sampling locations in the LRB considered in the present research.

In addition to the surface water collected from various rivers (major and tributaries) in the LRB, cumulative monthly rainwater samples were also collected for a period of 1 year (from October-2016 to September-2017) to determine the physico-chemical characteristics, and also to analyse the composition of stable isotopes such as deuterium (δD) and oxygen-18 ($\delta^{18}O$). Standard rainwater sampling procedures proposed by International Atomic Energy Agency (IAEA, 1992) was followed in order to set up the rainwater collection apparatus (Figure 3.3). Two 5L plastic containers washed with highly purified water were used to collect the cumulative monthly rainwater by fitting a funnel in its mouth. Rainwater was collected from the first day of the month till the last day of the month. Paraffin oil of 0.5cm thickness was put in the container to avoid evaporation through the walls. At the end of the month,

the rainwater collected had to be shaken, but not aggressively, before transferring the sample to the bottles to be sent for analysis. The transferring of samples should be carried out rapidly to reduce evaporation. After transferring the samples, the rain collector should be dried and kept to collect the next month rainwater. The cumulative monthly rainwater samples thus collected were stored in 4°C in 60ml high density polyethylene (HDPE) bottle for the analysis of δD and $\delta^{18}O$.

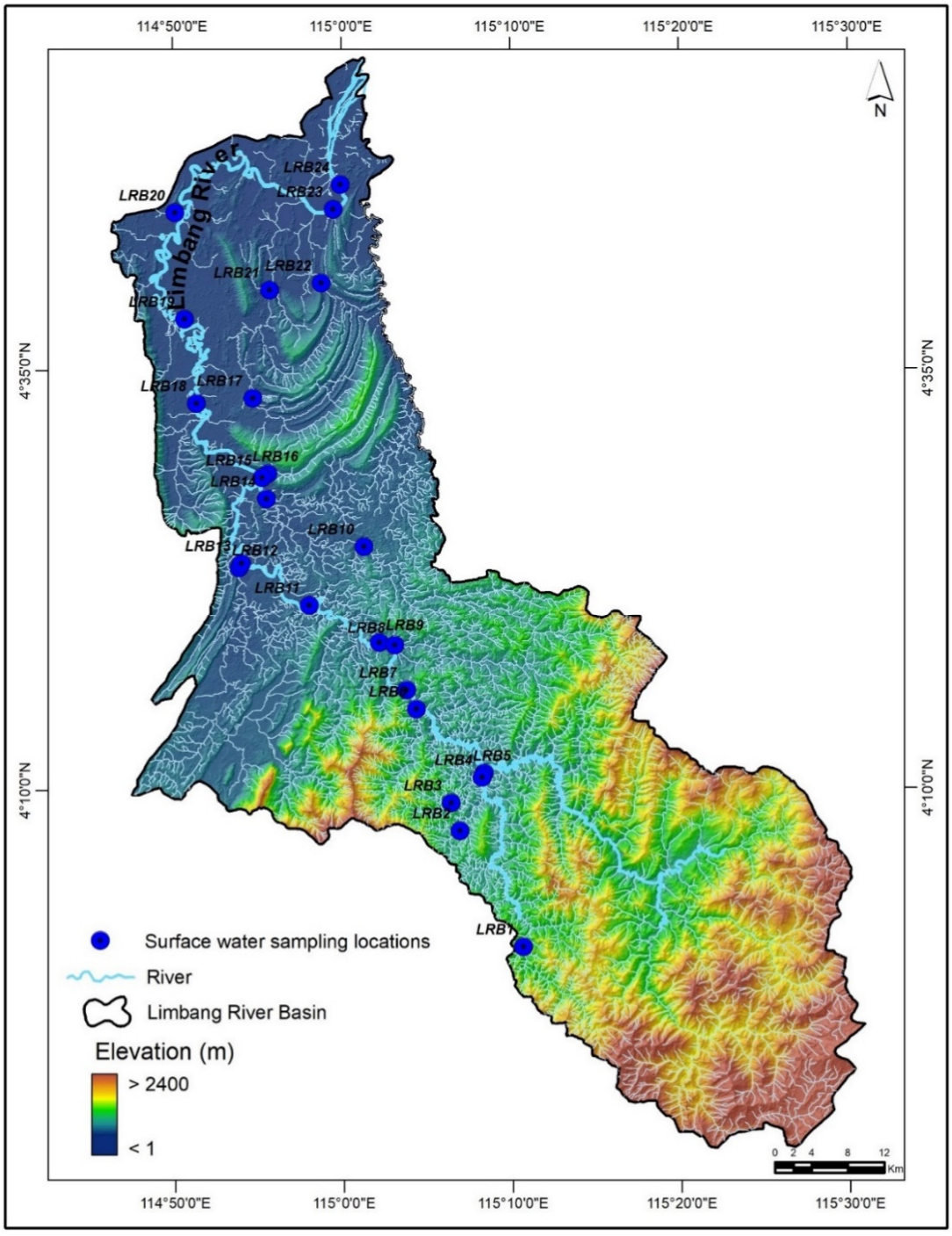

Figure 3.1: Map showing surface water collecting locations with drainage networks in the LRB.

Table 3.1: Details of surface water collection locations in the LRB.

SL No.	Sample No.	River	Location Details		Elevation	Condition of River / flow pattern	Characteristics
			Lat	Long			
1	LRB 01-SW	Limbang Tributary	4 00 32.5	115 10 50	366	Low water level - Clear water - Laminar flow	Incised river, boulders and bed rock exposed. Tropical forest cover both banks.
2	LRB 02-SW	Limbang Tributary	4 07 28.1	115 07 5.9	237	Low water level - Clear water - Laminar flow	Channel bottom exposed, small tributary with gravels and pebbles dominated.
3	LRB 03-SW	Limbang Tributary	4 09 7.5	115 06 34.5	218	Low water level - Clear water - Laminar flow	Gravel bedded Incised river, weathered rocks were found in both banks. One side of the river is cleared and the other side covered with secondary forest.
4	LRB 04-SW	Limbang Tributary	4 10 36.4	115 08 26.8	161	Low water level - Clear water - Laminar flow	Unpaired channel with bed rock exposed. Long houses and other buildings are present in both banks.
5	LRB 05-SW	Limbang	4 10 53.5	115 08 32.2	165	Low water level - Clear water - Laminar flow	Wide channel with bed rock exposed in some parts with huge boulders. River banks are flat and succeeded to higher elevated hills.
6	LRB 06-SW	Limbang Tributary	4 14 42.5	115 04 31.3	101	Low water level - Clear water - Laminar flow	River is enriched. Showing paired terrace covered with secondary forests. Bed rock exposed, river cross cutting the rocks. Small rapids are present.
7	LRB 07-SW	Limbang	4 15 14.6	115 03 57.2	90	Incised river - Clear water - Laminar flow	Highly incised river portion, cut across the bed rocks shown rapids elsewhere.
8	LRB 08-SW	Limbang Tributary	4 18 31.5	115 .3 15.3	76	Low water level - Clear water - Laminar flow	River meandering and small rapids present in the upstream. Unpaired terrace were found and shale is present in the left bank side of the terrace, dark color rock present in one side.
9	LRB 09-SW	Limbang	4 18 40.7	115 02 20.7	69	Low water level - Clear water - Laminar flow	River incised in nature, Both sides of the river are elevated and covered with vegetation. Channel bar present near downstream. Stream is meandering.
10	LRB 10-SW	Tributary Limbang	4 20 26.7	114 58 11.6	52	Low water level - Clear water - Laminar flow	Bolder bedded river, one side of the river is rock exposed and the other side boulders/ cobbles, meandering in nature.

11	LRB 11-SW	Limbang	4 24 24.8	115 01 28	30	Bank full discharge - Partially clear water - Turbulent flow	Wider river segment with flat river bank.
12	LRB 12-SW	Limbang Tributary	4 23 11.0	114 54 2.7	12	Bank full discharge - Partially clear water - Laminar flow	Black colour indicating the origin source might be a peat swamp. Both banks covered with tropical forest and showing increasing elevation.
13	LRB 13-SW	Limbang	4 23 26.8	114 54 10.4	14	Bank full discharge - Turbid water - Turbulent flow	Wide river segment with fine sediments in the river bank, mid-channel bars present (pebbles and cobbles).
14	LRB 14-SW	Limbang Tributary	4 27 16.3	114 55 40.8	24	Low water level - Turbid water - Turbulent flow	Unpaired terrace with bed rock exposed, small rapids were also present. Logged areas and settlements (logging camps) also seen in both banks.
15	LRB 15-SW	Limbang	4 28 46.1	114 55 25.7	17	Incised river - Turbid water - Turbulent flow	Channel bars formed, vast deposit of alluvial materials, enriched river, meandering nature.
16	LRB 16-SW	Limbang Tributary	4 28 46.9	114 55 46.8	11	Low water level - Clear water - Laminar flow	Slightly incised river.
17	LRB 17-SW	Limbang Tributary	4 33 16.1	114 54 53.4	18	Low water level - Turbid water - Turbulent flow	Incised river, originate from peat swamps, fine sediment deposit.
18	LRB 18-SW	Limbang	4 32 58	114 51 33.1	14	Bank full discharge - Turbid water - Turbulent flow	Wide stretch of flood plain in both sides of the river. Agricultural activates are limited.
19	LRB 19-SW	Limbang	4 37 58.3	114 50 51.4	14	Bank full discharge - Turbid water - Turbulent flow	Wide rive stretch with vast flat flood pains on both banks, river shows meandering and slight incision.
20	LRB 20-SW	Limbang	4 44 17.9	114 50 18.5	9	Bank full discharge - Turbid water - Turbulent flow	Flood plain area, deposit of alluvium were found both sides of the river.
21	LRB 21-SW	Limbang Tributary	4 39 40.7	114 55 54.6	15	Low water level - Turbid water - Turbulent flow	Peat swamp river, showing dark colour, fine alluvium deposited in both banks.
22	LRB 22-SW	Limbang Tributary	4 40 0.62	114 58 58.3	16	Low water level - Partially clear water - Stagnant	Peat swamp river, showing dark colour and slightly incised in nature.
23	LRB 23-SW	Limbang	4 44 28.8	114 59 40.8	11	Bank full discharge - Turbid water - Turbulent flow	Flood plain area, channel meander away from the point, area covered with vegetation (mangroves also), water transportation dominated.
24	LRB 24-SW	Limbang	4 45 55.8	115 00 06.3	10	Bank full discharge - Turbid water - Turbulent flow	Flood plain, alluvial river banks, human activity is present, mangroves in some part.

Figure 3.2: Field photographs showing selected surface water sampling locations.

Figure 3.2: Field photographs showing selected surface water sampling locations.

Next, the 1L rainwater corresponding to individual station for each month was stored in polyethylene bottles to analyse the physico-chemical characteristics in the laboratory. In the present research, rainwater was collected from five spatially separated locations in the LRB (Figure 3.4).

Figure 3.3: Experimental set up for cumulative sampling of precipitation for isotopic analysis (retrieved from IAEA, (1997), Technical Procedure for cumulative monthly sampling of precipitation for isotopic analysis).

3.2.2 Secondary data

Secondary data used in the present research are: daily rainfall, water level and evaporation data (13 rain gauge stations, 5 water level stations and 2 evaporation stations), collected from the Department of Irrigation and Drainage (DID) for a period of 69 years (1948-2016) (Table 3.2); topographical maps (1:50,000) of the study area published by Department of Survey and Mapping (JUPEM); Geological map (1:750,000) produced by Minerals and Geoscience Department (JMG) and soil textural map (1:50,000) published by Department of Agriculture (DoA), Sarawak, Malaysia. Satellite images (Landsat images) and digital elevation surface (30m Shuttle Radar Topographic Mission – SRTM-data) was collected from United States Geological Survey (https://earthexplorer.usgs.gov/). Distribution of rain gauges, water level measuring stations and evaporation gauges in the LRB is shown in Figure 3.5.

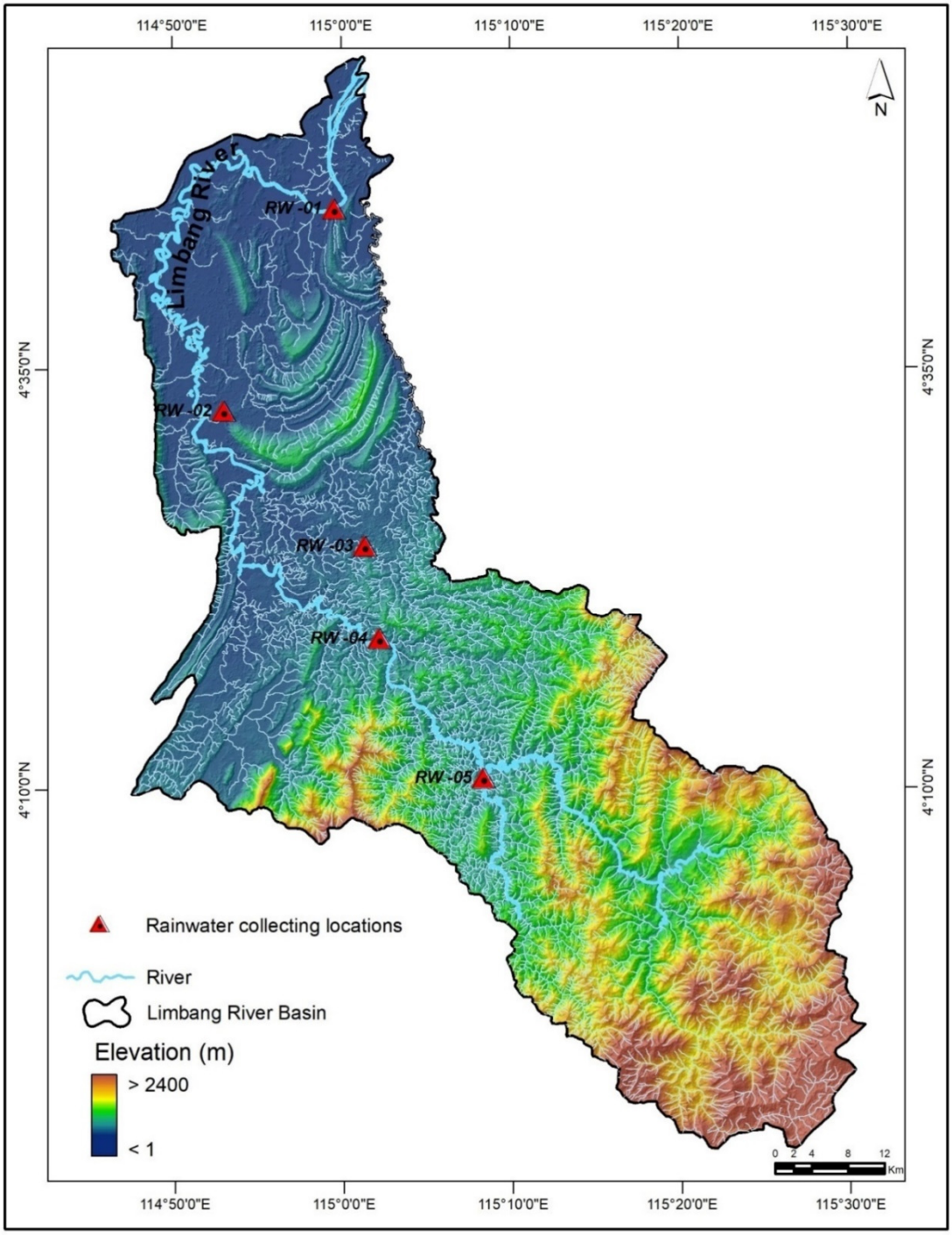

Figure 3.4: Map showing rainwater collecting locations with drainage networks in the LRB.

Table 3.2: Details of rain gauging, water level and evaporation measuring stations in the LRB.

Rain gauging stations	Data availability		Location attributes	
	From	To	Latitude	Longitude
Limbang DID	1980	2016	4.7444	114.9972
Pandaruan	1972	2016	4.6875	115.0194
Tegarai	1967	2016	4.6389	115.0250
Lubai Tengah	1972	2016	4.6097	114.9153
Ukong	1948	2016	4.3250	114.8944
Medamit Nanga	1963	2016	4.4819	114.9125
Lubok Lalang	1987	2016	4.4111	115.0222
Merbau	1990	2016	4.3500	115.0583
Ulu Medalam	1998	2016	4.3250	114.8944
Ulu Medamit	1993	2014	4.3416	115.1958
Setuan	1998	2016	4.2472	115.0750
Long Napir	1977	2016	4.1763	115.1389
Rutoh	1998	2016	4.0833	115.5111
Water level measuring stations				
Limbang DID	1988	2016	4.7458	114.9972
Batu Danau	1976	2015	4.6472	114.8208
Ukong	1976	2015	4.5514	114.8556
Saliban Nanga	1976	2016	4.4764	114.9236
Insungai Nanga	1980	2005	4.4000	114.8917
Evaporation measuring stations				
Limbang DID	1982	2016	4.7444	114.9972
Ukong	1970	2004	4.3250	114.8944

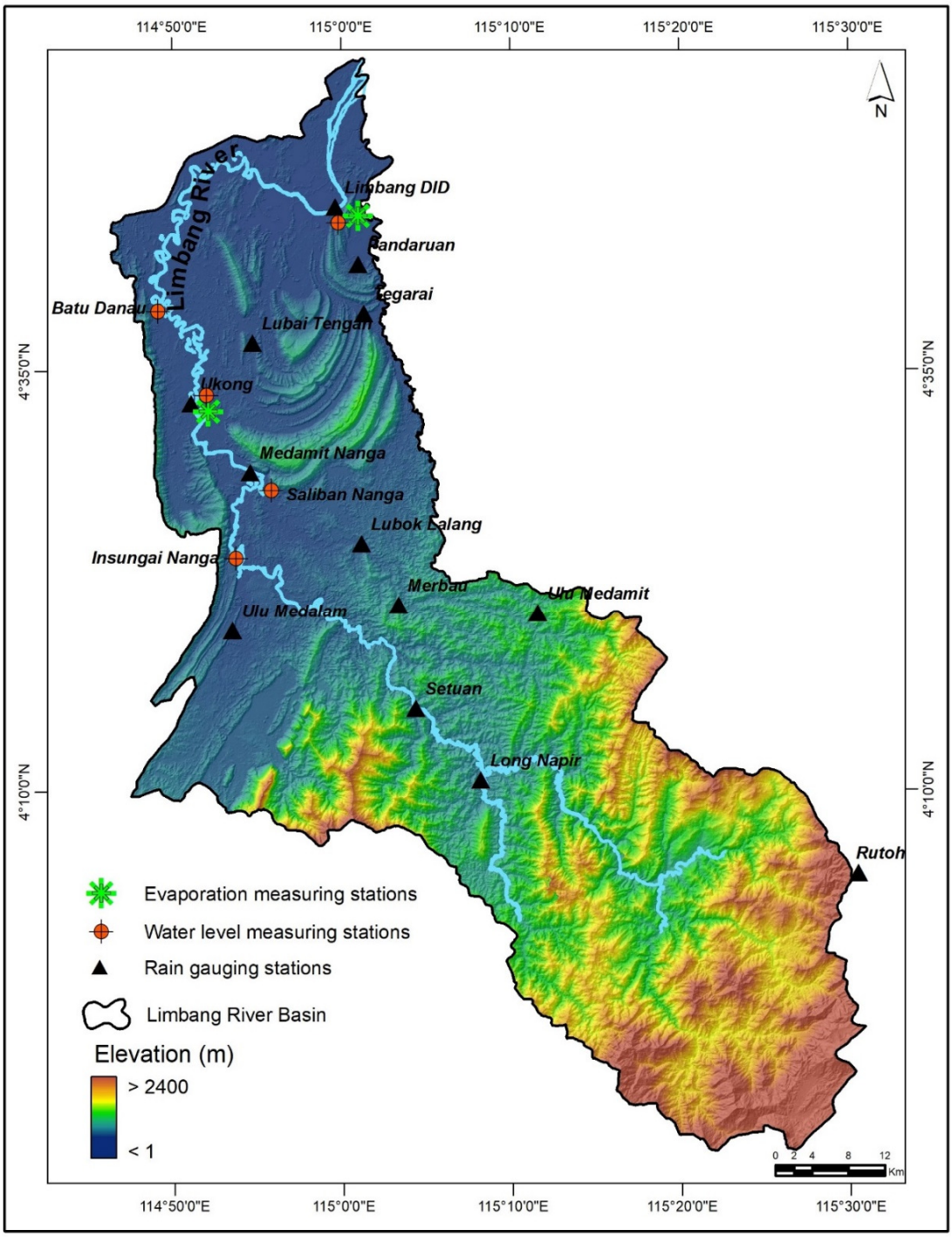

Figure 3.5: Map showing distribution of rain, water level and evaporation measuring stations in the LRB over digital elevation model (SRTM 30m data).

3.3 Methodology / Analysis Techniques

3.3.1 Rainfall trend analysis

Demonstration of changes in rainfall characteristics over a region in a statistical manner can be carried out through trend analysis methods. Trend analysis is used extensively to determine the impact of climate change and the changes caused in climatic variables in various parts of the world (Lettenmaier et al., 1994; Suppiah & Hennessy, 1998; Zhang et al., 2000; Crisci et al., 2002; Xu et al., 2006; Chaouche et al., 2010; Benestad, 2013; Yilmaz et al., 2014; Zhao et al., 2015; Chattopadhyay & Edwards, 2016; Dai et al., 2016; Dawood, 2017; Gao et al., 2017; Minaei & Irannezhad, 2018; Valipour & Sefidkouhi, 2018). Parametric and non-parametric tests are widely used for change detection (Morell & Fried, 2009; Kocsis et al., 2017). Parametric tests use data driven methods which requires many assumptions and is sensitive to outliers. At the same time, non-parametric tests use rank based methods which requires lesser assumption and is less sensitive to the outliers (Mann, 1945; Kendall, 1948; Lehmann & D'Abrera, 2006). In order to determine the hydrometeorological trend analysis, the non-parametric methods were preferred over the parametric methods because of the non-normally and censored distribution nature of the time series data. Mann Kendall test statistics are popularly used to assess the trend of hydrometeorological time series along with Spearman's Rho tests (Belle & Hughes, 1984; Yue et al., 2002; Shadmani et al., 2012; Gocic & Trajkovic, 2013; Kisi & Ay, 2014; Rahman et al., 2017; Dragićević et al., 2018; Kişi et al., 2018; Pandey & Khare, 2018). In the present study, non-parametric methods such as Mann Kendall and Spearman's Rho tests were used to determine the rainfall trend of the Limbang River Basin (LRB). Before proceeding to the statistical trend determination, homogeneity of rainfall data was tested with the lag-1 autocorrelation test. In addition, the gap in rainfall time series data was filled with the best suitable method. Results of trend analysis will help to forecast the pattern and severity of extreme events and also aid better management and mitigation measures to safeguard water resources.

3.3.1.1 Rainfall data homogeneity test (Lag-1 autocorrelation) and gap filling

Daily rainfall data from 13 rain gauging stations were collected from DID for a period of 69 years (1948-2016). Rainfall data for the thirteen rain gauges in the LRB were organised to ensure continuity and consistency of the data. Time series data, possesses certain correlations in the series, which will lead to over prediction of trend characteristics. Before processing the rainfall data, the lag-1 autocorrelation test was carried out at 95% significant level to test the randomness and homogeneity. The lag-1 autocorrelation coefficient can be

calculated as (Salas et al., 1980; Yue et al., 2002; Ishak, 2014; Yu et al., 2017, Sharma & Singh, 2017):

$$r = \frac{\sum_{t=1}^{N-1}[(x_t - \bar{X})(x_{t+1} - \bar{X})]}{\sum_{t=1}^{N}(x_t - \bar{X})^2}$$

$$\bar{X} = \frac{1}{N}\sum_{t=1}^{N} x_t$$

where, x_t represents the first $N-1$ observation with $t = 1, 2, \dots, N-1$ and x_{t+1} represents the second $N-1$ observations with $t+1 = 2, 3, \dots, N$.

The 95% significant value of two tailed lag-1 auto correlation can be obtained by the equation:

$$r_{(95\%)} = \frac{-1 \pm 1.96\sqrt{N-2}}{N-1}$$

where, N is the number of observations.

The result of lag-1 autocorrelation analysis indicates whether the original data should undergo any pre-processing before carrying out the trend test. Results of lag-1 autocorrelation shows that the data are homogenous and not correlated. Therefore, before applying the statistical measurements to determine the trend, no pre-processing is required (Tabari et al., 2012; Zhao et al., 2015). During the data arrangement, some of the daily rainfall observations were found to be missing and these values were replaced by the normal ratio method (NRM). This method is best suited for the calculation of missing rainfall, if the normal annual rainfall of the stations are lesser than 10% of any surrounding rain gauges (Paulhus & Kohler, 1952; Singh, 1992; Xia et al., 1999; Caldera et al., 2016). NRM was initially proposed by Paulhus and Kohler (1952), and later modified by Young (1992). The normal ratio method (NRM) can be written as:

$$P_x = \frac{1}{m}\sum_{i=1}^{m}\left[\frac{N_x}{N_i}\right] P_i$$

where, N_x is the normal annual rainfall at the x^{th} station. N_i and P_i are the normal annual rainfall and time series rainfall of m surrounding stations. The gap filled daily data were then converted into station wise monthly, seasonal and annual rainfall data to calculate

rainfall trend using statistical methods. In order to determine monthly, seasonal and annual rainfall trends, most widely used Mann Kendall and Spearman's Rho test were selected and applied in the rainfall data. Details about trend determining statistical methods are given below.

3.3.1.2 Mann Kendall test

The nonparametric monotonic trend of environmental, hydrological and climate variable can be calculated using the Mann Kendall trend test also known as Mann Kendall test (Mann, 1945; Kendall, 1948). The main strength of the test is its simple concept and it is also minimally affected by the departure from normality because of the 'no specific assumption of joint distribution' characteristic of the data. The advantage of Mann Kendall test is that, it allows missing values and any particular distribution is not needed. Another importance of this method is, if the data is reported as a trace or less than the detection limit, then the method is applicable, because Mann Kendall test uses relative magnitude of the data rather than the measured value (Gilbert, 1987; Mozejko, 2012). The null hypothesis, H_0 is that the data are independently and identically distributed (*iid*) i.e. no trend, is the main limitation of the trend but the non-acceptance of H_0 implies that the datasets are not to be taken as iid. Practically, the rejection of H_0 is taken as an alternative hypothesis, with H_1 indicating the evidence of a monotonic trend (Mann, 1945; Kendall, 1948; Asfaw et al., 2018; Gedefaw et al., 2018), which is given by,

Let X_1, X_2, X_3,…,X_n be the time series data, and the Mann Kendell statistics can be determined as:

$$S = \sum_{i=1}^{n-1} \sum_{j=i+1}^{n} \mathrm{sgn}(X_j - X_i)$$

where, X_i and X_j are i^{th} and j^{th} value of the data, n is the number of observations and $\mathrm{sgn}(X_j - X_i)$ is the sign function calculated as:

$$\mathrm{sgn}(X_j - X_i) = \begin{cases} +1 & if \quad X_j - X_i > 0 \\ 0 & if \quad X_j - X_i = 0 \\ -1 & if \quad X_j - X_i < 0 \end{cases}$$

If the number of observations $n \geq 8$, the statistics S is approximately normally distributed (Mann, 1945; Kendall, 1948), then the mean $(\mu(S))$ and the variance $(\sigma^2\,(S))$ are calculated using the following equation:

$$\mu(S) = 0$$

$$\sigma^2 = \frac{n(n-1)(2n+5) - \sum_{i=1}^{m} t_i(t_i-1)(2t_i+5)}{18}$$

where, t_i is the number of observations in the i^{th} tied group and m is the number of tied groups. If the number of ties are absent in the observation, then the variance is calculated as:

$$\sigma^2 = \frac{n(n-1)(2n+5)}{18}$$

The normalised standard test statistic is calculated as:

$$Z_s = \begin{cases} \frac{S-1}{\sigma} & if \quad S > 0 \\ 0 & if \quad S = 0 \\ \frac{S+1}{\sigma} & if \quad S < 0 \end{cases}$$

The Z_s value will provide information whether the observed data possess statistically significant trends. The positive value of Z_s indicates an increase in trend and negative value is used for decreasing trends. To test the positive or negative trend at α level of significance, the null hypothesis H_0 (absence of monotonic trend/ identical distribution) is rejected if the absolute value of $Z_s > Z_{s\,(1-\alpha/2)}$, and the alternative hypothesis H_1 (follow a monotonic trend) is accepted.

3.3.1.3 Spearman's Rho trend test

The rank based non-parametric Spearman's Rho test is used to understand the correlation between the variable and the time series by representing the monotonic trend (Sabzevari et al., 2015). This method is the same as Pearson product momentum correlation coefficient but possesses advantages over it. The SR test is unaffected by the distribution of population, i.e., the size and the interval or frequency of the data, because the method operates based on the rank of the data (Gauthier, 2001). The null hypothesis in this test (H_0) is that the time series data are independent and identically distributed which indicates no trend whereas the alternative hypothesis (H_1) is used if the data increases or decreases with *i* (time series) i.e. trend exist (Ahmad et al., 2015). In this test, the lowest to the highest ranks were assigned separately to each variable and the difference between ranks were calculated. Then the sum of the squares of the difference between the ranks was calculated. If the value is small this indicates the existence of correlation, and the value determines the significance

of the correlation. Equal rank was assigned to tie values (Sneyers, 1990; Gauthier, 2001; Hajani et al., 2014; Wang et al., 2015).

The test statistics can be calculated as:

$$r_s = 1 - \frac{6 \sum_{i=1}^{n} (R_i - i)^2}{n^3 - n}$$

where, R_i is the rank of i^{th} observation and n is the number of observations.

The equation becomes more complicated if ties are involved. But a significant difference will occur only by large number of ties occurs. If g is the number of tied groups and t_j is the number of tied data in the j^{th} group then the Spearman's Rho can be written as:

$$r_s = \frac{\frac{(n^3-3)}{6} - \sum_{i=1}^{n} (R_i - i)^2 - \sum T_x - \sum T_y}{\sqrt{\left[\frac{(n^3-3)}{6} - 2\sum T_x\right]\left[\frac{(n^3-3)}{6} - 2\sum T_y\right]}}$$

where, $\sum T_x / \sum T_y = \frac{\sum_{j=1}^{g} (t_j{}^3 - t_j)}{12}$ for x and y.

Under null hypothesis, the distribution of r_s is asymptotically normal with mean and variance as (Sneyers, 1990; Lehmann & D'Abrera, 2006):

$$\mu(r_s) = 0$$

$$\sigma^2 = \frac{1}{n-1}$$

The standardised statistics can be calculated using the equation:

$$Z_{SR} = r_s \sqrt{\frac{n-2}{1 - r_s^2}}$$

The positive value of Z_{SR} indicates increasing trend and negative value for decreasing trend. When $Z_{SR} > Z_{SR\,(n-2,1-\alpha/2),}$ which is the critical value, the null hypothesis H_0 is rejected indicating significant trend (Shadmani et al., 2012).

3.3.2 Rainfall-runoff modelling

The relationship between rainfall and runoff is the most complex phenomena in hydrology because of the interdependence of spatial and temporal variables and the pattern of precipitation. Precipitation (rainfall) is the principal input in the hydrological cycle, so the intensity, duration and amount of precipitation will directly influence runoff. Different models are provided to predict runoff from rainfall data. The accuracy of generated runoff is determined by the quality of input parameters. Artificial Neural Network modelling (ANN) has been employed widely for the generation of runoff from rainfall data in recent years (Halff et al., 1993; Smith & Eli, 1995). The technology used for ANN is adopted from the biological neuron system (McCulloch & Pitts, 1943; Gallant, 1993; Smith, 1993; Hassoun, 1995). The neural network structure constitutes of mainly neurons and its interconnections. Thus, the ANN is a layered system consisting of a minimum three layers i.e. one input, one output and a hidden layer and the main controlling parameters are the strength of the interneuron connections (weight and the biases) with a back propagation algorithm (Hsu et al., 1995; Anctil & Rat, 2005; Hung et al., 2009) (Figure 3.6).

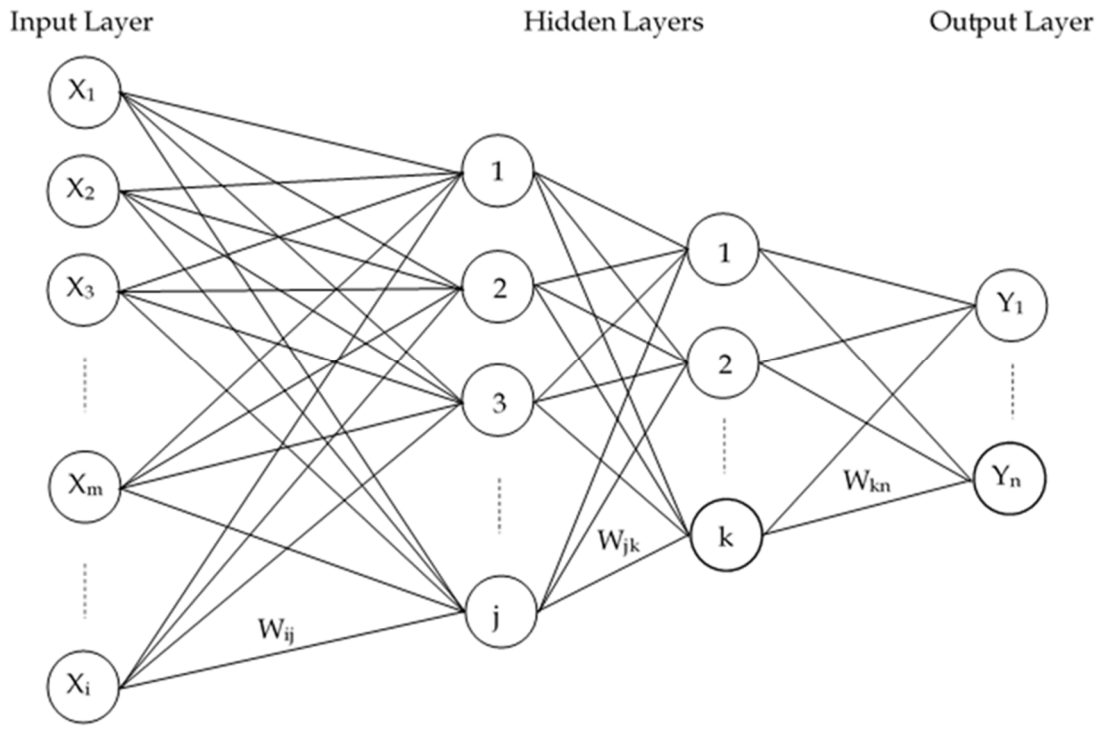

Figure 3.6: Schematic diagram of ANN model.

The best suitable value of the weights and the biases is established by minimizing the mean square error. Two phases such as learning phase and validation phase are associated with an ANN system. The learning phase, the most important and complicated in the ANN

system, learns the complex and highly nonlinear relationship from the input data. During learning, the input is combined with the weight and propagate to compute output (Zurada, 1992; Schalkoff, 1997). This output is subsequently compared with the original value to check the error value. The error is passed to each node in back propagation and will choose the appropriate weight which is used in the validation phase (Senthil Kumar et al., 2005). Different ANN models such as perceptron, feed forward, feedforward back propagation, recurrent model, radial basis function and self-organizing map are used at various conditions. In the present study, multilayer neural network (MNN) with the minimum description length (MDL) algorithm were considered to model the runoff.

3.3.2.1 Multilayer neural network (MNN)

Multilayer Neural Network (MNN) is a most commonly used supervised and feedforward neural network technique with more than one layer of hidden nodes in between the input and output nodes. Figure 3.7 shows the general scheme used in rainfall-runoff prediction modelling. The selection of input nodes in the input layer is of great important for the development of accurate neural network, which can be derive from the data set characteristics. The number of input nodes, hidden nodes, learning rate, momentum constant and the transfer function during training will influence the performance of MNN (Hsu et al., 1995; Patil & Valunjkar, 2014). The present neural network model consists of input layer connected to the input variables such as rainfall and discharge (calculated using stage discharge rating cure) x_i, hidden layer and the output layer connected to the runoff y_k. In the multilayer neural network, the data in the input layer transfers to the next consecutive layer and the activation function processes the signal which is sent by the input data and weight is associated with each input signal.

Consider n as input neurons $(x_1, x_2, x_3, \dots, x_n)$, $h$as hidden neurons $(z_1, z_2, z_3, \dots, z_h)$ and $m\ as$ output neurons $(y_1, y_2, y_3, \dots, y_m)$ in the MNN model. In the input layer each input neuron transmits the input signal to hidden layer and the hidden neurons in the hidden layer quantifies its weighted input signals (Ahmat Nor, 2005; Meher, 2014; Singh, 2014) as:

$$z_j = f_A\left(\sum_{i=1}^{n} x_i w_{ij} + \tau_j\right)$$

where, f_A is the activation function, w_{ij} is the weight of the connection from the input neuron x_i to hidden neuron z_j and τ_j is the bias for neuron z_j. This signal is transmitted to the output layer and is:

$$y_k = g_A\left(\sum_{j=1}^{h} z_j\beta_{jk} + \phi_k\right)$$

where, g_A is the activation function, β_{jk} is the weight of the connection from the hidden neuron z_j to output neuron y_k and ϕ_k is the bias for neuron y_k. Commonly used transfer function is the sigmoid function (Figure 3.8) and is given by the variables,

$$f(s) = \frac{1}{1 + e^{-s}}$$

In the present study, multilayer neural network model was designed with a single hidden layer, sigmoid activation function and a linear output (Minns & Hall, 1996; Patil, 2008). Then the signal transmitted to the output layer can be written as:

$$y_k = g_A\left(\sum_{j=1}^{h} f_A\left(\sum_{i=1}^{n} x_i w_{ij} + \tau_j\right)_j \beta_{jk} + \phi_k\right)$$

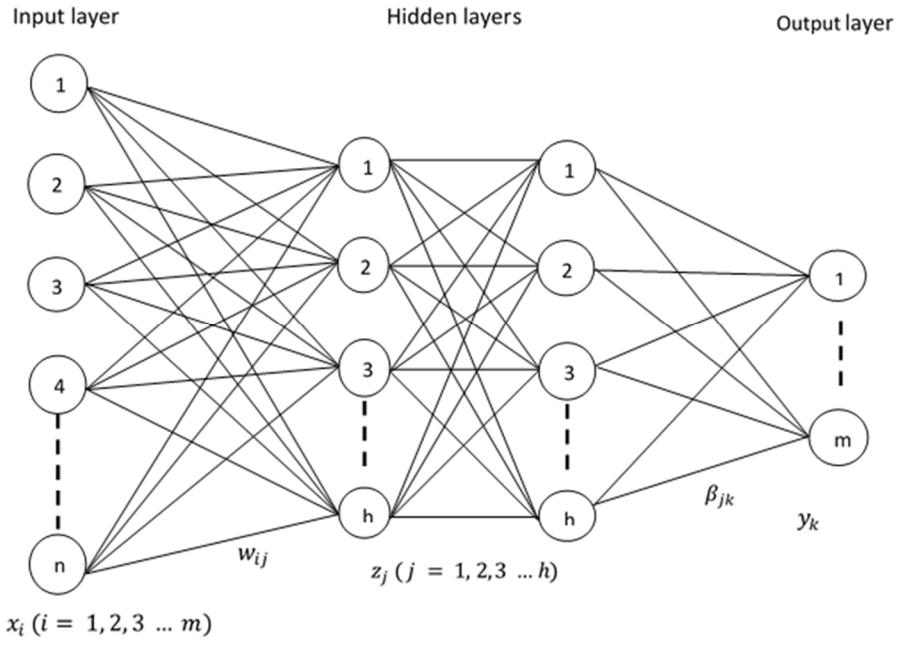

Figure 3.7: Schematic diagram of Multilayer Neural Network model with two hidden layers.

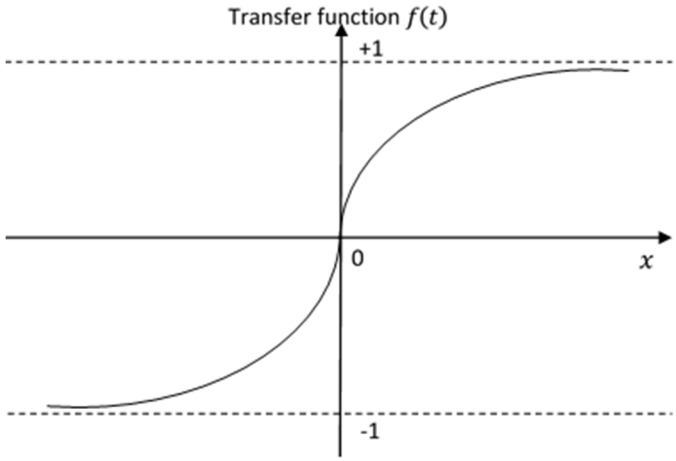

Figure 3.8: Sigmoid activation function.

Determination of the optimal weight vector for the network is a common feature of all the models. Training of MNN model helps to obtain the optimal weight vector for the network. There are a number of techniques available to train the MNN. In the present study, minimum description length (MDL), algorithm was considered to train the multilayer neural network. The MDL principle is used for estimation of both parameters and structure of the model (Rissanen, 1978, 1989; Lehtokangas et al., 1993; Bischof & Leonardis, 1998; Gao et al., 1998; Alippi, 2002; Small & Tse, 2002; Grünwald, 2005; Wu et al., 2010). The procedure for MDL will automatically protect against over fitting. The estimation of cost of specifying the model parameters and associated prediction error is the basic principle of MDL. The MDL provides the best compact description of a time series data. For an optimal model, the increase in model size leads to the decrease in model prediction. This indicates the tradeoff between the model complexity and the goodness of fit observed in MDL by avoiding the too simple model and overlay complex model. Let $E(k)$ and $M(k)$ be the cost of specifying the model prediction error and cost of describing the model. Then the description length can be defined (Judd & Mees, 1995; Yi & Small, 2006; de Rooij, 2008) as:

$$D(k) = E(k) + M(k)$$

The minimum description length states that the value of $D(k)$ is minimum for the optimal model.

Consider a time series of N measurements $\{y_i\}_{i=1}^{N}$ and scalar function of d variables $f(y_{i-1}, y_{i-2}, \dots, y_{i-d};\ \Lambda_k)$ described by k parameters $\Lambda_k = \lambda_1, \lambda_2, \dots, \lambda_k$. The prediction error can be defined as:

$$e_i = f(y_{i-1}, y_{i-2}, \dots, y_{i-d}; \Lambda_k) - y_i$$

For any Λ_k the description length of the model $f(.;\Lambda_k)$ is given by the description length of k parameters Λ_k (Judd & Mees, 1995; Small & Tse, 2002; Yi & Small, 2006),

$$M(k) = L(\Lambda_k) = \sum_{i=1}^{k} \ln \frac{\gamma}{\delta_j}$$

where, γ is a constant representing the number of bits in the exponent of the floating point of representation of λ_j and δ_j represents the optimal precision of λ_j and the optimal $(\delta_1, \delta_2, \dots, \delta_k)$ are given by the solution of,

$$\left(Q \begin{bmatrix} \delta_1 \\ \delta_2 \\ \vdots \\ \delta_k \end{bmatrix} \right)_j = \frac{1}{\delta_j}$$

where, $Q = D_{\Lambda_k \Lambda_k} E(k)$, the second derivative of the description length of model prediction error $E(k)$ with respect to model parameter Λ_k. $E(k)$ is the negative logarithm of the likelihood of the error $e = \{e_i\}_{i=d+1}^{N}$ under the assumed distribution of these errors (Rissanen,1989; Small & Judd, 1998),

$$E(k) = -\ln(e|\Lambda_k)$$

Assuming that the error are Gaussian distribution with mean zero and standard deviation σ then,

$$E(k) = \frac{N}{2} + \ln\left(\frac{2\pi}{N}\right)^{N/2} + \ln\left(\sum_{i=1}^{N} e_i^2\right)^{N/2}$$

The description length of a model is calculated by solving the equation for the precision δ_j and substituting it to calculate the description length of the model $M(k)$ and model prediction error $E(k)$.

3.3.2.2 Performance evaluation of the MNN model

The designed MNN MDL model for the simulation of rainfall-runoff relationship was evaluated by comparing the simulated output and the observed data because there is no specific test to evaluate the model performance. The prediction accuracy of the model was

evaluated using correlation coefficient, Nash Sutcliffe Efficiency (NSE), Root Mean Square Error (RMSE), Relative Root Mean Square Error (RRMSE), Mean Absolute Error (MAE), Mean Absolute Percentage Error (MAPE), Volumetric Error (EV) and Relative Peak Error (RPE). The formula for the calculation of statistical methods considered for the evaluation of accuracy of the MDL MNN model performance is given below (Sudheer & Jain, 2004; Cannas et al, 2006; Hejazi & Cai, 2009; Remesan et al., 2009; Napolitano, 2011; Kovačević et al., 2018).

Correlation coefficient:

$$CC = \frac{\sum_{t=1}^{n}\left[\left(Q_{o(t)} - \bar{Q}_{o(t)}\right)\left(Q_{s(t)} - \bar{Q}_{s(t)}\right)\right]}{\sqrt{\sum_{t=1}^{n}\left(Q_{o(t)} - \bar{Q}_{o(t)}\right)^2 \sum_{t=1}^{n}\left(Q_{s(t)} - \bar{Q}_{s(t)}\right)^2}}$$

Nash Sutcliffe Efficiency:

$$NSE = 1 - \frac{\sum_{t=1}^{n}\left(Q_{o(t)} - Q_{s(t)}\right)^2}{\sum_{t=1}^{n}\left(Q_{o(t)} - \bar{Q}_{o(t)}\right)^2}$$

Root Mean Square Error:

$$RMSE = \left[\frac{1}{n}\sum_{t=1}^{n}\left(Q_{o(t)} - Q_{s(t)}\right)^2\right]^{1/2}$$

Relative Root Mean Square Error:

$$RRMSE = \left[\frac{1}{n}\sum_{t=1}^{n}\left[\frac{\left(Q_{o(t)} - Q_{s(t)}\right)}{Q_{o(t)}}\right]^2\right]^{1/2}$$

Mean Absolute Error:

$$MAE = \frac{1}{n}\sum_{t=1}^{n}\left|\left(Q_{o(t)} - Q_{s(t)}\right)\right|$$

Mean Absolute Percentage Error:

$$MAPE = \frac{1}{n}\sum_{t=1}^{n}\left|\frac{\left(Q_{o(t)} - Q_{s(t)}\right)}{Q_{o(t)}}\right| \times 100\%$$

Volumetric Error:

$$EV = \frac{\left(\sum_{t=1}^{n} Q_{s(t)} - \sum_{t=1}^{n} Q_{o(t)}\right)}{\sum_{t=1}^{n} Q_{o(t)}} \times 100\%$$

Relative Peak Error:

$$RPE = \frac{Q_{op} - Q_{sp}}{Q_{op}}$$

where, $Q_{o(t)}$, $Q_{s(t)}$ are the observed and simulated value with $\bar{Q}_{o(t)}$ and $\bar{Q}_{s(t)}$ represents the average value of observed and simulated output. The number of observation was represented as n and the peak value of observed and simulated value were specified as Q_{op} and Q_{sp}. The most commonly used performance evaluation method in hydrological modelling is RMSE. The RMSE and RRMSE evaluate the models by comparing the estimated error between the observed value and the simulated output.

Though the LRB has five water level measuring stations namely Insungai Nanga, Saliban Nanga, Ukong, Batu Danau and Limbang, only Insungai Nanga has the proper measurements of river cross section, flow parameters and stage discharge rating curve (DID, 2015). Water levels data from the other stations are used to monitor the flood level (water level) in response to heavy rainfall in the basin. Considering the data limitation, in the present research, water level measuring station Insungai Nanga was selected to model the rainfall-runoff for the LRB, using artificial neural network. Cross section of the Limbang River at Insungai Naga was given in Figure 3.9. Available data were collected from DID, Sarawak and its standardisation and gap filling (missing value calculation) were carried out. The water level (stage height), and rainfall data for a period 1991-2000 were used to generate the runoff model at Insungai Nanga using MNN with MDL algorithm, because the stage discharge rating curve equation proposed by the DID, Sarawak was applicable to the period up to 2003. Details about the data characterisation can be found in chapter 4.

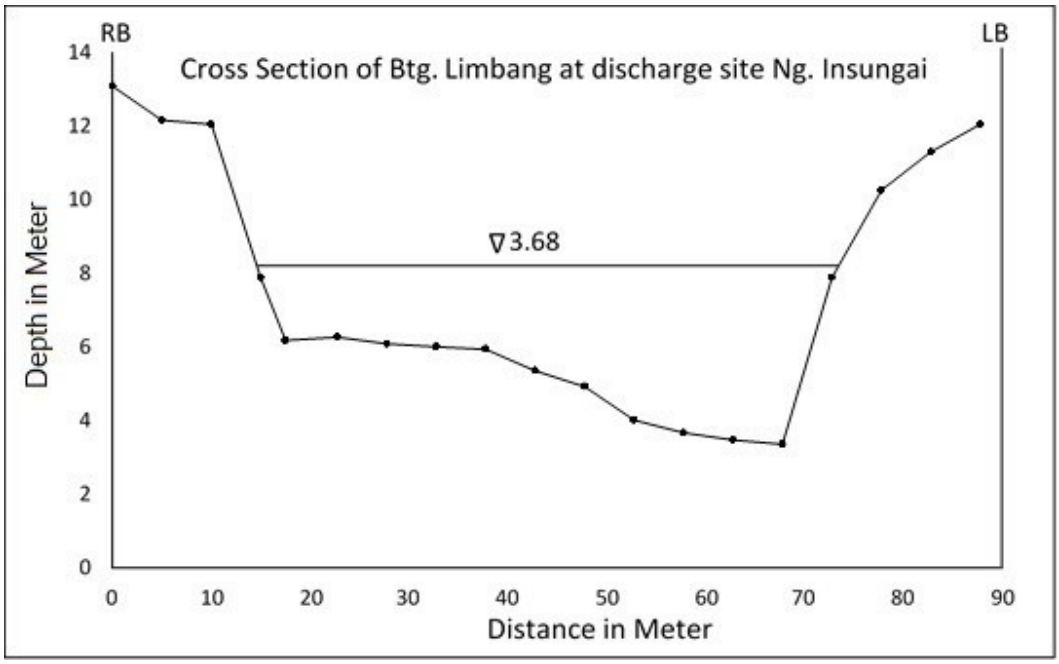

Figure 3.9: Cross section of the Limbang River at Insugai Nanga (Source: DID, Sarawak).

3.4 Hydrochemical Analysis of Surface Water and Rainwater

Physico-chemical parameters such as pH, electrical conductivity (EC), total dissolved solids (TDS), dissolved oxygen (DO), temperature (T) and turbidity of surface water were measured in the field and rainwater in the laboratory using portable pH, conductivity meter (Thermo Scientific Orion Star, 4 Star Plus Meter, and Hach meter). Carbonate, bicarbonate and chloride contents in the surface water and rainwater were determined by titrimetric method (APHA, 1995). Besides that, 100ml surface water samples were filtered using Whatman no.1 filter paper (11µm) to analyse the nutrients such as sulfate, phosphate, nitrate and ammonia. Nutrients were analysed in spectrophotometer using Hack Test Kits (Nitrate (NO_3^-) - Cadmium reduction method, Ammonia (NH_3) - Salicylate method, Phosphate (PO_4^{3-}) - Ascorbic acid method, Sulphate (SO_4^{2-}) - SulfaVer 4 method). Surface water and rainwater samples were filtered using 0.45µm Millipore filter paper and digested using 10ml con. Nitric acid (HNO_3) to lower the pH ~2 and make to 10ml by heating around 60 - 70 ˚C using hotplate. The concentrated sample is then remade to 100ml using ultra-pure water and kept in the refrigerator for the analysis of trace metals (Cu, Pb, Fe, Mn, Zn, Cd, Ni, Co, Na^+, K^+, Ca^{2+} and Mg^{2+}) in Atomic Absorption Spectrophotometer (AAS) (Perkin Elmer Analyst 400). A summary of parameters analysed and methodology adopted with instruments used are given in Table 3.3.

Table 3.3: Water quality parameters, analysis methodology with instruments used.

Parameter	**Methodology**	**Instrument**
pH, electrical conductivity (EC), total dissolved solids (TDS), dissolved oxygen (DO), temperature and turbidity	Sensor based field measurements.	Thermo Scientific's Orion Star and Hach® HQ40D portable meters
Carbonate (CO_3^{2-}), Bicarbonate (HCO_3^-) and Chloride (Cl^-)	Titrimetric Method (APHA, 1995, 2012)	---
Nitrate, Phosphate, Ammonia, Sulphate	Hack Test Kits	Hach® DR2800 spectrophotometer
Cu, Pb, Fe, Mn, Zn, Cd, Ni Co, Ca^{2+}, Mg^{2+}, Na^+ and K^+	Filtering of water sample with 0.45µm Millipore filter and acid digestion (adding HNO_3).	Atomic Absorption Spectrophotometer (AAS) (Perkin-Elmer Analyst 400).

Results of the physico-chemical parameters were interpreted with two approaches, such as quality based and process based to understand the chemical characteristics of water. The quality of the surface water was identified by comparing the concentration of the parameters with World Health Organization (WHO, 2011) standards and Malaysian Water Quality Standards (MWQS, 2009). WHO and MWQS values of the parameters are given in the Table 3.4.

Classification of collected surface water samples based on the suitability for irrigation and domestic purposes were carried out by calculating different parameters such as sodium percentage, sodium absorption ratio, residual sodium carbonate, permeability index, corrosivity ratio, Kelley's ratio, Larson ratio, magnesium ratio and chloro-alkaline indices. In order to understand the factors controlling the geochemistry of the water, standard methods such as Gibbs plot (surface water), Piper diagram (surface water) and factor analysis (rain and surface water) were applied in the present research. Partial pressure of carbon dioxide (pCO_2) and saturation index of carbonate minerals were also assessed. Variations in the concentration of different parameters between sampling locations and sampling periods were understood through the statistical method Analysis of Variance (two-way ANOVA) and interrelationship was determined through Pearson's correlation.

Table 3.4: The standard value of analysed parameters based on Malaysian Water Quality Standards (MWQS) and WHO standards.

Parameters	Malaysian water quality standards, 2009 (Raw water) Classes						WHO Standards (2011)
	I	IIA	IIB	III	IV	V	
pH	6.5 - 8.5	6 - 9	6 - 9	5 - 9	5 - 9	-	6.5 - 8.5
EC (µS/cm)	1000	100	-	-	6000	-	1000
TDS (mg/L)	500	100	-	-	4000	-	450
DO (mg/L)	7	5 - 7	5 - 7	3 - 5	< 3	< 1	NA
Turbidity (NTU)	5	50	50	-	-	1000NTU	<5
Sulfate (mg/L)	-	250	250	-	-	-	200
Nitrate (mg/L)	-	10	10	-	-	-	50
Ammonia (mg/L)	-	1.5	1.5	-	-	-	1.5
Phosphate	NA	-	-	-	-	-	NA
Bicarbonate	NA	-	-	-	-	-	NA
Chloride (mg/L)	-	250	250	-	-	-	250
Calcium (mg/L)	NA	-	-	-	-	-	200
Magnesium	NA	-	-	-	-	-	150
Sodium (mg/L)	NA	-	-	-	-	-	200
Potassium	NA	-	-	-	-	-	12
Cobalt (mg/L)	NA	-	-	-	-	-	2
Nickel (mg/L)	0.05 - 0.9	-	-	-	-	-	0.07
Cadmium (mg/L)	0.01	-	-	-	-	-	0.003
Iron (mg/L)	1	-	-	-	-	-	0.3
Manganese	0.1 - 0.2	-	-	-	-	-	0.5
Lead (mg/L)	0.01 - 0.05	-	-	-	-	-	0.01
Zinc (mg/L)	0.4 - 5	-	-	-	-	-	3
Copper (mg/L)	0.02	-	-	-	-	-	2

Water quality classes and its uses based on Malaysian Water Quality Standards are as flows:

Class 1: Conservation of natural environment. Water Supply I – Practically no treatment necessary. Fishery I – Very sensitive aquatic species.

Class II A: Water Supply II – Conventional treatment. Fishery II – Sensitive aquatic species.

Class IIB: Recreational use body contact.

Class III: Water Supply III – Extensive treatment required. Fishery III – Common, of economic value and tolerant species; livestock drinking.

Class IV: Irrigation

Class V: None of the above

3.4.1 Water quality indices

3.4.1.1 Sodium percentage (Na %)

For irrigation purposes, the concentration of sodium (Na^+) is very important. Percentage of Sodium (Na%) in water can be calculated as (Wilcox, 1955; Ogunfowokan et al., 2013; Shammi et al., 2016; Santacruz De León et al., 2017):

$$Na\,\% = \frac{Na^+ + K^+}{Ca^{2+} + Mg^{2+} + Na^+ + K^+} \times 100$$

where, Na^+, K^+, Ca^{2+} and Mg^{2+} are expressed in meq/L

3.4.1.2 Sodium absorption ratio (SAR)

The suitability of water for agricultural irrigation can be understood by sodium absorption ratio (SAR), which can be estimated by considering the concentration of Na^+, Ca^{2+} and Mg^{2+} as given below (Richards, 1954; Ogunfowokan et al., 2013; Shammi et al., 2016; Santacruz De León et al., 2017):

$$SAR = \frac{Na^+}{(Ca^{2+} + Mg^{2+})/2}$$

where, Na^+, Ca^{2+} and Mg^{2+} are expressed in meq/L

3.4.1.3 Residual sodium carbonate (RSC)

The excess amount of carbonate and bicarbonate covers the Ca^{2+} and Mg^{2+} in the water, which will affect agriculture unfavorably and that can be understood by calculating the residual sodium carbonate (RSC) value (Eaton, 1950; Santacruz De León et al., 2017):

$$RSC = HCO_3^- - (Ca^{2+} + Mg^{2+})$$

where, HCO_3^-, Ca^{2+} and Mg^{2+} are expressed in meq/L

3.4.1.4 Permeability index (PI)

Irrigation water quality can be evaluated by the parameter permeability index and can be calculated as (Doneen, 1964; Ogunfowokan et al., 2013; Santacruz De León et al., 2017):

$$PI = \frac{Na^+ + \sqrt{HCO_3^-}}{Ca^{2+} + Mg^{2+} + Na^+} \times 100$$

where, HCO_3^-, Na^+, Ca^{2+} and Mg^{2+} are expressed in meq/L

3.4.1.5 Corrosivity ratio (CR)

Corrosivity ratio will help to understand the transportation of water through metallic pipes and can be calculated as (Ryznar, 1944; Raman, 1983; Singaraja, 2017):

$$CR = \frac{\{(Cl^-/35.5) + (SO_4^{2-})\}}{2 \times HCO_3^-} \times 100$$

where, Cl^-, SO_4^{2-} and HCO_3^- are expressed in mg/L

3.4.1.6 Kelley's ratio

Kelley's ratio for excess level of sodium can be calculated as (Kelley, 1963; Shammi et al., 2016; Santacruz De León et al., 2017):

$$KR = \frac{Na^+}{(Ca^{2+} + Mg^{2+})}$$

where, Na^+, Ca^{2+} and Mg^{2+} are expressed in meq/L

3.4.1.7 Larson ratio (LnR)

Corrosiveness and aggressive nature of water can be identified through Larson Ratio and can be calculated as (Larson & Skold, 1958; Abbasnia et al., 2018):

$$LnR = \frac{2\,{SO_4}^{2-} + Cl^-}{{HCO_3}^-}$$

where, Cl^-, SO_4^{2-} and HCO_3^- are expressed in meq/L

3.4.1.8 Magnesium ratio (MR)

The suitability of the water for irrigation purpose can be understood by magnesium ratio and can be calculated as (Raghunath, 1987; Shammi et al., 2016; Santacruz De León et al., 2017):

$$MR = \frac{Mg^{2+} \times 100}{Ca^{2+} + Mg^{2+}}$$

where Ca^{2+} and Mg^{2+} are expressed in meq/L.

Normally Ca^{2+} and Mg^{2+} present in equilibrium in most of the water but the higher amount of Mg in water will adversely affect the quality of soil.

3.4.1.9 Chloro - alkaline indices (CAI)

Change in the composition of chemicals in the river water during its transportation can be understood through Chloro-alkaline indices (CAI-1 and 2). CAI-1 and CAI-2, suggested by Schoeller (1977), which indicates exchange of ion between the water and host environment during its flow and which can be calculated as (Ndoye et al., 2018):

$$CAI - 1 = \frac{Cl^- - (Na^+ + K^+)}{Cl^-}$$

$$CAI - 2 = \frac{Cl^- - (Na^+ + K^+)}{{SO_4}^{2-} + {HCO_3}^- + {CO_3}^{2-} + {NO_3}^-}$$

where, Ca^{2+}, Mg^{2+}, Na^+, K^+, HCO_3^-, CO_3^{2-}, NO_3^- and SO_4^{2-} are expressed in meq/L.

The CAI value can be positive or negative. The positive value indicates the exchange of Na^+ and K^+ ion from water with Ca^{2+} and Mg^{2+} of the rock whereas the negative value indicates the exchange of Ca^{2+} and Mg^{2+} of the water to Na^+ and K^+ of the rock (Kumar et al., 2007; Wu et al., 2015).

3.4.2 Analysis of geochemical processes

3.4.2.1 Gibbs plot

Gibbs (1970) introduced a diagram to understand the functional source of dissolved chemical constituents in surface water and groundwater by incorporating three dominant natural mechanisms such as precipitation, rock type and evaporation-crystallisation (Figure 3.10). In this, the first mechanism is atmospheric precipitation, which represents the chemical composition of low salinity sodium chloride water. The second process is rock weathering, which indicates the dissolution of rock and soil by rock water interaction and produces prime ions such as Ca^{2+} and HCO_3^-. Evaporation-crystallisation is the third mechanism controlling the water chemistry which is extended from Ca^{2+} rich medium salinity to Na^+ rich high salinity (Gibbs, 1970; Buckney & Tyler, 1973; Singh, 2002; Gowd, 2005; Aghazadeh & Mogaddam, 2010; Li et al., 2013; Wang et al., 2016; Asare-Donkor et al., 2018).

Gibbs plot uses the ratio of the dominant anion and cations against TDS (mg/L) to assess the dominant water chemistry controlling factor (Gibbs, 1970). In order to understand the percentage of components Gibbs introduced two ratios based on the dominants of cations and anions which can be obtained as:

$$Gibbs\ ratio\ I\ (for\ anion) = {Cl^-}/{(Cl^- + {HCO_3}^-)}$$

$$Gibbs\ ratio\ II\ (for\ cation) = {(Na^+ + K^+)}/{(Na^+ + K^+ + Ca^{2+})}$$

where, Na^+, K^+, Ca^{2+}, Cl^- and HCO_3^- are expressed in mg/L.

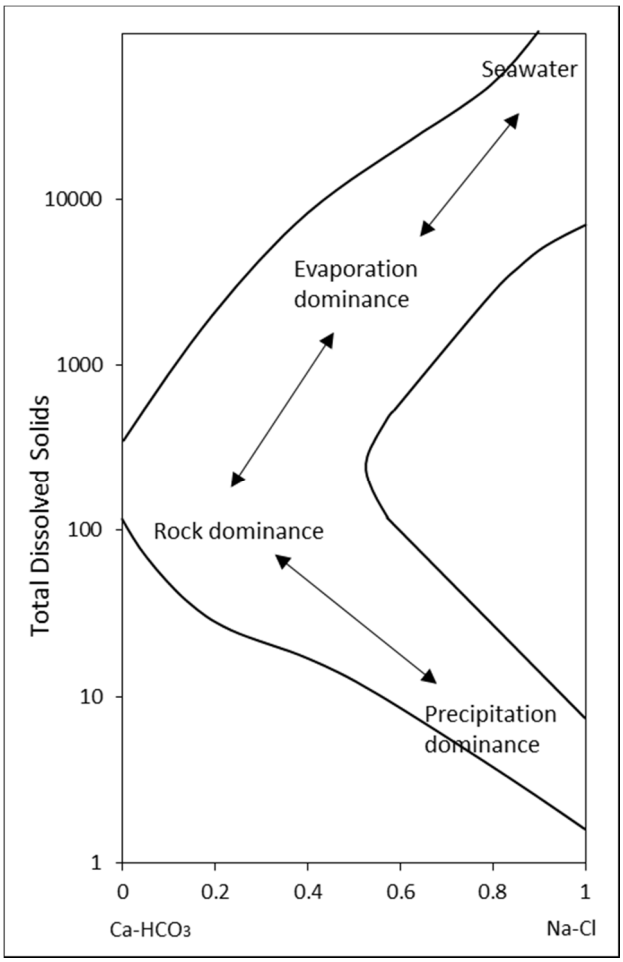

Figure 3.10: Gibbs diagram showing the dominant natural processes which control the chemistry of water.

3.4.2.2 Piper diagram

Geochemical composition of the water in different hydrological system can be inferred by piper diagram (Hill, 1940; Piper, 1944). Piper diagram is a visualisation of dominant ions in different water samples. The diagram is composed of three distinct fields includes two triangular fields and one diamond shaped field (Figure 3.11). The cations are expressed in the left triangle whereas the anions are in the right triangle. The cations and anions such as Ca^{2+}, Mg^{2+}, Na^{+}, K^{+}, HCO_3^{-}, CO_3^{-}, SO_4^{2-} and Cl^{-} were considered to plot the piper diagram. Characteristics of the water is inferred from the upper diamond shaped fields where the extension of the intersecting point from each triangular field which was projected along the line parallel to the upper margin. The upper diamond is divided into four quarters, representing four different chemical domains. The quarter I indicates Ca^{2+} - Mg^{2+}- Cl^{-} type water, quarter II indicates Ca^{2+}- Mg^{2+}- HCO_3^{-} type water whereas quarter III and IV indicates Na^{+}- K^{+} - Cl^{-} and Na^{+}- K^{+} - HCO_3^{-} type waters respectively (Razack & Dazy, 1990; Bakalowicz,

1994; Awad et al., 1997; Wang et al., 2011; Ravikumar et al., 2015; Tiwari et al., 2017; Al-Omran et al., 2018).

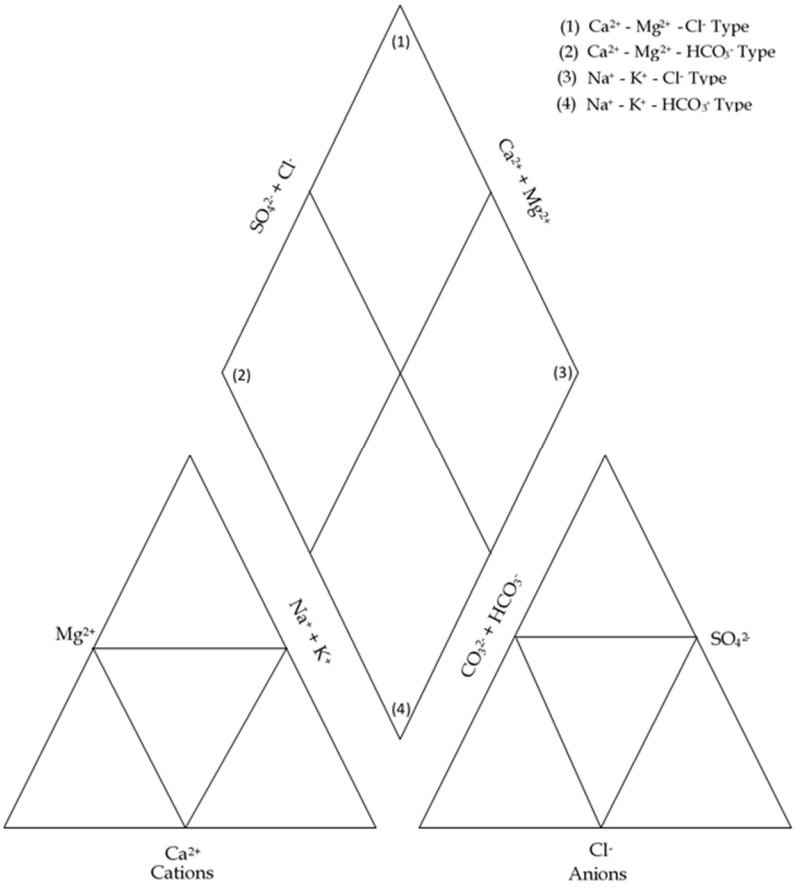

Figure 3.11: Basic structure of piper plot with dominant water types.

3.4.2.3 Partial pressure of carbon dioxide (pCO_2)

The pCO_2 can be calculated using pH and total dissolved carbon using the equation (Holland, 1978; Raymahashay, 1986; Stumm & Morgan, 1996; Ran et al., 2015):

$$pCO_2 = \frac{\propto H_2CO_3}{K_{CO_2}}$$

where, $\propto H_2CO_3$ is the sum of aqueous CO_2 and H_2CO_3 and K_{CO_2} is the thermodynamic dissolution constant. In the present research, the Log pCO_2 is calculated using WATEQ4F program (Truesdell & Jones, 1974; Plummer et al., 1976).

3.4.2.4 Saturation index of carbonate minerals

The thermodynamic stability of the surface water is characterised by the state of saturation index (SI) with respect to a particular mineral which helps to predict the reaction pathway. The SI of a particular mineral can be calculated as:

$$SI = log\frac{IAP}{K_{sp}}$$

where IAP is the ion activity product and K_{sp} is solubility product.

If, $SI = log\frac{IAP}{K_{sp}}$ < 0 undersaturation state (mineral dissolution condition).

$SI = log\frac{IAP}{K_{sp}}$ = 0 equilibrium state.

$SI = log\frac{IAP}{K_{sp}}$ < 0 oversaturation state (mineral precipitation state).

The SI of carbonate is analysed using WATEQ4F program (Truesdell & Jones, 1974; Plummer et al., 1976). During simulation in WATEQ4F, the total concentration of elements, log ratio for stability plots and distribution of aqueous species, and the amount of minerals (or other phases) transferred in or out of the aqueous phase with respect to specified mineral phases was calculated. The data required for the modelling include the concentration of dissolved constituents, temperature and pH. An iterative process using equilibrium constant based on the Gibbs (1970) free energy of reactions were used to calculate the aqueous speciation and the activity coefficients were estimated either by Davis or extended Debye Huckel equation (Garrels & Christ, 1965; Drever, 1988). Then the solubility equilibrium hypothesis was tested by computing ion activity product (IAP) from the activities of uncomplexed ions based on the stoichiometries of minerals and other solids in the WATEQ4F data base. The activity product is then compared to the solubility product (K_{sp}) for the same solid phases to validate the assumption that certain dissolved constituents in surface water are in equilibrium with particular minerals and amorphous solids (Deutsch et al., 1982).

3.4.3 Statistical analysis of the physico-chemical parameters

Variations in concentration of different parameters during sampling periods, locations and the interrelationship were statistically determined through applying analysis of variance, Pearson's correlation and factor analysis.

3.4.3.1 Analysis of variance (ANOVA)

The best way to determine the variation between and within the group of samples is the analysis of variance (ANOVA) (Sokol & Rohlf, 1969; Wonnacott & Wonnacott, 1990; Dominique et al., 1998; Calabrese et al., 2015). The null hypothesis in ANOVA is that the (population) mean of all groups under consideration is equal (McDonald, 2009). If the mean is not equal, the null hypothesis will be rejected and the alternative hypothesis is accepted. In the present study, two-way ANOVA test was considered to understand the variation in concentration of parameters between the sampling points and sampling periods.

Let X be the measurement with m rows and n columns, then the sum of squared deviation of all the measurement from the mean value of the measurement in the rows and columns can be calculated as:

$$SS_{row} = n \sum_{i=1}^{m} \left(\bar{X}_i - \bar{\bar{X}}\right)^2$$

and

$$SS_{col} = m \sum_{j=1}^{n} \left(\bar{X}_j - \bar{\bar{X}}\right)^2$$

where, $\bar{X}_i = \frac{\sum_{i=1}^{m} x_{ij}}{m}$ for $j = 1,2,\dots n$, $\bar{X}_j = \frac{\sum_{j=1}^{m} x_{ij}}{n}$ for $i = 1,2,\dots m$ and $\bar{\bar{X}} = \frac{1}{mn}\sum_{j=1}^{n}\sum_{i=1}^{m} x_{ij}$.

The sum of squares with in the measurements can be calculated as:

$$SS_E = \sum_{i=1}^{m}\sum_{j=1}^{n}\left(x_{ij} - \bar{X}_i - \bar{X}_j + \bar{\bar{X}}\right)^2$$

then total sum of square can be obtained as:

$$SS_T = SS_{row} + SS_{col} + SS_E$$

$$= \sum_{i=1}^{m}\sum_{j=1}^{n}\left(x_{ij} - \bar{\bar{X}}\right)^2$$

The percentage (%) of variance between the row and column can be obtained as:

$$\%\ of\ variance\ _{row} = \frac{SS_{row}}{SS_E}$$

$$\%\ of\ variance\ _{col} = \frac{SS_{col}}{SS_E}$$

The ratio between the sum of square and the degree of freedom will give the mean square value. The mean square between the row and column and within the measurement can be calculated as:

$$MS_{row} = \frac{SS_{row}}{m-1}$$

$$MS_{col} = \frac{SS_{col}}{n-1}$$

and

$$MS_E = \frac{SS_E}{(m-1)(n-1)}$$

the F- ratio value is used to determine the statistical significance and can be calculated as the row and column can be calculated as:

$$F_{row} = \frac{MS_{row}}{MS_E}$$

and $$F_{col} = \frac{MS_{col}}{MS_E}$$

the p value represents the probability to get accept or reject the statistics null hypothesis. If $p \leq 0.05$ (95% confidence level), the then the null hypothesis will reject.

3.4.3.2 Pearson's correlation

The strength of the linear relationship between two variables in a set of data can be explained with the help of Pearson's Correlation (Altman, 1990; Jäntschi & BOLBOACĂ, 2006; Moriasi et al., 2007; Hauke & Kossowski, 2011; Peña-Arancibia et al., 2016; Huang et al., 2017; Mirzaee et al., 2018).The theory of correlation was first introduced by Galton (1889) and the formula for Pearson correlation coefficient was introduced by Pearson (1895). Correlation coefficient (r) value ranges between -1 and +1. A strong negative linear relationship was indicated by -1 whereas +1 indicates a strong positive relationship (Lee Rodgers & Nicewander, 1988; Taylor, 1990; Mukaka, 2012; Meyers et al., 2016; Wiedermann &

Hagmann, 2016; Schober et al., 2018). Correlation value of 0 (zero) indicates no linear relationship and suggesting that the variables are independent of each other (Taylor, 1990).

Let X and Y are the two variables with n values $X_1, X_2, X_3, \dots, X_n$ and $Y_1, Y_2, Y_3, \dots, Y_n$ respectively. Then the Pearson correlation coefficient r can be written as:

$$r = \frac{\sum_{i=1}^{n}(X_i - \bar{X})(Y_i - \bar{Y})}{\sqrt{\sum_{i=1}^{n}(X_i - \bar{X})^2 \sum_{i=1}^{n}(Y_i - \bar{Y})^2}}$$

where, $\bar{X}$ and $\bar{Y}$ are the mean of X and Y respectively. Microsoft excel 2013 was used to calculate the Pearson's correlation coefficients.

3.4.3.3 Factor analysis

The influence of geochemical processes which control the geochemistry of water can be understood by factor analysis. Factor analysis is a multivariate statistical technique for variables with interdependent relationships. Factor analysis explains the correlation among the large number of variables in terms of a small number of underlying, unobservable random quantity called factor (Mardia et al., 1979; Oişte, 2014). In factor analysis, the variables in a particular group correlates strongly among themselves, but relatively insignificant correlation was observed with the different group variables (Johnson & Wichern, 1988; Brown, 1998; Belkhiri et al., 2011). Eigen value determines the number of factors to be considered and will represent the amount of variance accounted for each factor. The sum of Eigen values give the percentage of total variance. The factor with Eigen value <1 indicates less total variance than the variables, whereas Eigen value >1 indicates that the total variance in the data is greater than the individual variable. Therefore, factor with Eigen value >1 was only retained for interpretation (Vega et al., 1998; Usman et al., 2014). In each factor, the number of variables having high loading was minimised by an orthogonal rotation method called Varimax rotation. To optimize the relationship between the interdependent variables, Varimax rotation re-distribute the variance of each factor. Principal component analysis was considered as a method to extract each factor (Nosrati & Van Den Eeckhaut, 2012; Nolakana, 2016). Factors retained were extracted through Varimax rotation method. A Factor score of > +1 indicates the high influences by the process and the < -1 indicates the area is unaffected by the process. A value near to zero indicates moderate control of the area in the process. The matrix multiplication of the factor score coefficient with standardised data was used to

calculate the factor score corresponding to each sample. In the present study SPSS statistics 17.0 was used to carry-out the factor analysis of hydrochemical parameters of rainwater and surface water.

3.5 Analysis of Stable Isotopes in Precipitation

During the research, a total of 24 monthly rainwater samples were collected from two locations (12 samples / location) as per the International Atomic Energy Agency (IAEA) norms (IAEA/GNIP, 2014). Monthly accumulated rainwater samples collected were transferred to 60ml high density polyethylene (HDPE) bottles and stored at 4°C before sending for analysis. Among the total samples, three samples (July, August and September-2017) collected from the Limbang City were excluded from the analysis due to error in rainwater collection. First location was the Limbang City which was nearer to the coastal region (the South China Sea) and the second location is Kampong Salidong, located inside the tropical rainforest surrounded by high elevated hills. All remaining samples (9 from Limbang City and 12 from Kampong Salidong) were considered in the present research for subsequent analysis of stable isotopes, oxygen-18 ($\delta^{18}O$) and deuterium (δD) using Isotope Ratio Mass Spectrometer and interpretation.

The value of stable isotopes is generally represented by δ (expressed in terms of per mil, ‰) and is defined as (Craig, 1961; Coplen, 1994):

$$\delta = ((R_{sample} - R_{SMOW})/R_{SMOW}) * 10^3$$

where, R is D/H or $^{18}O/^{16}O$ and $SMOW$ is the standard Mean Ocean Water.

Isotopic fractionation results the variation of stable isotopes mainly because of the physical and chemical processes (Dansgaard, 1964; Gat & Gonfiantini, 1981; Rozanski et al., 1982). Condensation and evaporation are the major physical processes that lead to the isotopic fractionation. Equilibrium fractionation process helps to determine the isotopic composition of precipitation in clouds. The composition of isotopes of the condensing parent vapour and temperature are the two major factors which establish the stable isotopic composition of precipitation in a region (Ingraham, 1998; Warrier et al., 2010; Uemura et al., 2012; Yang & Yao, 2016). The meteoric history of the original air mass and its modification by upwind loss by precipitation, coupled with contributions due to the evapo-transpirational recycling influences the composition of the condensing vapours. Due to this, the isotopic composition of precipitation in the hydrological cycle is highly variable in space and time

(Warrier et al., 2010). In spite of these complexities, Craig (1961), defined a relationship between the stable isotopes $\delta^{18}O$ and δD and known as Global Meteoric Water Line (GMWL) which can be given as:

$$\delta\mathrm{D} = 8\,\delta^{18}O + 10$$

Slope of the GMWL is due to the ratio of isotopic fractionation factor of D and ^{18}O during condensation process, which is an equilibrium process (Clark & Fritz, 1997; Gupta & Deshpande, 2003; Hager & Foelsche, 2015). Even if the GMWL has global application, it is an average of Local Meteoric Water Line (LMWL) which differ from GMWL due to the difference in climatic and geographic conditions. The excess of Deuterium (d-excess) of atmospheric precipitation can be obtained as suggested by Dansgaard (1964):

$$d - excess = \delta\mathrm{D} - 8 \times \delta^{18}\mathrm{O}$$

The d-excess value mainly connected with the kinetic fractionation occurring during evaporation of falling rain drop and the vapour source region's meteorological condition (Unnikrishnan Warrier & Praveen Babu, 2012). Considering the variation in monthly rainfall characteristics, the volume weighted average of δ were calculated as (Dansgaard, 1964; IAEA, 1992; Wirmvem et al., 2017):

$$vw\delta = \frac{1}{P}\sum_{i=1}^{12} p_i\,\delta_i$$

where, P is the annual precipitation, p_i is the precipitation corresponding to the i^{th} month and the δ_i is the isotopic composition in i^{th} month.

The composition of stable isotopes (δD and $\delta^{18}O$) in monthly cumulative rainwater was analysed at the Isotope Hydrology Division of the Centre for water Resources Development and Management (CWRDM), India using continuous flow Isotope Ratio Mass Spectrometer (IRMS) (FINNIGAN DELTA^{PLUS} XP, Thermo Electric Corporation, Germany). CO_2-H_2O equilibrium method was used to analyse the oxygen isotope ($\delta^{18}O$) and H_2-H_2O equilibrium method using platinum catalyst support on a hydrophobic material was used to analyse the hydrogen isotope (δD). All measurements were made against secondary laboratory standards recommended by IAEA. The periodical calibration of the instrument was also conducted after 80 samples using international isotope standards. Analytical reproducibility of the results of δD is 0.5‰ and for $\delta^{18}O$ is 0.06‰.

Chapter 4 Results and Discussions

4.1 Drainage and Terrain Characteristics

The Limbang River, is the 6th largest river in Sarawak, Malaysian Borneo drain a total area of 3950km^2, originating from the Batu Lawi mountain ranges in southern Sarawak. The Limbang River flows 196km from the origin, initially flowing towards the northwest direction and then to northeast direction after middle reach, before finally debouching into the Brunei Bay in the South China Sea. The Limbang River Basin (LRB) is an 8th order river basin, showing an elongated shape with higher concentration of lower order streams in the central region of the basin (Figure 4.1a). At the same time, it shows the maximum width at the upper and middle part of the river basin than the lower reach. It was also observed that the drainage pattern exhibited by the lower order streams vary widely in close spatial proximity and the major pattern identified are parallel, dendritic, rectangular and trellis. Further up after the midland reach, the river follows a highly sinuous nature with numerous loops, meander cut-offs and ox-bow lakes. The presence of different drainage patterns in different segments of the river basin and well developed sinuous nature of the major river in the lower reach indicates the dominance of structural as well as lithological control over the development of peculiar drainage characteristics.

The LRB shows highly varying and undulating terrain characteristics. The terrain elevation of the river basin varies from below 1 to >2400 m above mean sea level, with a mean basin elevation of 495m (Figure 4.1b). More than 19% of the basin shows an elevation of less than 50m, 24% of the total area shows elevation in the range of 50-250m whereas 57% of the total area shows elevation above 250m. Lower elevation is found to be concentrated in the lower catchment region, which was dominated by flood plain, peat swamps and occasional small mounts. The middle portion of the basin shows comparatively moderate elevation, whereas the higher elevation in the river basin was found to be confined to the upper catchment region. In the LRB, Gunung Murud (2423m) and Batu Lawi (2046m) summits show maximum elevation. Besides the lower portion of the river basin, the terrain is quite varied with different kinds of continuous hills and valleys with varying slopes.

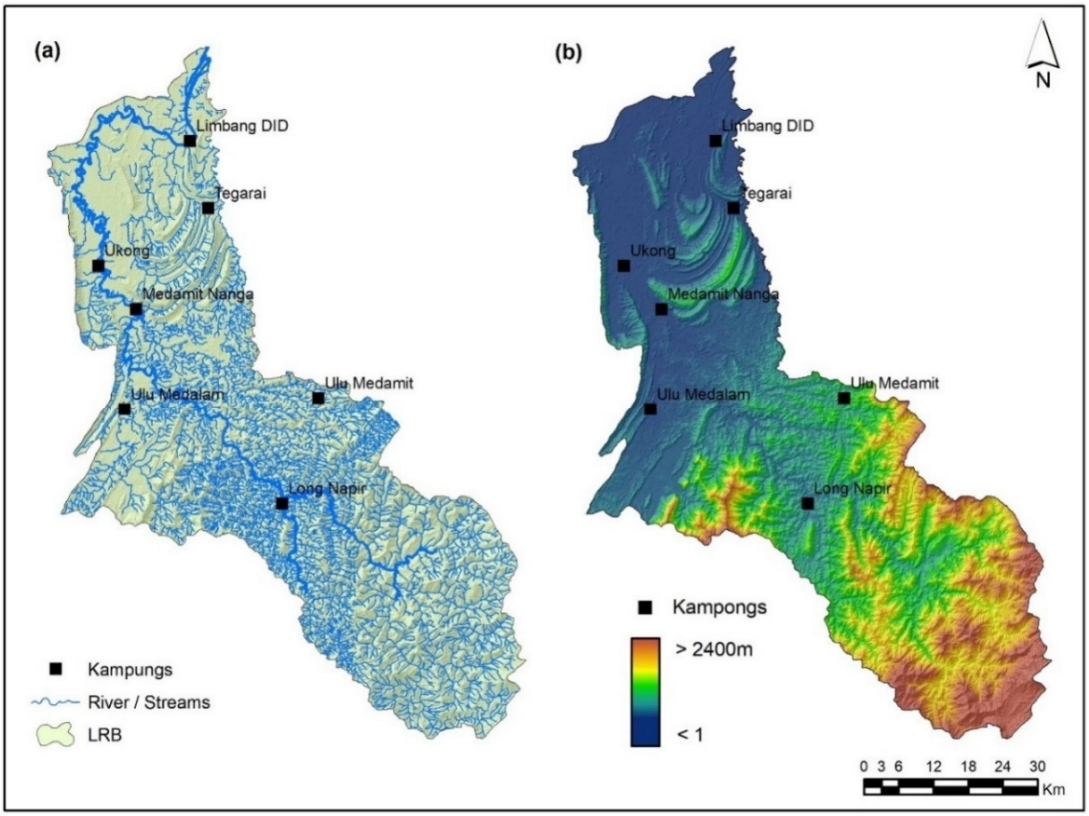

Figure 4.1: Distribution of (a) drainage networks and (b) elevation in the LRB.

Terrain slopes indicates the inclination of the land with respect to a horizontal. In the LRB, terrain slope ranges from 0 to 84^0, with a mean slope of 15^0. Higher degree of terrain slope is found to be clustered above middle part of the river basin especially in the upper catchment (Figure 4.2a). Relative relief indicates a change in elevation in the unit area, which controls the hydrological as well as erosional characteristics of a region or hill slope. Relative relief assessed in the LRB shows huge variation in its spatial patterns and value distribution. The relative relief map generated for the whole LRB varies in the range of 0-1074m/km^2 with a mean of 219m/km^2, indicating high variation in the relief aspect of the river basin (Figure 4.2b).

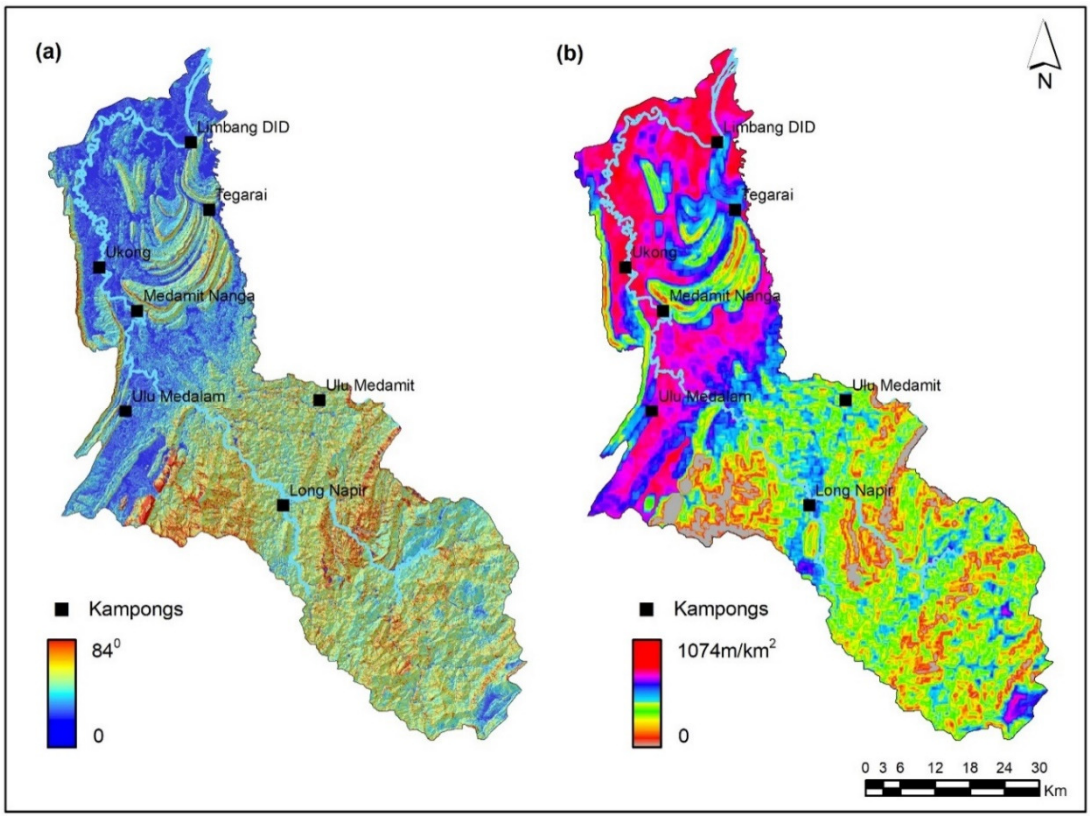

Figure 4.2: Distribution of (a) terrain slope in degree and (b) relative relief in the LRB.

4.2 Rainfall Trend Analysis

The daily rainfall data from thirteen well distributed rain gauging stations in the LRB were processed to identify the general rainfall distribution characteristics and monthly, seasonal and annual rainfall trends. General characteristics of rain gauging stations considered in the present research are given in the Table 4.1. Rainfall data ranging from of 19 to 69 years were collected from the Department of Irrigation and Drainage (DID), Sarawak, Malaysia. Rain gauging stations Tegarai, Ukong and Medamit Nanga possesses rainfall data of more than 50 years, in which rain gauging station Ukong shows the highest data (69 years). In the second group of rain gauges namely Pandaruan, Lubai Tengah and Long Napir, these stations only have rainfall data in the range of 40 to 50 years. Rain gauges such as Limbang DID and Lubok Lalang possesses rainfall data in the range of 30 to 40 years. The remaining five rain gauges namely Merbau, Ulu Medalam, Ulu Medamit, Setuan and Rutoh have daily rainfall data less than 30 years (vary between 19 to 22 years). In relation to the spatial location of each rain gauges, it shows varying elevation in its location which ranges from 7m (Limbang DID) to 1532m (Rutoh) above mean sea level. While cross checking and arranging the daily rainfall data, it was noted that each station in LRB shows

missing numbers in daily rainfall data. The daily rainfall data missing percentage in rain gauging stations which were considered in the present research ranges from 0.80% (Pandaruan) to 12.35% (Long Napir). Rain gauging stations namely Limbang DID, Pandaruan, Tegarai, Ukong, Medamit Nanga, Lubok Lalang, Ulu Medalam, Ulu Medamit, Setuan and Rutoh shows missing data of less than 5%, whereas other three stations Lubai Tengah, Merbau and Long Napir shows comparatively higher percentage of missing rainfall (8 to 12%). The lowest missing percentage in the daily rainfall data in rain gauging stations itself indicates the accuracy of data collection in the region (Suhaila et al., 2008; Presti et al., 2010).

Table 4.1: Details of rain gauging stations and rainfall data collected from DID.

Stations	Data availability		No. Years of data	Elevation (m)	Missing %
	From	To			
Limbang DID	1980	2016	37	7	3.63
Pandaruan	1972	2016	45	16	0.80
Tegarai	1967	2016	50	22	1.15
Lubai Tengah	1972	2016	45	31	8.28
Ukong	1948	2016	69	17	2.22
Medamit Nanga	1963	2016	54	20	1.99
Lubok Lalang	1987	2016	30	111	3.62
Merbau	1990	2016	27	290	9.67
Ulu Medalam	1998	2016	19	46	3.34
Ulu Medamit	1993	2014	22	509	4.14
Setuan	1998	2016	19	153	3.50
Long Napir	1977	2016	40	160	12.35
Rutoh	1998	2016	19	1532	3.98

However, in order to fill the gap in daily rainfall before processing the rainfall data, randomness and homogeneity of monthly rainfall data in all station were checked through lag-1 autocorrelation test at 95% confidence level. In the present research, rain gauges considered for the analysis possesses varying duration of rainfall data. Therefore the limit value of 95% confidence level suggests the acceptance of r_1 value shows variation. Table 4.2 shows lag-1 autocorrelation coefficients corresponding to monthly, seasonal and annual rainfall for each station in the LRB. In rain gauging station Limbang DID, lag-1 correlation coefficient of monthly rainfall varies in the range of -0.350 to 0.258 which falls within the limiting value of r_1 (95%) i.e. -0.350 to 0.294. Similarly the seasonal (SWM, NEM) and annual rainfall also shows r_1 value within the range (-0.117, 0.212 and 0.276 respectively).

Rain gauging station Pandaruan shows lag-1 autocorrelation coefficient of monthly rainfall in the range of -0.290 to 0.311, which falls in the range of r_1 -0.315 to 0.269 at 95% confidence level. Seasonal and annual rainfall also shows r_1 value within the limit of 95% confidence (-0.019, 0.100 and 0.224 for SWM, NEM and annual rainfall respectively). Lag-1 autocorrelation values assessed for monthly rainfall (-0.247 to 0.279) measured in rain gauging station Tegarai falls within the bounding limit of r_1 values (-0.298 to 0.257). The same characteristic was also shown by seasonal (0.122 and -0.102 for SWM and NEM respectively) and annual rainfall (0.246). Considering the rainfall in rain gauging station Lubai Tengah, monthly (-0.309 to 0.256), seasonal (0.035 and -0.020 for SWM and NEM) and annual (0.238) rainfall shows lag-1 correlation values within the bounding limit of -0.315 to 0.269. In Ukong, the lag-1 correlation coefficients of monthly rainfall varies in the range of -0.209 to 0.217, whereas the seasonal (SWM and NEM) and annual rainfall shows r_1 values -0.027, 0.069 and 0.210 respectively and all values fall within the range of limiting values -0.251 to 0.221. Lag-1 autocorrelation values of monthly (-0.273 to 0.250), seasonal (0.080 and 0.141 for SWM and NEM respectively) and annual rainfall (0.243) in Medamit Nanga also falls within the bounding limit of r_1 values (-0.286 to 0.248). Rainfall (monthly (-0.322 to 0.274), seasonal (-0.083 and -0.036) and annual (0.004)) measured in rain gauging station Lubok Lalang also shows lag-1 correlation values within the range of r_1 (-0.392 to 0.323).

Considering the monthly, seasonal and annual rainfall measured at rain gauging station Merbau, lag-1 autocorrelation values fall with the range of r_1 coefficients -0.415 to 0.338. Monthly rainfall in Merbau has lag-1 coefficient in the range of -0.206 to 0.243 whereas those for seasonal and annual rainfall are -0.128 (SWM), 0.029 (NEM) and 0.039 respectively. Rainfall data measured at rain gauging stations Ulu Medalam and Ulu Medamit show all values within the range of r_1 coefficients (-0.505 to 0.393 and -0.465 to 0.370 respectively). In Ulu Medalam, lag-1 correlation coefficient of monthly rainfall ranges from -0.471 to 0.123, whereas in Ulu Medamit it varies in the range of -0.320 to -0.029. At the same time, lag-1 coefficients of seasonal and annual rainfall show values of -0.179, -0.269 and 0.114 for Ulu Medalam and -0.260, 0.215 and -0.218 for Ulu Medamit. Lag-1 autocorrelation values of monthly (-0.495 to 0.258), seasonal (0.130 and -0.424 for SWM and NEM respectively) and annual (-0.171) rainfall in Setuan also within the bounding limit of r_1 values (-0.505 to 0.393). Rainfall data measured at rain gauging stations Long Napir and Rutoh show all values within the range of r_1 coefficients (-0.335 to 0.284 and -0.505 to 0.393 respectively). In Long Napir, lag-1 autocorrelation coefficients of monthly rainfall

ranges from -0.165 to 0.193, whereas in Rutoh it varies from -0.409 to 0.095. At the same time, lag-1 coefficients of seasonal and annual rainfall show values of 0.031, 0.281 and 0.218 for Long Napir and -0.100, -0.273 and -0.102 for Rutoh.

Results of lag-1 autocorrelation shows that, all analysed data falls within the limit of r_1 coefficients at 95% confidence levels, which indicate the acceptance of the null hypothesis (Salas et al., 1980; Mirza et al., 1998; Yue et al., 2002; Gocic & Trajkovic, 2013; Eymen & Köylü, 2018). This also indicates the homogeneous and non-correlated nature of rainfall data in the LRB. Therefore no pre-whitening technique is required before applying the Mann Kendall and Spearman's Rho tests for determining the statistical trends (Von Storch, 1999; Tabari et al., 2011; Zhao et al., 2015; Fathian et al., 2016; Yang et al., 2017; Araghi et al., 2018; Latif et al., 2018). Autocorrelation has no effect on time series rainfall data collected from all rain gauging stations in the LRB.

Subsequently, missing daily rainfall data values were replaced by normal ratio method (NRM), because NRM offered better calculation of missing rainfall in the region (De Silva et al., 2007). In order to understand the prediction accuracy of NRM in the calculation of missing rainfall time series data in the LRB, the two experimental regression plots with best fit and correlation between the observed and predicted rainfall in selected rain gauges (Limbang DID and Merbau) in the LRB using NRM method is given in Figure 4.3. Based on the findings, the observed (measured) rainfall data was considered as missing data and NRM method was applied to predict the monthly rainfall values. Three years of monthly rainfall data predicted using NRM shows best fit (R^2=0.71) and correlation (r=0.84) with observed (measured) data and is shown in Figure 4.3a. Similarly in the second case (Figure 4.3b), observed and predicted rainfall shows a comparatively high rate of best fit (R^2=0.74) and correlation (r=0.86). Considering the accuracy of NRM in missing data calculation, monthly missing rainfall values in each rain gauging station in the LRB is generated. Then the missing values were replaced and filled for the use of statistical analysis and trend determination of rainfall in the LRB.

Table 4.2: Lag–1 auto correlation coefficients for monthly, seasonal and annual rainfall data corresponding to rain gauging stations in the LRB.

Stations	Jan	Feb	Mar	Apr	May	Jun	Jul	Aug	Sep	Oct	Nov	Dec	SWM	NEM	Annual RF	Lag-1 auto correlations coefficient range at 95% confidence	
																From	To
Limbang DID	-0.158	-0.263	0.258	0.003	-0.281	0.045	-0.024	0.101	-0.350	-0.011	0.190	0.233	-0.117	0.212	0.276	-0.350	0.294
Pandaruan	-0.059	-0.105	0.311	0.214	-0.140	0.047	0.022	0.169	-0.030	0.031	-0.290	0.036	-0.019	0.1	0.224	-0.315	0.269
Tegarai	-0.205	-0.247	0.179	0.104	0.146	0.279	0.121	0.099	0.066	-0.054	0.011	-0.044	0.122	-0.102	0.246	-0.298	0.257
Lubai Tengah	-0.285	0.085	0.102	-0.027	-0.159	0.115	-0.017	0.256	0.081	-0.104	-0.309	-0.230	0.035	-0.02	0.238	-0.315	0.269
Ukong	-0.081	-0.025	0.043	0.066	-0.146	-0.125	-0.042	-0.007	-0.053	0.217	-0.209	0.100	-0.027	0.069	0.210	-0.251	0.221
Medamit Nanga	-0.273	0.056	0.250	-0.227	0.148	0.017	-0.108	0.034	0.049	-0.173	0.090	-0.061	0.08	0.141	0.243	-0.286	0.248
Lubok Lalang	-0.173	-0.122	-0.083	-0.249	-0.108	-0.322	-0.218	0.274	-0.141	-0.018	-0.062	-0.034	-0.083	-0.036	0.004	-0.392	0.323
Merbau	-0.206	0.101	-0.105	0.243	-0.038	-0.141	-0.021	0.089	-0.141	0.060	-0.064	-0.071	-0.128	0.029	0.039	-0.415	0.338
Ulu Medalam	-0.293	0.123	0.098	0.086	-0.113	-0.006	-0.221	-0.072	-0.242	-0.263	0.114	-0.471	-0.179	-0.269	0.114	-0.505	0.393
Ulu Medamit	-0.123	-0.047	-0.029	-0.306	-0.084	-0.115	-0.320	-0.201	-0.114	-0.311	-0.118	-0.286	-0.26	0.215	-0.218	-0.465	0.370
Setuan	-0.405	-0.041	-0.066	-0.070	0.151	0.258	-0.495	-0.022	-0.161	-0.010	-0.196	-0.244	0.13	-0.424	-0.171	-0.505	0.393
Long Napir	0.004	0.072	0.117	0.120	-0.058	0.069	-0.165	0.057	0.060	0.139	0.061	0.193	0.031	0.281	0.218	-0.335	0.284
Rutoh	-0.216	-0.056	-0.167	-0.177	-0.297	0.090	0.095	0.055	-0.219	0.012	-0.409	-0.012	-0.1	-0.273	-0.102	-0.505	0.393

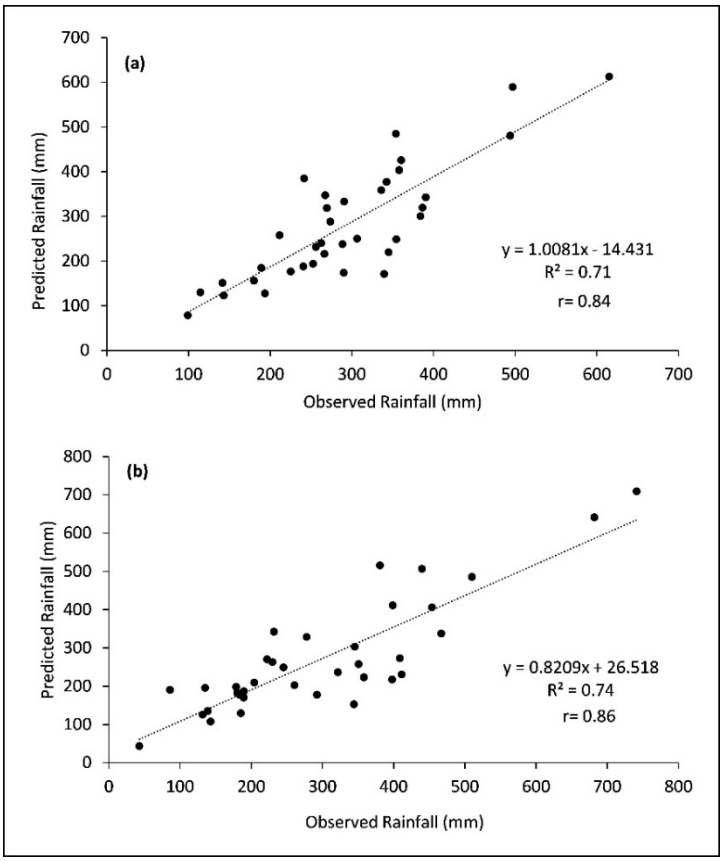

Figure 4.3: Prediction performance of NRM in calculating missing rainfall data of a) Limbang DID and b) Merbau.

General characteristics along with basic statistical properties of monthly, seasonal, inter-monsoon and annual rainfall in the LRB correspond to individual rain gauge is discussed in the following sections. Finally using the processed (gap filled) rainfall data, trend characteristics of monthly, seasonal, inter-monsoon and annual rainfall of thirteen rain gauging stations and the LRB as a whole were assessed by applying the Mann Kendall and Spearman's Rho tests at different significant levels (confidence level at 90%, 95% and 99%).

4.2.1 General characteristics of rainfall in the LRB

Characteristic variation was observed in monthly rainfall recorded at thirteen rain gauging stations in the LRB. Minimum and maximum monthly rainfall recorded at individual rain gauging stations are shown in Table 4.3. In the month of January, the lowest rainfall was observed in Limbang DID (14.50mm in the year 1998) and the highest rainfall was recorded in

Medamit Nanga (1152.60mm in the year 1963). Rainfall recorded at Medamit Nanga was the second highest monthly rainfall in the LRB. At the same time, Limbang DID recorded the lowest monthly rainfall (0.50mm in February-2008) among the stations and months, whereas rain gauging station Lubai Tengah recorded the highest rainfall (819.50mm in February-2000). In the month of March, rain gauging station Pandaruan recorded the lowest rainfall (1mm in the year 1998) and Ulu Medamit recorded the highest rainfall (801.50mm in the year 2008). In April, rain gauging station Ukong recorded minimum rainfall (35.30mm in the year 1963) and Tegarai recorded maximum rainfall (984.00mm in the year 1997). Rain gauging station Medamit Nanga has the lowest rainfall (28.50mm in the year 2012) during the month of May, whereas Tegarai has the highest rainfall (1315.50mm in the year 1993), which was the highest recorded monthly rainfall in the LRB.

It was noted that, rain gauges has the lowest and highest rainfall in the month of June was same as that of May and which varies in the range of 31.00 mm (Medamit Nanga in the year 1985) to 690.50mm (Tegarai in the year 2007). In the month of July, rain gauging station Lubai Tengah recorded minimum rainfall (20.70mm in the year 1972), whereas Lubok Lalang shown the maximum rainfall (717.00mm in the year 2010). During the month of August, the lowest rainfall was recorded by the rain gauging station Pandaruan (21mm in the year 1981) and the highest rainfall was reported in the rain gauging station Tegarai (959.00mm in the year 1996). In the month of September, Long Napir recorded the lowest rainfall (20.50mm in the year 1997) and Medamit Nanga shows the highest rainfall (879.40mm in the year 1973). Also in the month of October, rain gauging station Ukong has the lowest rainfall (32.00mm in the year 2016) and Ulu Medalam has the highest rainfall (906.50mm in the year 2008). During the month of November, rainfall in the LRB varies in the range of 52.00mm (Limbang DID in the year 1983) to 925.30mm (Tegarai in the year 1979). Rainfall for the month of December varies from 19.00mm (Tegarai in the year 2011) to 952.20mm (Lubai Tengah in the year 1977).

Considering the seasonal, inter-monsoon and annual rainfall in the LRB, large variations in seasonal rainfall among rain gauging stations were observed (Table 4.4 and Figure 4.4 a, b). In SWM, rainfall in the LRB varies in the range of 504.50mm (Long Napir in the year 1997) to 3098.50mm (Tegarai in the year 1993). At the same time, NEM has a higher value of rainfall and it varies from Long Napir (632.50mm in the year 1997) to Tegarai (3234mm in the year

1995). Considering the inter-monsoon month of April, rain gauging station Ukong recorded the minimum rainfall (35.30mm in the year 1963) and Tegarai recorded the maximum (984.00mm in the year 1997). During the second inter-monsoon month October, rainfall was found be varied in the range of 32.00mm (Ukong in the year 2016) to 906.50mm (Ulu Medalam in the year 2008). Annual rainfall in the LRB shows high variation between the stations (Table 4.4 and Figure 4.5 a, b). While considering the annual rainfall distribution, rain gauging station Long Napir recorded the lowest rainfall (1821.56mm in the year 1983) and Tegarai recorded the highest rainfall (6926mm in the year 1996).

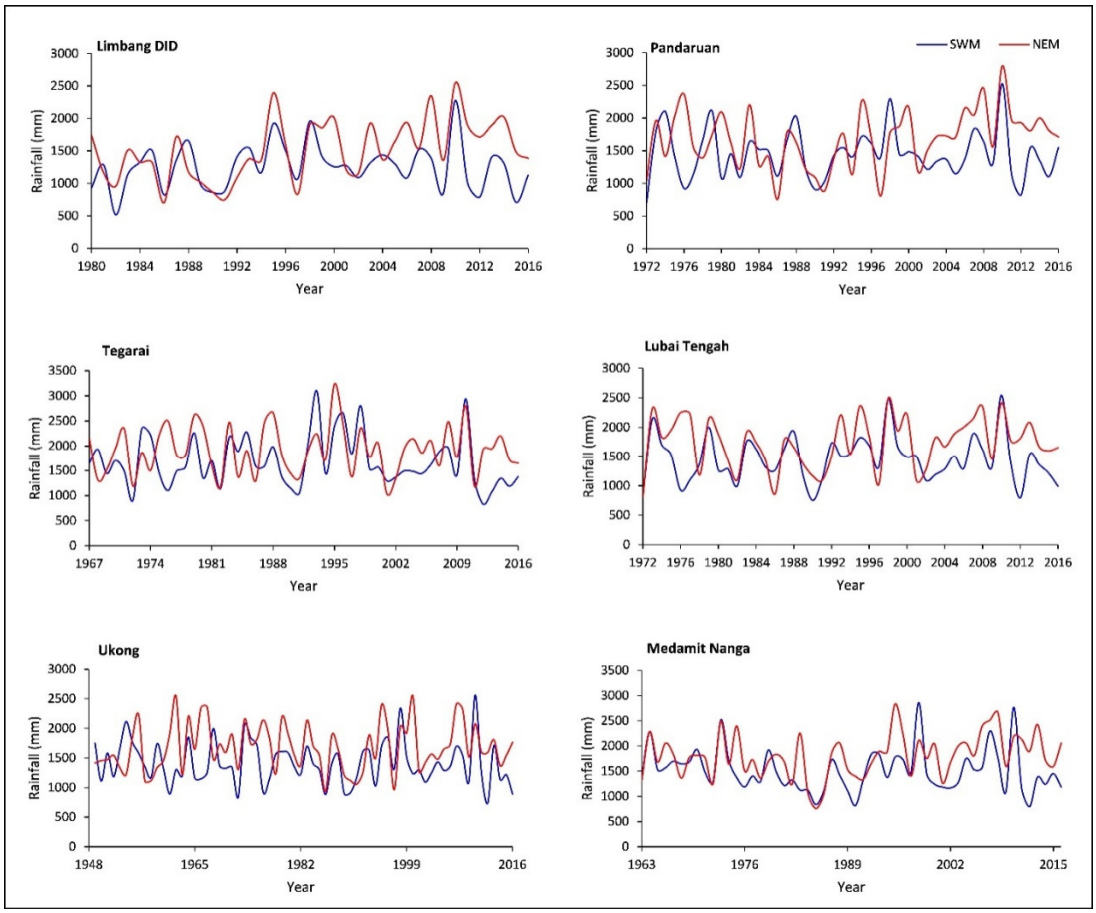

Figure 4.4a: Seasonal rainfall in individual stations in the LRB.

Table 4.3: Station-wise minimum and maximum monthly rainfall (mm) in the LRB.

Stations		**Jan**	**Feb**	**Mar**	**Apr**	**May**	**Jun**	**Jul**	**Aug**	**Sep**	**Oct**	**Nov**	**Dec**
Limbang DID	Min	14.50	0.50	4.00	113.00	64.50	43.00	70.00	25.00	84.50	39.50	52.00	109.00
	Max	774.50	585.50	617.50	503.00	687.50	425.00	452.00	636.50	708.00	673.00	741.50	512.50
Pandaruan	Min	42.50	16.70	1.00	113.50	130.50	50.50	45.60	21.00	89.00	119.50	188.50	81.00
	Max	810.50	793.20	667.50	686.50	743.70	640.40	575.50	843.00	864.80	683.50	825.50	623.50
Tegarai	Min	42.30	35.50	23.00	131.20	135.50	69.50	58.50	36.80	43.50	154.00	172.00	19.00
	Max	1118.50	658.60	637.00	984.00	1315.50	690.50	575.00	959.00	769.80	752.50	925.30	808.60
Lubai Tengah	Min	17.80	22.80	28.50	128.50	77.00	86.50	20.70	48.64	47.00	133.00	175.00	83.80
	Max	752.00	819.50	707.00	813.00	660.00	596.10	584.00	677.00	616.10	681.00	704.10	952.20
Ukong	Min	46.70	71.80	38.50	35.30	94.50	53.00	58.00	62.50	62.50	32.00	203.50	34.50
	Max	1061.90	604.00	739.50	652.00	584.50	578.70	650.50	708.50	693.00	665.70	877.50	782.50
Medamit Nanga	Min	16.40	30.00	45.50	51.00	28.50	31.00	31.10	41.50	51.50	135.20	156.00	85.00
	Max	1152.56	755.50	764.00	894.50	664.50	552.00	572.00	837.00	879.40	682.50	756.50	702.50
Lubok Lalang	Min	49.50	25.00	23.50	186.63	50.00	82.00	31.00	57.50	100.50	193.00	288.50	142.50
	Max	784.50	676.50	640.00	642.50	676.00	570.50	717.00	712.00	652.00	663.50	771.50	601.00
Merbau	Min	92.50	32.50	111.00	163.50	161.50	68.08	68.50	52.50	65.50	207.50	289.50	166.50
	Max	580.31	526.00	429.50	558.50	559.00	504.50	453.50	719.10	522.00	579.50	534.50	606.00
Ulu Medalam	Min	122.03	131.90	171.50	193.50	127.50	87.00	67.00	91.50	164.50	163.50	272.00	277.00
	Max	906.00	622.50	661.50	682.50	713.50	618.50	621.04	717.03	632.00	906.50	796.50	888.00
Ulu Medamit	Min	104.00	108.50	123.00	198.00	134.50	63.50	116.50	64.50	58.50	230.50	209.00	292.50
	Max	753.50	645.90	801.50	676.50	888.50	632.00	664.86	715.90	701.00	776.50	677.50	683.00
Setuan	Min	79.99	67.79	109.50	175.00	130.00	71.50	70.50	78.00	142.50	151.00	235.50	136.00
	Max	561.50	421.50	520.00	464.50	541.00	440.33	367.50	452.29	477.00	595.50	623.50	481.00
Long Napir	Min	38.50	25.50	56.50	84.14	83.00	58.50	42.50	27.00	20.50	62.50	56.50	115.00
	Max	521.50	502.00	426.50	444.00	573.50	393.00	447.50	465.50	387.00	450.00	564.79	511.50
Rutoh	Min	50.38	36.36	84.76	96.00	138.50	66.00	67.50	38.50	66.00	128.00	169.50	177.00
	Max	565.00	381.50	453.00	594.00	604.50	398.50	379.50	386.50	423.50	447.50	426.50	465.00

Table 4.4: Station-wise minimum and maximum seasonal, inter-monsoon and annual rainfall (mm) in the LRB.

Stations		Seasonal RF		Inter-monsoon RF		Annual RF
		SWM	NEM	Apr	Oct	
Limbang DID	Min	519.50	707.50	113.00	39.50	2148.00
	Max	2276.11	2552.00	503.00	673.00	4493.00
Pandaruan	Min	710.40	758.00	113.50	119.50	2630.00
	Max	2525.50	2797.50	686.50	683.50	5190.00
Tegarai	Min	827.50	1036.50	131.20	154.00	3172.50
	Max	3098.50	3234.00	984.00	752.50	6926.00
Lubai Tengah	Min	753.00	790.30	128.50	133.00	2722.00
	Max	2542.00	2486.00	813.00	681.00	5358.00
Ukong	Min	735.50	935.50	35.30	32.00	2322.50
	Max	2564.00	2550.00	652.00	665.70	5219.50
Medamit Nanga	Min	794.63	759.00	51.00	135.20	2190.42
	Max	2861.00	2832.00	894.50	682.50	5617.50
Lubok Lalang	Min	846.72	1173.50	186.63	193.00	2654.00
	Max	3003.00	2607.50	642.50	663.50	5334.50
Merbau	Min	798.50	1067.50	163.50	207.50	3158.00
	Max	2259.50	2100.50	558.50	579.50	4996.00
Ulu Medalam	Min	1199.00	1618.00	193.50	163.50	4106.50
	Max	2802.45	2815.00	682.50	906.50	5867.50
Ulu Medamit	Min	947.00	1437.00	198.00	230.50	4107.00
	Max	2952.00	2641.50	676.50	776.50	6078.00
Setuan	Min	896.50	1188.50	175.00	151.00	2865.37
	Max	1739.44	2098.50	464.50	595.50	4199.50
Long Napir	Min	504.50	632.50	84.14	62.50	1821.56
	Max	1663.77	1802.00	444.00	450.00	3598.50
Rutoh	Min	785.50	843.06	96.00	128.00	2163.25
	Max	1645.00	1818.50	594.00	447.50	3900.50

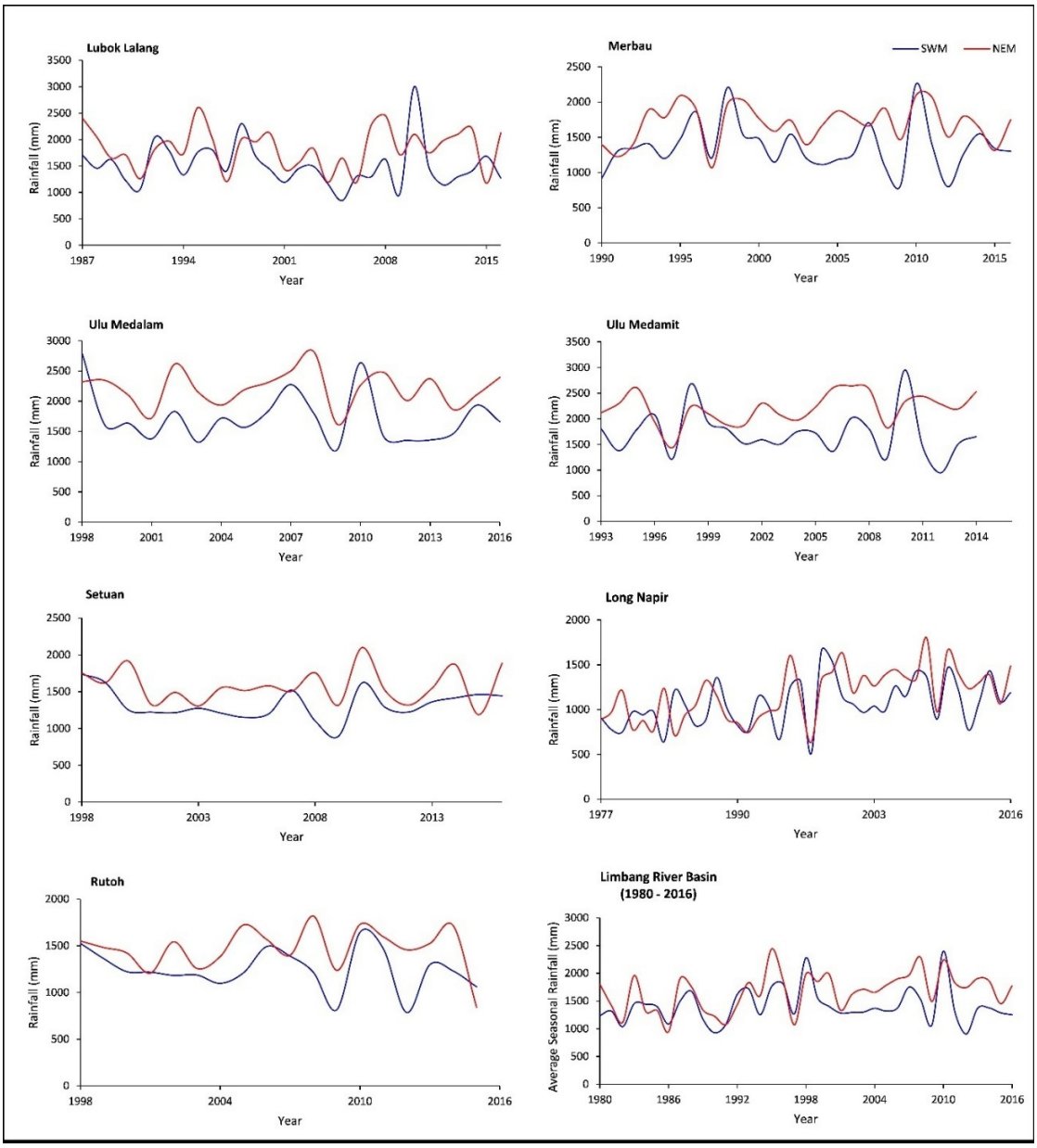

Figure 4.4b: Seasonal rainfall in individual stations and the LRB as a whole.

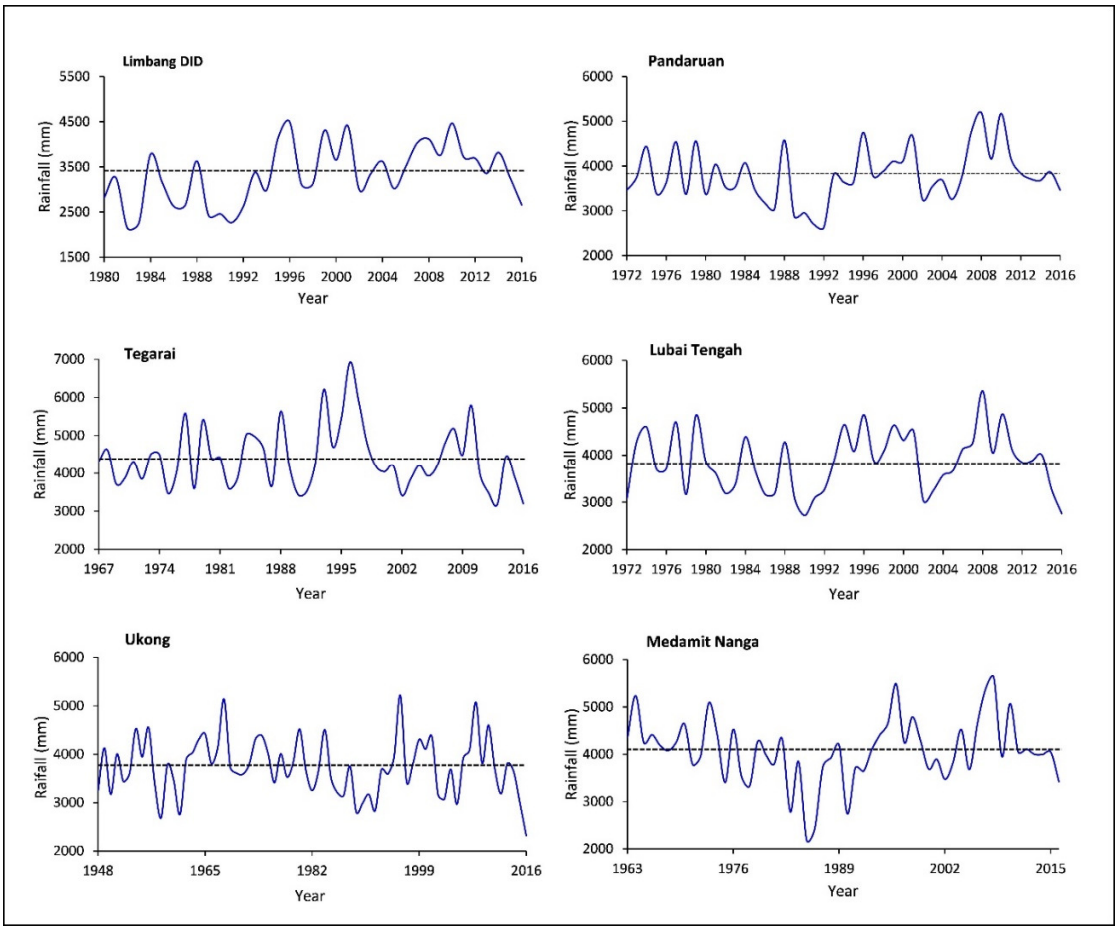

Figure 4.5a: Annual rainfall with long term average in individual stations in the LRB.

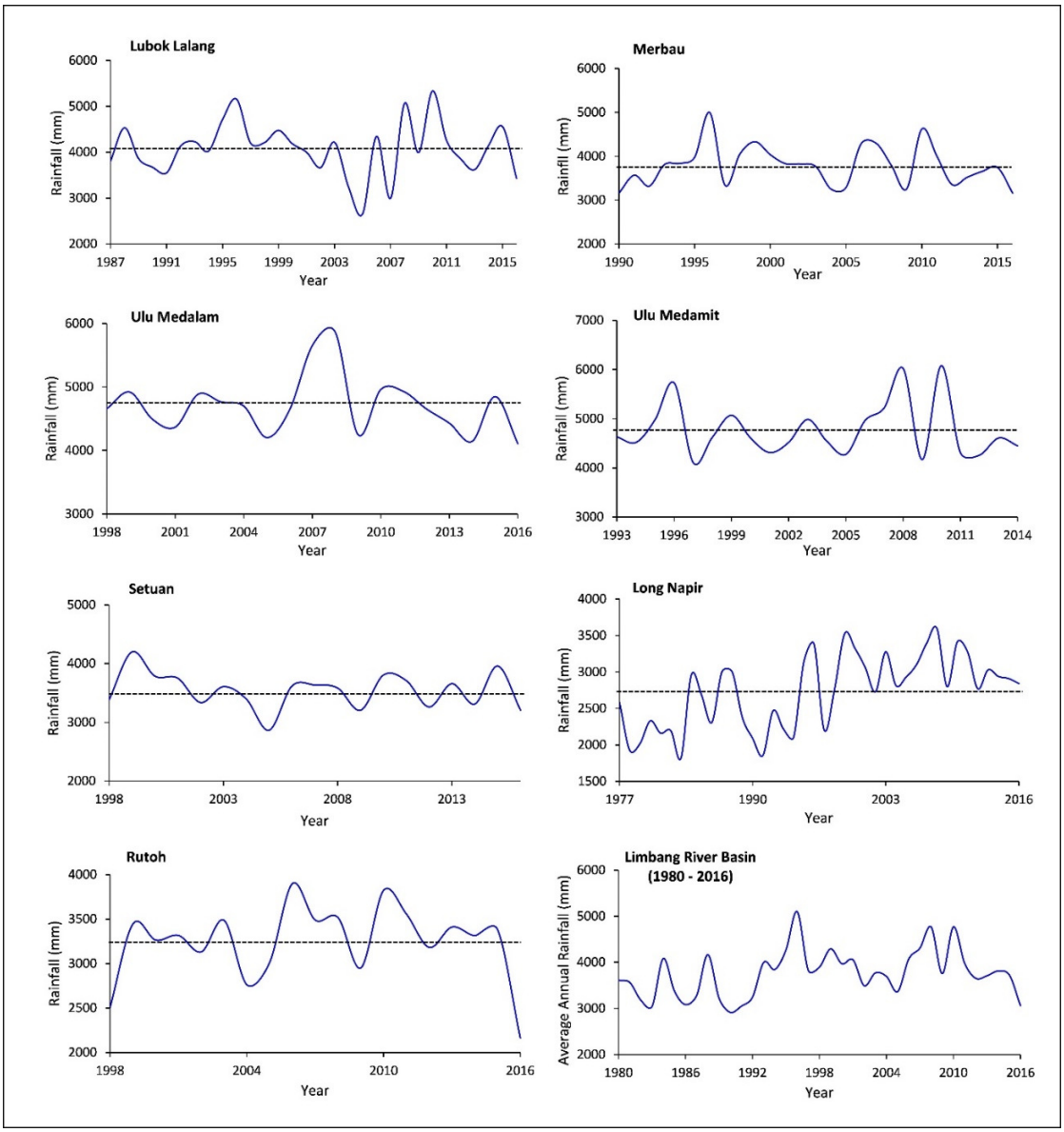

Figure 4.5b: Annual rainfall with long term average in individual stations and the LRB as a whole.

4.2.2 Basic statistical characteristics of rainfall in the LRB

Basic characteristics of monthly, seasonal, inter-monsoon and annual rainfall from thirteen rain gauging stations were assessed to create detailed understanding about the statistical characteristics of rainfall in the LRB. Statistical characteristics considered in this study are average, standard deviation, skewness, kurtosis and coefficient of variation (CV) and are discussed in detail in the following sections.

4.2.2.1 Average and standard deviation

Monthly average of rainfall in thirteen stations were calculated along with standard deviation and are given in Table 4.5 and shown in Figure 4.6 a, b. In the month of January, the average monthly rainfall in the LRB ranges from 244.89 (Long Napir) to 472.21mm (Ulu Medalam) and standard deviation lies between 118.89 (Long Napir) and 236.13mm (Tegarai). During the month of February, the average rainfall ranges between 183.53 (Long Napir) and 388.89mm (Ulu Medamit) with standard deviation of 86.81 (Setuan) and 174.1mm (Lubai Tengah). In the month of March, the average rainfall varies between 193.30 (Long Napir) and 402.76mm (Ulu Medalam) and shows the standard deviation in the range of 80.79 (Merbau) and 149.92mm (Tegarai). An average rainfall in the range of 247.81 (Long Napir) and 450.46mm (Ulu Medamit) was observed in April, which shows the standard deviation of 81.27 (Long Napir) and 171.79mm (Medamit Nanga). In the month of May, average rainfall varies between 237.41 and 403.75mm with standard deviation that ranges from 84.43 to 215.63mm in Long Napir and Tegarai respectively. Average rainfall during the month of June varies from 220.40 (Long Napir) to 354.27mm (Ulu Medamit) and standard deviation ranges from 84.26 (Rutoh) to 180.25mm (Ulu Medalam). In the month of July, average rainfall range from 187.79 (Long Napir) to 329.45 mm (Ulu Medalam) with standard deviation of 82.45 to 166.54mm in Long Napir and Ulu Medamit respectively. In August, average rainfall ranges from 205.18 (Long Napir) to 348.98mm (Ulu Medalam) and the standard deviation vary between 100.49 (Rutoh) and 210.47mm (Tegarai). During the month of September, the average rainfall varied in the range of 213.68 to 356.30mm in Long Napir and Tegarai whereas the standard deviation varies between 98.18 and 187.19mm in Setuan and Tegarai respectively. In October, the average rainfall varies in the range of 259.45 (Rutoh, but rain gauging station Long Napir also showed a similar value of 259.99 mm) to 436.08mm (Ulu Medamit) with standard deviation of 91.14 (Long Napir) to 189.99mm (Ulu Medalam). In the month of November, the average rainfall and standard deviation ranges from 290.70 (Long Napir) to 489.65mm (Tegarai) and 66.62 (Rutoh) to 175.83mm (Tegarai) respectively. Average rainfall during the month of December varies in the range of 248.26 (Long Napir) to 463.40mm (Ulu Medamit) and standard deviation ranges from 79.31 (Rutoh) to 163.70mm (Ulu Medalam).

Considering the seasonal, inter-monsoon and annual rainfall, a significant difference observed in average rainfall recorded in each rain gauging station (Table 4.6). During SWM, the

average rainfall varies from 1064.46 (Long Napir) to 1724.63mm (Ulu Medalam) and standard deviation in the range of 206.45 (Setuan) to 514.76mm (Tegarai). At the same time in NEM, average rainfall in the LRB was found to be varied in the range of 1169.65 (Long Napir) to 2216.61mm (Ulu Medalam) with standard deviation of 227.42 (Rutoh) to 484.93mm (Tegarai). Considering the inter-monsoon months, in the month of April, average rainfall varies from 247.81 (Long Napir) to 450.46mm (Ulu Medamit) with standard deviation of 81.27 (Long Napir) to 171.79mm (Medamit Nanga). In October, the average rainfall varies in the range of 259.45 (Rutoh) to 436.08mm (Ulu Medamit) with standard deviation of 91.14 (Long Napir) to 189.99mm (Ulu Medalam). While considering the annual rainfall, average rainfall in the LRB varies in the range of 2732.94 (Long Napir) to 4771.86mm (Ulu Medamit) and the standard deviation varies between 311.43 (Setuan) and 817.75mm (Tegarai) respectively.

While characterising the average monthly rainfall associated with rain gauging stations in the LRB, all the stations shown an average rainfall ≥200mm in all the months. Rain gauging station Long Napir shown the lowest average rainfall in all the months whereas Tegarai, Ulu Medalam and Ulu Medamit recorded the highest average monthly rainfall. The lowest average monthly rainfall in the LRB was observed during February (183.53mm in Long Napir) and the highest in November (489.65mm in Tegarai). Similarly, the lowest standard deviation in monthly rainfall data was observed in the month of November (66.62mm in Rutoh) and highest in the month of January (236.13mm in Tegarai). Considering the monsoon seasons, Long Napir and Ulu Medalam showed the lowest and highest average rainfall for both seasons (SWM and NEM), whereas in the inter-monsoon periods, rain gauging stations Long Napir and Ulu Medamit showed the lowest and highest average rainfall. Inter-monsoon periods also showed similar patterns of the monsoon seasons.

Table 4.5: Station-wise average and standard deviation of monthly rainfall (mm) in the LRB.

Stations		Jan	Feb	Mar	Apr	May	Jun	Jul	Aug	Sep	Oct	Nov	Dec
Limbang DID	Average	361.75	250.49	213.35	279.60	318.89	223.53	224.18	241.82	246.72	280.61	346.21	341.57
	Std Dev	211.65	148.41	135.26	104.67	145.36	106.62	123.32	168.91	121.46	134.42	132.27	113.86
Pandaruan	Average	389.66	290.96	256.12	326.96	346.29	273.94	255.08	263.01	309.60	337.88	404.10	347.63
	Std Dev	231.22	173.95	135.70	116.49	153.74	146.50	121.85	179.81	174.97	135.06	132.41	128.82
Tegarai	Average	400.98	308.04	287.04	381.63	403.75	306.35	311.83	307.89	356.30	414.95	489.65	426.84
	Std Dev	236.13	172.29	149.92	167.52	215.63	153.04	157.09	210.47	187.19	180.21	175.83	161.71
Lubai Tengah	Average	376.98	292.83	261.56	328.36	348.71	273.38	257.53	264.81	311.14	349.10	411.36	389.56
	Std Dev	209.01	174.11	135.55	144.15	130.20	132.98	126.70	158.33	155.00	134.15	132.36	154.34
Ukong	Average	360.66	274.95	249.69	306.26	326.04	271.96	256.01	249.77	305.83	352.06	412.22	376.96
	Std Dev	201.74	132.50	126.16	144.57	106.47	121.28	123.68	132.66	148.82	128.49	136.42	131.36
Medamit Nanga	Average	393.09	291.98	285.58	380.94	351.59	275.01	273.08	300.42	312.56	363.55	449.67	405.40
	Std Dev	210.39	153.89	123.32	171.79	156.14	136.39	138.52	168.32	170.46	119.81	142.55	137.07
Lubok Lalang	Average	364.63	302.03	313.12	368.67	351.30	278.78	271.42	295.08	312.85	370.74	466.27	376.77
	Std Dev	181.57	146.13	139.24	126.84	134.60	126.16	154.28	180.82	125.66	116.38	117.73	123.34
Merbau	Average	354.11	289.39	266.48	339.09	314.54	267.61	236.99	276.53	271.62	382.22	418.08	364.25
	Std Dev	140.26	118.32	80.79	99.26	97.14	114.04	106.41	165.60	112.86	92.10	77.16	125.46
Ulu Medalam	Average	472.21	365.71	402.76	443.34	371.60	328.11	329.45	348.98	346.50	376.47	470.38	453.96
	Std Dev	190.49	155.41	141.19	133.41	139.64	180.25	160.54	157.09	152.07	189.99	125.46	163.70
Ulu Medamit	Average	452.91	388.89	389.34	450.46	380.95	354.28	312.12	334.61	332.40	436.08	476.42	463.40
	Std Dev	154.59	123.38	144.42	129.75	161.38	165.12	166.54	164.57	170.54	142.02	112.62	100.08
Setuan	Average	299.63	252.33	292.90	323.48	297.43	247.33	239.90	253.41	289.39	353.74	368.26	324.37
	Std Dev	125.73	86.81	119.13	92.51	96.70	98.90	92.26	103.92	98.18	109.63	88.31	108.16
Long Napir	Average	244.89	183.53	193.30	247.81	237.41	220.40	187.79	205.18	213.68	259.99	290.70	248.26
	Std Dev	118.89	103.99	84.35	81.27	84.43	102.69	82.45	115.94	98.92	91.14	96.15	96.02
Rutoh	Average	320.57	242.60	257.73	319.29	306.71	234.44	220.08	218.39	255.21	259.45	293.21	315.79
	Std Dev	130.36	107.77	98.89	148.82	121.35	84.28	82.87	100.49	102.60	92.85	66.62	79.31

Table 4.6: Station-wise average and standard deviation of seasonal, inter-monsoon and annual rainfall (mm) in the LRB.

Stations		Seasonal RF		Inter-monsoon RF		Annual RF
		SWM	NEM	Apr	Oct	
Limbang DID	Average	1255.15	1517.55	279.60	280.61	3328.73
	Std Dev	359.34	460.08	104.67	134.42	658.05
Pandaruan	Average	1447.92	1682.16	326.96	337.88	3801.23
	Std Dev	377.60	446.18	116.49	135.06	604.39
Tegarai	Average	1686.12	1912.79	381.63	414.95	4395.26
	Std Dev	514.76	484.93	167.52	180.21	817.75
Lubai Tengah	Average	1455.57	1732.52	328.36	349.10	3865.32
	Std Dev	394.87	441.89	144.15	134.15	638.35
Ukong	Average	1409.62	1681.92	306.26	352.06	3742.42
	Std Dev	359.03	400.36	144.57	128.49	587.56
Medamit Nanga	Average	1512.66	1811.30	380.94	363.55	4082.87
	Std Dev	433.59	432.19	171.79	119.81	686.02
Lubok Lalang	Average	1509.43	1842.21	368.67	370.74	4071.66
	Std Dev	419.96	391.36	126.84	116.38	594.15
Merbau	Average	1367.29	1696.19	339.09	382.22	3780.92
	Std Dev	348.09	275.84	99.26	92.10	461.30
Ulu Medalam	Average	1724.63	2216.61	443.34	376.47	4709.46
	Std Dev	435.71	302.18	133.41	189.99	462.06
Ulu Medamit	Average	1714.36	2205.61	450.46	436.08	4771.86
	Std Dev	450.39	306.04	129.75	142.02	565.67
Setuan	Average	1327.47	1582.48	323.48	353.74	3542.18
	Std Dev	206.45	244.73	92.51	109.63	311.43
Long Napir	Average	1064.46	1169.65	247.81	259.99	2732.94
	Std Dev	262.20	288.87	81.27	91.14	500.50
Rutoh	Average	1234.83	1467.90	319.29	259.45	3243.47
	Std Dev	222.11	227.42	148.82	92.85	425.56

In the case of annual average rainfall, five rain gauges shows an average rainfall >4000mm, seven rain gauges shown an average rainfall between 3000 and 4000mm and the remaining one station showed an annual average rainfall ≥2700mm. However, considering the standard deviation of monthly, seasonal, inter-monsoon and annual rainfall in the LRB, each rain gauging station shows a lower value when compared with the average (mean rainfall). This indicates the less dispersed nature of rainfall data in the LRB.

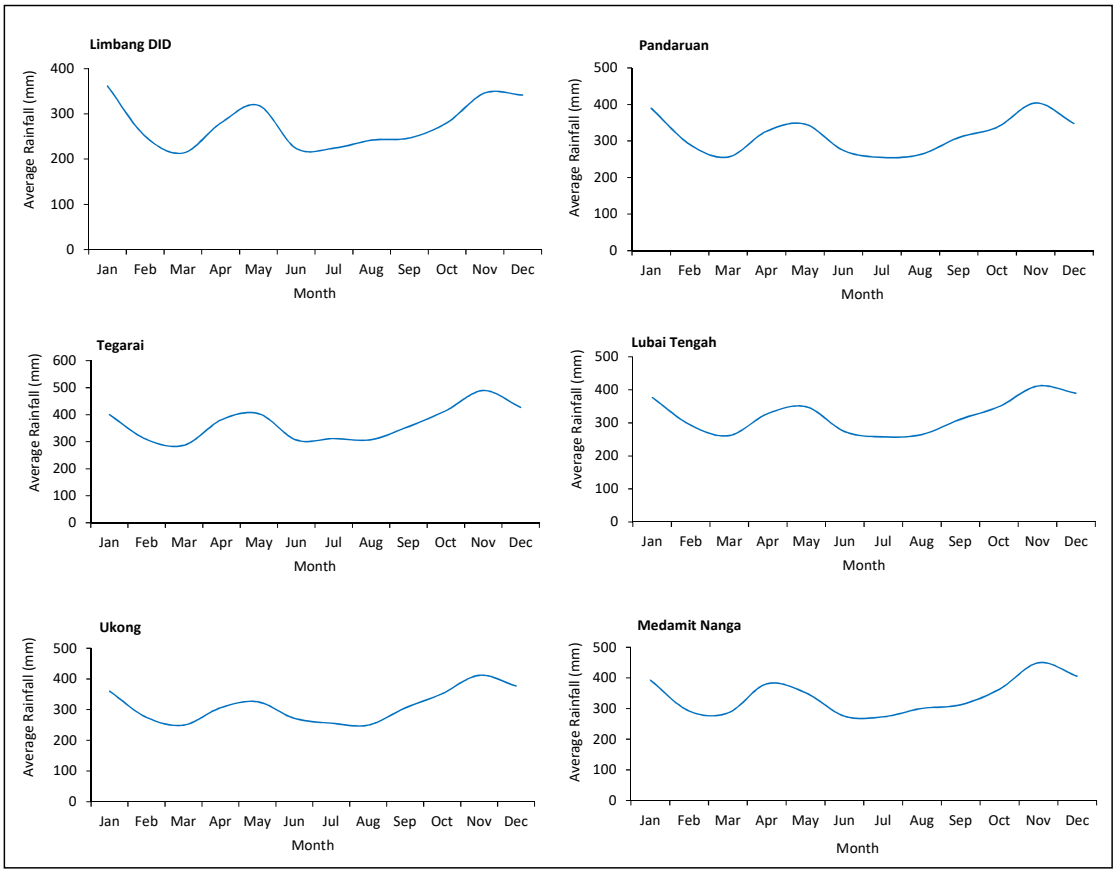

Figure 4.6a: Average monthly rainfall in individual station in the LRB.

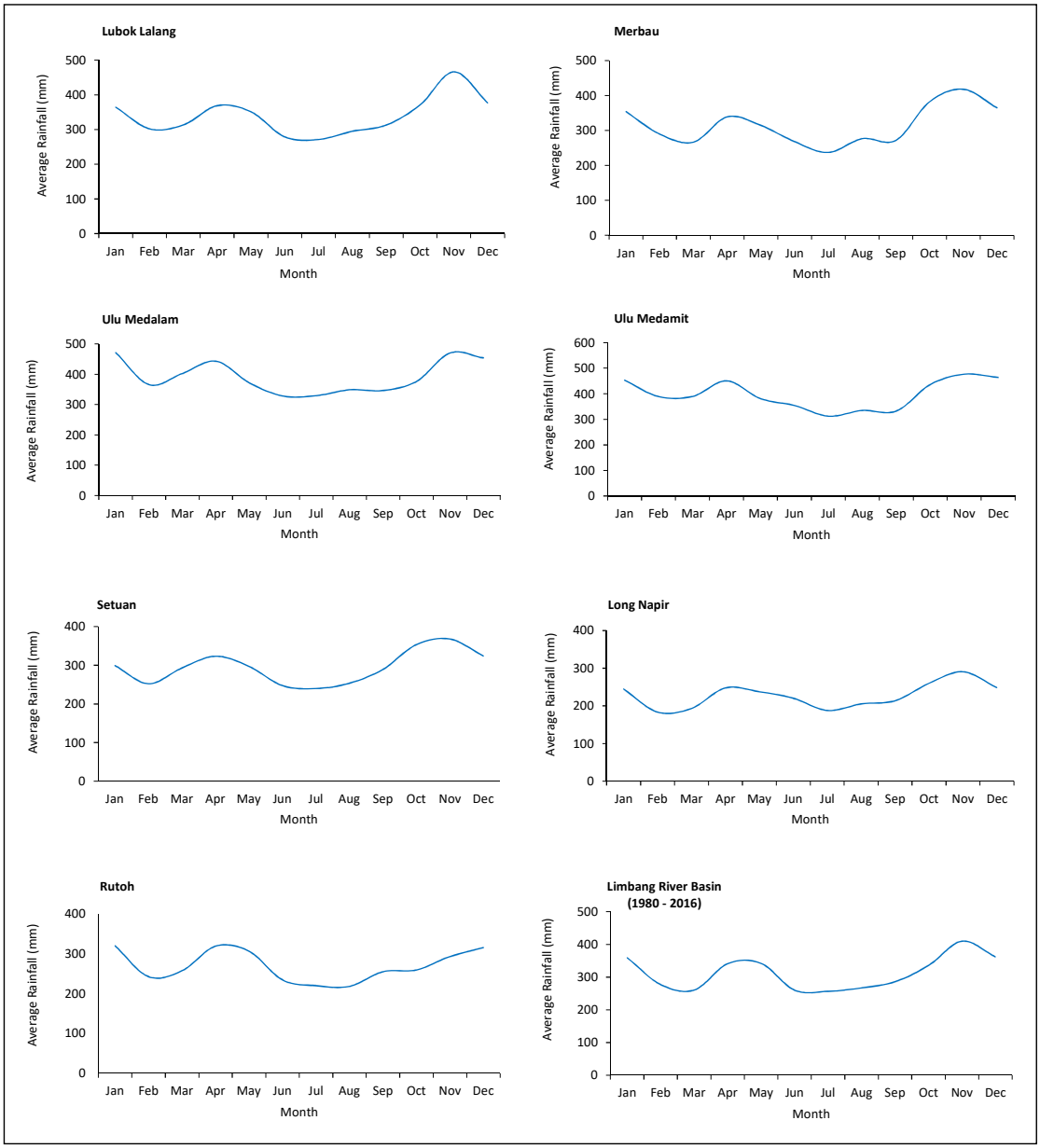

Figure 4.6b: Average monthly rainfall in individual stations and the LRB as a whole.

4.2.2.2 Skewness

Skewness of monthly, seasonal, inter-monsoon and annual rainfall from thirteen rain gauging stations were analysed to understand the rainfall distribution characteristics in the LRB. Results of monthly rainfall data analysed are given in Table 4.7 and are graphically represented in Figure 4.7. In the month of January, skewness of rainfall data varies from -0.45 (Rutoh) to 0.96 (Medamit Nanga) with most (ten) of the stations showing right skewness with a

positive value. A similar pattern was observed in the month of February with ten stations showing positive values indicating right skewed nature and the value of skewness in February varies in the range of -0.62 (Rutoh) to 0.94 (Long Napir). In the month of March, twelve rain gauges showed positive skewness and a single rain gauge (Merbau) showed negative skewness and varies in the range of -0.20 (Merbau) to 1.11 (Ukong). During the month of April, the skewness value ranges from -0.22 (Ulu Medamit) to 1.38 (Tegarai), with eleven stations showing positive skewness. Skewness value ranges from -0.12 (Ukong) to 2.24 (Tegarai) in the month of May with twelve stations showing positive skewness in rainfall data. In the month of June, skewness ranges from -0.16 (Setuan) to 0.64 (Tegarai) with most of the stations (eleven) showing positive skewness. In addition to Setuan, Rutoh (-0.12) also showed negative skewness in June.

Considering the month of July, rain gauging station Setuan shown negative skewness (-0.28) and remaining all stations shown positive skewness with maximum value was shown by Ukong (0.83). Similarly in the month of August, rain gauging station Rutoh (-0.19) only showed negatively skewed nature and all other stations shown positive skewness with maximum value was shown by Pandaruan (1.23). A similar pattern was followed in the month of September with twelve stations showing positive skewness with maximum value of 1.58 in Limbang DID and minimum in Long Napir (-0.24) with a negative skewness. At the same time during the month of October, all stations showed positive skewness with values ranging from 0.22 (Long Napir) to 1.45 (Limbang DID). In the month of November, skewness value ranges from -0.33 (Ulu Medamit) to 1.38 (Setuan) with eleven stations shows positive skewness and two stations namely Ulu Medamit and Merbau showed left skewness. Skewness value of rainfall during the month of December, ranges from -0.43 (Limbang DID) to 1.39 (Ulu Medalam) with nine stations showing positive skewness.

Table 4.7: Station-wise skewness assessed for monthly rainfall in the LRB.

Stations	Jan	Feb	Mar	Apr	May	Jun	Jul	Aug	Sep	Oct	Nov	Dec
Limbang DID	0.38	0.19	0.81	0.61	0.73	0.04	0.49	0.95	1.58	1.45	0.77	-0.43
Pandaruan	0.23	0.81	0.78	0.60	0.93	0.54	0.66	1.23	1.15	1.07	0.81	0.12
Tegarai	0.65	0.29	0.62	1.38	2.24	0.64	0.25	1.22	0.38	0.47	0.50	-0.07
Lubai Tengah	0.00	0.69	0.80	1.13	0.51	0.50	0.43	0.84	0.56	0.78	0.44	0.99
Ukong	0.72	0.44	1.11	0.45	-0.12	0.45	0.83	1.10	0.80	0.29	1.00	0.31
Medamit Nanga	0.96	0.54	0.89	0.55	0.21	0.15	0.25	0.67	1.18	0.37	0.40	0.03
Lubok Lalang	0.13	0.42	0.61	0.40	0.23	0.46	0.78	0.62	0.52	0.84	0.61	-0.19
Merbau	-0.23	0.36	-0.20	0.41	0.78	0.51	0.33	1.06	0.30	0.32	-0.19	0.38
Ulu Medalam	0.29	0.23	0.38	-0.19	0.82	0.34	0.19	0.51	0.59	1.14	0.70	1.39
Ulu Medamit	-0.31	-0.12	0.79	-0.22	1.51	0.23	0.73	0.56	0.61	0.94	-0.33	0.48
Setuan	0.09	-0.44	0.41	0.09	0.69	-0.16	-0.28	0.21	0.41	0.46	1.38	-0.20
Long Napir	0.38	0.94	0.74	0.36	1.65	0.27	0.76	0.61	-0.24	0.22	0.28	0.68
Rutoh	-0.45	-0.62	0.21	0.38	0.56	-0.12	0.38	-0.19	0.03	0.47	0.11	0.30

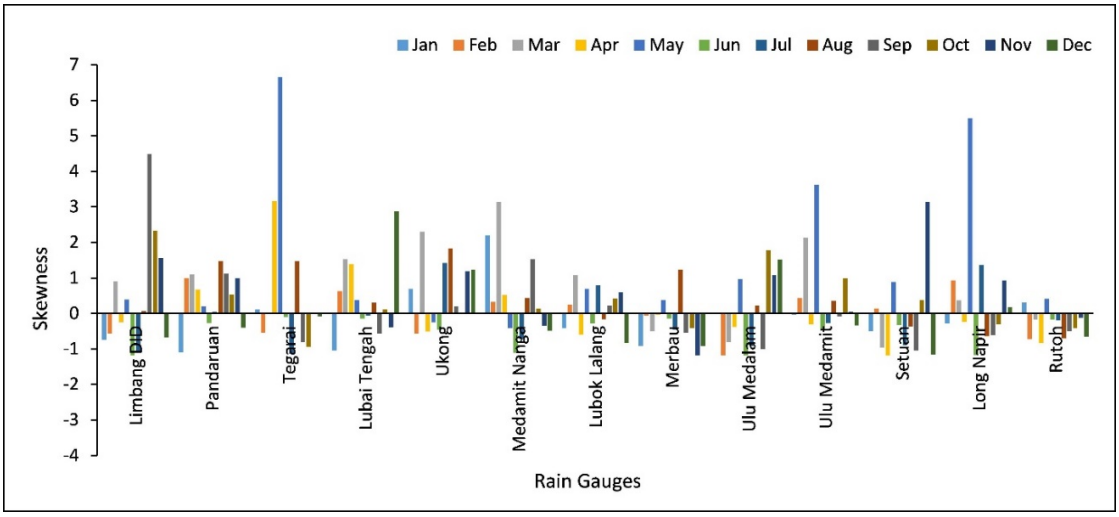

Figure 4.7: Graphical representation of station-wise skewness assessed for monthly rainfall in the LRB.

Skewness of seasonal, inter-monsoon and annual rainfall also shown comparable characteristics of monthly rainfall with majority of stations showing positively skewed rainfall distribution (Table 4.8 and Figure 4.8). During SWM, skewness value varies in the range of -0.28 (Rutoh) to 1.66 (Lubok Lalang) with twelve stations showing positively skewed rainfall distribution. At the same time, during the NEM, six stations shown positive skewness and seven stations shown negatively skewed rainfall distribution which varies in the range of -0.99 (Rutoh) to 0.41 (Setuan). During inter-monsoon periods, skewness value varies in the range of -0.22 (Ulu Medamit) to 1.38 (Tegarai) and 0.22 (Long Napir) to 1.45 (Limbang DID) for April and October respectively. It was noted that during the month of April, eleven stations shown positive skewness whereas in the month of October, all stations shown positive skewness. Considering the skewness value of annual rainfall data, it ranges from -0.99 to 1.20 for Rutoh and Ulu Medamit respectively with eight rain gauges shown positively skewed rainfall data.

Analysis of skewness of monthly, seasonal, inter-monsoon and annual rainfall data in the LRB revealed a dominant right skewed nature of rainfall data distribution with most of the stations showing positive values. This indicates similar distribution pattern of rainfall in the LRB.

Table 4.8: Station-wise skewness assessed for seasonal, inter-monsoon and annual rainfall in the LRB.

Stations	Seasonal RF		Inter-monsoon RF		Annual RF
	SWM	NEM	April	October	
Limbang DID	0.55	0.26	0.61	1.45	0.02
Pandaruan	0.66	-0.01	0.60	1.07	0.40
Tegarai	0.92	0.33	1.38	0.47	0.96
Lubai Tengah	0.66	-0.30	1.13	0.78	0.17
Ukong	0.70	0.35	0.45	0.29	0.22
Medamit Nanga	1.21	0.06	0.55	0.37	-0.26
Lubok Lalang	1.66	-0.20	0.40	0.84	-0.08
Merbau	0.96	-0.46	0.41	0.32	0.72
Ulu Medalam	1.34	-0.18	-0.19	1.14	1.10
Ulu Medamit	1.18	-0.54	-0.22	0.94	1.20
Setuan	0.20	0.41	0.09	0.46	-0.05
Long Napir	0.17	0.09	0.36	0.22	-0.19
Rutoh	-0.28	-0.99	0.38	0.47	-0.99

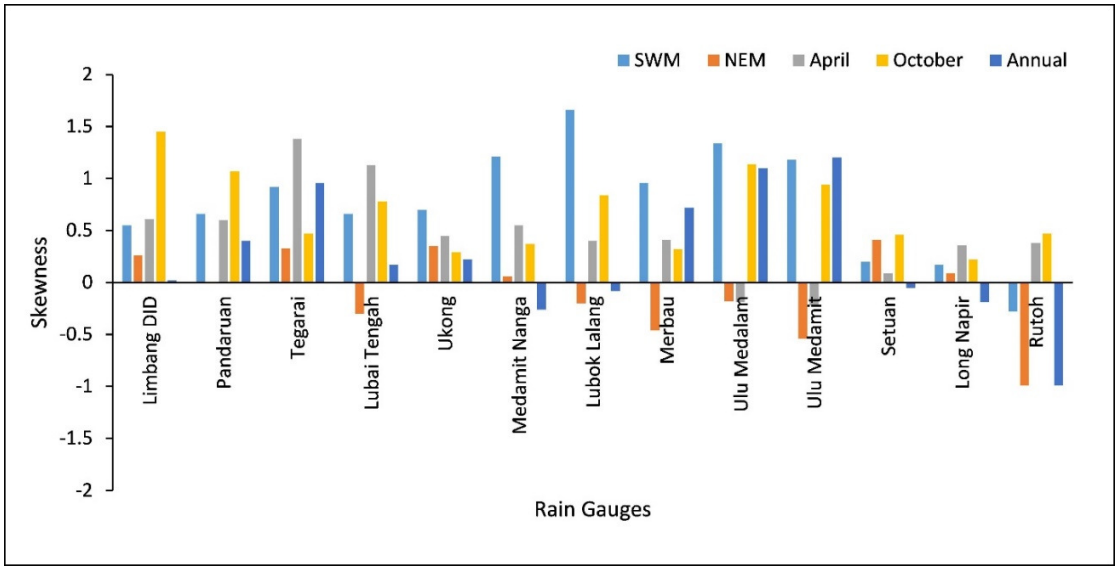

Figure 4.8: Graphical representation of station-wise skewness assessed for seasonal, inter-monsoon and annual rainfall in the LRB.

4.2.2.3 Kurtosis

Kurtosis analysis for monthly, seasonal, inter-monsoon and annual rainfall in different rain gauging stations was carried out to understand the peakness and flatness which indicates infrequent extreme deviations (higher values) and less distinct deviations (lower values). Result shows comparatively lower values in most cases (monthly, seasonal, inter-monsoon and annual rainfall) indicating less deviation of data but a few rain gauges in certain months and seasons show higher values due to high variation in the distribution of rainfall.

Results of Kurtosis derived for station-wise monthly rainfall were tabulated in Table 4.9 and shown in Figure 4.9. In the month of January, the Kurtosis value ranges from -1.10 (Pandaruan) to 2.20 (Medamit Nanga). During this month, most of the stations (nine) show negative values. Rain gauging station Ulu Medalam (-1.18) showed a minimum value of Kurtosis in February whereas the maximum value was noted in Pandaruan (1.00) while seven stations show positive values. In the month of March, Kurtosis value range from -0.97 (Setuan) to 3.14 (Medamit Nanga) and most of the stations (eight) showed positive Kurtosis. During the month of April, most of the stations (nine) show a negative value and the value of Kurtosis varies within the range of -1.19 (Setuan) to 3.17 (Tegarai). At the same time, the maximum value of Kurtosis among the months was noted during May and was shown by the rain gauging station Tegarai (6.66) and the minimum was noted in Medamit Nanga (-0.41). Eleven rain gauging stations showed positive Kurtosis values during this month. All rain gauging stations in June, show a negative value of Kurtosis and it ranges between -1.19 (Ulu Medalam) and -0.10 (Tegarai). In the month of July, the value of Kurtosis ranges from -1.14 (Tegarai) to 1.42 (Ukong) with most of the stations (nine) recording a negative Kurtosis. Kurtosis ranges from -0.71 (Rutoh) to 1.83 (Ukong) in the month of August with nine stations showing positive values. During the month of September, rain gauging station Limbang DID showed a comparatively higher value of Kurtosis (4.49) and Setuan showed the lower value of -1.04 with eight stations have negative values. In the month of October, Kurtosis ranges from -0.95 (Tegarai) to 2.33 (Limbang DID) with eight stations showing positive value whereas in November, it varies in the range of -1.18 (Merbau) to 3.14 (Setuan) with nine stations showing positive values. During the month of December, rain gauging station Lubai Tengah showed the highest value (2.88) and Setuan showed the lowest (-1.16) with most of the stations (nine) showing negative value of Kurtosis.

Table 4.9: Station-wise kurtosis assessed for monthly rainfall in the LRB.

Stations	Jan	Feb	Mar	Apr	May	Jun	Jul	Aug	Sep	Oct	Nov	Dec
Limbang DID	-0.75	-0.56	0.90	-0.25	0.39	-1.18	-1.07	0.06	4.49	2.33	1.56	-0.67
Pandaruan	-1.10	1.00	1.10	0.67	0.20	-0.27	0.04	1.48	1.12	0.53	1.00	-0.40
Tegarai	0.11	-0.54	-0.01	3.17	6.66	-0.10	-1.14	1.47	-0.82	-0.95	0.02	-0.08
Lubai Tengah	-1.04	0.63	1.53	1.39	0.38	-0.14	-0.07	0.30	-0.56	0.12	-0.39	2.88
Ukong	0.69	-0.57	2.30	-0.51	-0.25	-0.46	1.42	1.83	0.21	-0.01	1.19	1.23
Medamit Nanga	2.20	0.32	3.14	0.52	-0.41	-1.11	-0.73	0.43	1.53	0.14	-0.35	-0.49
Lubok Lalang	-0.42	0.25	1.07	-0.60	0.69	-0.28	0.79	-0.16	0.22	0.42	0.59	-0.84
Merbau	-0.91	-0.06	-0.50	-0.04	0.38	-0.14	-0.46	1.24	-0.55	-0.41	-1.18	-0.92
Ulu Medalam	-0.02	-1.18	-0.81	-0.38	0.97	-1.19	-0.92	0.22	-1.01	1.78	1.08	1.52
Ulu Medamit	-0.03	0.43	2.13	-0.31	3.62	-0.43	-0.27	0.36	-0.09	0.99	0.05	-0.34
Setuan	-0.50	0.14	-0.97	-1.19	0.89	-0.33	-0.89	-0.37	-1.04	0.38	3.14	-1.16
Long Napir	-0.29	0.93	0.37	-0.24	5.50	-1.17	1.37	-0.64	-0.61	-0.31	0.93	0.17
Rutoh	0.31	-0.73	-0.17	-0.84	0.41	-0.17	-0.19	-0.71	-0.50	-0.42	-0.12	-0.65

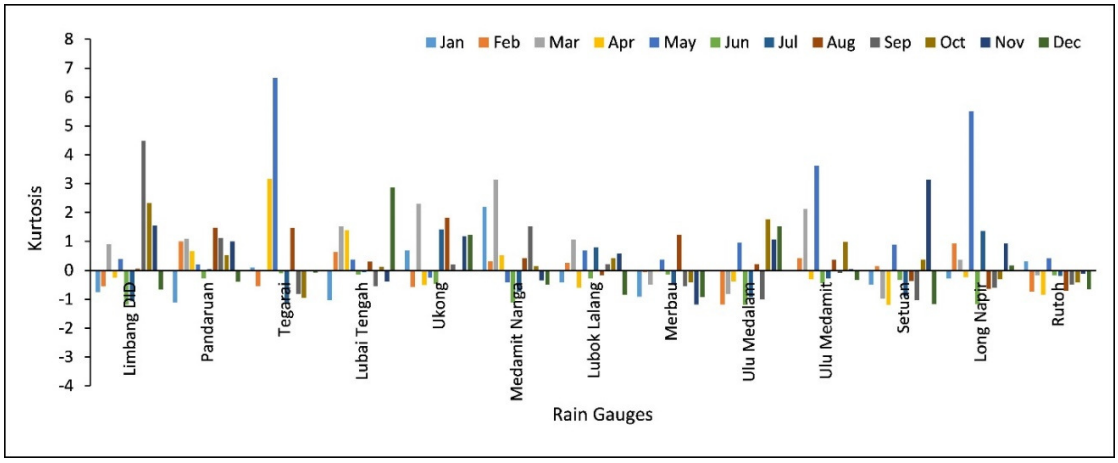

Figure 4.9: Graphical representation of station-wise kurtosis assessed for monthly rainfall in the LRB.

Kurtosis values of seasonal, inter-monsoon and annual rainfall show less variation in the data range compared to monthly rainfall (Table 4.10, Figure 4.10). In the case of seasonal rainfall, the Kurtosis ranges from -0.30 (Long Napir) to 4.63 (Lubok Lalang) for SWM and -0.73 (Long Napir) to 1.94 (Rutoh) for NEM. During SWM, twelve stations showed positive value of Kurtosis whereas in NEM, eleven stations showed negative value. Considering the IM periods, it varies in the range of -1.19 (Setuan) to 3.17 (Tegarai) and -0.95 (Tegarai) to 2.33 (Limbang DID) for April and October respectively. In the month of April, nine stations recorded negative Kurtosis and in October, eight stations exhibit positive Kurtosis. At the same time, Kurtosis of annual rainfall data ranges from -1.03 to 1.48 corresponding to the rain gauge stations Long Napir and Ulu Medalam with nine stations showing positive Kurtosis.

Considering the monthly, seasonal, inter-monsoon and annual rainfall data, Kurtosis values was found to fluctuate between negative and positive, but none showed higher value. However, considering the overall results, it can be concluded that most stations in the LRB possessed near normal distribution in rainfall with slight variation between months of May and September, particularly in stations namely Tegarai, Long Napir and Limbang DID.

Table 4.10: Station-wise kurtosis assessed for seasonal, inter-monsoon and annual rainfall in the LRB.

Stations	Seasonal RF		Inter-monsoon RF		Annual Rainfall
	SWM	NEM	April	October	
Limbang DID	0.94	-0.40	-0.25	2.33	-0.85
Pandaruan	0.80	-0.05	0.67	0.53	-0.05
Tegarai	0.56	-0.22	3.17	-0.95	0.84
Lubai Tengah	0.82	-0.69	1.39	0.12	-0.71
Ukong	0.81	-0.59	-0.51	-0.01	0.16
Medamit Nanga	1.94	-0.10	0.52	0.14	1.03
Lubok Lalang	4.63	-0.57	-0.60	0.42	0.55
Merbau	1.45	-0.45	-0.04	-0.41	0.43
Ulu Medalam	1.40	-0.04	-0.38	1.78	1.48
Ulu Medamit	2.25	0.31	-0.31	0.99	0.74
Setuan	0.07	-0.44	-1.19	0.38	0.35
Long Napir	-0.30	-0.73	-0.24	-0.31	-1.03
Rutoh	0.20	1.94	-0.84	-0.42	1.27

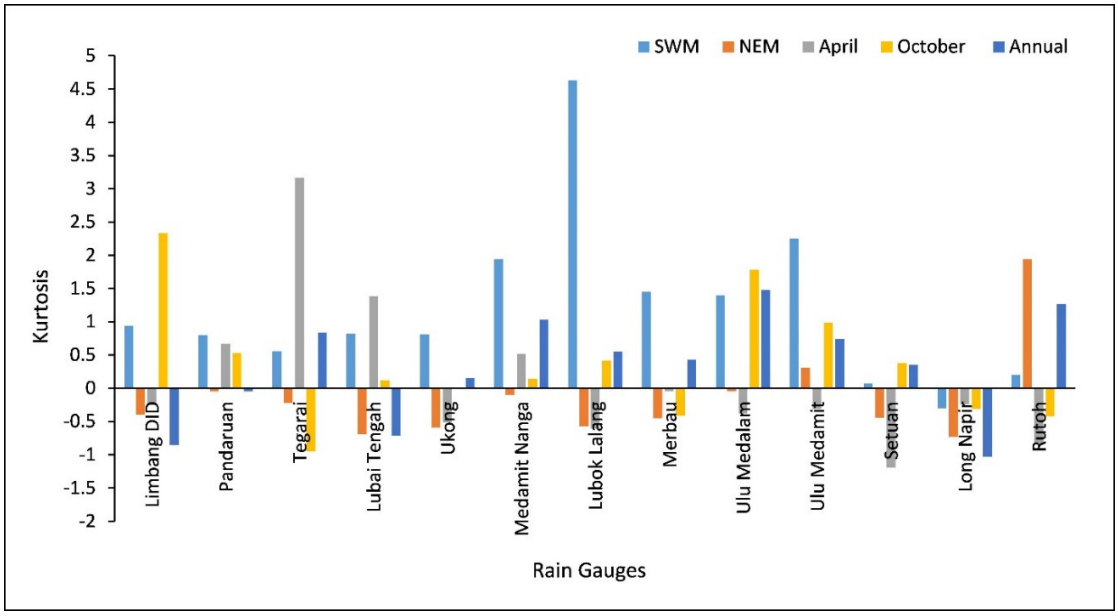

Figure 4.10: Graphical representation of station-wise kurtosis assessed for seasonal, inter-monsoon and annual rainfall in the LRB.

4.2.2.4 Coefficient of variation (CV)

Dispersion of the data from the mean value can be identified with the estimation of coefficient of variation (CV). Higher value of CV (≈1) indicates a greater dispersion of data from mean value i.e. very scattered nature of the data. In the present research, CV was analysed for the monthly, seasonal, inter-monsoon and annual rainfall data to understand the precision of data sets and its dispersion. It was noted that, CV of all the data set found to be very low compared to the limiting value 1.

Results of CV derived for station-wise monthly rainfall was tabulated in Table 4.11 and shown in Figure 4.11. Considering the monthly rainfall, in the month of January and February the minimum value of CV was showed by Ulu Medamit (0.34 and 0.32) and the maximum value by Pandaruan (0.59 and 0.60). In addition to Pandaruan, Limbang DID and Tegarai also shows the maximum CV in January. Minimum value (0.30) of CV in March was shown by Merbau and Limbang DID showed the maximum (0.63) value. In the month of April, rain gauging stations Merbau, Ulu Medamit and Setuan showed the lowest (0.29) value of CV and Ukong and Rutoh showed the highest (0.47) value. During the month of May, CV ranges between 0.31 (Merbau) and 0.53 (Tegarai). At the same time, rain gauging station Rutoh showed the minimum value of CV (0.36 and 0.38) in June and July months but the maximum value was shown by rain gauging station Ulu Medalam (0.55) in June and Lubok Lalang (0.57) in July. In the month of July, in addition to Rutoh, Setuan (0.38) also recorded the lowest value of CV. Similarly, the minimum value of CV in August and September was shown by the station Setuan (0.41 and 0.34) whereas the maximum value was associated with Limbang DID (0.70) and Pandaruan (0.57) in August and September respectively. In the month of October and November the rain gauging station Merbau recorded the least values of CV (0.24 and 0.18) but the highest values were recorded by Ulu Medalam (0.50) and Limbang DID (0.38) respectively. During the month of December, CV ranges between 0.22 (Ulu Medamit) and 0.40 (Lubai Tengah).

Table 4.11: Station-wise coefficient of variation (CV) assessed for monthly rainfall in the LRB.

Stations	Jan	Feb	Mar	Apr	May	Jun	Jul	Aug	Sep	Oct	Nov	Dec
Limbang DID	0.59	0.59	0.63	0.37	0.46	0.48	0.55	0.70	0.49	0.48	0.38	0.33
Pandaruan	0.59	0.60	0.53	0.36	0.44	0.53	0.48	0.68	0.57	0.40	0.33	0.37
Tegarai	0.59	0.56	0.52	0.44	0.53	0.50	0.50	0.68	0.53	0.43	0.36	0.38
Lubai Tengah	0.55	0.59	0.52	0.44	0.37	0.49	0.49	0.60	0.50	0.38	0.32	0.40
Ukong	0.56	0.48	0.51	0.47	0.33	0.45	0.48	0.53	0.49	0.36	0.33	0.35
Medamit Nanga	0.54	0.53	0.43	0.45	0.44	0.50	0.51	0.56	0.55	0.33	0.32	0.34
Lubok Lalang	0.50	0.48	0.44	0.34	0.38	0.45	0.57	0.61	0.40	0.31	0.25	0.33
Merbau	0.40	0.41	0.30	0.29	0.31	0.43	0.45	0.60	0.42	0.24	0.18	0.34
Ulu Medalam	0.40	0.42	0.35	0.30	0.38	0.55	0.49	0.45	0.44	0.50	0.27	0.36
Ulu Medamit	0.34	0.32	0.37	0.29	0.42	0.47	0.53	0.49	0.51	0.33	0.24	0.22
Setuan	0.42	0.34	0.41	0.29	0.33	0.40	0.38	0.41	0.34	0.31	0.24	0.33
Long Napir	0.49	0.57	0.44	0.33	0.36	0.47	0.44	0.57	0.46	0.35	0.33	0.39
Rutoh	0.41	0.44	0.38	0.47	0.40	0.36	0.38	0.46	0.40	0.36	0.23	0.25

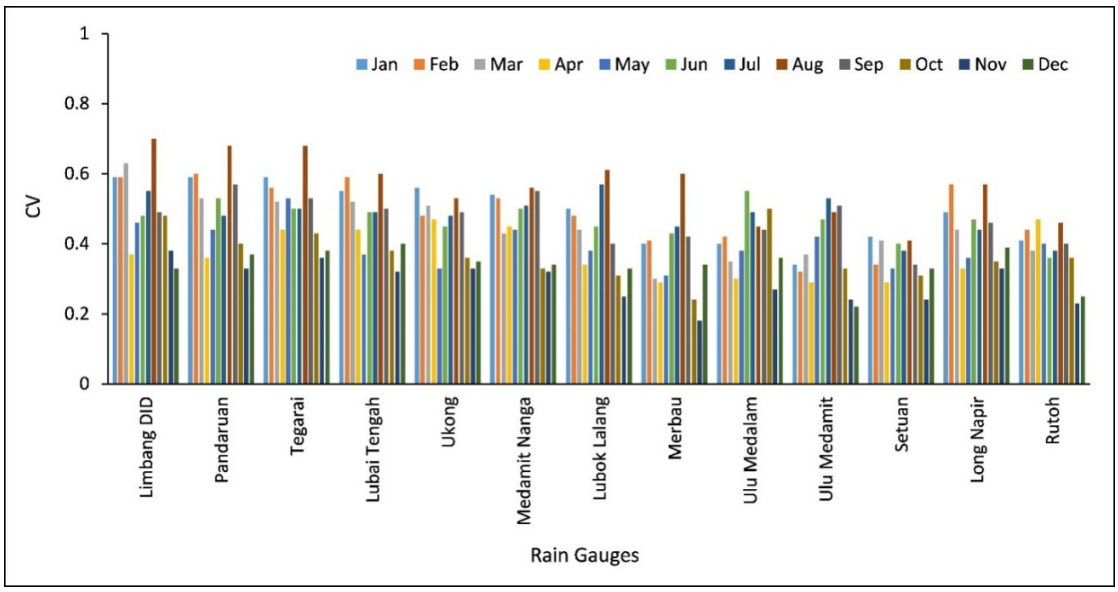

Figure 4.11: Graphical representation of station-wise coefficient of variation (CV) assessed for monthly rainfall in the LRB.

Considering the seasonal, inter-monsoon and annual rainfall, CV shows lower value than the monthly rainfall (Table 4.12 and Figure 4.12). During SWM, CV ranges between 0.16 (Setuan) and 0.31 (Tegarai). Low value of CV was recorded by Ulu Medalam and Ulu Medamit (0.14) in NEM whereas the highest value was shown by Limbang DID (0.30). Considering the inter-monsoon periods, CV ranges from 0.29 (Merbau, Ulu Medamit and Setuan) to 0.47 (Ukong and Rutoh) in April and 0.24 (Merbau) to 0.50 (Ulu Medalam) in October. In the case of annual rainfall, Setuan (0.09) shows the minimum value of CV, whereas Limbang DID (0.20) shows the maximum value.

The overall results of CV assessed for monthly, seasonal, inter-monsoon and annual rainfall shows a low value compared to the limiting value (1) which indicates that there is less dispersion in rainfall data collected from rain gauging stations in the LRB. This is also a signal of good precision of the data.

Table 4.12: Station-wise coefficient of variation (CV) assessed for seasonal, inter-monsoon and annual rainfall in the LRB.

Stations	Seasonal RF		Inter-monsoon RF		Annual Rainfall
	SWM	NEM	April	October	
Limbang DID	0.29	0.30	0.37	0.48	0.20
Pandaruan	0.26	0.27	0.36	0.40	0.16
Tegarai	0.31	0.25	0.44	0.43	0.19
Lubai Tengah	0.27	0.26	0.44	0.38	0.17
Ukong	0.25	0.24	0.47	0.36	0.16
Medamit Nanga	0.29	0.24	0.45	0.33	0.17
Lubok Lalang	0.28	0.21	0.34	0.31	0.15
Merbau	0.25	0.16	0.29	0.24	0.12
Ulu Medalam	0.25	0.14	0.30	0.50	0.10
Ulu Medamit	0.26	0.14	0.29	0.33	0.12
Setuan	0.16	0.15	0.29	0.31	0.09
Long Napir	0.25	0.25	0.33	0.35	0.18
Rutoh	0.18	0.15	0.47	0.36	0.13

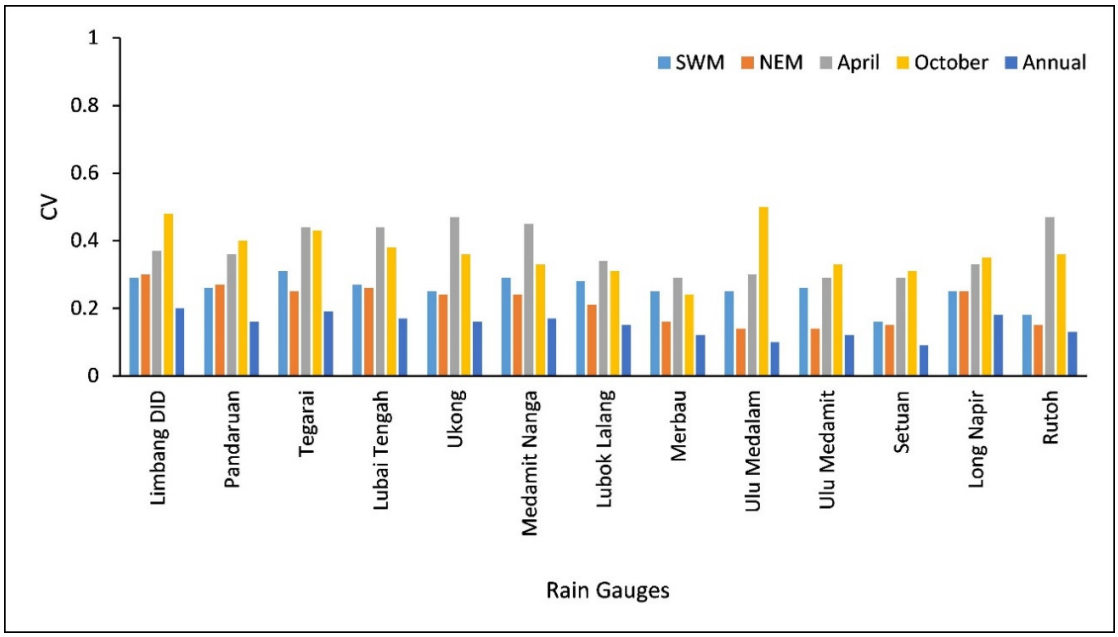

Figure 4.12: Graphical representation of station-wise coefficient of variation (CV) assessed for seasonal, inter-monsoon and annual rainfall in the LRB.

4.2.3 Spatial distribution of rainfall in the LRB

To understand the spatial distribution of rainfall in the LRB, average monthly, seasonal and annual rainfall corresponding to each rain gauging station, the data was spatially interpolated using ArcGIS 9.3 software (spatial analyst extension) to generate the spatial distribution map. Rainfall values were assigned to the corresponding rain gauges and spatially interpolated through the inverse distance weighted (IDW) method. IDW is a comparatively flexible and simplest method of interpolation and offers relatively accurate results when the observation point's density is very low compared with size of the study area (Burrough & McDonnell, 1998; Lu & Wong, 2008; Chen & Liu, 2012). IDW uses weighted average values from surrounding locations during interpolation to calculate the values for non-measured locations (Burrough & McDonnell, 1998; Apaydin et al., 2004; Ali et al., 2012; Yang et al., 2015). Results of spatial distribution of rainfall in the LRB are briefly discussed in the following sections.

4.2.3.1 Spatial distribution of monthly rainfall

Spatial pattern of average rainfall in each month was generated and shown in Figure 4.13. In general, spatial distribution of monthly rainfall in the LRB shows a common pattern (January to December) with slight variations in the total amount of rainfall received during each month. Considering the rainfall distribution in the month of January, it shows a domain of higher and lower rainfall located in the lower and upper catchment regions (245 to 472mm). Findings show regions above the rain gauging station Setuan experience domains of lower rainfall, constituted by Setuan, Long Napir and Rutoh whereas all other rain gauges contributed to moderate and high rainfall domain which is spatially spread in the lower catchment region. It was also noted that, rain gauging stations Ulu Medalam in the western side and Ulu Medamit in the eastern side of the LRB shows highly localised, high rainfall zones. In the month of February, the rainfall distribution showed slight variations in the low and high rainfall domains (186 to 389mm). Though the rain gauging stations Ulu Medalam and Ulu Medamit continued to remain as the foci of high rainfall, a few stations in lower catchment area started to show low rainfall (Limbang DID) along with those identified in the upper catchment area. In the months of March and April, rainfall distribution in the LRB shown a large variation with increase in the lower rainfall domains in lower catchment region (193 to 403mm and 248 to 450mm in March and April respectively). Along with Setuan, Long Napir, Rutoh and Limbang DID, the rain gauging stations Pandaruan and Ukong also have comparatively low rainfall. However, during

these months also Ulu Medalam and Ulu Medamit remains as the foci of high rainfall in the LRB.

During the month of May, rainfall distribution in the LRB showed comparatively larger domains of high rainfall in the middle to lower catchment region, with domains of low rainfall in the upper catchment (237 to 404mm). It was observed that, the boundary of high rainfall domain was controlled by rain gauging stations Tegarai, Ulu Medalam and Ulu Medamit. Considering the months June, July and August, rainfall distribution in the LRB was similar, with a central high rainfall domain bounded with low rainfall domains in lower and upper catchment (220 to 354mm, 188 to 329mm and 205 to 349mm in June, July and August respectively). Limbang DID and Pandaruan in the lower catchment and Setuan, Long Napir and Rutoh in the upper catchment controls the low rainfall domains whereas Tegarai, Ulu Medalam and Ulu Medamit contribute more to the high rainfall domain. It was observed that there were same patterns of rainfall distribution that prevailed in the months of September, October, November and December with high rainfall domain in middle catchment, and low rainfall domains in lower and upper catchment in the LRB (214 to 356mm, 260 t0 436mm, 291 to 490mm and 248 to 463mm in September, October, November and December respectively). As identified earlier, the high rainfall domains are controlled by Tegarai, Ulu Medalam and Ulu Medamit whereas the low rainfall domains are contributed by Limbang DID and Pandaruan in the lower catchment and Setuan, Long Napir and Rutoh in the upper catchment.

Overall, considering the monthly rainfall distribution pattern in the LRB, it was noted that though the basin receives similar rainfall in most stations, rainfall in the LRB shows a non-uniform distribution pattern. The dominant pattern identified was the clustering of rain gauges which defined domains of high and low rainfall. Notable characteristics in these domains are the orientation i.e. the high rainfall domain was mainly controlled by two rain gauges such as Ulu Medalam and Ulu Medamit (located in west and east side of middle catchment region in the LRB) along with Tegarai in the lower catchment region. At the same time, low rainfall domains in lower catchment was mainly controlled by Limbang DID and Pandaruan whereas those in the upper catchment by Long Napir. These facilitates the identification of rainfall corridor, which oriented in NE-SW direction and was mostly concentrated in the middle catchment in the LRB.

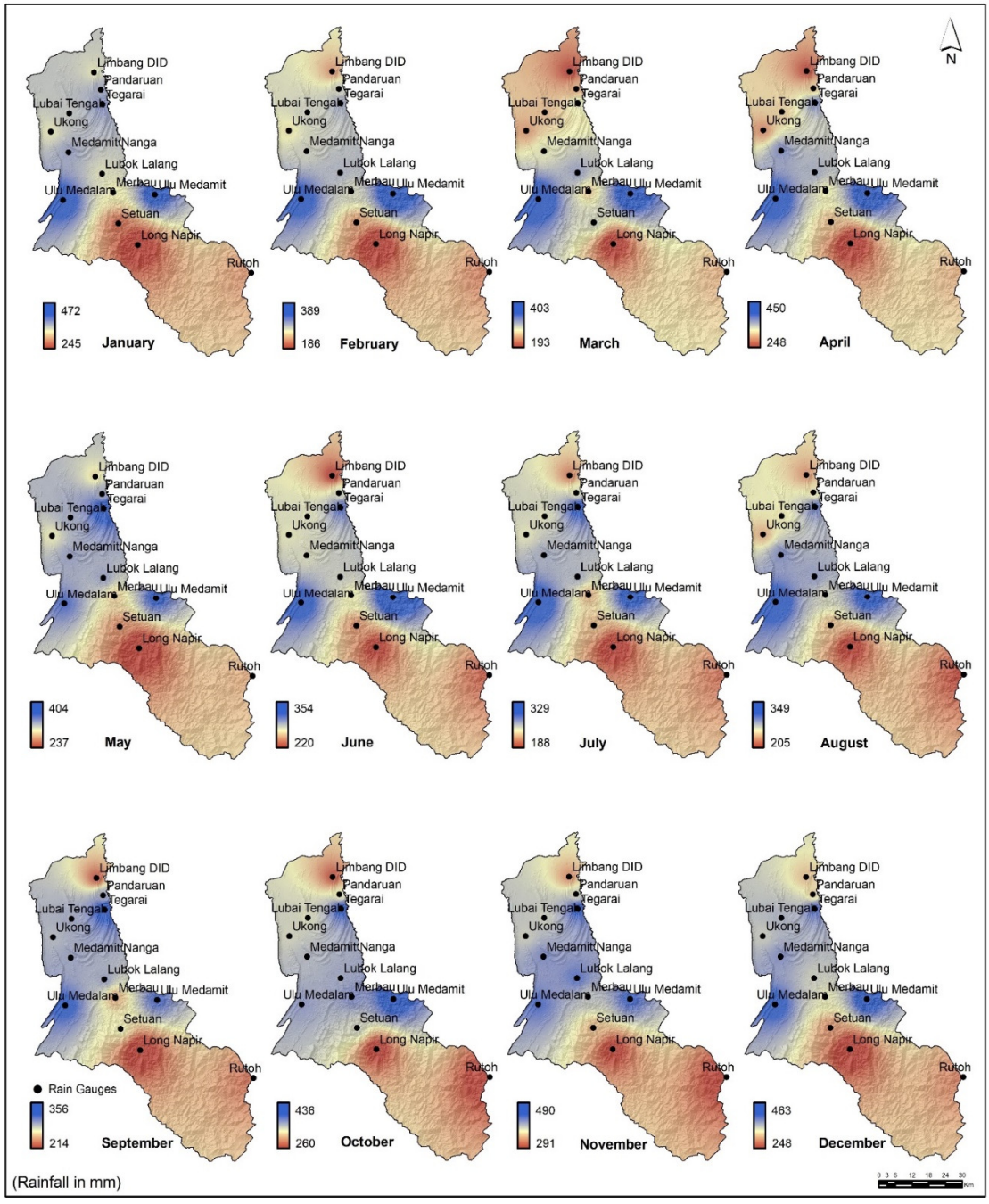

Figure 4.13: Spatial distribution of average monthly rainfall in the LRB.

4.2.3.2 Spatial distribution of seasonal and inter-monsoon rainfall

Monsoon rainfall in the LRB reflects accumulation of five months of total rainfall in SWM and NEM seasons, which not only shows the difference in total amount but also shows variation in distribution patterns (Figure 4.14). During SWM, spatial pattern of rainfall in the LRB shows a concise pattern in the months of May to September, with domain of high rainfall bound by low rainfall domains in the upper and lower catchment (1064 to 1725mm) (Figure 4.14a). As identified in the monthly rainfall patterns, the high rainfall domain during SWM was contributed mainly by three rain gauging stations namely Tegarai in the lower catchment and Ulu Medalam (west) and Ulu Medamit (east) in the middle catchment region. Limbang DID, Pandaruan and Ukong shows comparatively low rainfall in the lower catchment whereas Long Napir became the foci of lowest rainfall in the upper catchment along with Setuan and Rutoh. Rain gauging stations Lubai Tengah, Medamit Nanga and Lubok Lalang shows moderate rainfall and fall in the domain defined by high rainfall.

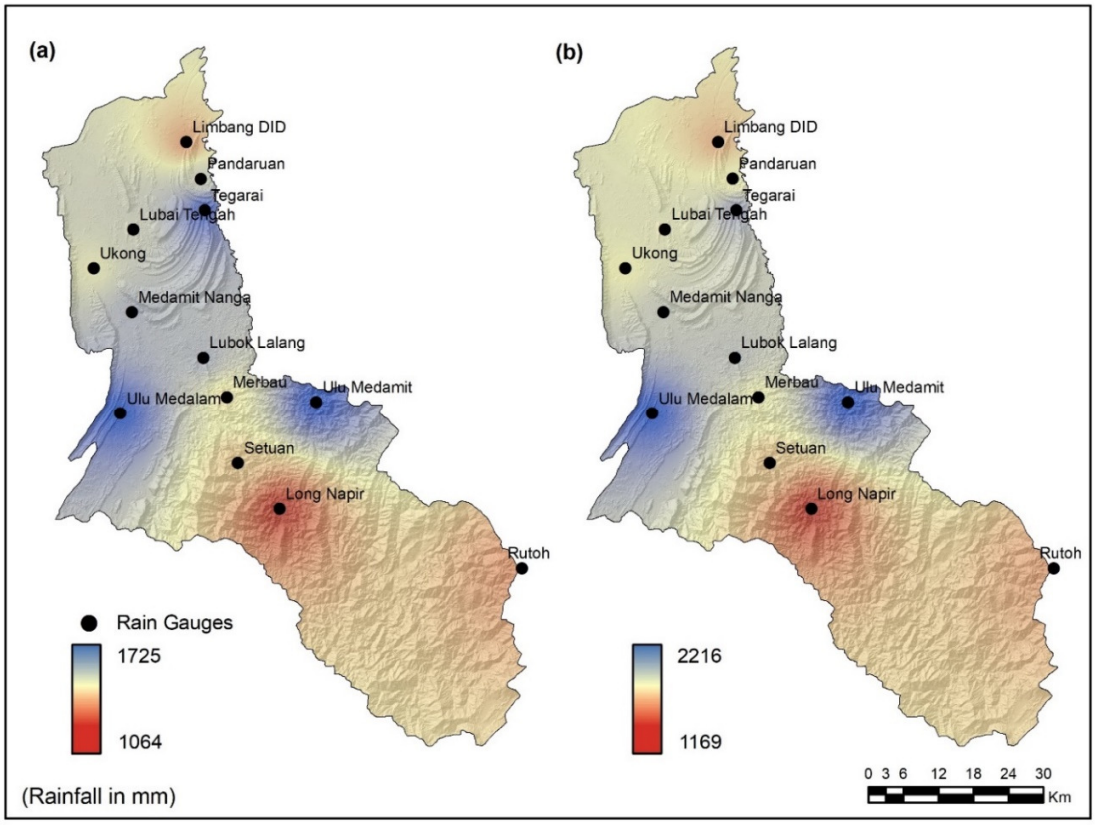

Figure 4.14: Spatial distribution of average seasonal rainfall in the LRB (a) SWM season and (b) NEM season.

Spatial pattern of rainfall distribution in NEM shows dissimilar spatial spread than SWM and reflects an overall distribution pattern observed in the months of November to March (Figure 4.14b). During this season, though the LRB recorded higher rainfall (1169 to 2216mm), spatial pattern indicates dominance of moderate and low rainfall. Higher rainfall domain shows a weak distribution with two prominent isolated locations around Ulu Medalam and Ulu Medamit in west and east side of the LRB in the middle catchment. Moderate rainfall domain in the lower catchment was controlled by Limbang DID, Pandaruan, Lubai Tengah and Ukong whereas in the middle catchment, areas around Merbau and Setuan show moderate rainfall. Long Napir remains as the focus of low rainfall in the upper catchment area.

Considering the inter-monsoon periods, both months show slightly different rainfall distribution patterns (Figure 4.15). During the month of April, high rainfall domain in the middle catchment region was dominant and Ulu Medalam and Ulu Medamit along with Tegarai, Medamit Nanga and Lubok Lalang defines the domain. Among these stations, Ulu Medalam and Ulu Medamit show comparatively high rainfall. At the same time, low rainfall domain in the lower catchment was contributed mainly by Limbang DID, Pandaruan and Ukong. Merbau and Setuan showed moderate rainfall distribution whereas Long Napir show localised lower rainfall in the upper catchment region. During the month of October, spatial distribution of rainfall in the LRB shows slender variation in the domain extent of low and high rainfall. Remarkable change was noted during this month. It was noted that though the middle catchment region showed high rainfall domain, rainfall distribution was found to be much localised around Tegarai and Ulu Medamit. Along with this, low rainfall domain in upper catchment showed more spatial coverage than April and was due to the combined effect of low rainfall in Long Napir and Rutoh. Moreover, in the lower catchment, low rainfall domain centered on the rain gauging station Limbang DID.

Overall, considering the rainfall distribution during monsoon and inter-monsoon periods in the LRB, a prevailing high rainfall domain in the middle catchment formed by the combination of rain gauging stations Tegarai, Ulu Medalam and Ulu Medamit was identified irrespective of seasons. This high rainfall domain shows variation in its spatial spread towards the lower catchment of the LRB, but not to the upper catchment region (above rain gauging station Setuan). It was also observed that the area around Long Napir consistently receives low

rainfall in the LRB (upper catchment). Regions around the rain gauging station Limbang DID in the lower catchment and Rutoh in upper catchment was also marked as domains of low rainfall.

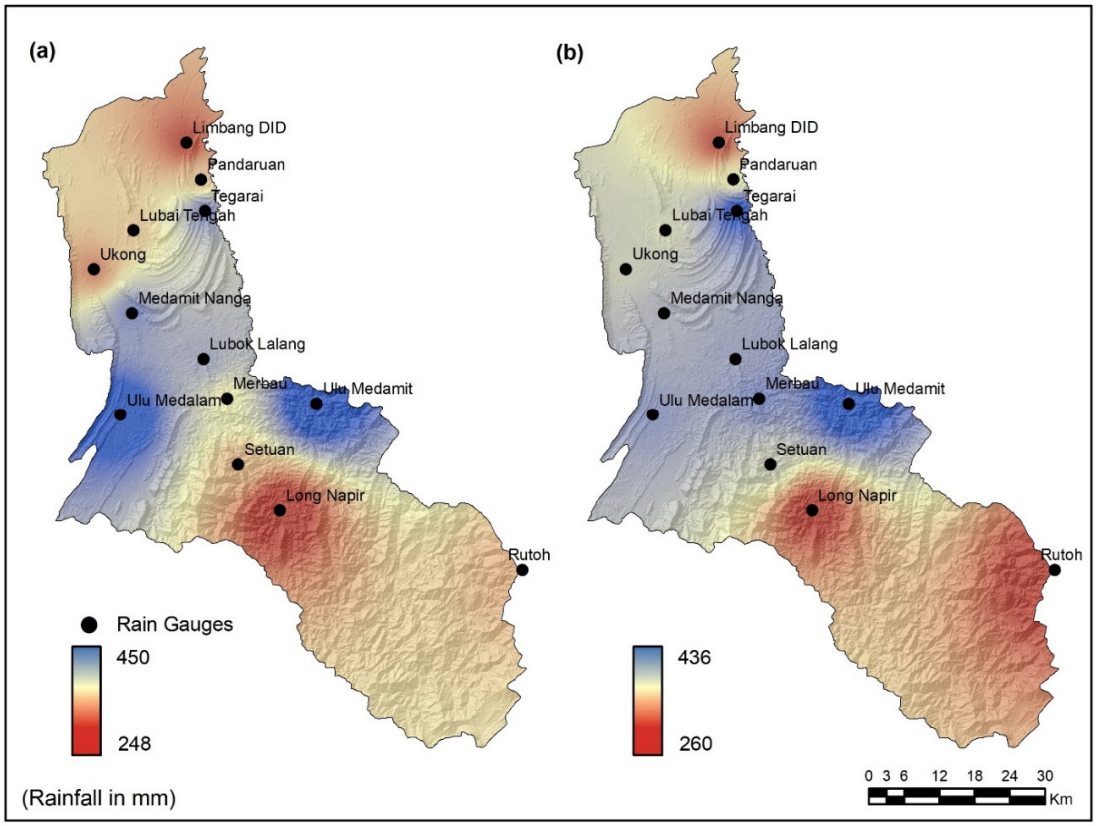

Figure 4.15: Spatial distribution of average inter-monsoon rainfall in the LRB (a) April and (b) October.

4.2.3.3 Spatial distribution of annual rainfall

Annual rainfall distribution in the LRB well reflected, with the cumulative effects of rain gauging stations receiving high and low rainfall throughout the year. The average annual rainfall in the LRB varies in the range of 2733 to 4772mm and shows distinct domains of high and low rainfall (Figure 4.16). Domains of high rainfall was found to be located in the middle catchment region of the river basin and was formed by the rain gauging stations namely Tegarai in the lower portion, Medamit Nanga and Lubok Lalang in the middle and Ulu Medalam and Ulu Medamit in west and east side of the LRB. Among this, high rainfall distribution was

concentrated around Tegarai, Ulu Medalam and Ulu Medamit. However, considering the occurrence of low rainfall domains in the LRB, regions around Limbang DID in the lower catchment and the area between Long Napir and Rutoh shows comparatively low rainfall distribution in the LRB. It was also noted that the area around Pandaruan, Lubai Tengah, Ukong and Merbau to Setuan shows moderate rainfall domain.

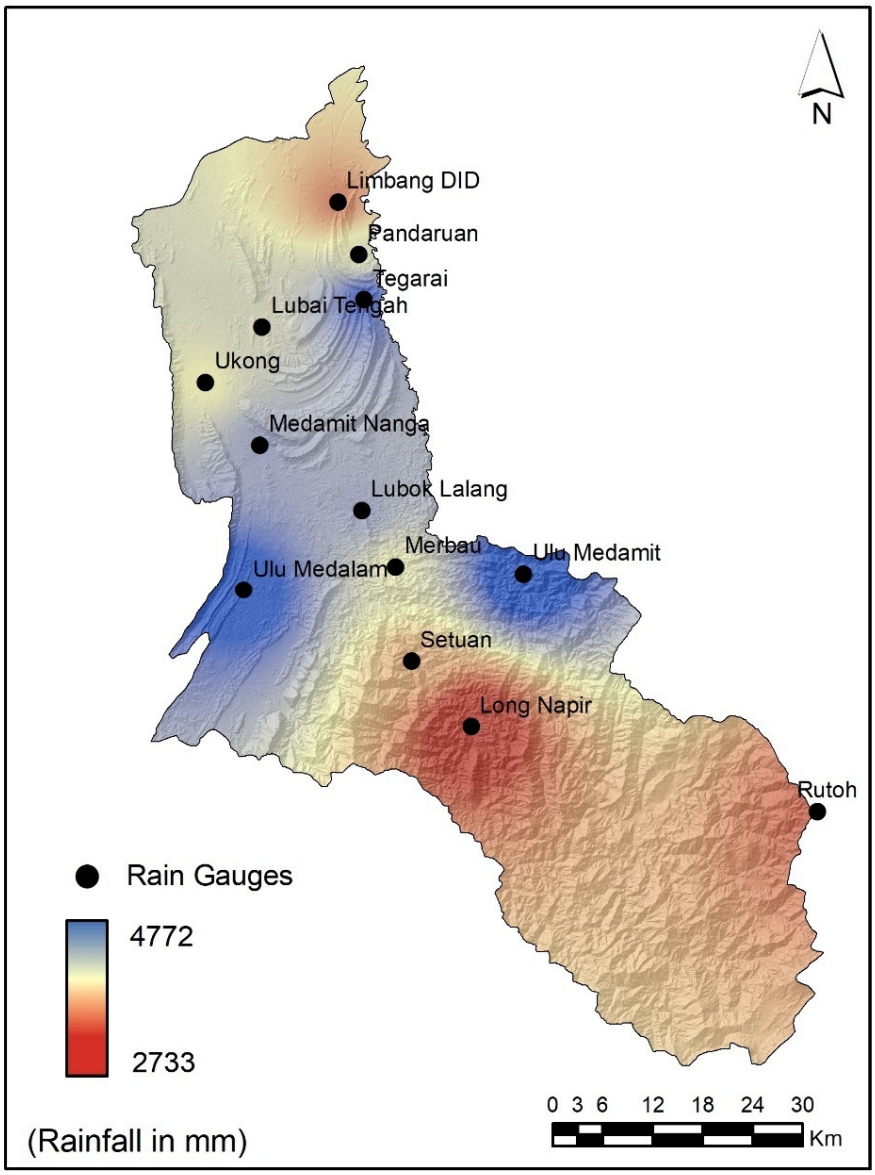

Figure 4.16: Spatial distribution of average annual rainfall in the LRB.

While considering the overall spatial pattern of annual rainfall distribution in the LRB, it can be concluded that the LRB possesses a specific high rainfall domain in the middle catchment area, encircled by low rainfall domains in the lower and upper catchment region. Though five stations contributed the high rainfall domain in the LRB, it was highly localised around rain gauging stations Tegarai, Ulu Medalam and Ulu Medamit.

4.2.4 Relationship between rainfall and elevation

In order to understand the relationship between rainfall and elevation in the LRB, linear regression and correlation analysis was performed. Elevation of each rain gauge location was extracted from the digital elevation surface (30m Shuttle Radar Topographic Mission - SRTM data) and the average annual rainfall data corresponding to the each rain gauge was used to analyse the relationship (Table 4.13).

Table 4.13: Rain gauging stations with elevation and average annual rainfall.

Stations	Elevation (m)	Average annual rainfall (mm)
Limbang DID	7	3328.73
Pandaruan	16	3801.20
Tegarai	22	4395.26
Lubai Tengah	31	3865.32
Ukong	17	3742.42
Medamit Nanga	20	4082.87
Lubok Lalang	111	4071.66
Merbau	290	3780.92
Ulu Medalam	46	4709.46
Ulu Medamit	509	4771.86
Setuan	153	3542.18
Long Napir	160	2732.94
Rutoh	1532	3243.47

Among the thirteen rain gauges, two are in higher elevation (Ulu Medamit (509m) and Rutoh (1532m)), while four stations shows elevation range of 100 to 290m, and remaining seven rain gauges are located in areas having elevations of below 50m. However, while analysing the inter-relationship between elevation and rainfall in the LRB, it was noted that rainfall was not well correlated with elevation (Figure 4.17). Rainfall and elevation in the LRB

show a very weak correlation with R^2 value of 0.048 and *r* of -0.22. At the same time, it was also noted that there was a clustering of rain gauges in lower elevation, which shows comparatively higher average annual rainfall.

However, considering the dominant cluster identified, it was noted that rain gauging stations located at elevations of less than 50m receives comparatively higher amount of rainfall than those recorded in the station above 100m which shows higher correlation (*r*=0.83) and best fit (R^2 = 0.68) (Figure 4.18). This indicates the occurrence of higher rainfall regime in lower elevation and middle catchment of the LRB, which is surrounded by high elevated hills. This inference was also supported by the high rainfall received in rain gauging station Ulu Medamit, though it shows an elevation higher than 500m, but it is located in middle catchment region. Spatial pattern maps of monthly, seasonal and annual rainfall also shows similar characteristics i.e. occurrence of higher rainfall regime in the middle to lower catchment, which was well discussed in the previous section. This suggests the requirement for further investigation of orographic effect on rainfall in the LRB along with wind directions throughout the year, particularly during the monsoon seasons.

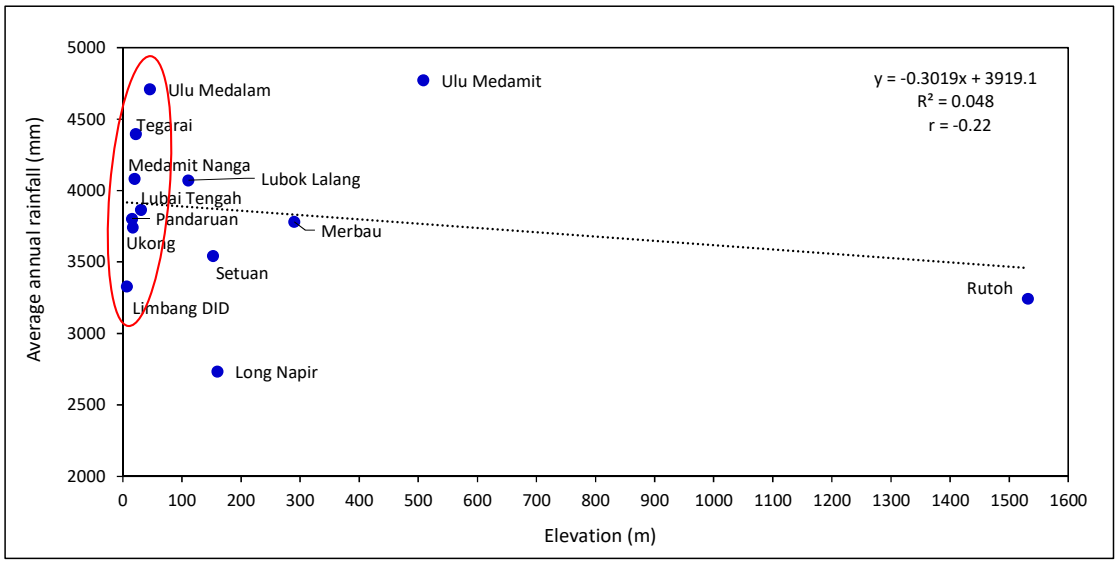

Figure 4.17: Linear plot explaining relationship between average annual rainfall and elevation in the LRB.

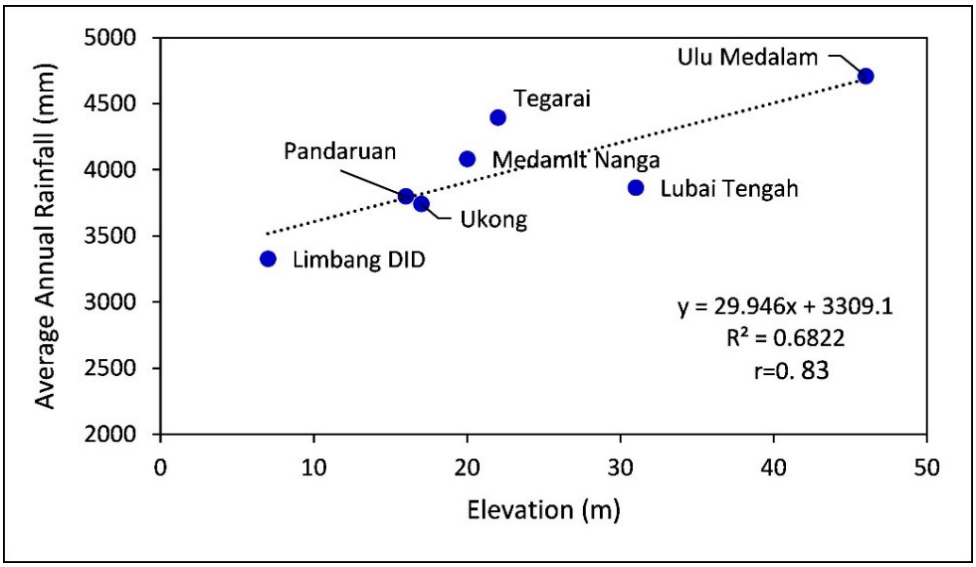

Figure 4.18: Linear plot explaining rain gauges showing higher correlation between average annual rainfall and elevation in the LRB.

4.2.5 Statistical rainfall trends

4.2.5.1 Monthly rainfall trend

Monthly rainfall measurements from each stations in the respective periods were considered for the analysis to determine the monthly trend of rainfall in the LRB. In order to run the Mann Kendall (MK) and Spearman's Rho (SR) tests, monthly rainfall of the individual stations were arranged separately and processed to determine the statistical trends at varying significance (confidence level ranging from 90 to 99%). Results of Mann Kendall (MK) and Spearman's Rho (SR) tests were shown in Table 4.14 and Figure 4.19 and 4.20. In general, it has been noted that, most of the stations show either increasing or decreasing trends in each month, but few stations show no trends in some months (trend ≤±0.05mm/year). At the same time, there are a few stations which consistently showing statistically significant trends throughout the year.

In the month of January, all stations except Lubai Tengah showed increasing trends in both tests (MK and SR tests). Among the stations, statistically significant increasing trends in both tests are shown by Long Napir (2.13 and 2.32mm/year) and Ulu Medamit (2.03 and 2.08mm/year) at 95% confidence level, whereas Rutoh recorded significant increasing trends in the SR test (1.60mm/year with 90% confidence). Rain gauging station Lubai Tengah showed a

non-significant decreasing trend (-0.39 and -0.31mm/year) in both tests. All other stations showed a non-significant increasing trend which ranges from 0.21 to 1.54mm/year and 0.24 to 1.54mm/year for MK and SR respectively. In the month of February, eleven stations were showing increasing trends and two stations showed decreasing trends. Rain gauging station Long Napir continued to show statistically significant increasing trends (1.70mm/year in SR test with 90% confidence), whereas all other stations showed non-significant increasing trends, which varies between 0.11 to 1.61mm/year in MK and 0.20 to 1.64mm/year in SR tests. At the same time, rain gauging stations Lubok Lalang (-1.18 and -1.33mm/year) and Setuan (-0.84 and -0.48mm/year) showed a non-significant decreasing trend. During the month of March, there was an increase in the number of stations showing decreasing trends. In March, seven stations show increasing trends and six stations were showing decreasing trends in rainfall. Among the stations, Limbang DID (2.42 and 2.30mm/year) and Long Napir (1.99 and 2.34mm/year) displayed a significant increasing trend at 95% confidence level in both MK and SR tests. At the same time, rain gauging station Ulu Medalam showed a significant decreasing trend of -1.54mm/year at 90% confidence level in MK test. Non-significant increasing trends during March range from 0.39 to 1.15mm/year in MK and 0.39 to 1.21mm/year in SR test. The non-significant decreasing trend varies in the range of -0.84 to -0.08mm/year in MK and -1.41 to -0.41mm/year in SR test. Rain gauging stations Merbau (-0.03mm/year), Rutoh (-0.02mm/year) and Setuan (0.01mm/year) shows no trend in SR test during the month. Considering the trend characteristics of rain gauges in the month of April, seven stations showed increasing trends and six stations recorded decreasing trends. During this month, rain gauging station Long Napir only shows a statistically significant increasing trend (1.86 and 1.95mm/year at 90% confidence level) in MK and SR tests. The non-significant increasing trends in April range between 0.08 to 1.26mm/year and 0.10 to 1.42mm/year for MK and SR tests respectively and the decreasing trend varies in the range of -1.56 to -0.25mm/year in MK and -1.64 to -0.16mm/year in SR test.

In the month of May, three stations had shown an increasing trend, eight stations shown decreasing trends and remaining two stations did not show any trend (zero or very low value in both tests). It is to be noted that, rain gauging station Long Napir continued the statistically significant increasing trends (2.07 and 2.06mm/year at 95% confidence level) and Setuan (0.84 and 0.60mm/year) and Ulu Medalam (0.63 and 0.62mm/year) continued to show non-significant increasing trends. Rain gauging stations which had shown statistically non-

significant decreasing trends vary in the range of -1.18 to -0.15mm/year and -1.35 to -0.10mm/year for MK and SR tests respectively. At the same time, rain gauging stations Tegarai and Lubai Tengah showed no trend in MK test (zero value) and no trend (0.03mm/year) and very weak decreasing trend (-0.16mm/year) in SR test. A drastic change in trend pattern was observed in the month of June with eight stations showing increasing trends, four stations showing decreasing trends and one station showing weak and no trend. It was also noted that none of the station had shown either a statistically significant increase or decrease in rainfall trend during this month. Rain gauging stations namely Limbang DID, Pandaruan, Tegarai, Lubai Tengah, Ukong, Medamit Nanga, Lubok Lalang and Long Napir shows non-significant increasing trends (0.18 to 1.52mm/year and 0.10 to 1.56mm/year in MK and SR respectively) whereas Ulu Medalam, Ulu Medamit, Setuan and Rutoh shows non-significant decreasing trends (-1.26 to -0.63mm/year and -1.24 to -0.70mm/year in MK and SR respectively). Rain gauging station Merbau shows very weak increasing trend in MK test (0.06mm/year) and no trend in SR test (-0.05mm/year). The non-significant nature of rainfall trend was continued to the month of July with a reversal in trend pattern i.e. most stations shown a non-significant decreasing trend. Among the rain gauges, two stations namely Long Napir (0.71 and 0.73mm/year) and Setuan (0.07 and 0.25mm/year) show a non-significant increase in rainfall trend, whereas eight stations show a non-significant decrease in rainfall trend. The decreasing trend in July ranges from -1.00 to -0.28mm/year and -0.97 to -0.34mm/year for MK and SR tests respectively. At the same time, rain gauging stations Lubai Tengah (-0.03 and -0.01mm/year) and Ulu Medalam (0.00 and -0.04mm/year) show no trend and Rutoh (-0.07mm/year in MK and SR) showed very weak decreasing trend in rainfall. Considering the trend patterns of rain gauging stations in the month of August, a sudden shift from the previous month was observed with ten stations showing non-significant increasing trend and three stations shown a non-significant decreasing trend. Among the stations, dominant non-significant increasing trends are shown by Limbang DID, Pandaruan, Lubai Tengah, Merbau, Ulu Medalam and Long Napir and the non-significant increasing trends vary in the range of 0.11 to 1.24mm/year in MK and 0.07 to 1.30mm/year in SR tests. Rain gauging stations Ukong (-0.13 and -0.11mm/year), Medamit Nanga (-0.12 and -0.25mm/year) and Rutoh (-0.28 and -0.34mm/year) show characteristics of non-significant decreasing trends.

In the month of September, rain gauging stations continued show a shifting trend pattern compared with previous months trend i.e. three stations show an increasing trend and ten stations shown decreasing trends. Increasing trends in rainfalls were shown by Merbau, Ulu Medamit and Long Napir in which Long Napir showed a statistically significant increasing trend (2.03 and 2.01mm/year in MK and SR tests at 95% confidence level). It is to be noted that during this month, few rain gauging stations started showing statistically significant decreasing trends. Among the stations, statistically significant decreasing trends were shown by Tegarai (-1.68 and -1.65mm/year in MK and SR tests at 90% confidence level), Medamit Nanga (-1.66mm/year in in SR test at 90% confidence level) and Ulu Medalam (-1.78 and -1.85mm/year in MK and SR tests at 95% confidence level). Dominant decreasing trend characteristics also continued in the month of October. In this month, three stations showed an increasing trend and the remaining ten stations showed decreasing trend. Rain gauging stations Limbang DID (1.15 and 1.04mm/year), Lubok Lalang (0.18 and 0.27mm/year) and Long Napir (1.25 and 1.43mm/year) showed a non-significant increasing trend. Considering the stations which showing decreasing trends, Ukong (-2.45 and -2.37mm/year) showed the most statistically significant decrease in rainfall at 95% confidence level. The non-significant decreasing trend in rainfall ranges between -1.52 to -0.18mm/year for MK test and -1.58 to -0.13mm/year for SR test respectively.

Table 4.14: Mann Kendall and Spearman's Rho test results for monthly rainfall in the LRB.

Stations	Trend Methods	Jan	Feb	Mar	Apr	May	Jun	Jul	Aug	Sep	Oct	Nov	Dec
Limbang DID	Mann Kendall	0.96	0.80	2.42**	1.19	-0.54	1.09	-0.67	1.24	-0.09	1.15	2.86***	1.83*
	Spearman's Rho	1.11	0.88	2.30**	1.17	-0.44	1.02	-0.75	1.3	-0.17	1.04	2.68***	1.75*
Pandaruan	Mann Kendall	0.93	1.61	1.15	0.45	-0.15	0.44	-0.28	0.88	-0.19	-0.68	0.09	0.29
	Spearman's Rho	0.99	1.64	1.11	0.42	-0.10	0.32	-0.34	0.85	-0.24	-0.61	0.13	0.13
Tegarai	Mann Kendall	0.34	0.95	0.39	1.26	0.00	0.39	-0.89	0.18	-1.68*	-1.10	-0.34	-0.90
	Spearman's Rho	0.32	0.97	0.39	1.42	0.03	0.41	-0.84	0.24	-1.65*	-1.26	-0.34	-0.96
Lubai Tengah	Mann Kendall	-0.39	1.14	0.77	-0.25	0.00	0.77	-0.03	0.95	-1.36	-0.25	0.99	0.04
	Spearman's Rho	-0.31	1.14	0.83	-0.16	-0.16	0.86	-0.01	0.99	-1.20	-0.37	0.86	0.06
Ukong	Mann Kendall	0.21	0.38	-0.44	-1.56	-0.78	0.25	-1.00	-0.13	-0.84	-2.45**	2.22**	0.03
	Spearman's Rho	0.24	0.37	-0.41	-1.64	-0.60	0.23	-0.97	-0.11	-0.83	-2.37**	2.13**	-0.05
Medamit Nanga	Mann Kendall	0.36	0.31	1.15	0.08	-0.55	0.57	-0.36	-0.12	-1.59	-0.18	2.47**	-0.60
	Spearman's Rho	0.35	0.35	1.21	0.10	-0.57	0.49	-0.42	-0.25	-1.66*	-0.13	2.43**	-0.60
Lubok Lalang	Mann Kendall	1.14	-1.18	-0.84	0.18	-1.18	0.18	-0.30	0.11	-0.48	0.18	0.00	0.11
	Spearman's Rho	1.14	-1.33	-0.96	0.24	-1.35	0.10	-0.36	0.07	-0.60	0.27	-0.07	0.15
Merbau	Mann Kendall	1.54	0.54	-0.08	-0.98	-0.31	0.06	-0.73	0.96	0.15	-1.52	0.04	-0.88
	Spearman's Rho	1.54	0.69	-0.03	-1.06	-0.65	-0.05	-0.93	1.07	0.25	-1.47	-0.07	-1.02
Ulu Medalam	Mann Kendall	0.35	0.77	-1.54*	-0.49	0.63	-0.63	0.00	0.84	-1.78**	-0.63	2.52***	-0.39
	Spearman's Rho	0.51	0.29	-1.41	-0.28	0.62	-0.70	-0.04	0.64	-1.85**	-0.57	2.49***	-0.48
Ulu Medamit	Mann Kendall	2.03**	0.11	0.73	-0.28	-0.68	-0.99	-0.68	0.11	0.79	-1.47	-0.06	0.11
	Spearman's Rho	2.08**	0.20	1.00	-0.45	-0.69	-1.24	-0.74	0.15	0.69	-1.58	-0.18	0.08
Setuan	Mann Kendall	0.91	-0.84	-0.14	-0.91	0.84	-1.26	0.07	0.63	-0.63	-1.33	0.77	-0.98
	Spearman's Rho	1.07	-0.48	0.01	-0.95	0.60	-1.19	0.25	0.42	-0.77	-1.36	0.84	-0.92
Long Napir	Mann Kendall	2.13**	1.49	1.99**	1.86*	2.07**	1.52	0.71	0.92	2.03**	1.25	2.13**	2.41**
	Spearman's Rho	2.32**	1.70*	2.34**	1.95*	2.06**	1.56	0.73	1.07	2.01**	1.43	2.21**	2.26**
Rutoh	Mann Kendall	1.47	0.21	-0.14	1.19	-0.49	-0.77	-0.07	-0.28	-0.84	-0.42	1.12	-1.26
	Spearman's Rho	1.60*	0.23	-0.02	1.27	-0.38	-0.95	-0.07	-0.34	-0.79	-0.61	0.98	-1.11
LRB (whole)	Mann Kendall	0.88	1.64	2.16**	0.56	-0.54	1.45	-0.17	1.16	-0.46	0.22	1.09	0.48
	Spearman's Rho	1.08	1.72*	2.23**	0.56	-0.56	1.35	-0.11	1.15	-0.46	0.22	1.11	0.42

(Statistically significant at ***99% confidence level; ** 95% confidence level and *90% confidence level).

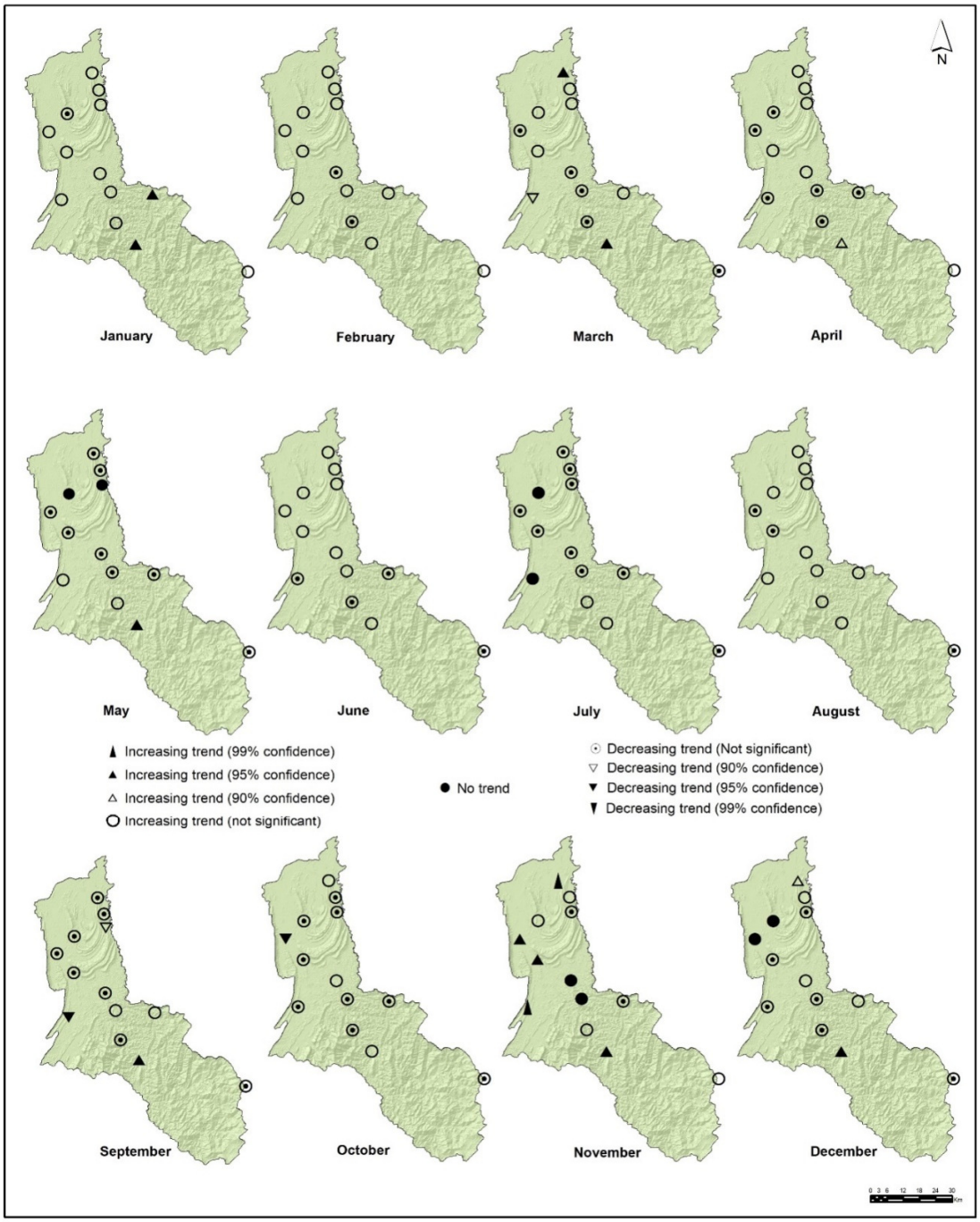

Figure 4.19: Map showing rain gauging stations with monthly rainfall trends with respect to Mann Kendall test.

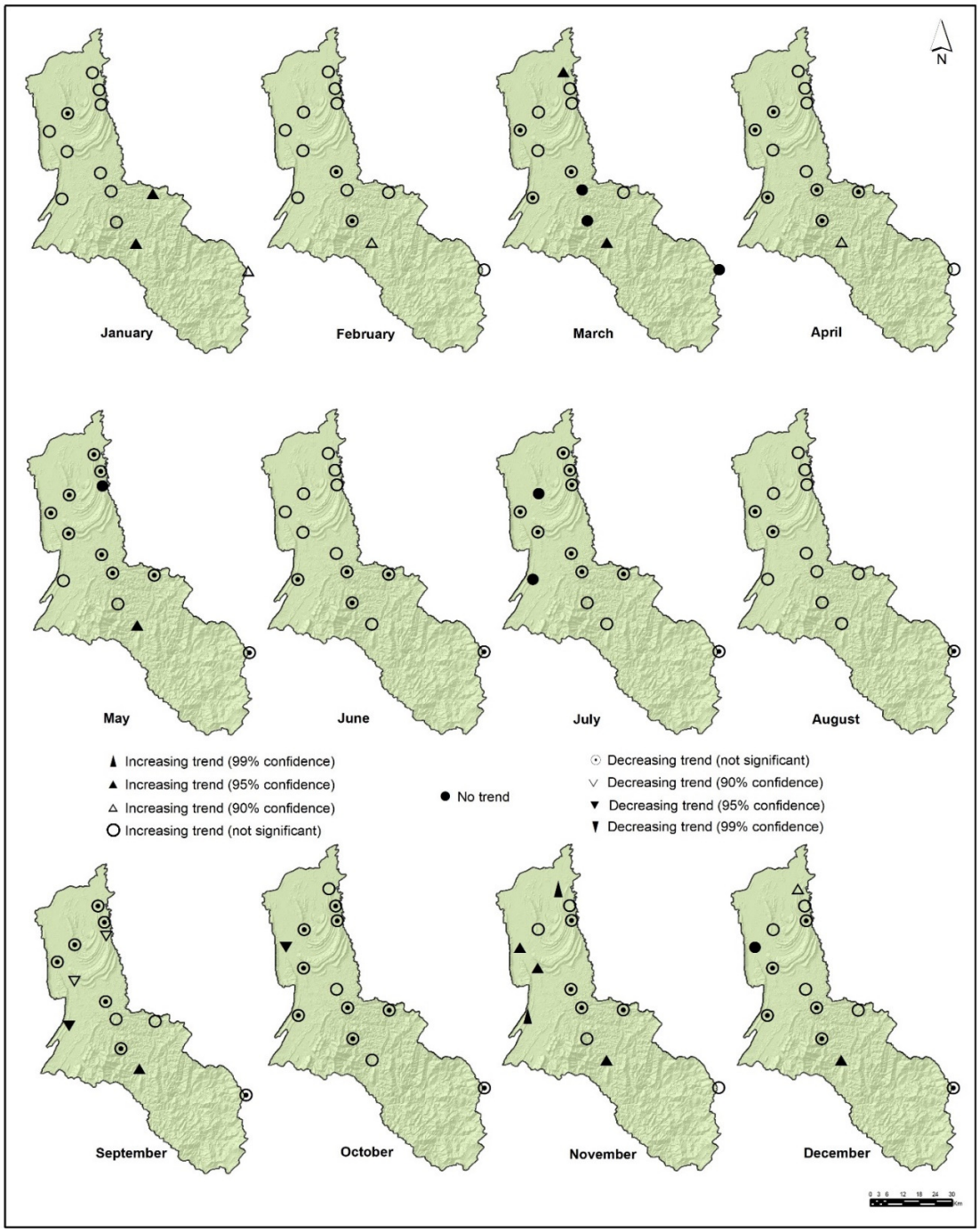

Figure 4.20: Map showing rain gauging stations with monthly rainfall trends with respect to Spearman's Rho test.

In the month of November, nine stations showed an increasing trend, two stations recorded decreasing trends and remaining two stations showed no or weak trend. It was also noted that, during this month, five stations showed statistically significant increasing trends at the highest (95 and 99%) confidence level. Rain gauging stations namely Limbang DID (2.86 and 2.68mm/year at 99% confidence), Ukong (2.22 and 2.13mm/year at 95% confidence), Medamit Nanga (2.47 and 2.43mm/year at 95% confidence), Ulu Medalam (2.52 and 2.49mm/year at 99% confidence) and Long Napir (2.13 and 2.21mm/year at 95% confidence) showed the highest increasing trends. Decreasing trends were recorded by Tegarai and Ulu Medamit, with a maximum value of -0.34mm/year in MK and SR tests and minimum value of -0.06 and -0.18mm/year in MK and SR tests respectively. The other two stations, namely Merbau (0.04 and -0.07mm/year) and Lubok Lalang (-0.07mm/year) show no and very weak decreasing trends during this month. In the month of December, five stations show an increasing trend, six stations showed decreasing trends and two stations shown no or weak increasing and decreasing trends. Rain gauging stations Limbang DID (1.83and 1.75mm/year at 90% confidence) and Long Napir (2.41 and 2.26mm/year at 95% confidence) shown a statistically significant increasing trend, whereas Pandaruan, Lubok Lalang and Ulu Medamit show a non-significant increasing trend. Non-significant decreasing trends vary in the range of -1.26 and -1.11mm/year (Rutoh) to -0.39 and -0.48mm/year (Ulu Medalam) for both tests. Similarly, rain gauging stations Lubai Tengah (0.04 and 0.06mm/year) and Ukong (0.03 and -0.05mm/year) show no and weak increasing trends.

Overall, while considering the monthly rainfall trend shown by each rain gauging station in the LRB, rain gauges show oscillating trend characteristics in different months. During January, February, June, August and November, the majority (≥8) of rain gauging stations showed an increasing (positive) trend whereas in the months May, July, September and October most stations (≥8) shown a decreasing trend. In the remaining months i.e. during March, April and December, rain gauging stations show both increasing (positive) and decreasing (negative) trends. It was also observed that, in the months of May, June, July, November and December, few stations shown no or a very weak trend. Considering the statistical significance, in the month of September, three stations show significant decreasing trends whereas in November, five rain gauging stations show significant increasing trends. In the remaining months, rain gauging stations with statistically significant trends varies between

nil and two. The detailed analysis of Mann Kendall and Spearman's Rho tests revealed that among the 13 stations, Long Napir has shown increasing trends at different significant levels (90 to 95% confidence level) in all the months except June, July, August and October compared to other stations. Trend values shown by Long Napir range between 0.71 to 2.41mm/year in MK and 0.73 to 2.34mm/year in SR tests. At the same time, while considering the maximum increase and decrease in rainfall trends, it found to vary between Limbang DID in November (2.86 and 2.68mm/year) and Ukong in October (-2.45 and -2.37mm/year).

An attempt has been taken to estimate overall monthly rainfall trend in the LRB as a whole, by considering the average monthly rainfall of all the stations. Results show nine months (January, February, March, April, June, August, October, November and December) with increasing trends and three months (May, July and September) with decreasing trends. The trend values varies between -0.54 to 2.16mm/year and -0.56 to 2.33mm/year in MK and SR tests respectively. It was noted that among the months which show increasing trends, February and March show statistically significant increasing trends (1.72mm/year in February with 90% confidence and 2.16 to 2.23mm/year in March with 95% confidence). But, decreasing trends associated with the months are non-significant and varies in the range of -0.54 and -0.56mm/year in May, -0.17 and -0.11mm/year in July and -0.46mm/year in September. Overall, it can be concluded that the LRB as a whole, shows an increasing trend in monthly rainfall.

4.2.5.2 Seasonal rainfall trend

The LRB possesses two distinct monsoon seasons separated by short inter-monsoon periods. The dominant monsoon seasons are the Southwest monsoon (May to September - 5 months) and Northeast monsoon (November to March - 5 months). The inter-monsoon (IM) periods are constituted by two individual months between the two monsoon seasons and are: April and October. The NEM receives more rainfall than SWM. In the present research, rainfall trends shown by each individual rain gauging stations during SWM, NEM and IM periods was assessed and the results are shown in Table 4.15 and Figure 4.21.

During SWM, three rain gauging stations show an increasing trend and ten rain gauging stations shows decreasing rainfall trends. Increasing trend characteristics associated with the

rain gauging stations vary in the range of 0.18 to 2.79mm/year and 0.14 to 2.88mm/year in MK and SR tests respectively. Among the three stations, Long Napir (2.79 and 2.88mm/year) shows statistically significant increasing trend at 99% confidence level in MK and SR tests. Other two stations, Limbang DID (0.18 and 0.14mm/year) and Setuan (0.00 and 0.25mm/year) show a non-significant increasing trend. It was noted that, rain gauging station Setuan shows no trend in the MK test. Considering the stations show decreasing rainfall trends, which ranges from -1.43 to -0.17mm/year in MK and -1.44 to -0.19mm/year in SR tests, results reveal that this not statistically significant. Among the ten stations, six shows comparatively higher value of non-significant decreasing trends in SWM rainfall which are Tegarai (-1.26 and -1.37mm/year), Ukong (-0.96 and -1.03mm/year), Medamit Nanga (-1.37 and -1.34mm/year), Lubok Lalang (-1.43 and -1.44mm/year), Ulu Medamit (-1.13 and -1.15mm/year) and Rutoh (-1.33 and -1.17mm/year). The other four stations, namely Pandaruan (-0.37 and -0.21mm/year), Lubai Tengah (-0.25 and -0.19mm/year), Merbau (-0.17 and -0.24mm/year) and Ulu Medalam (-0.42 and -0.63mm/year) show non-significant decreasing trends with the lowest values.

At the same time, during NEM season, twelve rain gauging stations recorded increasing trends and one rain gauging station showed decreasing trends. Increasing rainfall trends associated with the rain gauges in the LRB vary from 0.07 to 3.90mm/year and 0.05 to 3.95mm/year in MK and SR tests respectively. Among the stations showing increasing rainfall trends, statistically significant increasing trends were shown by Limbang DID (2.86 and 3.02mm/year at 99% confidence level), Pandaruan (1.82 and 1.87mm/year at 90% confidence level), Medamit Nanga (1.93 and 2.00mm/year at 90 and 95% confidence level) and Long Napir (3.90 and 3.95mm/year at 99% confidence level). Other stations namely Ukong (0.92 and 1.03mm/year) and Ulu Medamit (1.24 and 1.45mm/year) show higher values of increasing trends but are not statistically significant. Rain gauging stations Tegarai (0.12 and 0.14mm/year), Lubai Tengah (0.44 and 0.55mm/year), Lubok Lalang (0.32 and 0.39mm/year), Merbau (0.21 and 0.33mm/year) and Rutoh (0.21 and 0.34mm/year) show lower levels of non-significant increase in rainfall during NEM. The trend value associated with Ulu Medalam is very low (0.07 and 0.05mm/year) and can be consider as slightly increasing trend in MK test and as no trend in SR test. It is to be noted that, rain gauging station Setuan shows non-significant decreasing trends (-0.07 and -0.18mm/year) whereas it showed a very low non-significant decreasing trend in NEM.

Table 4.15: Mann Kendall and Spearman's Rho test results for seasonal and inter-monsoon rainfall in the LRB.

Stations	Trend Methods	Seasonal rainfall		Inter-monsoon periods	
		SW monsoon	NE monsoon	April	October
Limbang DID	Mann Kendall	0.18	2.86***	1.19	1.15
	Spearman's Rho	0.14	3.02***	1.17	1.04
Pandaruan	Mann Kendall	-0.37	1.82*	0.45	-0.68
	Spearman's Rho	-0.21	1.87*	0.42	-0.61
Tegarai	Mann Kendall	-1.26	0.12	1.26	-1.1
	Spearman's Rho	-1.37	0.14	1.42	-1.26
Lubai Tengah	Mann Kendall	-0.25	0.44	-0.25	-0.25
	Spearman's Rho	-0.19	0.55	-0.16	-0.37
Ukong	Mann Kendall	-0.96	0.92	-1.56	-2.45**
	Spearman's Rho	-1.03	1.03	-1.64	-2.37**
Medamit Nanga	Mann Kendall	-1.37	1.93*	0.08	-0.18
	Spearman's Rho	-1.34	2.00**	0.1	-0.13
Lubok Lalang	Mann Kendall	-1.43	0.32	0.18	0.18
	Spearman's Rho	-1.44	0.39	0.24	0.27
Merbau	Mann Kendall	-0.17	0.21	-0.98	-1.52
	Spearman's Rho	-0.24	0.33	-1.06	-1.47
Ulu Medalam	Mann Kendall	-0.42	0.07	-0.49	-0.63
	Spearman's Rho	-0.63	0.05	-0.28	-0.57
Ulu Medamit	Mann Kendall	-1.13	1.24	-0.28	-1.47
	Spearman's Rho	-1.15	1.45	-0.45	-1.58
Setuan	Mann Kendall	0	-0.07	-0.91	-1.33
	Spearman's Rho	0.25	-0.18	-0.95	-1.36
Long Napir	Mann Kendall	2.79***	3.90***	1.86*	1.25
	Spearman's Rho	2.88***	3.95***	1.95*	1.43
Rutoh	Mann Kendall	-1.33	0.21	1.19	-0.42
	Spearman's Rho	-1.17	0.34	1.27	-0.61
LRB (whole)	Mann Kendall	0.33	2.18**	0.56	0.22
	Spearman's Rho	0.13	2.24**	0.56	0.22

(Statistically significant at *** 99% confidence level; ** 95% confidence level and *90% confidence level)

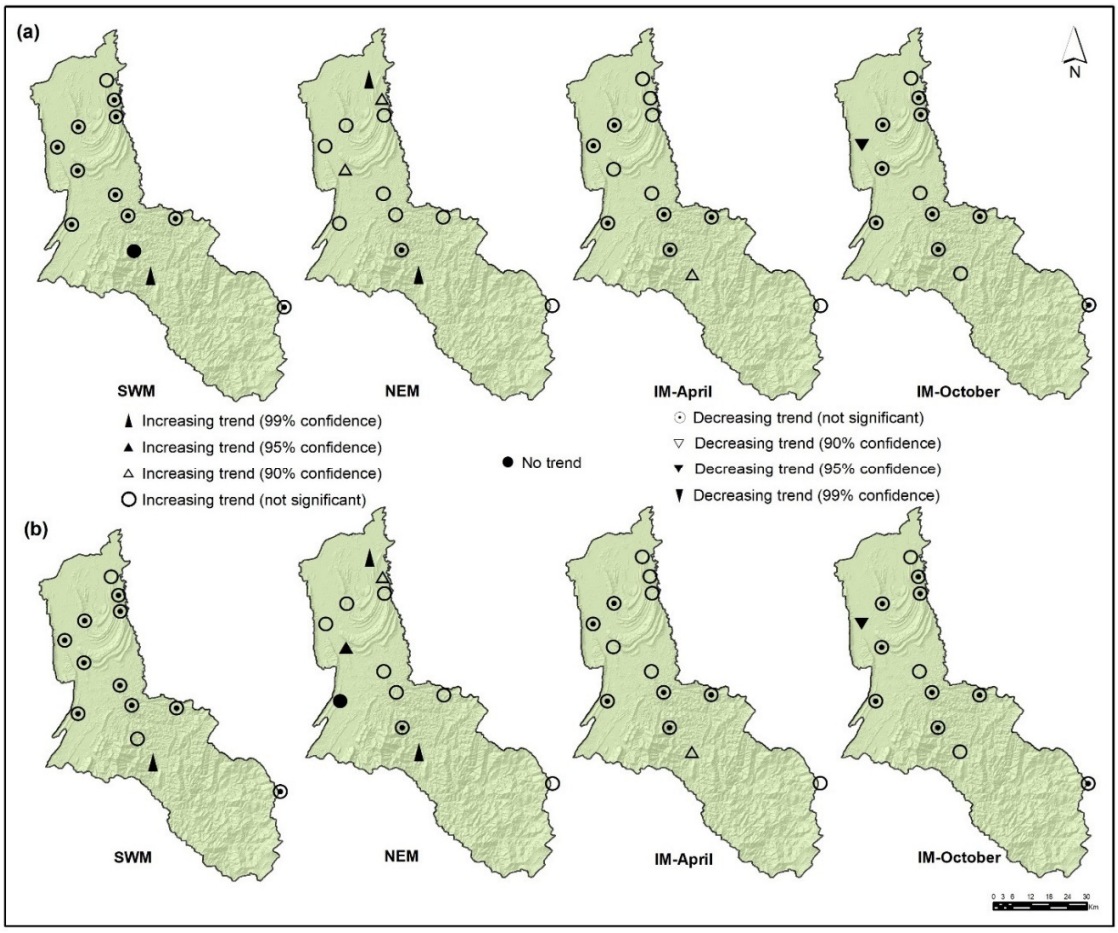

Figure 4.21: Map showing rain gauging stations with seasonal and inter-monsoon rainfall trends with respect to (a) Mann Kendall and (b) Spearman's Rho tests.

Considering the IM periods, in the month of April, seven rain gauging stations show increasing rainfall trends and six stations show decreasing trends. Increasing trend values associated with the rain gauging stations varies in the range of 0.08 to 1.86mm/year and 0.10 to 1.95mm/year in MK and SR tests respectively. Among the stations showing increasing trends, rain gauging station Long Napir show a statistically significant increasing trend (1.86 and 1.95mm/year at 90% confidence level) in MK and SR tests. It is to be noted that, rain gauging stations Limbang DID (1.19 and 1.17mm/year), Tegarai (1.26 and 1.42mm/year) and Rutoh (1.19 and 1.27mm/year) show higher values of non-significant increasing trends. Rain gauging stations Pandaruan (0.45 and 0.42mm/year), Medamit Nanga (0.08 and 0.10mm/year) and Lubok Lalang (0.18 and 0.24mm/year) show lower levels of increase (non-significant) in rainfall

trends. At the same time, decreasing trend values associated with the rain gauging stations range from -1.56 to -0.25mm/year and -1.64 to -0.16 mm/year in MK and SR tests respectively. Though six rain gauges show decreasing trends in rainfall, none was statistically significant. However, rain gauging stations Ukong (-1.56 and -1.64mm/year), Merbau (-0.98 and -1.06mm/year) and Setuan (-0.91 and -0.95mm/year) show higher values of non-significant decreasing trends. The other few stations namely Lubai Tengah (-0.25 and -0.16mm/year), Ulu Medalam (-0.49 and -0.28mm/year) and Ulu Medamit (-0.28 and -0.45mm/year) show lower levels of decreasing trends in rainfall.

At the same time, during the second IM month (October), three stations shown an increasing trend and ten stations shown decreasing trends. Increasing trend values associated with the rain gauging stations vary in the range of 0.18 to 1.25mm/year and 0.27 to 1.43mm/year in MK and SR tests respectively. Rain gauging stations Limbang DID (1.15 and 1.04mm/year), Lubok Lalang (0.18 and 0.27mm/year) and Long Napir (1.25 and 1.43mm/year) show a non-significant increasing trend in rainfall during October. Considering the decreasing trend characteristics shown by the rain gauge stations, the trend value varies in the range of -2.45 to -0.18mm/year and -2.37 to -0.13mm/year in MK and SR tests respectively. Among rain gauging stations which show decreasing trends, Ukong showed statistically significant decreasing trends (-2.45 and -2.37mm/year) at 95% confidence level. Rain gauging stations Tegarai (-1.10 and -1.26mm/year), Merbau (-1.52 and -1.47mm/year), Ulu Medamit (-1.47 and -1.58mm/year) and Setuan (-1.33 and -1.36mm/year) show higher values of non-significant decreasing trends. The remaining five rain gauges namely Pandaruan (-0.68 and -0.61mm/year), Lubai Tengah (-0.25 and -0.37mm/year), Medamit Nanga (-0.18 and -0.13mm/year), Ulu Medalam (-0.63 and -0.57mm/year) and Rutoh (-0.42 and -0.61mm/year) show lower levels of decrease (non-significant) in rainfall.

Characteristic variation in the rainfall trends were identified in the seasonal rainfall (SWM, NEM and IM period). It was noted that during NEM, higher number of stations show increasing rainfall trends with different significant levels compared to SWM. Rainfall trends during the IM period is the continuation of either SWM season or NEM season i.e. rainfall trend pattern in the month April follows the NEM rainfall trend and October follows the SWM rainfall trend. It was also noted that irrespective of seasons (SWM, NEM and IM month April), rain

gauging station Long Napir shows an increasing trend at varying confidence level (90 and 99%). In the IM period October, Long Napir showed a higher statistically non-significant increasing rainfall trend.

Considering the average rainfall in SWM, NEM and IM periods, trends associated with rain gauging stations were also estimated to understand rainfall trend in the LRB as a whole. Results revealed a characteristic increasing trend in rainfalls with different levels of significance and non-significance during SWM, NEM and IM rainfalls. A non-significant increasing trend (0.33 and 0.13mm/year in MK and SR tests respectively) were observed in the SWM, whereas NEM shows a statistically significant increasing trend (2.18 and 2.24mm/year at 95% confidence level) in MK and SR tests. Rainfall during the IM periods show a statistically non-significant increase of 0.56mm/year in April and 0.22mm/year for MK and SR tests in October.

4.2.5.3 Annual rainfall trend

Annual rainfall measured in each rain gauging station was considered individually, to detect the rainfall trend pattern in the LRB. Results of the statistical trend analysis are given in Table 4.16 and Figure 4.22. Annual trend patterns of individual rain gauging stations considered in the analysis show an increasing trend in five stations and decreasing trend in eight stations. Among the stations which shows increasing trends, Limbang DID (2.77 and 2.85mm/year) and Long Napir (3.65 and 3.77mm/year) show statistically significant (at 99% confidence level) increasing trends and Pandaruan (1.44 and 1.62mm/year), Lubai Tengah (0.52 and 0.58mm/year) and Rutoh (0.35 and 0.38mm/year) shown a non-significant increasing trends in MK and SR tests respectively. At the same time, decreasing trends shown by the rain gauging stations are non-significant and values ranges between -0.95 to -0.18mm/year in MK and -0.88to -0.17mm/year for SR tests. Rain gauging stations Ukong (-0.95 and -0.88mm/year), Merbau (-0.46 and -0.55mm/year), Ulu Medalam (-0.91 and -0.77mm/year), Ulu Medamit (-0.51 and -0.74mm/year) and Setuan (-0.63 and -0.74mm/year) shows notable decrease in rainfall trends. Other stations such as Tegarai (-0.46mm/year), Medamit Nanga (-0.24 and -0.27mm/year) and Lubok Lalang (-0.18 and -0.17mm/year) show the lowest non-significant decreasing trend in annual rainfall. However, considering the LRB as a whole unit, annual rainfall shows a statistically significant increasing trend (1.66 and 1.90mm/year at 90% confidence level) in both MK and SR tests.

Table 4.16: Mann Kendall and Spearman's Rho test results for annual rainfall in the LRB.

Stations	Trend Methods	Annual rainfall
Limbang DID	Mann Kendall	2.77***
	Spearman's Rho	2.85***
Pandaruan	Mann Kendall	1.44
	Spearman's Rho	1.62
Tegarai	Mann Kendall	-0.46
	Spearman's Rho	-0.46
Lubai Tengah	Mann Kendall	0.52
	Spearman's Rho	0.58
Ukong	Mann Kendall	-0.95
	Spearman's Rho	-0.88
Medamit Nanga	Mann Kendall	-0.24
	Spearman's Rho	-0.27
Lubok Lalang	Mann Kendall	-0.18
	Spearman's Rho	-0.17
Merbau	Mann Kendall	-0.46
	Spearman's Rho	-0.55
Ulu Medalam	Mann Kendall	-0.91
	Spearman's Rho	-0.77
Ulu Medamit	Mann Kendall	-0.51
	Spearman's Rho	-0.74
Setuan	Mann Kendall	-0.63
	Spearman's Rho	-0.74
Long Napir	Mann Kendall	3.65***
	Spearman's Rho	3.77***
Rutoh	Mann Kendall	0.35
	Spearman's Rho	0.38
LRB (whole)	Mann Kendall	1.66*
	Spearman's Rho	1.90*

(Statistically significant at *** 99% confidence level; ** 95% confidence level and *90% confidence level).

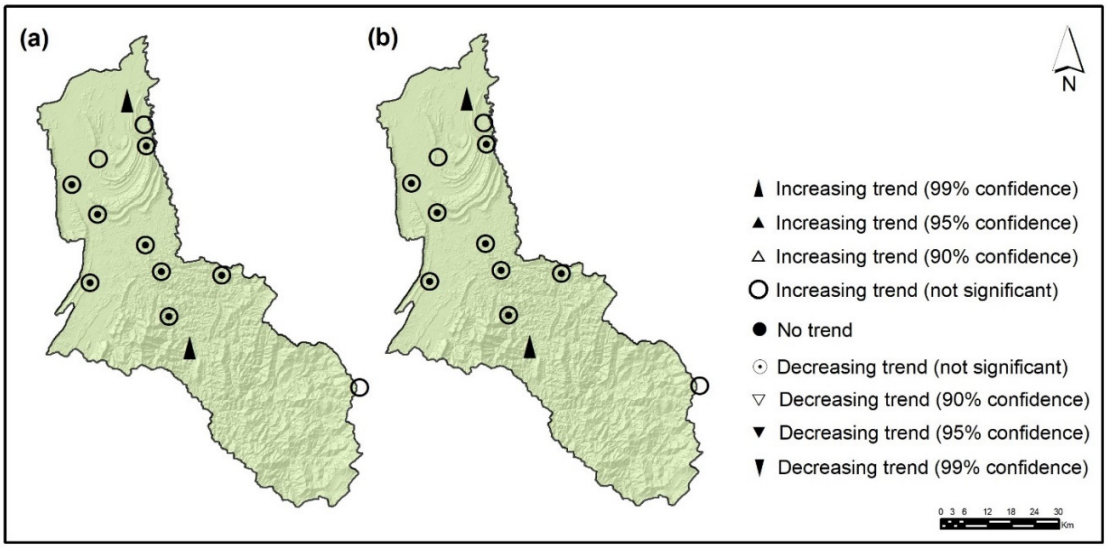

Figure 4.22: Map showing rain gauging stations with annual rainfall trend with respect to (a) Mann Kendall and (b) Spearman's Rho tests.

4.2.6 Spatial characteristics of rainfall trend in the LRB

Trend characteristics associated with each rain gauging station in the LRB was spatially interpolated in ArcGIS 9.3 software to identify the spatial pattern in monthly, seasonal, inter-monsoon and annual rainfall trends using the IDW interpolation technique as explained earlier. Spatial characteristics of rainfall trends during monthly, seasonal, inter-monsoon and annual are discussed in detail below.

Spatial pattern of monthly rainfall trend show specific characteristics in each month in both tests (Figure 4.23 and 4.24). However, considering the overall spatial distribution of rainfall trends, a dominant spatial pattern was observed in monthly rainfall trend in the LRB. The identified spatial pattern indicates two clusters of increasing rainfall trend in the lower and upper catchment and one major zone of decreasing rainfall trend in the central and upper part of the catchment. It is to be noted that the identified dominant zones are contributed by rain gauging stations showing comparatively higher rainfall trends (significant or non-significant) corresponding to increasing as well as decreasing trends. Clusters of increasing rainfall trend in the lower catchment is centered around rain gauging stations Limbang DID and Pandaruan (most months) and Long Napir in upper catchment. The low rainfall trend regime is formed by

rain gauging stations Ukong, Medamit Nanga, Lubok Lalang, Ulu Medamit, Ulu Medalam and Setuan. It was observed that during the month of November, besides the identified clusters of increasing rainfall trend, an elongated increasing rainfall trend corridor was noted in the western part of the study area and are formed by rain gauging stations Ukong, Medamit Nanga and Ulu Medalam in central part and Rutoh in upper part of the catchment. Identified clusters of high and low rainfall trends are observed in the spatial trend pattern during the months of February, March, April, June, August, October, November and December. Among this, in the month of April, spatial spread of an increasing trend in the upper catchment is prominent and was contributed by rain gauging stations Long Napir and Rutoh. At the same time, during the months January, May, July and September, the LRB showed spatial pattern dominated by decreasing rainfall trend with an isolated increasing trend in Long Napir.

Considering the spatial pattern of seasonal rainfall trends, during the southwest monsoon season (SWM), the LRB show a dominant decreasing trend in rainfall with an isolated foci of increasing rainfall trend in the spatial pattern of MK and SR tests (Figure 4.25). Though most areas show decreasing trend patterns, the dominance of decreasing trend was clustered around rain gauging stations Ukong, Medamit Nanga, Lubok Lalang, Ulu Medalam, Ulu Medamit and Rutoh. The region around rain gauging station Long Napir show increasing characteristics in rainfall trends. This pattern highly resembles the spatial pattern of rainfall trends observed in the months of January, May, July and September. In NEM, the rainfall trend pattern shows two clusters of increasing trends in the lower and upper catchment region and a dominant decreasing trend zone in central and upper part of the study area (Figure 4.25). As observed in most months, the increasing clusters are contributed by Limbang DID and Pandaruan in the lower catchment and Long Napir in the upper catchment. It was also noted that areas around rain gauging station Medamit Nanga shows an isolated increase in rainfall trend during NEM. The spatial spread of decreasing trend characteristics in the study area was controlled by Lubai Tengah, Ukong, Ulu Medalam and Setuan in the central part and Rutoh in the upper catchment. This pattern is common in MK and SR tests based surfaces.

However, considering the inter-monsoon (IM) months, April and October show an entirely different characteristics of spatial spread in both the tests (Figure 4.25). In April, spatial pattern of rainfall trend shows two dominant zones of increasing trend in the lower and upper

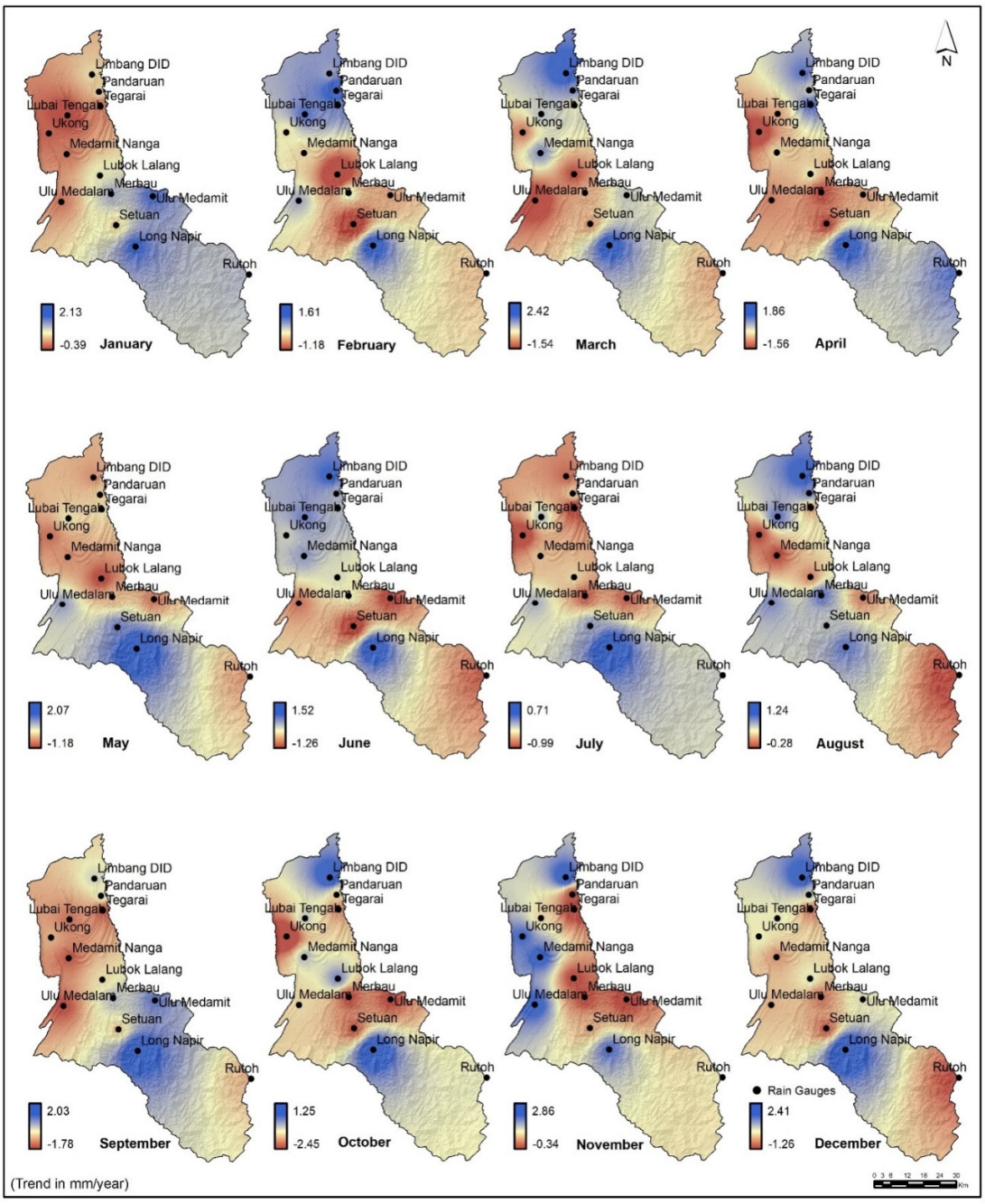

Figure 4.23: Spatial distribution of monthly rainfall trends in the LRB based on Mann Kendall test results.

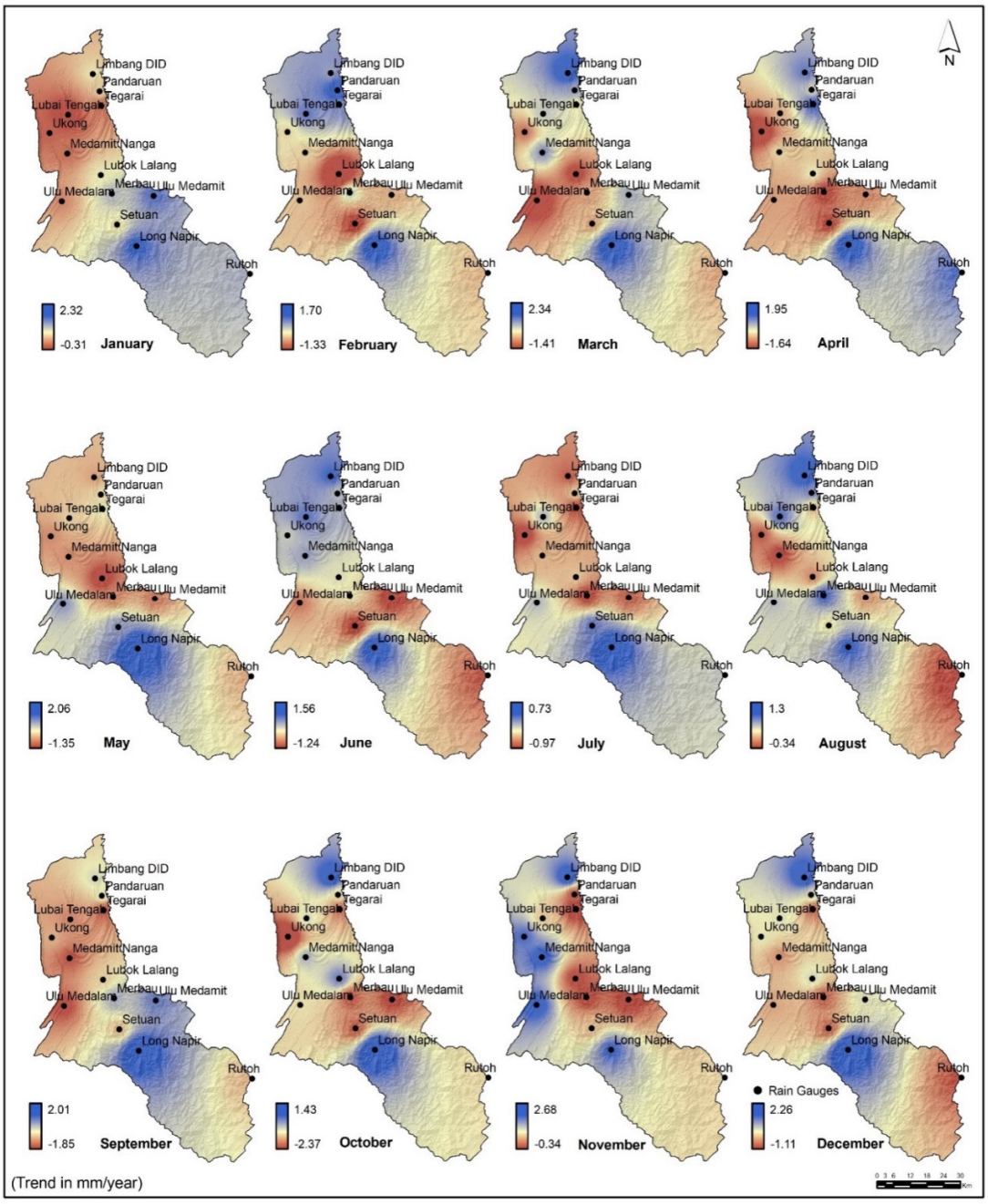

Figure 4.24: Spatial distribution of monthly rainfall trends in the LRB based on Spearman's Rho test results.

catchment region, separated by a prominent decreasing trend zone. Increasing trend zones in the lower catchment area is formed by rain gauging stations Limbang DID and Pandaruan and

those in the upper catchment was by Long Napir and Rutoh. The decreasing rainfall trend zones observed in the middle catchment region were contributed by Ukong, Ulu Medalam, Ulu Medamit and Setuan, which covers the northwest and central part of the catchment. Considering the IM month October, spatial pattern shows distinct clusters of increasing rainfall trend encircled by moderate and higher decreasing trend zones. Identified increasing clusters are around the rain gauging stations Limbang DID, Pandaruan, Medamit Nanga, Lubok Lalang and Long Napir. Decreasing rainfall trend zones are dominantly controlled by the rain gauging stations Ukong, Merbau, Ulu Medamit and Setuan whereas the moderate decreasing zones are contributed by Lubai Tengah, Ulu Medalam and Rutoh.

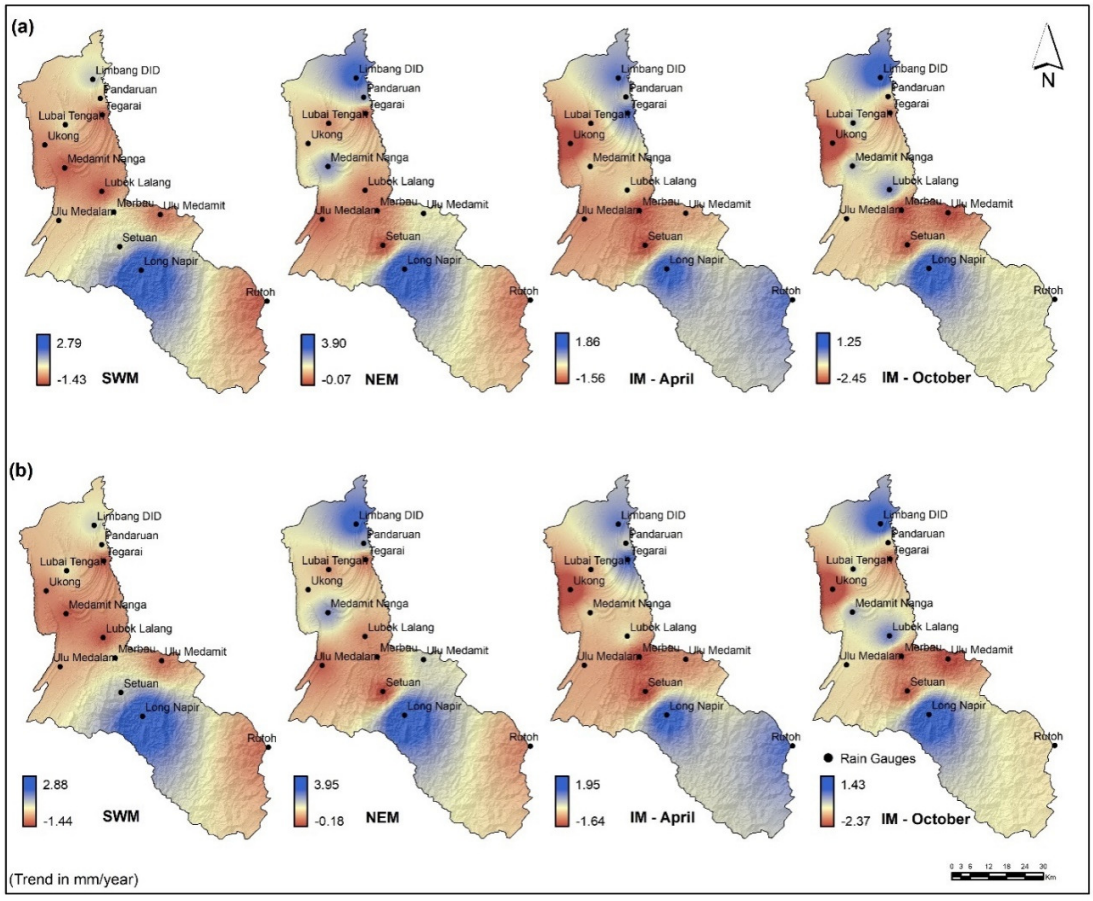

Figure 4.25: Spatial distribution of seasonal and inter-monsoon rainfall trends in the LRB based on (a) Mann Kendall and (b) Spearman's Rho tests.

Spatial pattern of annual rainfall trends derived in the study indicates similar characteristics in MK and SR tests (Figure 4.26). The spatial pattern of annual rainfall trends

also show two clusters of dominant increasing trends in the lower and the upper catchment which was separated by a prominent decreasing rainfall trend zone as like the monthly rainfall trend pattern. Moreover, moderate decreasing rainfall trend zones were also identified in the lower and upper catchment region of the LRB. Increasing rainfall trend cluster in lower catchment was contributed by Limbang DID and Pandaruan, whereas Long Napir alone control the increasing trend region in the upper catchment. The zone of decreasing rainfall trend in central part of the study area was contributed by the rain gauging stations Tegarai, Ukong, Medamit Nanga, Lubok Lalang, Merbau, Ulu Medalam, Ulu Medamit and Setuan. Areas around Lubai Tengah in lower and Rutoh in the upper part of the catchment show moderate decrease in rainfall trends. Overall, it can be concluded that, in the LRB, significant increasing trends in rainfall was confined in the lower catchment regions (area around Limbang DID) and upper catchment regions (area around Long Napir), whereas majority of the area shows non-significant decreasing trend in rainfall as observed in the spatial pattern maps.

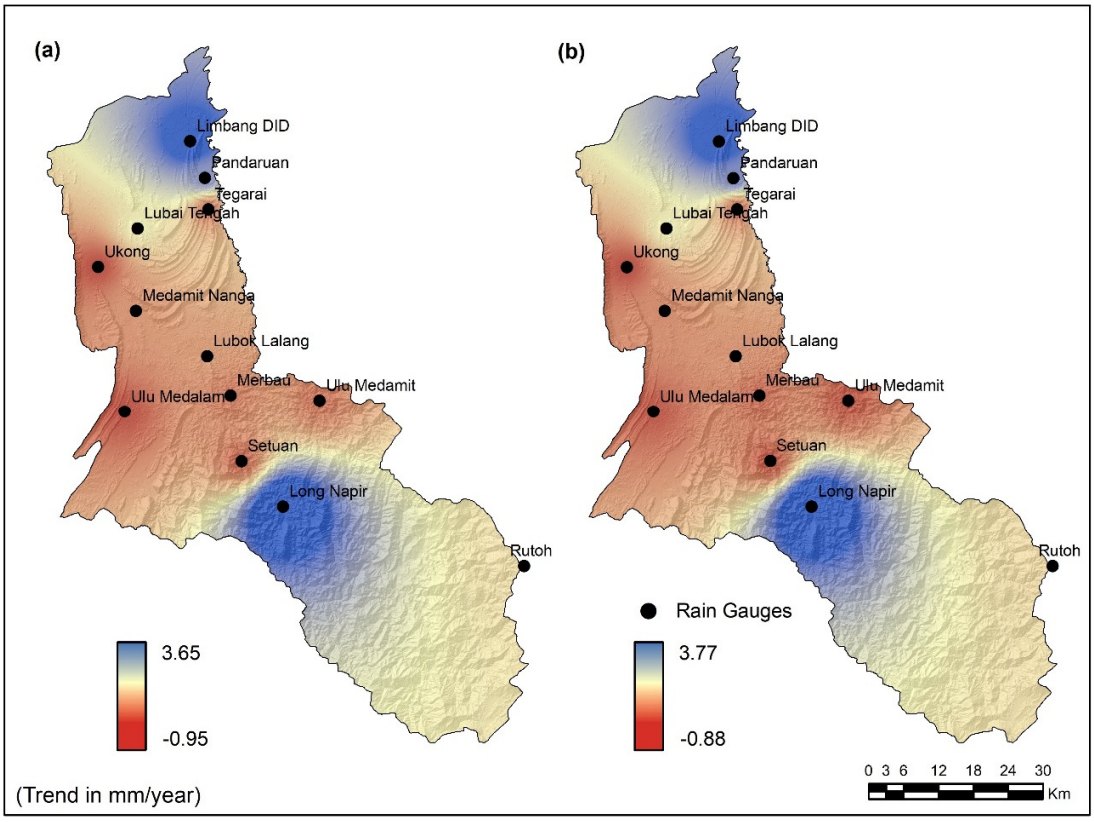

Figure 4.26: Spatial distribution of annual rainfall trend in the LRB based on (a) Mann Kendall and (b) Spearman's Rho tests.

4.3 Rainfall-Runoff Modelling

The Limbang River Basin, a forested river basin in northern Borneo has a lack of continuous and accurate information about the runoff, which received average annual rainfall of higher than 3851mm. Besides this, the Sarawak state government is going to construct two hydro-electric projects (HEP's) through the implementing agency, the Sarawak Energy Berhad (SEB), which not only alters the catchment characteristics but also heavily influence the runoff characteristics of the river basin (Shirley & Kammen, 2015; Chen, 2016). Considering this in the present research, rainfall and water level (stage height) data were obtained from the Department of Irrigation and Drainage (DID), Sarawak, Malaysia to generate the rainfall-runoff model using Multilayer Neural Network (MNN). Inventory of DID website to identify the discharge gauge information shows that five (Insungai Nanga, Saliban Nanga, Ukong, Batu Danau and Limbang) stage height measuring stations exist in Limbang River, and among those stations, only Insungai Nanga possesses a stage discharge rating curve equation. Insungai Nanga (4° 24' N and 114° 53' 30" E), is located at the middle reach of the Limbang River. Furthermore, referring to the hydrological year book of DID, Sarawak, it was noted that the stage discharge rating curve equation of Insungai Nanga was applicable for a period of 1985–2003 (Figure 4.27).

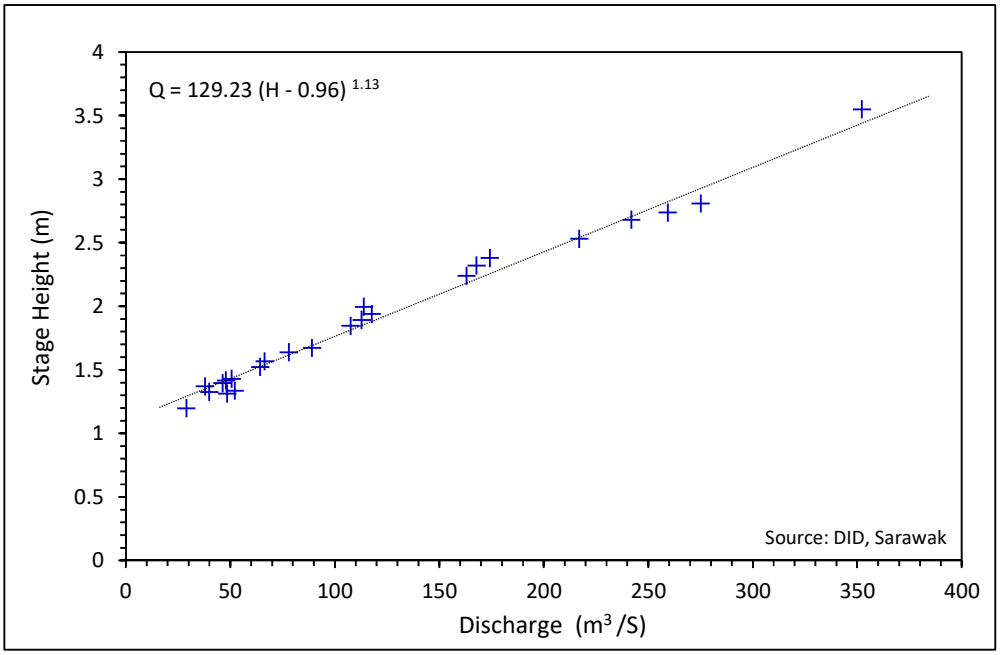

Figure 4.27: Stage height-discharge rating curve of the Insungai Nanga (Source: DID, Sarawak).

The rating curve was established by making a number of concurrent observations of stage and discharge over a period of time covering the expected range of stages at the river gauging section. From the stage height-discharge rating curve, the relationship between stage height and discharge was established and a rating curve equation to measure discharge from Insungai Naga was derived. The proposed rating curve equation is given as:

$$Q = 129.23(H - 0.96)^{1.13}$$

where, Q is the discharge and H is the stage height, the effective range of H is 1.20 to 5.67m.

Therefore, considering the validity of stage height-discharge rating curve equation and data availability in Insungai Nanga station, water level (stage height) and rainfall data for a period of 10 year (1991-2000) was collected from DID, Sarawak for rainfall-runoff modelling. In addition, using the rating curve equation and the stage height measurements, the corresponding relative discharge during the study period was generated for use in the ANN model.

4.3.1 Data preparation

The input data used in this research are daily rainfall data and discharge data calculated from the rating curve equation (1991-2000). The data collected was divided into fifteen sets of rainfall events by eliminating the missing values in order to ensure the continuity of the measurement. Rainfall events and equation based discharge measurements used is shown in Figure 4.28. It was noted that, the higher runoff calculated using the discharge rating curve equations correlate well with high rainfall events observed in the station.

Furthermore, in order to determine the input vectors and the network structure precisely, the selection of appropriate lags (days) of rainfall and runoff measurements has to be included in the ANN model to make the training process more effective. Therefore, it is necessary to investigate the statistical characteristics of input rainfall and runoff data to determine the correlation between input and output data (Hsu et al., 1995; Demuth & Beale, 1998). This is because, in the ANN model, runoff will be predicted by providing the input vector

as rainfall, antecedent rainfall and antecedent runoff values (Teschl & Randeu, 2006; Cobaner et al., 2009). Previous studies carried out by cross comparing the rainfall and runoff series revealed the high influence of antecedent rainfall over the predicted runoff (Istok & Boersma, 1986; Torres et al., 2011; Rodríguez-Blanco et al., 2012). Antecedent rainfall, which influence the quality of runoff output can be better determined through statistical measurements of correlations between the dependent and independent variable i.e. runoff and rainfall and will help to determine the significant lag values of input variable. The most general statistical measurements in the preparation of data in ANN models are cross-correlation function (CCF), auto-correlation function (ACF) and partial auto-correlation function (PACF).

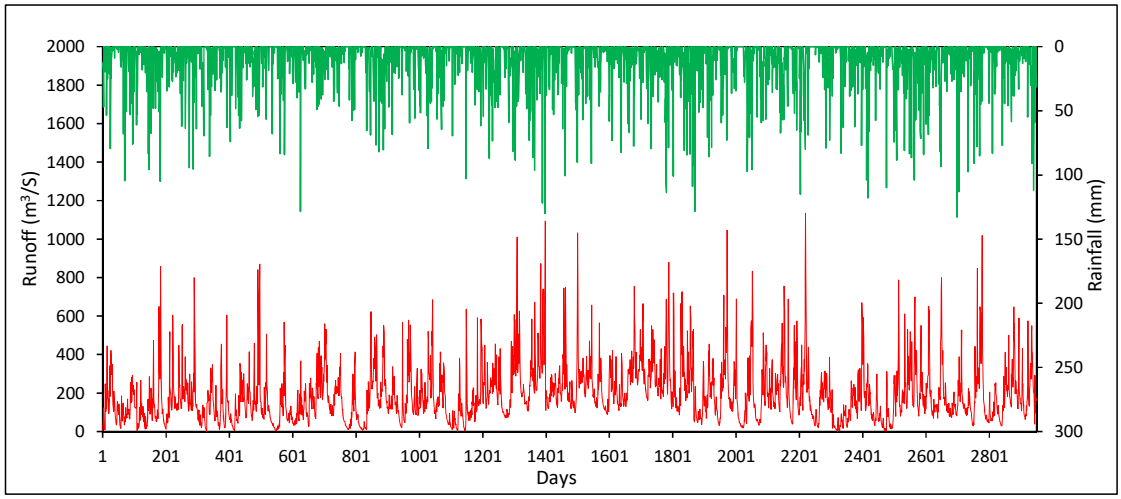

Figure 4.28: Time series plot of rainfall (top) and runoff (bottom) data used in the present research.

Cross correlation function (CCF) is the measure of similarity of two variables which considers the relative time between the variables. The cross correlation coefficient between rainfall and runoff, which was calculated by normalising the cross-correlation of the two variables, has been used to identify the time lag (offset) where the similarity is highest. Similarly, the autocorrelation function (ACF) describes the correlation between all the pairs of points in the time series with a given separation in time or time lag. At the same time, the partial autocorrelation functions (PACF) is the autocorrelation of a series with itself under stationary conditions while controlling the effect of intervening lags. This will reveal precise autocorrelation of a series with itself without the confounding effects of intervening lagged

autocorrelation (Hamilton, 1994; Wilks & Haman, 1996 a, b). Studies conducted by Sudheer et al. (2002) found that the qualitative examination of the cross-correlation curves between the rainfall and runoff series is capable of identifying the antecedent rainfall which heavily influences the runoff, whereas the autocorrelation function (ACF) and partial autocorrelation function (PACF) would suggest the influencing antecedent discharge patterns in the flow at a given time. All these statistical methods will help to determine the number of antecedent rainfall and runoff values that should be included in the input vector by avoiding the data variables that will not significantly influence the quality of output and performance of the model. Therefore in the present analysis, cross-correlation function (CCF), auto-correlation function (ACF) and partial auto-correlation function (PACF) between the input and output variables were carried out to find the significant lag values of input variables.

4.3.2 Results of statistical tests

Results of cross-correlation, autocorrelation and partial autocorrelation functions analysed for the rainfall and runoff data considered in the present study are given in Table 4.17. Cross correlation between the rainfall and runoff estimated between the lags -20 to 20 shows an initial increase in lag, and the rainfall intervals up to lag 3 (3 days) contributed to major part of the total variance (Figure 4.29). Lag time identified is the function of the time of concentration of water in the river basin and depends on basin characteristics such as contributing area, shape, slope, flow length, relative relief and land use (Mutlu et al., 2008).

Autocorrelation function and the corresponding 95% confidence interval from lag 1 to lag 20 (1 to 20 days) were estimated for the standardised runoff data (Table 4.17 and Figure 4.30). Standardisation of runoff data is required to ensure the uniformity of units in measured parameters because, parameters considered for the correlation analysis may be measured in different units. The standardisation process is capable of removing the arbitrary effects of similarity between the variables and making them dimensionless units (Raman & Sunilkumar, 1995; Sudheer et al., 2002). Autocorrelation analysis of runoff data shows a gradual decaying pattern with correlation coefficient values ranging from positive (0.76) to negative (-0.19). Correlation coefficient values up to lag 14 (14 days) shows a gradual decrease with positive values and had started showing negative value till lag 20 (20 days with -0.19). Autocorrelation function shows a significant correlation up to lag 12 (12 days) at 95% confidence levels and

thereafter fell within the confidence bands and then moved towards the negative correlation. The gradual decaying nature of the autocorrelation coefficient indicates the occurrence of dominant autoregressive process (Sudheer et al., 2002; Mutlu et al., 2008).

Table 4.17: Correlation coefficients between rainfall and runoff (CCF), and ACF and PACF of the runoff data.

Lag (days)	Cross correlation (CCF)	Autocorrelation (ACF)	Partial autocorrelation (PACF)
1	0.48	0.76	0.76
2	0.41	0.57	-0.01
3	0.34	0.43	0.01
4	0.24	0.36	0.08
5	0.23	0.29	-0.03
6	0.17	0.25	0.03
7	0.12	0.22	0.03
8	0.07	0.21	0.06
9	0.06	0.17	-0.07
10	0.10	0.13	0.01
11	0.12	0.14	0.08
12	0.13	0.10	-0.10
13	0.15	0.05	-0.05
14	0.14	-0.03	-0.09
15	0.16	-0.08	-0.06
16	0.13	-0.13	-0.05
17	0.07	-0.14	0.01
18	0.02	-0.16	-0.05
19	-0.07	-0.17	-0.03
20	-0.10	-0.19	-0.05

The partial autocorrelation function of runoff and corresponding 95% confidence level band was also analysed for lag 1 to lag 20 (Table 4.17 and Figure 4.31). The value of partial autocorrelation coefficient assessed for the runoff data varies in the range of 0.76 to -0.09. The partial autocorrelation plot showed a rapidly decaying nature concurrent with the gradual decaying nature of the autocorrelation plot and confirms the dominance of the autoregressive process, relative to the moving-average process (Sudheer et al., 2002; Mutlu et al., 2008). The partial autocorrelation function showed significant correlation up to lag 1 (1 day) and all other values corresponding the remaining lags fell within the 95% confidence level band. Results of autocorrelation and partial autocorrelation function of runoff data to establish the relationship

between the lag and correlation coefficient suggests the incorporation of runoff value of lag 1 (1 day) in the input vector in the ANN model.

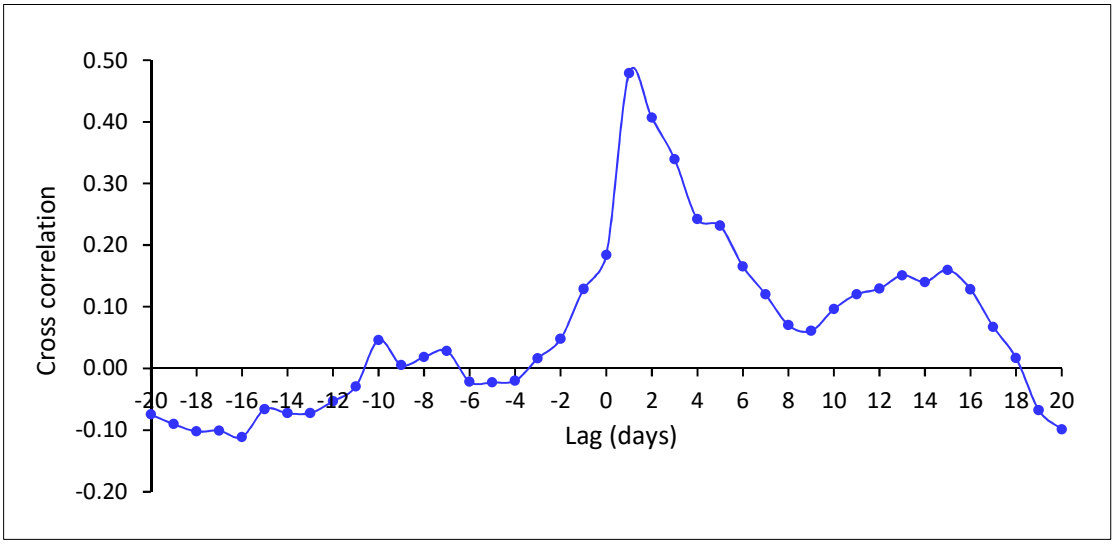

Figure 4.29: Cross correlation (CCF) plot of rainfall-runoff series of the Insungai Nanga.

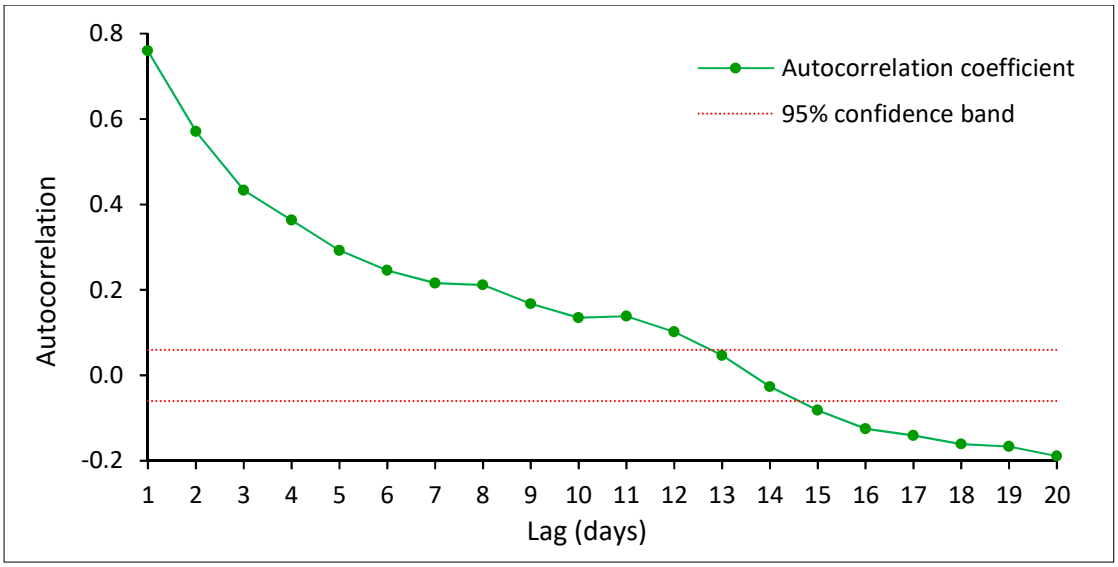

Figure 4.30: Autocorrelation (ACF) plot of runoff series in the Insungai Nanga.

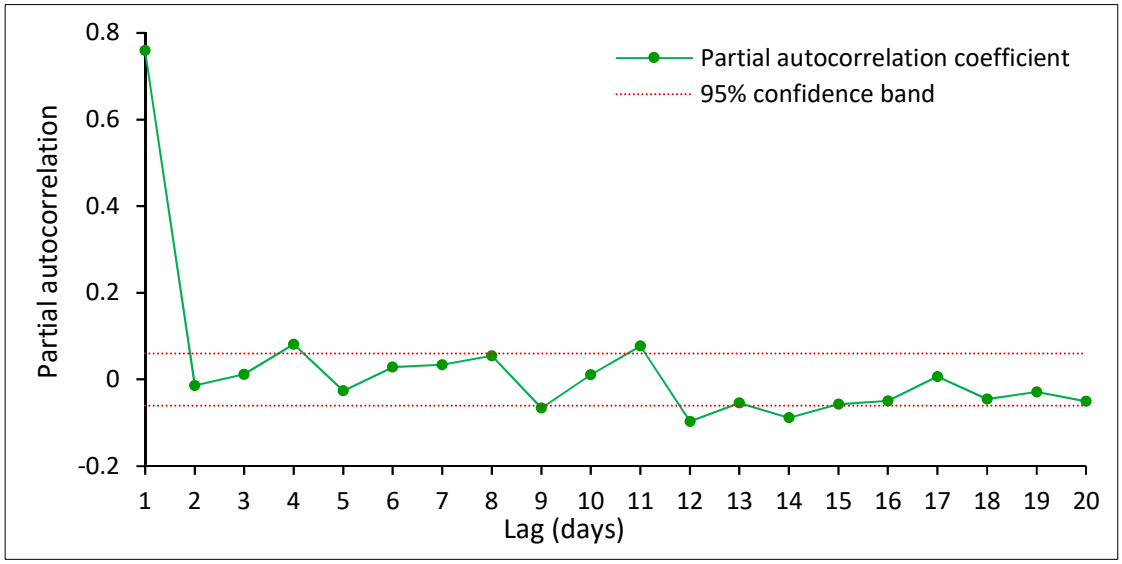

Figure 4.31: Partial autocorrelation (PACF) plot of runoff series in the Insungai Nanga.

4.3.3 Data preparation for runoff model generation

In ANN model, the input vector selection process is more cumbersome and will take more time through a long trial and error procedure to identify the suitable input vector which was relieved by the application of quantitative statistical methods (Mutlu et al., 2008; Papalaskaris & Kampas, 2017; Peng et al., 2017). The results of cross correlation, autocorrelation and partial autocorrelation functions enable the use of one antecedent runoff and three antecedent rainfall intervals together to form a four-element input vector in the minimum description length (MDL) based multilayer neural network (MNN) model. Hence in the present study, input considered for the MNN model is P(t-3), P(t-2), P(t-1) (antecedent rainfall) and Q(t-1), (antecedent runoff).

After finalising the input vectors, it is crucial to confirm the number of neurons in the hidden layer to be incorporated in the model. In the present model, only one hidden layer was considered. In order to fix the number of neurons in the hidden layer, a trial and error method was used. If the number of neurons are more, then the chance of the occurrence of over fitting is more. Similarly, if less number of neurons were considered compared to the complexity of the data then under fitting will occur (Muttil & Chau, 2006; Dawson & Wilby, 2001; Ma et al., 2015; Afram et al., 2017). So, the selection of the appropriate number of neurons in the hidden

layer is very crucial. In the present study, the number of neurons in the hidden layer was fixed as four. Transfer functions considered in the model are tangential sigmoid in the hidden layer and pure linear function at the output layer. The final structure of the MNN MDL model used in the present study is shown in Figure 4.32.

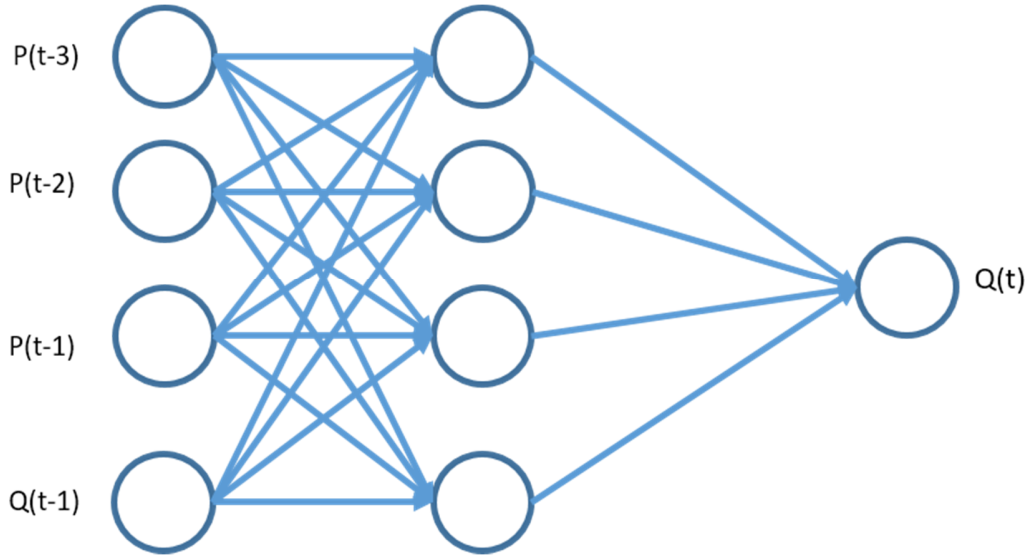

Figure 4.32: MNN MDL model explaining input vectors, hidden layer and neurons used in the runoff simulation of the Insungai Nanga.

Selection of data for training and testing using MNN MDL model is crucial due to the dependency of the complex and nonlinear behavior of the ANN model. Therefore appropriate selection of input data for training and testing is essential. As described in the earlier section, the events identified from the rainfall and runoff series by eliminating the missing values for a period of 1991-2000 were segmented into two i.e. event-1 to event-10 was used for prediction and modelling (training) and the remaining events (event-11 to 15) were used for validation (testing) of the results. Statistical characteristics of the data used for training and testing of MNN MDL model were shown in Table 4.18.

Table 4.18: Statistical characteristics of data used for the training and testing of the MNN MDL model.

	Training		Testing	
	Rainfall (mm)	**Runoff (m^3/S)**	**Rainfall (mm)**	**Runoff (m^3/S)**
Number of days	1865	1865	1080	1080
Min	0.00	1.55	0.00	1.55
Max	130.00	1093.79	133.00	1134.95
Average	10.79	197.28	12.33	190.09
Standard deviation	18.83	144.77	20.76	151.08
CV	1.75	0.73	1.68	0.79

A total of 1865 and 1080 rainfall and runoff data was considered in the training and testing of MNN MDL model. Rainfall shows a minimum value of 0.00 (zero) in training and testing data sets, whereas runoff shows a minimum of 1.55m^3/S in both data. At the same time in the training data set, rainfall and runoff shows a maximum value of 130.00mm and 1093.79m^3/S respectively. In the case of testing data, the maximum rainfall noted was 133.00mm and the runoff show peaked to a maximum value of 1134.95m^3/S. The average value of rainfall and runoff in training data set was 10.79mm and 197.28m^3/S which shows a standard deviation of 18.83mm and 144.77m^3/S respectively. Similarly in the testing data set, rainfall data shows an average value of 12.33mm with standard deviation of 20.76mm and the average runoff was 190.09m^3/S and shows a standard deviation of 151.08m^3/S. Coefficient of variation (CV) of rainfall and runoff series in training and testing data sets are 1.75, 1.68 and 0.73, 0.79.

4.3.4 Runoff model training and testing

MNN MDL model was trained and tested through its capability to simulate discharge (runoff) for the selected river section (Insungai Nanga) using the data sets described in the above section. The Nash Sutcliffe Efficiency (NSE) function adapted to high flow conditions as objective functions and enable the model to predict values that are different from mean. The determination coefficient R^2 were used for model testing (Nash & Sutcliffe, 1970; Chiew et al., 2009; Brocca et al., 2013; Shoaib et al., 2014; Alizadeh et al., 2017; Zadeh et al., 2017; Shoaib et

al., 2018). Results of runoff training and testing at Insungai Nanga are shown in Figure 4.33 and 4.34, shows comparatively higher agreement between observed and simulated runoff.

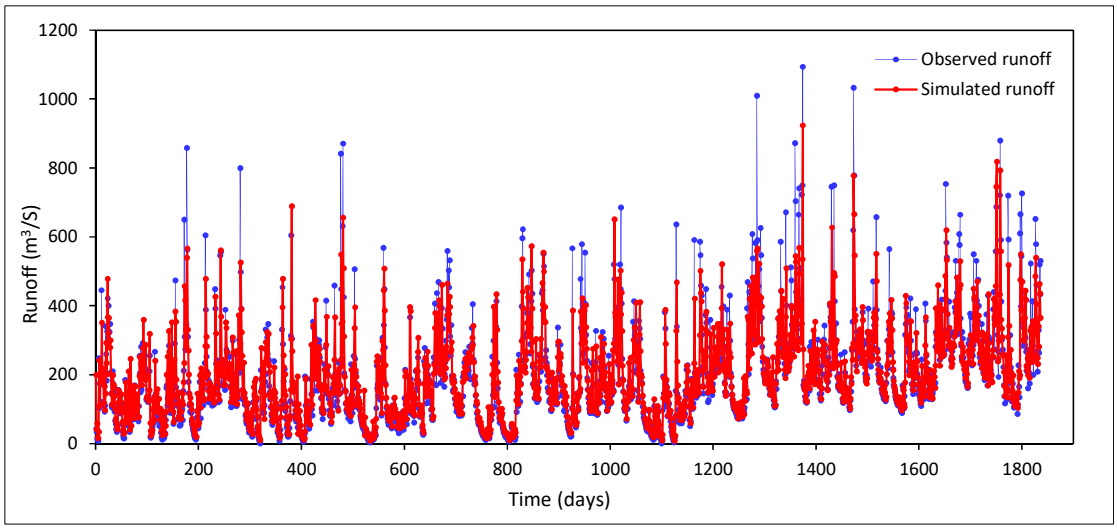

Figure 4.33: Comparison of observed and predicted results of runoff for training.

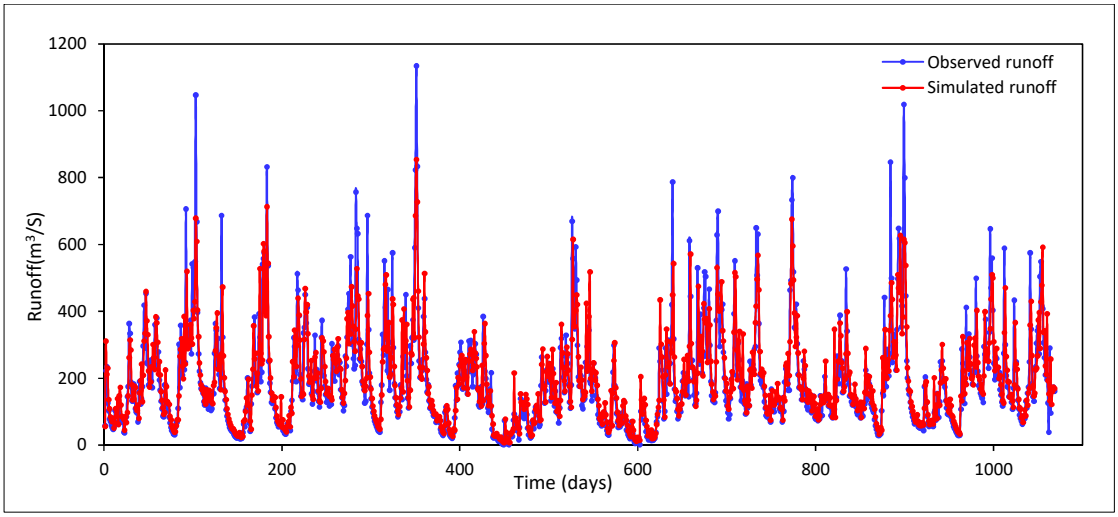

Figure 4.34: Comparison of observed and predicted results of runoff for testing.

While closely examining the training and testing results of observed and simulated runoff, the model shows comparatively higher performance in predicting most of the flow (discharge) conditions.

4.3.5 Evaluation of model performance

The prediction accuracy of the MNN MDL model in training and testing to simulate the runoff data was statistically evaluated by employing Pearson's correlation, Nash Sutcliffe Efficiency (NSE), Root Mean Square Error (RMSE), Relative RMSE (RRMSE), Mean Absolute Error (MAE), Mean Absolute Percentage Error (MAPE), Volumetric Error (EV) and Relative Peak Error (RPE) and the results are shown in Table 4.19. Along with this, scatter plots (regression plots) between observed and simulated runoff in training and testing is also generated and interpreted.

Table 4.19: Performance of MNN MDL model evaluated through statistical methods.

Statistical methods	**Training**	**Testing**
Correlation coefficient	0.84	0.85
NSE	0.70	0.73
RMSE	79.71	98.85
RRMSE	0.52	0.50
MAE	49.79	51.04
MAPE (%)	31.97	32.33
EV (%)	0.78	2.62
RPE	0.16	0.25

Linear regression plots of observed and simulated runoff for the training and testing data were shown in Figure 4.35 and 4.36. Both data sets shows comparatively satisfactory goodness of fit with R^2 values of 0.69 and 0.72 for training and testing respectively. In order to understand the correlation between observed and simulated runoff data, correlation analysis of training and testing data were carried out. Correlation coefficient values generally vary in the range of -1 to 1 and the negative value indicates negative correlation while positive values represent positive correlations whereas values close to zero indicate low or no correlation. In the present analysis, the correlation coefficients of simulated runoff in training and testing show a higher positive correlation with coefficients ≥0.80 (r=0.84 and 0.85 for training and testing respectively).

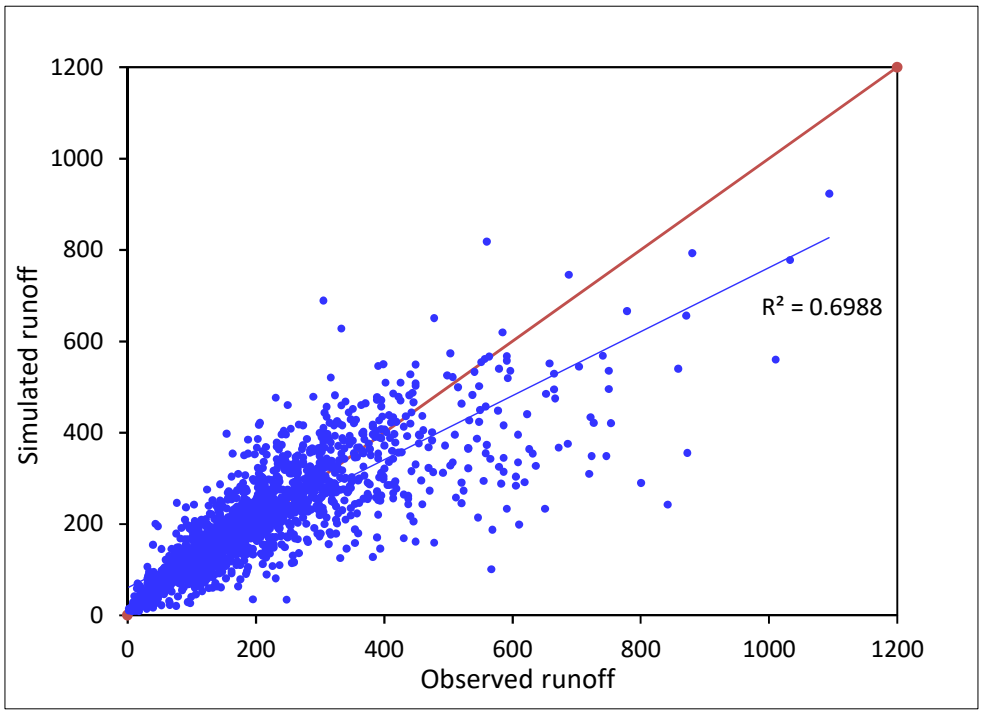

Figure 4.35: Correlation plot of observed and simulated runoff data (training).

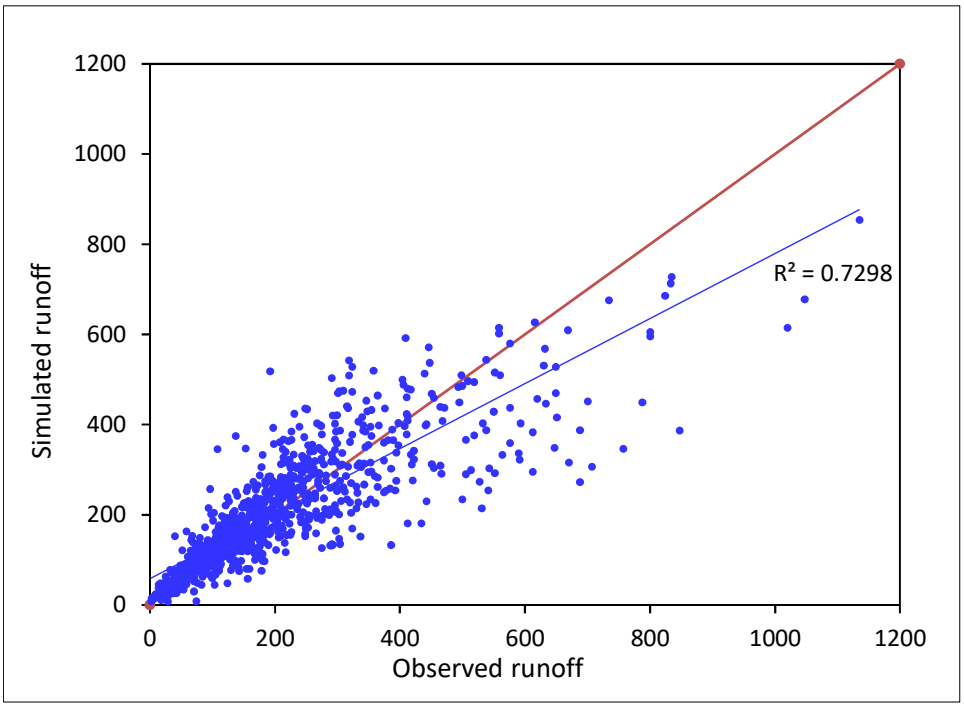

Figure 4.36: Correlation plot of observed and simulated runoff data (testing).

Nash Sutcliffe Efficiency (NSE) was generally used to assess the efficiency of the hydrological prediction model (i.e. coefficient of efficiency) and this value varies from –α to 1. If the value of NSE is close to 1, then the model prediction is more accurate whereas the value equal to 1 suggests a perfect association between the observed and the simulated data. If the prediction model is as accurate as the mean of the observed data, then the value of NSE become zero and the negative value of NSE indicates that the mean of the observed data is better than the predicted model. In current research, the NSE calculated for training and testing runoff data shows a value 0.70 and 0.73 respectively, indicating comparatively higher accuracy. This suggests the suitability of MNN MDL model for accurately predicting the runoff in similar kind of river basins.

Error estimation of the predicted runoff model carried out to assess the performance of MNN MDL model also yields comparatively good results (Table 4.19). Root mean square error (RMSE) assessed for the training and testing shows a value of 79.71 and 78.85 respectively. Considering the data range (1 to >1000) used to estimate the RMSE, the values corresponding to the training and testing data are considerably low, which indicates that the discrepancy generated in the simulated runoff by the MNN MDL model are insignificant and the resulted runoff data are acceptable. Similarly, the relative Root mean square error (RRMSE) was also used to understand the prediction accuracy of the model. If the observed and the simulated data are identical, then the value of RRMSE is 0. Deviation of the simulated value from the observed value will give RRMSE > 0. In the present analysis, the MNN model shows RRMSE value of 0.52 and 0.50 for training and testing data. This suggests that the simulated runoff has not really deviated from the observed runoff.

Mean absolute error (MAE) value varies from 0 to α based on the value range of data used in the analysis. Lower values of MAE suggest better accuracy of the simulated runoff data. Considering the training and testing data simulated, the MAE values estimated are in the range of 49.79 and 51.04. Though the MAE is comparatively high, while considering the date range used in the present model, simulated runoff by MNN MDL model is acceptable with comparatively good accuracy. At the same time, considering another statistical method of error estimation, the mean absolute percentage error (MAPE), which expresses the distortion of the simulated data from the observed data similar to RRMSE and the MAPE is expressed as

percentage. A value of zero (0) indicates no distortion between the simulated and observed runoff data and when the simulation shows variation from observed data, the value of MAPE becomes greater than zero. MAPE in the range of 5 to 10% indicates a very accurate prediction and values of around 30% indicates reasonable prediction (Johnson & King, 1988; Nor et al., 2007). MAPE estimated for training and testing of runoff data in the present study was 31.97% and 32.33% respectively. The results indicate a slight distortion of simulated runoff series when compared with observed data but was still in the acceptable limit. This confirms the suitability of MNN MDL model for the simulation of runoff in the present study.

Analysis of volumetric error (EV) is capable of evaluating and identifying the total errors in the modeled system which can be expressed as percentage error (Brath et al., 2004; Lohani et al., 2011; Chakravarti & Jain, 2014; Haile et al., 2016). The lower the percentage of EV, the lesser the error and vice versa. In the present analysis, the MNN MDL model shows an EV of 0.78% for training data and 2.62% for testing data, suggesting comparatively higher accuracy of the model in simulating the runoff in Insungai Nanga. At the same time, the relative peak error (RPE), calculates the prediction error between the peak discharge of observed and simulated runoff (Zakhrouf et al. 2016). Assessments of the RPE of training and testing runoff data shows comparatively lower values (0.16 and 0.25 respectively) and indicates that the simulated runoff values are acceptable.

The rainfall-runoff model generated for the Limbang River Basin using the rainfall and discharge rating curve based runoff measurement from the location Insungai Nang through MNN with MDL algorithm shows comparatively good accuracy and efficiency for the simulation of runoff when compared with the observed data series. Statistical measurements such as CCF, ACF and PACF helped to determine the input vectors. These methods eliminated the trial and error methods and suggested to use four input vectors (one antecedent runoff and three antecedent rainfall). Hidden layers essential for the ANN model was fixed as one and four neurons were used to define the model to simulate the single output (runoff). The results showed comparatively good agreement of prediction in training and testing of the simulated runoff. Furthermore, the efficiency and accuracy of the model evaluated through statistical techniques such as Pearson's correlation, NSE, RMSE, RRMSE, MAE, MAPE, EV and RPE indicate comparatively high accuracy of prediction with less error suggesting the acceptability of the

simulated runoff values. Hence it can be concluded that, the MNN MDL model is reasonably good for the simulation of runoff, particularly in forested catchments similar to the study area which lacks detailed and up to date discharge measurements.

4.4 Composition of Stable Isotopes in Rainwater

The composition of stable isotopes of oxygen-18 ($\delta^{18}O$) and deuterium (δD) in rainwater is capable of providing detailed information about the regional atmospheric circulation and effects of climate change (Ehhalt et al., 1963; Dansgaard, 1964; Lee et al., 2003; Vuille et al., 2005; Mayr et al., 2007; Wu et al., 2010; Li et al., 2012; Cui & Li, 2015; Ren et al., 2017; Marryanna et al., 2017; Gao et al., 2018). The global meteoric water line (GMWL) described by Craig (1961), identified a strong empirical relationship between the composition of $\delta^{18}O$ and δD, which created the standard to compare the isotopes composition in local rainfall (precipitation) referred to as local meteoric water line (LMWL). This is used to identify the source and origin of the moisture, evaporation and re-evaporation and movements. Considering the applicability of stable isotopes in understanding the regional climatic conditions in connection with large scale atmospheric phenomena such as monsoons and El Niño-Southern Oscillation (ENSO), an attempt was made in the present research to do so. Because of the criticality of the location of the study area (equatorial tropics and in Inter Tropical Convergence Zone (ITCZ)) and lack of IAEA /GNIP (International Atomic Energy Agency / Global Network of Isotopes in Precipitation) locations in the region during the study period, the present research attempt is highly valid.

4.4.1 Stable isotopes in rainfall over the LRB

In the present research, monthly cumulative rainwater collected from two distant locations in the LRB for a period of one year (October-2016 to September-2017) was analysed to understand the spatial and temporal variation in the composition of $\delta^{18}O$ and δD. Along with the spatial and temporal distribution characteristics, influence of latitude, altitude, continental and amount effects on stable isotopes in rainwater over the region was further investigated. Details of sampling locations along with basic meteorological and terrain characteristics are given in Table 4.20 and the locations are shown in Figure 4.37. The first location of rainwater collection is in Limbang City, located near to the Brunei Bay in the South China Sea (SCS) at a distance of approximately 6km (30km away from the SCS) and the second location Kampong

Salidong, located in the interior of tropical forest region and was about 70km away from the South China Sea. Both sampling sites are located at a distance of 50km apart. The two selected locations also differ in the elevation and the amount of rainfall received. Limbang City shows an elevation of 3m above mean sea level, whereas Kampong Salidong located at an elevation of 131m above mean sea level. Considering the total rainfall recorded during the study period (October-2016 to September-2017), rainfall received at both locations shows a difference of 1000mm in which the least amount of rainfall was recorded at Limbang City (3896mm) while Kampong Salidong recorded the high cumulative rainfall (4922mm).

Table 4.20: Details of rainwater collected locations.

Locations	**Latitude**	**Longitude**	**Height (m) (amsl)**	**Distance from the SCS (km)**	**Total RF (mm) during the study period**	**Type**	**Terrain and vegetation**
Limbang City	4°44′ 28.7″	114°59′40.7″	3	30.00 (6km away from Brunei Bay)	3896	Urban	Flat with orchards and home gardens
Kampong Salidong	4°18′53″	115°02′17.9″	131	70.00	4922	Rural	Undulating with rainforests

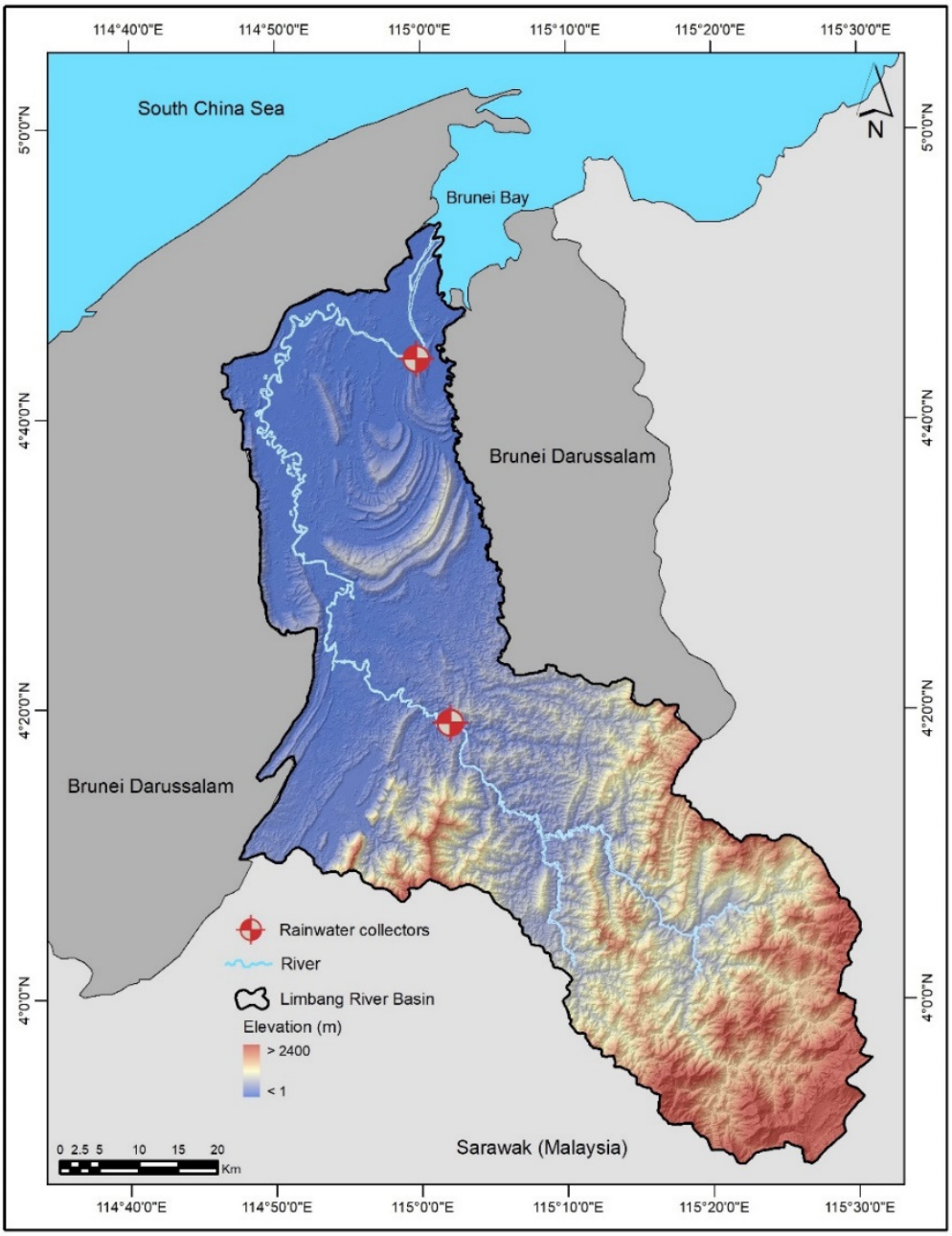

Figure 4.37: Rainwater collected locations with elevation.

4.4.2 Results of isotope analysis

Analysis results of δD and $\delta^{18}O$ with basic statistics (average and volume weighted average (VWA)) and monthly rainfall corresponding to each sampling location was given in the Table 4.21 and temporal variation is shown in Figure 4.38. During the sampling period, the

amount of monthly rainfall received in the sampling locations shows moderate variation. In Limbang City, the monthly rainfall varies in the range of 125mm (July-2017) to 531mm (May-2017) with an average of 325mm. Rainfall in Kampong Salidong shows comparatively higher range and it varies between 212mm (July-2017) to 615mm (August-2017) and shows a monthly average rainfall of 410mm. Though both stations show variation in monthly rainfall distribution and average rainfall, it shows a similar amount of inter-month rainfall variability i.e. 406 and 403mm respectively in Limbang City and Kampong Salidong.

Table 4.21: Results of stable isotopes against monthly rainfall in Limbang City and Kampong Salidong.

Sampling Period	**Limbang City**				**Kampong Salidong**			
	δD (‰)	$\delta^{18}O$ (‰)	d-excess (‰)	Rainfall (mm)	δD (‰)	$\delta^{18}O$ (‰)	d-excess (‰)	Rainfall (mm)
Oct. -2016	-66.50	-9.83	12.14	236	-72.05	-10.42	11.31	302
Nov.-2016	-54.48	-8.35	12.32	333	-56.62	-8.80	13.78	449
Dec.-2016	-59.09	-8.72	10.67	314	-77.67	-11.50	14.33	329
Jan.-2017	-51.46	-8.14	13.66	235	-58.75	-8.72	11.01	382
Feb.-2017	-50.12	-7.64	11.00	275	-50.76	-8.19	14.76	336
March-2017	-38.05	-5.81	8.43	289	-33.04	-5.50	10.96	539
April-2017	-38.86	-6.49	13.06	456	-59.85	-8.16	5.43	390
May-2017	-59.59	-8.69	9.93	531	-76.24	-10.61	8.64	606
June-2017	-68.43	-10.24	13.49	303	-88.48	-12.57	12.08	398
July-2017	N/A	N/A	N/A	125	-74.92	-10.54	9.40	212
Aug.-2017	N/A	N/A	N/A	387	-72.42	-10.93	15.02	615
Sept.-2017	N/A	N/A	N/A	416	-75.79	-11.24	14.13	364
Average	-54.06	-8.21	11.63	325	-66.38	-9.77	11.74	410
Volume-Weighted Average	-40.86	-6.21	8.80	----	-65.53	-9.66	11.76	----

Considering the location based composition of stable isotopes in rainwater collected in Limbang City, the value of δD ranges from -68.43‰ (June-2017) to -38.05‰ (March-2017) with an average value of -54.06‰ and VWA of -40.86‰. Similarly, the minimum value of δD in Kampong Salidong was observed in June-2017 (-88.48‰) and the maximum was noted in the month of March-2017 (-33.04‰) with an average and VWA of -66.38‰ and -65.53‰ respectively. A similar characteristics was noted in the composition of $\delta^{18}O$ in both the stations with a minimum in the month of June-2017 and the maximum during March-2017. The

composition of $\delta^{18}O$ in Limbang city ranges from -10.24 to -5.81‰ with an average of -8.21‰ and VWA of -6.21‰, whereas in the rainwater collected from the Kampong Salidong, $\delta^{18}O$ ranges from -12.57 to -5.50‰ with an average and VWA of -9.77‰ and -9.66‰ respectively. It was noted that, rainwater collected from Kampong Salidong shows comparatively lower value of δD and $\delta^{18}O$ in most of the months. The d-excess value calculated for the Limbang City ranges from 8.43‰ (March-2017) to 13.66‰ (January-2017) with an average of 11.63‰ and VWA of 8.80‰. At the same time, Kampong Salidong shows the minimum d-excess value of 5.43‰ in April-2017 and the maximum of 15.02‰ in August-2017 with an average and VWA of 11.74‰ and 11.76‰ respectively.

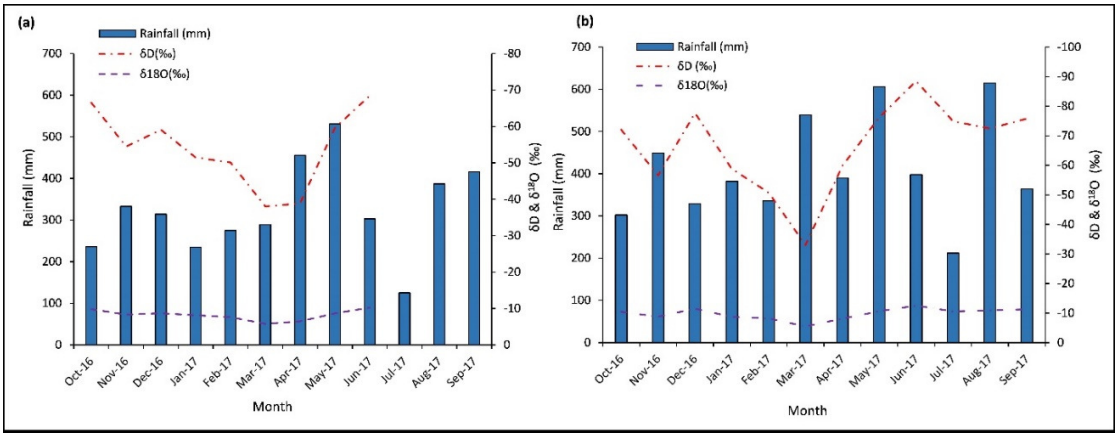

Figure 4.38: Monthly variation of δD and $\delta^{18}O$ and rainfall in the sampling locations a) Limbang City and b) Kampong Salidong.

Considering the isotopes values in the two locations, a slight difference in the average value of δD and $\delta^{18}O$ were identified. Average value of δD and $\delta^{18}O$ shows a decrease of 12.32‰ for δD and 1.55‰ for $\delta^{18}O$ between the locations Limbang City and Kampong Salidong. While comparing the average values of δD and $\delta^{18}O$ with respect to the latitudes and longitudes of the two stations, results show decreasing characteristics with decrease in latitude i.e. the closer to equatorial (positive relation) whereas the average value of δD and $\delta^{18}O$ shows a decreasing trend with increase in longitude (negative relation). Similar characteristics were identified in the VWA of δD and $\delta^{18}O$ with the latitudes and longitudes. At the same time, the average d-excess does not show any considerable difference with the latitude and longitude

difference in the present study and shows a very low difference of 0.10‰. It was also noted that the altitude difference of sampling locations influenced the composition of δD and $\delta^{18}O$. Kampong Salidong which is located at an elevation of 131m (a difference of 128m from Limbang City location), showing a reduction in average values of δD (-12.32‰) and $\delta^{18}O$ (-1.55‰). However, the altitude variation between the two sampling location does not have an influence over the average value of d-excess.

Continental effect (away from the coastal region) also influences the composition of stable isotopes in rainfall (Dansgaard, 1964; Rozanski et al., 1993; Winnick et al., 2014; Comas-Bru et al., 2016; Christner et al., 2018; Lacour et al., 2018). The location near to the coastal region shows comparatively high values of average δD and $\delta^{18}O$ whereas the location away from the coast (interior area), the average values of δD and $\delta^{18}O$ decreases. As observed in altitude effect, the continental effect does not have much influence over the d-excess value i.e. comparatively similar value of d-excess was observed in the two locations. Another factor affecting the value of δD and $\delta^{18}O$ is the amount of rainfall (Dansgaard, 1964; Rozanski et al., 1993; Johnson & Ingram, 2004; Risi et al., 2008; Breitenbach et al., 2010; Tan, 2014; Aggarwal et al., 2016; Tharammal et al., 2017; Jeelani et al., 2018). An inverse relation was identified between the amount of rainfall and the average value of δD and $\delta^{18}O$ (Moerman et al., 2013). In the present study, location Kampong Salidong showed lower δD and $\delta^{18}O$ values which received higher rainfall compared to Limbang City. Considering the sampling locations, no significant variation was observed between the average d-excess values, though both the stations showed higher variation in rainfall amount.

4.4.3 Local meteoric water line (LMWL)

The relationship between δD and $\delta^{18}O$ was analysed by plotting linear regression graphs for the two stations i.e. Limbang City and Kampong Salidong and were compared with the global meteoric water line (GMWL) shown in Figure 4.39. The local meteoric water line (LMWL) for Limbang City and Kampong Salidong, respectively were:

Limbang City	$\delta D = 7.46\,\delta^{18}O + 7.19$	$R^2 = 0.98$
Kampong Salidong	$\delta D = 7.62\,\delta^{18}O + 8.07$	$R^2 = 0.97$

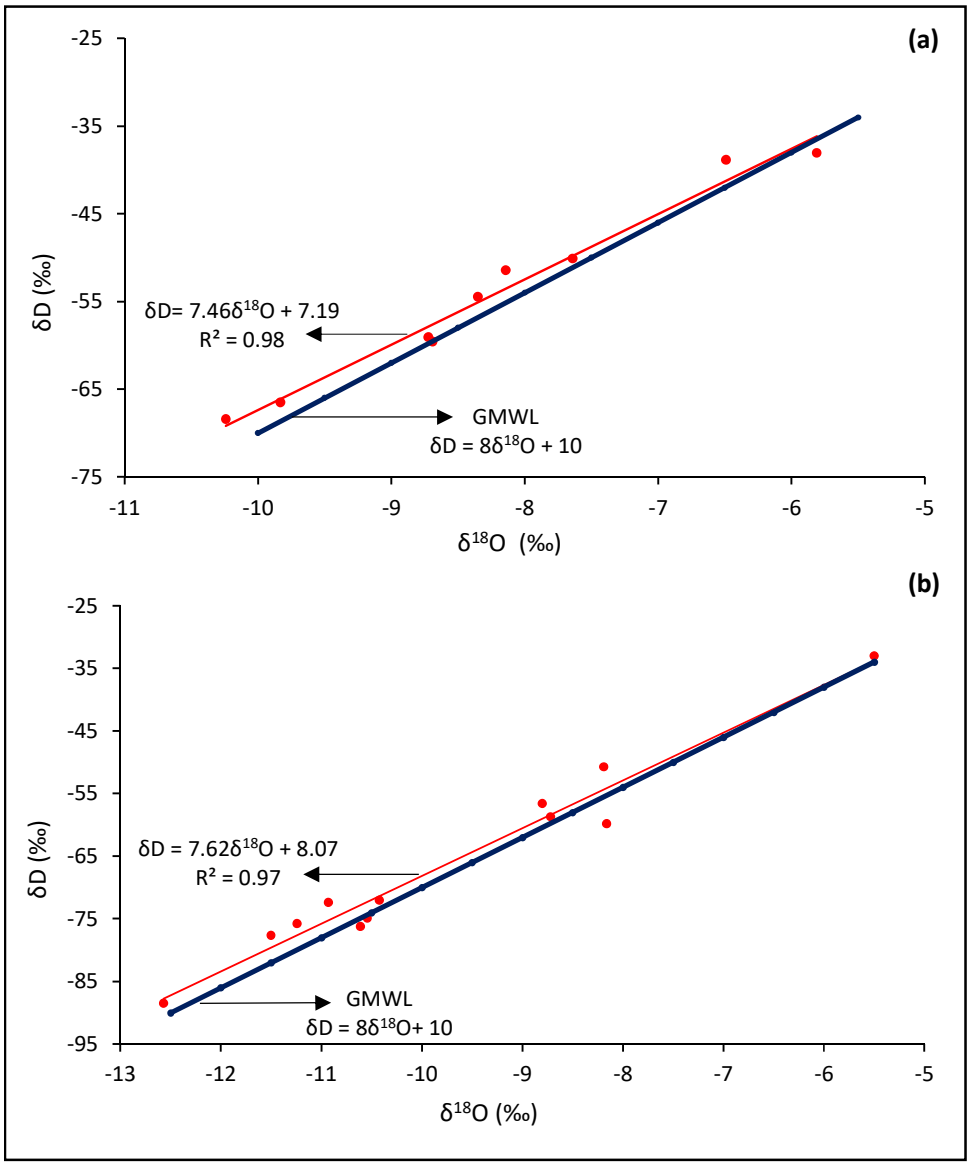

Figure 4.39: Relationship between δD and $\delta^{18}O$ in monthly rainwater collected from (a) Limbang City and (b) Kampong Salidong and its comparison with GMWL.

The linear equation (slope) of local meteoric water line (LMWL) derived for Limbang City and Kampong Salidong shows a slight variation from the value of global meteoric water line (GMWL) slope as defined by Craig (1961), but the d-intercept is comparatively lower. However, irrespective of location difference, the close values of the slope in two locations when compared to GMWL, indicates that the rain formation in the equatorial tropical region of Limbang occurred under the equilibrium condition i.e. at appropriate temperatures and steady

reaction rates with atmospheric boundary layers, vapors and liquids which control the fractionation of isotopes (Dansgaard, 1964). Comparatively higher slope values (close to GMWL) also indicate the non-significant influence of evaporation effect on the falling raindrops and suggesting enriched rain events (Craig, 1961; Dansgaard, 1964: Rozanski et al., 1993). Close similarity of slope values of independent locations in the study area suggests a common origin of rain formation with effect of secondary atmospheric processes in the composition of rainfall (Datta et al., 1991). At the same time, the difference in d-intercepts indicates the possibility of re-evaporation and changing condition of atmospheric moisture sources in these locations due to the evaporation of raindrops below the cloud layer (Rozanski et al., 1982).

4.4.4 Characteristic variation of δD, $\delta^{18}O$ and d-excess in the LRB

In order to understand the variation of δD and $\delta^{18}O$ in the LRB, the δD and $\delta^{18}O$ values of Limbang City and Kampong Salidong were combined and the average value which best represent the whole river basin was taken in to account. Results of average and volume weighted average values of δD, $\delta^{18}O$ and d-excess are given in Table 4.22.

Table 4.22: Rainfall and cumulative distribution of stable isotopes in the LRB.

Sampling period	δD (‰)	$\delta^{18}O$ (‰)	d-excess (‰)	Rainfall (mm)
October-16	-69.28	-10.13	11.73	268.90
November-16	-55.55	-8.58	13.05	390.90
December-16	-68.38	-10.11	12.50	321.00
January-17	-55.11	-8.43	12.34	308.38
February-17	-50.44	-7.92	12.88	305.63
March-17	-35.55	-5.66	9.70	413.75
April-17	-49.36	-7.33	9.25	422.88
May-17	-67.92	-9.65	9.29	568.50
June-17	-78.46	-11.41	12.79	350.13
July-17	-74.92	-10.54	9.40	168.38
August-17	-72.42	-10.93	15.02	500.75
September-17	-75.79	-11.24	14.13	389.75
Average	-62.76	-9.33	11.84	
Volume Weighted average	-62.32	-9.27	11.86	-----

Considering the LRB as a single whole unit, the δD measured from the rainfall collected during the study period varies from -78.46 (June-17) to -35.55‰ (March-17) with an average and VWA of -62.76‰ and -62.32‰ respectively. At the same time, the composition of $\delta^{18}O$ ranges between -11.41 (June-17) and -5.66‰ (March-17) with an average of -9.33‰ and VWA of -9.27‰. Similarly, the d-excess value ranges from 9.25 (April-17) to 15.02‰ (August-17) with an average and VWA of 11.84‰ and 11.86‰ respectively. In order to understand the temporal (monthly) distribution and variation of stable isotopes in the LRB, VWA of δD (vwδD), $\delta^{18}O$ (vw$\delta^{18}O$) and d-excess (vwd-excess) values were plotted against rainfall and are shown in Figure 4.40 a, b &c.

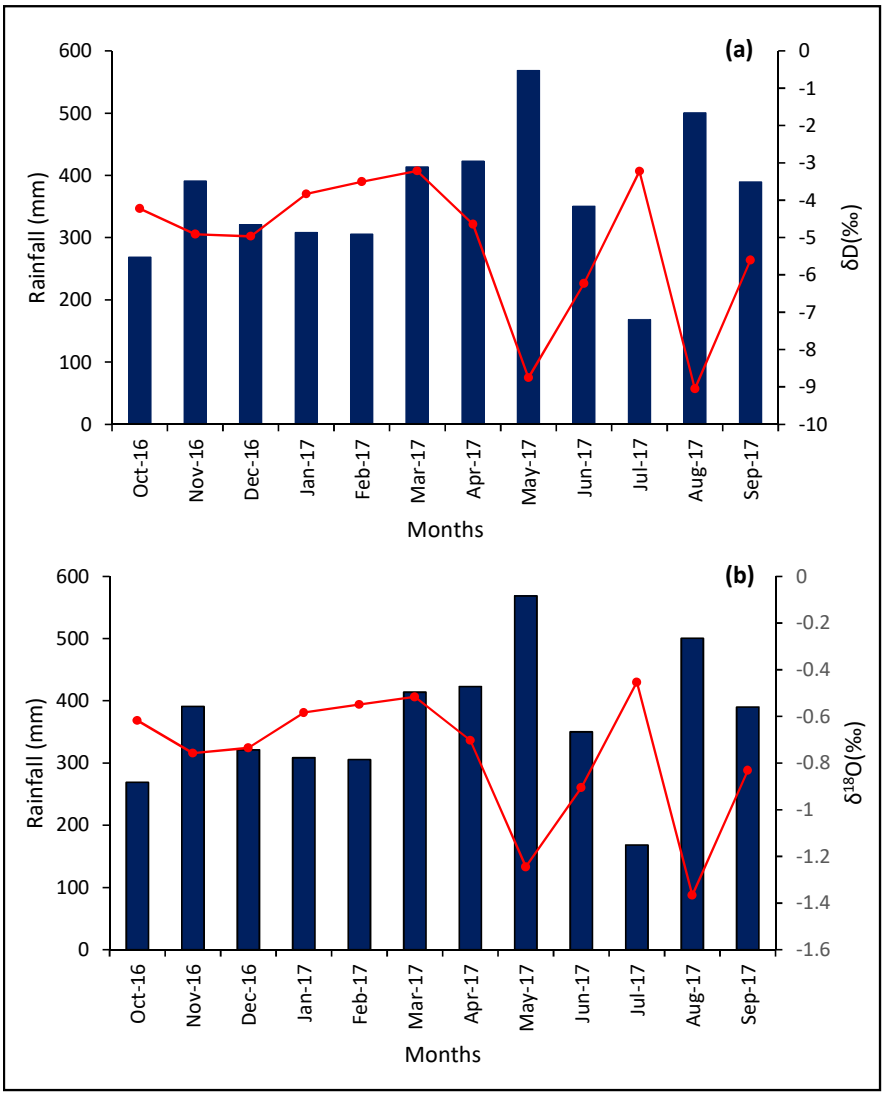

Figure 4.40: Temporal distribution of (a) vwδD and (b) vw$\delta^{18}O$ with rainfall during the study period.

It was noted that, lower amounts of rainfall were recorded with enriched composition of vwδD and vwδ^{18}O in January to March-17 and July-17 (Figure 4.40 a, b). Most depleted composition of vwδD and vwδ^{18}O was linked with the peak rainfall recorded during May-17 and August-17 during the study period. Furthermore, the characteristic depletion of vwδD and vwδ^{18}O generated a 'V' shape pattern during the months of May and August representing dominance of two rainy seasons in the area during the study period (Wirmvem et al., 2017). The characteristic pattern of depleted composition of vwδD and vwδ^{18}O also substantiated the concept of amount effect i.e. depletion of isotopes composition with the increase in amount of rainfall (Kumar et al., 2018).

While comparing the data with established monsoon seasons in the region i.e. southwest (May to September) and northeast (November to March), the present results of δ^{18}O and δD shows slight variation in monsoon characteristics in the region. Though the analysis of results reflected slight shifting in rainy seasonal characteristics, due to the limitation of the sampling periods, the exact seasonal influence and variation is not fully reflected. This is because, even one year monthly sample was considered in the analysis it does not followed the water year or hydrologic year (July to June) in Malaysia. Furthermore, the NE monsoon (November to March) in the region (including the LRB) was reported to receive a higher amount of rainfall and the SW monsoon (May to September) period receives comparatively lower rainfall (MMD, 2009). But it was noted during the study period of May and August which falls in the SWM season, this period recorded the highest rainfall than the other months especially November, December and January which was considered to be the wettest months in fall in the NEM season. This effect might be attributed to the overlapping of sampling period with two years seasons i.e. the sampling began in the inter-monsoon month of October-2016 and ended in September-2017. This not fully considered the seasonal rainfall within one year period like 2016-2017.

Assessment of the d-excess value which is the most useful stable isotope property, helps to determine the relative contribution of moisture source i.e. from inland or ocean (Gat & Carmi, 1970; Lee et al., 2003). Rainfall which originated from high humidity source regions by slow evaporation, show low d-excess values whereas regions of low humidity with fast evaporation show high d-excess values (Clark & Fritz, 1997). The value of d-excess nearer to

10‰ indicates that the condensation from ocean evaporation under equilibrium condition, has undergone non-equilibrium process of evaporation (Dansgaard, 1964; Clark & Fritz, 1997; Gautam et al., 2017). At the same time, variations from near 10‰ d-excess values explains the additional process involved in the generation of moisture (Dansgaard, 1964). Increased values of d-excess (>10‰) indicates the supply of recycled inland moisture to rainfall whereas the lower value of d-excess (<10‰) suggests the influence of evaporation of raindrops while falling down (Dansgaard, 1964). In addition to the re-evaporation, the lower values of d-excess also depends on the amount of rainfall, temperature and humidity (Kumar et al., 2018).

In the present study most of the months (October-16 to February-17, June-17, August-17 and September-17) show the d-excess value >10‰, which indicates the processes of increased convective activity with less re-evaporation in the LRB (Figure 4.40c).

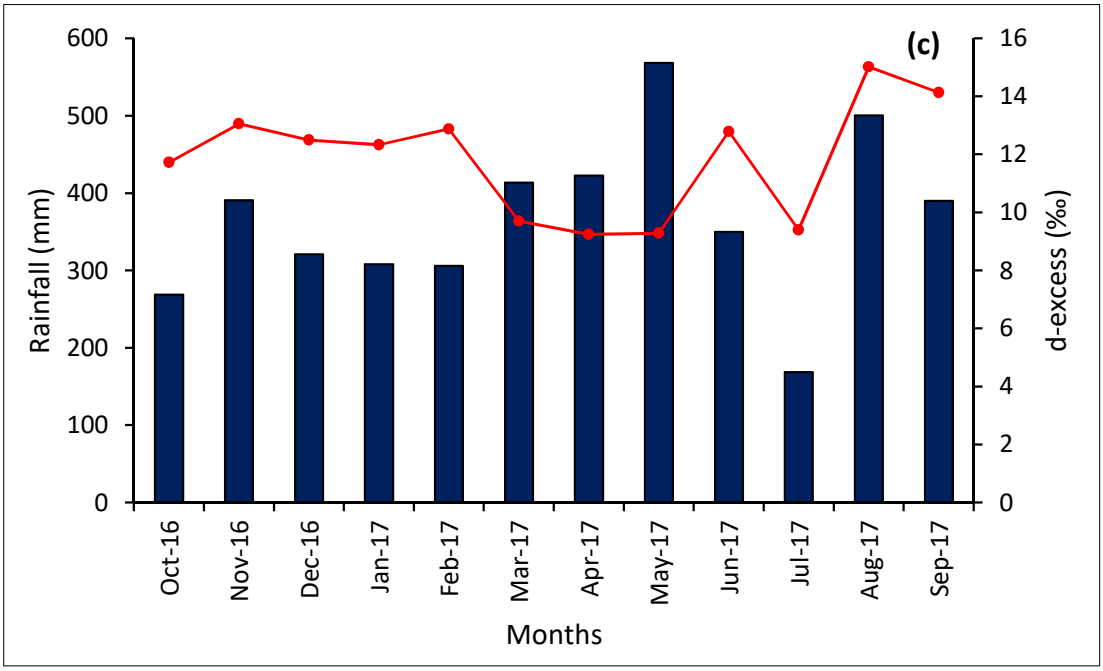

Figure 4.40: Temporal distribution of (c) vwd-excess with rainfall during the study period.

In addition to that, the influence of the recycled moisture from equatorial tropical rainforests and the net effect of evaporation from the river and precipitation cycle is also the reason for higher d-excess values in the LRB (Salati et al., 1979; Liu et al., 2014). During the months of March-17 to May-17 and July-17, the d-excess shows value is <10‰ (or≈10‰).

Among this, compared to other months, lower rainfall was recorded in July-17. Lower values of d-excess during these months can be attributed to the limited supply of inland moisture in the rainfall or due to the increased evaporation of raindrops when it transferred from cloud to land, lower amount of rainfalls and slow evaporation at source region due to high humidity (Clark & Fritz, 1997; Lee et al., 2003).

4.4.4.1 Amount effect

The relationship between the amount of rainfall and composition of stable isotopes in rainwater can be well explained by correlation plot, which is known as amount effect (Dansgaard, 1964). Amount effect occurs mainly due to the removal of water from the atmosphere in different amounts (Unnikrishnan Warrier & Praveen Babu, 2012). The correlation plot between the amount of rainfall in each month with composition of δD and $\delta^{18}O$ in the LRB was given in Figure 4.41. Regression line with the best fit (R^2) values and correlation coefficients (r) is as follows:

$\delta D = -0.01Pm + 0.10$	$R^2 = 0.60$	$r = -0.77$
$\delta^{18}O = -0.002Pm + 0.01$	$R^2 = 0.63$	$r = -0.80$

The linear regression plot explained a comparatively good fit and high negative correlation between the monthly rainfall and composition of δD and $\delta^{18}O$ (volume weighted average). The regression plot between δD with rainfall shows an inverse relationship with comparatively good best fit (R^2=0.60) with a slope of -0.01, which indicates an average rate of depletion of 1‰ of δD per 100mm of rainfall. However, the correlation analysis conducted revealed a strong negative correlation (r=-0.77) between monthly rainfall and δD. Considering the relationship between monthly rainfall and $\delta^{18}O$, an inverse relationship was noted with comparatively good best fit (R^2=0.63) as observed in the case of δD. Linear equation shown a slope value of -0.002, which indicates that the $\delta^{18}O$ value shows an average rate of depletion of 0.2‰ per 100mm of rainfall with a strong negative correlation with amount of rainfall (r=-0.80). The linear regression and correlation analysis reveals that the composition of δD and $\delta^{18}O$ will deplete with increase in rainfall amount (Dansgaard, 1964; Lawrence & White, 1991).

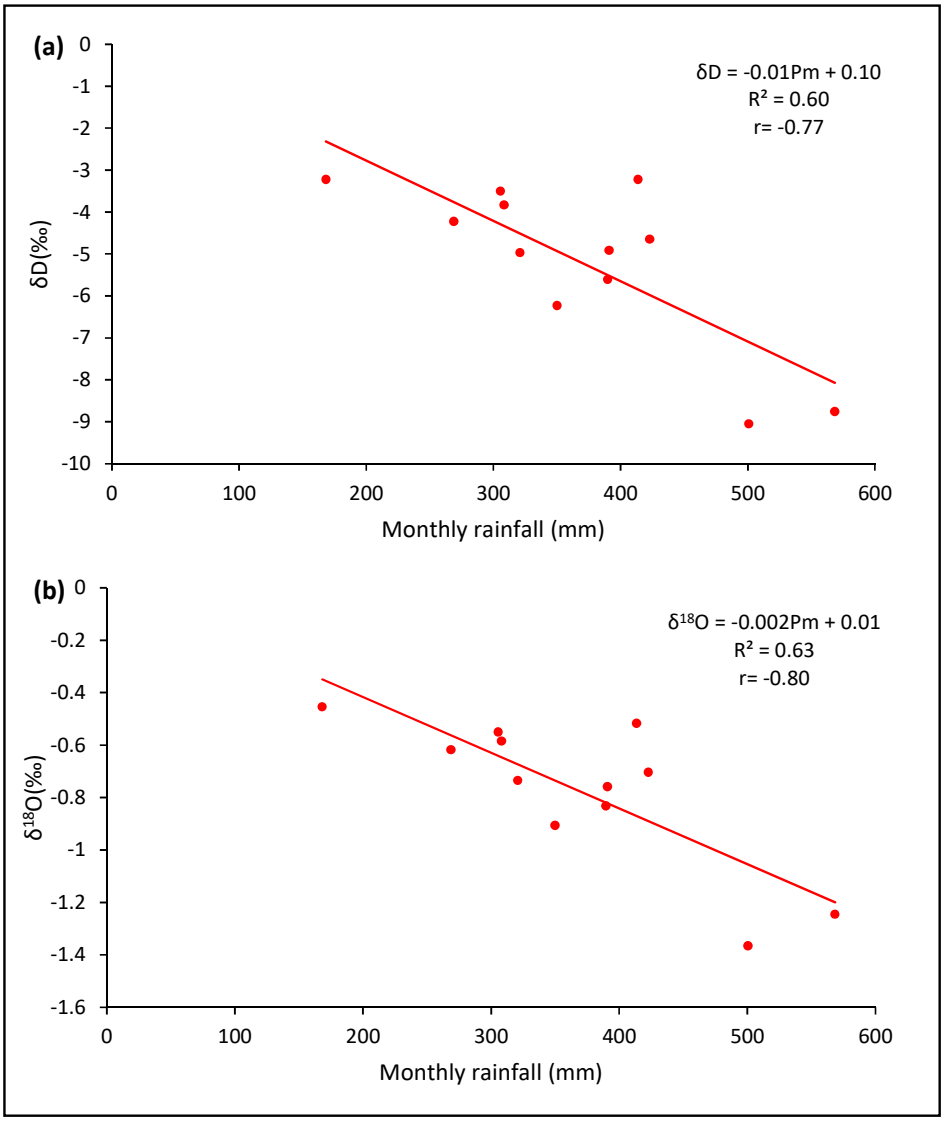

Figure 4.41: Explaining the relationship between rainfall amount and composition of δD and $\delta^{18}O$.

4.4.4.2 Temperature and humidity dependence of δD and $\delta^{18}O$ composition

The correlation between volume weighted average of δD and $\delta^{18}O$ in rainfall against monthly average values of atmospheric temperature and relative humidity was established by regression analysis (Figure 4.42). Regression plots of δD and $\delta^{18}O$ show a negative slope value of -3.59‰ and -0.46‰ respectively with regards to temperature and show very low goodness of fit with low R^2 values of 0.24 and 0.19 (Figure 4.42a & b). Regression equations also indicate that the average rate of depletion in δD and $\delta^{18}O$ were 3.59‰ and 0.46‰ per 1°C of

temperature. Correlation analysis of δD and $\delta^{18}O$ also showed a moderate inverse correlation (negative relation) with temperature i.e. r=-0.49 and -0.43 respectively. A similar characteristic relationship was also identified between the composition of δD and $\delta^{18}O$ with humidity (Figure 4.42 c & d). Linear regression plots identified a very weak negative relationship between humidity and composition of δD and $\delta^{18}O$ with no goodness of fit (R^2=0.03 and 0.04 respectively). At the same time, it was noted that the correlation coefficient also returned a very weak inverse correlation (negative relation) between humidity and the composition of δD and $\delta^{18}O$ (r=-0.16 and -0.19 for δD and for $\delta^{18}O$ respectively). The slope values of the linear regression equation between δD and $\delta^{18}O$ with humidity indicates that the δD and $\delta^{18}O$ show an average depletion of 0.28‰ and 0.05‰ per 1% of relative humidity.

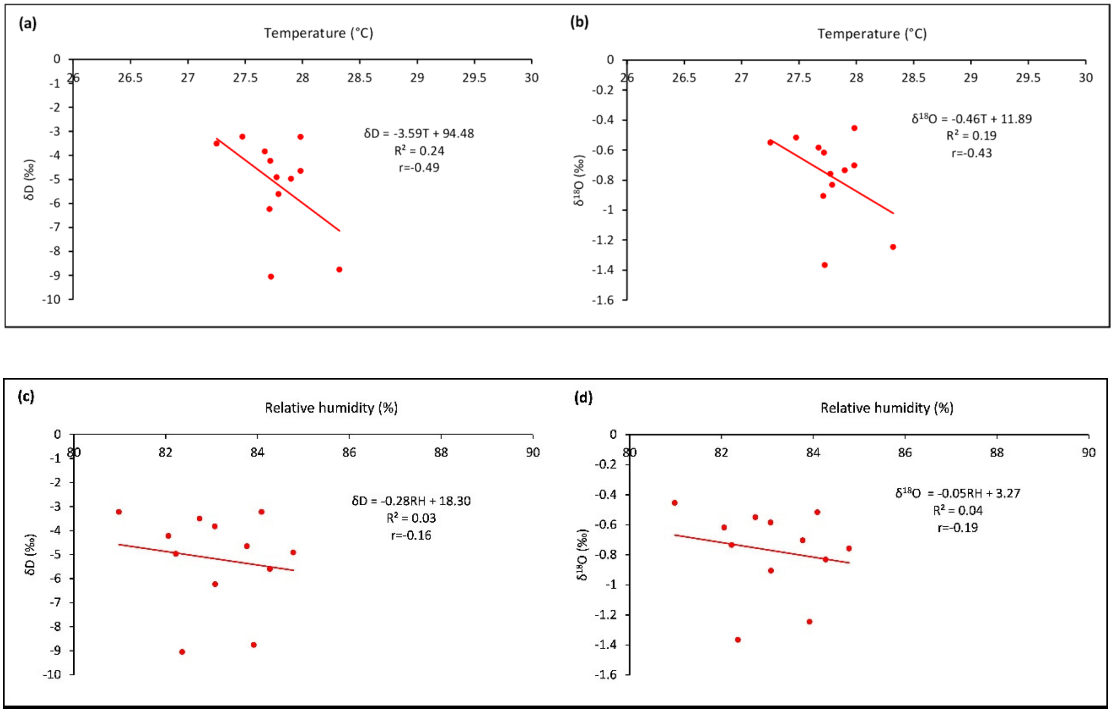

Figure 4.42: Linear regression plots explaining the relationship between volume weighted composition of δD and $\delta^{18}O$ with (a & b) temperature and (c & d) relative humidity during the sampling period.

Temperature vs δD and $\delta^{18}O$

δD = -3.59T + 94.48	R^2 = 0.24	r= -0.49
$\delta^{18}O$ = -0.46T + 11.89	R^2 = 0.19	r= -0.43

Relative humidity vs δD and $\delta^{18}O$

δD = -0.28RH + 18.30	R^2 = 0.03	r= -0.16
$\delta^{18}O$ = -0.05RH + 3.27	R^2 = 0.04	r= -0.19

The results suggest that there is no significant correlation that exists between the composition of δD and $\delta^{18}O$ with temperature and humidity in the LRB and suggests a near equilibrium condensation of ocean evaporation.

4.4.4.3 Seasonal variation of δD, $\delta^{18}O$ and d-excess in the LRB

As discussed earlier the study area experiences two dominant monsoon seasons (southwest monsoon - SWM and northeast monsoon - NEM) which covers a total of 10 months with short inter-monsoon periods of one month each. In order to understand the seasonal distribution characteristics of δD, $\delta^{18}O$ and d-excess in the LRB, monthly composition of δD and $\delta^{18}O$ were cumulated into seasonal averages (volume weighted averages) and the d-excess was calculated by considering the total of seasonal rainfall. Results of the composition of δD, $\delta^{18}O$ and d-excess calculated for seasonal rainfall are given in Table 4.23.

Table 4.23: Season based average and volume weighted average composition of δD and $\delta^{18}O$ with d-excess value.

Seasons	Average			Volume-Weighted Average			Seasonal Rainfall (mm)
	δD (‰)	**$\delta^{18}O$ (‰)**	**d-excess (‰)**	**δD (‰)**	**$\delta^{18}O$ (‰)**	**d-excess (‰)**	
Southwest monsoon (SWM)	-73.90	-10.75	12.12	-73.07	-10.67	12.32	1977.50
Northeast monsoon (NEM)	-53.00	-8.14	12.09	-52.18	-8.02	11.99	1739.65
Inter-monsoon (October)	-69.28	-10.13	11.73	-	-	-	268.90
Inter-monsoon (April)	-49.36	-7.33	9.25	-	-	-	422.88

During the southwest monsoon (SWM), δD shows an average value of -73.90‰ and the VWA of -73.07‰ whereas in the northeast monsoon (NEM) season, the average and VWA of δD was -53.00‰ and -52.18‰ respectively. During the inter-monsoon periods, average values of δD was -69.28‰ and -49.36‰ for October and April respectively. It was noted that, the most depleted values of δD were observed in SWM followed by the inter-monsoon month October. At the same time, the higher δD observed in the inter-monsoon month April, could have been the continuation of the northeast monsoon (NEM). A similar characteristics was observed in the composition of $\delta^{18}O$. During SWM, $\delta^{18}O$ shows a depleted value for the average (-10.75‰) and VWA (-10.67‰) compared to other seasons. In inter-monsoon period October, the $\delta^{18}O$ shows a low value of -10.13‰ whereas during April, it shows comparatively higher composition of -7.33‰. At the same time, during the NEM season, $\delta^{18}O$ showed an average and VWA composition of -8.14‰ and -8.02‰ respectively. Variations in the composition of δD and $\delta^{18}O$ is highly correlated with the amount of rainfall received during these seasons. During the study period, considering the seasonal rainfall, SWM season recorded the highest rainfall than NEM season, which may be the reason for depleted composition of δD and $\delta^{18}O$. In addition to that, higher vertical velocity of ascending air masses and lesser exchange effect of falling raindrops in atmospheric air could also a reason for the depleted values of δD and $\delta^{18}O$ (Rozanski et al., 1993). The enriched values of δD and $\delta^{18}O$ are due to evaporation of raindrops during rainfall and higher exchange effect of falling raindrops and atmospheric air (Taupin et al., 2000; Gat, 2010).

Average and VWA of d-excess during SWM were 12.12‰ and 12.32‰ whereas in NEM season it shows a slight variation and are 12.09‰ and 11.99‰ respectively. During inter-monsoon months October and April, the d-excess value shows high difference i.e. 11.73‰ and 9.25‰ respectively. Higher values of d-excess (>10‰) observed in SWM and NEM seasons indicate an additional source of moisture and higher convective activity with less re-evaporation and dominance of vapor from adjacent sea surface along with high relative humidity during the study period (Liu et al., 2010; Guan et al., 2013). In addition to that, the influence of regional winds, dominated oscillation of ITCZ (Inter Tropical Convergent Zone) and re-evaporation from tropical rainforests in the study area also influenced the composition of isotopes in rainfall in this region. Considering the inter-monsoon periods, the low value of d-

excess observed in the month of April might be due to the effect of partial evaporation of raindrops when falling from the cloud (Gat & Dansgaard, 1972).

4.4.5 Comparison of LMWL with nearby locations of IAEA

In order to assure the quality of present research, an attempt has been made to cross validate the analysis results of the present study with the stable isotope data available in IAEA /GNIP (International Atomic Energy Agency / Global Network of Isotopes in Precipitation). IAEA /GNIP operating in three sampling locations in northern Borneo namely Kuching, Mulu (Sarawak) and Kota Kinabalu (Sabah), and the available daily and monthly data of δD and $\delta^{18}O$ was retrieved to compare the LMWL with that of the present study. Figure 4.43 shows IAEA /GNIP sampling locations, along with location of rainwater samples collected for the present research. Kuching and Mulu are located in southwest side of the present study area whereas Kota Kinabalu is located at the northeastern side. Among the locations, Mulu is very close to

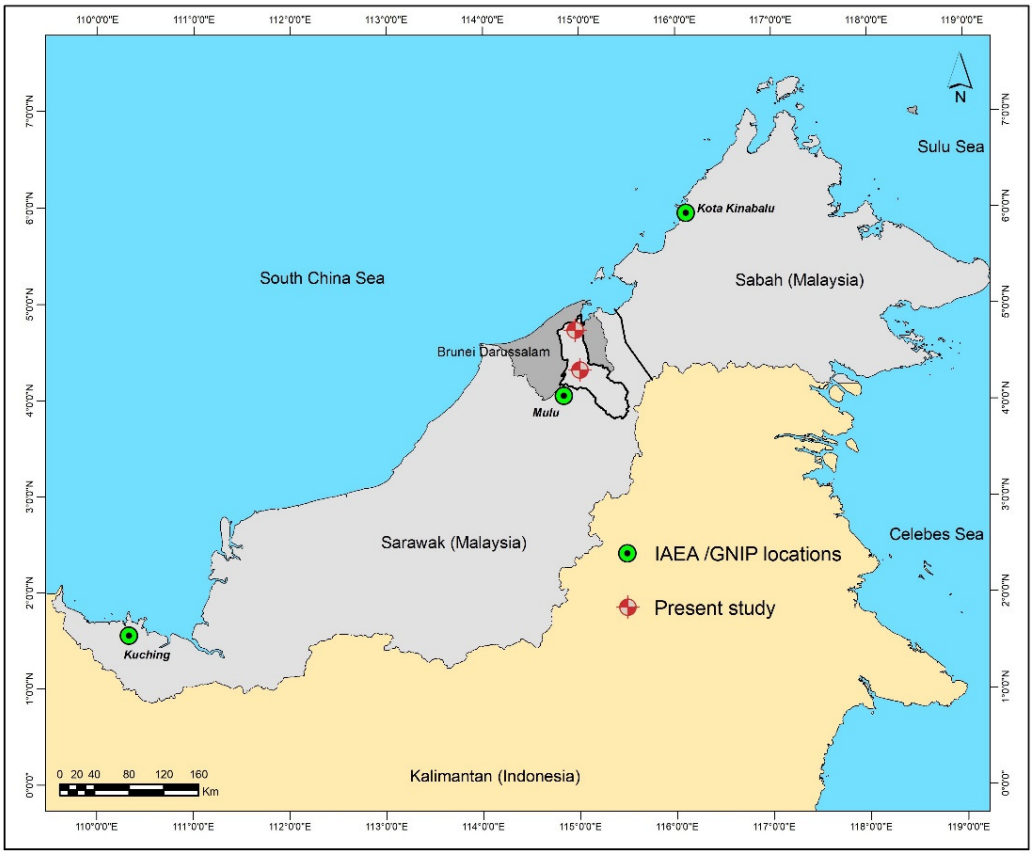

Figure 4.43: Selected IAEA /GNIP locations in East Malaysia along with rainwater sampling locations in the present research.

the present study area. IAEA /GNIP stations at Kuching and Kota Kinabalu have monthly isotope measurements for a period of 4 years (2013 to 2016), whereas the station Mulu has daily data over the range of 6 years (2006 to 2011).

After collecting δD and $\delta^{18}O$ values corresponding to the locations in East Malaysia, LMWL for all the four data sets (including the present research) was drawn and compared with GMWL (Figure 4.44). Though the δD and $\delta^{18}O$ measurements considered in the comparison study represented slightly different years, the LMWL of the different rainfall location shows more similar characteristics with comparable slope values. But the d-intercept showed a slight variation in its value among the datasets compared.

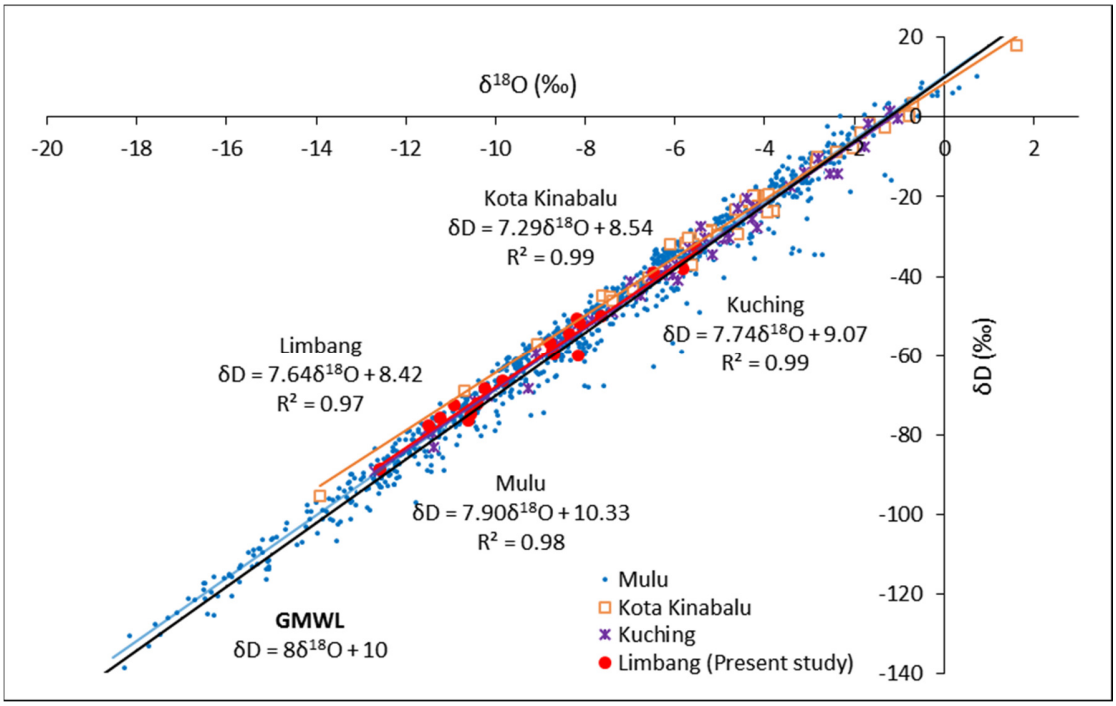

Figure 4.44: Comparison plot of LMWL of four locations in East Malaysia (GMWL also shown).

The linear regression equation derived by plotting δD and $\delta^{18}O$ of the locations considered are given below:

Location	LMWL	Goodness of fit	Correlation
Kota Kinabalu (2013-2016)	$\delta D = 7.29\delta^{18}O + 8.54$	R^2 = 0.99	r = 0.99
Kuching (2013-2016)	$\delta D = 7.74\delta^{18}O + 9.07$	R^2 = 0.99	r = 0.99
Mulu (2006-2011)	$\delta D = 7.90\delta^{18}O + 10.33$	R^2 = 0.98	r = 0.99
Limbang (2016-2017) (Present Study)	$\delta D = 7.64\delta^{18}O + 8.42$	R^2 = 0.97	r = 0.99

Slope of the above four equations are almost similar (7.29 to 7.90) and are very close to the slope value of GMWL i.e. 8. This suggests the equilibrium condition of rain formation in the equatorial tropical region. At the same time, slight variations in the value of the slope of four locations suggests the evaporation effects on the falling rain drops but was not significant. It was noted that the lowest slope value was shown by the rainfall received at Kota Kinabalu (7.29) and the highest value was associated with rainfall in Mulu (7.90). In addition, the LMWL of Mulu shows close similarity with GMWL. LMWL of Kuching station show a slope value of 7.74, which was the second highest slope value observed among the stations considered. Further, it was observed that the LMWL derived for the present study area shows a slope value of 7.64 which fall between the slope value of Kota Kinabalu and Kuching. However, it shows a slight variation when compared with LMWL of Mulu which can be attributed to the higher resolution of data samples in Mulu. Daily rainwater samples were collected from Mulu for the analysis whereas in the present study monthly cumulative rainwater was used to determine the composition of δD and $\delta^{18}O$. Accuracy of isotopes composition measurements in rainfall was highly dependent on the resolution of the sampling.

However, while considering the d-intercept of the four LMWL, it showed variation between the stations and also with GMWL. Among the stations, Mulu showed the highest and closer d-intercept value of GMWL (10.33) whereas the present study showed the lowest intercept value of 8.42. The other two d-intercept values come in close range but shows lower values with comparable difference from the intercept of GMWL (8.54 and 9.07 for Kota Kinabalu and Kuching respectively). The low d-intercept was observed in the present study may be due to the attribution of additional moisture source and re-evaporation process as discussed earlier.

Overall, the results of stable isotopes in rainfall in the LRB indicate a common source of moisture origin for the two locations. At the same time, LMWL of the study area is very close to the GMWL value with a slight deviation in the intercept. This indicates that the rain formation in this region is under equilibrium condition (near equilibrium) even though the evaporation occurs through non equilibrium processes. It was noted that rainfall and composition of stable isotopes show a strong negative correlation in the present study also as observed in other researches around the world (Breitenbach et al., 2010; Tan, 2014; Aggarwal et al., 2016; Tharammal et al., 2017; Jeelani et al., 2018; Zhao et al., 2018). Similarly, temperature and relative humidity does not have much influence on the composition of δD and $\delta^{18}O$ in the study area. At the same time, a comparison of present results with IAEA /GNIP locations that exists in the region (East Malaysia) showed a good agreement between the LMWL's slope but slightly different in d-intercept. Variations in the slope (very low) and d-intercept values in the present research can be attributed to the re-evaporation effect and change in the source condition of the atmospheric moisture. Though the present research has shown overall good accuracy, but due to the limitation of sampling periods and resolution, more detailed information about the effect of climate change on seasonal rainfall characteristics is not possible. Therefore it is suggested that, in order to acquire better understanding of the seasonal variation and reconstruction of palaeo climates, highly accurate and higher resolution (event based and daily) rainwater sampling for long period is required.

4.5 Rainwater Chemistry

4.5.1 Rainwater quality

An attempt has been made to assess the quality of rainwater collected in the LRB by analysing physico-chemical parameters. For the purpose, monthly accumulated rainwater from spatially separated 5 locations in the LRB was collected for a period of one year. The parameters pH, EC, TDS, DO, Turbidity, Carbonate (CO_3^{2-}), Bicarbonate (HCO_3^-), Chloride (Cl^-), Calcium (Ca^{2+}), Magnesium (Mg^{2+}), Sodium (Na^+), Potassium (K^+), Cobalt (Co), Nickel (Ni), Iron (Fe), Manganese (Mn), Lead (Pb), Cadmium (Cd), Zinc (Zn) and Copper (Cu) were analysed for the rainwater samples. Results are given in Table 4.24 and its spatial and temporal variations are shown in Figures 4.45 to 4.65.

4.5.1.1 Physical parameters

pH

pH in the RW-01 samples ranges from 5.33 (March-17) to 7.14 (November-16) during the sampling period, with a mean of 6.07. In RW-02, pH ranges from 5.68 (February-17) to 7.22 (October-16) with a mean of 6.09. The pH value in RW-03 ranges from 5.48 (January-17) to 6.86 (September-17) with a mean value of 6.01. In the sampling point RW-04, the mean value of pH is 5.95, which varies from 5.70 (October-16) to 6.24 (April-17). In the case RW-05, pH shows a minimum of 5.25 in November-16 and the maximum is 7.23 in September-17 with a mean of 5.95. The rainwater collected from locations near to the coastal area (RW-01 and RW-02) shows comparatively higher value of pH than other sampling points except the location RW-05, which is in the upper catchment region of the river basin.

EC

Rainwater collected from RW-01 shows the minimum value of the EC in the month of November-16 (58.17µS/cm) and the maximum value in September-17 (117.16µS/cm), with a mean of 87.56µS/cm. In the sampling location RW-02, EC ranges from 57.1 µS/cm to 109.45µS/cm which shows the same months as showed by the RW-01 with maximum and minimum EC values. The mean value of EC in RW-02 is 86.43µS/cm. In RW-03, the minimum value was observed in the month of October -16 (44.94µS/cm) and the maximum value in September-17 (148.94µS/cm) with a mean of 88.63µS/cm. In the case of samples collected from RW-04, the EC value ranges from 49.42µS/cm (November-16) to 131.13µS/cm (May-17) with a mean of 87.57µS/cm. EC value ranges from 49.73µS/cm (October -16) to 260.77 µS/cm (June-17) in location RW-05 with a mean of 104.07µS/cm. Among the sampling location RW-05 shown the highest value of EC.

TDS

TDS of monthly rainwater samples from five locations shows temporal and spatial variation. TDS in RW-01 ranges from 40.72 (November-16) to 82.01mg/L (September-17) with a mean of 61.29mg/L. In RW-02 the minimum value of TDS was observed in November-16 (40.03mg/L) and maximum values was recorded in September-17 (76.61mg/L). RW-02 samples show a mean TDS of 60.50mg/L. Comparatively, a small variation was observed in the TDS value of RW-03 samples and ranges from 31.46 (October-16) to 104.26 (September-17) mg/L with a mean of 62.04mg/L. TDS in RW-04 ranges from 34.60 (November-16) to 91.79 (May-17)

mg/L with a mean average of 61.30mg/L. At the same time, RW-05 shows the large variation in the TDS values and ranges between 34.81 (October-16) to 182.54 (June-17) mg/L. The mean TDS is 72.85mg/L for RW-05 samples.

DO

DO shows almost similar range of distribution in rainwater during the entire period of collection. The samples collected from of RW-01, DO value ranges from 3.40 (October-16) to 9.19 (November-17) mg/L with a mean of 6.92mg/L. DO in RW-02 from 4.60 (August-17) to 8.71 (October-16) mg/L with a mean of 7.19mg/L. In RW-03, the DO value ranges from 5.60 (June-17) to 8.07 (November-16) mg/L with a mean of 7.04mg/L. Samples collected from RW-04 shows maximum values in the months of February-17 and March-17 (7.60mg/L) and the minimum value in August-17 and September-17 (3.70mg/L) and shows a mean of 6.36mg/L. Rainwater samples collected from RW-05 shows a maximum in the month of March-17 (7.60mg/L) and the minimum value was recorded in August-17 (4.40mg/L) with a mean of 6.83mg/L.

Turbidity

Very low or negligible value of turbidity was observed in rainwater samples of five collecting locations. The Turbidity value ranges from 0.06 (March-17) to 4.11NTU (August-17) and 0.42 (August-17) to 3.30 (January-17) NTU for RW-01 and RW-02 respectively. The mean of turbidity for RW-01 is 1.31NTU and RW-02 is 1.13NTU. In RW-03, the samples show turbidity in the ranges of 0.03 (October-16) to 1.02 (March-17) NTU with a mean of 0.24NTU. Among the sampling sites the lowest value range of turbidity was observed in RW-04 and ranges from 0.04 (November-16) to 0.68NTU (August-17) with a mean of 0.30NTU. In the location RW-05, turbidity value ranges from 0.31 (March-17) to 4.92 (August-17) NTU and shows a mean of 1.60NTU.

4.5.1.2 Major Ions

Bicarbonate (HCO_3^-)

Rainwater samples analysed indicate the absence of carbonate concentration, whereas the HCO_3^- shows varying degree in concentration. Concentration of HCO_3^- in RW-01 samples ranges from 18.30 (November-16) to 41.18 (September-17) mg/L with mean of 32.77mg/L. In RW-02, HCO_3^- ranges from 18.30 (November-16) to 43.19 (January-17) mg/L with a mean of

31.68mg/L. At the same time, HCO_3^- shows a range from 9.15 (October-16) to 50.33 (September-17) mg/L in RW-03 with a mean of 30.28mg/L. In RW-04, the concentration of HCO_3^- ranges from 15.25 (October-16) to 41.18 (May-17) mg/L and a mean of 30.50mg/L. In the case of location RW-05 HCO_3^- ranges from 15.25 (November-16) to 59.48 (June-17) mg/L with a mean of 34.80 mg/L.

Chloride (Cl^-)

In sampling location RW-01, Cl^- concentration ranges from 15.62mg/L (January-17 and February-17) to 42.54mg/L (April-17) with a mean of 26.67mg/L. In RW-02, Cl^- value ranges from 13.29 (October-16) to 42.54 (July-17) mg/L with a mean of 26.98mg/L. In the case of RW-03, the Cl^- concentration ranges from 14.20mg/L (January-17) to 48.70mg/L (April-17) with a mean of 28.62mg/L. In RW-04, Cl^- ranges from 13.29 (November-16) to 49.63mg/L (May-17) and the mean value is 28.46mg/L. Sampling location RW-05 shows the concentration of Cl^- in the range of 12.78 (March-17) to 69.13mg/L (June-17). The mean value of Cl^- in RW-05 is 29.37mg/L.

Calcium (Ca^{2+})

Higher concentration of Ca^{2+} in RW-01 and RW-02 was identified in same month (November-16), and are 1.25mg/L and 1.03mg/L. But the minimum value in RW-01 was observed on February-17 (0.46mg/L) and January-17 in RW-02 (0.40mg/L). The mean concentration of Ca^{2+} in RW-01 is 0.74mg/L and 0.71mg/L in RW-02. In the case of remaining sampling locations namely RW-03, RW-04 and RW-05, the maximum concentration of Ca^{2+} was observed in the month of September-17 and is 17.16mg/L, 1.21mg/L, and 1.48mg/L respectively. The minimum concentration of Ca^{2+} in RW-03 is 0.28 mg/L (January-17), which shows a mean of 2.04mg/L. In the case of RW-04, the minimum values were observed in the month of July-17 (0.43mg/L) and the mean is 0.74mg/L. The sampling location RW-05 shows a minimum value of 0.35mg/L (December-16) with mean value of 0.64mg/L. Among the locations and samples, RW-03 samples show the highest concentration of Ca^{2+}.

Magnesium (Mg^{2+})

In the sampling locations RW-01 and RW-02, maximum concentration of Mg^{2+} was observed in the month of November-16 (0.76mg/L and 0.69mg/L) and the minimum in June-17 (0.19mg/L) and in August-17 (0.13mg/L) for RW-01 and RW-02 respectively. The mean

concentration in RW-01 is 0.29mg/L and in RW-02 is 0.27mg/L. In the case of RW-03, Mg^{2+} ranges from 0.15 (July-17) to 0.77mg/L (October-16) with a mean of 0.28mg/L. The minimum and maximum value of Mg^{2+} in RW-04 was 0.14 (August-17) and 1.98mg/L (March-17) with a mean of 0.43mg/L. In the case of RW-05 the value ranges from 0.19 (April-17) to 3.49mg/L (August-17) and shows mean of 0.57mg/L.

Sodium (Na^+)

Na^+ concentration in RW-01 ranges from 0.30 (April-17) to 2.47mg/L (November-16) with a mean value of 0.62mg/L. In RW-02, Na^+ ranges from 0.30 (May-17) to 2.02mg/L (November-16) with a mean of 0.69mg/L. It was observed that the Na^+ concentration in RW-03, ranges from 0.22 (July-17) to 2.30mg/L (October-16) with mean of 0.67mg/L. In RW-04, Na^+ shows minimum and maximum concentration of 0.26 (August-17) to 4.69mg/L (September-17) with mean of 1.05mg/L. Rainwater collected from RW-05 shows comparatively higher concentration of Na^+ in June-17 and July-17, and it ranges from 0.27 (April-17) to 46.44mg/L (June-17) with a mean of 6.34mg/L.

Potassium (K^+)

Concentration of K^+ in all months of each sampling location is comparatively lower than other major ions. In sampling location RW-01, K^+ ranges from 0.06 (February-17) to 0.52mg/L (July-17) with a mean of 0.20mg/L. Rainwater samples collected from RW-02 possess a mean of 0.18mg/L and the concentration of K^+ ranges from 0.06 (March-17) to 0.31mg/L (January-17). In RW-03, maximum value of K^+ is measured as 0.41mg/L (September-17) and the minimum as 0.06mg/L (December-16) with a mean of 0.15mg/L. In RW-04, the minimum and maximum concentration of K^+ is observed in March-17 (0.04mg/L) and February-17 (0.27mg/L) with a mean of 0.12mg/L. In RW-05, comparatively higher concentration of K^+ was observed in the months of June-17 and July-17 and it ranges from 0.08mg/L (March-17) to 6.68mg/L (June-17) with a mean of 1.12mg/L.

4.5.1.3 Trace Metals

Cobalt (Co)

Co concentration at different station shows almost similar characteristics with maximum and minimum value in the same months in most stations. Samples from RW-01 show Co in the range of 0.008 (July-17) to 0.051mg/L (February-17) with a mean of 0.025mg/L. In

RW-02, the minimum concentration was observed in August-17 (0.011mg/L) and maximum in November-16 (0.055mg/L) with a mean of 0.024mg/L. Co concentration in the ranges of 0.005 (July-17) to 0.056mg/L (November-16) was observed in samples collected from RW-03 with a mean of 0.022mg/L. In sampling location RW-04, the minimum and maximum Co concentration observed is 0.007mg/L (July-17) and 0.054mg/L (December-17) with a mean of 0.028mg/L. Samples collected from RW-05 shows Co in the ranges of 0.007mg/L (July-17) to 0.048mg/L (November-16) with a mean of 0.022mg/L.

Nickel (Ni)

Ni shown almost similar concentrations in most months, in most sampling locations. In RW-01 and RW-02 the maximum concentration was observed in the month of January-17 (0.212mg/L and 0.194mg/L), whereas RW-01 shows a minimum in June-17 (0.083mg/L) and RW-02 in July-17 (0.103mg/L). Mean concentration observed in these locations were 0.146mg/L and 0.142mg/L respectively. In RW-03, Ni ranges from 0.063 (July-17) to 0.207mg/L (January-17) with a mean of 0.138mg/L. Rainwater samples from RW-04 shows the minimum and maximum concentration in the ranges of 0.082 (August-17) to 0.219mg/L (February-17) with a mean of 0.142mg/L. Ni concentration in RW-05, show the minimum value in the month of August-17 (0.066mg/L) and the maximum in January-17 (0.199mg/L). The mean observed in RW-05 is 0.12mg/L.

Cadmium (Cd)

Concentration of Cd ranges from 0.003 (August-17) to 0.010 (September-17) mg/L with mean of 0.006mg/L in rainwater collected from RW-01. In RW-02, the minimum and maximum concentration of 0.003 and 0.009mg/L in the months August-17 and September-17 was similar to RW-01. RW-02 shows a mean of 0.005mg/L. In RW-03, the minimum concentration was observed in the month of August-17 (0.002mg/L) and the maximum value in the month of October-16 (0.009mg/L) with a mean of 0.004mg/L. Rainwater samples from RW-04 shows the minimum concentration of Cd in two consecutive months, namely June and July-17 (0.003mg/L) and the maximum concentration was measured in October-16 (0.008mg/L) with a mean of 0.005mg/L. Similar to sampling locations RW-01 and RW-02, the samples from RW-05 also show the minimum and maximum value in the month of August (0.002mg/L) and September -17 (0.011mg/L) with a mean of 0.005mg/L.

Iron (Fe)

Fe concentration in rainwater collected from the location RW-01 ranges from 0.96 (December-16) to 1.61mg/L (November-16) with a mean of 1.09mg/L. The lowest concentration of Fe in RW-02 and RW-03 samples were measured in the month of March-17 (0.68mg/L and 0.83mg/L), whereas the maximum was obtained in the months of October-16 (1.62mg/L) in RW-02 and November-16 (1.64mg/L) in RW-03. The mean concentration of Fe in RW-02 and RW-03 is 1.05mg/L and 1.10mg/L respectively. In RW-04 and RW-05, the minimum concentration of Fe was measured in the months of September-17 (0.73mg/L and 0.63mg/L) with maximum value recorded in October-16 (1.58mg/L and 1.71mg/L). The mean for RW-04 is 1.08mg/L and for RW-05 is 0.95mg/L.

Manganese (Mn)

The Mn concentration in samples collected from RW-01 ranges from 0.022 (April-17) to 0.042mg/L (December-16) with a mean of 0.030mg/L. In location RW-02, Mn ranges from 0.016 (March-17) to 0.042mg/L (December-16) with a mean value of 0.027mg/L. In RW-03, the minimum value of Mn was noted in the month of September-17 (0.016mg/L) and the maximum value recorded in the months November-16, December-16 and January-17 (0.036mg/L) with a mean value 0.027mg/L. Similarly, in RW-04, the minimum value was noted in September-17 (0.016mm/L) and the maximum value in August-17 (0.045mg/L) with a mean of 0.032mg/L. In RW-05, the minimum value of Mn was shown in August-17 (0.017mg/L) and the maximum Mn concentration were observed in different months such as December-16, January-17 and March-17 (0.037mg/L). RW-05 shows a mean of 0.028mg/L.

Lead (Pb)

The concentration of Pb in RW-01 ranges from 0.012 (July-17) to 0.115mg/L (November-16) with a mean of 0.035mg/L. In the case of RW-02, the value ranges from 0.007 (February-17) to 0.109mg/L (October-16) with mean of 0.039mg/L. The minimum and maximum values of Pb in RW-03 is 0.012 (July-17) to 0.108mg/L (November-16) with a mean of 0.037mg/L. In the case of RW-04, the minimum value was observed in the month of April-17 (0.018mg/L) and maximum in October-17 (0.097mg/L). The mean in RW-04 is 0.038mg/L. In RW-05, Pb ranges from 0.016 (December-16) to 0.079mg/L (October-16) with a mean of 0.034mg/L. Higher Pb concentration were noted in the sampling locations near to the coastal region and the locations away from the coastal zone shows comparatively lower concentration.

Zinc (Zn)

Concentration of Zn in samples collected from RW-01 shows that the value ranges from 0.002 (June-17) to 0.030mg/L (October-16) with a mean of 0.014mg/L. In RW-02, the minimum and maximum value noted is 0.006mg/L (June-17) and 0.033mg/L (November-16) with a mean of 0.017mg/L. At the same time, in RW-03, Zn value range of 0.001 to 0.031mg/L with a mean of 0.015mg/L. In RW-04, the minimum value was observed in the months of April-17 and July-17 (0.003mg/L) and maximum was observed in the month of November-16 (0.029mg/L) with mean value of 0.015mg/L. In sampling location RW-05, Zn concentrations ranged from 0.001 (June-17) to 0.025mg/L (November-16) with a mean of 0.014mg/L.

Copper (Cu)

Cu concentration in rainwater collected from location RW-01 varies from 0.007 (June-17) to 0.026mg/L (March-17) with a mean value of 0.015mg/L. In the case of RW-02, the minimum and maximum value of Cu concentration is 0.007 (September-17) and 0.020mg/L (January-17) with a mean of 0.012mg/L. In RW-03 samples, Cu ranges from 0.003 (April-17) to 0.020 mg/L (March-17) with a mean of 0.012mg/L. The minimum value noted in rainwater collected from RW-04 is 0.007mg/L (May-17) and the maximum is 0.019mg/L (January-17) and shows a mean of 0.012mg/L. In location RW-05, the Cu in the rainwater samples ranges from 0.006 (June-17) to 0.019mg/L (March-17) with a mean of 0.012mg/L. In the case of Cu, higher concentration is observed in the samples collected near the coastal region, similar to those of Pb.

Table 4.24: Results of physico-chemical parameters of rainwater collected from sampling locations RW-01, RW-02 and RW-03.

Parameters	RW-01				RW-02				RW-03			
	Min	Max	Mean	Std. Dev	Min	Max	Mean	Std. Dev	Min	Max	Mean	Std. Dev
pH	5.33	7.14	6.07	0.48	5.68	7.22	6.09	0.49	5.48	6.86	6.01	0.34
EC (µS/cm)	58.17	117.16	87.56	20.41	57.19	109.45	86.43	20.61	44.94	148.94	88.63	31.69
TDS (mg/L)	40.72	82.01	61.29	14.29	40.03	76.61	60.50	14.43	31.46	104.26	62.04	22.18
DO (mg/L)	3.40	9.19	6.92	1.52	4.60	8.71	7.19	1.26	5.60	8.07	7.04	0.80
Turbidity (NTU)	0.06	4.11	1.31	1.16	0.42	3.30	1.13	0.78	0.03	1.02	0.24	0.27
Bicarbonate (mg/L)	18.30	41.18	32.77	5.95	18.30	43.19	31.68	6.41	9.15	50.33	30.28	11.07
Chloride (mg/L)	15.62	42.54	26.67	10.35	13.29	42.54	26.98	11.51	14.20	48.74	28.62	12.26
Ca (mg/L)	0.46	1.25	0.74	0.21	0.40	1.03	0.71	0.20	0.28	17.16	2.04	4.77
Mg (mg/L)	0.19	0.76	0.29	0.15	0.13	0.69	0.27	0.18	0.15	0.77	0.28	0.21
Na (mg/L)	0.30	2.47	0.62	0.60	0.30	2.02	0.69	0.60	0.22	2.30	0.67	0.69
K (mg/L)	0.06	0.52	0.20	0.14	0.06	0.31	0.18	0.08	0.06	0.41	0.15	0.09
Co (mg/L)	0.008	0.051	0.025	0.015	0.011	0.055	0.024	0.013	0.005	0.056	0.022	0.012
Ni (mg/L)	0.083	0.212	0.146	0.051	0.103	0.194	0.142	0.035	0.063	0.207	0.138	0.043
Cd (mg/L)	0.003	0.010	0.006	0.002	0.003	0.009	0.005	0.002	0.002	0.009	0.004	0.002
Fe (mg/L)	0.96	1.61	1.09	0.17	0.68	1.62	1.05	0.30	0.83	1.64	1.10	0.248
Mn (mg/L)	0.022	0.042	0.030	0.006	0.016	0.042	0.027	0.007	0.016	0.036	0.027	0.007
Pb (mg/L)	0.012	0.115	0.035	0.028	0.007	0.109	0.039	0.034	0.012	0.108	0.037	0.031
Zn (mg/L)	0.002	0.030	0.014	0.010	0.006	0.033	0.017	0.009	0.001	0.031	0.015	0.010
Cu (mg/L)	0.007	0.026	0.015	0.006	0.007	0.020	0.012	0.004	0.003	0.020	0.012	0.005

Table 4.24: Results of physico-chemical parameters of rainwater collected from sampling locations RW-04 and RW-05.

Parameters	RW-04				RW-05			
	Min	Max	Mean	Std. Dev	Min	Max	Mean	Std. Dev
pH	5.70	6.24	5.95	0.18	5.25	7.23	5.95	0.58
EC (µS/cm)	49.42	131.13	87.57	25.84	49.73	260.77	104.07	58.25
TDS (mg/L)	34.60	91.79	61.30	18.09	34.81	182.54	72.85	40.78
DO (mg/L)	3.70	7.60	6.36	1.62	4.40	7.60	6.83	1.00
Turbidity (NTU)	0.04	0.68	0.30	0.21	0.31	4.92	1.60	1.49
Bicarbonate (mg/L)	15.25	41.18	30.50	7.52	15.25	59.48	34.80	12.61
Chloride (mg/L)	13.29	49.63	28.46	13.12	12.78	69.13	29.37	18.12
Ca (mg/L)	0.43	1.21	0.74	0.27	0.35	1.48	0.64	0.31
Mg (mg/L)	0.14	1.98	0.43	0.52	0.19	3.49	0.57	0.94
Na (mg/L)	0.26	4.69	1.05	1.27	0.27	46.44	6.34	13.86
K (mg/L)	0.04	0.27	0.12	0.07	0.08	6.68	1.12	2.10
Co (mg/L)	0.007	0.054	0.028	0.015	0.007	0.048	0.022	0.012
Ni (mg/L)	0.082	0.219	0.142	0.053	0.066	0.199	0.123	0.049
Cd (mg/L)	0.003	0.008	0.005	0.001	0.002	0.011	0.005	0.002
Fe (mg/L)	0.73	1.58	1.08	0.26	0.63	1.71	0.95	0.32
Mn (mg/L)	0.016	0.045	0.032	0.009	0.017	0.037	0.028	0.007
Pb (mg/L)	0.018	0.097	0.038	0.028	0.016	0.079	0.034	0.023
Zn (mg/L)	0.003	0.029	0.015	0.010	0.001	0.025	0.014	0.007
Cu (mg/L)	0.007	0.019	0.012	0.004	0.006	0.019	0.012	0.004

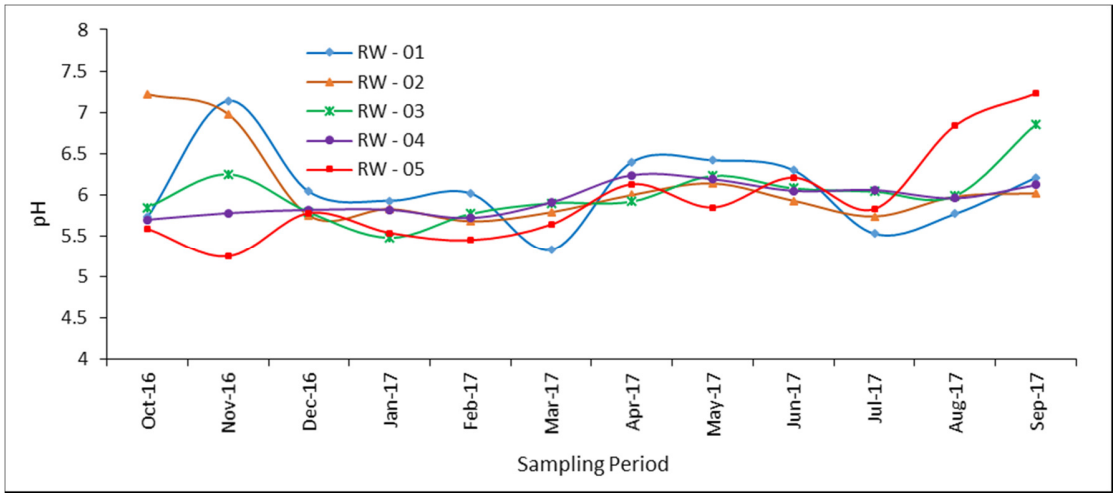

Figure 4.45: Spatial and temporal variation in pH.

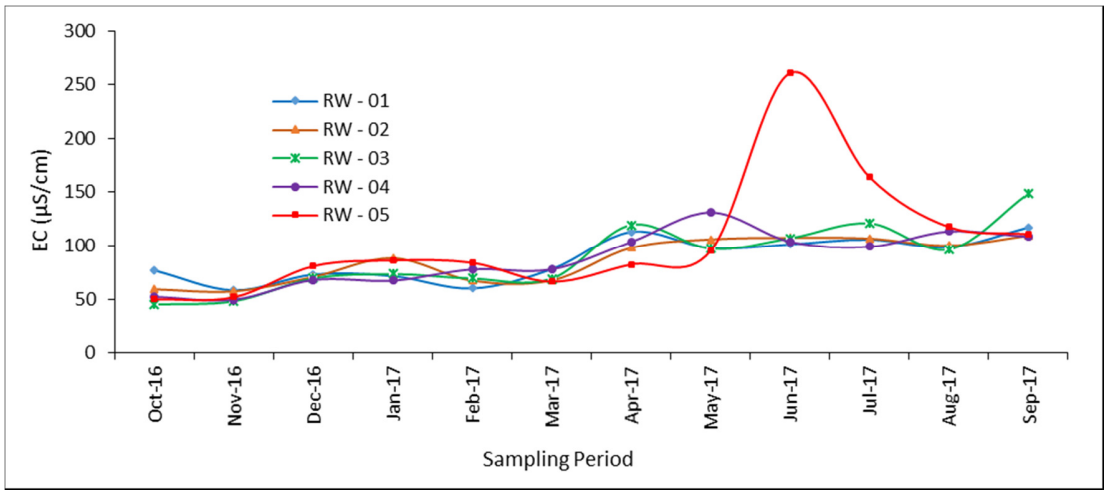

Figure 4.46: Spatial and temporal variation in EC.

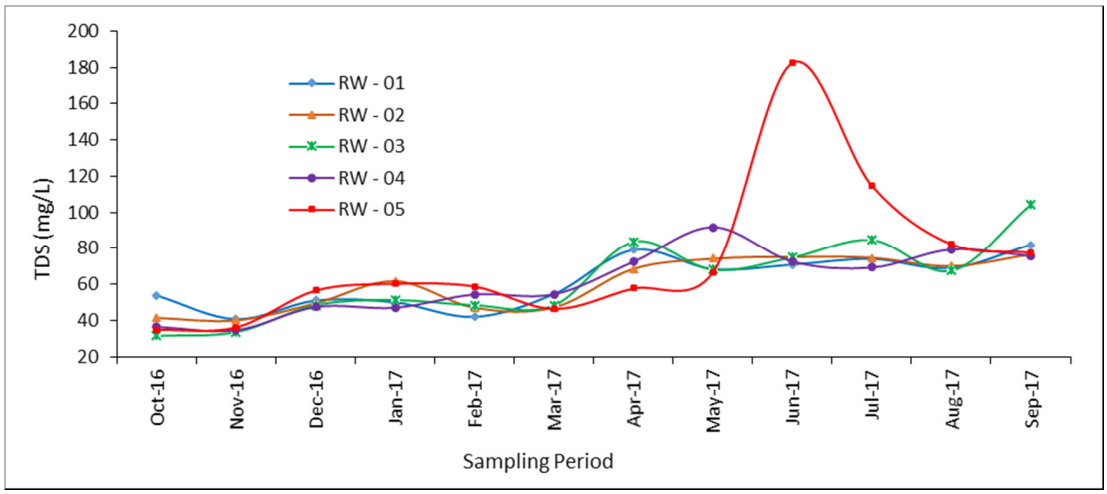

Figure 4.47: Spatial and temporal variation in TDS.

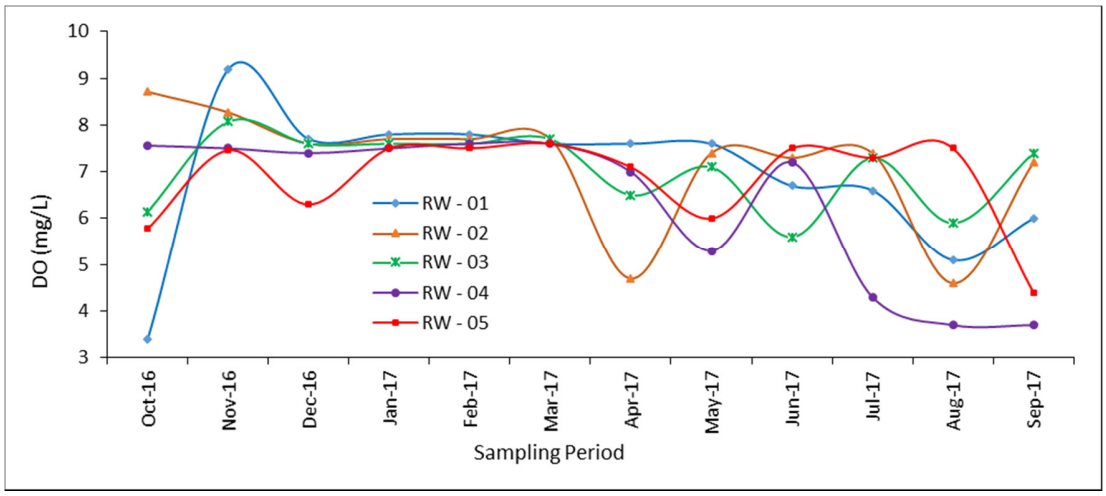

Figure 4.48: Spatial and temporal variation in DO.

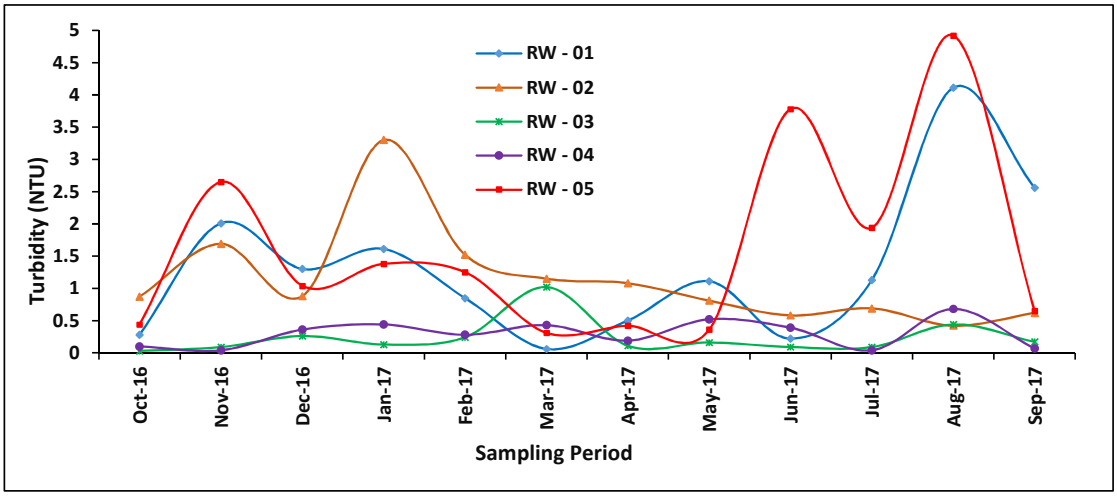

Figure 4.49: Spatial and temporal variation in Turbidity.

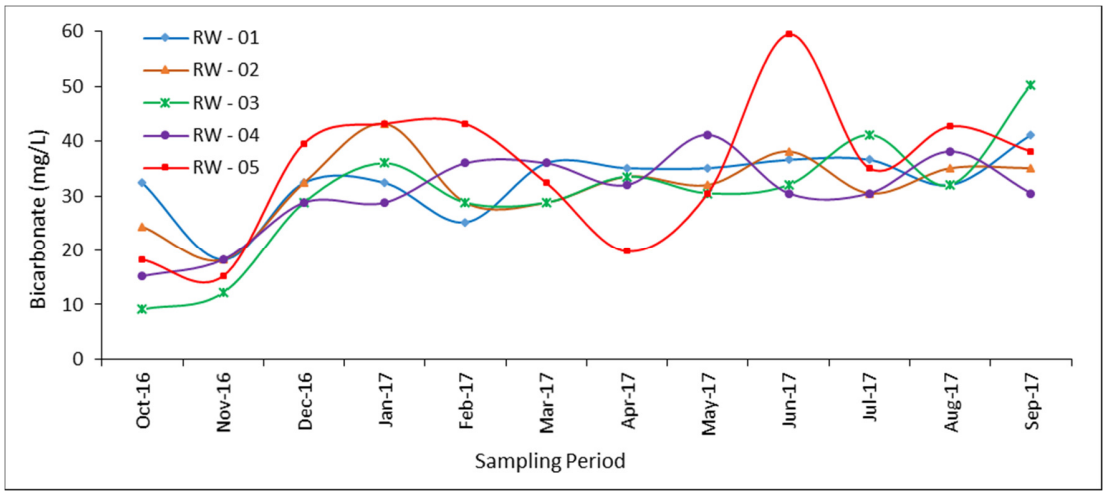

Figure 4.50: Spatial and temporal variation in Bicarbonate.

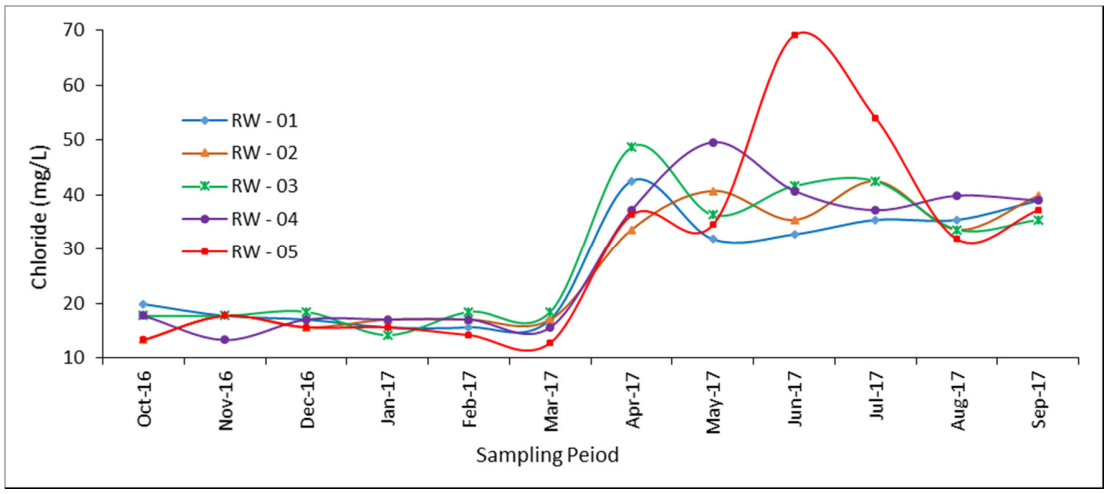

Figure 4.51: Spatial and temporal variation in Chloride.

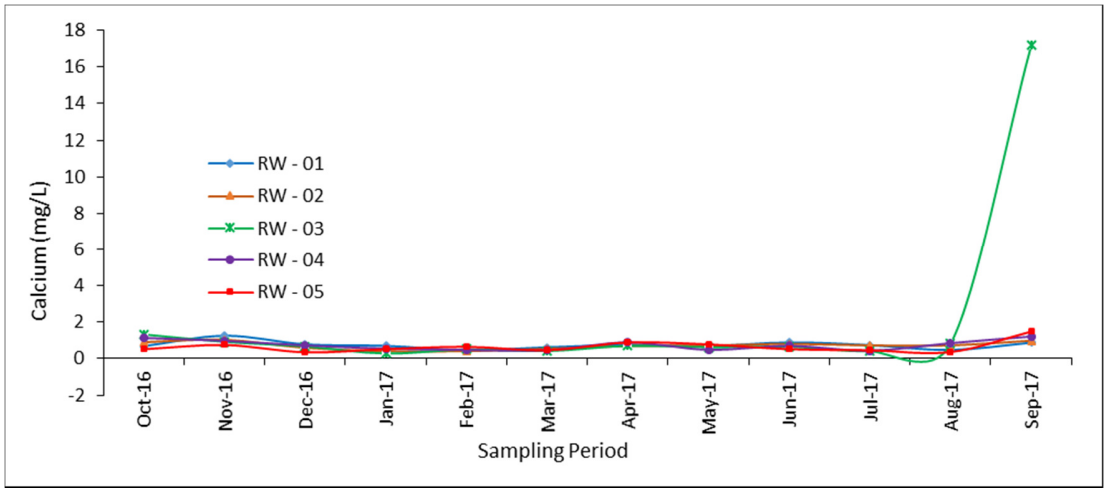

Figure 4.52: Spatial and temporal variation in Calcium.

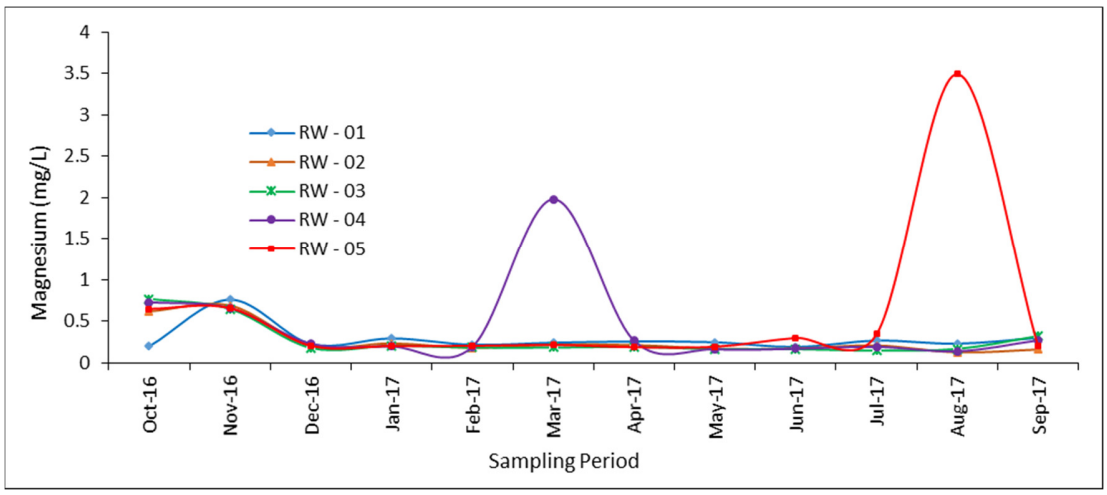

Figure 4.53: Spatial and temporal variation in Magnesium.

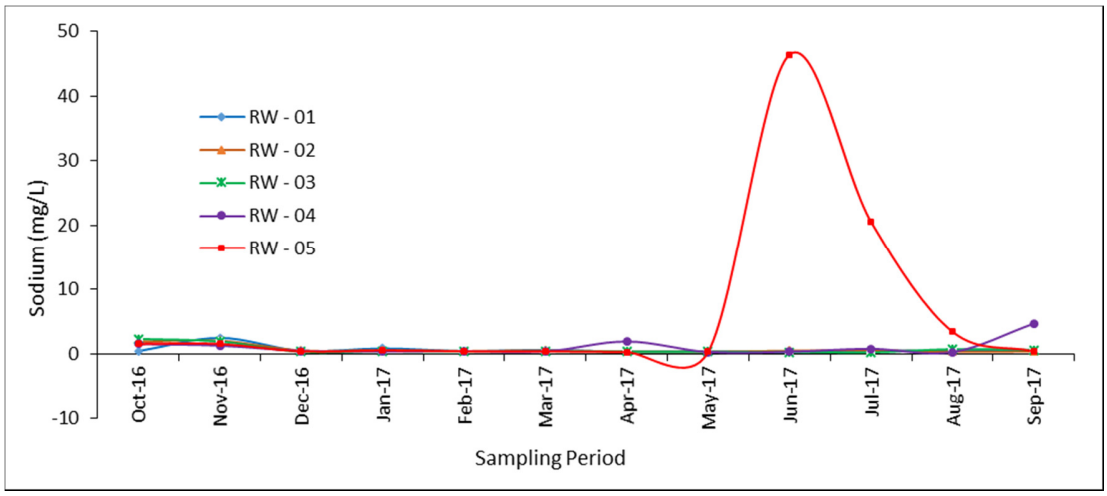

Figure 4.54: Spatial and temporal variation in Sodium.

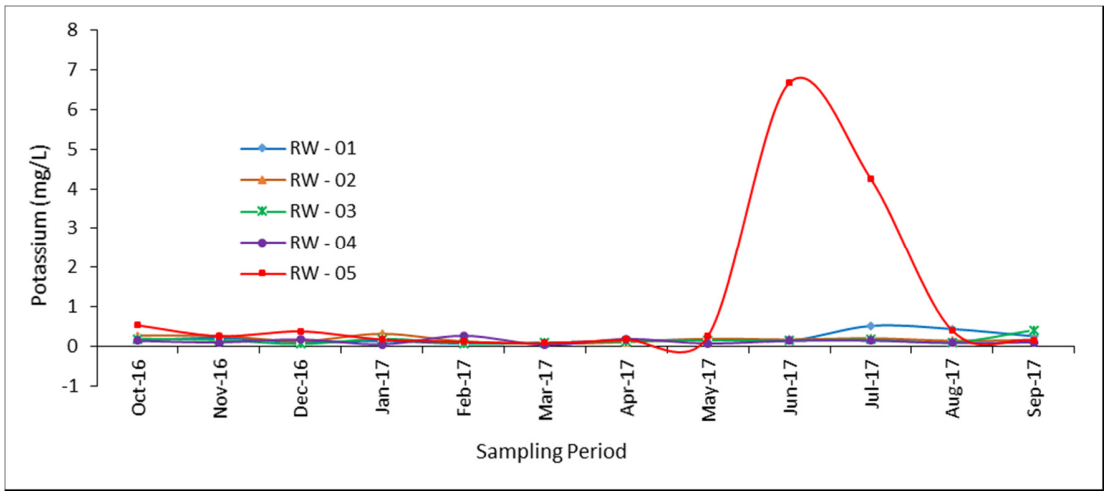

Figure 4.55: Spatial and temporal variation in Potassium.

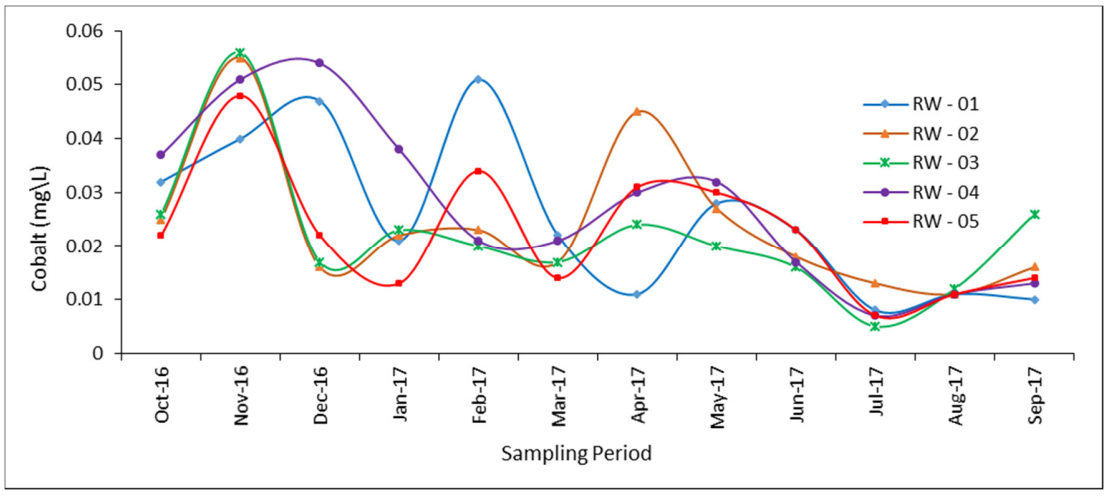

Figure 4.56: Spatial and temporal variation in Cobalt.

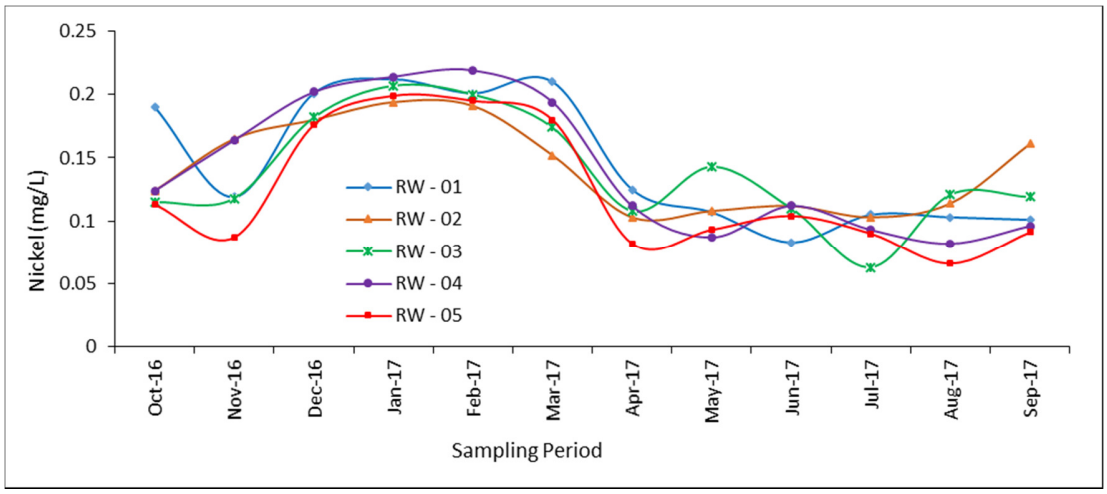

Figure 4.57: Spatial and temporal variation in Nickel.

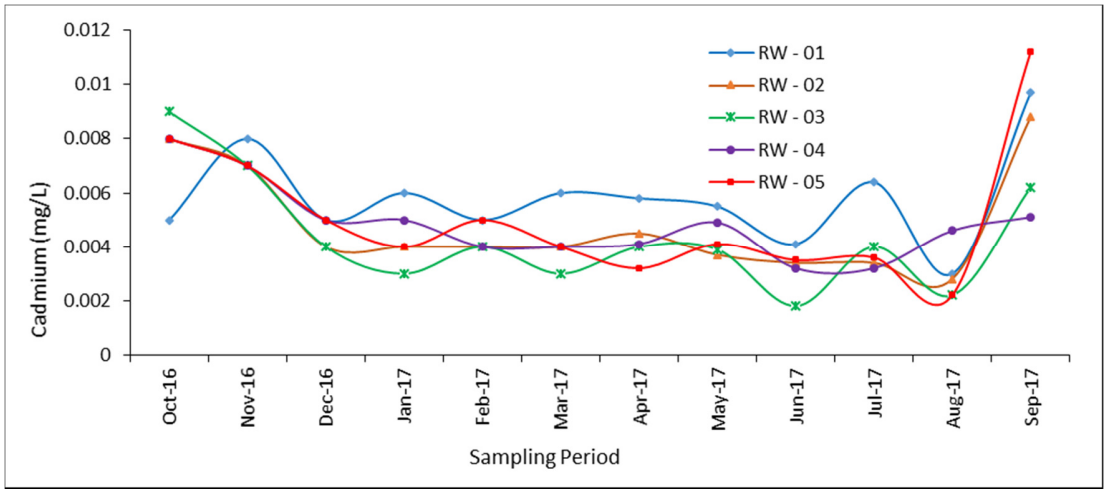

Figure 4.58: Spatial and temporal variation in Cadmium.

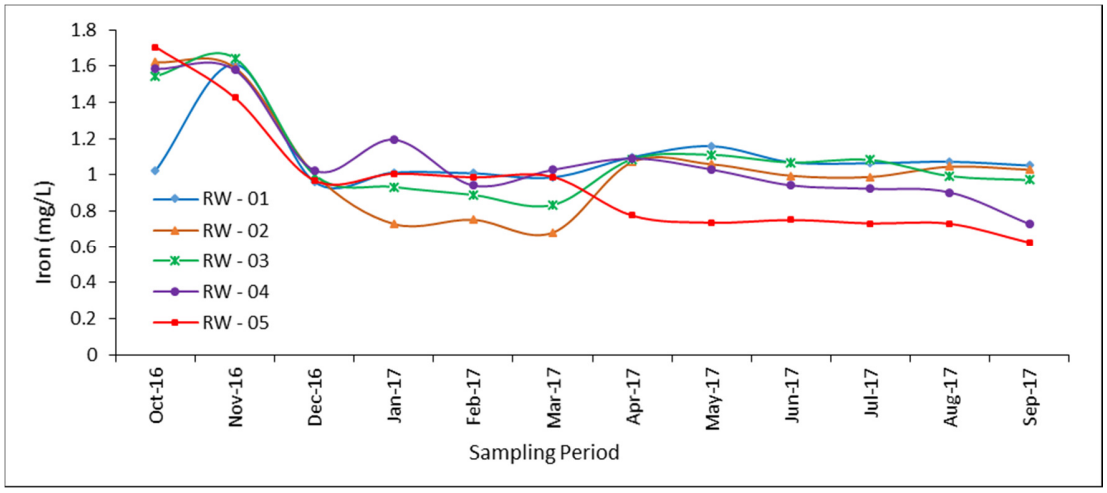

Figure 4.59: Spatial and temporal variation in Iron.

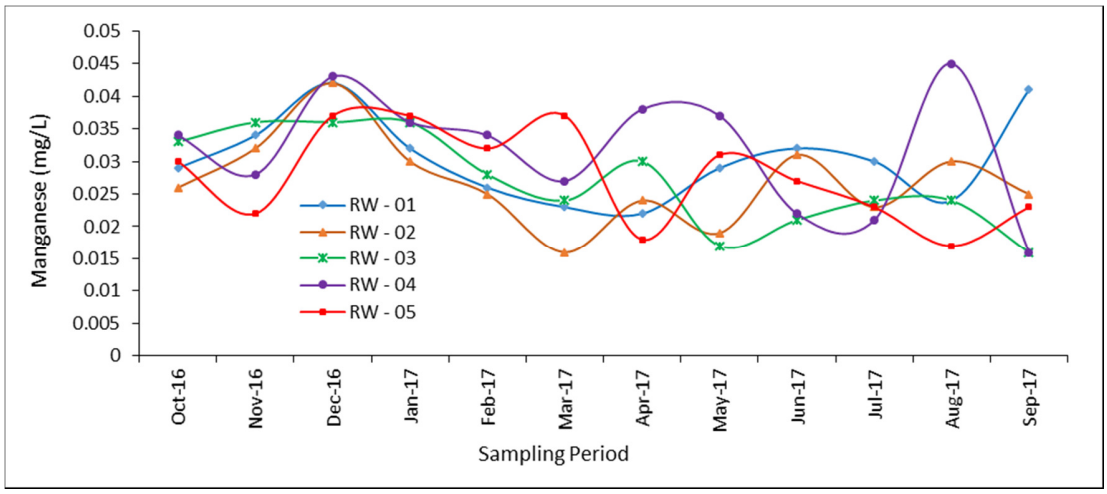

Figure 4.60: Spatial and temporal variation in Manganese.

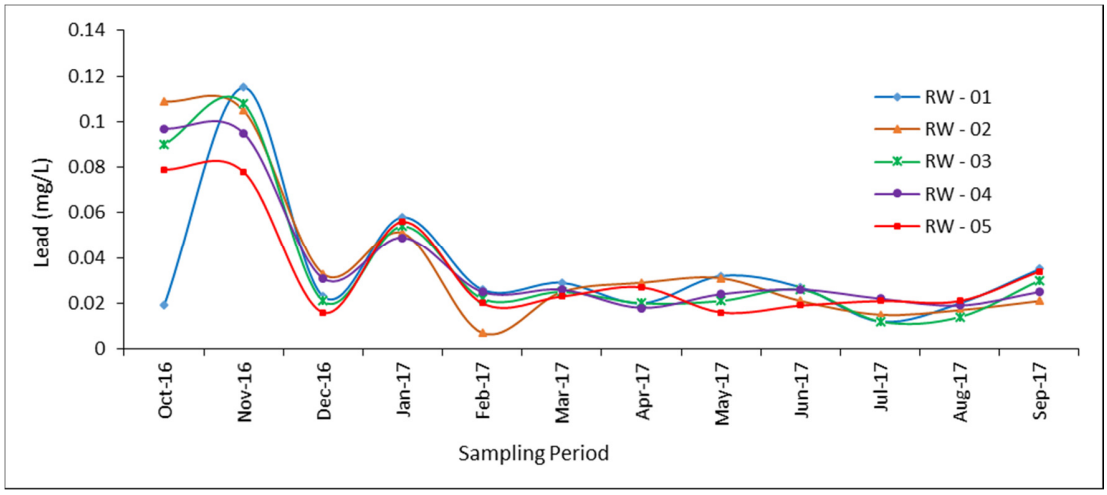

Figure 4.61: Spatial and temporal variation in Lead.

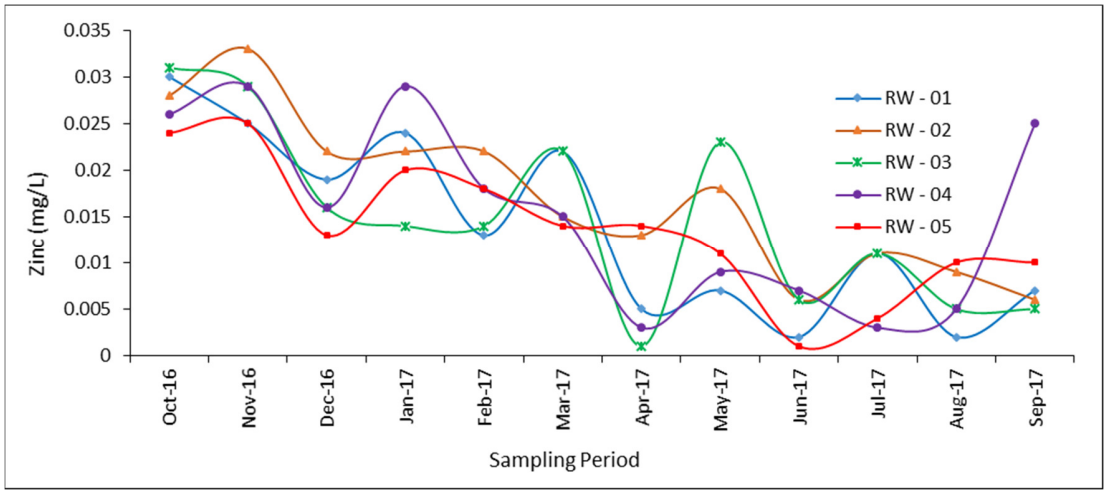

Figure 4.62: Spatial and temporal variation in Zinc.

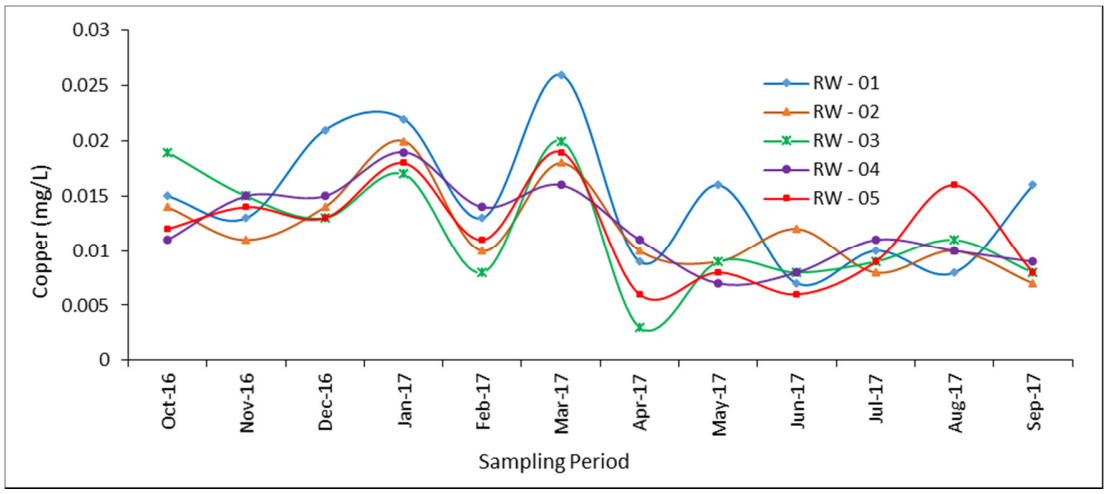

Figure 4.63: Spatial and temporal variation in Copper.

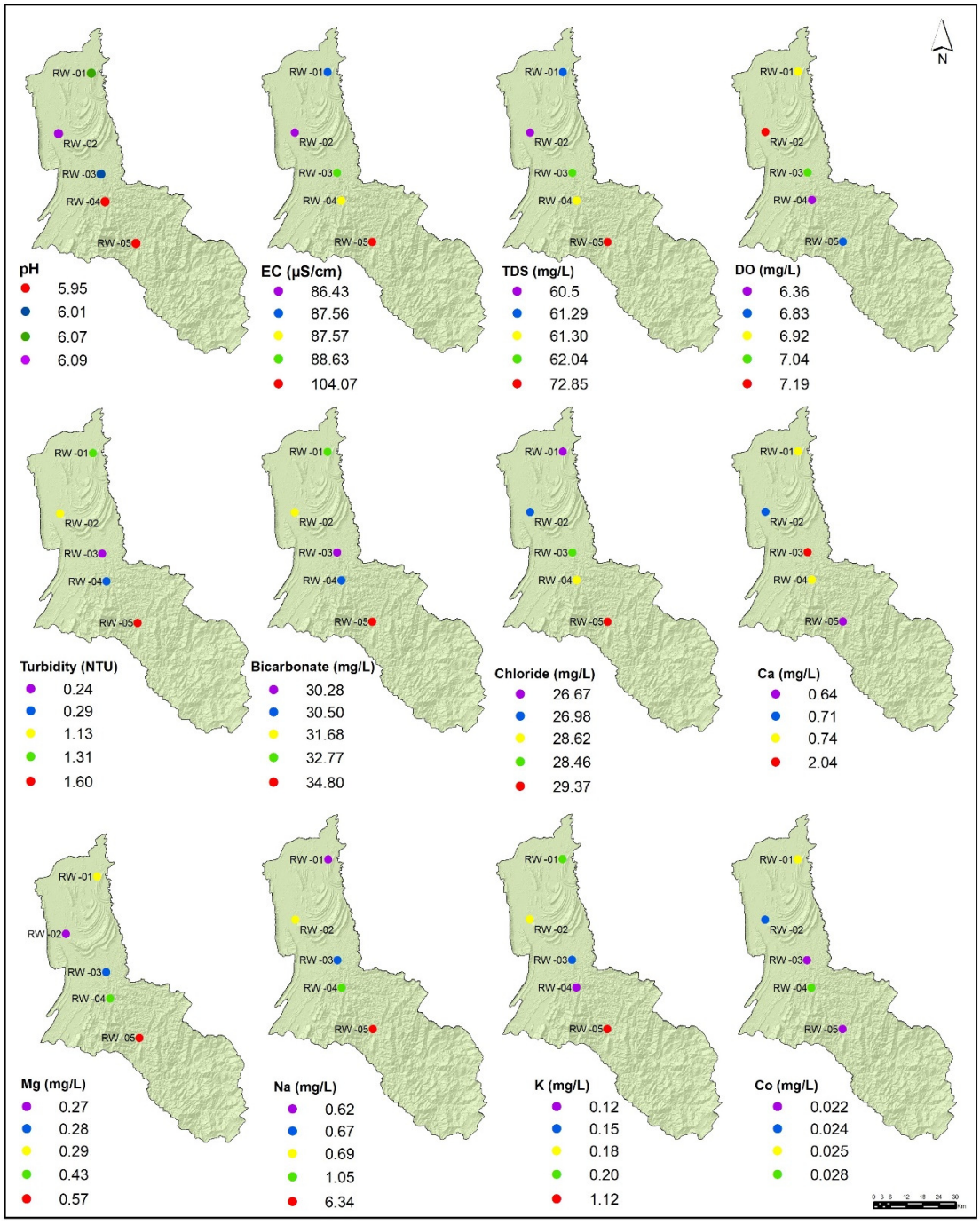

Figure 4.64: Spatial distribution of mean values of physico-chemical parameters of rainwater collected from different locations in the LRB.

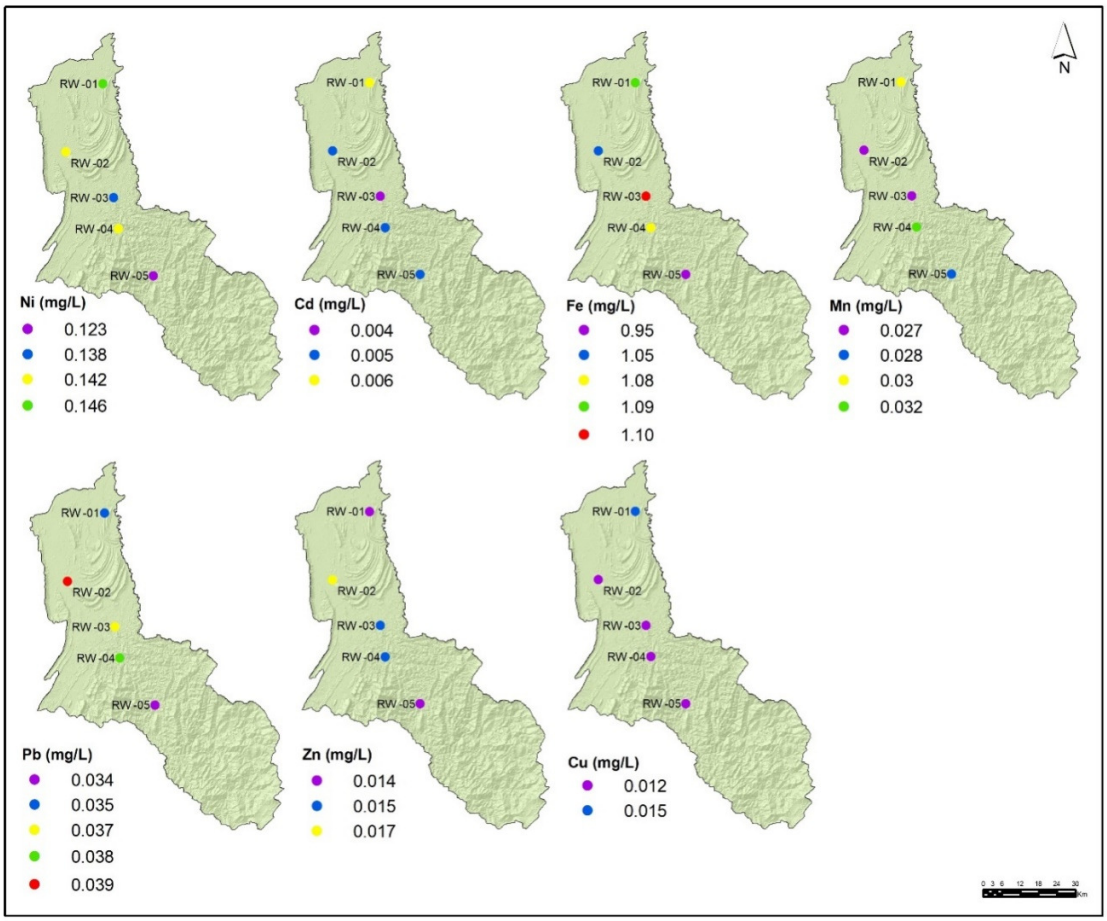

Figure 4.65: Spatial distribution of mean values of chemical parameters of rainwater collected from different locations in the LRB.

Results of physico-chemical characteristics of rainwater collected from different locations in the LRB show slight variation in its concentration. It was also noted that, besides showing variations among the sampling locations, rainwater collected in different months also shows variations in concentration. Mean concentration of pH in the LRB is found to be varied in the range of 5.95 to 6.09. It was suggested that, rainwater falling through clean atmosphere shows pH value 5.6 which can be attributed to the dissolution of CO_2 present in the rain droplets (Boubel et al., 1994; Al-Khashman, 2009). Among the rainwater samples, those collected from comparatively near coastal region (RW-01, RW-02, and RW-03) shows slightly higher mean pH (>6.0) than those collected from interior regions i.e. from inside the tropical rainforests (RW-04 and RW-05). This might be due to the local influence of evaporation over

rainfall characteristics in the specific locations and also due to the presence of increased amount of particulate matter in the atmosphere (Galloway et al., 1982; Sanhueza et al., 1989; Rajeev et al., 2016). The acidity of the rainwater can be decreased by the CO_3^{2-} and HCO_3^- of Ca^{2+} concentration in the suspended particulate matter (Kulshrestha et al., 2003; Al Obaidy & Joshi, 2006). At the same time, considering the electrical conductivity (EC) and total dissolved solids (TDS) in the rainwater samples, it shows a mean value in the range of 86.43 to 104.07µS/cm and 60.50 to 72.85mg/L for EC and TDS respectively. EC is directly proportional to TDS, which heavily depends on the concentration of dissolved ions, ionic strength and temperature of water (Marandi et al., 2013; Rusydi, 2018). Among the sampling locations, the lowest value of EC and TDS was noted in RW-02, whereas the highest value was recorded in the location RW-05. The variability in the value range can be attributed to the local influence. EC and TDS measured at different locations in the LRB shows lower values, and indicates the relatively clear nature of the rainwater with comparatively less concentration of dissolved ions (Abulude et al., 2018).

Rainfall in the LRB is comparatively rich in dissolved oxygen content and the mean concentration of DO measured in rainwater collected from different locations in the LRB vary between 6.36 to 7.19mg/L. Concentration of dissolved oxygen in rainwater was controlled by the structure of the raincloud and is also linked to the mechanism of raindrop formation and height of cloud base (Komabayasi, 1959). As an equatorial tropical rain region, the study area experiences different weather and atmospheric processes compared to other regions. Among the rainwater sampling locations, the rainwater collected in the middle part of the river basin shows comparatively higher mean DO whereas the location inside the tropical forest and upper catchment region shows a lower amount of DO. This might be due to the influence of local climatic phenomenon, which influences the cloud formation and rainfall characteristics. At the same time, considering the turbidity of rainwater, samples collected from all the locations show comparatively low turbidity, which varies in the range of 0.24 to 1.60NTU. Turbidity of rainwater was contributed by the suspended particulate matter present in the atmosphere (Cobbina et al., 2013). However, considering the mean turbidity, the rainfall received in the region is considered to be poor and devoid of much suspended particulate matter. This indicates an almost clear atmospheric environment over the river basin.

Concentration of six major ions (HCO_3^-, Cl^-, Ca^{2+}, Mg^{2+}, Na^+ and K^+) present in the rainwater samples shows variation between sampling locations. Among the major ions, HCO_3^- and Cl^- shows higher concentration in all the sampling location and samples analysed. Mean concentration of HCO_3^- vary between 30.28 to 34.80mg/L, in which the highest mean concentration was measured in the rainwater collected from sampling location RW-05 whereas the location RW-03 shows the lowest concentration. Higher concentration of HCO_3^- due to the increased amount of CO_2 in atmosphere, which react with water vapor to form HCO_3^-, and the major driving force behind the mechanism might be the biomass burning in Southeast Asian countries (Hu et al., 2003; Khoon et al., 2011). The mean concentration of Cl^- in rainwater samples varies in the range of 26.67 to 29.37mg/L which shows a gradual increase from the sampling locations near coastal region (RW-01) to those interior forests (RW-05). In general, there is higher concentration of Cl^- in rainwater was due to the marine contribution i.e. sea-salt particles (Al Obaidy & Joshi, 2006; Khoon et al., 2011). Considering this, the higher concentration of Cl^- in rainwater samples collected from the LRB can be attributed by the marine contribution (evaporation water from the South China Sea) and local evaporation from land region which contains soil and rocks of calcareous origin.

Analysed rainwater samples show low concentration of Ca^{2+} in most months in all locations, and the mean concentration ranges from 0.64 to 2.04mg/L. Among the sampling stations, rainwater collected at location RW-03, shows the highest mean concentration of Ca^{2+} whereas the samples collected from location RW-05 shows the lowest mean concentration. Ca^{2+} concentration in rainwater was mainly contributed by dust originating from calcareous soil and construction activities (Matawle et al., 2015; Rao et al., 2016). In the LRB, most of the areas are covered with calcareous soils and the concentration of Ca^{2+} observed in the rainwater samples collected from these regions can be attributed to the dominance of dust particles which evolved from calcareous soils along with rapid evaporation at local scale and re-precipitation which is typical in Borneo. Similarly, rainwater samples shows lower concentration of Mg^{2+} and the mean concentration varies in the range of 0.26 (RW-02) to 0.57 (RW-05) mg/L. Dispersion of soil and biological fragments and excess emission of alkaline dust are the major sources of dissolved Mg^{2+} and Ca^{2+} in rainwater (Tsukuda et al. 2006; Sapek, 2014). As discussed previously, calcareous soil in the region along with local and site specific

evaporation, which contributes to the precipitation in the region controls the Ca^{2+} and Mg^{2+} concentration of the rainwater in the region.

Na^{+} and K^{+} in rainwater samples collected from the LRB shows a lower concentration, and the mean concentration in different sampling locations varies from the range of 0.62 to 6.34mg/L and 0.12 to 1.12mg/L respectively. Concentration of Na^{+} and K^{+} in rainwater is mainly of marine contribution and are due to the presence of aerosols and evaporation based sea salts in the atmosphere (Cerqueira et al., 2014). The study area is very close to the South China Sea and most of the time the cloud movement in the region was controlled by wind blowing from the South China Sea. Marine evaporation along with soil dust particles that evolved from the land surface might also contribute to the occurrence of Na^{+} and K^{+} in rainwater samples collected from the LRB.

Rainwater samples analysed also shown trace metals such as Co, Ni, Cd, Fe, Mn, Pb, Zn and Cu at lower concentrations. Human activities and industrial development such as combustion of fossil fuel, pollution from motor vehicles, and mining and forest fires are major sources of trace metal pollution in the atmosphere (Farahmandkia et al., 2010; Sabuti & Mohamed, 2016). Few trace metals are lithogenic and originated and are contributed by the dust particle blowing from the bare earth (Jeffries & Snyder, 1981). The mean centration of Co in rainwater samples varies in the range of 0.022 (RW-03 and 05) to 0.028mg/L (RW-04), whereas Ni varies in the range of 0.123 (RW-05) to 0.146mg/L (RW-01). At the same time, the mean concentration of Cd and Fe varies in the range of 0.004 (RW-03) to 0.006mg/L (RW-01) and 0.95 (RW-05) to 1.10mg/L (RW03) respectively. Mn and Pb shows comparatively lower mean concentration in rainwater samples collected from different locations and varies within the range of 0.027 (RW-02 and 03) to 0.032mg/L (RW-04) and 0.034 (RW-05) to 0.039mg/L (RW-02) respectively. A similar nature was observed in the mean concentration of Zn and Cu, which vary from 0.014 (RW-01 and 05) to 0.017mg/L (RW-02) and 0.012 (RW-02, 03, 04 and 05) to 0.015mg/L (RW-01). Concentration of trace metals in rainwater was controlled by the closeness to the contributing source, wind direction (direction of air masses) and the amount of precipitation. Regions which receives rain after long period of dryness shows higher concentration of trace metals compared to regions that receives regular rainfall (Al-Khashman, 2009; Koulousaris et al., 2009). Considering the study area, petro-chemical (off shore stations)

and other industrial activities, heavy use of fossil fuel, shipping activity in the South China Sea and soil dust from local areas due non-protected nature of interior roads in the forest region (logging roads) along with regional monsoon winds, contribute the trace metals in rainwater.

Furthermore, it was also noted that the mean concentration of major ions in rainwater collected at different locations in the LRB shows variation in its concentration (Table 4.25). In location RW-01, RW-02 and RW-03, concentration of major ions follow the order of $HCO_3^- > Cl^- > Ca^{2+} > Na^+ > Mg^{2+} > K^+$. At the same time, in location RW-04 the ionic concentration varies in the order of $HCO_3^- > Cl^- > Na^+ > Ca^{2+} > Mg^{2+} > K^+$ whereas in location RW-05, ions follow an order of $HCO_3^- > Cl^- > Na^+ > K^+ > Ca^{2+} > Mg^{2+}$. It was also noted that, besides the variation in the concentration of major ions, trace metal also show variations in its mean concentration among the sampling locations. Rainwater collected at location RW-01, trace metal follows the order of Fe > Ni > Pb > Mn > Co > Cu > Zn > Cd. Trace metal concentration in rainwater samples collected at locations RW-02, RW-03, RW-04 and RW-05 follows the order of Fe > Ni > Pb > Mn > Co > Zn > Cu > Cd. Variation in the mean concentration of major ions and trace metals in rainwater samples collected from different locations in the river basin was caused by the variation in the source and amount of precipitation along with evaporation of rain while falling down and also local site specific input such as soil dust. In addition forest burning also contributes to this variation to a certain extent (Migliavacca et al., 2005; Thakur et al., 2018; Meng et al. 2019).

Table 4.25: Concentration (order) of major ions and trace metals in rainwater samples.

Sampling locations	Major ions	Trace metals
RW-01	$HCO_3^- > Cl^- > Ca^{2+} > Na^+ > Mg^{2+} > K^+$	Fe> Ni> Pb> Mn> Co> Cu> Zn> Cd
RW-02	$HCO_3^- > Cl^- > Ca^{2+} > Na^+ > Mg^{2+} > K^+$	Fe> Ni> Pb> Mn> Co> Zn> Cu> Cd
RW-03	$HCO_3^- > Cl^- > Ca^{2+} > Na^+ > Mg^{2+} > K^+$	Fe> Ni> Pb> Mn> Co> Zn> Cu> Cd
RW-04	$HCO_3^- > Cl^- > Na^+ > Ca^{2+} > Mg^{2+} > K^+$	Fe> Ni> Pb> Mn> Co> Zn> Cu> Cd
RW-05	$HCO_3^- > Cl^- > Na^+ > K^+ > Ca^{2+} > Mg^{2+}$	Fe> Ni> Pb> Mn> Co> Zn> Cu> Cd

4.5.2 Statistical analysis of rainwater quality parameters

4.5.2.1 Analysis of variance (ANOVA)

The significant and non-significant variation of the parameters between the station and sampling periods was identified by two-way ANOVA test (Table 4.26). Ni, Fe and Cu showed significant variation (at 95% confidence level) between the sampling locations and sampling periods. pH, EC, TDS, DO, HCO_3^-, Cl^-, Co, Cd, Mn, Pb and Zn shows significant variations during the sampling periods. Turbidity and K^+ showed significant variation between sampling locations. All other parameters (Ca^{2+}, Mg^{2+} and Na^+) showed a statistically non-significant variation during sampling period and sampling locations.

Table 4.26: Two- way ANOVA of rainwater quality parameters.

		% of total variation	*SS*	*MS*	*F*	*P-value*	*Significa-nce*
pH	Between stations	0.035	0.422	0.084	0.563	0.728	No
	Between months	0.287	3.486	0.317	2.115	0.034	Yes
EC (µS/cm)	Between stations	0.044	3222.758	644.552	1.369	0.250	No
	Between months	0.603	44160.654	4014.605	8.526	0.000	Yes
TDS (mg/L)	Between stations	0.044	1579.152	315.830	1.369	0.250	No
	Between months	0.603	21638.720	1967.156	8.526	0.000	Yes
DO (mg/L)	Between stations	0.050	5.749	1.150	0.995	0.429	No
	Between months	0.397	45.544	4.140	3.584	0.001	Yes
Turbidity (NTU)	Between stations	0.298	20.435	4.087	6.051	0.000	Yes
	Between months	0.161	11.075	1.007	1.491	0.162	No
Bicarbonat e (mg/L)	Between stations	0.033	178.756	35.751	0.956	0.452	No
	Between months	0.584	3136.787	285.162	7.629	0.000	Yes
chloride (mg/L)	Between stations	0.011	125.968	25.194	0.865	0.510	No
	Between months	0.845	9443.532	858.503	29.482	0.000	Yes
Ca (mg/L)	Between stations	0.068	18.419	3.684	1.025	0.412	No
	Between months	0.206	56.043	5.095	1.418	0.191	No
Mg (mg/L)	Between stations	0.061	0.910	0.182	0.899	0.488	No
	Between months	0.190	2.825	0.257	1.269	0.267	No
Na (mg/L)	Between stations	0.127	312.884	62.577	1.900	0.109	No
	Between months	0.137	336.121	30.556	0.928	0.521	No
K (mg/L)	Between stations	0.152	8.870	1.774	2.463	0.044	Yes
	Between months	0.167	9.746	0.886	1.230	0.290	No
Co (mg/L)	Between stations	0.021	0.000	0.000	0.744	0.594	No
	Between months	0.667	0.009	0.001	10.684	0.000	Yes

Ni (mg/L)	Between stations	0.041	0.007	0.001	3.471	0.008	Yes
	Between months	0.829	0.140	0.013	31.940	0.000	Yes
Cd (mg/L)	Between stations	0.050	0.00	0.000	2.315	0.056	No
	Between months	0.712	0.0002	0.000	14.990	0.000	Yes
Fe (mg/L)	Between stations	0.057	0.297	0.059	2.902	0.021	Yes
	Between months	0.727	3.786	0.344	16.817	0.000	Yes
Mn (mg/L)	Between stations	0.069	0.000	0.000	1.430	0.228	No
	Between months	0.400	0.002	0.000	3.769	0.000	Yes
Pb (mg/L)	Between stations	0.008	0.000	0.000	0.616	0.688	No
	Between months	0.854	0.045	0.004	30.908	0.000	Yes
Zn (mg/L)	Between stations	0.012	0.000	0.000	0.394	0.851	No
	Between months	0.644	0.005	0.000	9.358	0.000	Yes
Cu (mg/L)	Between stations	0.095	0.000	0.000	3.813	0.005	Yes
	Between months	0.630	0.001	0.000	11.466	0.000	Yes

4.5.2.2 Correlation analysis

Correlation of 19 parameters analysed from a one year sample collected from five locations were calculated separately in the present analysis (Table 4.27). Strong negative and positive correlation (r≥±0.70) was identified and is discussed in the following sections. In the first sampling location RW-01, strong positive correlation (r≥0.70) were identified between EC and TDS (r=1), Mg^{2+} with Na^{+} (r=0.97), Cl^{-} with EC and TDS (r=0.95), Na^{+} with Pb (r=0.95), Mg^{2+} with Fe (r=0.94), Mg^{2+} with Pb (r=0.93), Na^{+} with Fe (r=0.89), Fe with Pb (r=0.85), HCO_3^{-} with EC and TDS (r=0.80), pH with Fe (r=0.79), Ca^{2+} with Mg^{2+} (r=0.79), Ca^{2+} with Fe (r=0.76), Ni with Cu (r=0.75), Ca^{2+} with Pb (r=0.73), Ca^{2+} with Na^{+} (r=0.73), Ni with Zn (r=0.73) and pH with Ca^{2+} (r=0.72) and Pb (r=0.70). Strong negative correlation (r ≥ -0.70) identified in RW-01 were between EC and TDS with Co (r=-0.83), Cl^{-} with Ni (r=-0.82), Cl^{-} with Zn (r=-0.81), Cl^{-} with Co (r=-0.77), HCO_3^{-} with Na^{+} (r=-0.76), EC and TDS with Zn (r=-0.75) and EC and TDS with Ni (r=-0.70). At the same time, considering the samples collected from location RW-02, strong positive correlations were identified between EC with TDS (r=1), Mg^{2+} with Na^{+} (r=0.99), Mg^{2+} with Pb (r=0.96), Na^{+} with Pb (r=0.95), pH with Fe (r=0.93), EC and TDS with Cl^{-} (r=0.93), pH with Pb (r=0.92), pH with Mg^{2+} (r=0.91), pH with Na^{+} (r=0.91), Na^{+} with Fe (r=0.83), Mg^{2+} with Fe (r=0.83), Pb with Fe (r=0.82), Ca^{2+} with Fe (r=0.80), Mg^{2+} with Zn (r=0.78), Pb with Zn (r=0.77) and Na^{+} with Zn (r=0.75). But a strong negative correlation in RW-02 are between EC and TDS

with Zn (r=-0.84), Cl^- with Zn (r=-0.76), HCO_3^- with Mg^{2+} (r=-0.75), HCO_3^- with Na^+ (r=-0.74) and Cl^- with Cu (r=-0.71).

In RW-03, strong correlation were observed between the parameters such as EC with TDS (r=1), Mg^{2+} with Na^+ (r=0.98), Mg^{2+} with Pb (r=0.92), Mg^{2+} with Cd (r=0.90), Na^+ with Pb (r=0.90), Ca^{2+} with K^+ (r=0.88), Mg^{2+} with Fe (r=0.88), Na^+ with Fe (r=0.88), EC and TDS with HCO_3^- (r=0.87), Fe with Pb (r=0.84), EC and TDS with Cl^- (r=0.83), Co with Pb (r=0.83), Na^+ with Cd (r=0.83), pH with Ca^{2+} (r=0.80), Cd with Fe (r=0.76), Cd with Pb (r=0.74), Zn with Cu (r=0.73), pH with K^+ (r=0.71), Mg^{2+} with Co (r=0.71) and Pb with Zn (r=0.70). At the same time, a strong negative correlations were noted between Cl^- with Cu (r=-0.81), EC and TDS with Zn (r=-0.80), HCO_3^- with Na^+ (r=-0.78), HCO_3^- with Zn (r=-0.78), HCO_3^- with Fe (r=-0.74), EC and TDS with Cupper (r=-0.74), HCO_3^- with Pb (r=-0.73), HCO_3^- with Mg^{2+} (r=-0.72), EC and TDS with Mn (r=-0.71) and $Cl^-$with Ni (r=-0.71).

Considering the water samples from RW-04, parameters showing strong positive correlations are EC and TDS (r=1), EC and TDS with Cl^- (r=0.95), Fe with Pb (r=0.93), Cd with Pb (r=0.89), Ni with Cu (r=0.88), pH with Cl^- (r=0.87), pH with EC and TDS (r=0.86), Cd with Fe (r=0.80), EC and TDS with HCO_3^- (r=0.77), DO with Ni (r=0.74), Ca^{2+} with Na^+ (r=0.74), Pb with Zn (r=0.72) and Cd with Zn (r=0.71). Strong negative correlations (r≥-0.70) were also observed between HCO_3^- with Pb (r=-0.89), Cl^- with Cu (r=-0.86), Cl^- with Ni (r=-0.86), HCO_3^- with Fe (r=-0.78), EC and TDS with Pb (r=-0.77), EC and TDS with Cu (r=-0.74), HCO_3^- with Cd (r=-0.74), EC and TDS with Fe (r=-0.73), DO with Cl^- (r=-0.72), EC and TDS with Zn (r=-0.71), EC and TDS with DO (r=-0.70), EC and TDS with DO (r=-0.70) and pH with Ni (r=-0.70) in location RW-04. Parameters analysed in rainwater collected from RW-05, shows a strong positive correlation between EC and TDS (r=1), Na^+ with K^+ (r=0.99), EC and TDS with Na^+ (r=0.94), EC and TDS with K^+ (r=0.92), EC and TDS with Cl^- (r=0.91), Ni with Mn (r=0.88), Cl^- with K^+ (r=0.84), Fe with Pb (r=0.84), Cl^- with Na^+ (r=0.83), Fe with Zn (r=0.82), Pb with Zn (r=0.78), EC and TDS with HCO_3^- (r=0.74), Turbidity with Mg^{2+} (r=0.73) and Ca^{2+} with Cd (r=0.70). Some other parameters show a strong negative correlation and are Cl^- with Zn (r=-0.85), EC and TDS with Zn (r=-0.85), DO with Cd (r=-0.78) and K^+ with Zn (r=-0.71).

Table 4.27: Correlation analysis results (r≥±0.70) of physico-chemical parameters of rainwater collected from location RW-01 RW-02 and RW-03.

RW - 01						RW - 02						RW - 03					
Positive Correlation			Negative Correlation			Positive Correlation			Negative Correlation			Positive Correlation			Negative Correlation		
Parameters		r	Parameters		r	Parameters		r	Parameters		r	Parameters		r	Parameters		r
EC	TDS	1.00	Co	EC	-0.83	EC	TDS	1.00	Zn	EC	-0.84	EC	TDS	1.00	Cl	Cu	-0.81
Mg	Na	0.97	Co	TDS	-0.83	Mg	Na	0.99	Zn	TDS	-0.84	Mg	Na	0.98	Zn	EC	-0.80
Na	Pb	0.95	Cl	Ni	-0.82	Mg	Pb	0.96	HCO_3	Mg	-0.75	Mg	Pb	0.92	Zn	TDS	-0.80
Cl	EC	0.95	Cl	Zn	-0.81	Na	Pb	0.95	Cl	Zn	-0.76	Na	Pb	0.90	HCO_3	Zn	-0.78
Cl	TDS	0.95	Cl	Co	-0.77	pH	Fe	0.93	HCO_3	Na	-0.74	Mg	Cd	0.90	HCO_3	Na	-0.78
Mg	Fe	0.94	HCO_3	Na	-0.76	Cl	EC	0.93	Cl	Cu	-0.71	Mg	Fe	0.88	HCO_3	Fe	-0.74
Mg	Pb	0.93	Zn	EC	-0.75	Cl	TDS	0.93				Ca	K	0.88	HCO_3	Pb	-0.73
Fe	Na	0.89	Zn	TDS	-0.75	pH	Pb	0.92				Na	Fe	0.88	Cu	EC	-0.73
Fe	Pb	0.85	Ni	EC	-0.70	pH	Mg	0.91				HCO_3	EC	0.87	Cu	TDS	-0.73
HCO_3	EC	0.80	Ni	TDS	-0.70	pH	Na	0.91				HCO_3	TDS	0.87	HCO_3	Mg	-0.72
HCO_3	TDS	0.80				Fe	Mg	0.83				Fe	Pb	0.84	Cl	Ni	-0.71
pH	Fe	0.79				Fe	Na	0.83				Cl	EC	0.83	Mn	EC	-0.71
Ca	Mg	0.79				Fe	Pb	0.82				Cl	TDS	0.83	Mn	TDS	-0.71
Ca	Fe	0.76				Fe	Ca	0.80				Na	Cd	0.83			
Ni	Cu	0.75				Zn	Mg	0.78				Co	Pb	0.83			
Ni	Zn	0.73				Zn	Pb	0.77				pH	Ca	0.80			
Ca	Pb	0.73				Zn	Na	0.75				Cd	Fe	0.76			
Ca	Na	0.73										Cd	Pb	0.74			
Ca	pH	0.72										Cu	Zn	0.73			
pH	Pb	0.70										pH	K	0.71			
												Pb	Zn	0.70			
												Mg	Co	0.70			

Table 4.27: Correlation analysis results (r≥±0.70) of physico-chemical parameters of rainwater collected from location RW-04 and RW-05.

RW - 04						RW - 05					
Positive Correlation			Negative Correlation			Positive Correlation			Negative Correlation		
Parameters		r	Parameters		r	Parameters		r	Parameters		r
EC	TDS	1.00	HCO_3	Pb	-0.89	EC	TDS	1.00	Zn	EC	-0.85
Cl	EC	0.95	Cl	Ni	-0.86	Na	K	0.99	Zn	TDS	-0.85
Cl	TDS	0.95	Cl	Cu	-0.86	EC	Na	0.94	Cl	Zn	-0.85
Pb	Fe	0.93	HCO_3	Fe	-0.78	TDS	Na	0.94	DO	Cd	-0.78
Pb	Cd	0.89	Pb	EC	-0.77	EC	K	0.92	K	Zn	-0.71
Ni	Cu	0.88	Pb	TDS	-0.77	TDS	K	0.92			
pH	Cl	0.87	Cu	EC	-0.74	EC	Cl	0.91			
pH	EC	0.86	Cu	TDS	-0.74	TDS	Cl	0.91			
pH	TDS	0.86	HCO_3	Cd	-0.74	Ni	Mn	0.88			
Cd	Fe	0.80	Fe	EC	-0.73	Cl	K	0.84			
HCO_3	EC	0.77	Fe	TDS	-0.73	Fe	Pb	0.84			
HCO_3	TDS	0.77	DO	Cl	-0.72	Cl	Na	0.83			
DO	Ni	0.74	Zn	EC	-0.71	Fe	Zn	0.82			
Ca	Na	0.74	Zn	TDS	-0.71	Pb	Zn	0.78			
Zn	Pb	0.72	DO	EC	-0.70	EC	HCO_3	0.74			
Zn	Cd	0.71	DO	TDS	-0.70	TDS	HCO_3	0.74			
			Ni	EC	-0.70	Turbidity	Mg	0.73			
			Ni	TDS	-0.70	Ca	Cd	0.70			
			pH	Ni	-0.70						

Overall, variation in the amount of correlation among the parameters in rainwater collected at different locations was observed in the study area. Among the locations, rainwater collected from RW-03 showed the maximum number of positive correlations between the parameters whereas the samples collected from location RW-04 show the maximum number of negative (inverse) correlations. Though the different sampling locations received almost same amount of rainfall during the sampling periods, variation in concentration of parameters and inter-relationships suggests the contribution of local input in the moisture source of rainfall collected at spatially separated but unique rainfall regime of the LRB.

4.5.2.3 Factor analysis

Monthly cumulative rainwater collected from five different sampling location was used in the factor analysis to determine the dominant component which controls the chemistry of rainwater. Factor analysis was performed with principal component analysis as the extraction method and varimax with Kaiser Normalization as the rotation method (eigenvalue >1) using the physico-chemical parameters of rainwater. The result of factor analysis revealed five components (factors) in RW-01, RW-02 and RW-05 and four components (factors) in RW-03 and RW-04 (Table 4.28). Parameters showing significant loading (≥±0.50) in different sampling locations were considered to explain the processes which control the chemistry of rainwater in the LRB. (Factor loading between ±0.50 to ±0.70 is considered as good loading and ≥±0.70 is considered as strong loading in the present research).

In RW-01 (rainwater collected at sampling location 01), the components explained a cumulative of 90.69% variance. Parameters such as pH, Ca^{2+}, Mg^{2+}, Na^{+}, Fe and Pb showed a strong positive loading along with DO and Cd having good positive loading whereas HCO_3^{-} showed good negative loading in Factor 1 which alone explained 32.06% of total variance. Water samples collected during the month of November-16 show dominance of these elements. EC, TDS, HCO_3^{-}, Cl^{-} shown strong positive loading whereas Co, Ni and Zn shown strong and good negative loading in Factor 2, which altogether explained 28.36% of total variance. Rainwater analysed in the months of April-17, July-17 and September-17 shows dominance of these elements. For Factor 3, Cu showed strong positive loading whereas Ni and Zn shows good positive loading indicating 12.00% of total variance. Rainwater collected during the periods of January-17 and March-17 was dominated with the Cu, Ni and Zn contents. A strong positive loading of Turbidity and K^{+} was observed in Factor 4 which

contributed 10.29% of total variance and rainwater collected in August-17 shows comparatively higher concentration of these parameters. However, it was also noted that Mn alone showed a strong positive loading in Factor 5 with 7.98% of total variance. Rainwater samples of December-16 and September-17 shown higher concentration of Mn.

A cumulative of 90.14% variance was explained by the factor components in RW-02. Parameters such as pH, HCO_3^-, Ca^{2+}, Mg^{2+}, Na^+, K^+, Co, Cd, Fe, Pb and Zn showed significant loading in Factor 1 which explained 36.64% of total variance. Among the parameters except HCO_3^-, all showed strong to good positive loading whereas the later showed a good negative loading. Rainwater samples collected in the months of October-16 and November-16 shows dominance of these parameters. In Factor 2, EC, TDS, HCO_3^- and Cl^- shows significant negative loading (strong and good) whereas Ni and Zn shows significant positive (good) loading which together explained 26.08% of the total variance. Rainwater in the month of December-16, February-17 and March-17 shows the dominance of these parameters. Factor 3 explained 14.72% of the total variance with significant positive (strong and good) loading of Turbidity, K^+ and Cu which can be linked with the rainwater collected in the month of January-17. In Factor 4, Mn shows a strong positive loading which explain 6.46% of total variance and rainwater rich in Mn was noted in the month of December-16. Factor 5 explained 6.23% of total variance with good positive loading of DO and rainwater of September-17 showed a higher amount of DO.

The factor components of rainwater collected in location RW-03, shows a cumulative of 88.60% variance. Parameters such as Mg^{2+}, Na^+, Co, Cd, Fe, Pb and Zn showed strong positive loading and EC, TDS and HCO_3^- shown significant (good) negative loading in Factor 1 with 39.88% of the total variance. Rainwater samples during October-16 and November-16 showed the dominance of these parameters. Factor 2 was contributed by pH, EC, TDS, HCO_3^-, Ca^{2+} and K^+ which showed significant positive (strong and good) loading which explained 23.80% of total variance. Rainwater collected in the month of September-17 showed the dominance of pH, Ca^{2+}, and K^+ which showed strong positive loading in the Factor 2. In Factor 3, DO and Ni showed strong positive loading, whereas Cl^- showed strong negative loading which altogether contributed to 15.00% of total variance. These parameters are dominant in rainwater samples collected in the months of January-17 and February-17. Turbidity and Cu with significant positive loading explained 9.93% of total variance and contributed by Factor 4. Rainwater enriched with Cu was found in the month of March-17.

Factor analysis explained a cumulative of 84.24% variance in rainwater samples collected from location RW-04. Factor 1 show 33.39% of the total variance with significant positive (strong and good) loading of DO, Ni, Zn, Cu and strong negative loading of pH, EC, TDS and Cl^-. Rainwater samples in January-17, February-17 and March-17 show the dominance of these parameters. For the second factor (Factor 2), parameters such as Ca^{2+}, Co, Cd, Fe, Pb and Zn showed significant positive loading whereas EC, TDS and HCO_3^- show significant negative loading which together explained 28.36% of the total variance. Rainwater samples collected during the period of October-16 and September-17, show comparatively higher concentration of these parameters. In Factor 3, Turbidity and Mn showed strong positive loading and Na^+ showed strong negative loading which contributed to 14.01% of the total variance. It was observed that, rainwater samples during the period of May-17 and August-17 show dominance of these parameters. However, in Factor 4, Mg^{2+} showed good positive loading and K^+ showed strong negative loading together which contributed to 8.49% of total variance, and rainwater samples collected in March-17 shows reasonable concentration of these parameters.

Further considering the physico-chemical parameters of rainwater samples collected from location RW-05, factor analysis explained a cumulative of 92.34% variance. In Factor 1, parameters such as EC, TDS, Cl^-, Na^+, K^+ and HCO_3^- show strong and good positive loading whereas Zn and Cu shown good negative loading which together contributed to 31.14% of the total variance. All the parameters shows loading in Factor 1 was found to be dominated in the rainwater samples collected during June-17 and July-17. At the same time, Factor 2 explained 17.46% of the total variance with strong positive loading of DO and significant negative loading of pH, Ca^{2+} and Cd that can be attributed to rainwater of August-17 which showed dominance of these parameters. A significant positive (strong and good) loading of Fe, Pb and Zn was observed in Factor 3, which explained 16.69% of the total variance. It was noted that Fe, Pb and Zn showed comparatively higher concentration in rainwater samples collected during October-16 and November-16. Factor 4 contributed to 16.54% of the total variance with significant positive loading of pH, turbidity and Mg^{2+} and strong negative loading of Ni and Mn. Rainwater sample collected during August-17 shows dominance of these parameters. Factor 5 explains good positive loading of HCO_3^-, Mg^{2+} and Cu and strong negative loading of Co with 10.50% of the total variance. Rainwater samples in August-17 showed comparatively higher concentration of these parameters.

Individual factor components with parameters showing strong positive loading in rainwater samples collected from different locations indicate variation in the processes that dominantly controls the rainwater chemistry. In location RW-01, parameters such as pH, DO, Ca^{2+}, Mg^{2+}, Na^{+}, Cd, Fe and Pb dominate in Factor 1. pH and DO are the physical parameters which determine the overall water chemistry by dissolution of other major ions and trace metals. Ca^{2+} and Mg^{2+} in the rainwater indicates the origin from soil dust whereas the Na^{+} loading suggest the contribution from sea salt through the evaporation (De Mello, 2001; Al-Khashman, 2009). Furthermore, the loading of trace metals such as Cd, Fe and Pb can be attributed by the anthropogenic-pollution based factors such as fossil fuel burning (petrochemical industries and transportation) and forest fires in the region as well as that carried from long distance by cloud winds (Cheng et al., 2011). Positive loading of EC and TDS in Factor 2 might be due to the increased amount of total suspended solids in the atmosphere which originated either from local sources or from distant sources which were carried by the dominating monsoon wind. HCO_3^- and Cl^- indicates both anthropogenic and natural contribution. High concentration of HCO_3^- in rainwater in this region was contributed by the increased amount of CO_2 in the atmosphere due to forest fires as well as the soil dust rich in carbonate (Lewis Jr, 1981; Shrestha et al., 2013) whereas the Cl^- concentration indicates traces of marine contribution (Wang & Han, 2011; Pearce et al., 2015; Khan et al., 2018). Dominance of Ni, Zn and Cu in Factor 3 indicates that the transportation of pollutants from distant sources originate from industrial and traffic activities (Vuai & Tokuyama, 2011; Ghadimi et al., 2013). Factor 4 showed sole loading of K^{+}, which is of terrestrial origin and due to the forest fire or biomass combustion (Zhang et al., 2007; Lu et al., 2011). In Factor 5, the total variance was defined by Mn and the contribution can be from anthropogenic (iron and steel manufacturing industry, fossil fuel combustion and mining) activities as well as from natural factors such as sea salt spray, forest fire, windblown dust rich in Mn (Nriagu, 1989; Ressler et al., 2000).

Rainwater samples collected at location RW-02 shows completely different loading of factor components. In Factor 1, physical parameter pH was loaded along with major ions Ca^{2+}, Mg^{2+}, Na^{+}, K^{+} and trace metals such as Co, Cd, Fe, Pb and Zn. As discussed earlier, Ca^{2+} and Mg^{2+} might be from dust particles whereas Na^{+} from the sea-salt fraction and K^{+} from the biomass burning. Higher loading of trace metals in the first factor indicates the increased effect of anthropogenic processes, along with dust particle from the land surface carried by flowing wind. However, the second Factor was dominated by trace metals Ni and

Zn indicating increased effect of atmospheric pollution by anthropogenic activities such as increased traffic and industrial discharge. Positive loading of K^+ and Cu in Factor 3, might be due to the local contribution of forest clearing through forest burning and regional industrial and traffic emission (Espinosa et al., 2004; Cheng et al., 2011). Loading of turbidity in Factor 3, indicates a presence of higher suspended particulate matter in the atmosphere originating from the forest burning, regional traffic activities and dust carried by wind. It was noted that, Mn alone explained the total variance percentage in Factor 4, originating from the dissolution of windblown dust rich in Mn, fossil fuel combustion, mining and forest fire (Nriagu, 1989; Moreda-Piñeiro et al., 2014). The fifth factor in rainwater samples collected from location RW-02, shows enrichment of DO, indicating local influence over the mechanism of raindrop formation, height of cloud base and the structure of the rain cloud (Komabayasi, 1959).

Variations in the loading of major ions and trace metals in different factors were found in the rainwater samples collected from location RW-03. In Factor 1, the total variance was contributed by Mg^{2+}, Na^+, Co, Cd, Fe, Pb and Zn. Parameters such as Mg^{2+} and Na^+ was contributed by natural processes such as soil dust and sea salt contribution through evaporation (Al-Khashman, 2009). Furthermore, the loading of trace metals such as Co, Cd, Fe, Pb and Zn indicates increased atmospheric pollution caused by anthropogenic processes such as emission from vehicles, petro-chemical industries, forest (biomass) burning along with dust particles transported from distant palaces as well as from local areas. In Factor 3, DO and Ni showed good loading which indicates the nature of cloud formation and its base elevation and anthropogenic activities such as increased traffic and industrial discharge. Turbidity and Cu loaded in Factor 4 indicates the source such as the dust particle and suspended particulate matter generated due to natural and anthropogenic activities as well as regional industrial and traffic emission.

Factor loading of various parameters in rainwater collected from location RW-04, gives four factors with loading of different parameters than other samples. Factor 1 was made by DO and trace metals such as Ni, Zn and Cu. DO indicates the variation in cloud formation and local influence over the rainfall whereas the presence of trace metal indicates the influence of anthropogenic processes such industrial and traffic activities. Factor 2 was defined by Ca^{2+} and trace metals like Co, Cd, Fe, Pb and Zn, which indicates contributions from soil dust and anthropogenic processes such as pollution from vehicles, petro-chemical industries, forest (biomass) burning along with dust particles transported

from distant palaces as well as from local areas. Turbidity and Mn contribute to the variance explained by Factor 3, indicating increased concentration of suspended particulate matter derived locally or contributed by wind blowing from long distances. Mn contributions can be from anthropogenic (iron and steel manufacturing industry, fossil fuel combustion and mining) as well as natural factors such as sea salt spray and forest fires (Moreda-Piñeiro et al., 2014). Mg^{2+} loaded in Factor 5 might be contributed by sea and land, as evaporation of saltwater and dust originates from the logged and unprotected areas.

Rainwater samples collected at location RW-05 shows five factor components. Factor 1 was constituted by EC, TDS, HCO_3^-, Cl^-, Na^+ and K^+. Among this EC and TDS are physical parameters which are contributed by the suspended particles in the atmosphere caused due to natural and anthropogenic activities. HCO_3^- in rainwater in this region was contributed by the increased amount of CO_2 in the atmosphere due to forest fires as well as the soil dust rich in carbonate contents formed by anthropogenic activities. At the same time, Cl^- concentration indicates marine contribution (Khoon et al., 2011). Loading of Na^+ suggests the contribution of sea salt through evaporation whereas K^+ originates from the forest fire or biomass combustion in the region. Factor 2 is contributed by pH and DO, indicating the overall water chemistry by dissolution of major ions and trace metals and local influence over the cloud formation. Trace metals such as Fe, Pb and Zn dominate the Factor 3, mainly contributed by anthropogenic activities such as fossil fuel burning (petrochemical industries and transportation) and forest fire in the region as well as that carried from long distance by cloud winds. Factor 4 shows strong loading of Turbidity and Mg^{2+} which indicates increased concentration of suspended particulate matter derived locally or contributed by wind blowing from long distances and evaporation of saltwater and dust that originates from the logged areas. HCO_3^- and Cu loaded in Factor 5 indicates increased pollution caused by anthropogenic processes in the region and industrial and traffic activities.

Overall, it can be concluded that rainwater chemistry in the LRB was controlled by natural as well as anthropogenic processes but the variation of water chemistry between the sampling locations were observed. Factor analysis facilitated the identification of major processes which controls the chemistry of rainwater in the region and are: (a) higher concentration of suspended particulate matter (dust) in the region (b) contribution of soil dust through wind and sea salt through evaporation (c) anthropogenic-pollution based

factors such as fossil fuel burning (petrochemical industries and transportation) and forest fire in the region as well as that carried from long distance by cloud winds and (d) vehicle emission. Though these are the major factors controlling the chemical characteristics of rainwater in the region, specific characteristics of location and the local addition of natural and anthropogenic processes have influenced the variation in chemical characteristics in different locations. For example, rainwater collected from location RW-01 has more influence of sea spray and pollution caused by industrial and vehicle traffic as it was located in the city. At the same time, rainwater collected at location RW-05 shows more influence of soil dust particles due to logging activity and local forest burning for agricultural activity.

Table 4.28: Varimax component loadings of factors and the percentage of variance explained for rainwater samples RW - 01 and RW - 02.

	RW - 01						**RW - 02**					
	Communalities	Component					Communalities	Component				
		1	2	3	4	5		1	2	3	4	5
pH	0.93	**0.77**	-0.03	-0.47	-0.19	0.28	0.94	**0.95**	0.20	-0.02	-0.05	0.00
EC	0.99	-0.23	**0.94**	-0.20	0.09	0.06	0.99	-0.28	***-0.95***	-0.10	-0.03	-0.04
TDS	0.99	-0.23	**0.94**	-0.20	0.09	0.06	0.99	-0.28	***-0.95***	-0.10	-0.03	-0.04
DO	0.56	**0.58**	-0.17	-0.01	-0.44	0.01	0.82	0.34	0.42	0.27	-0.13	**0.66**
Turbidity	0.78	0.14	0.04	-0.18	**0.83**	0.19	0.93	-0.02	0.26	**0.93**	0.01	-0.04
Bicarbonate	0.97	***-0.58***	**0.75**	0.20	-0.09	0.19	0.93	***-0.60***	***-0.59***	0.39	0.25	0.06
Chloride	0.98	-0.07	**0.89**	-0.40	0.16	-0.03	0.96	-0.10	***-0.88***	-0.35	-0.18	-0.10
Ca	0.87	**0.84**	0.13	0.02	-0.09	0.38	0.93	**0.79**	-0.29	-0.45	0.07	0.12
Mg	0.99	**0.96**	-0.17	0.07	0.17	0.04	0.98	**0.88**	0.44	0.12	-0.02	-0.01
Na	0.99	**0.91**	-0.33	0.13	0.16	-0.02	0.96	**0.87**	0.44	0.09	0.03	0.06
K	0.86	0.04	0.44	-0.09	**0.80**	-0.14	0.92	**0.65**	-0.16	**0.65**	0.16	0.18
Co	0.94	0.10	***-0.87***	-0.14	-0.32	0.24	0.76	**0.60**	0.24	0.14	-0.12	***-0.55***
Ni	0.94	-0.30	***-0.68***	**0.56**	-0.27	-0.06	0.78	-0.19	**0.57**	0.42	0.30	0.39
Cd	0.83	**0.57**	0.34	0.47	-0.05	0.40	0.71	**0.70**	0.09	-0.11	-0.03	0.45
Fe	0.96	**0.95**	-0.08	-0.19	0.13	-0.07	0.98	**0.95**	0.07	-0.22	0.15	-0.10
Mn	0.97	0.17	-0.04	0.11	0.09	**0.96**	0.98	0.10	0.14	0.07	**0.97**	-0.02
Pb	0.94	**0.91**	-0.30	0.12	0.05	0.10	0.96	**0.88**	0.35	0.27	0.06	0.01
Zn	0.86	0.21	***-0.60***	**0.67**	-0.05	0.01	0.90	**0.51**	**0.71**	0.36	0.05	-0.07
Cu	0.85	-0.10	-0.32	**0.80**	-0.26	0.20	0.70	-0.18	0.45	**0.68**	0.04	0.09
% of variance		32.06	28.36	12.00	10.29	7.98		36.64	26.08	14.72	6.46	6.23
Cumulative % of variance		32.06	60.43	72.42	82.71	90.69		36.64	62.73	77.45	83.90	90.14

Table 4.28: Varimax component loadings of factors and the percentage of variance explained for rainwater samples RW - 03 and RW - 04.

	RW - 03					RW - 04				
	Communalities	Component				Communalities	Component			
		1	2	3	4		1	2	3	4
pH	0.87	0.13	**0.89**	-0.24	-0.01	0.76	***-0.77***	-0.40	-0.10	0.04
EC	0.99	***-0.58***	**0.66**	-0.36	-0.30	0.98	***-0.82***	***-0.54***	0.11	0.01
TDS	0.99	***-0.58***	**0.66**	-0.36	-0.30	0.98	***-0.82***	***-0.54***	0.11	0.01
DO	0.71	0.06	0.14	**0.83**	0.06	0.70	**0.78**	0.22	0.19	-0.10
Turbidity	0.84	-0.33	-0.07	0.16	**0.84**	0.86	-0.15	-0.34	**0.80**	0.29
Bicarbonate	0.95	***-0.78***	**0.56**	0.03	-0.17	0.89	-0.32	***-0.80***	0.37	0.11
Chloride	0.94	-0.42	0.31	***-0.73***	-0.37	0.97	***-0.93***	-0.32	0.03	-0.07
Ca	0.92	0.01	**0.95**	0.12	-0.05	0.77	-0.31	**0.71**	-0.41	-0.08
Mg	0.97	**0.98**	0.07	0.01	0.01	0.69	0.43	0.00	-0.15	**0.69**
Na	0.95	**0.97**	-0.03	-0.07	0.08	0.78	-0.33	0.24	***-0.78***	-0.02
K	0.88	0.20	**0.90**	0.03	-0.19	0.92	0.20	-0.13	-0.13	***-0.92***
Co	0.73	**0.74**	0.12	0.34	-0.22	0.71	0.44	**0.63**	0.33	-0.10
Ni	0.84	-0.22	-0.32	**0.80**	0.22	0.91	**0.94**	-0.06	0.14	-0.01
Cd	0.84	**0.86**	0.28	0.08	-0.08	0.94	0.11	**0.96**	-0.02	0.11
Fe	0.97	**0.93**	-0.07	-0.22	-0.21	0.84	0.37	**0.83**	0.12	0.07
Mn	0.85	0.43	***-0.62***	0.46	-0.27	0.84	0.06	0.19	**0.87**	-0.20
Pb	0.94	**0.94**	-0.06	0.22	-0.06	0.92	0.34	**0.89**	-0.11	0.10
Zn	0.82	**0.73**	-0.24	0.25	0.41	0.72	**0.50**	**0.59**	-0.28	0.22
Cu	0.84	0.48	-0.25	0.37	**0.64**	0.82	**0.88**	0.05	0.11	0.19
% of variance		39.88	23.80	15.00	9.93		33.39	28.36	14.01	8.49
Cumulative % of variance		39.88	63.67	78.67	88.60		33.39	61.74	75.75	84.24

Table 4.28: Varimax component loadings of factors and the percentage of variance explained for rainwater sample RW - 05.

RW - 05						
	Communalities	Component				
		1	2	3	4	5
pH	0.96	0.16	***-0.50***	-0.45	**0.53**	0.45
EC	0.99	**0.93**	0.07	-0.29	0.12	0.14
TDS	0.99	**0.93**	0.07	-0.29	0.12	0.14
DO	0.88	0.13	**0.93**	0.02	0.00	-0.09
Turbidity	0.89	0.43	0.47	0.09	**0.59**	0.35
Bicarbonate	0.84	**0.58**	0.15	-0.39	-0.22	**0.53**
Chloride	0.98	**0.84**	-0.10	-0.36	0.34	-0.09
Ca	0.84	-0.09	***-0.85***	-0.15	0.18	-0.22
Mg	0.96	-0.16	0.36	0.02	**0.74**	**0.50**
Na	0.99	**0.98**	0.16	-0.02	0.05	0.01
K	0.98	**0.98**	0.15	-0.03	0.03	-0.01
Co	0.72	-0.16	0.06	0.31	0.06	***-0.77***
Ni	0.92	-0.23	0.24	0.03	***-0.87***	0.21
Cd	0.93	-0.13	***-0.86***	0.42	-0.06	0.04
Fe	0.94	-0.27	0.10	**0.90**	-0.15	-0.16
Mn	0.94	-0.13	0.12	0.08	***-0.93***	0.18
Pb	0.93	-0.21	-0.15	**0.92**	0.08	-0.09
Zn	0.96	***-0.67***	0.03	**0.67**	-0.14	-0.19
Cu	0.90	***-0.52***	0.45	0.32	-0.21	**0.54**
% of variance		31.14	17.46	16.69	16.54	10.50
Cumulative % of variance		31.14	48.61	65.30	81.84	92.34

4.5.3 Comparison of rainwater chemical characteristics with different locations in the world

An attempt has been also carried out to compare the chemical characteristics of rainwater in the LRB with selected areas in the world. For that, results of the studies carried out in Brazil, Indonesia, Jordan, United States, South Korea, England, China and India were extracted from research publications (Table 4.29). It is noted that most of the studies do not include all the physico-chemical parameters considered in the present research. Considering the mean pH, the LRB shows higher values than all other places except Jordan, England and India. Similarly, Jordan also shows a higher value of EC compared with the LRB. Most locations show the alkaline nature of rainwater except in Indonesia, US and China which showed a pH value < 5.6 (neutral for rainwater). Higher values of EC in the LRB indicates the presence of more suspended particulate matter in the atmosphere and rainwater. In the case of major anion concentration, most of the studies do not consider HCO_3^-, but rainwater in the LRB shows comparatively higher concentration of HCO_3^-. There is also a higher concentration of chloride when compared with other regions except for India, which showed a moderate value. Similarly, the concentration of major cations shows moderate concentrations compared to Jordan, England and India. This indicates a comparatively higher input from sea, land and anthropogenic activities in those regions. At the same time, trace metal in rainwater collected from the LRB shows higher concentration than all other places. It was noted that, rainfall in Jordan also shows comparatively close values to the LRB. However, considering the concentration of trace metal in the region and comparing this with the industrial development in the LRB, there is a higher concentration of trace metals compared to industrially developed countries. Contributions of trace metals in the region can be attributed to the monsoon winds originating from long distances, the presence of petro-chemical industries in the region, especially in the South China Sea and also by regional forest fire (biomass burning) in South East Asia. Overall, while comparing the rainwater chemistry of the LRB with spatially and regionally separated locations in the world, shows that the rainwater in the LRB is also polluted due to the anthropogenic activities.

Table 4.29: Comparison of mean concentration of physico-chemical parameters of rainwater in the LRB with selected locations in the world.

Parameters	Limbang River Basin, Borneo	Thames river, South eastern England	Ghore El-Safi, Jordan	Newark, New Jersey, US	Nanping Mangdang Mountain, China	Palampur Dist., Himachal Pradesh, India	Juiz de Fora City, Brazil	GIST campus, Gwangju, Korea	Bandung City, Indonesia
pH	6.01	6.13	6.91	4.57	4.81	6.11	5.77	5.78	4.67
EC (µS/cm)	90.85	48.5	95	-	20.01	33.62	11.30	27.82	17.79
TDS (mg/L)	63.60	-	-	-	-	-	-	-	-
DO (mg/L)	6.87	-	-	-	-	-	-	-	-
Turbidity(NTU)	0.91	-	-	-	-	-	-	-	-
Bicarbonate (mg/L)	32.01	-	8.153	-		-	1.80	-	-
Chloride (mg/L)	28.02	7.925	5.053	1.08	0.205	15.30	0.614	4.4	0.292
Ca (mg/L)	0.97	3.29	3.3064	0.21	0.605	3.95	0.792	0.7	0.684
Mg (mg/L)	0.37	0.565	1.117	0.05	0.074	0.14	0.289	0.2	0.060
Na (mg/L)	1.87	3.85	3.003	0.60	0.163	0.2	0.575	1.4	0.114
K (mg/L)	0.35	0.405	3.3232	0.06	0.208	0.9	0.278	0.3	0.233
Co (mg/L)	0.024	0.00155	0.43	0.00002	0.00005	-	-	-	0.006
Ni (mg/L)	0.138	0.00405	0.003	0.0055	0.001	0.183	-	0.00028	0.0059
Cd (mg/L)	0.005		0.052	0.00003	-	0.00022	BDL	0.00009	0.0057
Fe (mg/L)	1.054	0.019	0.43	0.00835	0.0153	-	-	0.011	0.0348
Mn (mg/L)	0.029	0.01365	-	-	0.0062	-	-	0.00458	-
Pb (mg/L)	0.037	0.0012	0.066	0.00047	0.0096	0.00385	BDL	0.00310	0.0767
Zn (mg/L)	0.015	0.1231	0.21	0.00660	0.065	-	0.007	0.01878	0.0335
Cu (mg/L)	0.012	0.00245	0.073	0.00282	0.0038	0.0011	0.004	0.00169	0.0088
Reference	Present study	Neal et al. (2004).	Al-Khashman (2009).	Song and Gao (2009).	Cheng et al. (2011).	Singh (2011).	Cerqueira et al. (2014).	Chon et al., (2015).	Hasan et al. (2017).

4.6 Surface Water Chemistry

4.6.1 Surface water quality

In order to determine the spatial and temporal characteristics of water quality of the Limbang River, three sampling periods (November 2016, March 2017 and September 2017) samples were collected from 24 locations from the LRB, considering the tributaries and major river. Results of analysed parameters are given in Tables 4.30 and its spatial and temporal variations are shown in Figures 4.66 to 4.92. The results of quality parameters analysed are then compared with Malaysian Water Quality Standards (MWQS) and World Health Organization (WHO) standards to assess the suitability of water for various purposes (Table 4.31).

4.6.1.1 Physical parameters

pH

The pH was found to be varying spatially and temporally (in different sampling periods and sampling locations). In the first sampling period (S1), pH ranges from 4.41 to 7.55 with a mean of 6.77. During the second sampling period (S2) pH varies in the range of 4.77 to 7.03 with a mean of 6.60. At the same time, in the third sampling period (S3), pH in the surface water varies from 5.78 to 7.28 with a mean of 6.72. Comparing the measured values with Malaysian and WHO water quality standards, 19 samples in S1 and S3 and 18 in S2 come under the class I category of Malaysian Water Quality Standards (MWQS) and within the permissible limit of the WHO standards. 5 samples in S1, 4 samples in S2 and 3 in S3 fall in the class IIA category of MWQS. None of the samples show alkaline nature, in fact LRB SW- 17 (4.41, 4.77) in S1 and S2 shows acidic nature (pH < 5). At the same time, LRB SW- 17(5.89) in S3, LRB SW-21 (5.42, 5.78) in S1 and S3 and LRB SW-24 (5.98) in S2 are also slightly acidic in nature and comes in the class IV category of MWQS. The lower value of pH may be due to the dilution caused by the direct input of rainwater to the river water. In addition to that, the dissolution of carbon dioxide and its reaction with water will generate carbonic acid and this might also be a reason for the acidic nature of river water in general.

EC

Electrical conductivity (EC) which directly relates to the concentration of dissolved ions in the water are found to vary spatially and temporally. Measured values of EC was found to range from 77.14 to 160.38µS/cm with a mean of 101.66µS/cm in S1. In S2, EC varies between

86.23 to 139.94µS/cm with a mean of 108.62µS/cm. During S3, EC varies from 107.76 to 178.37µS/cm with a mean of 129.28µS/cm. According to MWQS and WHO standards, all values of EC are comparatively lower than the guideline value of both standards. Considering the seasonal difference, EC values measured during S3 shows comparatively higher than the other two seasons.

TDS

Total dissolved solids (TDS) measures the amount of dissolved ions in the water samples. In the LRB during S1, TDS ranges from 54.00 to 112.27mg/L with a mean of 71.16mg/L. In S2, TDS varies between 60.36 and 97.96mg/L with a mean of 76.04mg/L. During S3, TDS was found to vary between 75.43 to 124.86mg/L with a mean of 90.49mg/L. Similar to EC, TDS also shows comparatively higher value in S3. TDS values also indicate that the water samples belong to class I according to MWQS and are within the tolerable limits of WHO standards.

DO

Dissolved oxygen measures the amount of gaseous oxygen dissolved in the water sample. During S1, S2 and S3, DO ranges from 5.48 to 8.44mg/L, 4.60 to 9.40mg/L and 4.00 to 7.60mg/L respectively. At the same time, the mean DO shows variation between the season S1, S2 and S3 as 7.50mg/L, 7.82mg/L and 5.88mg/L. In all sampling periods, most of the samples fall within the Class I and Class IIA category of MWQS. LRB SW-02 in S2 and LRB SW-08, 09, 12 and 23 in S3, are in Class III category of MWQS. DO values found to be comparatively lower during S3 than the other two sampling periods.

Temperature

Temperature of the water samples were measured in-situ and found to be vary in the range of 24.80˚C (LRB SW-01) to 30.30˚C (LRB SW-08) in S1, 23.90˚C (LRB SW-01) to 32.00˚C (LRB SW-23) in S2 and 24.20˚C (LRB SW-01) to 27.90˚C (LRB SW-22) in S3 sampling period. The mean temperature of S1, S2 and S3 is 27.97˚C, 26.90˚C and 26.50˚C respectively. It was noted that the temperature of the surface water varies depending on the time of measurement. Moreover, the LRB samples in the lower catchment shows a higher temperature than the headwater region.

Turbidity

Clarity of the water can be understood by measuring the turbidity. The turbidity ranges from 4.23 to 310.00NTU in S1 with a mean of 68.37NTU. During S2, turbidity varies from 3.34 to 821.00 (Above Measurable Unit) NTU with a mean of 184.81NTU. At the same time in S3, turbidity ranges from 2.82 to 120.00NTU with a mean of 33.17NTU. According to MWQS, very few number of samples fall under class I category. These samples are collected from the upper reaches of the river basin. However, a number of samples fall in the Class IIA category of MWQS. Moreover, all stations possess higher values than that of WHO standards (≤ 5NTU). High turbidity value was marked in S2, then S1 and S3, in which the least value was observed in S3. During S2, most samples show values beyond the measurable limit of the instrument (highly turbid in nature).

4.6.1.2 Nutrients

Sulfate

Sulfate concentration in the samples range from BDL to 11.00mg/L in S1, BDL to 10.00mg/L in S2 and BDL to 7.00mg/L in S3. The mean concentration of sulfate are 3.42mg/L in S1, 3.13mg/L in S2 and 2.63mg/L in respectively. While comparing with the MWQS, the water samples collected during the three sampling periods show very low values and are below the maximum desirable limit.

Nitrate

Nitrate is found to vary between BDL to 0.050mg/L, 0.010 to 0.580mg/L and 0.010 to 0.090mg/L in S1, S2 and S3 respectively. The mean of nitrate concentration are 0.020mg/L in S1, 0.093mg/L in S2 and 0.030mg/L in S3. Nitrate values of the samples are below the maximum desirable limit of MWQS. Water samples collected during S1, show lower values compared to the other seasonal samples.

Ammonia

Ammonia content in water samples collected during S1 ranges from 0.030 to 0.200mg/L with a mean of 0.076mg/L. During S2, the concentration of ammonia varies from 0.050 to 1.500mg/L with a mean of 0.275mg/L. However, in S3, the ammonia concentration ranges from BDL to 0.110mg/L with a mean of 0.036mg/L. Comparing the seasonal variation, samples collected during S2 contains comparatively higher concentration of ammonia but are

within the maximum desirable limit of MWQS and WHO standards. The least value of ammonia concentration was observed in S3 samples. However, all the samples are within the limit of MWQS and WHO standards (Class II according to MWQS).

Phosphate

Phosphate concentration in the water samples ranges from 0.120 to 0.360mg/L in S1, 0.170 to 0.550mg/L in S2 and 0.090 to 0.240mg/L in S3. In addition, the mean of phosphate concentration in the LRB shows variation among the seasons and is 0.223mg/L during S1, 0.233mg/L during S2 and 0.162mg/L during S3. Considering the sampling periods, comparatively lower concentration of phosphate was observed in S3 compared to the other two sampling periods.

4.6.1.3 Major ions

Bicarbonate (HCO_3^-)

Surface water samples analysed indicate the absence of carbonate concentration, whereas the HCO_3^- shows varying degree in concentration. In S1 samples, the HCO_3^- ranges from 27.45 to 61.00mg/L with a mean of 36.60mg/L. During S2, HCO_3^- varies in the range of 39.59 to 61.18mg/L and shows a mean concentration of 47.09mg/L. Concentration of HCO_3^- during S3 ranges from 30.50 to 68.63mg/L with a mean of 39.65mg/L. It was noted that HCO_3^- shows moderately higher concentration in S2 than S1 and S3.

Chloride (Cl^-)

Cl^- concentration in the surface water was found to vary in the range of 13.29 to 26.59mg/L in S1 with a mean of 20.68mg/L. During S2, the Cl^- varies from 14.20 to 24.14mg/L with a mean of 18.11mg/L. At the same time, in S3, the Cl^- concentration ranges from 31.91 to 46.09mg/L with a mean of 37.08mg/L which is comparatively higher than S1 and S2. According to Malaysian and WHO water quality standards, the Cl^- concentration is very low compared to the desirable limit and falls under the Class II category of MWQS.

Calcium (Ca^{2+})

Concentration of Ca^{2+} in S1 samples varies from 0.16 to 12.95mg/L with a mean of 1.73mg/L. During S2, Ca^{2+} concentration ranges between 0.29 to 9.40mg/L with a mean of 1.76mg/L. In S3, Ca^{2+} ranges from 0.32 to 19.84mg/L S3 which shows a mean of 1.58mg/L.

Considering the sampling periods, the S3 sample shows higher concentration of Ca^{2+}. Water samples collected from the LRB show comparatively higher concentration of Ca^{2+} in all the sampling periods compared to other cations concentration.

Magnesium (Mg^{2+})

Mg^{2+} concentration in S1 samples ranges from 1.93 to 4.63mg/L with a mean of 2.99mg/L. During S2, the concentration of Mg^{2+} varies from 1.31 to 2.91mg/L with a mean of 2.25mg/L. Considering the water samples collected during S3, Mg^{2+} concentration ranges from 1.35 to 44.64mg/L with mean of 4.95mg/L. The highest Mg^{2+} concentration in water was observed in S3 sample (LRB SW-06) and the lowest concentration was observed in the S2 samples.

Sodium (Na^{+})

The Na^{+} concentration in S1 samples shows a variation in the range of 3.03 to 7.21mg/L with a mean of 4.75mg/L. At the same time, during S2, Na^{+} ranges from 1.67 to 4.27mg/L with a mean of 2.75mg/L. During the sampling period S3, Na^{+} ranges from 2.11 to 7.46mg/L with a mean concentration of 3.82mg/L. The lowest value range of Na^{+} was observed in S2 samples compared to the other two sampling periods.

Potassium (K^{+})

K^{+} concentration in the sampling period S1 varies from 0.39 to 1.33mg/L with a mean of 0.76mg/L. During S2, K^{+} varies in the range of 0.28 to 1.88mg/L with a mean of 0.64mg/L. However, S3 samples show concentration in the range of 0.37 to 0.90mg/L with a mean of 0.60mg/L. Among the sampling periods, the lowest concentration of K^{+} was observed in S3.

4.6.1.4 Trace metals

Cobalt (Co)

Concentration of Co in S1 samples varies from 0.018 to 0.061mg/L, S2 from 0.018 to 0.066mg/L and S3 from 0.012 to 0.042mg/L. The mean concentration of Co in S1, S2 and S3 were 0.038mg/L, 0.030mg/L and 0.023mg/L respectively. When comparing the three sampling periods, the lowest Co concentration was observed in S3 samples.

Nickel (Ni)

Ni concentration in S1 samples range from 0.103 to 0.146mg/L with a mean of 0.123mg/L. During S2, Ni ranges from 0.104 to 0.214mg/L with a mean of 0.159mg/L. Considering the S3 samples, Ni concentration ranges between 0.069 to 0.156mg/L with a mean of 0.111mg/L. Among the sampling periods, S2 shows the highest concentration of Ni. Compared to MWQS and WHO standards, all the samples in the three seasons were above the permissible limit, except LRB SW-8 during S3 (which comes with in the guideline value of WHO standard).

Cadmium (Cd)

Concentration of the Cd in S1 ranges from 0.005 to 0.009mg/L, S2 from 0.003 to 0.006mg/L and S3 from 0.002 to 0.008mg/L. The mean concentration of Cd during the sampling periods are 0.007mg/L in S1, 0.004mg/L in S2 and 0.005mg/L during S3. Samples collected in all sampling periods are within the permissible limit of MWQS and WHO standards.

Iron (Fe)

Fe concentration in the samples ranges from 1.57 to 1.94mg/L, 0.78 to 1.29mg/L and 0.98 to 1.24mg/L for S1, S2 and S3 respectively. However, the mean concentration of Fe during the sampling periods S1, S2 and S3 were 1.77mg/L, 1.03mg/L and 1.13mg/L respectively. All the samples in all the seasons show values above the permissible limit of the WHO standard. Considering the MWQS, in S2, most of the samples show Fe concentration in the Class II category (LRB SW-01, 03, 04, 05, 07, 10, 11, 13, 14, and 16) but the values are very close to the permissible limit of Class II category. All the samples in S1 and S3 (except LRB SW-13) fall in the class IV category of MWQS.

Manganese (Mn)

Concentration of Mn in S1, S2 and S3 samples ranges from 0.019 to 0.140mg/L, 0.031 to 0.127mg/L and 0.016 to 0.121mg/L respectively. The mean concentration of the Mn was 0.037mg/L during S1, 0.051mg/L during S2 and 0.038mg/L during S3 respectively. Most of the samples in three seasons fall under the Class II category of the MWQS except in two locations (LRB SW-17 and 21). These water samples fall in the class IV category. At the same time, all the samples are within the permissible limit of the WHO standards.

Lead (Pb)

Pb concentration in the S1 samples ranges from 0.079 to 0.131mg/L with a mean of 0.099mg/L whereas in S2, the concentration of Pb ranges from 0.023 to 0.056mg/L with a mean of 0.040mg/L respectively. Considering the S3 samples, concentration of Pb ranges from 0.013 to 0.030mg/L with a mean of 0.022mg/L. It was noted that, none of the sample falls in the permissible limit of the WHO standard. Comparing the seasonal concentration of Pb, S1 samples shows higher values compared to the other two seasons and are in the class IV category of the MWQS. S2 samples except the location LRB SW-17 and the S3 samples are within the permissible limit of Class II of the MWQS.

Zinc (Zn)

In S1, the value of Zn ranges from 0.019 to 0.426mg/L, in S2 it ranges from 0.009 to 0.030mg/L and in S3 from 0.003 to 0.032mg/L. Zn shows a mean concentration of 0.059mg/L, 0.016mg/L and 0.018mg/L during S1, S2 and S3 respectively. All the samples fall in the Class II category of the MWQS and are within the limit of the WHO standards. Among the samples, the highest value was observed in S1 samples, especially in LRB SW-17.

Copper (Cu)

Cu concentration in water samples collected during different sampling periods range from 0.011 to 0.040mg/L, 0.014 to 0.042mg/L and 0.003 to 0.017mg/L in S1, S2 and S3 respectively. However, the mean concentration of Cu during the sampling periods S1, S2 and S3 are 0.020mg/L, 0.023mg/L and 0.009mg/L respectively. During S3, all the samples fall in the permissible limit of Class II category of the MWQS. 50% of the samples in S1 and S2 were above the limit of Class II category of the MWQS. But while compared to the WHO standards, all the samples collected during the three sampling periods are within the permissible limit.

Table 4.30: Results of physico-chemical parameters of surface water collected from 24 locations in the LRB during S1, S2 and S3.

Parameters	Sampling Period-1 (S1)				Sampling Period-2 (S2)				Sampling Period-3 (S3)			
	Min	Max	Mean	Std. Dev	Min	Max	Mean	Std. Dev	Min	Max	Mean	Std. Dev
pH	4.41	7.55	6.77	0.73	4.77	7.03	6.60	0.48	5.78	7.28	6.72	0.40
EC(µS/cm)	77.14	160.38	101.66	18.22	86.23	139.94	108.62	15.30	107.76	178.37	129.28	17.15
TDS(mg/L)	54.00	112.27	71.16	12.75	60.36	97.96	76.04	10.71	75.43	124.86	90.49	12.01
DO(mg/L)	5.48	8.44	7.50	0.85	4.60	9.40	7.82	1.04	4.00	7.60	5.88	1.03
Temperature (˚C)	24.80	30.30	27.97	1.11	23.90	32.00	26.90	1.56	24.20	27.90	26.50	0.87
Turbidity (NTU)	4.23	310.00	68.67	71.83	3.34	821.00(AU)	184.81	251.22	2.82	120.00	33.17	30.96
Sulfate (mg/L)	BDL	11.00	3.42	3.28	BDL	10.00	3.13	2.77	BDL	7.00	2.63	2.26
Nitrate (mg/L)	BDL	0.050	0.020	0.016	0.010	0.580	0.093	0.145	0.010	0.090	0.030	0.020
Ammonia (mg/L)	0.030	0.200	0.076	0.044	0.050	1.500	0.275	0.306	BDL	0.110	0.036	0.027
Phosphate (mg/L)	0.120	0.360	0.223	0.063	0.170	0.550	0.233	0.077	0.090	0.240	0.162	0.035
Bicarbonate (mg/L)	27.45	61.00	36.60	9.26	39.59	61.18	47.09	6.62	30.50	68.63	39.65	7.50
Chloride(mg/L)	13.29	26.59	20.68	4.27	14.20	24.14	18.11	2.88	31.91	46.09	37.08	3.50
Ca (mg/L)	0.16	12.95	1.73	3.14	0.29	9.40	1.76	2.29	0.32	19.84	1.58	3.90
Mg (mg/L)	1.93	4.63	2.99	0.63	1.31	2.91	2.25	0.42	1.35	44.64	4.95	8.47
Na (mg/L)	3.03	7.21	4.75	0.95	1.67	4.27	2.75	0.62	2.11	7.46	3.82	1.17
K (mg/L)	0.39	1.33	0.76	0.25	0.28	1.88	0.64	0.31	0.37	0.90	0.60	0.14
Co (mg/L)	0.018	0.061	0.038	0.011	0.018	0.066	0.030	0.011	0.012	0.042	0.023	0.008
Ni (mg/L)	0.103	0.146	0.123	0.009	0.104	0.214	0.159	0.036	0.069	0.156	0.111	0.020
Cd (mg/L)	0.005	0.009	0.007	0.001	0.003	0.006	0.004	0.001	0.002	0.008	0.005	0.002
Fe (mg/L)	1.57	1.94	1.77	0.09	0.78	1.29	1.03	0.11	0.98	1.24	1.13	0.05
Mn (mg/L)	0.019	0.140	0.037	0.027	0.031	0.127	0.051	0.025	0.016	0.121	0.038	0.026
Pb (mg/L)	0.079	0.131	0.099	0.013	0.023	0.056	0.040	0.008	0.013	0.030	0.022	0.004
Zn (mg/L)	0.019	0.426	0.059	0.085	0.009	0.030	0.016	0.006	0.003	0.032	0.018	0.009
Cu (mg/L)	0.011	0.040	0.020	0.006	0.014	0.042	0.023	0.006	0.003	0.017	0.009	0.003

Table 4.31: Comparison of water quality parameters of the LRB during S1, S2 and S3 with Malaysian and WHO water quality standards.

Parameters	Observed value range			Malaysian Standard (2009)	WHO Standard (2011)	No of location showing beyond range of MWQS		
	S1	S2	S3			S1	S2	S3
pH	4.41 -7.55	4.77 - 7.03	5.78 – 7.28	6.0 - 9.0	6.5 - 8.5	2 stations	2 stations	Nil
EC (µS/cm)	77.14 - 160.38	86.23 - 139.94	107.76 – 178.37	1000 - 6000	100	Nil	Nil	Nil
TDS (mg/L)	54.00 - 112.27	60.36 - 97.96	75.43 - 124.86	500 - 4000	450	Nil	Nil	Nil
DO (mg/L)	5.48 -8.44	4.60 - 9.40	4.00 – 7.60	5 - 7	NA	18 stations	20 stations	8 stations
Turbidity (NTU)	4.23 - 310	3.34 - 821	2.82 - 120	5 - 1000	<5	Nil	Nil	Nil
Sulfate (mg/L)	BDL - 11	BDL - 10	BDL - 7	250	200	Nil	Nil	Nil
Nitrate (mg/L)	BDL - 0.05	0.01 - 0.58	0.01 - 0.09	10	50	Nil	Nil	Nil
Ammonia (mg/L)	0.03 - 0.20	0.05 - 1.5	BDL - 0.11	1.5	1.5	Nil	Nil	Nil
Phosphate (mg/L)	0.12 - 0.36	0.17 - 0.55	0.09 - 0.24	NA	NA	NA	NA	NA
Bicarbonate (mg/L)	27.45 – 61.00	39.59 - 61.18	30.50 - 68.23	NA	NA	NA	NA	NA
Chloride (mg/L)	13.29 - 26.59	14.20 - 24.15	31.91 - 46.09	NA	250	NA	NA	NA
Ca (mg/L)	0.16 - 12.95	0.29 - 9.40	0.32 - 19.84	NA	200	NA	NA	NA
Mg (mg/L)	1.93 - 4.63	1.31 - 2.91	1.35 - 44.64	NA	150	NA	NA	NA
Na (mg/L)	3.03 - 7.21	1.67 - 4.27	2.11 - 7.46	NA	200	NA	NA	NA
K (mg/L)	0.39 - 1.33	0.28 - 1.88	0.37 - 0.90	NA	12	NA	NA	NA
Co (mg/L)	0.018 - 0.061	0.018 - 0.066	0.012 - 0.042	NA	2	NA	NA	NA
Ni (mg/L)	0.103 - 0.146	0.104 - 0.214	0.069 - 0.156	0.05 - 0.9	0.02	Nil	Nil	Nil
Cd (mg/L)	0.005 - 0.009	0.003 - 0.006	0.002 - 0.008	0.01	0.003	Nil	Nil	Nil
Fe (mg/L)	1.57 - 1.94	0.78 - 1.29	0.98 - 1.24	1	0.3	All stations	13 stations	23 stations
Mn (mg/L)	0.019 - 0.140	0.031 - 0.127	0.016 - 0.121	0.1 - 0.2	0.5	Nil	Nil	Nil
Pb (mg/L)	0.079 - 0.131	0.023 - 0.056	0.013 - 0.030	0.01 - 0.05	0.01	All stations	1 stations	Nil
Zn (mg/L)	0.019 - 0.426	0.009 - 0.030	0.003 - 0.032	0.4 - 5	3	Nil	Nil	Nil
Cu (mg/L)	0.011 - 0.040	0.014 - 0.042	0.003 - 0.017	0.02	2	11 stations	17 stations	Nil

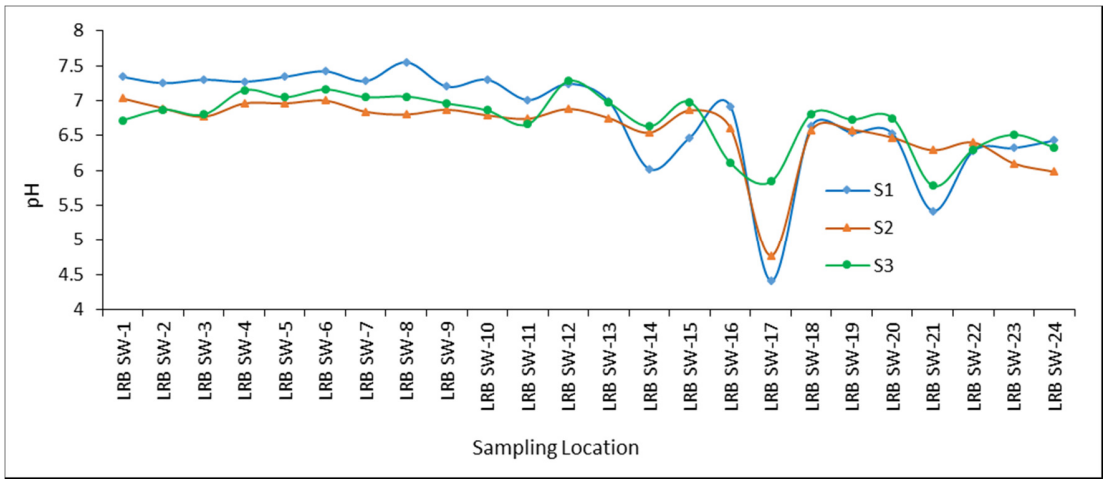

Figure 4.66: Spatial and temporal variation in pH.

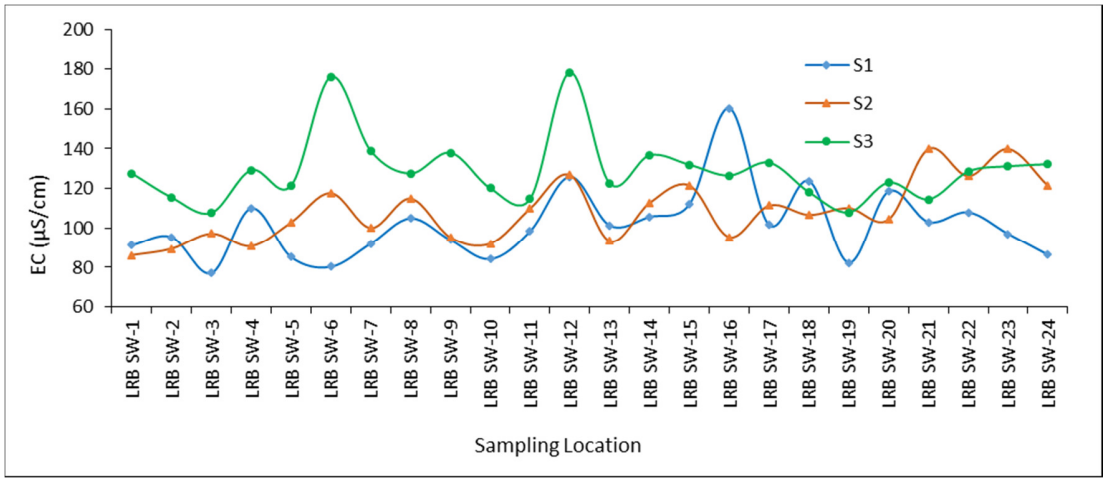

Figure 4.67: Spatial and temporal variation in EC.

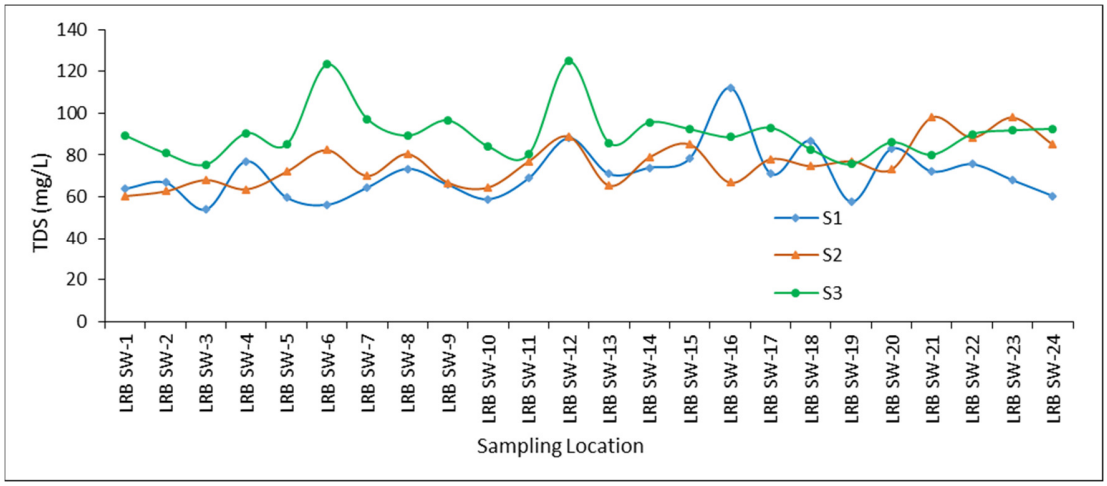

Figure 4.68: Spatial and temporal variation in TDS.

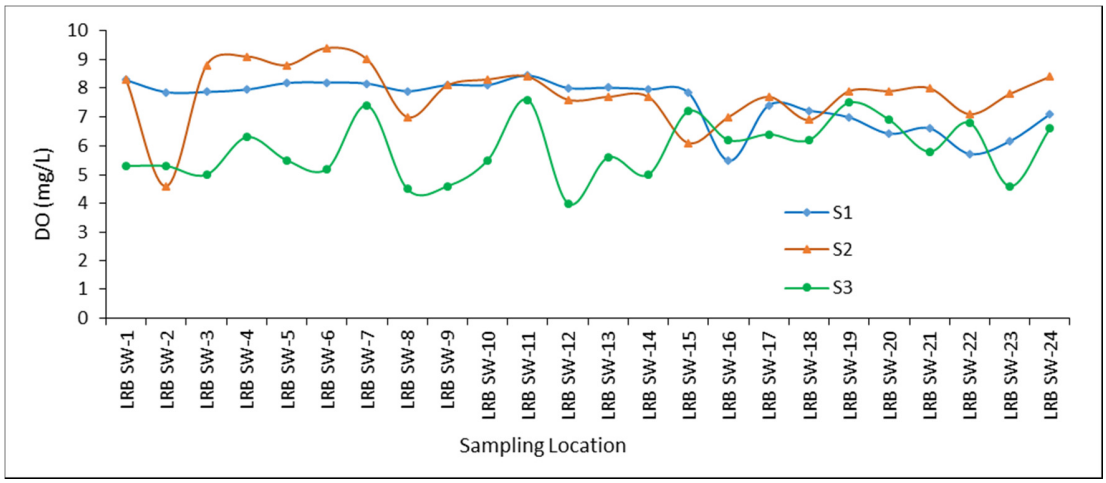

Figure 4.69: Spatial and temporal variation in DO.

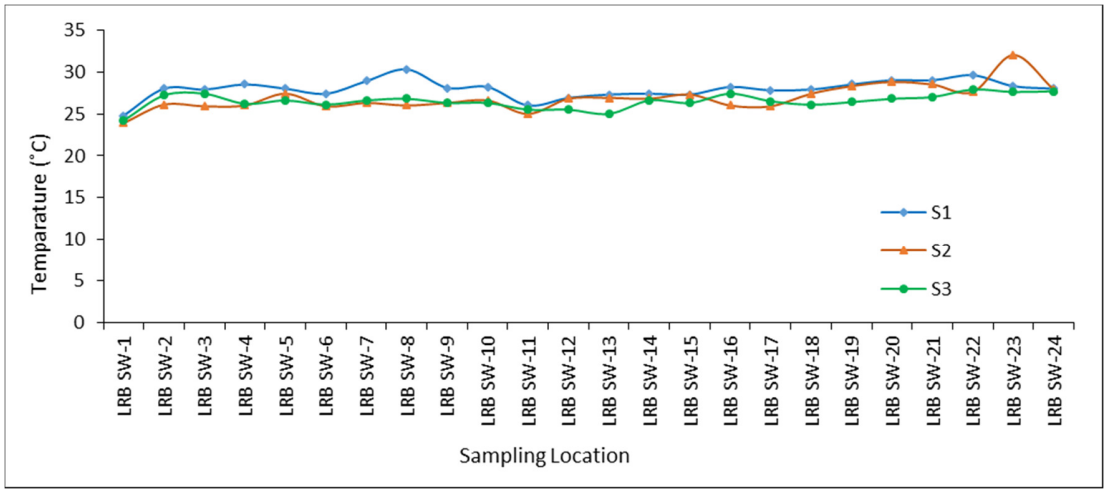

Figure 4.70: Spatial and temporal variation in Temperature.

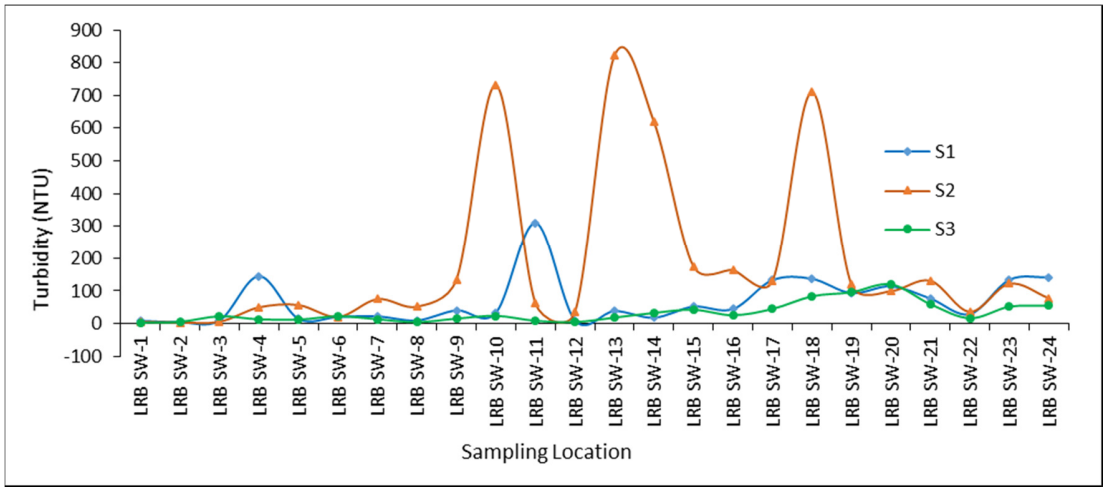

Figure 4.71: Spatial and temporal variation in Turbidity.

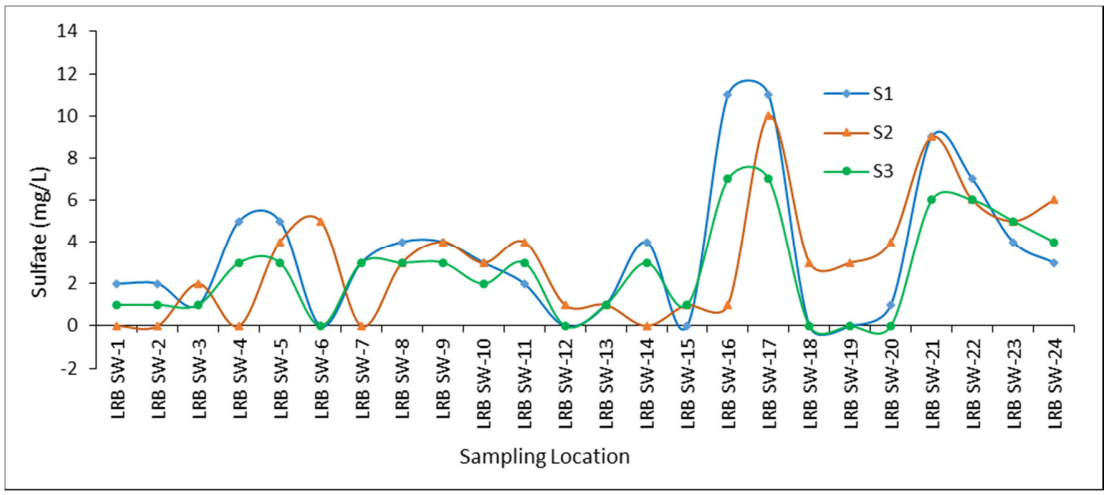

Figure 4.72: Spatial and temporal variation in Sulphate.

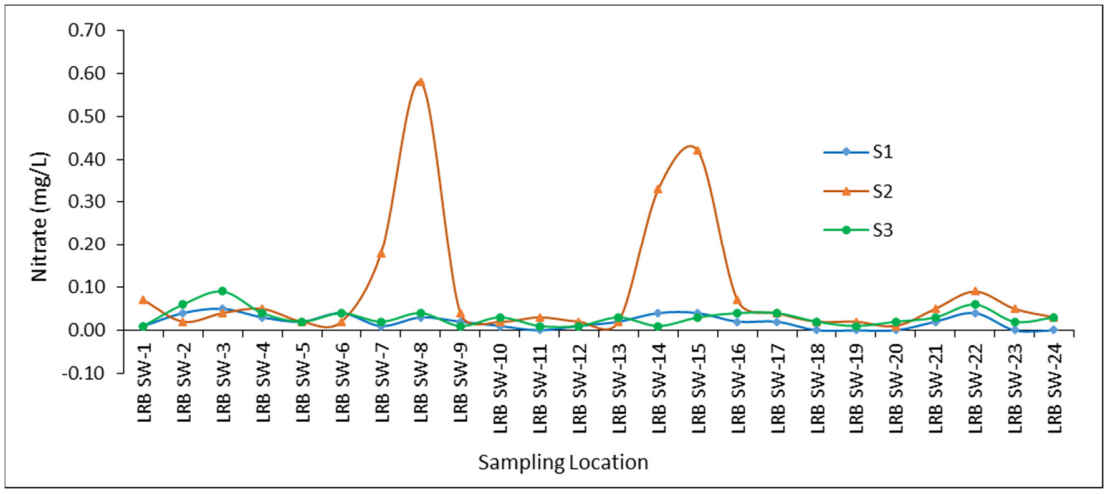

Figure 4.73: Spatial and temporal variation in Nitrate.

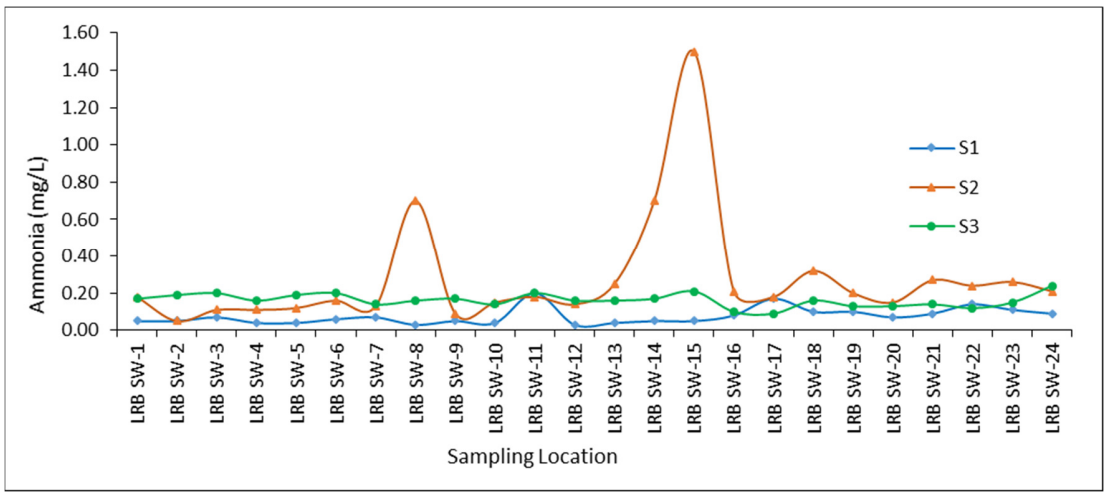

Figure 4.74: Spatial and temporal variation in Ammonia.

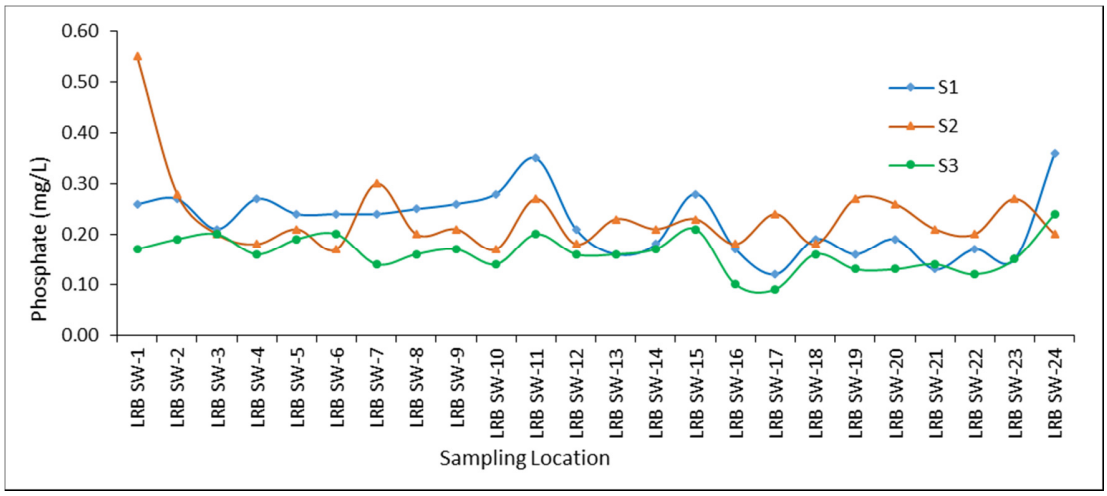

Figure 4.75: Spatial and temporal variation in Phosphate.

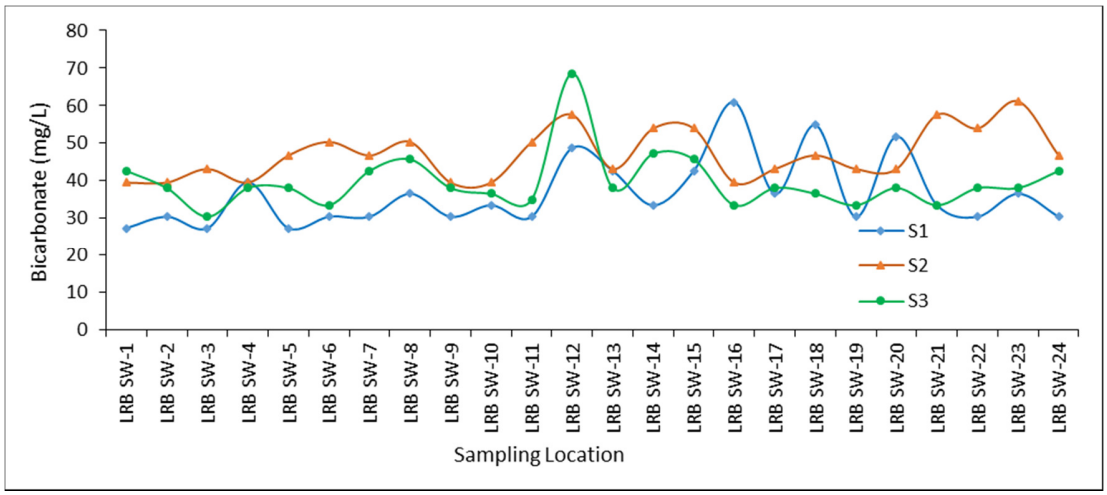

Figure 4.76: Spatial and temporal variation in Bicarbonate.

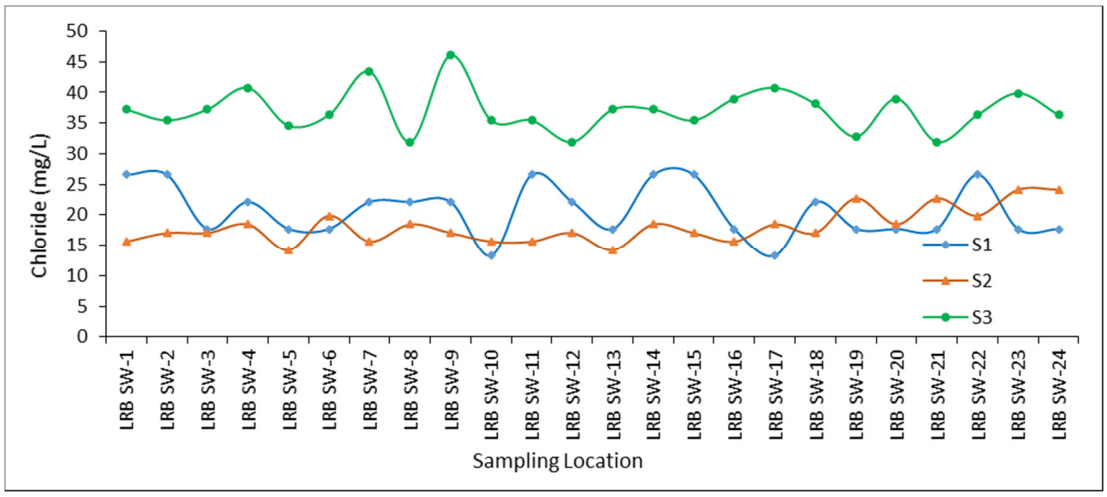

Figure 4.77: Spatial and temporal variation in Chloride.

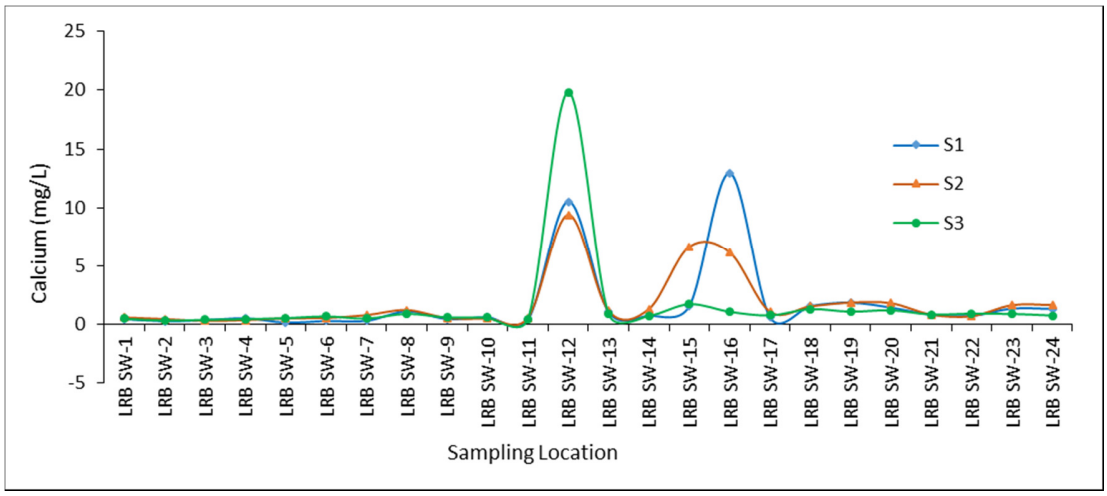

Figure 4.78: Spatial and temporal variation in Calcium.

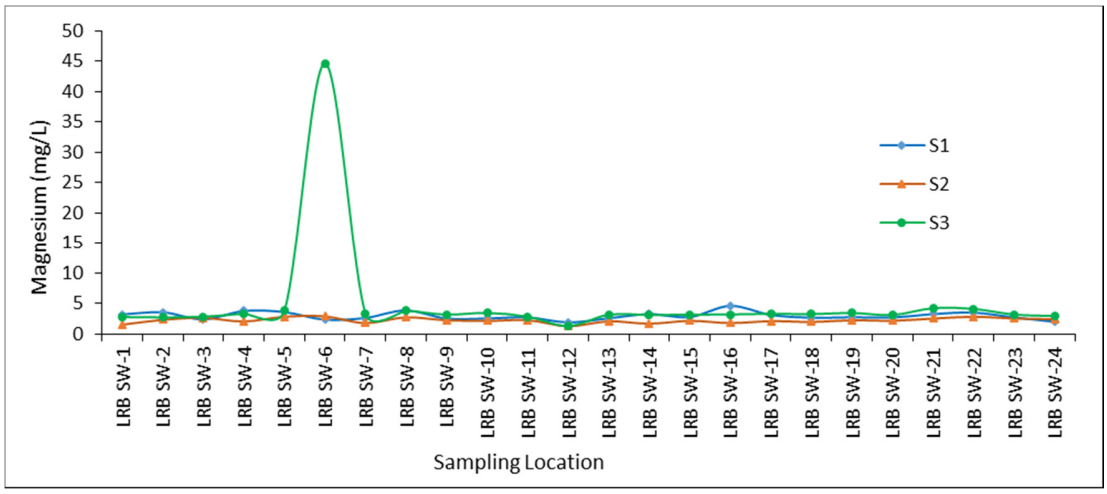

Figure 4.79: Spatial and temporal variation in Magnesium.

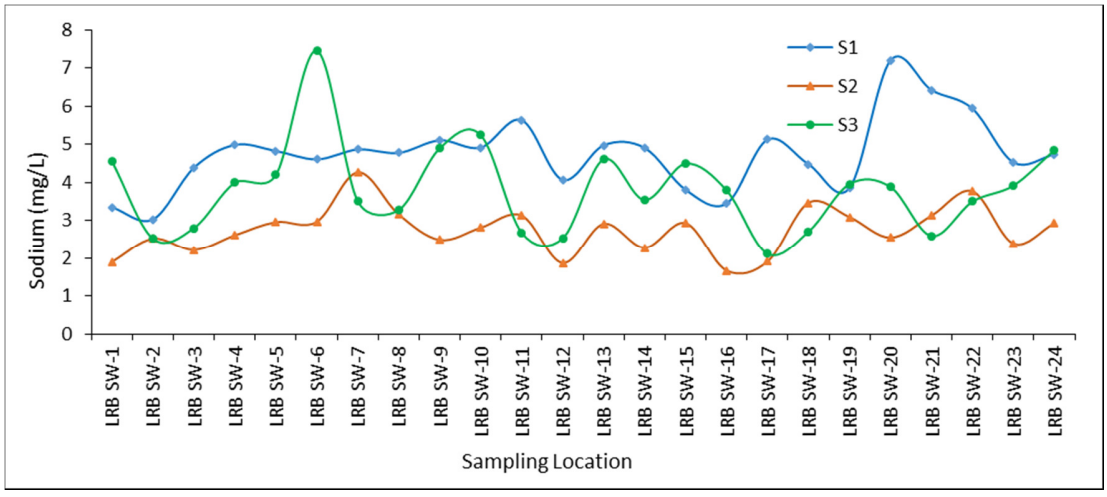

Figure 4.80: Spatial and temporal variation in Sodium.

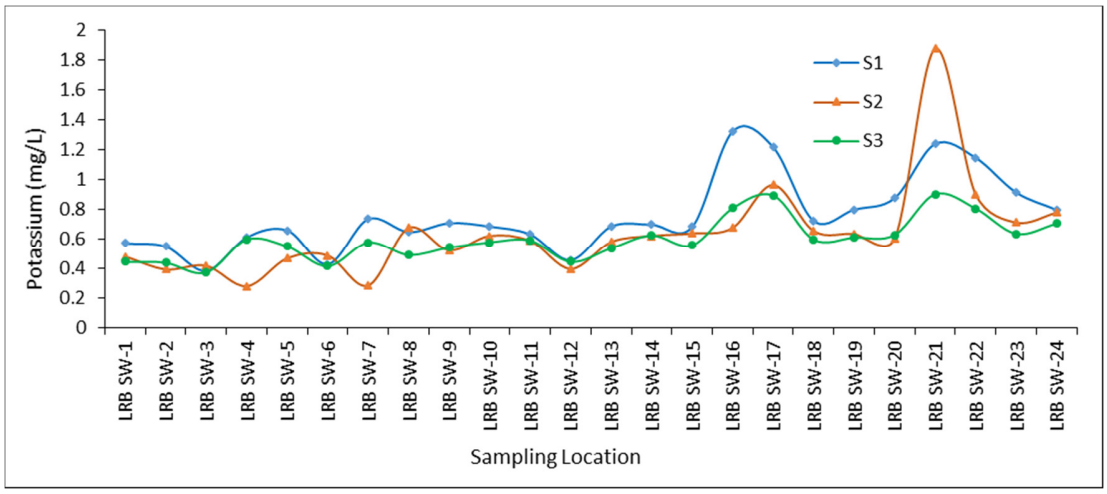

Figure 4.81: Spatial and temporal variation in Potassium.

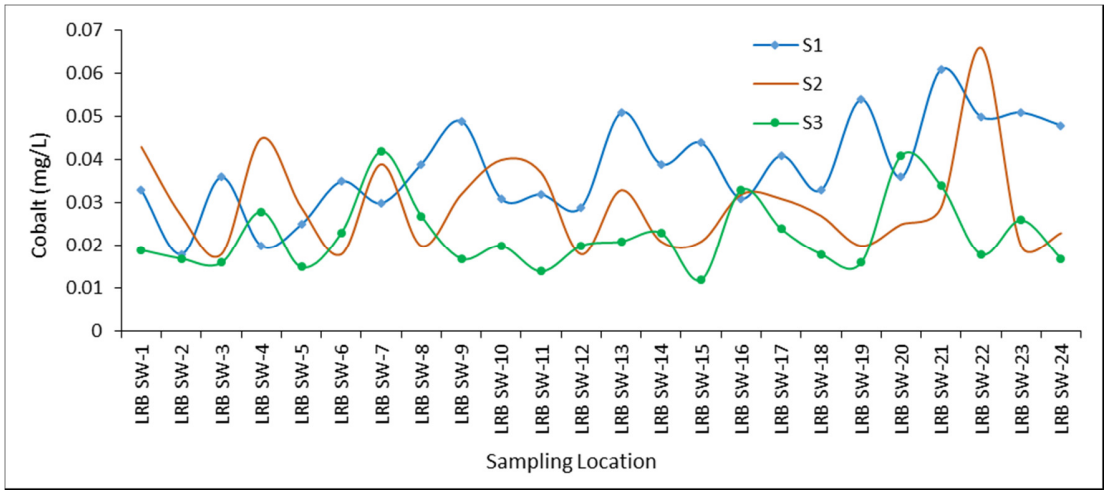

Figure 4.82: Spatial and temporal variation in Cobalt

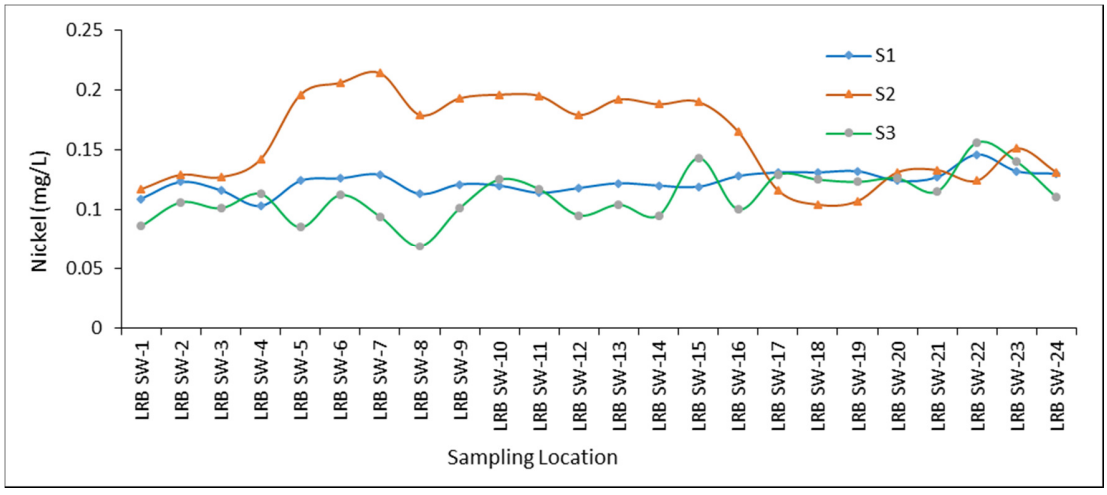

Figure 4.83: Spatial and temporal variation in Nickel.

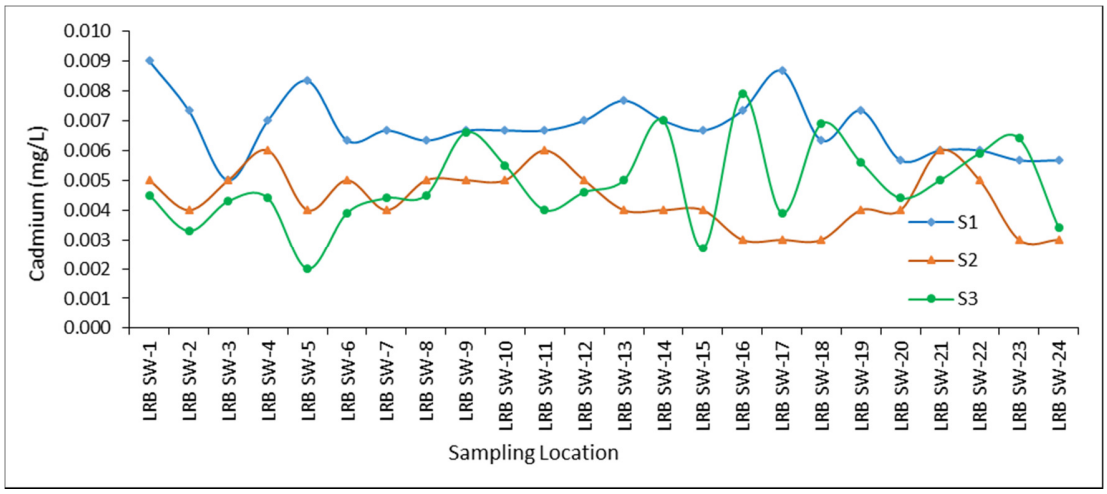

Figure 4.84: Spatial and temporal variation in Cadmium.

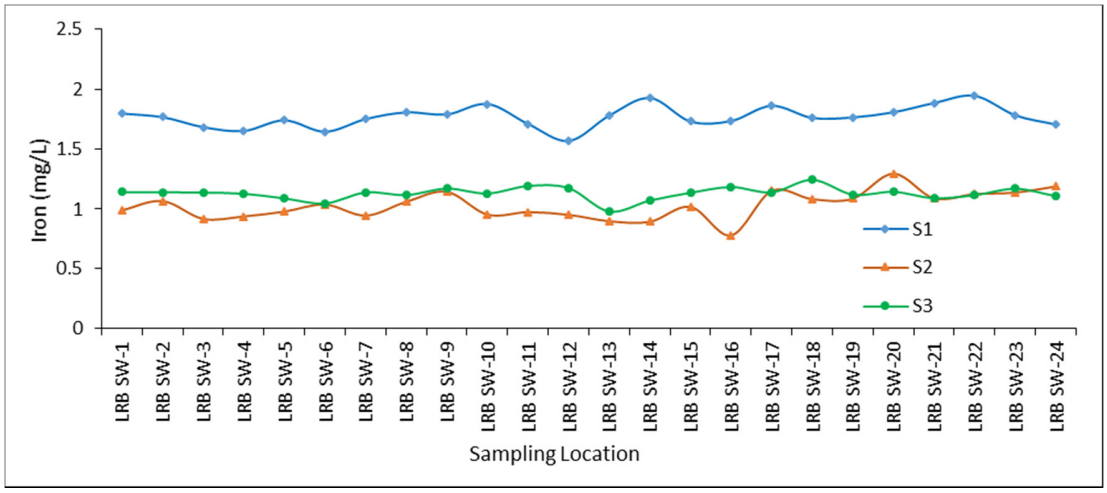

Figure 4.85: Spatial and temporal variation in Iron.

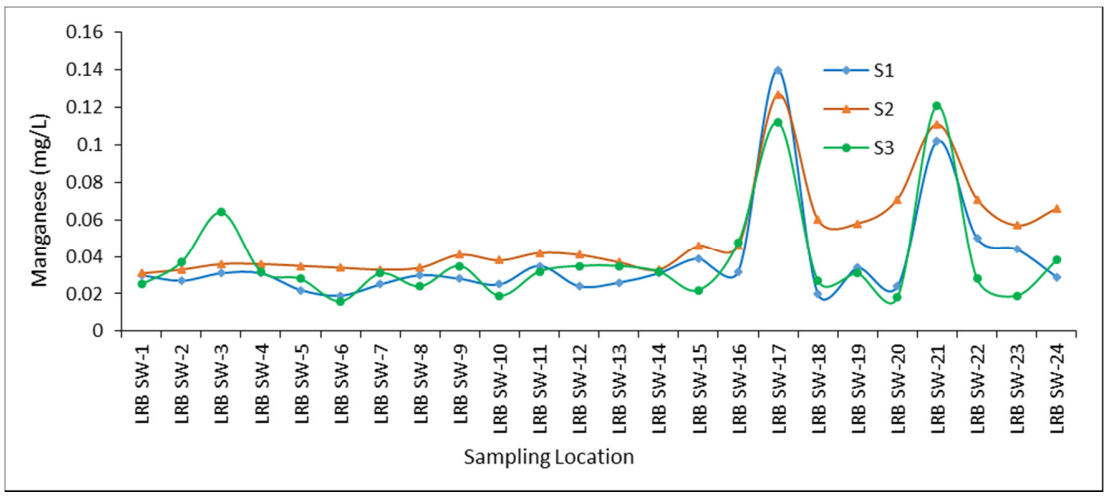

Figure 4.86: Spatial and temporal variation in Manganese.

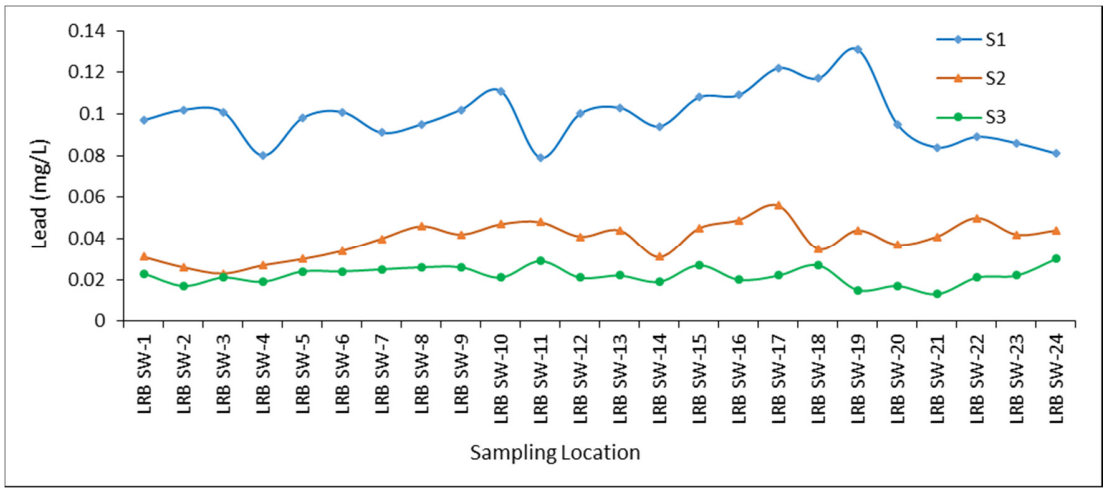

Figure 4.87: Spatial and temporal variation in Lead.

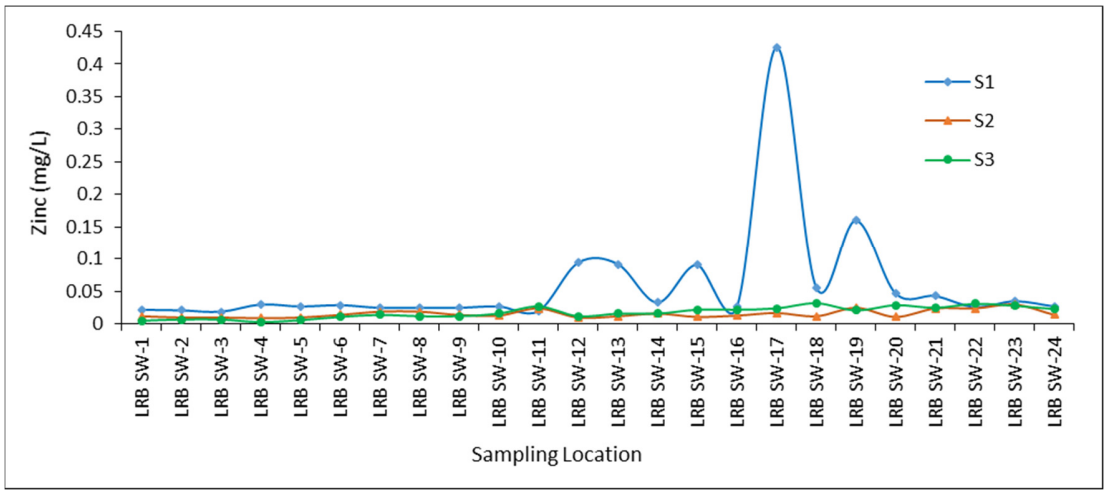

Figure 4.88: Spatial and temporal variation in Zinc.

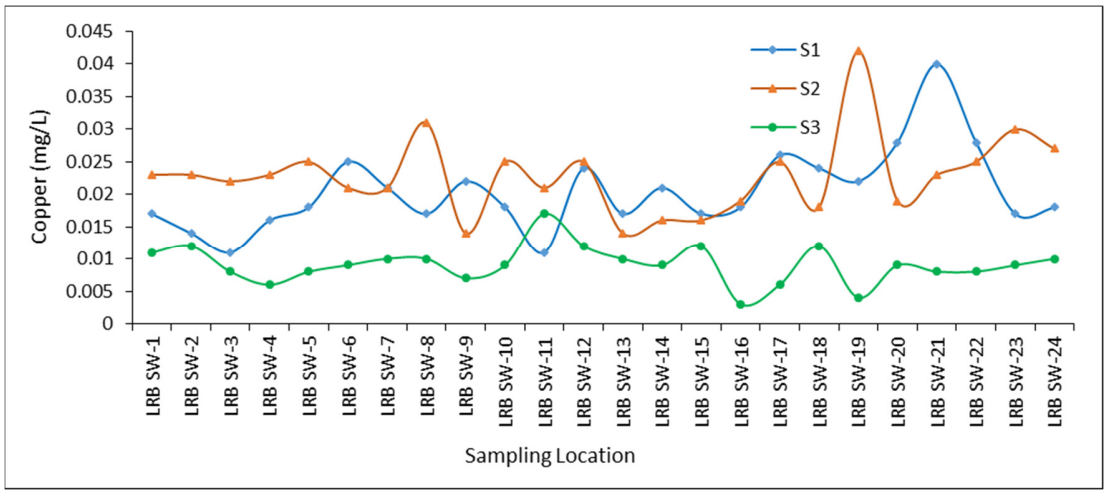

Figure 4.89: Spatial and temporal variation in Copper.

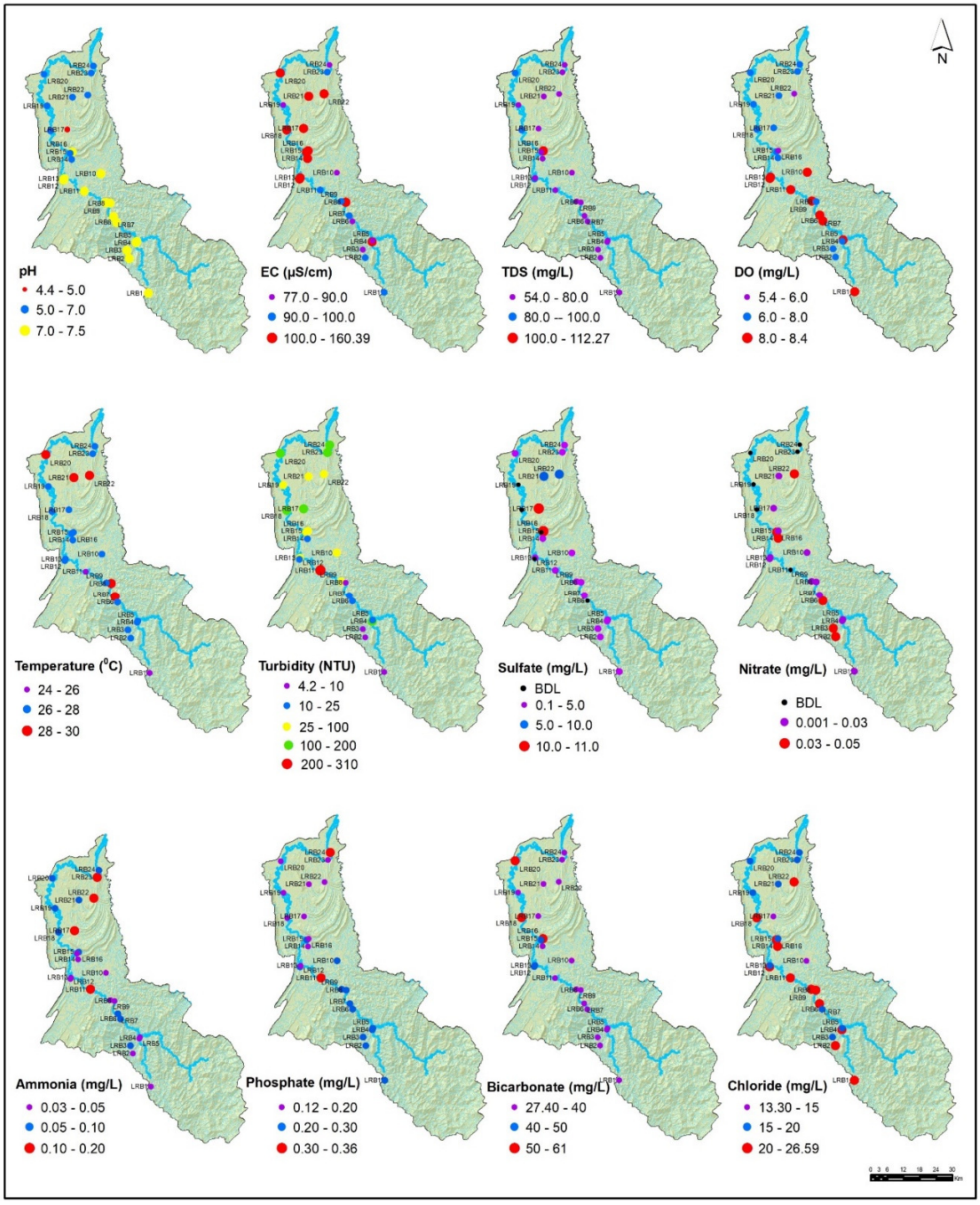

Figure 4.90: Spatial distribution of physico-chemical parameters of surface water collected during S1.

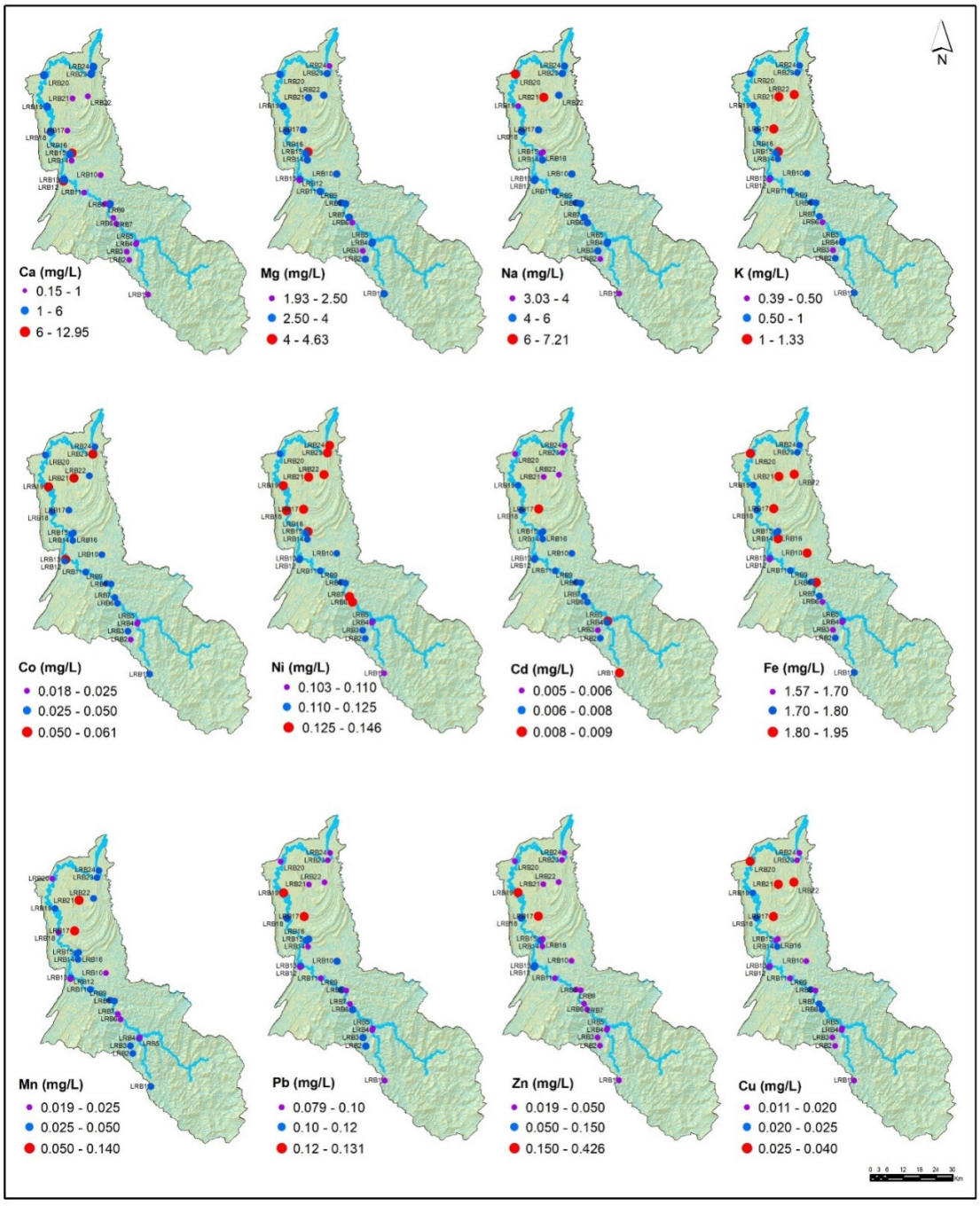

Figure 4.90: Spatial distribution of physico-chemical parameters of surface water collected during S1.

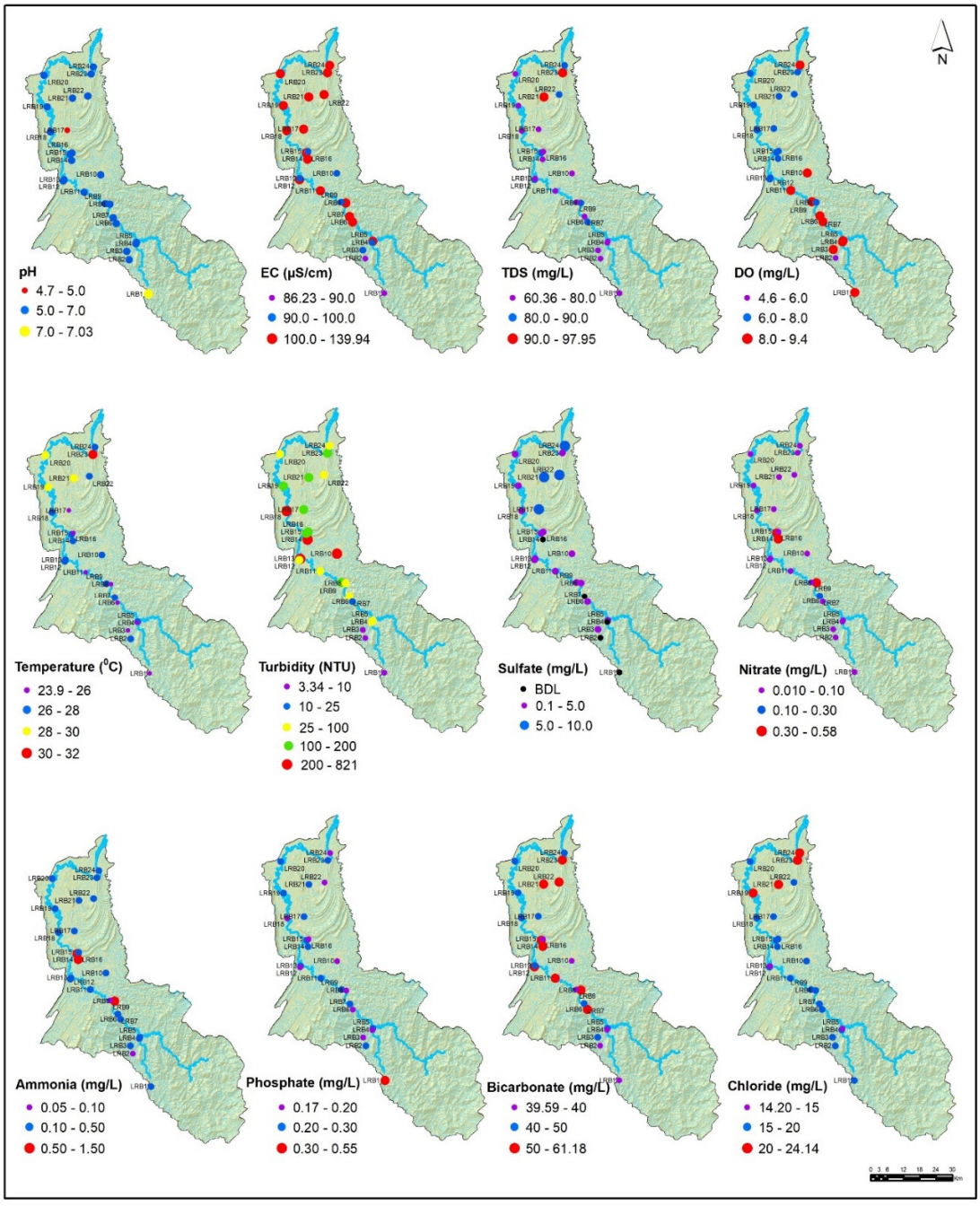

Figure 4.91: Spatial distribution of physico-chemical parameters of surface water collected during S2.

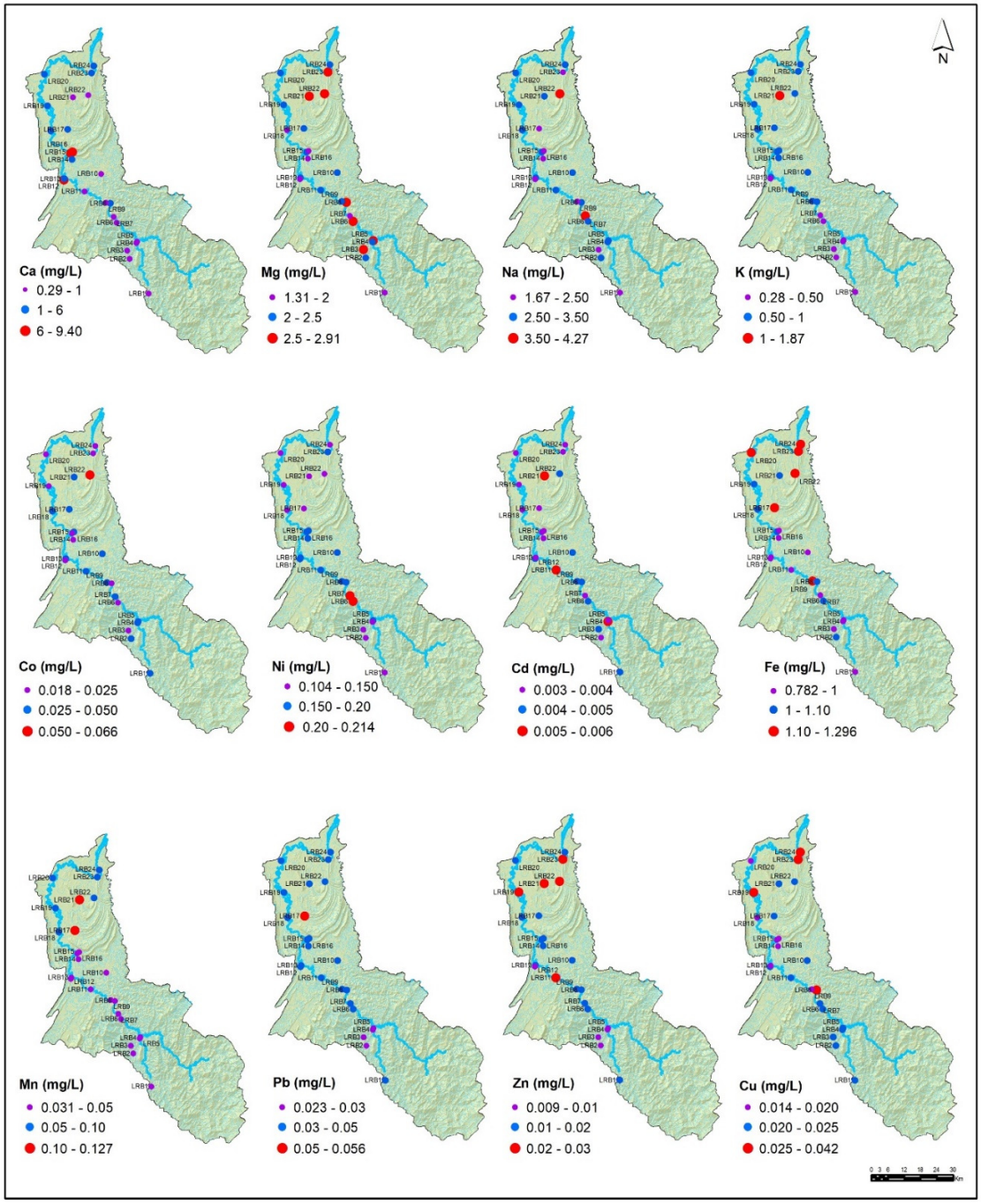

Figure 4.91: Spatial distribution of physico-chemical parameters of surface water collected during S2.

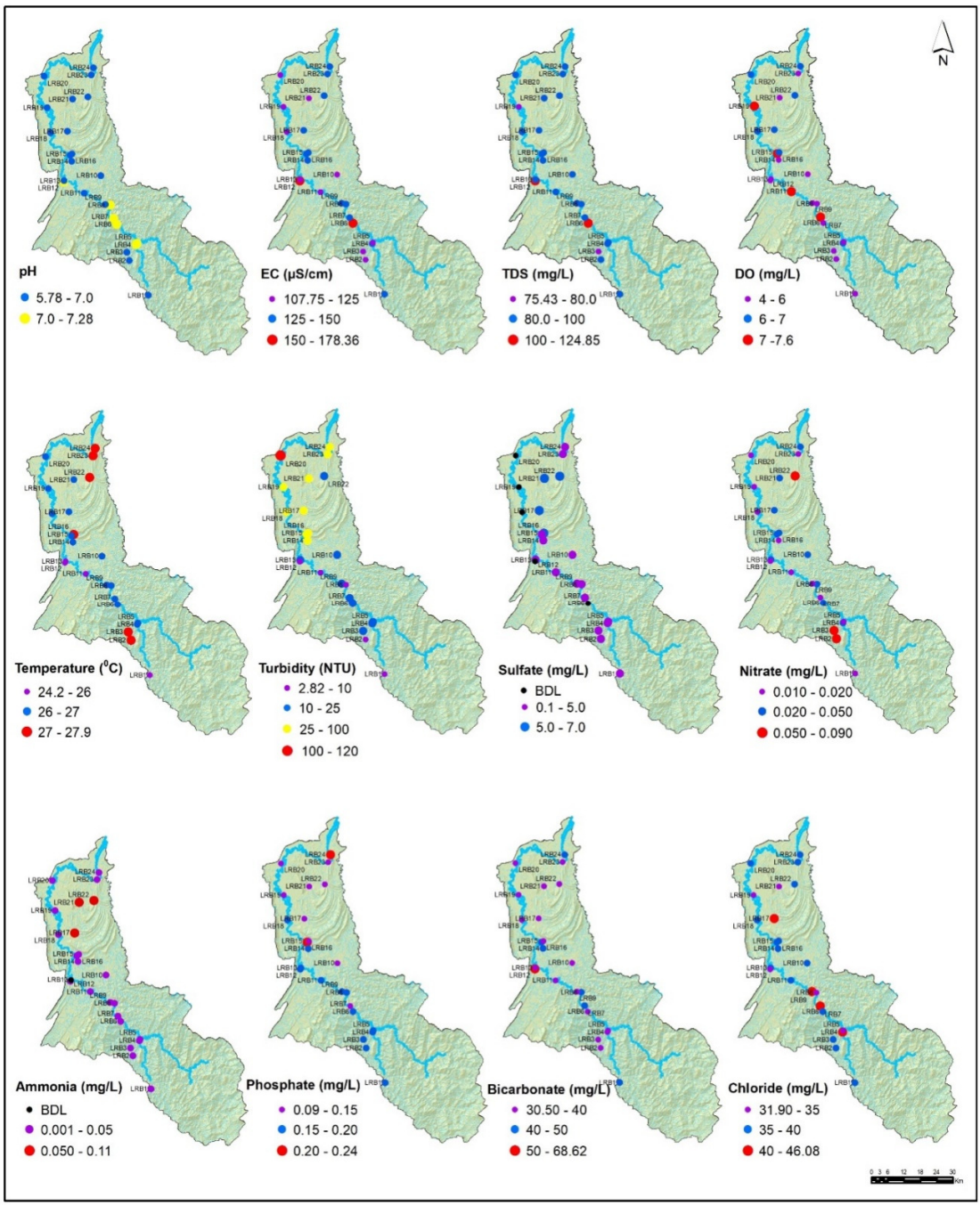

Figure 4.92: Spatial distribution of physico-chemical parameters of surface water collected during S3.

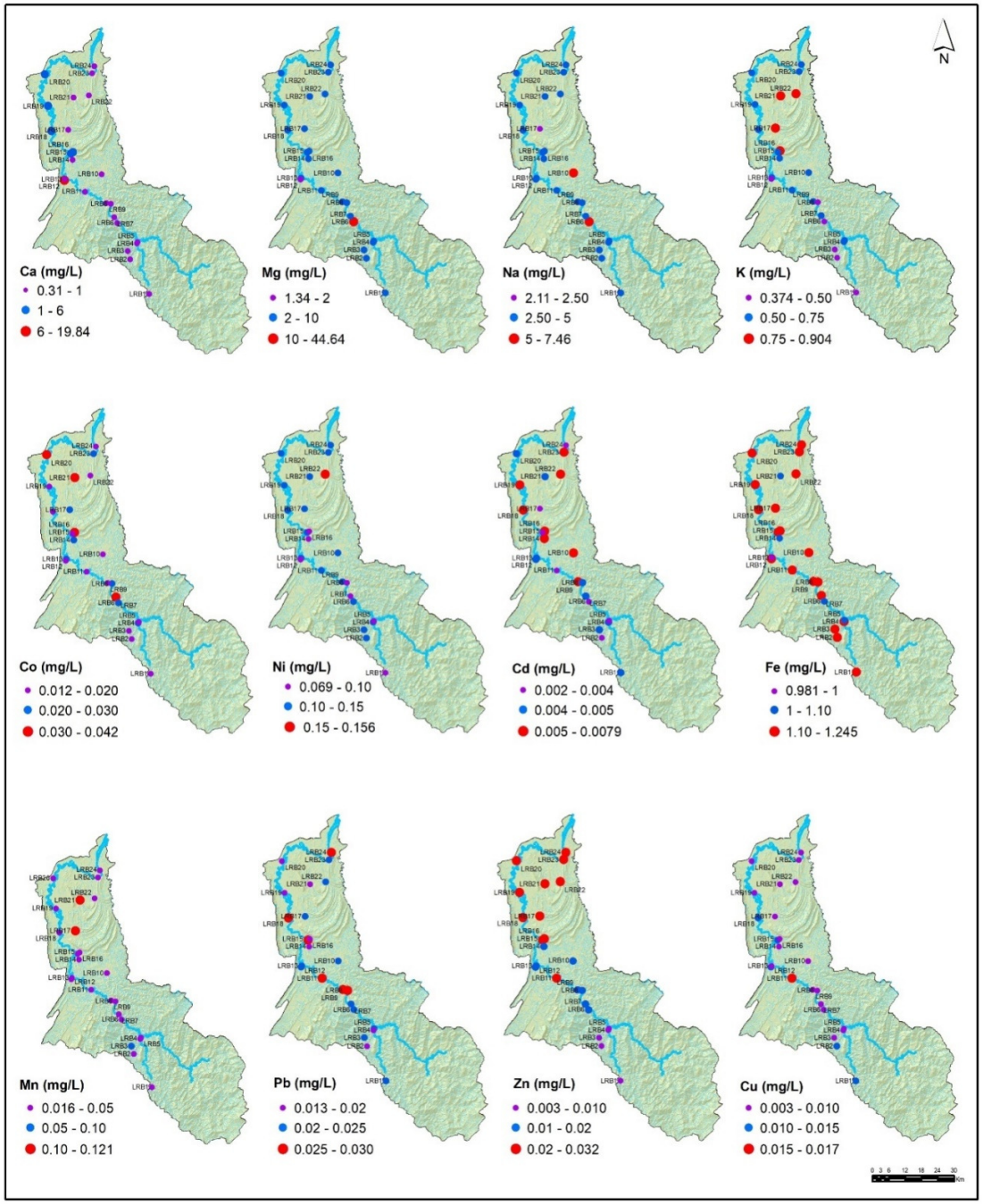

Figure 4.92: Spatial distribution of physico-chemical parameters of surface water collected during S3.

The pH level in surface water was controlled by the concentration of H^+ and OH^- ions, which determine the characteristics of other elements in the water (UNEP, 2006; Davie, 2008). Water samples collected during three sampling periods shows slightly acidic or neutral nature with pH value higher than 6.5. This can be attributed to the reaction of water (H_2O) with HCO_3^- that originates from the vast limestone deposit in the river basin, which produces comparatively higher OH^- ions that changes the quality of surface water in the region. However, it was also noted that surface water samples collected at location SW-17 in two sampling periods show acidic nature (pH≈4.4). These samples were collected from the low land tributary of the Limbang River, which originates and flows through lower peat swamps of reducing environment. Surface water samples collected from all sampling periods shows comparatively higher pH levels and indicates a higher amount of dissolved ion concentrations, ionic strength, and temperature of measurements (Hem, 1985). This indicates a higher rate of mineral dissolution in the region which depends on the rainfall input and lithology.

Electrical Conductivity (EC) and concentration of Total Dissolved Solids (TDS) are depend each other i.e. if the concentration of soluble salts (total dissolved salts) in surface water is high it show higher EC (Purandara et al., 2003; Harila et al., 2004; Gupta et al., 2008; Ravikumar et al., 2013). Dissolved salts in the water are contributed by natural processes of weathering, erosion, leaching and dissolution along with input from anthropogenic sources (Chigor et al., 2012; Misaghi, et al., 2017). Dominant dissolved solids present in the water are major ions, nutrients, trace metals and organic matter (Ameli & Creed, 2017; Majeed et al., 2018; Mao et al., 2019). Though EC and TDS showed comparatively higher values in all the sampling periods, the highest value was noted in S3 than other two sampling periods. The higher values of EC and TDS in the surface water samples can be linked with the increased rate of erosion and sediment load in the water.

Dissolved Oxygen (DO) concentration indicates an overall quality of water with respect to aquatic life. The addition of different pollutants and sediment through anthropogenic and natural processes might affect the DO level (Rajkumar et al., 2009). Moreover, the oxygen in water might be trapped through impact of rainfall (splash) and also when it flows through rapids or water falls (Hall Jr. et al., 2012). In the LRB, surface water samples collected from sampling locations in the upper river basin during S1 and S2 show comparatively higher DO

(>7mg/L) than those collected at lower part of the river and S3. The variation in DO levels between the upper and lower reach of the basin can be attributed to the water level in the river and flow mechanism (presence of rapids, small falls and exposure of bed rocks and huge boulders) and water temperature. The amount of DO decreases with the increase of water temperature and comparatively colder water possess higher DO (Peirce et al., 2003; Said et al., 2004; Gandaseca et al., 2014). The lower catchment region of the Limbang River is flat and shows a higher water temperature whereas the upper catchment regions are cooler and shows high undulations in the river channel. However, the lower DO values in the upper river basin sampling locations during S3 might be due to the higher water levels in response to higher rainfall in the region during the sampling period.

The temperature of surface water depends on the time of measurements and exposure of the surface to direct sunlight. During the sampling, higher variations in temperature was observed in S2 than S1 and S3. In fact, the samples collected from higher elevation locations (upper river basin) show comparatively lower temperatures than those collected from downstream locations. This was due to the variation in sample collection time and overall temperature in the region. The turbidity of the water is the measure of its clarity, indicating the level of suspended materials present in the water (Mays, 1996). Higher level of turbidity results the increase in water temperature and reduction of the amount of dissolved oxygen in it (Paaijmans et al., 2008). Turbidity of the surface water samples collected from various locations and seasons in the LRB shows highly varying characteristics with poor and clear water in a few locations in the upper river basin and highly turbid water in middle and lower reach. Turbidity in the surface water samples collected from the LRB was due to the severe terrain alteration in relation to the intense logging process in the region. During heavy erosive rainfall events, most of the loose and altered material flows downstream and contributes to the higher concentration of suspended material and higher turbidity.

The concentration of nutrients in the surface water samples shows comparatively low concentration, which indicates less or no contribution from anthropogenic sources. It was also observed that sulfate in surface water samples show comparatively lower concentrations (<11mg/L) in all the samples and sampling periods indicate purely natural (geologic) contributions. The natural sulfate in the region were formed by the sedimentary rock

formations through oxidation of iron sulphides and dissolution of limestone present in the river basin (Rice & Bricker, 1995; Peters et al., 2006). Variations in the concentration between the sampling locations may be due to the variation in the terrain conditions and input from tributaries. Ammoniacal nitrogen indicates the presence of nitrogen in the form of ammonia. Findings reveal that the surface water samples of all the three sampling period show comparatively lower concentrations of Ammona suggesting its natural origin than the anthropogenic contribution. Being in a pristine environment in terms of agricultural activity with higher fertilizer use, the concentration of ammonia in the surface water samples might be of hydrolysis of organic nitrogen i.e. decomposition of microorganisms and the aerobic decomposition of organic nitrogenous matter (Marzluf, 1997; Geisseler et al., 2010). Phosphate concentration in fresh (non-polluted) water is comparatively low and may occur either due to natural as well as anthropogenic processes. Thermodynamically stable forms of phosphate is orthophosphate; and water samples collected from different locations in the LRB during different sampling periods show comparatively lower concentration (<0.23mg/L) of phosphate. In the LRB, the anthropogenic activity (agricultural) is lesser and the phosphate concentration in surface water might be due to the atmospheric deposition, natural decomposition of rocks and minerals, weathering of soluble inorganic materials, decaying biomass, runoff, sedimentation and forest fires (Manahan, 1993; Mueller et al., 1995; Fadiran et al., 2008).

Major ion (HCO_3^-, Cl^-, Ca^{2+}, Mg^{2+}, Na^+ and K^+) concentration in surface water samples collected at different sampling locations shown seasonal variation. The HCO_3^- in surface water samples collected during S2 shows higher concentration than S1 and S3. While comparing with other major ions, HCO_3^- shows higher concentration. HCO_3^-, in the river water might be contributed by the dissolution of sedimentary rocks rich in biogenic marine material and carbonate present in the river basin (Wedepohl, 1995). Also, the formation of carbonic acid (H_2CO_3), through hydration of dissolved CO_2 and its dissociation, also produces HCO_3^- (Langmuir, 1997; England et al., 2011). Surface water samples collected from different locations in the LRB at different sampling periods show comparatively higher concentration of Cl^- compared to other ions except HCO_3^-. Among the sampling periods, S3 shows higher concentration of Cl^- than S1 and S2. Cl^- concentration in the surface water samples was derived from natural sources such as water interaction with calcareous rocks, leaching and minor atmospheric contributions (Mullaney et al., 2009). Ca^{2+} in the surface water samples show

comparatively lower concentration than HCO_3^- and Cl^-, and also shows spatial as well as temporal variation in its concentration. As observed earlier, the source of Ca^{2+} in surface water samples is the interaction of water with calcareous rocks present in the catchment area and leaching and mixing through rainfall and runoff.

Mg^{2+}, Na^+ and K^+ also present in lower concentrations in surface water samples collected from various locations at the LRB. Among these major ions, Na^+ showed higher concentration than the other two. The concentration of Mg^{2+} in surface water samples shows variation between sampling periods, and S3 showed higher concentrations. Source contribution of Mg^{2+} in the Limbang River water is mineral dissolution of dolomite and soil rich in Mg^{2+} content (Blum et al., 1998). At the same time, the mean concentration of Na^+ was higher in S1 samples than S2 and S3 and it also shows variation between the sampling locations. A similar characteristics was observed in the case of K^+, showing comparatively lower concentrations in all the sampling periods. Surface water samples collected during S1, shows slightly higher concentration compared to other seasons. As observed, anthropogenic activity in the river basin is negligible and the contribution of Na^+ and K^+ can also be attributed to the natural process of mineral dissolution and leaching from organic matter (Bowser & Jones, 2002; Sun et al., 2014).

Trace metals such as Co, Ni, Cd, Fe, Mn, Pb, Zn and Cu, were also present in the surface water samples collected from different locations and sampling periods. The concentration of trace metals in surface water might influenced by anthropogenic processes such as industrial development, combustion of fossil fuel, pollution from motor vehicles, mining and forest fire and also from natural processes i.e. from the rock present in the river basin as product of weathering and leaching (Jeffries & Snyder, 1981; Demirak et al., 2006; Sabuti & Mohamed, 2016). It was also noted that, rainwater rich in trace metals also contributes to the surface water (Koulousaris et al., 2009). The highest mean concentration (0.038mg/L) of Co in surface water samples collected from the LRB was observed in S1 samples than S2 and S3. At the same time, Ni showed the mean highest concentration (0.159mg/L) in S2 samples than S1 and S3. Cd in surface water samples collected in three sampling period shows lower mean concentration than all other trace metals and the samples collected during S1 shows higher mean concentration of 0.007mg/L. It was observed that, among the trace metals analysed in the

present research, Fe show comparatively higher mean concentration in surface water samples collected during all the three sampling periods, and water samples of S1 showed the highest mean concentration of 1.77mg/L. The concentration of Mn in surface water samples collected during the sampling periods shown fluctuation in its concentration and water samples collected during S2 shows higher mean concentration of 0.051mg/L. Pb, Zn and Cu concentration in the surface water samples correspond to different sampling period also showed variation in its concentration. Pb and Mn are found to be higher in S1 water samples (0.099mg/L and 0.059mg/L respectively) whereas Cu shown higher mean concentration in S2 samples (0.023mg/L). In the LRB, the major source of trace metals in surface water is the process of weathering and erosion of sedimentary rocks present in the region along with atmospheric fallout due to forest burning and petro-chemical industries in the region.

Considering the mean concentration of major ions in surface water collected from different locations in the major river and its tributaries, the LRB shows variations in different sampling periods (Table 4.32). During the sampling periods S1 and S2, major ion concentrations in surface water samples are in the decreasing order of HCO_3^- > Cl^- > Na^+ > Mg^{2+} > Ca^{2+} > K^+ whereas in S3, major ions shown variation in its concentration and followed the decreasing order of HCO_3^- > Cl^- > Mg^{2+} > Na^+ > Ca^{2+} > K^+. At the same time, considering the mean concentration of trace metals in surface water samples, it also showed variations between the sampling periods. Trace metal concentrations in surface water collected during S1 shows the decreasing order of Fe > Ni > Pb > Zn > Co > Mn > Cu > Cd whereas in the sampling period S2, the mean concentration of trace metals follow the decreasing order of Fe > Ni > Mn > Pb > Co > Cu > Zn > Cd. However, considering the surface water samples collected during S3, the mean concentration of trace metal varies in the order of Fe > Ni > Mn > Co > Pb > Zn > Cu > Cd. Though the water sampling locations are similar in three sampling periods, the variation observed in the concentration of major ions and trace metals indicate a change in the source region in response to the seasonal rainfall characteristics of the LRB. In the river basin, the water chemistry is mainly dependent on the natural process of weathering, erosion and sedimentation which was controlled by the rainfall in the region. Though the samples were collected during the monsoon seasons (NEM and SWM), variations in rainfall amount, availability of eroded material and dissolution also contributed to the overall fluctuation in surface water chemistry of the LRB.

Table 4.32: Concentration (order) of major ions and trace metals in surface water samples.

Sampling period	Major ions	Trace metals
S1	$HCO_3^- > Cl^- > Na^+ > Mg^{2+} > Ca^{2+} > K^+$	Fe > Ni > Pb > Zn > Co > Mn > Cu > Cd
S2	$HCO_3^- > Cl^- > Na^+ > Mg^{2+} > Ca^{2+} > K^+$	Fe > Ni > Mn > Pb > Co > Cu > Zn > Cd
S3	$HCO_3^- > Cl^- > Mg^{2+} > Na^+ > Ca^{2+} > K^+$	Fe > Ni > Mn > Co > Pb > Zn > Cu > Cd

4.6.2 Water quality indices

Water quality indices were calculated for water samples collected during different sampling periods, and are given in Table 4.33. The interpretation is as follows:

a. Sodium percentage (Na%)

Understanding about the concentration of Na^+ in water is necessary for using it in irrigation purposes. The water was classified into five categories based on the Sodium percentage as: excellent (0-20), good (20-40), permissible (40-60), doubtful (60-80) and unsuitable (> 80) (Tijani, 1994; Khan & Abbasi, 2013). Considering the water samples collected in the present research, during the first sampling period (S1), Na% ranges from 15.18 to 53.08. Among 24 samples, one sample falls in the excellent category (SW-16), 6 samples belong to the good and 17 samples are in the permissible class. In S2 and S3, Na% ranges from 13.69 to 50.47 and 8.29 to 45.11 respectively. In S2 and S3, two samples (SW-12, SW-16 in S2 and SW-06, SW-12 in S3 respectively) belongs to the excellent category. At the same time, 16 samples in S2 and 17 samples in S3 falls in the good category and 6 samples in S2 and 5 samples in S3 in the permissible category.

b. Sodium absorption ratio (SAR)

The concentration of Na^+ reduces the soil permeability, soil structure and the SAR helps to measure the suitability of water for agricultural irrigation (Richards, 1954; Todd & Mays, 1980; Essington, 2015). Based on the SAR value, the water is classified into four classes such as excellent (0-10), good (10-18), doubtful (18-26) and unsuitable (>26). The SAR in S1 ranges from 0.21 to 0.81, in S2 from 0.15 to 0.60 and in S3 from 0.15 to 0.57. Results indicate that, all samples in the three sampling periods fall under the excellent category.

Table 4.33: Water quality indices calculated for surface water samples (S1, S2 and S3) collected from the LRB.

Category	Number of samples in sampling period		
	Fist season (S1)	Second Season (S2)	Third Season (S3)
Sodium Percentage (%)			
Excellent (0-20)	1	2	2
Good (20-40)	6	16	17
Permissible (40-60)	17	6	5
Doubtful (60-80)	0	0	0
Unsuitable (>80)	0	0	0
Sodium Absorption Ratio			
Excellent (0-10)	24	24	24
Good (10-18)	0	0	0
Doubtful (18-26)	0	0	0
Unsuitable (>26)	0	0	0
Residual Sodium Carbonate (meq/L)			
Safe (< 1.25)	24	24	24
Moderate (1.25 – 2.5)	0	0	0
Unsuitable (>2.5)	0	0	0
Corrosivity Ratio			
Suitable (<1)	15	24	1
Unsuitable (>1)	9	0	23
Kelley's ratio (KR)			
Suitable (<1)	7	19	18
Unsuitable (>1)	17	5	6
Permeability Index (%)			
Class I (excellent) (>75)	24	24	23
Class II (Good) (25 to 75)	0	0	1
Class III (Unsuitable) (<25)	0	0	0
Larson Ratio			
Strong Corrosion (>1)	7	0	17
Slight Corrosion (0.2 to 1)	17	24	7
No Corrosion (<0.2)	0	0	0
Magnesium Ratio			
Soft (0 – 60)	2	3	1
Moderate (60-120)	22	21	23
Hard (120 -180)	0	0	0
Very Hard (>180)	0	0	0
Chloro - Alkaline Indices			
Positive	24	24	24
Negative	0	0	0

c. Residual sodium carbonate (RSC)

The combination of alkaline earth metals such as Ca^{2+} and Mg^{2+}, with carbonates and bicarbonates will limit the favorable condition of water for agricultural use (Eaton, 1950; Raghunath, 1987). Based on RSC values, the water can be classified into safe (<1.25meq/L), moderate (1.25-2.5meq/L) and unsuitable (>2.5meq/L). In the LRB, RSC in S1 ranges from -0.027 to 0.601meq/L, 0.19 to 0.71meq/L in S2 and -3.16 to 0.48meq/L in S3. Based on RSC classification, all samples in three sampling periods comes under the safe (RSC < 1.25meq/L) category.

d. Permeability index (PI)

The Permeability index of the water explains the suitability of water for irrigation purposes and categorises the water into three classes such as Class I (>75%), Class II (25 to 75%) and Class III (<25%) (Doneen, 1964; Vasanthavigar et al., 2010). In S1, PI values ranges from 97.69 to 231.45 and all samples fall in the class I category. In S2, PI value in the range of 159.98 to 369.48 and all samples are in the class I category with excellent condition. At the same time in S3, PI values ranges from 26.45 to 256.42, except one sample (SW-06) in S3, all other samples fall in class I which indicates the excellent condition of the water samples.

e. Corrosivity ratio (CR)

The suitability of transportation of water through metallic pipes can be explained with the help of corrosivity ratio (Ryznar, 1944; Tahlawi et al., 2014). During S1 period, the CR value ranges from 0.49 to 1.40 and 15 samples are appropriate for transportation through metallic pipes and the remaining 9 samples are unsuitable. At the same time, in S2, the CR value ranges from 0.43 to 0.79 and all the samples are suitable for transportation through metallic pipes. But in S3, 23 samples are unsuitable and only one sample is suitable for the transportation through metallic pipes as the CR value ranges from 0.65 to 1.75.

f. Kelley's ratio (KR)

The suitability of water for irrigation purposes can be explained with the help of Kelley's ratio (KR) (Kelley, 1951; Kadyampakeni et al., 2018). KR classifies the water samples into two classes such as the value <1 suitable for irrigation and >1 unsuitable for irrigation purpose. In S1, the KR value ranges from 0.20 to 1.79; 0.17 to 1.63 in S2 and 0.12 to 1.39 in S3 respectively.

Among the samples 7 in S1, 19 in S2 and 18 in S3 are suitable for irrigation purposes and rest of the samples are unsuitable for irrigation purposes.

g. Larson ratio (LnR)

Potentiality towards corrosion of water were explained with the help of Larson ratio (LnR) (Larson & Skold, 1958; Larson, 1975; Stets et al., 2018). In S1, the LnR ranges from 0.38 to 1.33 in which 7 samples show strong potential towards corrosion and 17 samples shows slight potentiality towards corrosion. All samples in S2 show slight potential towards corrosion which shows LnR value in the ranges of 0.33 to 0.89. In S3, 17 samples shown strong potential towards corrosion and 7 samples have slightly potential towards corrosion with LnR in the range of 0.46 to 1.58

h. Magnesium ratio (MR)

Mg^{2+} concentration in water samples determines the hardness of the water which adversely affects the crop yield (Paliwal, 1972; Hem, 1985). The value of MR ranges from 23.21 to 97.45, 18.68 to 93.68 and 10.05 to 99.08 for S1, S2 and S3 respectively. Most of the samples in the three seasons i.e. 22 samples in S1, 21 samples in S2 and 23 samples in S3 fall under the moderate hardness category.

i. Chloro-alkaline indices (CAI)

The exchange of Na^+ and K^+ ions with Ca^{2+} and Mg^{2+} ions from the water samples to rock and vice versa, can be identified with the help of Chloro-alkaline Indices. Positive values of Chloro-alkaline Indices indicate an exchange of Na^+ and K^+ from the water to Ca^{2+} and Mg^{2+} of the rock whereas the negative value indicates exchange of Ca^{2+} and Mg^{2+} from the water to Na^+ and K^+ of the rock (Ishaku et al., 2011). Two types of Chloro-Alkaline Indices were proposed by Schoeller (1965, 1977) such as CAI-1 and CAI-2, to understand the ion exchange between the water and rock. In the present study, all the samples in three sampling periods shown positive indices. In the sampling period S1, the CAI-1 value ranges from 0.32 to 0.81 and CAI-2 from 0.15 to 1.20. CAI-1 and CAI-2 for S2, ranges from 0.56 to 0.82 and 0.31 to 0.64 respectively. Similarly, in S3, the CAI-1 range from 0.67 to 0.90 and CAI-2 from 0.69 to 1.76. All results indicate exchange of Na^+ and K^+ ions from the water to Ca^{2+} and Mg^{2+} from the rock.

4.6.3 Analysis of geochemical processes

4.6.3.1 Piper diagram

In order to determine and classify the major water types in the LRB, the Piper-Hill diagram was plotted for all seasonal samples (Hill, 1940; Piper, 1944). Spatial and temporal variation in the classification of ionic water type observed between the sampling periods indicate that most of the samples in S1 and S3 periods were classified as mixed Ca^{2+}-Mg^{2+}-Cl^{-} type water and samples in S2 is classified as Ca^{2+}-Mg^{2+}-HCO_3^{-} type. Different water types were observed in S1 samples (Figure 4.93). Among that, the majority of the samples were categorized as mixed Ca^{2+}-Mg^{2+}-Cl^{-} water type and a few samples were classified as Ca^{2+}-Mg^{2+}-HCO_3^{-} type. Very small number of samples show characteristics of mixed Na^{+}-K^{+}-HCO_3^{-} and Na^{+}-K^{+}-Cl^{-} water type. In the case of S2, a majority of the water samples were classified as Ca^{2+}-Mg^{2+}-HCO_3^{-} water type with very few samples showing mixed Ca^{2+}-Mg^{2+}-Cl^{-} type and mixed Na^{+}-K^{+}-HCO_3^{-} water type (Figure 4.94).

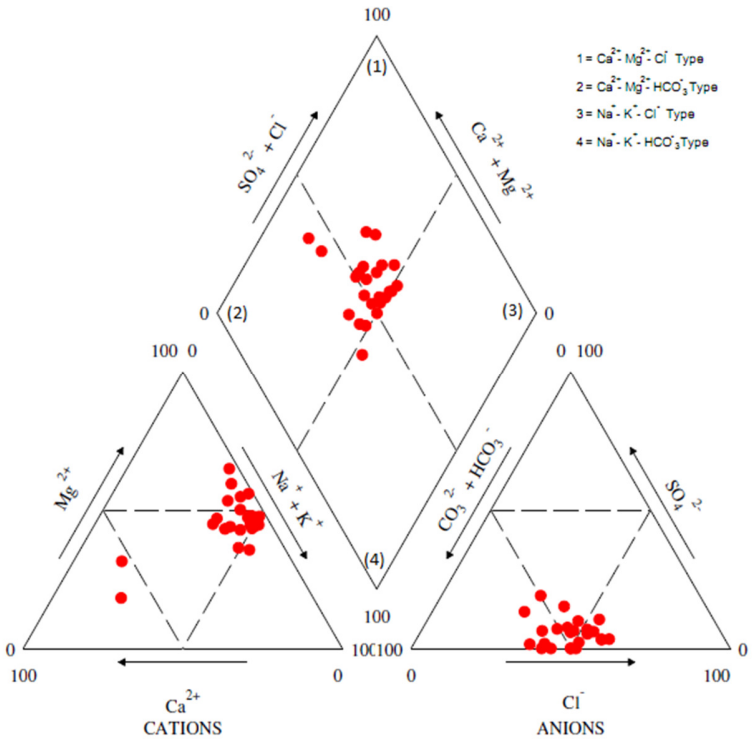

Figure 4.93: Piper Diagram for the sampling period S1.

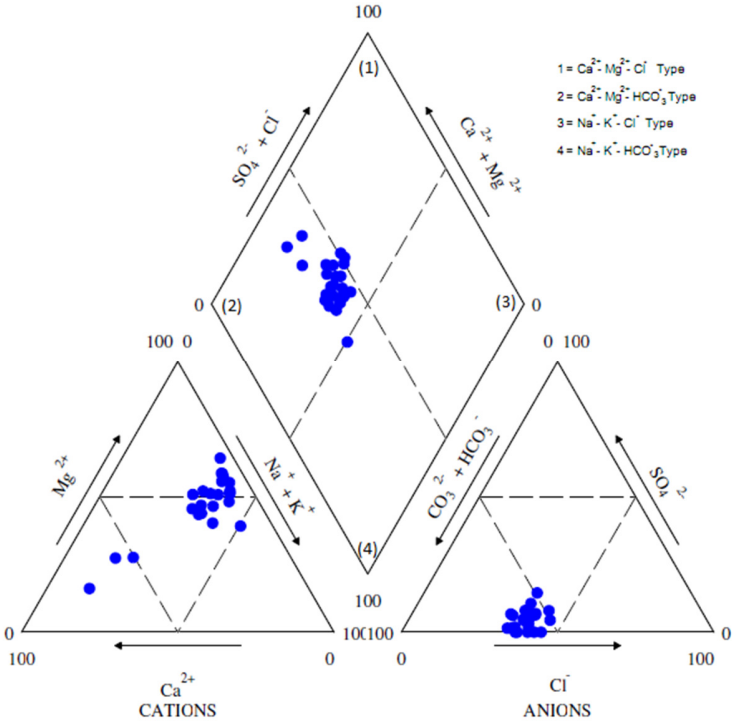

Figure 4.94: Piper Diagram for the sampling period S2.

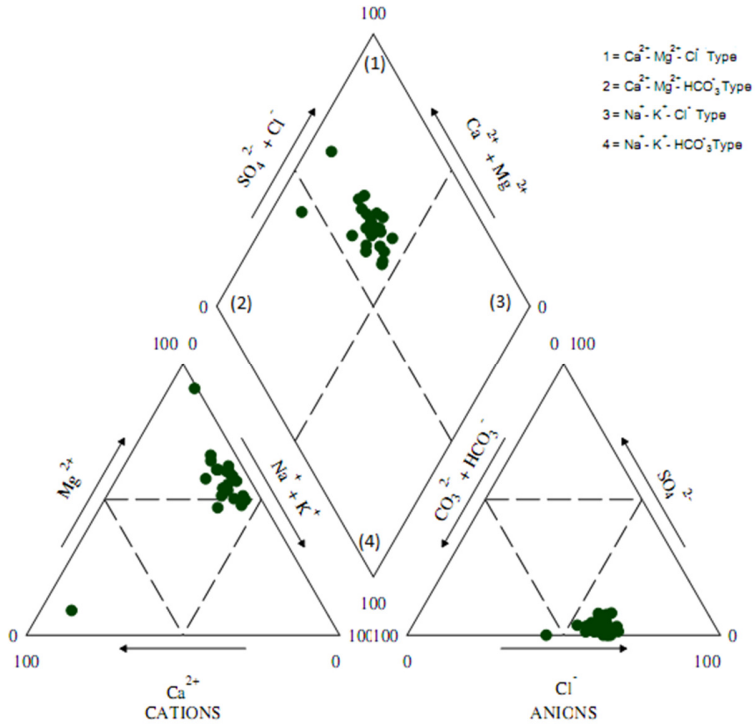

Figure 4.95: Piper Diagram for the sampling period S3.

At the same time, while considering the S3 samples, it shows an entirely different nature and most of the water samples were categorised as mixed Ca^{2+}-Mg^{2+}-Cl^{-} water type, except one which is classified as Ca^{2+}-Mg^{2+}-HCO_3^{-} water type (Figure 4.95).

Based on the above results, it was clear that water samples collected from the LRB were dominated by two major water types such as Ca^{2+}-Mg^{2+}-HCO_3^{-} type and mixed Ca^{2+}-Mg^{2+}-Cl^{-} type water. This points towards the occurrence of Ca^{2+} and Mg^{2+} rich rock types in the river basin and mineral dissolution, which produced HCO_3^{-} and Cl^{-} in the river water (Sultan, 2012). In general, the hydro-chemical characteristics of surface water in the LRB was controlled by the processes described below. The dominance of Ca^{2+} and Mg^{2+} ions in the surface water were observed, which is an indication of exchange of ions from the water to rock due to the weathering, leaching and mineral dissolution process which were supported by the results of Chloro-alkaline indices. HCO_3^{-} and Cl^{-} are the dominant anions in the surface water samples. Rainwater, weathering of silicate minerals and rock and decomposition of vegetation are the main input of Cl^{-} in the surface water. The presence of limestone in the study may be the reason for comparatively higher concentrations of HCO_3^{-} in the surface water samples. In addition to that, the dissolution CO_2 in rainwater also contributed HCO_3^{-} to the surface water (Lima et al., 2017).

4.6.3.2 Gibbs plot

Dominant natural process which controls the chemistry of river water can be explained with the help of the Gibbs plot (Gibbs, 1970). According to Gibbs plot, the river water is divided into atmospheric precipitation dominance, rock weathering dominance and evaporation and fractional crystallization dominant types. In Gibbs plot, TDS were plotted against the ratio of (Na+K)/(Na+K+Ca) and Cl/(Cl+HCO_3). In the present research, surface water samples collected during different sampling periods were used to generate the Gibbs plot. It was observed that, most of the samples in three sampling periods fell in the precipitation dominant class. In the sampling period S1, most of the water samples fall under the precipitation dominant category, and only one sample in the boundary of rock-water interaction dominant class (Figure 4.96).

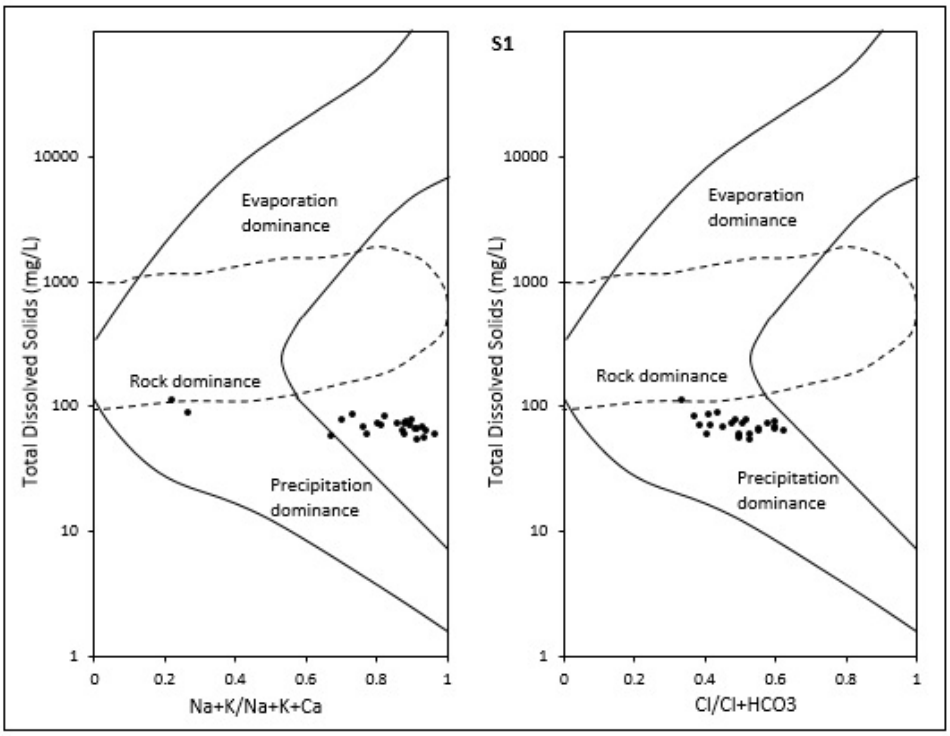

Figure 4.96: Gibbs plot for the sampling period S1.

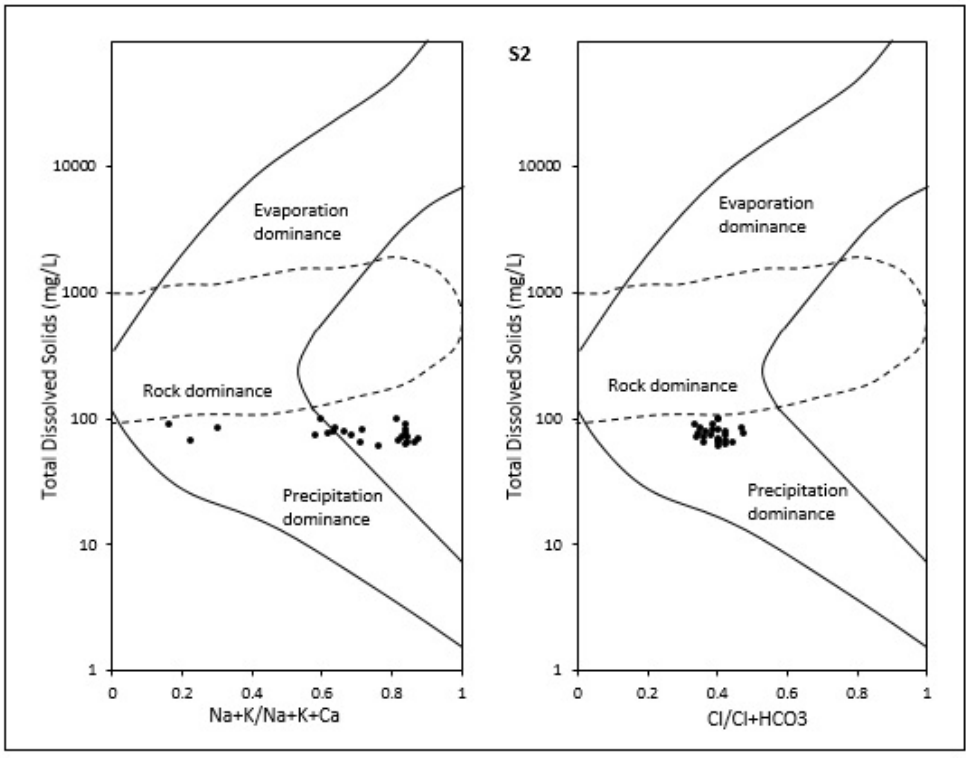

Figure 4.97: Gibbs plot for the sampling period S2.

In the case of sampling period S2, water samples showed a different nature than S1 samples i.e. all the samples fall in the category of precipitation dominant (Figure 4.97). However, while considering the S3 samples, most of the samples showed precipitation dominant characteristics with one sample in the rock-water interaction domain boundary (Figure 4.98). From the Gibbs plot, it can be concluded that the concentration of major ions in the water samples collected from different sampling locations during different sampling period was mainly influenced by precipitation. Heavy precipitation in the region has higher influence over the weathering and evaporation process.

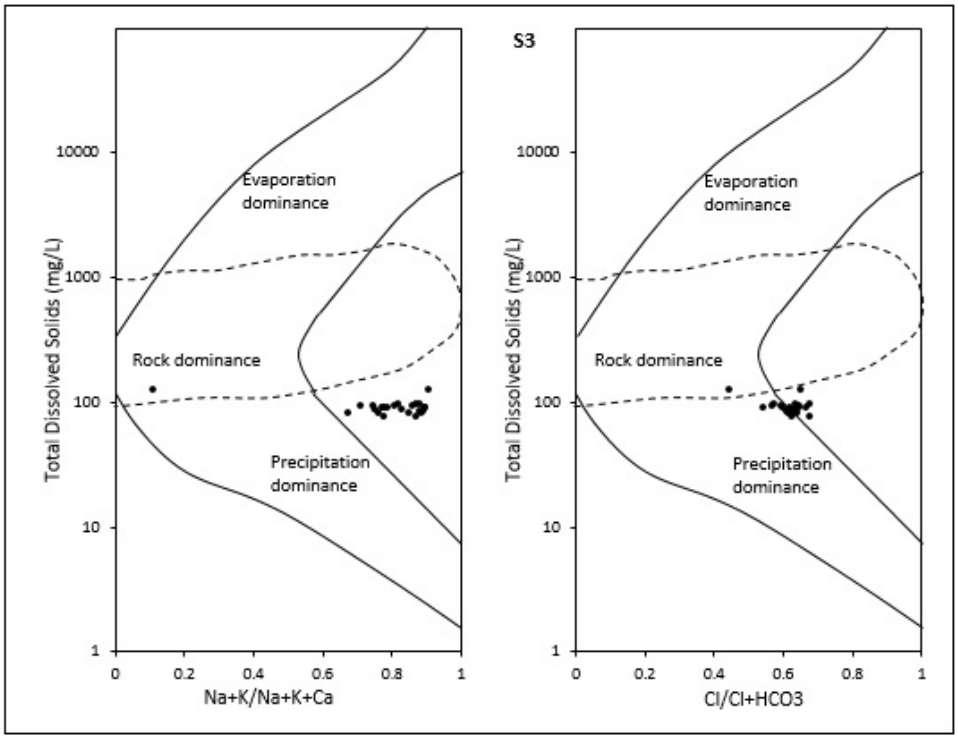

Figure 4.98: Gibbs plot for the sampling period S3.

4.6.3.3 Partial pressure of carbon dioxide (pCO_2)

The concentration of CO_2 in surface water depends on the dissolution of carbonate minerals, microbial oxidation of organic carbon and CO_2 from the plants through respiration, in addition to the atmospheric CO_2. Generally, the partial pressure of CO_2 (pCO_2) in surface water shows a non-equilibrium with the atmosphere due to the supply of high amount of CO_2 from groundwater and the relatively slow rate of re-equilibrium with the atmosphere caused by the

release of excess CO_2. Estimation of pCO_2 will help to gain a better understanding of the state of recharge and its relation to the geochemical process.

The Log pCO_2 for the surface water samples in all the three sampling periods were calculated to understand the recharge process. The Log pCO_2 value ranges from -2.94 to 0.19 with an average of -2.18 in S1, -2.42 to -0.11 with an average value of -1.91 in S2 and -2.63 to -1.23 with an average of -2.11 in S3. In all the three sampling periods, the samples collected from upstream are close to the atmospheric Log pCO_2 value (i.e. -3.5), which indicates recent recharge of water by the rainfall (Figure 4.99). Samples belonging to middle to downstream areas show considerably higher Log pCO_2 values, suggesting longer residence time of mixed water, in which the additional CO_2 has been acquired due to the interaction of water with the river sediments (Park et al., 1969; Jones Jr. et al., 2003; Chidambaram et al. 2011; Tao, 2017). Therefore, the increasing trend of Log pCO_2 values from upstream to downstream samples shows the direct recharge of rainwater with lower Log pCO_2 values in the upstream side and mixed water with higher Log pCO_2 in the downstream side.

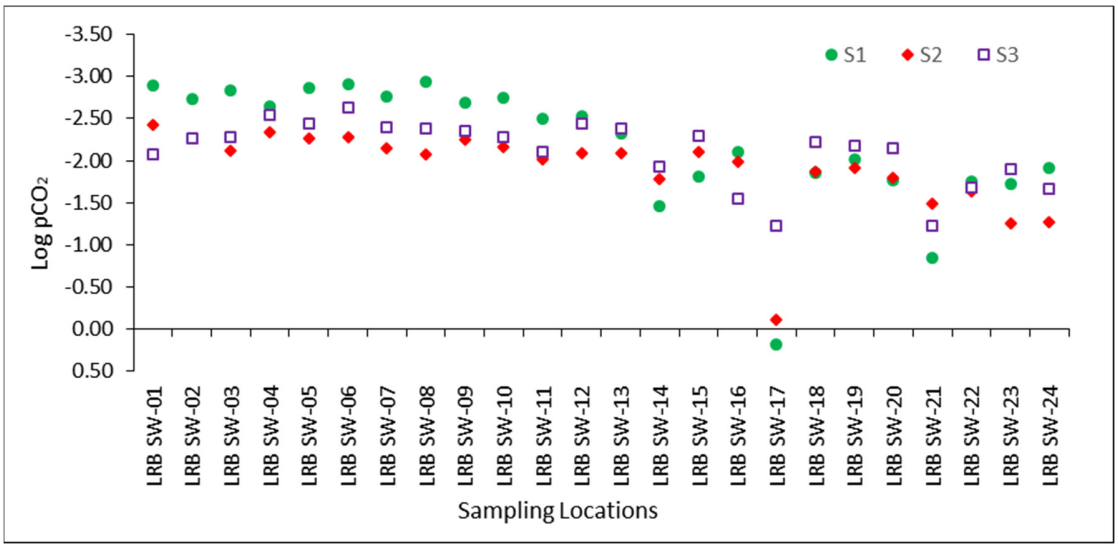

Figure 4.99: Spatial and temporal distribution of the Log pCO_2 values in the LRB.

4.6.3.4 Saturation index of carbonate minerals

The primary source of CO_2^{2-} dissolved in natural water is from the earth atmosphere. When CO_2^{2-} gas is in contact with water, it will dissolve until the equilibrium is reached. The

solubility of CO_2^{2-} gas in water contributes the neutral $H_2CO_3^-$ and the two anions HCO_3^- (bicarbonate) and CO_3^{2-} (carbonate). The neutral species $H_2CO_3^-$ and the two anions allow $CaCO_3$ to be dissolved and transported under certain conditions, redepositing at the same point as $CaCO_3$ again. Change in the pH of water results in the precipitation of $CaCO_3$. As dissolution of Carbonate minerals takes place, there is an increase in pH and HCO_3^-. The water generally becomes charged with CO_2^{2-} due to the contact with atmosphere or soil zone or when it comes in contact with Carbonate minerals in a zone isolated from gaseous CO_2^{2-}. In a closed system dissolution process, Carbonic acid is consumed and not replenished from outside the system as dissolution proceeds. Hence the pCO_2 declines as the reaction proceeds towards equilibrium (Wigley & Plummer, 1976; Raymahashay, 1996; Al et al., 2000; Sand et al., 2016). So, Carbonate minerals are lesser soluble under closed system and have higher equilibrium pH values.

The disequilibrium indices i.e. saturation index (SI) of Carbonate minerals like Aragonite, Calcite, Dolomite and Magnesite were represented from the data bank of WATEQ4F and was used to study the dissociation factors in the surface water samples collected from the LRB. The SI value of Magnesite ranges from -5.03 to -1.74 with an average of -2.70, Dolomite ranges from -10.52 to -3.59 with an average of -5.69, Calcite ranges from -5.54 to -1.36 with an average of -3.03 and Aragonite varies in the range of -5.68 to -1.50 with average of -3.18 during S1. In S2, the SI value of Magnesite ranges from -4.81 to -2.37 with an average of -2.90, Dolomite varies from -9.65 to -4.41 with an average of -5.84, Calcite ranges from -4.88 to -1.69 with average value of -2.99 and Aragonite ranges from -5.02 to -1.84 with an average of -3.13. In S3, the SI value of Magnesite varies from -3.59 to -1.27 with an average of -2.67, Dolomite varies from -7.61 to -3.23 with an average of -5.71, Calcite ranges from -4.07 to -0.94 with an average of -3.08 and Aragonite varies from -4.21 to -1.08 with an average of -3.22. Figure 4.100 shows the saturation index of carbonate minerals in the surface water for all the three seasons. The SI values show variation in the four Carbonate minerals considered and the saturation state of Carbonate minerals is in the following order of: $SI_{Magnesite} > SI_{Calcite} > SI_{Aragonite} > SI_{Dolomite}$. Overall, the surface water samples are in the under-saturated state for all the carbonate minerals, indicating the effect of dilution through monsoon rainfall.

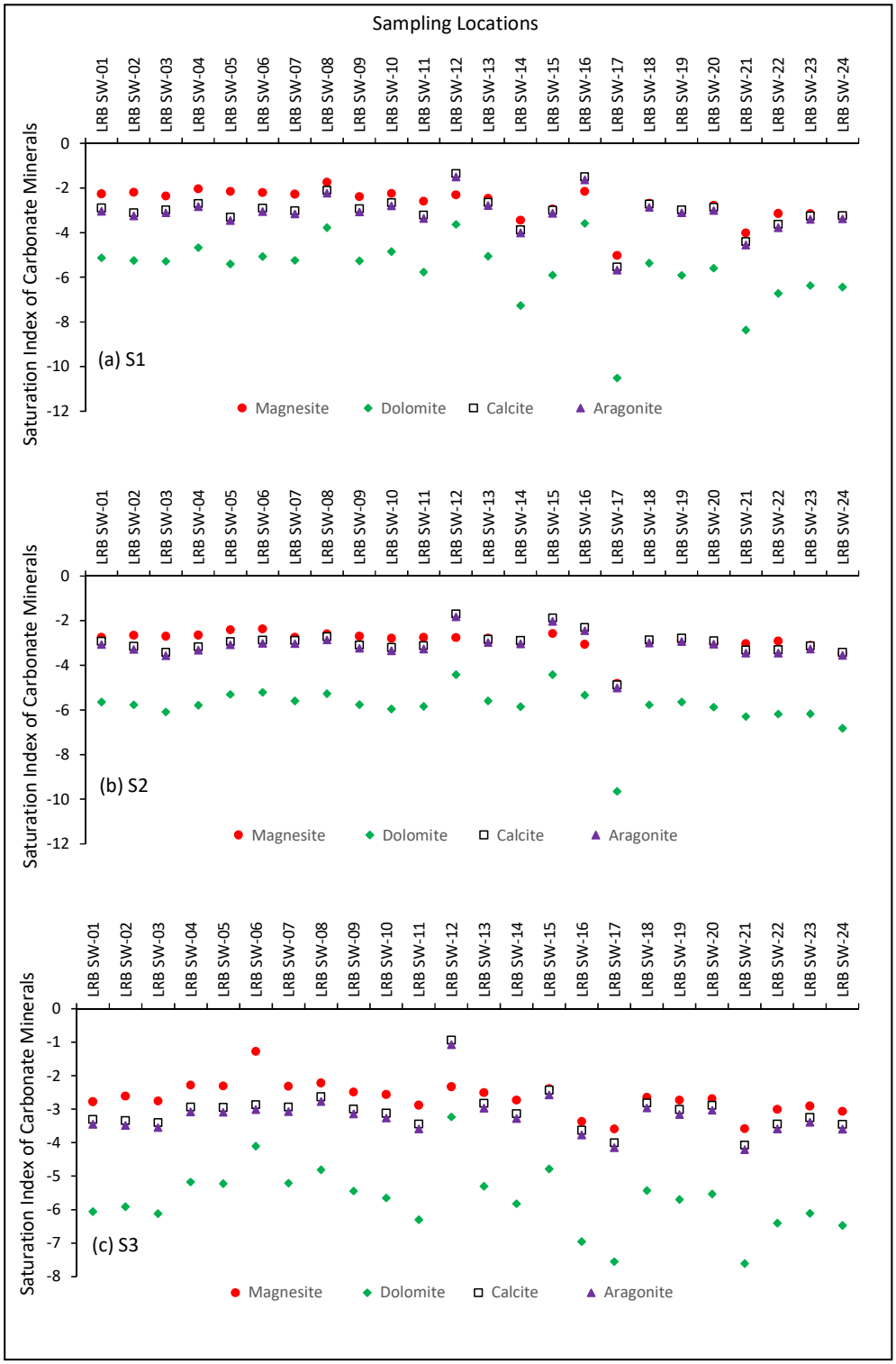

Figure 4.100: Spatial and temporal distribution of the saturation index (SI) of carbonate minerals in the LRB.

4.6.3.5 Relationship between surface water and rainwater chemical characteristics

Before proceeding to the statistical analysis to determine the major processes governing the geochemistry of surface water in the LRB, a spider plot (ratio plot) of chemical characteristics of surface water against rainwater was carried out. If the ratio of chemical constituents in surface water and rainwater shows unity, then there are no additional processes influencing the chemistry of surface water, and rainfall is the sole source contributing chemical constituent to the surface water (Van Wyk et al., 1992; Soderberg, 2003). In other cases, if the ratio is above or below unity, it indicates the possibility of an additional process which controls the geochemistry of surface water. Ratio above unity indicates the enrichment of chemical constituents caused due to oxidation, dissolution and leaching processes, whereas the ratio below unity indicates reduction or removal of chemical constituents supplied by rainwater through the process of adsorption (Van Wyk et al., 1992; Soderberg, 2003). Considering the surface water and rainwater chemistry of the LRB, both shows dominance of similar major ions and trace metal concentration.

Spider plot of chemical characteristics of surface water and rainwater samples was generated season wise to determine the temporal variation in processes controlling the geochemistry of surface water. In S1, pH, EC, TDS, DO, Cl^-, Ni and Mn in most locations show a ratio near unity suggesting rainfall as the major source controlling the geochemistry of surface water (Figure 4.101a). Turbidity, HCO_3^-, Na^+, K^+, Mg^{2+}, Co, Cd, Fe, Mn, Pb, Zn and Cu in most locations show ratio above unity which indicates the enrichment of these parameters to surface water due to oxidation, dissolution and leaching. Few parameters such as Cl^-, Ca^{2+}, Co, Ni and Mn shows ratio below unity in most locations that indicates removal of these elements due to adsorption process controlled by the colloidal particles. It is also noted that, few parameters like Ca^{2+} and Mn shows, high variation than unity (fluctuates above and below) suggesting combined influence of all the processes described above.

In S2, pH, EC, TDS, DO, Co, Ni, Cd and Fe in most locations show a ratio near unity suggesting rainfall is the major source controlling the geochemistry of surface water (Figure 4.101b). Turbidity, HCO_3^-, Mg^{2+}, Na^+, K^+, Co, Ni, Mn, Pb, Zn and Cu in most locations shows ratio above unity, which indicates the enrichment of these parameters as explained earlier in the case of S1 samples. Few parameters such as Cl^-, Ca^{2+}, K^+, Ni, Cd, Pb, Zn and Fe show ratio below

unity in most locations that indicates removal of these elements due to adsorption process. It is also noted that, a few parameters like Ca^{2+}, Co, Ni, Cd, Pb and Zn shows high variation than unity (fluctuates above and below) suggesting combined influence of all the processes in controlling the concentration of a particular element in surface water.

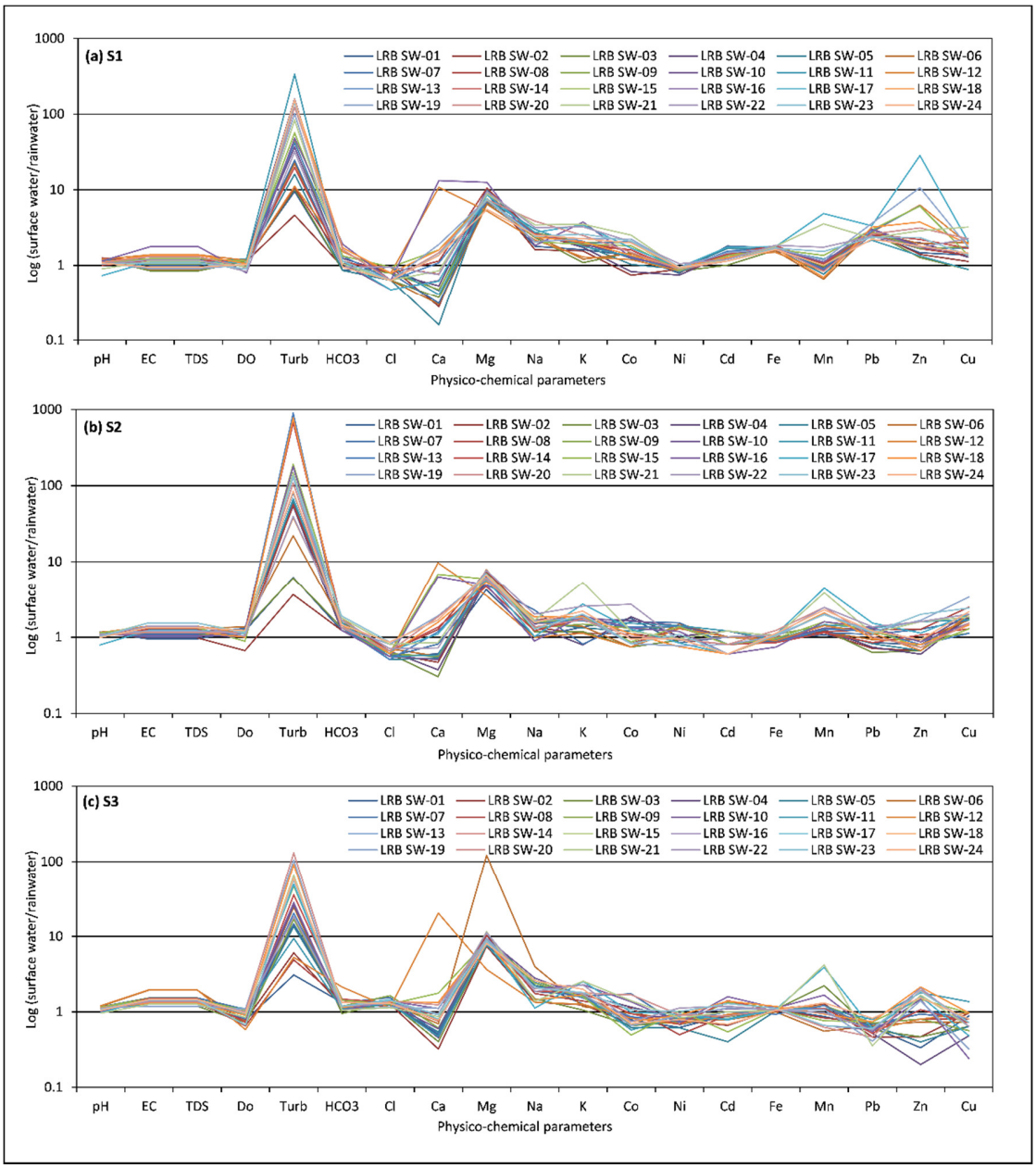

Figure 4.101: Spider plot (ratio plot) of chemical parameters of surface water normalized by rainwater.

Considering S3, pH, DO, Fe and Ni, most locations shows a ratio near unity suggesting the sole contribution of rainfall (Figure 4.101c). Turbidity, EC, TDS, HCO_3^-, Cl^-, Mg^{2+}, Na^+, K^+, Co, Ni, Cd, Mn and Zn in most locations show ratio above unity due to enrichment of these parameters to surface water through the processes of oxidation, dissolution and leaching. Few parameters such as Ca^{2+}, Co, Ni, Cd, Mn, Pb, Zn and Cu shows ratio below unity in most locations, which indicates removal of these elements by adsorption. It is also noted that, few parameters like Ca^{2+}, Co, Ni, Cd, Mn and Zn shows high variation than unity (fluctuates above and below) suggesting combined influence of all the processes described above.

The results of the spider plots (ratio plots) indicates the different possible processes and mechanism which might have a control over the geochemistry of surface water. Therefore, findings deducted from ratio plot will aid the statistical analysis (Factor Analysis) to explain the plausible processes which control the geochemistry of surface water in the LRB.

4.6.4 Statistical analysis of surface water quality parameters

4.6.4.1 Analysis of variance (ANOVA)

Variation in concentration of different parameters between the sampling locations and sampling periods (seasons) were carried out through two-way analysis of variance (Two Way ANOVA) at 95% confidence level. The results revealed four notable relationships between the parameters considered (Table 4.34). This includes significant and non-significant relationships. In the first case, parameters such as temperature, K^+ and Mn showed variation between the sampling locations and sampling periods at 95% confidence level. In the second case, parameters such as EC, TDS, DO, turbidity, Nitrate, Ammonia, Phosphate, HCO_3^-, Cl^-, Na^+, Co, Ni, Cd, Fe, Pb, Zn and Cu shows significant variations only between the sampling periods and not among the sampling locations. pH, Sulfate and Ca^{2+} concentration shows significant variation between the sampling locations, pointing to the third case. Among the parameters, magnesium showed no significant variation between the sampling periods and sampling locations. From the statistical analysis of two-way ANOVA, it is clear that most of the parameters do not vary spatially but show significant temporal variations (vary during sampling periods).

Table 4.34: Two-way ANOVA of water quality parameters of the Limbang River.

Parameters	Category	% of total variation	SS	MS	F	P-value	Significance
pH	Between stations	81.63	17.59	0.76	9.77	0.00	Yes
	Between seasons	1.66	0.36	0.18	2.29	0.11	No
EC (µS/cm)	Between stations	28.81	8549.08	371.70	1.52	0.11	No
	Between seasons	33.36	9900.91	4950.46	20.28	0.00	Yes
TDS (mg/L)	Between stations	28.81	4189.05	182.13	1.52	0.11	No
	Between seasons	33.36	4851.45	2425.72	20.28	0.00	Yes
DO (mg/L)	Between stations	19.60	23.13	1.01	1.08	0.40	No
	Between seasons	44.14	52.09	26.04	28.00	0.00	Yes
Temperature (˚C)	Between stations	51.65	66.80	2.90	3.84	0.00	Yes
	Between seasons	21.46	27.76	13.88	18.35	0.00	Yes
Turbidity (NTU)	Between stations	29.41	557289.29	24229.97	1.08	0.40	No
	Between seasons	15.96	302309.49	151154.74	6.72	0.00	Yes
Sulfate (mg/L)	Between stations	73.08	401.78	17.47	5.73	0.00	Yes
	Between seasons	1.40	7.69	3.85	1.26	0.29	No
Nitrate (mg/L)	Between stations	31.81	0.18	0.01	1.16	0.33	No
	Between seasons	13.38	0.08	0.04	5.61	0.01	Yes
Ammonia (mg/L)	Between stations	23.42	0.70	0.03	0.93	0.56	No
	Between seasons	26.30	0.79	0.40	12.03	0.00	Yes
Phosphate (mg/L)	Between stations	35.80	0.12	0.01	1.68	0.07	No
	Between seasons	21.64	0.07	0.04	11.70	0.00	Yes
Bicarbonate (mg/L)	Between stations	33.94	1924.36	83.67	1.64	0.08	No
	Between seasons	24.63	1396.69	698.34	13.68	0.00	Yes
Chloride (mg/L)	Between stations	3.78	225.59	9.81	0.68	0.84	No
	Between seasons	85.07	5081.19	2540.59	175.43	0.00	Yes
Ca (mg/L)	Between stations	77.74	543.07	23.61	7.00	0.00	Yes
	Between seasons	0.06	0.44	0.22	0.06	0.94	No
Mg (mg/L)	Between stations	31.93	561.23	24.40	1.02	0.46	No
	Between seasons	5.35	93.96	46.98	1.96	0.15	No
Na (mg/L)	Between stations	21.13	23.03	1.00	1.22	0.27	No
	Between seasons	44.33	48.32	24.16	29.52	0.00	Yes
K (mg/L)	Between stations	72.19	3.25	0.14	7.06	0.00	Yes
	Between seasons	7.35	0.33	0.17	8.26	0.00	Yes
Co (mg/L)	Between stations	22.66	0.00	0.00	0.94	0.56	No
	Between seasons	28.93	0.00	0.00	13.75	0.00	Yes
Ni (mg/L)	Between stations	14.64	0.01	0.00	0.67	0.85	No
	Between seasons	41.81	0.03	0.01	22.08	0.00	Yes
Cd (mg/L)	Between stations	12.62	0.00	0.00	0.62	0.89	No

	Between seasons	46.78	0.00	0.00	26.50	0.00	Yes
Fe (mg/L)	Between stations	2.65	0.22	0.01	1.35	0.19	No
	Between seasons	93.43	7.74	3.87	548.19	0.00	Yes
Mn (mg/L)	Between stations	83.70	0.04	0.00	15.50	0.00	Yes
	Between seasons	5.50	0.00	0.00	11.71	0.00	Yes
Pb (mg/L)	Between stations	2.75	0.00	0.00	1.25	0.26	No
	Between seasons	92.82	0.08	0.04	482.72	0.00	Yes
Zn (mg/L)	Between stations	30.21	0.06	0.00	1.10	0.38	No
	Between seasons	14.85	0.03	0.01	6.22	0.00	Yes
Cu (mg/L)	Between stations	11.18	0.00	0.00	0.70	0.82	No
	Between seasons	57.04	0.00	0.00	41.28	0.00	Yes

4.6.4.2 Correlation analysis

Results of physico-chemical parameters of surface water samples collected from 24 different locations in the LRB during three sampling periods were statistically processed (independently) through Pearson's correlation analysis to determine the inter-relationship between the parameters. Analysis revealed significant positive and negative correlations (r≥0.50) between the parameters (Table 4.35). During all the sampling periods, EC and TDS show a strong positive correlation. In the first sampling period (S1), significant positive correlations (r≥0.50) were observed between EC and TDS (r=1), HCO_3^- with EC and TDS (r=0.89), K^+ with Sulfate (r=0.81), Ca^{2+} with TDS and EC (r=0.76), Zn with Mn (r=0.74), Ammonia with turbidity (r=0.73), Ca^{2+} with HCO_3^- (r=0.69), Mn with Sulfate (r=0.68) and K^+ (r=0.65), Mg^{2+} with Sulfate (r=0.64), Ni with K^+ (r=0.59), Zn with Pb (r=0.57), Fe with K^+ (r=0.56), Phosphate with pH (r=0.55) and DO (r=0.53), Cu with Na^+ and K^+ (r=0.54), Ammonia with Mn (r=0.53) and Mn with Cu (r=0.50). Similarly, significant negative correlations were observed between pH with Mn (r=-0.86), Zn (r=-0.70), K^+ (r=-0.71), Ammonia (r=-0.57), Cu (r=-0.56), Sulfate (r=-0.53), Co and Fe (r=-0.52), DO with K^+ (r=-0.79), Ni with DO (r=-0.66), Phosphate with Cu (r=-0.56), Nitrate with turbidity (r=-0.54), K^+ with Phosphate (r=-0.54) and DO with EC and TDS (r=-0.51).

During the second sampling period (S2), EC showed the highest positive correlation with TDS (r=1). Other strong positive correlations were observed are HCO_3^- with EC and TDS (r=0.91), Sulfate with Mn (r=0.84), Ammonia and Nitrate (r=0.80), K^+ with Mn (r=0.78) and Sulfate (r=0.73), Cl^- with EC and TDS (r=0.70), temperature with EC, TDS and Cl^- (r=0.64), Fe with

Table 4.35: Correlation analysis results (significant) of physico-chemical parameters of surface water sampled during S1, S2 and S3.

First Sampling Period (S1)						Second Sampling Period (S2)						Third Sampling Period (S3)					
Positive Correlation			Negative Correlation			Positive Correlation			Negative Correlation			Positive Correlation			Negative Correlation		
Parameters		r	Parameters		r	Parameters		r	Parameters		r	Parameters		r	Parameters		r
TDS	EC	1.00	pH	Mn	-0.86	TDS	EC	1.00	pH	Mn	-0.85	TDS	EC	1.00	pH	K	-0.86
HCO_3	EC	0.89	DO	K	-0.79	HCO_3	EC	0.91	pH	SO_4	-0.72	HCO_3	Ca	0.83	pH	SO_4	-0.76
HCO_3	TDS	0.89	pH	K	-0.71	HCO_3	TDS	0.91	pH	Pb	-0.53	SO_4	K	0.80	pH	Mn	-0.71
K	SO_4	0.81	pH	Zn	-0.70	SO_4	Mn	0.84	pH	K	-0.52	Ni	Zn	0.69	K	PO_4	-0.58
Ca	EC	0.76	Ni	DO	-0.66	NH_4	NO_3	0.80	Ni	Mn	-0.52	Na	Mg	0.67	pH	NH_4	-0.57
Ca	TDS	0.76	NH_4	pH	-0.57	K	Mn	0.78	Ca	Mg	-0.50	SO_4	NH_4	0.66	pH	Zn	-0.57
Zn	Mn	0.74	pH	Cu	-0.56	K	SO_4	0.73				Zn	K	0.65	PO_4	Co	-0.54
NH_4	Turbidity	0.73	PO_4	Cu	-0.56	Cl	EC	0.70				Zn	Turbidity	0.64	PO_4	Cd	-0.52
Ca	HCO_3	0.69	NO_3	Turbidity	-0.54	Cl	TDS	0.70				HCO_3	EC	0.62	Na	Mn	-0.51
Mn	SO_4	0.68	K	PO_4	-0.54	Temperature	EC	0.64				Ca	EC	0.61			
Mn	K	0.65	SO_4	pH	-0.53	Temperature	TDS	0.64				Ca	TDS	0.61			
Mg	SO_4	0.64	pH	Co	-0.52	Temperature	Cl	0.64				K	NH_4	0.61			
Ni	K	0.59	pH	Fe	-0.52	Fe	SO_4	0.61				K	Mn	0.58			
Zn	Pb	0.57	DO	EC	-0.51	Zn	EC	0.61				Mn	NH_4	0.57			
Fe	K	0.56	DO	TDS	-0.51	Zn	TDS	0.61				PO_4	Cu	0.56			
PO_4	pH	0.55				K	EC	0.60				Mg	EC	0.55			
Na	Cu	0.54				K	TDS	0.60				Mg	TDS	0.55			
K	Cu	0.54				Cl	Fe	0.58				SO_4	Mn	0.54			
PO_4	DO	0.53				Cl	Zn	0.58				PO_4	Pb	0.52			
NH_4	Mn	0.53				SO_4	EC	0.57				Temperature	NO_3	0.51			
Mn	Cu	0.50				SO_4	TDS	0.57				Temperature	SO_4	0.50			
						Mn	Fe	0.55				Cu	Pb	0.50			
						Cu	Cl	0.54									
						HCO_3	Zn	0.53									
						HCO_3	Temperature	0.53									
						SO_4	Cl	0.52									
						SO_4	Mg	0.52									
						K	Cl	0.50									

Sulfate (r=0.61), Zn with EC and TDS (r=0.61), K^+ with EC and TDS (r=0.60), Cl^- with Fe and Zn (r=0.58), Sulfate with EC and TDS (r=0.57), Mn with Fe (r=0.55), Cu with Cl^- (r=0.54), HCO_3^- with Zn and temperature (r=0.53), Sulfate with Cl^- and Mg^{2+} (r=0.52) and K^+ with Cl^- (r=0.50). Significant negative correlations were observed among pH with Mn (r=-0.85), Sulfate (r=-0.72), Pb (r= -0.53) and K^+ (r=-0.52), Ni with Mn (r=-0.52) and Ca^{2+} with Mg^{2+} (r=-0.50).

In the third sampling period (S3), strong positive correlations between parameters shown by EC with TDS (r=1), HCO_3^- with Ca^{2+} (r=0.83), Sulfate with K^+ (r=0.80), Ni with Zn (r=0.69), Na^+ with Mg^{2+} (r=0.67), Sulfate with Ammonia (r=0.66) and Mn (r=0.54), Zn with K^+ (r=0.65) and Turbidity (r=0.64), HCO_3^- with EC (r=0.62), Ca^{2+} with EC and TDS (r=0.61), K^+ with Ammonia (r=0.61) and Mn (r=0.58), Mn with Ammonia (r=0.57), Phosphate with Cu (r=0.56), Mg^{2+} with EC and TDS (r=0.55), Phosphate with Pb (r=0.52), temperature with Nitrate (r=0.51) and Sulfate (r=0.50) and Cu with Pb (r=0.50). Significant negative correlations were observed among pH with K^+ (r=-0.86), Sulfate (r=-0.76), Ammonia and Zn (r=-0.57), K^+ (r=-0.76) and Mn (r=-0.71), K^+ with Phosphate (r=-0.58), Phosphate with Co (r=-0.54) and Cd (r=-0.52) and Na^+ with Mn (r=-0.51).

Correlation analysis of physico-chemical parameters of surface water samples collected from different locations in the LRB revealed highly varying relationships among parameters between the three sampling periods. Results of the correlation analysis indicate maximum number of positive correlation among the parameters during S2 than S1 and S3. However, higher number of inverse (negative) correlation was observed in S1 samples followed by S3. Variation in inter-relationship between the physico-chemical parameters can be attributed by the variation in sampling periods, which showed high fluctuation in overall rainfall characteristics and water level in the river. During the S1 sampling, rainfall in the LRB was comparatively low and most of the sampling locations have less water. At the same, during S2 sampling most of the river showed a slightly higher water level in response to the higher amount of rainfall. During S3 sampling, the same situation prevailed. Further, it was also noted that, the effect of rainfall during the sampling time (before or on time of sampling) might also influence the variation of physico-chemical characteristics of surface water. Furthermore, source variability of eroded material due to variation in rainfall characteristics within the river basin also have an influence on the variation in the correlation among the parameters. It was also noted that, two sampling i.e. S1 and S2 were carried out in the beginning and ending of the northeast monsoon season whereas the S3 was in the end period of the southwest monsoon season. One of the reasons for the

variation in the chemical composition may be due to the difference in the moisture source. As a high temperature and high humid region, weathering of rock and erosion of soil is more common and which will also contribute to the seasonal variation of chemical composition in surface water because SWM is the classified as dry period compare to NEM.

4.6.4.3 Factor analysis

Results of physico-chemical parameters in surface water samples collected during three sampling periods were used in the factor analysis to determine the dominant process which controls the geochemistry of water in the LRB. Factor analysis was performed with principal component analysis as the extraction method and varimax with Kaiser Normalization as the rotation method (eigenvalue >1). In general, factor analysis revealed six factor components in S1, and seven factor components in S2 and S3 (Table 4.36 to 4.41). Parameters showing significant loading (≥±0.50) in different sampling periods were considered to explain the processes controlling the geochemistry of surface water in the LRB.

In S1, factor components showed a cumulative of 80.89% variance contributed by six factor components. Parameters such as EC, TDS, HCO_3^- and Ca^{2+} shows significant positive loading in Factor 1, which together contributed 18.24% of total variance. Surface water samples collected from locations SW-12, SW-16, SW-18 and SW-20 indicates the dominance of these parameters. In Factor 2, sulfate, Mg^{2+}, K^+, Fe and Mn shows strong positive loading with 14.81% contribution towards the total variance. Surface water samples from locations SW-14, SW-16, SW-17, SW-21 and SW-20 showed comparatively higher concentration of these parameters. K^+, Co and Ni show strong and good positive loading along with a good negative loading of DO in Factor 3, which explained 14.11% of the total variance. These parameters are dominant in surface water samples collected from locations SW-19, SW-22 and SW-23. A significant good and strong positive loading of Cd, Mn, Pb and Zn in Factor 4 explained 12.97% of total variance. Surface water samples collected from SW-17 and SW-19 shows higher concentration of Cd, Mn, Pb and Zn. In Factor 5, a strong positive loading by Turbidity and Ammonia and a good negative loading by Nitrate explained 11.08% of total variance. These parameters show comparatively higher concentration in surface water samples collected from locations SW-11 and SW-17. In Factor 6, Na^+ and Cu show strong positive loading which explained 9.69% of total variance and surface water samples from locations SW-20 and SW-21 was dominated by Na^+ and Cu

concentration. It was observed that, the result indicates a strong correlation of the factor component with the parameters and surface water samples from locations SW-16, SW-17, SW-19, SW-20, SW-21 and SW-22 showed a dominant nature in more than one factor component.

Factor analysis of S2 surface water samples showed a cumulative of 80.18% variance with seven factor components. Strong positive loading of EC, TDS, HCO_3^- and good positive loading of Cl^- and Zn was observed in Factor 1, which explained 19.24% of the total variance. Surface water samples collected from locations SW-06, SW-12, SW-21 and SW-23 shows the dominant nature of these parameters. In the case of Factor 2, Sulfate, K^+, Fe and Mn showed strong positive loading whereas pH and Ni show a significant negative loading and contributed 18.62% of the total variance. It was observed that, surface water samples collected from locations SW-17, SW-20, SW-21 and SW-22 show the dominance of parameters loaded in Factor 2. At the same time, in Factor 3, Mg^{2+} and Na^+ show strong positive loadings and Ca^{2+} show good negative loading which explained 9.98% of the total variance. Samples collected from SW-06, SW-08 and SW-22 show comparatively high concentration of Mg^{2+} and Na^+. Factor 4 explained 9.66% of the total variance with good and strong positive loading of Nitrate and Ammonia and strong negative loading of DO. It was noted that, surface water samples collected from locations SW-02, SW-08, SW-14 and SW-15 show the dominant nature of these elements. In Factor 5, Phosphate and Cu shows significant positive loading, whereas Turbidity and Ni showed significant negative loading which together explained 8.47% of the total variance. Parameters loaded in Factor 5 is prevalent in surface water samples collected from locations SW-01, SW-02, SW-19 and SW-23. A 7.33% of the total variance was explained by Factor 6, with good and strong positive loadings of Co, Pb and Zn. Higher concentration of these parameters was found in surface water samples collected from locations SW-07, SW-10, SW-11 and SW-22. It was also noted that, Cd and Co showed a strong and good positive loading in Factor 7 which explained 6.88% of total variance. Samples collected from the locations SW-01, SW-04, SW-11, SW-21 and SW-22 showed comparatively higher concentrations. Besides that, it was observed that sampling locations SW-01, SW-02, SW-06, SW-08, SW-11, SW-21, SW-22 and SW-23 shows dominant presence in most of the factor components loading.

The factor analysis of S3 samples revealed seven factor components which explained a cumulative of 81.98% variance. Among that, Factor 1 showed 17.41% of the total variance with significant strong positive loading of Sulfate, Ammonia, K^+, Mn and

strong negative loading of pH. Parameters loaded in Factor 1 was found to be dominant in surface water samples collected from locations SW-17, SW-21 and SW-22. Factor 2 explained 15.16% of the total variance with strong positive loading of EC, TDS, HCO_3^- and Ca^{2+}. Higher concentration of loaded variables was observed in the surface water sample collected from location SW-12. A strong positive loading of DO, turbidity, Ni and Zn is found in Factor 3 which explained 13.13% of total variance. Surface water samples collected from locations SW-15, SW-18, SW-19, SW-20 and SW-22 show dominance of these parameters. In Factor 4, Mg^{2+} and Na^+ shows strong positive loading, EC, TDS showed good positive loading and Fe shows good negative loading which together contributed 12.09% of the total variance. Dominance of parameters loaded in Factor 4 is found in surface water collected from LRB SW-06. Cd shows a strong positive loading and phosphate and Cu showed good negative loading in Factor 5 with 8.72% of the total variance. Surface water samples collected from SW-09, SW-16 and SW-23 show dominance of these parameters. Factor 6 explained 7.77% of total variance with strong positive loading of Cl^- and Pb. Higher concentration of Cl^- and Pb was observed in surface water samples collected from locations SW-07, SW-09 and SW-11. A strong positive loading of Co with 7.68% of the total variance contributed to Factor 7 and surface water samples collected from sampling locations SW-07 and SW-20 shows comparatively higher concentration of Co. Overall, it was noted that surface water samples collected from SW-07, SW-09, SW-20 and SW-22 shows dominance in the factor components with more than one occurrence as a factor loading.

Factor analysis of surface water quality parameters facilitated the identification of complex linear relationship that exists between the parameters (physico-chemical). This also explained the correlation of elements present in the surface water samples collected from different locations and different sampling periods in the LRB. In S1, Factor 1 showed positive loading of EC, TDS, HCO_3^- and Ca^{2+}. EC and TDS, which are controlled by the dissolved ions and was contributed by the primary source of rainwater chemistry followed by dissolution of river sediments. In general, loading of HCO_3^- indicates the role of partial pressure of CO_2 of air, bio-respiration and equilibrium balance of carbonate minerals in soil solution (Langmuir, 1997; Kim et al., 2005) whereas Ca^{2+} indicate the dissolution of carbonate rocks (Wedepohl, 1995; Blum et al., 1998; Sun et al., 2014). In the LRB, carbonate and calcareous rocks forms major parts of all the rock formations and dissolution of limestone contributed to a comparatively higher concentration of Ca^{2+} and HCO_3^- in the surface water (Semwal & Jangwan, 2009; Jin et al., 2011; Abdalla & Scheytt, 2012; Berhe et al., 2017; Rasool & Xiao, 2019). A similar observation was also noted in the results of

rainwater chemistry, which showed the dominance of HCO_3^- in most samples, suggesting a contribution from rainfall as well. Factor 2 shows the strong positive loading of sulfate, Mg^{2+}, K^+, Fe and Mn which indicates the dissolution of sediment and rocks in the river basin (Eocene to Miocene formations). Oxidation of iron sulphide, dissolution of limestone (dolomites) and K-feldspars and leaching of shale and mudstone contributed these parameters to surface water (Rochelle et al., 1987; Blum et al., 1998; Sun et al., 2014). Dissolution and leaching of shale, sandstone and mudstone present in the river basin along with rainfalls contributed K^+, Co and Ni in surface water samples, which form Factor 3. Strong loading of Pb, Zn and good loading of Cd and Mn in Factor 4 indicates the coupled contribution from the atmosphere, through rainfalls caused by vehicle transport, fossil fuel and forest burning as well as inputs from leaching of carbonates, shale and mudstones present in the river basin (Cheng et al., 2011). Factor 5 shows good loading of turbidity and ammonia and negative loading of nitrate. This indicates increased contribution of suspended sediments in relation to severe terrain alteration, erosive rainfall and hydrolysis of organic nitrogen through decomposition of microorganisms and the aerobic decomposition of organic nitrogenous matter (Marzluf, 1997; Brady & Weil, 2008; Geisseler et al., 2010). Loading of Na^+ and Cu in Factor 6 suggests dissolution of silicate minerals, carbonates and shale in the river basin.

Surface water samples collected during S2 showed seven factor components. Factor 1 was contributed by EC, TDS, HCO_3^-, Cl^- and Zn. EC and TDS, which indicates the highly turbid nature of the surface water with dissolved solids derived through erosion, as explained previously. HCO_3^- and Cl^- loading suggests dissolution of carbonate rocks along with a contribution from rainfall and Zn added as leaching from shale and mudstone present in the river basin (Saleem et al., 2014). Factor 2 showed higher positive loading of Sulfate, K^+, Mn and Fe and negative loading of pH and Ni suggesting dissolution of sulfate and silicate minerals mainly from shale and sandstone present in the river basin. Factor 3 shows strong loading of Mg^{2+} and Na^+ and negative loading of Ca^{2+}, indicating dissolution of carbonate rocks (dolomite) and silicate minerals (Bowser & Jones, 2002; Moral et al., 2008). Strong loadings of Nitrate and Ammonia and negative loading of DO in Factor 4 indicates hydrolysis of organic nitrogen i.e. decomposition of microorganisms and the aerobic decomposition of organic nitrogenous matter. Factor 5 shows good loading of phosphate and Cu and negative loading of turbidity and Ni suggesting decaying of bio-mass and atmospheric deposition (forest fire, burning of fuel oil and petrochemical industries) along with leaching of shale (Manahan, 1993; Mueller et al., 1995; Fadiran et al., 2008). Loading

of Co, Pb and Zn in Factor 6 and Co and Cd in Factor 7, indicates leaching from shale, mudstones and sandstone in the river basin and atmospheric input through rainfall (due to anthropogenic activities especially through vehicle emission, petrochemical industries and forest fire).

Considering the factor analysis results of surface water samples collected during S3, variations in factor loading was observed and it explained seven factor components. Factor 1 was formed by good positive loading of Sulfate, Ammonia, K^+, Mn and negative loading of pH suggesting dissolution of sulfate and silicate minerals and hydrolysis of organic nitrogen. EC, TDS, HCO_3^- and Cl^- shows good positive loading in Factor 2, indicating dissolution of carbonate rocks along with a contribution from rainfall. DO, Turbidity, Ni and Zn contributed Factor 3, indicates atmospheric contribution along with leaching of shale and mudstone (dissolution of silicate minerals). Factor 4 shows good positive loading of EC, TDS, Mg^{2+}, Na^+ and negative loading of Fe, indicating dissolution of carbonate rocks (dolomite) and silicate minerals. Factor 5 shows good positive loading of Cd and negative loading of phosphate and Cu, good positive loading of Cl^- and Pb in Factor 6, and Co in Factor 7 suggesting dissolution and leaching of carbonate rocks, shale and mudstone and atmospheric deposition.

The geochemistry of surface water in the LRB was controlled by dominant natural (geological) process with less contribution from anthropogenic activities. Major natural processes which control the geochemistry of surface water is (a) high rate of sediment load in the river due to severe erosive rainfall (b) mineral dissolution and leaching from dominant rocks (carbonates, shale and mudstones) (c) hydrolysis of organic nitrogen through decomposition of microorganisms and the aerobic decomposition of organic nitrogenous matter and (d) atmospheric deposition (act as major contributor of trace metals). Forest fire, biomass burning and atmospheric pollution from petrochemical industries and fossil fuel burning are the main sources of metal in rainwater. Seasonal variation in the geochemistry of surface water samples in the LRB was mainly controlled by the rainfall characteristics. Depending on the amount of rainfall and its spatial variation, erosion and transportation of weathered materials from distinct locations in the LRB vary, thus changing the overall geochemical characteristics of the water. Furthermore, the time of sampling also has an effect on the water chemistry because if the sampling was carried out after a long break of rainfall and the first rainy day, surface water shows comparatively higher concentration of parameters than the samples collected during flooding and

continuous rainfall periods. These findings were well supported by the results of Piper plots and Gibbs diagrams, which clearly indicate variations in chemical characteristics of surface water collected during different sampling periods (S1, S2 and S3).

Table 4.36: Varimax component loadings of factors and the percentage of variance explained for surface water samples collected during S1.

Sampling Period – S1							
	Communalities	Component					
		1	2	3	4	5	6
pH	0.84	0.02	-0.47	-0.39	-0.48	-0.34	-0.34
EC	0.96	**0.94**	0.25	0.02	-0.05	0.05	0.01
TDS	0.96	**0.94**	0.25	0.02	-0.05	0.05	0.01
DO	0.90	-0.48	-0.28	***-0.74***	0.09	-0.13	-0.12
Turbidity	0.93	0.03	0.00	-0.07	-0.06	**0.95**	0.10
Sulfate	0.81	0.21	**0.83**	0.13	0.15	0.07	0.18
Nitrate	0.60	-0.20	0.36	-0.06	-0.15	***-0.62***	-0.15
Ammonia	0.89	-0.11	0.29	0.35	0.11	**0.80**	-0.05
Phosphate	0.74	-0.26	-0.27	-0.49	-0.46	0.24	-0.30
Bicarbonate	0.90	**0.93**	-0.10	0.03	0.11	0.05	0.10
Chloride	0.50	-0.04	0.20	-0.18	-0.52	-0.01	-0.39
Ca	0.80	**0.87**	-0.08	0.05	0.10	-0.07	-0.16
Mg	0.83	0.32	**0.78**	-0.08	-0.14	-0.20	-0.22
Na	0.86	-0.11	0.14	0.11	-0.20	0.28	**0.84**
K	0.93	0.35	**0.62**	**0.52**	0.19	0.24	0.25
Co	0.63	-0.20	0.04	**0.65**	0.13	0.10	0.37
Ni	0.82	0.02	0.09	**0.88**	0.15	0.11	0.03
Cd	0.71	-0.05	0.32	-0.45	**0.58**	0.05	-0.22
Fe	0.66	-0.25	**0.61**	0.41	0.05	-0.09	0.23
Mn	0.87	-0.11	**0.60**	0.17	**0.54**	0.26	0.34
Pb	0.81	0.13	-0.16	0.22	**0.76**	-0.22	-0.31
Zn	0.90	-0.02	0.22	0.05	**0.89**	0.24	0.07
Cu	0.75	0.13	0.18	0.41	0.19	-0.10	**0.70**
% of Variance		18.24	14.81	14.11	12.97	11.08	9.69
Cumulative % of Variance		18.24	33.05	47.16	60.13	71.21	80.89

Table 4.37: Varimax component loadings of factors and the percentage of variance explained for surface water samples collected during S2.

Sampling Period – S2								
	Communalities	Component						
		1	2	3	4	5	6	7
pH	0.84	-0.13	***-0.79***	0.08	0.08	0.01	-0.26	0.35
EC	0.97	**0.91**	0.34	0.04	0.12	0.00	0.07	-0.02
TDS	0.97	**0.91**	0.34	0.04	0.12	0.00	0.07	-0.02
DO	0.66	0.14	-0.21	0.17	***-0.72***	-0.08	0.05	0.20
Turbidity	0.61	-0.28	-0.03	-0.02	0.15	***-0.61***	0.29	-0.22
Sulfate	0.92	0.37	**0.79**	0.27	-0.26	-0.10	0.12	0.01
Nitrate	0.76	0.25	-0.28	0.12	**0.77**	-0.02	0.09	0.02
Ammonia	0.86	0.29	-0.10	-0.06	**0.85**	-0.18	0.02	-0.01
Phosphate	0.71	-0.32	-0.05	-0.16	0.11	**0.72**	0.15	0.17
Bicarbonate	0.86	**0.89**	0.05	-0.01	0.22	-0.05	0.08	0.11
Chloride	0.80	**0.60**	0.44	0.24	-0.08	0.33	-0.10	-0.26
Ca	0.83	0.36	-0.15	***-0.76***	0.25	-0.11	-0.01	-0.14
Mg	0.80	0.26	0.20	**0.79**	-0.06	-0.05	-0.23	0.02
Na	0.72	0.13	-0.13	**0.73**	0.13	-0.08	0.34	0.11
K	0.80	0.38	**0.74**	0.07	0.10	-0.09	0.18	0.23
Co	0.76	-0.39	0.11	0.16	-0.10	0.11	**0.53**	**0.51**
Ni	0.78	0.19	***-0.64***	0.03	0.00	***-0.52***	0.18	0.17
Cd	0.82	0.11	-0.21	0.15	-0.17	0.08	-0.09	**0.83**
Fe	0.66	0.15	**0.62**	0.36	0.05	0.27	-0.14	-0.17
Mn	0.94	0.21	**0.93**	-0.04	-0.06	-0.01	0.18	-0.03
Pb	0.79	0.25	0.34	-0.10	0.09	-0.15	**0.75**	-0.14
Zn	0.85	**0.54**	0.21	0.32	-0.05	0.32	**0.55**	-0.03
Cu	0.75	0.34	0.04	0.22	-0.22	**0.62**	0.13	-0.37
% of Variance		19.24	18.62	9.98	9.66	8.47	7.33	6.88
Cumulative % of Variance		19.24	37.86	47.84	57.50	65.97	73.30	80.18

Table 4.38: Varimax component loadings of factors and the percentage of variance explained for surface water samples collected during S3.

Sampling Period – S3								
	Communalities	Component						
		1	2	3	4	5	6	7
pH	0.84	***-0.77***	0.23	-0.36	0.19	-0.14	0.09	-0.07
EC	0.98	0.00	**0.82**	-0.14	**0.51**	0.02	0.17	0.06
TDS	0.98	0.00	**0.82**	-0.14	**0.51**	0.02	0.17	0.06
DO	0.74	0.07	-0.36	**0.63**	-0.08	-0.35	0.15	0.24
Turbidity	0.81	-0.14	-0.18	**0.77**	-0.04	0.13	-0.27	0.29
Sulfate	0.87	**0.86**	-0.11	0.00	-0.13	0.16	0.24	0.13
Nitrate	0.60	0.37	-0.38	-0.28	0.14	-0.02	-0.25	-0.39
Ammonia	0.82	**0.88**	0.05	0.10	0.18	0.02	-0.01	-0.05
Phosphate	0.79	-0.39	-0.02	-0.19	0.17	***-0.59***	0.14	-0.45
Bicarbonate	0.90	-0.16	**0.88**	-0.16	-0.23	-0.12	-0.02	0.03
Chloride	0.73	0.06	-0.21	-0.08	0.09	0.28	**0.70**	0.33
Ca	0.91	-0.12	**0.89**	-0.07	-0.20	0.06	-0.24	-0.08
Mg	0.83	-0.03	0.10	0.00	**0.90**	-0.05	-0.02	-0.08
Na	0.86	-0.33	-0.08	-0.01	**0.84**	0.04	0.19	0.01
K	0.92	**0.74**	-0.10	0.48	-0.15	0.15	0.01	0.28
Co	0.76	0.20	0.04	0.02	0.04	0.12	-0.02	**0.84**
Ni	0.78	0.24	-0.10	**0.78**	0.13	0.11	0.00	-0.26
Cd	0.82	0.01	0.06	0.14	-0.11	**0.88**	0.12	0.02
Fe	0.65	-0.06	0.14	0.25	***-0.56***	0.27	0.39	-0.16
Mn	0.75	**0.76**	-0.08	-0.05	-0.23	-0.05	-0.30	0.12
Pb	0.86	-0.15	0.13	0.00	0.04	-0.35	**0.77**	-0.32
Zn	0.90	0.27	0.02	**0.88**	-0.17	0.11	0.10	-0.02
Cu	0.75	-0.30	0.29	0.10	-0.23	***-0.58***	0.22	-0.36
% of Variance		17.41	15.16	13.13	12.09	8.72	7.77	7.68
Cumulative % of Variance		17.41	32.57	45.70	57.79	66.52	74.29	81.98

Table 4.39: Factor scores associated with sampling location correspond to S1.

Sampling Period - S1						
	Score					
	Factor-1	Factor-2	Factor-3	Factor-4	Factor-5	Factor-6
LRB SW-1	-0.65	0.50	-1.24	0.20	-0.37	-1.04
LRB SW-2	-0.48	0.60	-0.25	-0.42	-0.82	-1.95
LRB SW-3	-1.04	-0.87	0.23	-0.30	-0.92	-0.40
LRB SW-4	0.49	0.72	-2.30	-0.84	0.26	0.50
LRB SW-5	-0.62	0.34	-0.82	0.15	-0.70	-0.16
LRB SW-6	-0.77	-1.26	0.13	-0.02	-0.91	0.29
LRB SW-7	-0.48	-0.28	-0.10	-0.32	-0.11	0.00
LRB SW-8	0.04	0.52	-0.60	-0.79	-1.00	0.11
LRB SW-9	-0.56	-0.24	-0.10	-0.15	-0.41	0.39
LRB SW-10	-0.60	-0.64	-0.35	0.47	-0.51	0.35
LRB SW-11	-0.54	0.12	-1.22	-1.25	**3.37**	-0.65
LRB SW-12	1.83	-1.78	-0.92	0.70	-0.44	0.36
LRB SW-13	0.03	-0.63	-0.23	0.83	-0.59	0.47
LRB SW-14	-0.37	1.11	-0.14	-0.44	-0.97	0.16
LRB SW-15	0.19	-0.09	-0.18	0.17	-0.30	-0.86
LRB SW-16	**3.41**	1.25	0.61	-0.08	-0.26	-1.34
LRB SW-17	-0.42	**1.91**	-0.22	**3.56**	1.26	0.42
LRB SW-18	1.20	-1.10	0.74	0.17	0.70	-0.30
LRB SW-19	-0.58	-1.11	1.63	1.56	0.27	-1.09
LRB SW-20	1.11	-0.76	0.09	-0.50	0.42	2.18
LRB SW-21	-0.18	1.33	0.80	-0.19	-0.22	**2.78**
LRB SW-22	-0.37	1.65	**2.37**	-1.40	-0.19	-0.14
LRB SW-23	-0.05	-0.29	1.46	-0.37	0.98	-0.13
LRB SW-24	-0.59	-0.99	0.62	-0.72	1.46	0.05

Table 4.40: Factor scores associated with sampling location correspond to S2.

Sampling Period - S2							
	Score						
	Factor-1	Factor-2	Factor-3	Factor-4	Factor-5	Factor-6	Factor-7
LRB SW-1	-1.60	-0.29	-1.23	0.23	**2.68**	0.18	1.42
LRB SW-2	-1.55	0.14	0.29	1.05	1.09	-1.57	-0.45
LRB SW-3	-0.31	-0.32	0.24	-0.80	-0.01	-2.07	0.18
LRB SW-4	-0.76	-0.63	0.11	-0.88	0.31	-0.81	1.10
LRB SW-5	-0.09	-0.73	0.90	-0.84	-0.60	-0.81	-0.05
LRB SW-6	1.11	-0.71	1.02	-1.20	-0.83	-1.26	0.20
LRB SW-7	-0.24	-1.65	0.66	-0.25	0.32	1.76	-0.01
LRB SW-8	0.81	-0.80	1.36	1.84	0.47	0.08	-0.29
LRB SW-9	-0.73	0.13	0.27	-0.42	-0.69	-0.34	0.64
LRB SW-10	-0.92	-0.45	0.37	-0.74	-1.29	1.23	-0.11
LRB SW-11	0.40	-0.56	0.21	-0.63	0.12	1.29	1.37
LRB SW-12	1.74	-0.90	-2.99	-0.75	-0.03	-0.46	0.19
LRB SW-13	-1.16	-0.40	-0.06	0.03	-1.70	0.97	-0.19
LRB SW-14	0.35	-0.71	-0.53	1.11	-0.94	-0.11	-0.23
LRB SW-15	0.78	-0.35	-0.65	**3.21**	-0.63	-0.33	0.27
LRB SW-16	-0.57	-0.21	-2.05	-0.15	-0.64	0.70	-0.66
LRB SW-17	-0.58	**2.75**	-0.88	-0.42	-0.22	0.95	-0.95
LRB SW-18	-0.91	0.71	0.35	0.70	-0.99	-0.20	-1.04
LRB SW-19	0.43	-0.28	0.54	-0.57	1.99	0.68	-1.84
LRB SW-20	-0.62	1.07	-0.04	0.00	0.17	-1.09	-0.16
LRB SW-21	1.62	2.16	0.21	-0.07	-0.27	-0.20	**2.21**
LRB SW-22	0.35	1.01	1.27	0.44	0.53	**1.49**	1.36
LRB SW-23	**1.92**	0.13	0.16	-0.38	1.04	0.35	-1.47
LRB SW-24	0.54	0.91	0.45	-0.51	0.13	-0.42	-1.48

Table 4.41: Factor scores associated with sampling location correspond to S3.

Sampling Period - S3							
	Score						
	Factor-1	Factor-2	Factor-3	Factor-4	Factor-5	Factor-6	Factor-7
LRB SW-1	-0.75	-0.07	-1.03	-0.31	-0.01	0.43	0.09
LRB SW-2	-0.31	-0.70	-1.07	-0.68	-0.65	-1.01	-0.96
LRB SW-3	0.03	-1.50	-1.50	-0.41	0.07	-0.96	-1.58
LRB SW-4	-0.03	-0.54	-0.97	0.27	0.03	0.18	0.88
LRB SW-5	-0.35	-0.54	-1.10	-0.02	-1.21	-0.19	0.17
LRB SW-6	-0.26	0.67	-0.04	**4.18**	-0.26	-0.09	-0.43
LRB SW-7	-0.02	0.18	-0.51	-0.17	-1.00	**1.60**	**2.46**
LRB SW-8	-0.09	0.25	-1.45	-0.49	-0.21	-0.14	-0.05
LRB SW-9	-0.25	-0.06	-0.90	0.20	1.62	2.02	-0.16
LRB SW-10	-0.42	-0.43	0.13	0.33	0.93	-0.19	-0.63
LRB SW-11	-0.10	-0.21	0.95	-1.19	-1.70	1.39	-1.01
LRB SW-12	-0.52	**4.13**	-0.58	-0.92	0.21	-1.09	-0.38
LRB SW-13	-0.70	-0.56	-0.48	0.46	-0.34	-0.65	0.40
LRB SW-14	-0.16	0.50	-0.40	-0.07	0.63	-0.24	0.48
LRB SW-15	-0.57	0.25	1.22	0.17	-1.39	0.34	-1.00
LRB SW-16	0.84	-0.43	-0.24	-0.32	**2.07**	0.54	0.87
LRB SW-17	**2.76**	0.23	0.31	-0.27	-0.13	0.24	0.47
LRB SW-18	-1.10	-0.08	1.60	-1.07	0.89	0.78	-0.90
LRB SW-19	-1.32	-0.93	1.42	-0.11	0.91	-1.88	0.41
LRB SW-20	-1.12	-0.20	**1.73**	-0.01	-0.21	-0.74	2.16
LRB SW-21	2.17	-0.18	0.43	-0.35	-0.46	-2.01	0.81
LRB SW-22	1.84	0.05	1.07	0.51	0.68	0.07	-1.45
LRB SW-23	0.05	0.17	0.75	-0.02	1.25	0.73	-0.32
LRB SW-24	0.38	0.01	0.67	0.29	-1.72	0.85	-0.33

Chapter 5 Summary and Conclusion

5.1 Summary

The Limbang River Basin, located in the equatorial tropical island Borneo facing environmental degradation due to anthropogenic activities and climate change. The effects of these activities and phenomena are greater in the hydrological regime and are well reflected as change in quality and quantity aspects of surface water and variation in the amount of precipitation characteristics. In the present research, hydroclimatic characteristics of the Limbang River Basin were successfully characterised through analysis and interpretation of hydrometeorological (rainfall trend and runoff) and hydrochemical (rainwater chemistry, stable isotopes and surface water chemistry) components. The salient findings of the research are summarised below.

The LRB receives an annual average rainfall of 3851mm, which is higher than the national (2000mm) and global average (750mm) annual rainfall (Borhanazad et al., 2013). The LRB experiences two dominant monsoon seasons, each consists of five-month duration separated with short inter-monsoon periods of single month duration. The northeast monsoon (November to March) is wetter than the southwest monsoon (May to September) and the inter-monsoon periods (April and October) also receives higher amount of rainfall (Hashim et al., 2016; MMD, 2017). Detailed analysis of rainfall characteristics provides a better understanding of the rainfall patterns and statistical trend characteristics at the local (station) and regional (basin) scale. The LRB has monthly rainfall data for a period of 19 to 69 years from thirteen rain gauging stations located at spatially separate places, having elevation in the range of 7m to above 1532m. Homogeneity and continuity of data characterised through Lag-1 autocorrelation test at 95% confidence level do not identify any correlation in rainfall data. Considering the missing percentage, rainfall data show very little missing values (0.80% to 12.35%) and were filled using the normal ratio method (NRM), which offered higher accuracy (R^2>0.71 and r>0.84). Basic statistical analysis (skewness, kurtosis and coefficient of variation) revealed homogenous and consistent data with less dispersion and good precision. Monthly rainfall in the basin showed comparatively higher range of variation (0.50mm to 1315.50mm), which is also reflected in seasonal rainfall (504.50mm to 3234mm) and annual rainfall (1821.56mm to 6926mm).

Statistical rainfall trends assessed for monthly, seasonal and annual rainfall at the individual rain gauge and the LRB as a whole showed varying characteristics such as no trend,

non-significant increasing or decreasing trend and significantly increasing and decreasing trends. Considering the monthly rainfall trend, most of the stations (≥8) showed an increasing trend during the months January, February, June, August and November, and decreasing trends in the months of May, July, September and October. Rain gauging stations showed a mixed trend (increasing and decreasing trend) in the months of March, April and December. It was also observed that rainfall recorded at few stations showed no or very weak trends in the months May, June, July, November and December. Among the gauging stations, rainfalls recorded at Long Napir shows a consistent increase in rainfall in all months. Statistically significant highest increasing trend in monthly rainfall was observed in Limbang DID (2.86mm/year in November) and lowest in Ukong (-2.45mm/year in October). At the basin scale, rainfall in nine months (January, February, March, April, June, August, October, November and December) show increasing trends and three months (May, July and September) shown decreasing trends. Among this, rainfall recorded during the months February and March showed statistically significant increasing trends (1.72mm/year at 90% confidence and 2.23mm/year at 95% confidence level). Considering the seasonal rainfall trends, during SWM, most (ten) stations showed decreasing trends and three showed an increasing trend in which rainfall at Long Napir showed the maximum increase of 2.88mm/year. In NEM season, twelve rain gauging stations showed increasing trends and one showed decreasing trends while the Long Napir station showed the highest increase of 3.95mm/year. Rainfalls occurring during the IM periods in April, seven gauging stations showing increasing rainfall trends and six stations show decreasing trends whereas in October, three stations showed an increasing trend and ten stations showed decreasing trends. Annual rainfall showed an increasing trend in five stations and decreasing trend in eight stations and rainfall recorded at Long Napir showed the highest increase of 3.77mm/year. However, the LRB as a whole, during SWM, NEM, IM and annual rainfall, showed statistically significant and non-significant increasing trends. Significant and higher trends was noted in NEM (2.24mm/year) and annual (1.90mm/year) rainfall. Overall, rainfall in the LRB shows a consistent increasing trend.

Runoff, which is predominantly dependent on the amount of rainfall along with terrain and channel characteristics such as slope (its steepness and length), direction of the slope, relief variation, width and depth of the channels. Further, human intervention as modification of terrain characteristics for agriculture, developmental activities and logging also influences the runoff characteristics. In the LRB, a few water level measuring stations are operating for monitoring flood events and issuing pre-caution in the lower river basin

areas. In the research, the water level for a period of 10 years (1991-2000) from the Insungai Nanga was used to model the runoff by selecting minimum description length based multilayer neural network (MDL MNN). The calculated discharge is based on stage height rating curve equation for the period considered in the research range from 1.55m^3/S to 1134.95m^3/S and the daily rainfall varies from 0 to 133mm. The whole data is divided into 20 lags, by considering the continuity, and missing in the data and is used to determine the structure of the model (input variables). Statistical models such as cross correlation function (CCF), autocorrelation function (ACF) and partial autocorrelation function (PACF) was applied, and three antecedent rainfalls and one antecedent runoff were fixed as input variables and by trial and error methods, four neurons were also selected in the hidden layer. Before proceeding to runoff modelling, the whole 10 years data was split into two i.e. 60% data for training the model and 40% to test the runoff model output. Runoff modelling using MNN MDL gives comparable results with discharge calculated using rating curve equation. In training and testing, the observed and predicted runoff shows an average value of 197 and 198m^3/S and 190 and 195m^3/S respectively. Correlation coefficients of simulated runoff in training and testing showed a higher positive correlation (r=0.84 and 0.85 for training and testing respectively) suggesting the efficiency of the model to predict the runoff from Insungai Nanga at given conditions. Furthermore, different statistical tests were applied to assess the prediction accuracy of the MNN MDL model in training and testing in simulating the runoff data. Pearson's correlation, Nash Sutcliffe Efficiency (NSE), Root Mean Square Error (RMSE), Relative RMSE (RRMSE), Mean Absolute Error (MAE), Mean Absolute Percentage Error (MAPE), Volumetric Error (EV) and Relative Peak Error (RPE) were calculated and all showed comparatively higher accuracy of the results of modelling. This indicates the efficiency of the model and also suggests the replicability of MNN MDL model in forested catchments which lack detailed and up to date discharge measurements.

Effects of climate change can be clearly understood by analysing the pattern, amount and chemical characteristics of rainwater, because rainfall is the dominant hydrological variable which reflects the effects of climate change. Assessment of the composition of stable isotopes in rainwater gives valid clues about the source, movement and variation in climatic patterns. Identifying the importance of the composition of stable isotopes in rainwater, oxygen-18 ($\delta^{18}O$) and deuterium (δD) in monthly cumulative rainwater collected from two locations (Limbang City near to the South China Sea and Kampong Salidong in interior forest) in the LRB for a period of one year was characterised in the present research. Rainfall during the period of research (October-2016 to September-2017) varies in the range of 125mm

(July-2017) to 615mm (August-2017) with an average of 410mm. Composition of δD ranges from -68.43‰ (June-2017) to -38.05‰ (March-2017) and $\delta^{18}O$ ranges from -10.24 to -5.81‰ in Limbang City. In Kampong Salidong, δD ranges from -88.48‰ (June-2017) to -33.04 ‰ (March-2017) and $\delta^{18}O$ ranges from -12.57 to -5.50‰. Considering the d-excess values in Limbang City it ranges from 8.43‰ (March-2017) to 13.66‰ (January-2017) and for Kampong Salidong it varies between 5.43‰ (April-2017) and 15.02‰ (August-2017) with an average of 11.74‰. The local meteoric water line (LMWL) generated for both locations shows comparatively similar slope values and are close to that of global meteoric water line (GMML) ($\delta D = 7.46\ \delta^{18}O + 7.19$; $\delta D = 7.62\ \delta^{18}O + 8.07$ and $\delta D = 8\delta^{18}O + 10$ for Limbang City, Kampong Salidong and GMWL respectively), suggesting equilibrium condition of rain formation in this region. However, the difference in d-intercepts indicates the possibility of re-evaporation and changing conditions of atmospheric moisture source in these locations due to the evaporation of raindrops below the cloud layer. Further, considering the volume weighted composition, lower amount of rainfalls show enriched vwδD and vw$\delta^{18}O$ and higher amount of rainfalls show depleted vwδD and vw$\delta^{18}O$ which indicates the amount effect over the composition of δD and $\delta^{18}O$, but no significant correlation observed with temperature and humidity. Furthermore, the temporal pattern indicates dominance of two rainy seasons (also includes comparatively dry seasons) in the LRB during the study period. Variation in d-excess >10‰ observed in few months indicates increased convective activity with less re-evaporation whereas d-excess <10‰ or ≈10‰) noted during remaining months, indicates a limited supply of inland moisture to the rainfall. However this could also be due to the increased evaporation of raindrops and high humidity in the region. The composition of δD and $\delta^{18}O$ shows seasonal variation caused by variations in the source of moisture in connection with the regional monsoon characteristics, amount of rainfall as well as local input through re-evaporation.

Rainwater and surface water also shows the influence of climate change as the variation in quality and quantity aspects. As discussed earlier, any hydrological system is driven by input from rainfall and the variation in rainfall amount and patterns will affect overall characteristics of the hydrological system. Therefore, in the present research, chemical characteristics of rainwater and surface water collected from the LRB was analysed for physical parameters (pH, EC, TDS, DO and Turbidity), chemical parameters including major ions (CO_3^{2-}, HCO_3^-, Cl^-, Ca^{2+}, Mg^{2+}, Na^+ and K^+) and trace metals (Co, Ni, Cd, Fe, Mn, Pb, Zn and Cu). Rainfall, the scavenger of atmospheric pollutants, not only reflect the chemical composition of the atmosphere above an area but also help to identify the source of chemical

constituents. In general, chemical constituents in rainwater was contributed by windblown dust from distant locations originating from various natural and anthropogenic activities. Rainwater collected from 5 locations in the LRB showed slightly alkaline nature with mean pH higher than 5.8. All other physical and chemical parameters showed spatial and temporal variation in its concentration. The observed spatial and temporal variation in the chemical characteristics of rainwater was caused by the changes in the source and amount of rainfall along with evaporation of rain while falling down, and local site specific input such as soil dust and forest burning. Considering the mean concentration of major ions and trace metals, bicarbonate (HCO_3^-) and chloride (Cl^-) are the dominant major ions and Fe and Ni are the dominant trace metals. The mean concentration of major ions and trace metals in rainwater follows the decreasing order, $HCO_3^- > Cl^- > Na^+ > Ca^{2+} > Mg^{2+} > K^+$ and Fe > Ni > Pb > Mn > Co > Zn > Cu > Cd. Statistical analysis (Pearson's correlation) revealed a strong correlation between parameters, suggesting a common source of chemical constituents along with local input in the moisture source and mutual relationship between the variables. At the same time, two-way ANOVA identified significant variation (95% confidence level) in the concentration of Ni, Fe and Cu in sampling locations and sampling periods, and certain parameters (Turbidity and K^+) between sampling locations and others (pH, EC, TDS, DO, HCO_3^-, Cl^-, Co, Cd, Mn, Pb and Zn) between sampling periods. Some other parameters like Ca^{2+}, Mg^{2+} and Na^+ do not show any significant variation during the period of sample collection. Factor analysis revealed different loading of factor components and provided information about the major processes controlling the chemistry of rainwater in the LRB. Chemical characteristics of rainfall in the LRB is controlled by contribution from sea and barren land (sea salt spray, evaporation and dust particles), monsoon winds originating from long distance, the presence of petro-chemical industries, transportation based pollutions (both land and sea) and regional forest fire (biomass burning) in South East Asia. A comparison of chemical characteristics of rainwater in the LRB with other locations showed slightly higher concentration of trace metals, which indicates slightly polluted nature of rainwater due to the anthropogenic activities in the region, as explained earlier.

Surface water samples collected during the three different sampling periods (November-2016, March-2017 and September-2017), from 24 locations in the LRB representing northeast monsoon and southwest monsoon seasons also showed spatial and temporal variations in physico-chemical parameters. Surface water in the LRB is slightly acidic with mean pH less than 6.8. A comparison of surface water chemistry with Malaysian Water Quality Standards (MWQS) and World Health Organization (WHO) standards indicate

comparatively good quality of water with an exception in turbidity. It was also observed that pH, DO, Fe, Pb, and Cu shows variation in a few locations in all sampling periods when compared with the water quality standards. Higher turbidity of surface water is related to sediment load caused by intense logging and terrain alteration processes in the river basin. Moreover, concentration of nutrients in the surface water samples are very low, suggesting nil or minimal contribution from anthropogenic sources (agricultural activities) and points towards the mineral dissolution and decaying of biomass. As observed in the rainwater, bicarbonate (HCO_3^-) and chloride (Cl^-) are the dominant major ions and Fe and Ni are the dominant trace metals. The mean concentration of major ions and trace metals in surface water follows the decreasing order of $HCO_3^- > Cl^- > Na^+ > Mg^{2+} > Ca^{2+} > K^+$ and Fe > Ni > Pb > Mn > Zn > Co > Cu > Cd. In addition, the application of water quality indices aided the classification of surface water in moderate to good class, which indicates the usability of water for various purposes. The identification of major geochemical processes in the LRB through Piper diagram, Gibbs plot, partial pressure of CO_2 (Log pCO_2) and saturation index showed variation in the intensity of processes in response to rainfall patterns and amount. Piper diagram identified two dominant types of water (mixed Ca^{2+}- Mg^{2+}- Cl^- and Ca^{2+}- Mg^{2+}- HCO_3^-) in three sampling periods and the Gibbs plots indicates precipitation (rainfall) dominance with rock-water interaction as the process controls the surface water chemistry. This was supported by the results of the Log pCO_2, which showed lower Log pCO_2 values in the upstream side indicating direct recharge of rainwater, whereas the higher Log pCO_2 in the downstream side points towards mixed water. The saturation index indicates the effect of dilution through monsoon rainfall by showing the under-saturated state for the carbonate minerals in the order of $SI_{Magnesite} > SI_{Calcite} > SI_{Aragonite} > SI_{Dolomite}$. Normalisation of surface water chemistry with rainwater chemistry also supports the findings by showing enrichment and depletion in certain elements. Significant relationships (correlation) and variance (Two-way ANOVA) shown by the statistical analysis (correlation and two-way ANOVA) suggests a common source as well as variations in rainfall amount, availability of eroded material and dissolution contributed to the overall fluctuation in surface water chemistry. Factor Analysis revealed different loadings of factor components in surface water samples collected during different sampling periods from different locations in the LRB. However, association of parameters in different factors indicates that the surface water's geochemistry is controlled by the dominance of high sediment loads in response to severe rainfall, weathering, leaching and dissolution of bed rocks, hydrolysis of organic nitrogen through decomposition of microorganisms and the aerobic decomposition of organic nitrogenous matter and atmospheric fallout as the product of forest fires, biomass burning,

discharge from petrochemical industries and fossil fuel burning. Overall, surface water in the LRB is of good quality and the processes which govern the geochemistry is controlled by the rainfall characteristics of the basin.

5.2 Conclusion

The present research is a first time attempt to understand and characterise the comprehensive hydroclimatic condition of the Limbang River Basin. All the declared aim and objectives were successfully completed by addressing the individual research questions. Overall it can be concluded that, an increasing trend in rainfall in the LRB indicates the effect of climate change which increases the runoff from land and streams in the region. This increased runoff which carries a high amount of sediment derived through intense terrain alteration and weathering process, ultimately controls the chemistry of surface water in the LRB. Variations in the rainfall amount, the dominance of monsoon winds and the anthropogenic activities controls the isotope composition as well as chemistry of rainwater. The findings of present research can be used as baseline information to tackle the adverse effects of climate change by planning and implementing better management - agricultural, developmental and hazard risk reduction - schemes and measurements. In addition, the findings will also serve as an authentic scientific document which details the pre-dam hydroclimatological scenario in the LRB.

5.3 Scope for Future Research

Though the present research successfully characterised the hydroclimatic conditions of the LRB, however, due to the limitations in secondary data (rainfall, runoff, evaporation and temperature etc.) and the limited period of primary data collection, the effect of climate change over this region is not fully recognised. Certain aspects of research need to be strengthened with augmentation of accurate datasets related to temperature and hourly rainfall data. Furthermore, long term and continuous monitoring of event based and daily rainfall data are essential for the identification of the effects of climate change over rainfall characteristics in the region. Along with this, continuous monitoring of water level and discharge is essential for better forecasting of flood events and also for the development of proper mitigation measures. These will help to reduce the flashflood hazards in the lower reach of the river basin. It is also recommended to monitor the surface water chemistry regularly to assure the water quality to avoid health hazards of people who continuously use the river water for their daily needs. During the field data collection, it is observed that, most part of the river basin facing severe terrain degradation connected to logging activities.

Logging not only altered the terrain characteristics but also contributed a heavy load of sediment to the river. Unfortunately, there is no instrumentation facility available to quantify the sediment discharge through rivers. Considering these facts together, it is essential and necessary to model the spatial and temporal characteristics of soil erosion and sediment delivery in the LRB. Moreover, the impact of land cover alteration over terrain erosion needs to be studied to detect the trend of erosion characteristics in the LRB. Overall, the LRB is facing impacts of climate change and adverse effects of human intervention at various levels, which needs to be understood with the analysis of higher resolution and accurate geo-environmental, hydrological and atmospheric variables to tackle the adverse effects by implementing better management, agricultural and developmental schemes.

References

Abaje, I. B., Ishaya, S., & Usman, S. U. (2010). An analysis of rainfall trends in Kafanchan, Kaduna State, Nigeria. *Research Journal of Environmental and Earth Sciences*, *2*(2), 89-96.

Abbasnia, A., Yousefi, N., Mahvi, A. H., Nabizadeh, R., Radfard, M., Yousefi, M., & Alimohammadi, M. (2018). Evaluation of groundwater quality using water quality index and its suitability for assessing water for drinking and irrigation purposes: Case study of Sistan and Baluchistan province (Iran). *Human and Ecological Risk Assessment: An International Journal*, 1-18.

Abdalla, F. A., & Scheytt, T. (2012). Hydrochemistry of surface water and groundwater from a fractured carbonate aquifer in the Helwan area, Egypt. *Journal of Earth System Science*, 121(1), 109-124.

Abulude, F., Ndamitso, M. M., & Abdulkadir, A. (2018). Environmental situation of an agricultural area in Akure, Nigeria, based on physico-chemical properties of rainwater. *Pollution*, *4*(2), 317-325.

Adame, M. F., Fry, B., & Bunn, S. E. (2016). Water isotope characteristics of a flood: Brisbane River, Australia. *Hydrological Processes*, *30*(13), 2033-2041.

Afram, A., Janabi-Sharifi, F., Fung, A. S., & Raahemifar, K. (2017). Artificial neural network (ANN) based model predictive control (MPC) and optimization of HVAC systems: A state of the art review and case study of a residential HVAC system. *Energy and Buildings*, *141*, 96-113.

Agarwal, A., & Singh, R. D. (2004). Runoff modelling through back propagation artificial neural network with variable rainfall-runoff data. *Water Resources Management*, *18*(3), 285-300.

Aggarwal, P. K., Romatschke, U., Araguas-Araguas, L., Belachew, D., Longstaffe, F. J., Berg, P., ... & Funk, A. (2016). Proportions of convective and stratiform precipitation revealed in water isotope ratios. *Nature Geoscience*, *9*(8), 624.

Aghazadeh, N., & Mogaddam, A. A. (2010). Assessment of groundwater quality and its suitability for drinking and agricultural uses in the Oshnavieh area, Northwest of Iran. *Journal of Environmental Protection*, *1*(01), 30.

Ahmad, I., Tang, D., Wang, T., Wang, M., & Wagan, B. (2015). Precipitation trends over time using Mann-Kendall and spearman's rho tests in swat river basin, Pakistan. *Advances in Meteorology*, *2015*.

Ahmat Nor, N. I. B. (2005). *Rainfall runoff modelling using Artificial Neural network method* (Doctoral dissertation, Universiti Teknologi Malaysia (Malaysia))

Aichouri, I., Hani, A., Bougherira, N., Djabri, L., Chaffai, H., & Lallahem, S. (2015). River flow model using artificial neural networks. *Energy Procedia*, *74*, 1007-1014.

Akoto, O., Darko, G., & Nkansah, M. A. (2011). Chemical composition of rainwater over a mining area in Ghana. *International Journal of Environmental Research*, *5*(4), 847-854.

Akpan, A. O., Udosen, E. D., & Offiong, N. A. O. (2018). Rainwater chemistry within the vicinity of Qua Iboe estuary, Nigeria. *CLEAN–Soil, Air, Water*, *46*(3), 1700114.

Al Charideh, A. R., & Abou Zakhem, B. (2010). Distribution of tritium and stable isotopes in precipitation in Syria. *Hydrological sciences journal*, *55*(5), 832-843.

Al Mamoon, A., & Rahman, A. (2017). Rainfall in Qatar: Is it changing?. *Natural Hazards*, *85*(1), 453-470.

Al Obaidy, A. H. M. J., & Joshi, H. (2006). Chemical composition of rainwater in a tropical urban area of northern India. *Atmospheric Environment*, *40*(35), 6886-6891.

Al, T. A., Martin, C. J., & Blowes, D. W. (2000). Carbonate-mineral/water interactions in sulfide-rich mine tailings. *Geochimica et Cosmochimica Acta*, *64*(23), 3933-3948.

Aldrian, E., & Djamil, Y. S. (2008). Spatio-temporal climatic change of rainfall in East Java Indonesia. *International Journal of Climatology: A Journal of the Royal Meteorological Society*, *28*(4), 435-448.

Ali, S. M., Mahdi, A. S., & Shaban, A. H. (2012). Wind speed estimation for Iraq using several spatial interpolation methods. *Environmental Protection*, *1*, 2.

Alippi, C. (2002). Selecting accurate, robust, and minimal feedforward neural networks. *IEEE Transactions on Circuits and Systems I: Fundamental Theory and Applications*, *49*(12), 1799-1810.

Alizadeh, M. J., Kavianpour, M. R., Kisi, O., & Nourani, V. (2017). A new approach for simulating and forecasting the rainfall-runoff process within the next two months. *Journal of Hydrology*, *548*, 588-597.

Al-Khashman, O. A. (2009). Chemical characteristics of rainwater collected at a western site of Jordan. *Atmospheric Research*, *91*(1), 53-61.

Al-Khashman, O. A., Jaradat, A. Q., & Salameh, E. (2013). Five-year monitoring study of chemical characteristics of wet atmospheric precipitation in the southern region of Jordan. *Environmental Monitoring and Assessment*, *185*(7), 5715-5727.

Al-Omran, A. M., Mousa, M. A., AlHarbi, M. M., & Nadeem, M. E. (2018). Hydrogeochemical characterization and groundwater quality assessment in Al-Hasa, Saudi Arabia. *Arabian Journal of Geosciences*, *11*(4), 79.

Altman, D. G. (1990). *Practical statistics for medical research*. United States of America: CRC press.

Ameli, A. A., & Creed, I. F. (2017). Quantifying hydrologic connectivity of wetlands to surface water systems. *Hydrology & Earth System Sciences*, *21*(3).

American Public Health Association (APHA) (1995). *Standard methods for the examination of water and waste water*, 19th ed. APHA, Washington DC, USASS.

American Public Health Association (APHA) (2012). *Standard methods for the examination of water and waste water.* 22nd ed. APHA, American Water Works Association, Water Environment Federation

Anctil, F., & Rat, A. (2005). Evaluation of neural network streamflow forecasting on 47 watersheds. *Journal of Hydrologic Engineering*, *10*(1), 85-88.

André, F., Jonard, M., & Ponette, Q. (2007). Influence of meteorological factors and polluting environment on rain chemistry and wet deposition in a rural area near Chimay, Belgium. *Atmospheric Environment*, *41*(7), 1426-1439.

Anil, I., Alagha, O., & Karaca, F. (2017). Effects of transport patterns on chemical composition of sequential rain samples: trajectory clustering and principal component analysis approach. *Air Quality, Atmosphere & Health*, *10*(10), 1193-1206.

Antar, M. A., Elassiouti, I., & Allam, M. N. (2006). Rainfall-runoff modelling using artificial neural networks technique: a Blue Nile catchment case study. *Hydrological Processes: An International Journal*, *20*(5), 1201-1216.

Apaydin, H., Sonmez, F. K., & Yildirim, Y. E. (2004). Spatial interpolation techniques for climate data in the GAP region in Turkey. *Climate Research*, *28*(1), 31-40.

Araghi, A., Martinez, C. J., Adamowski, J., & Olesen, J. E. (2018). Spatiotemporal variations of aridity in Iran using high-resolution gridded data. *International Journal of Climatology*, *38*(6), 2701-2717.

Asare-Donkor, N. K., Kwaansa-Ansah, E. E., Opoku, F., & Adimado, A. A. (2015). Concentrations, hydrochemistry and risk evaluation of selected heavy metals along the Jimi River and its tributaries at Obuasi a mining enclave in Ghana. *Environmental Systems Research*, *4*(1), 12.

Asare-Donkor, N. K., Ofosu, J. O., & Adimado, A. A. (2018). Hydrochemical characteristics of surface water and ecological risk assessment of sediments from settlements within the Birim River basin in Ghana. *Environmental Systems Research*, 7(1), 9.

Asfaw, A., Simane, B., Hassen, A., & Bantider, A. (2018). Variability and time series trend analysis of rainfall and temperature in northcentral Ethiopia: A case study in Woleka sub-basin. *Weather and Climate Extremes*, *19*, 29-41.

Asikoglu, O. L., & Ciftlik, D. (2015). Recent rainfall trends in the Aegean region of Turkey. *Journal of Hydrometeorology*, *16*(4), 1873-1885.

Asnani, G. C. (1993). Tropical meteorology, vol. 1. *Indian Institute of Tropical Meteorology, Pune, India*. p.1202.

Awad, M. A., El Arabi, N. E., & Hamza, M. S. (1997). Use of Solute Chemistry and Isotopes to Identify Sources of Ground-Water Recharge in the Nile Aquifer System, Upper Egypt. *Groundwater*, *35*(2), 223-228.

Báez, A., Belmont, R., García, R., Padilla, H., & Torres, M. D. C. (2007). Chemical composition of rainwater collected at a southwest site of Mexico City, Mexico. *Atmospheric Research*, *86*(1), 61-75.

Baig, M. A. A., Mallikarjuna, P., & Krishna Reddy, T. V. (2008). Rainfall-runoff modelling: a case study. *ISH Journal of Hydraulic Engineering*, *14*(2), 18-35.

Bakalowicz, M. (1994). Water geochemistry: water quality and dynamics. *Groundwater Ecology*, *1*, 97.

Baltas, E. A. (2016). Variability analysis of hydrometeorological parameters under a climate change scenario in Northern Greece. *International Journal of Global Environmental Issues*, *15*(1-2), 70-80.

Barakat, A., El Baghdadi, M., Rais, J., Aghezzaf, B., & Slassi, M. (2016). Assessment of spatial and seasonal water quality variation of Oum Er Rbia River (Morocco) using multivariate statistical techniques. *International Soil and Water Conservation Research*, *4*(4), 284-292.

Barnett, T., Malone, R., Pennell, W., Stammer, D., Semtner, B., & Washington, W. (2004). The effects of climate change on water resources in the west: introduction and overview. *Climatic Change*, *62*(1-3), 1-11.

Barzegar, R., Moghaddam, A. A., & Tziritis, E. (2016). Assessing the hydrogeochemistry and water quality of the Aji-Chay River, northwest of Iran. *Environmental Earth Sciences*, *75*(23), 1486.

Başak, B., & Alagha, O. (2004). The chemical composition of rainwater over Büyükçekmece Lake, Istanbul. *Atmospheric Research*, *71*(4), 275-288.

Bavil, S. S., Zeinalzadeh, K., & Hessari, B. (2018). The changes in the frequency of daily precipitation in Urmia Lake basin, Iran. *Theoretical and Applied Climatology*, *133*(1-2), 205-214.

Belkhiri, L., Boudoukha, A., & Mouni, L. (2011). A multivariate statistical analysis of groundwater chemistry data. *International Journal of Environmental Research*, *5*(2), 537-544.

Belle, G., & Hughes, J. P. (1984). Nonparametric tests for trend in water quality. *Water Resources Research*, *20*(1), 127-136.

Benestad, R. E. (2013). Association between trends in daily rainfall percentiles and the global mean temperature. *Journal of Geophysical Research: Atmospheres*, *118*(19), 10-802.

Bergamaschi, P., Brenninkmeijer, C. A. M., Hahn, M., Röckmann, T., Scharffe, D. H., Crutzen, P. J., ... & Worthy, D. E. J. (1998). Isotope analysis based source identification for atmospheric CH4 and CO sampled across Russia using the Trans-Siberian railroad. *Journal of Geophysical Research: Atmospheres*, *103*(D7), 8227-8235.

Berhe, B. A., Dokuz, U. E., & Çelik, M. (2017). Assessment of hydrogeochemistry and environmental isotopes of surface and groundwaters in the Kütahya Plain, Turkey. *Journal of African Earth Sciences*, 134, 230-240.

Besaw, L. E., Rizzo, D. M., Bierman, P. R., & Hackett, W. R. (2010). Advances in ungauged streamflow prediction using artificial neural networks. *Journal of Hydrology*, *386*(1-4), 27-37.

Beysens, D., Mongruel, A., & Acker, K. (2017). Urban dew and rain in Paris, France: Occurrence and physico-chemical characteristics. *Atmospheric research*, *189*, 152-161.

Bhutiyani, M. R., Kale, V. S., & Pawar, N. J. (2010). Climate change and the precipitation variations in the northwestern Himalaya: 1866–2006. *International Journal of Climatology: A Journal of the Royal Meteorological Society*, *30*(4), 535-548.

Bischof, H., & Leonardis, A. (1998). Finding optimal neural networks for land use classification. *IEEE transactions on Geoscience and Remote Sensing*, *36*(1), 337-341.

Blum, J. D., Gazis, C. A., Jacobson, A. D., & Page Chamberlain, C. (1998). Carbonate versus silicate weathering in the Raikhot watershed within the high Himalayan Crystalline Series. *Geology*, *26*(5), 411-414.

Boé, J., & Terray, L. (2008). Uncertainties in summer evapotranspiration changes over Europe and implications for regional climate change. *Geophysical Research Letters*, *35*(5).

Boggs, D. A., Boggs, G. S., Knott, B., & Eliot, I. (2007). The hydrology and hydrochemistry of six small playas in the Yarra Yarra drainage system of Western Australia. *Journal of the Royal Society of Western Australia*, *90*, 15.

Bordalo, A. A., Nilsumranchit, W., & Chalermwat, K. (2001). Water quality and uses of the Bangpakong River (Eastern Thailand). *Water Research*, *35*(15), 3635-3642.

Borhanazad, H., Mekhilef, S., Saidur, R., & Boroumandjazi, G. (2013). Potential application of renewable energy for rural electrification in Malaysia. *Renewable Energy*, *59*, 210-219.

Boubel, R. W., Fox, D. L., Turner, D. B., & Stern, A. C. (1994). Fundamentals of air pollution. United States: Academic Press.

Bowser, C. J., & Jones, B. F. (2002). Mineralogic controls on the composition of natural waters dominated by silicate hydrolysis. *American Journal of Science*, *302*(7), 582-662.

Brady, N. C., & Weil, R. R. (2008). The soils around us. *The Nature and Properties of Soils, 14th ed.* New Jersey and Ohio: Pearson Prentice Hall, 1-31.

Brahim, Y. A., Bouchaou, L., Sifeddine, A., Khodri, M., Reichert, B., & Cruz, F. W. (2016). Elucidating the climate and topographic controls on stable isotope composition of meteoric waters in Morocco, using station-based and spatially-interpolated data. *Journal of Hydrology*, *543*, 305-315.

Brath, A., Montanari, A., & Toth, E. (2004). Analysis of the effects of different scenarios of historical data availability on the calibration of a spatially-distributed hydrological model. *Journal of Hydrology*, 291(3-4), 232-253.

Breitenbach, S. F., Adkins, J. F., Meyer, H., Marwan, N., Kumar, K. K., & Haug, G. H. (2010). Strong influence of water vapor source dynamics on stable isotopes in precipitation observed in Southern Meghalaya, NE India. *Earth and Planetary Science Letters*, *292*(1-2), 212-220.

Brocca, L., Liersch, S., Melone, F., Moramarco, T., & Volk, M. (2013). Application of a model-based rainfall-runoff database as efficient tool for flood risk management. *Hydrology and Earth System Sciences*, *17*(8), 3159-3169.

Brown, C. (1998). *Applied multivariate statistics in geohydrology and related sciences*. New York: Springer.

Buckney, R. T., & Tyler, P. A. (1973). Chemistry of Tasmanian inland waters. *Internationale Revue der Gesamten Hydrobiologie und Hydrographie*, *58*(1), 61-78.

Burrough, P. A., & McDonnell, R. A. (1998). *Principles of Geographic Information Systems. UK. Oxford University Press, Oxford.*

Burford, J. E., Déry, S. J., & Holmes, R. D. (2009). Some aspects of the hydroclimatology of the Quesnel River Basin, British Columbia, Canada. *Hydrological Processes: An International Journal*, *23*(10), 1529-1536.

Burnik Šturm, M., Ganbaatar, O., Voigt, C. C., & Kaczensky, P. (2017). First field-based observations of $\delta^{2}H$ and $\delta^{18}O$ values of event-based precipitation, rivers and other water bodies in the Dzungarian Gobi, SW Mongolia. *Isotopes in Environmental and Health Studies*, *53*(2), 157-171.

Calabrese, F., Van Der Doelen, R. H., Guidotti, G., Racagni, G., Kozicz, T., Homberg, J. R., & Riva, M. A. (2015). Exposure to early life stress regulates Bdnf expression in SERT mutant rats in an anatomically selective fashion. *Journal of Neurochemistry*, *132*(1), 146-154.

Caldera, H. P. G. M., Piyathisse, V. R. P. C., & Nandalal, K. D. W. (2016). A comparison of methods of estimating missing daily rainfall data. *Engineer: Journal of the Institution of Engineers, Sri Lanka*, *49*(4).

Caloiero, T. (2015). Analysis of rainfall trend in New Zealand. *Environmental Earth Sciences*, *73*(10), 6297-6310.

Caloiero, T., Coscarelli, R., & Ferrari, E. (2018). Application of the innovative trend analysis method for the trend analysis of rainfall anomalies in southern Italy. *Water Resources Management*, *32*(15), 4971-4983.

Caloiero, T., Coscarelli, R., Ferrari, E., & Mancini, M. (2011). Trend detection of annual and seasonal rainfall in Calabria (Southern Italy). *International Journal of Climatology*, *31*(1), 44-56.

Cannas, B., Fanni, A., See, L., & Sias, G. (2006). Data preprocessing for river flow forecasting using neural networks: wavelet transforms and data partitioning. *Physics and Chemistry of the Earth, Parts A/B/C*, *31*(18), 1164-1171.

Carroll, D. (1962). *Rainwater as a chemical agent of geologic processes: a review*. Washington: US Government Printing Office.

Cerqueira, M. R. F., Pinto, M. F., Derossi, I. N., Esteves, W. T., Santos, M. D. R., Matos, M. A. C., ... & Matos, R. C. (2014). Chemical characteristics of rainwater at a southeastern site of Brazil. *Atmospheric Pollution Research*, *5*(2), 253-261.

Chahine, M. T. (1992). The hydrological cycle and its influence on climate. *Nature*, *359*(6394), 373- 380.

Chakraborty, S., Sinha, N., Chattopadhyay, R., Sengupta, S., Mohan, P. M., & Datye, A. (2016). Atmospheric controls on the precipitation isotopes over the Andaman Islands, Bay of Bengal. *Scientific Reports*, *6*, 19555.

Chakravarti, A., & Jain, M. K. (2014). Experimental investigation and modeling of rainfall runoff process. *Indian Journal of Science and Technology*, *7*(12), 2096.

Chaouche, K., Neppel, L., Dieulin, C., Pujol, N., Ladouche, B., Martin, E., ... & Caballero, Y. (2010). Analyses of precipitation, temperature and evapotranspiration in a French Mediterranean region in the context of climate change. *Comptes Rendus Geoscience*, *342*(3), 234-243.

Chattopadhyay, S., & Edwards, D. (2016). Long-term trend analysis of precipitation and air temperature for Kentucky, United States. *Climate*, *4*(1), 10.

Che Ros, F., Tosaka, H., Sidek, L. M., & Basri, H. (2016). Homogeneity and trends in long-term rainfall data, Kelantan River Basin, Malaysia. *International Journal of River Basin Management*, *14*(2), 151-163.

Chen, C. A., Long, S. M., & Rosli, N. M. (2012). Spatial distribution of tropical estuarine nematode communities in Sarawak, Malaysia (Borneo). *Raffles Bulletin of Zoology*, 60(1). 173–181.

Chen, F. W., & Liu, C. W. (2012). Estimation of the spatial rainfall distribution using inverse distance weighting (IDW) in the middle of Taiwan. *Paddy and Water Environment*, *10*(3), 209-222.

Chen, S. (2016). Rural Electrification in Sarawak, Malaysia: Potential & Challenges for Mini-Hydro & Solar Hybrid Solutions. https://www.eclareon.com/sites/default/files/Presentations/04_chen_shiun.pdf. Acceded on 05/10/2018.

Cheng, M. C., You, C. F., Lin, F. J., Huang, K. F., & Chung, C. H. (2011). Sources of Cu, Zn, Cd and Pb in rainwater at a subtropical islet offshore northern Taiwan. *Atmospheric Environment*, *45*(11), 1919-1928.

Chetelat, B., Liu, C. Q., Zhao, Z. Q., Wang, Q. L., Li, S. L., Li, J., & Wang, B. L. (2008). Geochemistry of the dissolved load of the Changjiang Basin rivers: anthropogenic impacts and chemical weathering. *Geochimica et Cosmochimica Acta*, *72*(17), 4254-4277.

Chidambaram, S., Prasanna, M. V., Karmegam, U., Singaraja, C., Pethaperumal, S., Manivannan, R., ... & Tirumalesh, K. (2011). Significance of pCO 2 values in determining carbonate chemistry in groundwater of Pondicherry region, India. *Frontiers of Earth Science*, *5*(2), 197.

Chidambaram, S., Prasanna, M. V., Ramanathan, A. L., Vasu, K., Hameed, S., Warrier, U. K., ... & Johnsonbabu, G. (2009). A study on the factors affecting the stable isotopic composition in precipitation of Tamil Nadu, India. *Hydrological Processes: An International Journal*, *23*(12), 1792-1800.

Chidambaram, S., Prasanna, M. V., Singaraja, C., Thilagavathi, R., Pethaperumal, S., & Tirumalesh, K. (2012). Study on the saturation index of the carbonates in the groundwater using WATEQ4F, in layered coastal aquifers of Pondicherry. *Journal of the Geological Society of India*, *80*(6), 813-824.

Chiew, F. H. S., Teng, J., Vaze, J., Post, D. A., Perraud, J. M., Kirono, D. G. C., & Viney, N. R. (2009). Estimating climate change impact on runoff across southeast Australia: Method, results, and implications of the modeling method. *Water Resources Research*, *45*(10).

Chigor, V. N., Umoh, V. J., Okuofu, C. A., Ameh, J. B., Igbinosa, E. O., & Okoh, A. I. (2012). Water quality assessment: surface water sources used for drinking and irrigation in Zaria, Nigeria are a public health hazard. *Environmental Monitoring and Assessment*, *184*(5), 3389-3400.

Chon, K., Kim, Y., Bae, D. H., & Cho, J. (2015). Confirming anthropogenic influences on the major organic and inorganic constituents of rainwater in an urban area. *Drinking Water Engineering and Science*, *8*(2), 35-48.

Christner, E., Aemisegger, F., Pfahl, S., Werner, M., Cauquoin, A., Schneider, M., ... & Schädler, G. (2018). The Climatological Impacts of Continental Surface Evaporation, Rainout, and Subcloud Processes on δD of Water Vapor and Precipitation in Europe. *Journal of Geophysical Research: Atmospheres*, *123*(8), 4390-4409.

Chughtai, M., Mustafa, S., & Mumtaz, M. (2014). Study of physicochemical parameters of rainwater: A case study of Karachi, Pakistan. *American Journal of Analytical Chemistry*, *5*(04), 235.

Chung, S. Y., Venkatramanan, S., Park, N., Ramkumar, T., Sujitha, S. B., & Jonathan, M. P. (2016). Evaluation of physico-chemical parameters in water and total heavy metals in sediments at Nakdong River Basin, Korea. *Environmental Earth Sciences*, *75*(1), 50.

Cigizoglu, H. K. (2008). Artificial neural networks in water resources. In *Integration of Information for Environmental Security*, 115-148. Springer, Dordrecht.

Clark, I. D., & Fritz, P. (1997). *Environmental Isotopes in Hydrogeology*. United States of America: CRC Press.

Cobaner, M., Unal, B., & Kisi, O. (2009). Suspended sediment concentration estimation by an adaptive neuro-fuzzy and neural network approaches using hydro-meteorological data. *Journal of Hydrology*, *367*(1-2), 52-61.

Cobbina, S. J., Michael, K., Salifu, L., & Duwiejua, A. B. (2013). Rainwater quality assessment in the Tamale municipality. *International Journal of Scientific and Technological Research*, *2*, 1-10.

Comas-Bru, L., McDermott, F., & Werner, M. (2016). The effect of the East Atlantic pattern on the precipitation δ^{18}O-NAO relationship in Europe. *Climate Dynamics*, *47*(7-8), 2059-2069.

Coplen, T. B. (1994). Reporting of stable hydrogen, carbon, and oxygen isotopic abundances (technical report). *Pure and Applied Chemistry*, *66*(2), 273-276.

Craig, H. (1961). Isotopic variation in meteoric waters. *Science*, *133*, 1833-1834.

Crawford, J., Hollins, S. E., Meredith, K. T., & Hughes, C. E. (2017). Precipitation stable isotope variability and subcloud evaporation processes in a semi-arid region. *Hydrological Processes*, *31*(1), 20-34.

Crisci, A., Gozzini, B., Meneguzzo, F., Pagliara, S., & Maracchi, G. (2002). Extreme rainfall in a changing climate: regional analysis and hydrological implications in Tuscany. *Hydrological Processes*, *16*(6), 1261-1274.

Cui, B. L., & Li, X. Y. (2015). Stable isotopes reveal sources of precipitation in the Qinghai Lake Basin of the northeastern Tibetan Plateau. *Science of the Total Environment*, *527*, 26-37.

Dai, S., Shulski, M. D., Hubbard, K. G., & Takle, E. S. (2016). A spatiotemporal analysis of Midwest US temperature and precipitation trends during the growing season from 1980 to 2013. *International Journal of Climatology*, *36*(1), 517-525.

Daliakopoulos, I. N., & Tsanis, I. K. (2016). Comparison of an artificial neural network and a conceptual rainfall–runoff model in the simulation of ephemeral streamflow. *Hydrological Sciences Journal*, *61*(15), 2763-2774.

Dansgaard, W. (1964). Stable isotopes in precipitation. *Tellus*, *16*(4), 436-468.

Darbandi, S., & Pourhosseini, F. A. (2018). River flow simulation using a multilayer perceptron-firefly algorithm model. *Applied Water Science*, *8*(3), 85.

Datta, P. S., Tyagi, S. K., & Chandrasekharan, H. (1991). Factors controlling stable isotope composition of rainfall in New Delhi, India. *Journal of Hydrology*, *128*(1-4), 223-236.

Davie, T. (2008). *Fundamentals of hydrology*. London: Routledge.

Dawood, M. (2017). Spatio-statistical analysis of temperature fluctuation using Mann–Kendall and Sen's slope approach. *Climate Dynamics*, *48*(3-4), 783-797.

Dawson, C. W., & Wilby, R. L. (2001). Hydrological modelling using artificial neural networks. *Progress in Physical Geography*, *25*(1), 80-108.

De Jongh, I. L., Verhoest, N. E., & De Troch, F. P. (2006). Analysis of a 105-year time series of precipitation observed at Uccle, Belgium. *International Journal of Climatology*, *26*(14), 2023-2039.

De Luis, M., Raventós, J., González-Hidalgo, J. C., Sánchez, J. R., & Cortina, J. (2000). Spatial analysis of rainfall trends in the region of Valencia (East Spain). *International Journal of Climatology*, *20*(12), 1451-1469.

De Mello, W. Z. (2001). Precipitation chemistry in the coast of the Metropolitan Region of Rio de Janeiro, Brazil. *Environmental Pollution*, *114*(2), 235-242.

de Mello, W. Z., & de Almeida, M. D. (2004). Rainwater chemistry at the summit and southern flank of the Itatiaia massif, Southeastern Brazil. *Environmental Pollution*, *129*(1), 63-68.

de Rooij, S. (2008). *Minimum Description Length Model Selection* (Doctoral dissertation, University of Amsterdam (Amsterdam)).

De Silva, R. P., Dayawansa, N. D. K., & Ratnasiri, M. D. (2007). A comparison of methods used in estimating missing rainfall data. *Journal of Agricultural Sciences*, *3*(2).

de Souza, E. L., Galvão, P., de Almeida, R., Pinheiro, C., Baessa, M., & Cabral, M. (2015). Stable Isotopes Studies in the Urucu Oil Province, Amazon Region, Brazil. *Journal of Water Resource and Protection*, *7*(03), 131.

Delpla, I., Jung, A. V., Baures, E., Clement, M., & Thomas, O. (2009). Impacts of climate change on surface water quality in relation to drinking water production. *Environment International*, *35*(8), 1225-1233.

Demirak, A., Yilmaz, F., Tuna, A. L., & Ozdemir, N. (2006). Heavy metals in water, sediment and tissues of Leuciscus cephalus from a stream in southwestern Turkey. *Chemosphere*, *63*(9), 1451-1458.

Demuth, H., & Beale, M. (1998). *MATLAB: The Language of Technical Computing; Neutral Network Toolbox; User's Guide; Version 3*. MathWorks.

Deutsch, W. J., Jenne, E. A., & Krupka, K. M. (1982). Solubility equilibria in basalt aquifers: the Columbia Plateau, eastern Washington, USA. *Chemical Geology*, *36*(1-2), 15-34.

Dibike, Y. B., & Solomatine, D. P. (2001). River flow forecasting using artificial neural networks. *Physics and Chemistry of the Earth, Part B: Hydrology, Oceans and Atmosphere*, *26*(1), 1-7.

DID (2015). The Sarawak Hydrological Yearbook 2015. 42 Department of Irrigation & Drainage, Sarawak.

Dinka, M. O., Loiskandl, W., & Ndambuki, J. M. (2015). Hydrochemical characterization of various surface water and groundwater resources available in Matahara areas, Fantalle Woreda of Oromiya region. *Journal of Hydrology: Regional Studies*, *3*, 444-456.

DoA (1972). Soil map of Sarawak (1:50,000 scale). Published by the *Department of Agriculture*, Sarawak, Malaysia.

Dominique, J. F., Roozendaal, B., & McGaugh, J. L. (1998). Stress and glucocorticoids impair retrieval of long-term spatial memory. *Nature*, *394*(6695), 787.

Doneen, L. D. (1964). *Notes on water quality in agriculture*. Department of Water Science and Engineering, University of California, Davis.

Dragićević, S., Ghirardelli, E., & Ranzi, R. (2018). Hydrometeorological monitoring in west Morava river basin (Serbia). *Editura Politehnica 2018*, 67.

Dragun, Z., Roje, V., Mikac, N., & Raspor, B. (2009). Preliminary assessment of total dissolved trace metal concentrations in Sava River water. *Environmental Monitoring and Assessment*, *159*(1-4), 99.

Drever, J. I. (1988). *The geochemistry of natural waters* (Vol. 437). Englewood Cliffs: Prentice Hall.

Eaton, F. M. (1950). Significance of carbonates in irrigation waters. *Soil Science*, *69*(2), 123-134.

Ehhalt, D., Knott, K., Nagel, J. F., & Vogel, J. C. (1963). Deuterium and oxygen 18 in rain water. *Journal of Geophysical Research*, *68*(13), 3775-3780.

Elganiny, M. A., & Eldwer, A. E. (2018). Enhancing the forecasting of monthly streamflow in the main key stations of the river Nile Basin. *Water Resources*, *45*(5), 660-671.

England, A. H., Duffin, A. M., Schwartz, C. P., Uejio, J. S., Prendergast, D., & Saykally, R. J. (2011). On the hydration and hydrolysis of carbon dioxide. *Chemical Physics Letters*, *514*(4-6), 187-195.

Engström, J., & Waylen, P. (2017). The changing hydroclimatology of Southeastern US. *Journal of Hydrology*, *548*, 16-23.

Espinosa, A. J. F., Rodríguez, M. T., & Álvarez, F. F. (2004). Source characterisation of fine urban particles by multivariate analysis of trace metals speciation. *Atmospheric Environment*, *38*(6), 873-886.

Essington, M. E. (2015). *Soil and water chemistry: an integrative approach*. United States of America: CRC press.

Etteieb, S., Cherif, S., & Tarhouni, J. (2017). Hydrochemical assessment of water quality for irrigation: a case study of the Medjerda River in Tunisia. *Applied Water Science*, *7*(1), 469-480.

Eymen, A., & Köylü, Ü. (2018). Seasonal trend analysis and ARIMA modeling of relative humidity and wind speed time series around Yamula Dam. *Meteorology and Atmospheric Physics*, 1-12.

Fadiran, A. O., Dlamini, S. C., & Mavuso, A. (2008). A comparative study of the phosphate levels in some surface and ground water bodiesof Swaziland. *Bulletin of the Chemical Society of Ethiopia*, *22*(2).

Farahmandkia, Z., Mehrasbi, M. R., & Sekhavatjou, M. S. (2010). Relationship between concentrations of heavy metals in wet precipitation and atmospheric pm10> particles in Zanjan, Iran. *Iranian Journal of Environmental Health, Science and Engineering*, *8*(1), 49-56.

Fathian, F., Dehghan, Z., Bazrkar, M. H., & Eslamian, S. (2016). Trends in hydrological and climatic variables affected by four variations of the Mann-Kendall approach in Urmia Lake basin, Iran. *Hydrological Sciences Journal*, *61*(5), 892-904.

Fathian, F., Morid, S., & Kahya, E. (2015). Identification of trends in hydrological and climatic variables in Urmia Lake basin, Iran. *Theoretical and Applied Climatology*, *119*(3-4), 443-464.

Fatichi, S., & Caporali, E. (2009). A comprehensive analysis of changes in precipitation regime in Tuscany. *International Journal of Climatology: A Journal of the Royal Meteorological Society*, *29*(13), 1883-1893.

Feng, F., Feng, Q., Liu, X., Wu, J., & Liu, W. (2017). Stable isotopes in precipitation and atmospheric moisture of Pailugou Catchment in northwestern China' s Qilian Mountains. *Chinese Geographical Science*, *27*(1), 97-109.

Fischer, B. M., van Meerveld, H. I., & Seibert, J. (2017). Spatial variability in the isotopic composition of rainfall in a small headwater catchment and its effect on hydrograph separation. *Journal of Hydrology*, *547*, 755-769.

Fisher, D. W. (1967). *Annual variations in chemical composition of atmospheric precipitation, eastern North Carolina and southeastern Virginia* (No. 1535-M). Washington: US Government Printing Office.

Forti, M. C., Melfi, A. J., Astolfo, R., & Fostier, A. H. (2000). Rainfall chemistry composition in two ecosystems in the northeastern Brazilian Amazon (Amapá State). *Journal of Geophysical Research: Atmospheres*, *105*(D23), 28895-28905.

Frazier, A. G., & Giambelluca, T. W. (2017). Spatial trend analysis of Hawaiian rainfall from 1920 to 2012. *International Journal of Climatology*, *37*(5), 2522-2531.

Fuller, M., Ali, J. R., Moss, S. J., Frost, G. M., Richter, B., & Mahfi, A. (1999). Paleomagnetism of Borneo. *Journal of Asian Earth Sciences*, *17*(1-2), 3-24.

Gaagai, A., Boudoukha, A., Boumezbeur, A., & Benaabidate, L. (2017). Hydrochemical characterization of surface water in the Babar watershed (Algeria) using environmetric techniques and time series analysis. *International Journal of River Basin Management*, *15*(3), 361-372.

Gallant, S. I., (1993). *Neural network learning and expert systems*. United States of America: MIT press.

Galloway, J. N., Likens, G. E., Keene, W. C., & Miller, J. M. (1982). The composition of precipitation in remote areas of the world. *Journal of Geophysical Research: Oceans*, *87*(C11), 8771-8786.

Galton, F. (1889). *Natural inheritance*. London: Macmillan.

Gandaseca, S., Rosli, N., Ngayop, J., & Arianto, C. I. (2011). Status of water quality based on the physico-chemical assessment on river water at Wildlife Sanctuary Sibuti Mangrove Forest, Miri Sarawak. *American Journal of Environmental Sciences*, *7*(3), 269.

Gandaseca, S., Rosli, N., Pazi, A. M. M., & Arianto, C. I. (2014). Effects of land use on river water quality of Awat-Awat Lawas Mangrove Forest Limbang Sarawak Malaysia. *International Journal of Physical Sciences*, *9*(17), 386-396.

Gao, J., He, Y., Masson-Delmotte, V., & Yao, T. (2018). ENSO effects on annual variations of summer precipitation stable isotopes in Lhasa, southern Tibetan Plateau. *Journal of Climate*, *31*(3), 1173-1182.

Gao, X. M., Ovaska, S. J., Lehtokangas, M., & Saarinen, J. (1998). Modeling of speech signals using an optimal neural network structure based on the PMDL principle. *IEEE Transactions on Speech and Audio Processing*, *6*(2), 177-180.

Gao, Z., He, J., Dong, K., & Li, X. (2017). Trends in reference evapotranspiration and their causative factors in the West Liao River basin, China. *Agricultural and Forest Meteorology*, *232*, 106-117.

Garrels, R. M., & Christ, C. L. (1965). Solutions, minerals and equilibria. New York: Harpers Geoscience Series, Harper & Row.

Gat, J. (2010). *Isotope hydrology: a study of the water cycle* (Vol. 6). Singapore: World Scientific.

Gat, J. R. (1995). Stable isotopes of fresh and saline lakes. In *Physics and chemistry of lakes,* 139-165. Springer, Berlin, Heidelberg.

Gat, J. R., & Carmi, I. (1970). Evolution of the isotopic composition of atmospheric waters in the Mediterranean Sea area. *Journal of Geophysical Research*, *75*(15), 3039-3048.

Gat, J. R., & Dansgaard, W. (1972). Stable isotope survey of the fresh water occurrences in Israel and the northern Jordan Rift Valley. *Journal of Hydrology*, *16*(3), 177-211.

Gat, J. R., & Gonfiantini, R. (1981). *Stable isotope hydrology. Deuterium and oxygen-18 in the water cycle*. Vienna: IAEA.

Gautam, A. S., Negi, R. S., Singh, S., Srivastava, A. K., Tiwari, S., & Bisht, D. S. (2018). Chemical characteristics of atmospheric aerosol at Alaknanda Valley (Srinagar) in the Central Himalaya Region, India. *International Journal of Environmental Research*, *12*(5), 681-691.

Gautam, M. K., Lee, K. S., Bong, Y. S., Song, B. Y., & Ryu, J. S. (2017). Oxygen and hydrogen isotopic characterization of rainfall and throughfall in four South Korean cool temperate forests. *Hydrological Sciences Journal*, *62*(12), 2025-2034.

Gautam, M. R., Acharya, K., & Tuladhar, M. K. (2010). Upward trend of streamflow and precipitation in a small, non-snow-fed, mountainous watershed in Nepal. *Journal of Hydrology*, *387*(3-4), 304-311.

Gauthier, T. D. (2001). Detecting trends using Spearman's rank correlation coefficient. *Environmental Forensics*, *2*(4), 359-362.

Gedefaw, M., Yan, D., Wang, H., Qin, T., Girma, A., Abiyu, A., & Batsuren, D. (2018). Innovative trend analysis of annual and seasonal rainfall variability in Amhara Regional State, Ethiopia. *Atmosphere*, *9*(9), 326.

Geisseler, D., Horwath, W. R., Joergensen, R. G., & Ludwig, B. (2010). Pathways of nitrogen utilization by soil microorganisms–a review. *Soil Biology and Biochemistry*, *42*(12), 2058-2067.

Ghadimi, F., Ghomi, M., Ranjbar, M., & Hajati, A. (2013). Sources of contamination in rainwater by major and heavy elements in Arak, Iran. *Journal of Water Sciences, Research,* 5(2), 67 – 82.

Ghorbani, M. A., Zadeh, H. A., Isazadeh, M., & Terzi, O. (2016). A comparative study of artificial neural network (MLP, RBF) and support vector machine models for river flow prediction. *Environmental Earth Sciences*, *75*(6), 476.

Ghosh, S., Luniya, V., & Gupta, A. (2009). Trend analysis of Indian summer monsoon rainfall at different spatial scales. *Atmospheric Science Letters*, *10*(4), 285-290.

Gibbs, R. J. (1970). Mechanisms controlling world water chemistry. *Science*, *170*(3962), 1088-1090.

Gilbert, R. O. (1987). *Statistical methods for environmental pollution monitoring*. United states of America: John Wiley & Sons.

Gioda, A., Mayol-Bracero, O. L., Scatena, F. N., Weathers, K. C., Mateus, V. L., & McDowell, W. H. (2013). Chemical constituents in clouds and rainwater in the Puerto Rican rainforest: potential sources and seasonal drivers. *Atmospheric Environment*, *68*, 208-220.

Gocic, M., & Trajkovic, S. (2013). Analysis of changes in meteorological variables using Mann-Kendall and Sen's slope estimator statistical tests in Serbia. *Global and Planetary Change*, *100*, 172-182.

Gocic, M., & Trajkovic, S. (2013). Analysis of precipitation and drought data in Serbia over the period 1980–2010. *Journal of Hydrology*, *494*, 32-42.

Gökbulak, F., Şengönül, K., Serengil, Y., Yurtseven, İ., Özhan, S., Cigizoglu, H. K., & Uygur, B. (2015). Comparison of rainfall-runoff relationship modeling using different methods in a forested watershed. *Water Resources Management*, *29*(12), 4229-4239.

Gowd, S. S. (2005). Assessment of groundwater quality for drinking and irrigation purposes: a case study of Peddavanka watershed, Anantapur District, Andhra Pradesh, India. *Environmental Geology*, *48*(6), 702-712.

Grünwald, P. (2005). A tutorial introduction to the minimum description length principle. *Advances in Minimum Description Length: Theory and Applications*, 3-81.

Guan, H., Zhang, X., Skrzypek, G., Sun, Z., & Xu, X. (2013). Deuterium excess variations of rainfall events in a coastal area of South Australia and its relationship with synoptic weather systems and atmospheric moisture sources. *Journal of Geophysical Research: Atmospheres*, *118*(2), 1123-1138.

Guettaf, M., Maoui, A., & Ihdene, Z. (2017). Assessment of water quality: a case study of the Seybouse River (North East of Algeria). *Applied Water Science*, *7*(1), 295-307.

Gupta, S. K., & Deshpande, R. D. (2003). Synoptic hydrology of India from the data of isotopes in precipitation. *Current Science*, 1591-1595.

Gupta, S., Mahato, A., Roy, P., Datta, J. K., & Saha, R. N. (2008). Geochemistry of groundwater, Burdwan District, West Bengal, India. *Environmental Geology*, *53*(6), 1271-1282.

Hager, B., & Foelsche, U. (2015). Stable isotope composition of precipitation in Austria. *Austrian Journal of Earth Sciences*, *108*(2).

Haile, A. T., Tefera, F. T., & Rientjes, T. (2016). Flood forecasting in Niger-Benue basin using satellite and quantitative precipitation forecast data. *International Journal of Applied Earth Observation and Geoinformation*, *52*, 475-484.

Haile, N. S. (1974). Borneo. *Geological Society, London, Special Publications*, *4*(1), 333-347.

Hajani, E., Rahman, A., & Haddad, K. (2014). Trend analysis for extreme rainfall events in New South Wales, Australia. *International Journal of Environmental, Chemical, Ecological, Geological and Geophysical Engineering*, *8*(12), 834-839.

Hajani, E., Rahman, A., & Ishak, E. (2017). Trends in extreme rainfall in the state of New South Wales, Australia. *Hydrological Sciences Journal*, *62*(13), 2160-2174.

Halff, A. H., Halff, H. M., & Azmoodeh, M. (1993). Predicting runoff from rainfall using neural networks. In *Engineering Hydrology*, 760-765. ASCE.

Hall Jr, R. O., Kennedy, T. A., & Rosi-Marshall, E. J. (2012). Air–water oxygen exchange in a large whitewater river. *Limnology and Oceanography: Fluids and Environments*, 2(1), 1-11.

Hall, R. (1996). Reconstructing Cenozoic SE Asia. *Geological Society, London, Special Publications*, *106*(1), 153-184.

Hall, R. (2013). Contraction and extension in northern Borneo driven by subduction rollback. *Journal of Asian Earth Sciences*, *76*, 399-411.

Hall, R., & Nichols, G. (2002). Cenozoic sedimentation and tectonics in Borneo: climatic influences on orogenesis. *Geological Society, London, Special Publications*, *191*(1), 5-22.

Hall, R., van Hattum, M. W., & Spakman, W. (2008). Impact of India–Asia collision on SE Asia: the record in Borneo. *Tectonophysics*, *451*(1-4), 366-389.

Hamada, J. I., D Yamanaka, M., Matsumoto, J., Fukao, S., Winarso, P. A., & Sribimawati, T. (2002). Spatial and temporal variations of the rainy season over Indonesia and their link to ENSO. *Journal of the Meteorological Society of Japan. Ser. II*, *80*(2), 285-310.

Hamilton, J. D. (1994). *Time series analysis* (Vol. 2, pp. 690-696). Princeton, NJ: Princeton university press

Hamilton, W. B. (1979). *Tectonics of the Indonesian region* (No. 1078). Washington: US Government Printing Office

Hamlaoui-Moulai, L., Mesbah, M., Souag-Gamane, D., & Medjerab, A. (2013). Detecting hydro-climatic change using spatiotemporal analysis of rainfall time series in Western Algeria. *Natural Hazards*, *65*(3), 1293-1311.

Harilal, C. C., Hashim, A., Arun, P. R., & Baji, S. (2004). Hydrogeochemistry of two rivers of Kerala with special reference to drinking water quality. *Ecology Environment and Conservation*, *10*, 187-192.

Hasan, N. Y., Driejana, D., & Sulaeman, A. (2017). Composition of ions and trace metals in rainwater in Bandung City, Indonesia. *IPTEK Journal of Proceedings Series*, *3*(6).

Hashim, M., Reba, N., Nadzri, M., Pour, A., Mahmud, M., Mohd Yusoff, A., ... & Hossain, M. (2016). Satellite-based run-off model for monitoring drought in Peninsular Malaysia. *Remote Sensing*, *8*(8), 633.

Hassoun, M. H. (1995). *Fundamentals of artificial neural networks*. United States of America: MIT press.

Hauke, J., & Kossowski, T. (2011). Comparison of values of Pearson's and Spearman's correlation coefficients on the same sets of data. *Quaestiones Geographicae*, *30*(2), 87-93.

Hejazi, M. I., & Cai, X. (2009). Input variable selection for water resources systems using a modified minimum redundancy maximum relevance (mMRMR) algorithm. *Advances in Water Resources*, *32*(4), 582-593.

Hem, J. D. (1985). *Study and interpretation of the chemical characteristics of natural water* (Vol. 2254). Department of the Interior, US Geological Survey.

Hidalgo, J. G., De Luis, M., Raventós, J., & Sánchez, J. R. (2003). Daily rainfall trend in the Valencia Region of Spain. *Theoretical and Applied Climatology*, *75*(1-2), 117-130.

Hidayat, R., & Kizu, S. (2010). Influence of the Madden–Julian oscillation on Indonesian rainfall variability in austral summer. *International Journal of Climatology*, *30*(12), 1816-1825.

Hill, R. A. (1940). Geochemical patterns in Coachella valley. *Eos, Transactions American Geophysical Union*, *21*(1), 46-53.

Holland, H. D. (1978). *The chemistry of the atmosphere and oceans*. New York: Wiley Inter Sciences, 351

Hollins, S. E., Hughes, C. E., Crawford, J., Cendón, D. I., & Meredith, K. M. (2018). Rainfall isotope variations over the Australian continent–Implications for hydrology and isoscape applications. *Science of the Total Environment*, *645*, 630-645.

Hsu, K. L., Gupta, H. V., & Sorooshian, S. (1995). Artificial neural network modeling of the rainfall-runoff process. *Water Resources Research*, *31*(10), 2517-2530.

Hu, G. P., Balasubramanian, R., & Wu, C. D. (2003). Chemical characterization of rainwater at Singapore. *Chemosphere*, *51*(8), 747-755.

Hua, T. M., Hui, R. C. Y., & Husen, R. (2013). Trends of rainfall in Sarawak from 1999 to 2008. In *Proceedings of the International Conference on Social Science Research, ICSSR*.

Huang, S., Kumar, R., Flörke, M., Yang, T., Hundecha, Y., Kraft, P., ... & Strauch, M. (2017). Evaluation of an ensemble of regional hydrological models in 12 large-scale river basins worldwide. *Climatic Change*, *141*(3), 381-397.

Huang, X. F., Li, X., He, L. Y., Feng, N., Hu, M., Niu, Y. W., & Zeng, L. W. (2010). 5-Year study of rainwater chemistry in a coastal mega-city in South China. *Atmospheric Research*, *97*(1-2), 185-193.

Huang, Y. F., Puah, Y. J., Chua, K. C., & Lee, T. S. (2015). Analysis of monthly and seasonal rainfall trends using the Holt's test. *International Journal of Climatology*, *35*(7), 1500-1509.

Hung, N. Q., Babel, M. S., Weesakul, S., & Tripathi, N. K. (2009). An artificial neural network model for rainfall forecasting in Bangkok, Thailand. *Hydrology and Earth System Sciences*, *13*(8), 1413-1425.

Huo, M., Sun, Q., Bai, Y., Xie, P., Liu, Z., Li, J., ... & Lu, S. (2010). Chemical character of precipitation and related particles and trace gases in the North and South of China. *Journal of Atmospheric Chemistry*, *67*(1), 29.

Hutchison, C. S. (1989). *Geological evolution of South-east Asia* (Vol. 13, p. 368). Oxford: Clarendon Press.

Hutchison, C. S. (1996). The 'Rajang accretionary prism'and 'Lupar Line'problem of Borneo. *Geological Society, London, Special Publications*, *106*(1), 247-261.

Hutchison, C. S. (2005). *Geology of North-West Borneo: Sarawak, Brunei and Sabah*. Netherland: Elsevier.

Hutchison, C. S., Bergman, S. C., Swauger, D. A., & Graves, J. E. (2000). A Miocene collisional belt in north Borneo: uplift mechanism and isostatic adjustment quantified by thermochronology. *Journal of the Geological Society*, *157*(4), 783-793.

IAEA/GNIP. (2014). Precipitation Sampling Guide (V2.02). Vienna: IAEA.

Ichiyanagi, K., Tanoue, M., & Isotope Mapping Working Group of the Japanese Society of Hydrological Science (IMWG/JAHS). (2016). Spatial analysis of annual mean stable isotopes in precipitation across Japan based on an intensive observation period throughout 2013. *Isotopes in Environmental and Health Studies*, *52*(4-5), 353-362.

Ingraham, N. L. (1998). Isotopic variations in precipitation: In: *Isotope Tracers in Catchment Hydrology*. Elsevier, 87-118.

International Atomic Energy Agency (IAEA) (1992). *Statistical treatment of data on environmental isotopes in precipitation*. Technical Report Series. 331, pp. 781.

International Atomic Energy Agency (IAEA) (1997). *Technical procedure for cumulative monthly sampling of precipitation for isotopic analyses*. IAEA, Vienna, November 1997. www-naweb.iaea.org/NAALIHL/docs/tech_info/Precipitation%20Sampling97.pdf. Accessed on 15.7.2016.

Ishak, E. H. (2014). *Effects of climate variability and change on flood magnitude and frequency in Australia* (Doctoral dissertation, University of Western Sydney (Australia)).

Ishaku, J. M., Ahmed, A. S., & Abubakar, M. A. (2011). Assessment of groundwater quality using chemical indices and GIS mapping in Jada area, Northeastern Nigeria. *Journal of Earth Sciences and Geotechnical Engineering*, *1*(1), 35-60.

Istok, J. D., & Boersma, L. (1986). Effect of antecedent rainfall on runoff during low-intensity rainfall. *Journal of Hydrology*, *88*(3-4), 329-342.

Jäntschi, L., & BOLBOACĂ, S. D. (2006). Pearson versus Spearman, Kendall's tau correlation analysis on structure-activity relationships of biologic active compounds. *Leonardo Journal of Sciences*, *5*(9), 179-200.

Jeelani, G., Deshpande, R. D., Galkowski, M., & Rozanski, K. (2018). Isotopic composition of daily precipitation along the southern foothills of the Himalayas: impact of marine and continental sources of atmospheric moisture. *Atmospheric Chemistry and Physics*, *18*(12), 8789-8805.

Jeffries, D. S., & Snyder, W. R. (1981). Atmospheric deposition of heavy metals in central Ontario. *Water, Air, and Soil Pollution*, *15*(2), 127-152.

Jimeno-Sáez, P., Senent-Aparicio, J., Pérez-Sánchez, J., & Pulido-Velazquez, D. (2018). A comparison of SWAT and ANN models for daily runoff simulation in different climatic zones of peninsular Spain. *Water*, *10*(2), 192.

Jin, Z., You, C. F., Yu, J., Wu, L., Zhang, F., & Liu, H. C. (2011). Seasonal contributions of catchment weathering and eolian dust to river water chemistry, northeastern Tibetan Plateau: chemical and Sr isotopic constraints. *Journal of Geophysical Research: Earth Surface*, 116(F4).

Johnson, D., & King, M. (1988). *Basic forecasting techniques*: Great Britain: Butterworth & Co. (Publishers) Ltd.

Johnson, K. R., & Ingram, B. L. (2004). Spatial and temporal variability in the stable isotope systematics of modern precipitation in China: implications for paleoclimate reconstructions. *Earth and Planetary Science Letters*, *220*(3-4), 365-377.

Johnson, R. A., & Wichern, D. W. (1988). Factor analysis and inference for structured covariance matrices. *Applied Multivariate Statistical Analysis, 2nd ed. Prentice Hall, Englewood Cliffs, NJ*, 378-430.

Jones Jr, J. B., Stanley, E. H., & Mulholland, P. J. (2003). Long-term decline in carbon dioxide supersaturation in rivers across the contiguous United States. *Geophysical Research Letters*, *30*(10).

Judd, K., & Mees, A. (1995). On selecting models for nonlinear time series. *Physica D: Nonlinear Phenomena*, *82*(4), 426-444.

Kadyampakeni, D., Appoh, R., Barron, J., & Boakye-Acheampong, E. (2018). Analysis of water quality of selected irrigation water sources in northern Ghana. *Water Science and Technology: Water Supply*, *18*(4), 1308-1317.

Kamruzzaman, M., Rahman, A. S., Ahmed, M. S., Kabir, M. E., Mazumder, Q. H., Rahman, M. S., & Jahan, C. S. (2018). Spatio-temporal analysis of climatic variables in the western part of Bangladesh. *Environment, Development and Sustainability*, *20*(1), 89-108.

Kashani, M. H., Ghorbani, M. A., Dinpashoh, Y., & Shahmorad, S. (2014). Comparison of Volterra model and artificial neural networks for rainfall–runoff simulation. *Natural Resources Research*, *23*(3), 341-354.

Kelley, W. P. (1951). *Alkali soils; their formation, properties, and reclamation* (No. 04; RMD, S595 K4.). New York: Reinhold.

Kelley, W. P. (1963). Use of saline irrigation water. *Soil Science*, *95*(6), 385-391.

Kendall, M. G. (1948). *Rank correlation methods*. Oxford, England: Griffin

Kerr, T., Srinivasan, M. S., & Rutherford, J. (2015). Stable water isotopes across a transect of the southern Alps, New Zealand. *Journal of Hydrometeorology*, *16*(2), 702-715.

Khaledian, Y., Ebrahimi, S., Natesan, U., Basatnia, N., Nejad, B. B., Bagmohammadi, H., & Zeraatpisheh, M. (2018). Assessment of water quality using multivariate statistical analysis in the Gharaso River, Northern Iran. In *Urban Ecology, Water Quality and Climate Change*, 227-253. Springer, Cham.

Khan, M. F., Maulud, K. N. A., Latif, M. T., Chung, J. X., Amil, N., Alias, A., ... & Hassan, H. (2018). Physicochemical factors and their potential sources inferred from long-term rainfall measurements at an urban and a remote rural site in tropical areas. *Science of The Total Environment*, *613*, 1401-1416.

Khan, T. A., & Abbasi, M. A. (2013). Synthesis of parameters used to check the suitability of water for irrigation purposes. *International Journal of Environmental Sciences*, *3*(6), 2131-2138.

Kharroubi, O., Blanpain, O., Masson, E., & Lallahem, S. (2016). Application of artificial neural networks to predict hourly flows: Case study of the Eure basin, France. *Hydrological Sciences Journal-Journal des Sciences Hydrologiques*, *61*(3), 541-550.

Khatibi, R., Ghorbani, M. A., & Pourhosseini, F. A. (2017). Stream flow predictions using nature-inspired Firefly Algorithms and a Multiple Model strategy–Directions of innovation towards next generation practices. *Advanced Engineering Informatics*, *34*, 80-89.

Khemani, L. T., & Ramana Murty, B. V. (1968). Chemical composition of rain water and rain characteristics at Delhi. *Tellus*, *20*(2), 284-292.

Khoon, S. H., Issabayeva, G. I., & Lee, L. W. (2011). Measurement of rainwater chemical composition in Malaysia based on ion chromatography method. *World Academy of Science, Engineering and Technology*, *11*, 161-168.

Kim, K., Rajmohan, N., Kim, H. J., Kim, S. H., Hwang, G. S., Yun, S. T., ... & Lee, S. H. (2005). Evaluation of geochemical processes affecting groundwater chemistry based on mass balance approach: a case study in Namwon, Korea. *Geochemical Journal*, *39*(4), 357-369.

Kimaro, T. A., Tachikawa, Y., & Takara, K. (2005). Distributed hydrologic simulations to analyze the impacts of land use changes on flood characteristics in the Yasu River Basin in Japan. *Journal of Natural Disaster Sciences*, *27*(2), 85-94.

Kirono, D. G. C. (2004). Principal component analysis for identifying period of seasons in Indonesia. *Indonesian Journal of Geography*, *36*(2004).

Kisi, O., & Ay, M. (2014). Comparison of Mann–Kendall and innovative trend method for water quality parameters of the Kizilirmak River, Turkey. *Journal of Hydrology*, *513*, 362-375.

Kişi, Ö., Guimarães Santos, C. A., Marques da Silva, R., & Zounemat-Kermani, M. (2018). Trend analysis of monthly streamflows using Şen's innovative trend method. *Geofizika*, *35*(1), 53-68.

Knapp, A. K., Hoover, D. L., Wilcox, K. R., Avolio, M. L., Koerner, S. E., La Pierre, K. J., ... & Smith, M. D. (2015). Characterizing differences in precipitation regimes of extreme wet and dry years: implications for climate change experiments. *Global Change Biology*, *21*(7), 2624-2633.

Kocsis, T., Kovács-Székely, I., & Anda, A. (2017). Comparison of parametric and non-parametric time-series analysis methods on a long-term meteorological data set. *Central European Geology*, *60*(3), 316-332.

Komabayasi, M. (1959). Dissolved oxygen in rainwater and its relation to the raincloud structure (I). precipitation from September to March. *Journal of the Meteorological Society of Japan. Ser. II*, *37*(1), 22-34.

Köppen, W. (1900). Versuch einer Klassifikation der Klimate, vorzugsweise nach ihren Beziehungen zur Pflanzenwelt. *Geographische Zeitschrift*, *6*(11. H), 593-611.

Koulousaris, M., Aloupi, M., & Angelidis, M. O. (2009). Total metal concentrations in atmospheric precipitation from the Northern Aegean Sea. *Water, Air, and Soil Pollution*, *201*(1-4), 389.

Kovačević, M., Ivanišević, N., Dašić, T., & Marković, L. (2018). Application of artificial neural networks for hydrological modelling in karst. *Građevinar*, *70*(01), 1-10.

Krishnakumar, K. N., Rao, G. P., & Gopakumar, C. S. (2009). Rainfall trends in twentieth century over Kerala, India. *Atmospheric Environment*, *43*(11), 1940-1944.

Kulshrestha, U. C., Kulshrestha, M. J., Sekar, R., Sastry, G. S. R., & Vairamani, M. (2003). Chemical characteristics of rainwater at an urban site of south-central India. *Atmospheric Environment*, *37*(21), 3019-3026.

Kumar, A., Tiwari, S. K., Verma, A., & Gupta, A. K. (2018). Tracing isotopic signatures (δD and δ18O) in precipitation and glacier melt over Chorabari Glacier–Hydroclimatic

inferences for the Upper Ganga Basin (UGB), Garhwal Himalaya. *Journal of Hydrology: Regional Studies*, *15*, 68-89.

Kumar, M., Kumari, K., Ramanathan, A. L., & Saxena, R. (2007). A comparative evaluation of groundwater suitability for irrigation and drinking purposes in two intensively cultivated districts of Punjab, India. *Environmental Geology*, *53*(3), 553-574.

Kuok, K. K., & Bessaih, N. (2007). Artificial neural networks (ANNS) for daily rainfall runoff modelling. *Journal-The Institution of Engineers, Malaysia*, *68*(3).

Lacour, J. L., Risi, C., Worden, J., Clerbaux, C., & Coheur, P. F. (2018). Importance of depth and intensity of convection on the isotopic composition of water vapor as seen from IASI and TES δD observations. *Earth and Planetary Science Letters*, *481*, 387-394.

Langmuir, D. (1997). *Aqueous environmental Geochemistry.* Upper Saddle River, NJ: Prentice Hall.

Langner, A., Miettinen, J., & Siegert, F. (2007). Land cover change 2002–2005 in Borneo and the role of fire derived from MODIS imagery. *Global Change Biology*, *13*(11), 2329-2340.

Lara, L. B. L. S., Artaxo, P., Martinelli, L. A., Victoria, R. L., Camargo, P. B. D., Krusche, A., ... & Ballester, M. V. (2001). Chemical composition of rainwater and anthropogenic influences in the Piracicaba River Basin, Southeast Brazil. *Atmospheric Environment*, *35*(29), 4937-4945.

Larson, T. E. (1975). *Corrosion by Domestic Waters.* State of Illinois Department of Registration and Education, Illinois State Water Survey, Urbana, IL

Larson, T. E., & Skold, R. V. (1958). Laboratory studies relating mineral quality of water to corrosion of steel and cast iron. *Corrosion*, *14*(6), 43-46.

Latif, Y., Yaoming, M., & Yaseen, M. (2018). Spatial analysis of precipitation time series over the Upper Indus Basin. *Theoretical and Applied Climatology*, *131*(1-2), 761-775.

Lavee, H., Imeson, A. C., & Sarah, P. (1998). The impact of climate change on geomorphology and desertification along a Mediterranean-arid transect. *Land Degradation & Development*, *9*(5), 407-422.

Lawrence, J. R., & White, J. W. C. (1991). The elusive climate signal in the isotopic composition of precipitation. *Stable Isotope Geochemistry: A Tribute to Samuel Epstein*, *3*, 169-185.

Le, T. D. H., Kattwinkel, M., Schützenmeister, K., Olson, J. R., Hawkins, C. P., & Schäfer, R. B. (2018). Predicting current and future background ion concentrations in German surface water under climate change. *Philosophical Transactions of the Royal Society B*, *374*(1764), 20180004.

Lee Rodgers, J., & Nicewander, W. A. (1988). Thirteen ways to look at the correlation coefficient. *The American Statistician*, *42*(1), 59-66.

Lee, K. S., Grundstein, A. J., Wenner, D. B., Choi, M. S., Woo, N. C., & Lee, D. H. (2003). Climatic controls on the stable isotopic composition of precipitation in Northeast Asia. *Climate Research*, *23*(2), 137-148.

Lee, K. S., Kim, J. M., Lee, D. R., Kim, Y., & Lee, D. (2007). Analysis of water movement through an unsaturated soil zone in Jeju Island, Korea using stable oxygen and hydrogen isotopes. *Journal of Hydrology*, *345*(3-4), 199-211.

Lehmann, A., & Rode, M. (2001). Long-term behaviour and cross-correlation water quality analysis of the river Elbe, Germany. *Water Research*, *35*(9), 2153-2160.

Lehmann, E. L., & D'Abrera, H. J. (2006). *Nonparametrics: statistical methods based on ranks*. New York: Springer. p. 464.

Lehtokangas, M., Saarinen, J., Huuhtanen, P., & Kaski, K. (1993). Neural network optimization tool based on predictive MDL principle for time series prediction. In *Proceedings of 1993 IEEE Conference on Tools with Al (TAI-93)*, 338-342. IEEE.

Lettenmaier, D. P., Wood, E. F., & Wallis, J. R. (1994). Hydro-climatological trends in the continental United States, 1948-88. *Journal of Climate*, *7*(4), 586-607.

Levin, N. E., Zipser, E. J., & Cerling, T. E. (2009). Isotopic composition of waters from Ethiopia and Kenya: insights into moisture sources for eastern Africa. *Journal of Geophysical Research: Atmospheres*, *114*(D23).

Levshina, S. (2018). An assessment of metal-humus complexes in river waters of the Upper Amur basin, Russia. *Environmental Monitoring and Assessment*, *190*(1), 18.

Lewis Jr, W. M. (1981). Precipitation chemistry and nutrient loading by precipitation in a tropical watershed. *Water Resources Research*, *17*(1), 169-181.

Li, M., Xia, J., Chen, Z., Meng, D., & Xu, C. (2013). Variation analysis of precipitation during past 286 years in Beijing area, China, using non-parametric test and wavelet analysis. *Hydrological Processes*, *27*(20), 2934-2943.

Li, P., Qian, H., Wu, J., Zhang, Y., & Zhang, H. (2013). Major ion chemistry of shallow groundwater in the Dongsheng Coalfield, Ordos Basin, China. *Mine Water and the Environment*, 32(3), 195-206.

Li, X. F., Zhang, M. J., Ma, Q., Li, Y. J., Wang, S. J., & Wang, B. L. (2012). Characteristics of stable isotopes in precipitation over northeast China and its water vapor sources. *Huan jing ke xue= Huanjing kexue*, *33*(9), 2924-2931.

Lim, Y. H., & Lye, L. M. (2003). Regional flood estimation for ungauged basins in Sarawak, Malaysia. *Hydrological Sciences Journal*, 48(1), 79-94.

Lima, A. D. O., Lima-Filho, F. P., Dias, N. D. S., REGO, P. R., ARAGÃO, D., BLANCO, F. F., & FERREIRA NETO, M. I. G. U. E. L. (2017). Mechanisms controlling surface water quality in the Cobras river sub-basin, northeastern Brazil. *Revista Caatinga*, *30*(1), 181-189.

Liong, T.E (1982). Soil classification in Sarawak. Technical paper no.6, Soil division research branch, *Department of Agriculture*, Sarawak, Malaysia

Lioubimtseva, E., & Henebry, G. M. (2009). Climate and environmental change in arid Central Asia: Impacts, vulnerability, and adaptations. *Journal of Arid Environments*, *73*(11), 963-977.

Liu, J., Fu, G., Song, X., Charles, S. P., Zhang, Y., Han, D., & Wang, S. (2010). Stable isotopic compositions in Australian precipitation. *Journal of Geophysical Research: Atmospheres*, *115*(D23).

Liu, J., Xiao, C., Ding, M., & Ren, J. (2014). Variations in stable hydrogen and oxygen isotopes in atmospheric water vapor in the marine boundary layer across a wide latitude range. *Journal of Environmental Sciences*, *26*(11), 2266-2276.

Liu, Q., Yang, Z., & Cui, B. (2008). Spatial and temporal variability of annual precipitation during 1961–2006 in Yellow River Basin, China. *Journal of Hydrology*, *361*(3-4), 330-338.

Lohani, A. K., Goel, N. K., & Bhatia, K. K. S. (2011). Comparative study of neural network, fuzzy logic and linear transfer function techniques in daily rainfall-runoff modelling under different input domains. *Hydrological Processes*, 25(2), 175-193.

Longobardi, A., & Villani, P. (2010). Trend analysis of annual and seasonal rainfall time series in the Mediterranean area. *International Journal of Climatology*, *30*(10), 1538-1546.

Loo, Y. Y., Billa, L., & Singh, A. (2015). Effect of climate change on seasonal monsoon in Asia and its impact on the variability of monsoon rainfall in Southeast Asia. *Geoscience Frontiers*, *6*(6), 817-823.

Lu, X., Li, L. Y., Li, N., Yang, G., Luo, D., & Chen, J. (2011). Chemical characteristics of spring rainwater of Xi'an city, NW China. *Atmospheric Environment*, *45*(28), 5058-5063.

Lu, G. Y., & Wong, D. W. (2008). An adaptive inverse-distance weighting spatial interpolation technique. *Computers & geosciences*, *34*(9), 1044-1055.

Ma, X., Tao, Z., Wang, Y., Yu, H., & Wang, Y. (2015). Long short-term memory neural network for traffic speed prediction using remote microwave sensor data. *Transportation Research Part C: Emerging Technologies*, *54*, 187-197.

Machado, F., Mine, M., Kaviski, E., & Fill, H. (2011). Monthly rainfall–runoff modelling using artificial neural networks. *Hydrological Sciences Journal–Journal des Sciences Hydrologiques*, *56*(3), 349-361.

Madsen, H., Lawrence, D., Lang, M., Martinkova, M., & Kjeldsen, T. R. (2014). Review of trend analysis and climate change projections of extreme precipitation and floods in Europe. *Journal of Hydrology*, *519*, 3634-3650.

Majeed, S., Rashid, S., Qadir, A., Mackay, C., & Hayat, F. (2018). Spatial patterns of pollutants in water of metropolitan drain in Lahore, Pakistan, using multivariate statistical techniques. *Environmental Monitoring and Assessment*, *190*(3), 128.

Malaysian Meteorological Department (MMD) (2009). *Climate change scenarios for Malaysian 2001-2090*. Malaysian Meteorological Department, Scientific Report, Petaling Jaya Malaysia, 1-84.

Malaysian Meteorological Department (MMD) (2017). Malaysia's Climate: Seasonal rainfall variation in Sabah and Sarawak. http://www.met.gov.my *accessed on 12.07.2017.*

Malaysian Water Quality Standards (MWQS) (2009). Malaysian Ministry of Health (MMOH). *National drinking water quality standard*, Engineering Services Division, Ministry of Health, Malaysia.

Maloney, E. D., & Shaman, J. (2008). Intraseasonal variability of the West African monsoon and Atlantic ITCZ. *Journal of Climate*, *21*(12), 2898-2918.

Manahan, S. E. (1993). Fundamentals of environmental chemistry. United States: CRC Press

Mann, H. B. (1945). Nonparametric tests against trend. *Econometrica: Journal of the Econometric Society*, 245-259.

Mao, G., Zhao, Y., Zhang, F., Liu, J., & Huang, X. (2019). Spatiotemporal variability of heavy metals and identification of potential source tracers in the surface water of the Lhasa River basin. *Environmental Science and Pollution Research*, 1-11.

Marandi, A., Polikarpus, M., & Jõeleht, A. (2013). A new approach for describing the relationship between electrical conductivity and major anion concentration in natural waters. *Applied Geochemistry*, *38*, 103-109.

Mardia, K. V. Kent, J. T., & Bibby, J. M. (1979). Multivariate Analysis*. Probability and Mathematical Statistics.* London: Academic Press.

Marescaux, A., Thieu, V., Borges, A. V., & Garnier, J. (2018). Seasonal and spatial variability of the partial pressure of carbon dioxide in the human-impacted Seine River in France. *Scientific Reports*, *8*(1), 13961.

Marryanna, L., Kosugi, Y., Itoh, M., Noguchi, S., Takanashi, S., Katsuyama, M., ... & Siti-Aisah, S. (2017). Temporal variation in the stable isotopes in precipitation related to the rainfall pattern in a tropical rainforest in Peninsular Malaysia. *Journal of Tropical Forest Science*, 349-362.

Martin, N. J., Conroy, J. L., Noone, D., Cobb, K. M., Konecky, B. L., & Rea, S. (2018). Seasonal and ENSO influences on the stable isotopic composition of Galápagos precipitation. *Journal of Geophysical Research: Atmospheres*, *123*(1), 261-275.

Martinez-Tavera, E., Rodriguez-Espinosa, P. F., Shruti, V. C., Sujitha, S. B., Morales-Garcia, S. S., & Muñoz-Sevilla, N. P. (2017). Monitoring the seasonal dynamics of physicochemical parameters from Atoyac River basin (Puebla), Central Mexico: multivariate approach. *Environmental Earth Sciences*, *76*(2), 95.

Martino, G. D., Fontana, N., Marini, G., & Singh, V. P. (2012). Variability and trend in seasonal precipitation in the continental United States. *Journal of Hydrologic Engineering*, *18*(6), 630-640.

Martins, E. H., Nogarotto, D. C., Mortatti, J., & Pozza, S. A. (2018). Chemical composition of rainwater in an urban area of the southeast of Brazil. *Atmospheric Pollution Research, 10*(2), 520- 530.

Marzluf, G. A. (1997). Genetic regulation of nitrogen metabolism in the fungi. *Microbiology and Molecular Biology Reviews*, *61*(1), 17-32.

Matawle, J. L., Pervez, S., Dewangan, S., Shrivastava, A., Tiwari, S., Pant, P., ... & Pervez, Y. (2015). Characterization of PM2. 5 source profiles for traffic and dust sources in Raipur, India. *Aerosol Air Quality Research*, *15*, 2537-2548.

Maurer, E. P., Brekke, L., Pruitt, T., & Duffy, P. B. (2007). Fine-resolution climate projections enhance regional climate change impact studies. *Eos, Transactions American Geophysical Union*, *88*(47), 504-504.

Mayr, C., Lücke, A., Stichler, W., Trimborn, P., Ercolano, B., Oliva, G., ... & Janssen, S. (2007). Precipitation origin and evaporation of lakes in semi-arid Patagonia (Argentina) inferred from stable isotopes (δ18O, δ2H). *Journal of Hydrology*, *334*(1-2), 53-63.

Mays, L. W. (1996). *Water Resources Handbook*. New York: McGraw-Hill.

McCulloch, W. S., & Pitts, W. (1943). A logical calculus of the ideas immanent in nervous activity. *The Bulletin of Mathematical Biophysics*, *5*(4), 115-133.

McDonald, J. H. (2009). *Handbook of biological statistics* (Vol. 2, pp. 173-181). Baltimore, MD: sparky house publishing.

Meher, J. (2014). *Rainfall and runoff estimation using hydrological models and ANN techniques* (Doctoral dissertation, National Institute of Technology (India)).

Meng, Y., Zhao, Y., Li, R., Li, J., Cui, L., Kong, L., & Fu, H. (2019). Characterization of inorganic ions in rainwater in the megacity of Shanghai: Spatiotemporal variations and source apportionment. *Atmospheric Research*.

Meshram, S. G., Singh, V. P., & Meshram, C. (2017). Long-term trend and variability of precipitation in Chhattisgarh State, India. *Theoretical and Applied Climatology*, *129*(3-4), 729-744.

Metellus, W. (2016). *Long-term Changes and Influences of Climate Variability on Rainfall Extremes of Different Durations* (Doctoral dissertation, Florida Atlantic University (Florida)).

Meyers, L. S., Gamst, G., & Guarino, A. J. (2016). *Applied multivariate research: Design and interpretation*. United States of America: Sage publications.

MGDM (2013). Geological map of Sarawak (1: 1:750,000 scale). Published by *Minerals and Geoscience Department*, Sarawak, Malaysia

Migliavacca, D., Teixeira, E. C., Wiegand, F., Machado, A. C. M., & Sanchez, J. (2005). Atmospheric precipitation and chemical composition of an urban site, Guaiba hydrographic basin, Brazil. *Atmospheric Environment*, *39*(10), 1829-1844.

Milly, P. C. D., & Dunne, K. A. (2017). A hydrologic drying bias in water-resource impact analyses of anthropogenic climate change. *JAWRA Journal of the American Water Resources Association*, *53*(4), 822-838.

Milsom, J., Holt, R., Hutchison, C. S., Bergman, S. C., Swauger, D. A., & Graves, J. E. (2001). Discussion of a Miocene collisional belt in north Borneo: uplift mechanism and isostatic adjustment quantified by thermochronology: Journal, Vol. 157, 2000, 783–793. *Journal of the Geological Society*, *158*(2), 396-400.

Minaei, M., & Irannezhad, M. (2018). Spatio-temporal trend analysis of precipitation, temperature, and river discharge in the northeast of Iran in recent decades. *Theoretical and Applied Climatology*, *131*(1-2), 167-179.

Minns, A. W., & Hall, M. J. (1996). Artificial neural networks as rainfall-runoff models. *Hydrological Sciences Journal*, *41*(3), 399-417.

Mirza, M. Q., Warrick, R. A., Ericksen, N. J., & Kenny, G. J. (1998). Trends and persistence in precipitation in the Ganges, Brahmaputra and Meghna river basins. *Hydrological Sciences Journal*, *43*(6), 845-858.

Mirzaee, S., Yousefi, S., Keesstra, S., Pourghasemi, H. R., Cerdà, A., & Fuller, I. C. (2018). Effects of hydrological events on morphological evolution of a fluvial system. *Journal of Hydrology*, *563*, 33-42.

Moerman, J. W., Cobb, K. M., Adkins, J. F., Sodemann, H., Clark, B., & Tuen, A. A. (2013). Diurnal to interannual rainfall $\delta^{18}O$ variations in northern Borneo driven by regional hydrology. *Earth and Planetary Science Letters*, *369*, 108-119.

Mohamed, A. A., Mwevura, H., Rahman, I. A., Hoon, L. L., & Ali, H. R. (2016). Determination of physico-chemical parameters in rainwater in urban-west region of Zanzibar Island. *ARPN Journal of Science and Technology*, 6(2), 55-59.

Molina-Carpio, J., Espinoza, J. C., Vauchel, P., Ronchail, J., Gutierrez Caloir, B., Guyot, J. L., & Noriega, L. (2017). Hydroclimatology of the Upper Madeira River basin: spatio-temporal variability and trends. *Hydrological Sciences Journal*, *62*(6), 911-927.

Moral, F., Cruz-Sanjulián, J. J., & Olías, M. (2008). Geochemical evolution of groundwater in the carbonate aquifers of Sierra de Segura (Betic Cordillera, southern Spain). *Journal of Hydrology*, *360*(1-4), 281-296.

Moreda-Piñeiro, J., Alonso-Rodríguez, E., Moscoso-Pérez, C., Blanco-Heras, G., Turnes-Carou, I., López-Mahía, P., ... & Prada-Rodríguez, D. (2014). Influence of marine, terrestrial and anthropogenic sources on ionic and metallic composition of rainwater at a suburban site (northwest coast of Spain). *Atmospheric Environment*, *88*, 30-38.

Morell, O., & Fried, R. (2009). On nonparametric tests for trend detection in seasonal time series. In *Statistical Inference, Econometric Analysis and Matrix Algebra*, 19-39. Physica-Verlag HD.

Morgan, M. D., & Good, R. E. (1988). Stream chemistry in the New Jersey Pinelands: the influence of precipitation and watershed disturbance. *Water Resources Research*, *24*(7), 1091-1100.

Moriasi, D. N., Arnold, J. G., Van Liew, M. W., Bingner, R. L., Harmel, R. D., & Veith, T. L. (2007). Model evaluation guidelines for systematic quantification of accuracy in watershed simulations. *Transactions of the ASABE*, *50*(3), 885-900.

Moron, V., Robertson, A. W., & Qian, J. H. (2010). Local versus regional-scale characteristics of monsoon onset and post-onset rainfall over Indonesia. *Climate Dynamics*, *34*(2-3), 281-299.

Moss, S. J., & Chambers, J. L. (1999). Tertiary facies architecture in the Kutai basin, Kalimantan, Indonesia. *Journal of Asian Earth Sciences*, *17*(1-2), 157-181.

Mostafaei, A. (2014). Application of multivariate statistical methods and water-quality index to evaluation of water quality in the Kashkan River. *Environmental Management*, *53*(4), 865-881.

Mozejko, J. (2012). Detecting and estimating trends of water quality parameters. In *Water Quality Monitoring and Assessment*. IntechOpen.

Mueller, D. K., Hamilton, P. A., Helsel, D. R., Hitt, K. J., & Ruddy, B. C. (1995). Nutrients in ground water and surface water of the United States: an analysis of data through 1992. *Water-Resources Investigations Report*, *95*, 4031.

Muhammad Noor Hisyam, B. A. H. (2010). *Water level predictio for Limbang basin using multilayer perceptron (mlp) and radial basis function (rbf) neural network*. Universiti Malaysia Sarawak, UNIMAS.

Mukaka, M. M. (2012). A guide to appropriate use of correlation coefficient in medical research. *Malawi Medical Journal*, *24*(3), 69-71.

Mullaney, J. R., Lorenz, D. L., & Arntson, A. D. (2009). *Chloride in groundwater and surface water in areas underlain by the glacial aquifer system, northern United States* (p. 41). Reston, VA: US Geological Survey.

Munksgaard, N. C., Zwart, C., Kurita, N., Bass, A., Nott, J., & Bird, M. I. (2015). Stable isotope anatomy of tropical cyclone Ita, North-Eastern Australia, April 2014. *PloS one*, *10*(3), e0119728.

Mustapha, A., Aris, A. Z., Juahir, H., Ramli, M. F., & Kura, N. U. (2013). River water quality assessment using environmentric techniques: case study of Jakara River Basin. *Environmental Science and Pollution Research*, *20*(8), 5630-5644.

Mutlu, E., Chaubey, I., Hexmoor, H., & Bajwa, S. G. (2008). Comparison of artificial neural network models for hydrologic predictions at multiple gauging stations in an agricultural watershed. *Hydrological Processes: An International Journal*, *22*(26), 5097-5106.

Muttil, N., & Chau, K. W. (2006). Neural network and genetic programming for modelling coastal algal blooms. *International Journal of Environment and Pollution*, 28(3-4), 223-238.

Nacar, S., Hınıs, M. A., & Kankal, M. (2018). Forecasting daily streamflow discharges using various neural network models and training algorithms. *KSCE Journal of Civil Engineering*, *22*(9), 3676-3685.

Naimabadi, A., Shirmardi, M., Maleki, H., Teymouri, P., Goudarzi, G., Shahsavani, A., ... & Zarei, M. R. (2018). On the chemical nature of precipitation in a populated Middle Eastern Region (Ahvaz, Iran) with diverse sources. *Ecotoxicology and Environmental Safety*, *163*, 558-566.

Napolitano, G. (2011). *An exploration of neural networks for real-time flood forecasting* (Doctoral dissertation, University of Leeds (England)).

Nash, J. E., & Sutcliffe, J. V. (1970). River flow forecasting through conceptual models part I—A discussion of principles. *Journal of Hydrology*, *10*(3), 282-290.

Nawaz, N., Harun, S., Othman, R., & Heryansyah, A. (2016). Rainfall runoff modeling by multilayer perceptron neural network for LUI river catchment. *Jurnal Teknologi*, *78*(6-12), 37-42.

Ndoye, S., Fontaine, C., Gaye, C., & Razack, M. (2018). Groundwater Quality and Suitability for Different Uses in the Saloum Area of Senegal. *Water*, *10*(12), 1837.

Neal, C., Skeffington, R., Neal, M., Wyatt, R., Wickham, H., Hill, L., & Hewitt, N. (2004). Rainfall and runoff water quality of the Pang and Lambourn, tributaries of the River Thames, south-eastern England. *Hydrology and Earth System Sciences Discussions*, *8*(4), 601-613.

Ngah, M., Reid, I., & Hashim, M. (2012). Rainfall trend analysis using 50 years historical data in newly developed catchment in peninsular Malaysia. *Middle-East Journal of Scientific Research*, *11*(5), 668-673.

Nienie, A. B., Sivalingam, P., Laffite, A., Ngelinkoto, P., Otamonga, J. P., Matand, A., ... & Poté, J. (2017). Seasonal variability of water quality by physicochemical indexes and traceable metals in suburban area in Kikwit, Democratic Republic of the Congo. *International Soil and Water Conservation Research*, *5*(2), 158-165.

Niu, H., He, Y., Lu, X. X., Shen, J., Du, J., Zhang, T., ... & Chang, L. (2014). Chemical composition of rainwater in the Yulong Snow Mountain region, Southwestern China. *Atmospheric Research*, *144*, 195-206.

Nkiaka, E., Nawaz, N. R., & Lovett, J. C. (2017). Analysis of rainfall variability in the Logone catchment, Lake Chad basin. *International Journal of Climatology*, *37*(9), 3553-3564.

Nolakana, P. (2016). Geochemical assessment of groundwater quality and suitability for drinking and irrigation purposes in Newcastle, Kwazulu-Natal, South Africa.

Nor, N. I., Harun, S., & Kassim, A. H. (2007). Radial basis function modeling of hourly streamflow hydrograph. *Journal of Hydrologic Engineering*, *12*(1), 113-123.

Nosrati, K., & Van Den Eeckhaut, M. (2012). Assessment of groundwater quality using multivariate statistical techniques in Hashtgerd Plain, Iran. *Environmental Earth Sciences*, *65*(1), 331-344.

Nriagu, J. O. (1989). A global assessment of natural sources of atmospheric trace metals. *Nature*, *338*(6210), 47.

O'Gorman, P. A. (2015). Precipitation extremes under climate change. *Current Climate Change Reports*, *1*(2), 49-59.

Ogunfowokan, A. O., Obisanya, J. F., & Ogunkoya, O. O. (2013). Salinity and sodium hazards of three streams of different agricultural land use systems in Ile-Ife, Nigeria. *Applied Water Science*, *3*(1), 19-28.

Oguntunde, P. G., & Abiodun, B. J. (2013). The impact of climate change on the Niger River Basin hydroclimatology, West Africa. *Climate Dynamics*, *40*(1-2), 81-94.

Oguntunde, P. G., Abiodun, B. J., & Lischeid, G. (2016). A numerical modelling study of the hydroclimatology of the Niger River Basin, West Africa. *Hydrological Sciences Journal*, *61*(1), 94-106.

Oguntunde, P. G., Friesen, J., van de Giesen, N., & Savenije, H. H. (2006). Hydroclimatology of the Volta River Basin in West Africa: Trends and variability from 1901 to 2002. *Physics and Chemistry of the Earth, Parts A/B/C*, *31*(18), 1180-1188.

Oişte, A. M. (2014). Groundwater quality assessment in urban environment. *International Journal of Environmental Science and Technology*, *11*(7), 2095-2102.

Okoya, A., Osungbemiro, B., & Ologunorisa, T. (2017). Spatial and temporal variation of rainwater chemistry in Ile-Ife and its environ, Osun State, Nigeria. *Journal of Sustainable Development*, 10, 203. 10.5539/jsd.v10n2p203.

Olowoyo, D. N. (2011). Physicochemical characteristics of rainwater quality of Warri axis of Delta state in western Niger Delta region of Nigeria. *Journal of Environmental Chemistry and Ecotoxicology*, *3*(12), 320-322.

Paaijmans, K. P., Takken, W., Githeko, A. K., & Jacobs, A. F. G. (2008). The effect of water turbidity on the near-surface water temperature of larval habitats of the malaria mosquito Anopheles gambiae. *International Journal of Biometeorology*, *52*(8), 747-753.

Paliwal, K. V. (1972). *Irrigation with saline water* (p. 198). Monogram no. 2 (New series). New Delhi: IARI.

Pandey, B. K., & Khare, D. (2018). Identification of trend in long term precipitation and reference evapotranspiration over Narmada river basin (India). *Global and Planetary Change*, *161*, 172-182.

Pant, R. R., Zhang, F., Rehman, F. U., Wang, G., Ye, M., Zeng, C., & Tang, H. (2018). Spatiotemporal variations of hydrogeochemistry and its controlling factors in the Gandaki River Basin, Central Himalaya Nepal. *Science of the Total Environment*, *622*, 770-782.

Papalaskaris, T., & Kampas, G. (2017). Time series analysis of water characteristics of streams in Eastern Macedonia–Thrace, Greece. *European Water*, 57, 93-100.

Park, J. H., Duan, L., Kim, B., Mitchell, M. J., & Shibata, H. (2010). Potential effects of climate change and variability on watershed biogeochemical processes and water quality in Northeast Asia. *Environment International*, *36*(2), 212-225.

Park, P. K., Gordon, L. I., Hager, S. W., & Cissell, M. C. (1969). Carbon dioxide partial pressure in the Columbia River. *Science*, *166*(3907), 867-868.

Partal, T., & Kahya, E. (2006). Trend analysis in Turkish precipitation data. *Hydrological Processes*, *20*(9), 2011-2026.

Patil, S. R. (2008). *Regionalization of an event based Nash cascade model for flood predictions in ungauged basins* (Doctoral dissertation, Institut für Wasserbau der Universität Stuttgart (Germany)).

Patil, S., & Valunjkar, S. (2014). Farecasting of daily runoff using artificial neural networks. *International Journal of Civil Engineering and Technology (IJCIET), ISSN*, 0976-6308.

Paulhus, J. L., & Kohler, M. A. (1952). Interpolation of missing precipitation records. *Monthly Weather Review*, *80*(8), 129-133.

Pearce, C. R., Parkinson, I. J., Gaillardet, J., Chetelat, B., & Burton, K. W. (2015). Characterising the stable (d88/86Sr) and radiogenic (87Sr/86Sr) isotopic composition of strontium in rainwater. *Chemical Geology*, 409, 54-60.

Pearson, K. (1895). Notes on Regression and Inheritance in the Case of Two Parents. *Proceedings of the Royal Society of London*, *58*(347-352), 240-242.

Peirce, J. J., Weiner, R., Matthews, R., & Vesilind, P. A. (2003). *Environmental engineering*. United States of America: Butterworth-Heinemann.

Pelig-Ba, K. B. (2009). Analysis of stable isotope contents of surface and underground water in two main geological formations in the Northern region of Ghana. *West African Journal of Applied Ecology*, *15*(1).

Peña-Arancibia, J. L., Mainuddin, M., Kirby, J. M., Chiew, F. H., McVicar, T. R., & Vaze, J. (2016). Assessing irrigated agriculture's surface water and groundwater consumption by combining satellite remote sensing and hydrologic modelling. *Science of the Total Environment*, *542*, 372-382.

Peng, T., Zhou, J., Zhang, C., & Fu, W. (2017). Streamflow forecasting using empirical wavelet transform and artificial neural networks. *Water*, *9*(6), 406.

Perona, E., Bonilla, I., & Mateo, P. (1999). Spatial and temporal changes in water quality in a Spanish river. *Science of The Total Environment*, *241*(1-3), 75-90.

Peters, N. E., Shanley, J. B., Aulenbach, B. T., Webb, R. M., Campbell, D. H., Hunt, R., ... & Walker, J. F. (2006). Water and solute mass balance of five small, relatively undisturbed watersheds in the US. *Science of the Total Environment*, *358*(1-3), 221-242.

Petersen, T., Devineni, N., & Sankarasubramanian, A. (2018). Monthly hydroclimatology of the continental United States. *Advances in Water Resources*, *114*, 180-195.

Peterson, T. C., Easterling, D. R., Karl, T. R., Groisman, P., Nicholls, N., Plummer, N., ... & Vincent, L. (1998). Homogeneity adjustments of in situ atmospheric climate data: a review. *International Journal of Climatology: A Journal of the Royal Meteorological Society*, *18*(13), 1493-1517.

Piper, A. M. (1944). A graphic procedure in the geochemical interpretation of water-analyses. *Eos, Transactions American Geophysical Union*, *25*(6), 914-928.

Plummer, L. N., Jones, B. F., & Truesdell, A. H. (1976). *WATEQF; a FORTRAN IV version of WATEQ: a computer program for calculating chemical equilibrium of natural waters* (No. 76-13). Department of the Interior, Geological Survey, Water Resources Division

Potter, N. J., Chiew, F. H. S., & Frost, A. J. (2010). An assessment of the severity of recent reductions in rainfall and runoff in the Murray–Darling Basin. *Journal of Hydrology*, *381*(1-2), 52-64.

Presti, R. L., Barca, E., & Passarella, G. (2010). A methodology for treating missing data applied to daily rainfall data in the Candelaro River Basin (Italy). *Environmental Monitoring and Assessment*, *160*(1-4), 1.

Purandara, B. K., Varadarajan, N., & Jayashree, K. (2003). Impact of sewage on ground water quality-A case study. *Pollution Research*, *22*(2), 189-197.

Qaisar, F. U. R., Zhang, F., Pant, R. R., Wang, G., Khan, S., & Zeng, C. (2018). Spatial variation, source identification, and quality assessment of surface water geochemical composition in the Indus River Basin, Pakistan. *Environmental Science and Pollution Research*, *25*(13), 12749–12763.

Qin, T., Yang, P., Groves, C., Chen, F., Xie, G., & Zhan, Z. (2018). Natural and anthropogenic factors affecting geochemistry of the Jialing and Yangtze Rivers in urban Chongqing, SW China. *Applied Geochemistry*, *98*, 448-458.

Qishlaqi, A., Kordian, S., & Parsaie, A. (2017). Hydrochemical evaluation of river water quality—a case study. *Applied Water Science*, *7*(5), 2337-2342.

Raghunath, H.M. (1987). *Groundwater*. Wiley Eastern Ltd., Delhi.

Rahman, M. A., Yunsheng, L., & Sultana, N. (2017). Analysis and prediction of rainfall trends over Bangladesh using Mann–Kendall, Spearman's rho tests and ARIMA model. *Meteorology and Atmospheric Physics*, *129*(4), 409-424.

Raj, P. N., & Azeez, P. A. (2012). Trend analysis of rainfall in Bharathapuzha River basin, Kerala, India. *International Journal of Climatology*, *32*(4), 533-539.

Raja, N. B., & Aydin, O. (2018). Trend analysis of annual precipitation of Mauritius for the period 1981–2010. *Meteorology and Atmospheric Physics*, 1-17.

Rajeev, P., Rajput, P., & Gupta, T. (2016). Chemical characteristics of aerosol and rain water during an El Niño and PDO influenced Indian summer monsoon. *Atmospheric Environment*, *145*, 192-200.

Rajkumar, M., Perumal, P., Prabu, V. A., Perumal, N. V., & Rajasekar, K. T. (2009). Phytoplankton diversity in Pichavaram mangrove waters from south-east coast of India. *Journal of Environmental Biology*, *30*(4).

Rajurkar, M. P., Kothyari, U. C., & Chaube, U. C. (2002). Artificial neural networks for daily rainfall—runoff modelling. *Hydrological Sciences Journal*, *47*(6), 865-877.

Raman, H., & Sunilkumar, N. (1995). Multivariate modelling of water resources time series using artificial neural networks. *Hydrological Sciences Journal*, *40*(2), 145-163.

Raman, V. (1983). Impact of corrosion in the conveyance and distribution of water. *Journal of Indian Water Works Association*, *15*(1), 115-121.

Ran, L., Lu, X. X., Richey, J. E., Sun, H., Han, J., Yu, R., ... & Yi, Q. (2015). Long-term spatial and temporal variation of CO2 partial pressure in the Yellow River, China. *Biogeosciences*, *12*(4), 921-932.

Rana, A., Uvo, C. B., Bengtsson, L., & Sarthi, P. P. (2012). Trend analysis for rainfall in Delhi and Mumbai, India. *Climate Dynamics*, *38*(1-2), 45-56.

Rangin, C., Bellon, H., Benard, F., Letouzey, J., Muller, C., & Sanudin, T. (1990). Neogene arc-continent collision in Sabah, northern Borneo (Malaysia). *Tectonophysics*, *183*(1-4), 305-319.

Rao, P. S. P., Tiwari, S., Matwale, J. L., Pervez, S., Tunved, P., Safai, P. D., ... & Hopke, P. K. (2016). Sources of chemical species in rainwater during monsoon and non-monsoonal periods over two mega cities in India and dominant source region of secondary aerosols. *Atmospheric Environment*, *146*, 90-99.

Rasool, A., & Xiao, T. (2019). Distribution and potential ecological risk assessment of trace elements in the stream water and sediments from Lanmuchang area, southwest Guizhou, China. *Environmental Science and Pollution Research*, 26(4), 3706-3722.

Ravikumar, P., Mehmood, M. A., & Somashekar, R. K. (2013). Water quality index to determine the surface water quality of Sankey tank and Mallathahalli lake, Bangalore urban district, Karnataka, India. *Applied Water Science*, *3*(1), 247-261.

Ravikumar, P., Somashekar, R. K., & Prakash, K. L. (2015). A comparative study on usage of Durov and Piper diagrams to interpret hydrochemical processes in groundwater from SRLIS river basin, Karnataka, India. *Elixir International Journal*, *80*, 31073-31077.

Raymahashay, B. C. (1986). Geochemistry of bicarbonate in river water. *Journal of the Geological Society of India*, *27*(1), 114-118.

Raymahashay, B. C. (1996). Geochemistry for hydrologists. New Delhi: Allied Publishers.

Razack, M., & Dazy, J. (1990). Hydrochemical characterization of groundwater mixing in sedimentary and metamorphic reservoirs with combined use of Piper's principle and factor analysis. *Journal of Hydrology*, *114*(3-4), 371-393.

Remesan, R., Shamim, M. A., Han, D., & Mathew, J. (2009). Runoff prediction using an integrated hybrid modelling scheme. *Journal of Hydrology*, *372*(1-4), 48-60.

Ren, W., Yao, T., Xie, S., & He, Y. (2017). Controls on the stable isotopes in precipitation and surface waters across the southeastern Tibetan Plateau. *Journal of Hydrology*, *545*, 276-287.

Ressler, T., Wong, J., Roos, J., & Smith, I. L. (2000). Quantitative speciation of Mn-bearing particulates emitted from autos burning (methylcyclopentadienyl) manganese tricarbonyl-added gasolines using XANES spectroscopy. *Environmental Science & Technology*, *34*(6), 950-958.

Rezaeianzadeh, M., Stein, A., Tabari, H., Abghari, H., Jalalkamali, N., Hosseinipour, E. Z., & Singh, V. P. (2013). Assessment of a conceptual hydrological model and artificial neural networks for daily outflows forecasting. *International Journal of Environmental Science and Technology*, *10*(6), 1181-1192.

Riad, S., Mania, J., Bouchaou, L., & Najjar, Y. (2004). Rainfall-runoff model using an artificial neural network approach. *Mathematical and Computer Modelling*, *40*(7-8), 839-846.

Rice, K. C., & Bricker, O. P. (1995). Seasonal cycles of dissolved constituents in streamwater in two forested catchments in the mid-Atlantic region of the eastern USA. *Journal of Hydrology*, *170*(1-4), 137-158.

Richards, L. A. (1954). *Diagnosis and improvement of saline and alkali soils*. Handbook No. 60. US Department of Agriculture, Washington, DC.

Risi, C., Bony, S., & Vimeux, F. (2008). Influence of convective processes on the isotopic composition (δ18O and δD) of precipitation and water vapor in the tropics: 2. Physical interpretation of the amount effect. *Journal of Geophysical Research: Atmospheres*, *113*(D19).

Rissanen, J. (1978). Modeling by shortest data description. *Automatica*, *14*(5), 465-471.

Rissanen, J. (1989). *Stochastic complexity in statistical inquiry*. River Edge, New Jersey, USA: World Scientific Publishing Co., Inc. ©1989 ISBN:9971508591.

Ritzema, H., & Wösten, H. (2002). Hydrology of Borneo's peat swamps. In *Strategies for implementing sustainable management of peatlands in Borneo. Proceedings STRAPEAT Partners Workshop, Palangka Raya, Kalimantan, Indonesia and Sibu, Sarawak, Malaysia*.

Robertson, A. W., Moron, V., Qian, J. H., Chang, C. P., Tangang, F., Aldrian, E., ... & Juneng, L. (2011). The maritime continent monsoon. The global monsoon system: research and forecast. *World Scientific Series on Asia-Pacific Weather and Climate*, *5*, 608.

Robins, P. E., Skov, M. W., Lewis, M. J., Gimenez, L., Davies, A. G., Malham, S. K., ... & Jago, C. F. (2016). Impact of climate change on UK estuaries: A review of past trends and potential projections. *Estuarine, Coastal and Shelf Science*, *169*, 119-135.

Rochelle, B. P., Church, M. R., & David, M. B. (1987). Sulfur retention at intensively studied sites in the US and Canada. *Water, Air, and Soil Pollution*, *33*(1-2), 73-83.

Rodgers, P., Soulsby, C., Waldron, S., & Tetzlaff, D. (2005). Using stable isotope tracers to assess hydrological flow paths, residence times and landscape influences in a nested mesoscale catchment. *Hydrology and Earth System Sciences Discussions*, *9*(3), 139-155.

Rodríguez-Blanco, M. L., Taboada-Castro, M. M., & Taboada-Castro, M. T. (2012). Rainfall–runoff response and event-based runoff coefficients in a humid area (northwest Spain). *Hydrological Sciences Journal*, *57*(3), 445-459.

Rozanski, K., Araguás-Araguás, L., & Gonfiantini, R. (1993). Isotopic patterns in modern global precipitation. *Climate Change in Continental Isotopic Records*, *78*, 1-36.

Rozanski, K., Sonntag, C., & Münnich, K. O. (1982). Factors controlling stable isotope composition of European precipitation. *Tellus*, *34*(2), 142-150.

Rusydi, A. F. (2018). Correlation between conductivity and total dissolved solid in various type of water: A review. In *IOP Conference Series: Earth and Environmental Science* (Vol. 118, No. 1, p. 012019). IOP Publishing.

Ryznar, J. W. (1944). A new index for determining amount of calcium carbonate scale formed by a water. *Journal-American Water Works Association*, *36*(4), 472-483.

Sa'adi, Z., Shahid, S., Ismail, T., Chung, E. S., & Wang, X. J. (2017a). Trends analysis of rainfall and rainfall extremes in Sarawak, Malaysia using modified Mann–Kendall test. *Meteorology and Atmospheric Physics*, 1-15.

Sa'adi, Z., Shahid, S., Chung, E. S., & bin Ismail, T. (2017b). Projection of spatial and temporal changes of rainfall in Sarawak of Borneo Island using statistical downscaling of CMIP5 models. *Atmospheric Research*, *197*, 446-460.

Sabuti, A. A., & Mohamed, C. A. R. (2016). Distribution and source of trace elements in marine aerosol of Mersing, Johor, Malaysia. *Journal of Oceanography and Marine Research*, *4*(146), 2.

Sabzevari, A. A., Zarenistanak, M., Tabari, H., & Moghimi, S. (2015). Evaluation of precipitation and river discharge variations over southwestern Iran during recent decades. *Journal of Earth System Science*, *124*(2), 335-352.

Said, A., Stevens, D. K., & Sehlke, G. (2004). An innovative index for evaluating water quality in streams. *Environmental Management*, *34*(3), 406-414.

Sajikumar, N., & Thandaveswara, B. S. (1999). A non-linear rainfall–runoff model using an artificial neural network. *Journal of Hydrology*, *216*(1-2), 32-55.

Salahuddin, A., & Curtis, S. (2011). Climate extremes in Malaysia and the equatorial South China Sea. *Global and Planetary Change*, *78*(3-4), 83-91.

Salamalikis, V., Argiriou, A. A., & Dotsika, E. (2015). Stable isotopic composition of atmospheric water vapor in Patras, Greece: A concentration weighted trajectory approach. *Atmospheric research*, *152*, 93-104.

Salas, J. D. Delleur, J. W., Yevjevich, V., & Lane, W. L. (1980). *Applied modeling of hydrologic time series*. United States of America: Water Resources Publication.

Salati, E., Dall'Olio, A., Matsui, E., & Gat, J. R. (1979). Recycling of water in the Amazon basin: an isotopic study. *Water Resources Research*, *15*(5), 1250-1258.

Saleem, M., Iqbal, J., & Shah, M. H. (2014). Dissolved concentrations, sources, and risk evaluation of selected metals in surface water from Mangla lake, Pakistan. *The Scientific World Journal*, *2014*.

Sánchez-Murillo, R., Birkel, C., Welsh, K., Esquivel-Hernández, G., Corrales-Salazar, J., Boll, J., ... & Arce-Mesén, R. (2016). Key drivers controlling stable isotope variations in daily precipitation of Costa Rica: Caribbean Sea versus Eastern Pacific Ocean moisture sources. *Quaternary Science Reviews*, *131*, 250-261.

Sánchez-Murillo, R., Brooks, E. S., Elliot, W. J., & Boll, J. (2015). Isotope hydrology and baseflow geochemistry in natural and human-altered watersheds in the Inland Pacific Northwest, USA. *Isotopes in Environmental and Health Studies*, *51*(2), 231-254.

Sand, K. K., Tobler, D. J., Dobberschutz, S., Larsen, K. K., Makovicky, E., Andersson, M. P., ... & Stipp, S. L. S. (2016). Calcite Growth Kinetics: Dependence on Saturation Index, Ca2+:

CO32–Activity Ratio, and Surface Atomic Structure. *Crystal Growth & Design*, *16*(7), 3602-3612.

Sanhueza, E., Elbert, W., Rondón, A., Arias, M. C., & Hermoso, M. (1989). Organic and inorganic acids in rain from a remote site of the Venezuelan savannah. *Tellus B: Chemical and Physical Meteorology*, *41*(2), 170-176.

Sankarasubramanian, A., & Vogel, R. M. (2002). Annual hydroclimatology of the United States. *Water Resources Research*, *38*(6), 19.1-12.

Santacruz De León, G., Ramos Leal, J. A., Morán Ramírez, J., López Álvarez, B., & Santacruz de León, E. E. (2017). Quality indices of groundwater for agricultural use in the Soconusco, Chiapas, Mexico. *Earth Sciences Research Journal*, *21*(3), 117-127.

Sanusi, A., Wortham, H., Millet, M., & Mirabel, P. (1996). Chemical composition of rainwater in eastern France. *Atmospheric Environment*, *30*(1), 59-71.

Sapek, B. (2014). Calcium and magnesium in atmospheric precipitation, groundwater and the soil solution in long-term meadow experiments. *Journal of Elementology*, *19*(1).

Sapin, F., Pubellier, M., Lahfid, A., Janots, D., Aubourg, C., & Ringenbach, J. C. (2011). Onshore record of the subduction of a crustal salient: example of the NW Borneo Wedge. *Terra Nova*, *23*(4), 232-240.

Scarsbrook, M. R., McBride, C. G., McBride, G. B., & Bryers, G. G. (2003). Effects of climate variability on rivers: consequences for long term water quality analysis. *JAWRA Journal of the American Water Resources Association*, *39*(6), 1435-1447.

Schalkoff, R. J. (1997). *Artificial neural networks* (Vol. 1). New York: McGraw-Hill.

Schober, P., Boer, C., & Schwarte, L. A. (2018). Correlation coefficients: appropriate use and interpretation. *Anesthesia & Analgesia*, *126*(5), 1763-1768.

Schoeller, H. (1965). Qualitative evaluation of groundwater resources. *Methods and Techniques of Groundwater Investigations and Development. UNESCO*, *5483*.

Schoeller, H. (1977). Geochemistry of groundwater. In 'Groundwater Studies–an International Guide for Research and Practice'.(Eds RH Brown, AA Konoplyantsev, J. Ineson, and VS Kovalevsky.) pp. 1–18.

SEB Annual Report (2010). Sarawak Energy Berhad Annual Report. https://www.sarawakenergy.com/AnnualReport/SEBAR10.pdf. Accessed on 20.02.2018.

Semwal, N., & Jangwan, J. S. (2009). Major ion chemistry of river Bhagirathi and river Kosi in the Uttarakhand Himalaya. *International Journal of Chemical Science*, 7(2), 607-616.

Senthil Kumar, A. R., Sudheer, K. P., Jain, S. K., & Agarwal, P. K. (2005). Rainfall-runoff modelling using artificial neural networks: comparison of network types. *Hydrological Processes: An International Journal*, *19*(6), 1277-1291.

Serrano, A., Mateos, V. L., & Garcia, J. A. (1999). Trend analysis of monthly precipitation over the Iberian Peninsula for the period 1921–1995. *Physics and Chemistry of the Earth, Part B: Hydrology, Oceans and Atmosphere*, *24*(1-2), 85-90.

Shadmani, M., Marofi, S., & Roknian, M. (2012). Trend analysis in reference evapotranspiration using Mann-Kendall and Spearman's Rho tests in arid regions of Iran. *Water Resources Management*, *26*(1), 211-224.

Shah, A., Zhafri, M., Delson, J., & Navakanesh, B. (2018). Major Strike-Slip faults identified using satellite data in Central Borneo, SE Asia. *Geosciences*, *8*(5), 156.

Shammi, M., Rahman, R., Rahman, M. M., Moniruzzaman, M., Bodrud-Doza, M., Karmakar, B., & Uddin, M. K. (2016). Assessment of salinity hazard in existing water resources for irrigation and potentiality of conjunctive uses: a case report from Gopalganj District, Bangladesh. *Sustainable Water Resources Management*, *2*(4), 369-378.

Shamseldin, A. Y., O'CONNOR, K. M., & Nasr, A. E. (2007). A comparative study of three neural network forecast combination methods for simulated river flows of different rainfall—runoff models. *Hydrological Sciences Journal*, *52*(5), 896-916.

Shanmugasundram, S. (2012). *Statistical analysis to detect climate change and its implications on water resources* (Doctoral dissertation, Victoria University (Australia)).

Sharma, S., & Singh, P. (2017). Long term spatiotemporal variability in rainfall trends over the State of Jharkhand, India. *Climate*, *5*(1), 18.

Shelton, M. L. (2009). *Hydroclimatology: perspectives and applications*. Cambridge, UK: Cambridge University Press.

Shirley, R., & Kammen, D. (2015). Energy planning and development in Malaysian Borneo: Assessing the benefits of distributed technologies versus large scale energy mega-projects. *Energy Strategy Reviews*, *8*, 15-29.

Shoaib, M., Shamseldin, A. Y., & Melville, B. W. (2014). Comparative study of different wavelet based neural network models for rainfall–runoff modeling. *Journal of Hydrology*, *515*, 47-58.

Shoaib, M., Shamseldin, A. Y., Khan, S., Khan, M. M., Khan, Z. M., Sultan, T., & Melville, B. W. (2018). A comparative study of various hybrid wavelet feedforward neural network models for runoff forecasting. *Water Resources Management*, *32*(1), 83-103.

Shoaib, M., Shamseldin, A. Y., Khan, S., Khan, M. M., Khan, Z. M., & Melville, B. W. (2018). A wavelet based approach for combining the outputs of different rainfall–runoff models. *Stochastic Environmental Research and Risk Assessment*, *32*(1), 155-168.

Shrestha, S., Prasad Pandey, V., Yoneyama, Y., Shrestha, S., & Kazama, F. (2013). An evaluation of rainwater quality in Kathmandu Valley, Nepal. *Sustainable Environment Research*, 23(5).

Sidauruk, P., Pratikno, B., & Pujiindiyati, E. R. (2018). Isotopic Characterization of Precipitation, Inflow, and Outflow of Lake Toba as a First Assessment of Lake Water Balance Study. *atom indonesia*, *44*(1), 1-7.

Sillapapiromsuk, S., & Chantara, S. (2010). Chemical composition and seasonal variation of acid deposition in Chiang Mai, Thailand. *Environmental Engineering Research*, *15*(2), 93-98.

Simeonov, V., Stratis, J. A., Samara, C., Zachariadis, G., Voutsa, D., Anthemidis, A., ... & Kouimtzis, T. (2003). Assessment of the surface water quality in Northern Greece. *Water research*, *37*(17), 4119-4124.

Singaraja, C. (2017). Relevance of water quality index for groundwater quality evaluation: Thoothukudi District, Tamil Nadu, India. *Applied Water Science*, *7*(5), 2157-2173.

Singh, A. K. (2002). Quality assessment of surface and subsurface water of Damodar river basin. *Indian Journal of Environmental Health*, *44*(1), 41-49.

Singh, K. (2011). *Chemical Composition of Atmospheric Precipitation in Different Environments of Palampur* (Masters dissertation, CSKHPKV Palampur (India))

Singh, P. V. (2014). *Multilayer perceptron and single multiplicative neuron based artificial neural network rainfall-runoff models for a Himalayan watershed* (Doctoral dissertation, GB Pant University of Agriculture and Technology, Pantnagar-263145 (Uttarakhand)).

Singh, V. P. (1992). *Elementary hydrology*. United Kingdom: Pearson College Division.

Sjostrom, D. J., & Welker, J. M. (2009). The influence of air mass source on the seasonal isotopic composition of precipitation, eastern USA. *Journal of Geochemical Exploration*, *102*(3), 103-112.

Small, M., & Judd, K. (1998). Comparisons of new nonlinear modeling techniques with applications to infant respiration. *Physica D: Nonlinear Phenomena*, *117*(1-4), 283-298.

Small, M., & Tse, C. K. (2002). Minimum description length neural networks for time series prediction. *Physical Review E*, *66*(6), 066701.

Smith, J., & Eli, R. N. (1995). Neural-network models of rainfall-runoff process. *Journal of Water Resources Planning and Management*, *121*(6), 499-508.

Smith, M. (1993). *Neural networks for statistical modeling*. New York: John Wiley & Sons, Inc..

Sneyers, R. (1990). *On the statistical analysis of series of observations* (No. 143). Geneva: World Meteorological Organisation.

Soderberg, K. (2003). *Geochemistry of the fynbos ecosystem in a Table Mountain Group sub catchment of the Olifants River, Western Cape, South Africa* (Doctoral dissertation, University of Cape Town (South Africa)).

Sokol, R. R., & Rohlf, F. J. (1969). *The principles and practice of statistics in biological research*. San Francisco: W.H. Freeman and Company.

Solomatine, D. P., & Dulal, K. N. (2003). Model trees as an alternative to neural networks in rainfall—runoff modelling. *Hydrological Sciences Journal*, *48*(3), 399-411.

Song, F., & Gao, Y. (2009). Chemical characteristics of precipitation at metropolitan Newark in the US East Coast. *Atmospheric Environment*, *43*(32), 4903-4913.

Srinivasulu, S., & Jain, A. (2006). A comparative analysis of training methods for artificial neural network rainfall–runoff models. *Applied Soft Computing*, *6*(3), 295-306.

Stets, E. G., Lee, C. J., Lytle, D. A., & Schock, M. R. (2018). Increasing chloride in rivers of the conterminous US and linkages to potential corrosivity and lead action level exceedances in drinking water. *Science of the Total Environment*, *613*, 1498-1509.

Stumm, W., & Morgan, J. J. (1996). *Aquatic Chemistry–chemical equilibria and rates in natural waters* 3rd edition. New York: John Wiley & Sons.

Stumpp, C., Klaus, J., & Stichler, W. (2014). Analysis of long-term stable isotopic composition in German precipitation. *Journal of Hydrology*, *517*, 351-361.

Subash, N., Ram Mohan, H. S., & Sikka, A. K. (2011). Decadal frequency and trends of extreme excess/deficit rainfall during the monsoon season over different meteorological sub-divisions of India. *Hydrological Sciences Journal*, *56*(7), 1090-1109.

Sudheer, K. P., & Jain, A. (2004). Explaining the internal behaviour of artificial neural network river flow models. *Hydrological Processes*, *18*(4), 833-844.

Sudheer, K. P., Gosain, A. K., & Ramasastri, K. S. (2002). A data-driven algorithm for constructing artificial neural network rainfall-runoff models. *Hydrological Processes*, *16*(6), 1325-1330.

Sudheer, K. P., Nayak, P. C. & Rangan, D. M. (2000). *Rainfall runoff modelling using artificial neural network technique*. Unpublished report by National Institute of Hydrology, Roorkee. 1999 – 2000.

Suhaila, J., Sayang, M. D., & Jemain, A. A. (2008). Revised spatial weighting methods for estimation of missing rainfall data. *Asia-Pacific Journal of Atmospheric Sciences*, *44*(2), 93-104.

Suhaimi, S., & Bustami, R. A. (2009). Rainfall Runoff Modeling using Radial Basis Function Neural Network for Sungai Tinjar Catchment, Miri, Sarawak. *Journal of Civil Engineering, Science and Technology*, *1*(1), 1-7.

Sultan, K. (2012). Hydrochemistry and baseline values of major and trace elements in tropical surface waters of the Terengganu River (Malaysia). *Water International*, *37*(1), 1-15.

Sun, H., Alexander, J., Gove, B., Pezzi, E., Chakowski, N., & Husch, J. (2014). Mineralogical and anthropogenic controls of stream water chemistry in salted watersheds. *Applied Geochemistry*, *48*, 141-154.

Suppiah, R., & Hennessy, K. J. (1998). Trends in total rainfall, heavy rain events and number of dry days in Australia, 1910–1990. *International Journal of Climatology: A Journal of the Royal Meteorological Society*, *18*(10), 1141-1164.

Szép, R., Bodor, Z., Miklóssy, I., Niță, I. A., Oprea, O. A., & Keresztesi, Á. (2019). Influence of peat fires on the rainwater chemistry in intra-mountain basins with specific atmospheric circulations (Eastern Carpathians, Romania). *Science of The Total Environment*, *647*, 275-289.

Szép, R., Mateescu, E., Nechifor, A. C., & Keresztesi, Á. (2017). Chemical characteristics and source analysis on ionic composition of rainwater collected in the Carpathians "Cold Pole," Ciuc basin, Eastern Carpathians, Romania. *Environmental Science and Pollution Research*, *24*(35), 27288-27302.

Tabari, H., Abghari, H., & Hosseinzadeh Talaee, P. (2012). Temporal trends and spatial characteristics of drought and rainfall in arid and semiarid regions of Iran. *Hydrological Processes*, *26*(22), 3351-3361.

Tabari, H., Somee, B. S., & Zadeh, M. R. (2011). Testing for long-term trends in climatic variables in Iran. *Atmospheric Research*, *100*(1), 132-140.

Tahir, T., Hashim, A. M., & Yusof, K. W. (2018). Statistical downscaling of rainfall under transitional climate in Limbang River Basin by using SDSM. In *IOP Conference Series: Earth and Environmental Science,* 140(1), 012037. IOP Publishing.

Tahlawi, M. R., Mohamed, M. A., Boghdadi, G. Y., Rabeiy, R. E., & Saleem, H. A. (2014). Groundwater quality assessment to estimate its suitability for different uses in Assiut Governorate, Egypt. *International Journal of Recent Technology and Engineering*, *3*, 2277-3878.

Talabi, A. O., Afolagboye, O. L., Tijani, M. N., Aladejana, J. A., & Ogundana, A. K. (2013). Hydrogeochemical assessment of surface water in the central part of Ekiti-State, Southwestern Nigeria.". *American Journal of Water Resource*, *1*(4), 56-65.

Talaee, P. H. (2014). Iranian rainfall series analysis by means of nonparametric tests. *Theoretical and Applied Climatology*, *116*(3-4), 597-607.

Tan, D. N. K. (1979). Lupar Valley, West Sarawak, Malaysia. *Geological Survey of Malaysia, Report*, *13*, 39-49.

Tan, M. (2014). Circulation effect: response of precipitation δ 18 O to the ENSO cycle in monsoon regions of China. *Climate Dynamics*, *42*(3-4), 1067-1077.

Tang, L., Duan, X., Kong, F., Zhang, F., Zheng, Y., Li, Z., ... & Hu, S. (2018). Influences of climate change on area variation of Qinghai Lake on Qinghai-Tibetan Plateau since 1980s. *Scientific reports*, *8*(1), 7331-7331.

Tangang, F. T., Juneng, L., Salimun, E., Vinayachandran, P. N., Seng, Y. K., Reason, C. J. C., ... & Yasunari, T. (2008). On the roles of the northeast cold surge, the Borneo vortex, the Madden-Julian oscillation, and the Indian Ocean Dipole during the extreme 2006/2007 flood in southern Peninsular Malaysia. *Geophysical Research Letters*, *35*(14).

Taniguchi, M., Nakayama, T., Tase, N., & Shimada, J. (2000). Stable isotope studies of precipitation and river water in the Lake Biwa basin, Japan. *Hydrological Processes*, *14*(3), 539-556.

Tao, F. (2017). Air–water CO 2 flux in an algae bloom year for Lake Hongfeng, Southwest China: implications for the carbon cycle of global inland waters. *Acta Geochimica*, *36*(4), 658-666.

Tapper, N. (1999). Atmospheric issues for fire management in eastern Indonesia and northern Australia. In *ACIAR Proceedings* (pp. 21-30). ACIAR; 1998.

Tardy, Y., Bustillo, V., Roquin, C., Mortatti, J., & Victoria, R. (2005). The Amazon. Bio-geochemistry applied to river basin management: part I. Hydro-climatology, hydrograph separation, mass transfer balances, stable isotopes, and modelling. *Applied Geochemistry*, *20*(9), 1746-1829.

Taupin, J. D., Coudrain-Ribstein, A., Gallaire, R., Zuppi, G. M., & Filly, A. (2000). Rainfall characteristics ($\delta^{18}O$, $\delta^{2}H$, ΔT and ΔHr) in western Africa: Regional scale and influence of irrigated areas. *Journal of Geophysical Research: Atmospheres*, *105*(D9), 11911-11924.

Taxak, A. K., Murumkar, A. R., & Arya, D. S. (2014). Long term spatial and temporal rainfall trends and homogeneity analysis in Wainganga basin, Central India. *Weather and Climate Extremes*, *4*, 50-61.

Taylor, R. (1990). Interpretation of the correlation coefficient: a basic review. *Journal of Diagnostic Medical Sonography*, *6*(1), 35-39.

Tayyab, M., Dong, X., Ahmad, I., Zahra, A., Zhou, J., Zeng, X., & Shakoor, A. (2019). Identifying Half-Century Precipitation Trends in a Chinese Lake Basin. *Polish Journal of Environmental Studies*, *28*(3).

Tayyab, M., Zhou, J., Zeng, X., & Adnan, R. (2016). Discharge forecasting by applying artificial neural networks at the Jinsha river basin, China. *European Scientific Journal, ESJ*, *12*(9), 108.

Teschl, R., & Randeu, W. L. (2006). A neural network model for short term river flow prediction. *Natural Hazards and Earth System Science*, *6*(4), 629-635.

Thakur, D., Bartarya, S. K., & Nainwal, H. C. (2018). Tracing ionic sources and geochemical evolution of groundwater in the Intermountain Una basin in outer NW Himalaya, Himachal Pradesh, India. *Environmental Earth Sciences*, 77(20), 720.

Tharammal, T., Bala, G., & Noone, D. (2017). Impact of deep convection on the isotopic amount effect in tropical precipitation. *Journal of Geophysical Research: Atmospheres*, *122*(3), 1505-1523.

Tian, C., Wang, L., Kaseke, K. F., & Bird, B. W. (2018). Stable isotope compositions (δ 2 H, δ 18 O and δ 17 O) of rainfall and snowfall in the central United States. *Scientific Reports*, *8*(1), 6712.

Tie, S. T. (2010). *Water Quality Assessment of Trusan and Limbang Basins, Sarawak* (Doctoral dissertation, Universiti Malaysia Sarawak (Malaysia)).

Tijani, M. N. (1994). Hydrogeochemical assessment of groundwater in Moro area, Kwara state, Nigeria. *Environmental Geology*, *24*(3), 194-202.

Tiwari, A. K., Singh, A. K., Singh, A. K., & Singh, M. P. (2017). Hydrogeochemical analysis and evaluation of surface water quality of Pratapgarh district, Uttar Pradesh, India. *Applied Water Science*, *7*(4), 1609-1623.

Tiwari, S., Chate, D. M., Bisht, D. S., Srivastava, M. K., & Padmanabhamurty, B. (2012). Rainwater chemistry in the North Western Himalayan Region, India. *Atmospheric Research*, *104*, 128-138.

Todd, D. K., & Mays, L. W. (1980). *Groundwater hydrology*. New York: John Willey Sons. Inc.

Tokar, A. S., & Markus, M. (2000). Precipitation-runoff modeling using artificial neural networks and conceptual models. *Journal of Hydrologic Engineering*, *5*(2), 156-161.

Topçu, S., Incecik, S., & Atimtay, A. T. (2002). Chemical composition of rainwater at EMEP station in Ankara, Turkey. *Atmospheric Research*, *65*(1-2), 77-92.

Torres, I. B. L. T., Amatya, D. M., Sun, G., & Callahan, T. J. (2011). Seasonal rainfall–runoff relationships in a lowland forested watershed in the southeastern USA. *Hydrological Processes*, *25*(13), 2032-2045.

Tositti, L., Pieri, L., Brattich, E., Parmeggiani, S., & Ventura, F. (2018). Chemical characteristics of atmospheric bulk deposition in a semi-rural area of the Po Valley (Italy). *Journal of Atmospheric Chemistry*, *75*(1), 97-121.

Trenberth, K. E. (2011). Changes in precipitation with climate change. *Climate Research*, *47*(1-2), 123-138.

Truesdell, A. H., & Jones, B. F. (1974). WATEQ, a computer program for calculating chemical equilibria of natural waters. Journal of Research of the U.S. Geological Survey, *2*(2), 233-248.

Tsukuda, S., Sugiyama, M., Harita, Y., & Nishimura, K. (2006). Atmospheric phosphorus deposition in Ashiu, Central Japan–source apportionment for the estimation of true input to a terrestrial ecosystem. *Biogeochemistry*, *77*(1), 117-138.

Uemura, R., Yonezawa, N., Yoshimura, K., Asami, R., Kadena, H., Yamada, K., & Yoshida, N. (2012). Factors controlling isotopic composition of precipitation on Okinawa Island,

Japan: Implications for paleoclimate reconstruction in the East Asian Monsoon region. *Journal of Hydrology*, *475*, 314-322.

Uhlenbrook, S. (2006). Catchment hydrology—a science in which all processes are preferential. *Hydrological Processes: An International Journal*, *20*(16), 3581-3585.

United Nations Environment Programme (UNEP) (2006). Water Quality for Ecosystem and Human Health, USA, p.132.

Unnikrishnan Warrier, C., & Praveen Babu, M. (2012). A study on the spatial variations in stable isotopic composition of precipitation in a semiarid region of Southern India. *Hydrological Processes*, *26*(25), 3791-3799.

Unnikrishnan Warrier, C., Praveen Babu, M., Sudheesh, M., & Deshpande, R. D. (2016). Studies on stable isotopic composition of daily rainfall from Kozhikode, Kerala, India. *Isotopes in Environmental and Health Studies*, *52*(3), 219-230.

Usman, U. N., Toriman, M. E., Juahir, H., Abdullahi, M. G., Rabiu, A. A., & Isiyaka, H. (2014). Assessment of groundwater quality using multivariate statistical techniques in Terengganu. *Science and Technology*, *4*(3), 42-49.

Uygur, N., Karaca, F., & Alagha, O. (2010). Prediction of sources of metal pollution in rainwater in Istanbul, Turkey using factor analysis and long-range transport models. *Atmospheric Research*, *95*(1), 55-64.

Valipour, M., & Sefidkouhi, M. A. G. (2018). Temporal analysis of reference evapotranspiration to detect variation factors. *International Journal of Global Warming*, *14*(3), 385-401.

van de Weerd, A. A., & Armin, R. A. (1992). Origin and evolution of the Tertiary hydrocarbon-bearing basins in Kalimantan (Borneo), Indonesia (1). *AAPG bulletin*, *76*(11), 1778-1803.

Van Hattum, M. W. A., Hall, R., Pickard, A. L., & Nichols, G. J. (2013). Provenance and geochronology of Cenozoic sandstones of northern Borneo. *Journal of Asian Earth Sciences*, *76*, 266-282.

Van Wyk, D. B., Lesch, W., & Stock, W. D. (1992). Fire and catchment chemical budgets. In *Fire in South African Mountain Fynbos*, 240-257. Berlin, Heidelberg: Springer.

Vasanthavigar, M., Srinivasamoorthy, K., Vijayaragavan, K., Ganthi, R. R., Chidambaram, S., Anandhan, P., ... & Vasudevan, S. (2010). Application of water quality index for groundwater quality assessment: Thirumanimuttar sub-basin, Tamilnadu, India. *Environmental Monitoring and Assessment*, *171*(1-4), 595-609.

Vega, M., Pardo, R., Barrado, E., & Debán, L. (1998). Assessment of seasonal and polluting effects on the quality of river water by exploratory data analysis. *Water research*, *32*(12), 3581-3592.

Vlastos, D., Antonopoulou, M., Lavranou, A., Efthimiou, I., Dailianis, S., Hela, D., ... & Kassomenos, P. (2019). Assessment of the toxic potential of rainwater precipitation: First evidence from a case study in three Greek cities. *Science of The Total Environment*, *648*, 1323-1332.

Vodila, G., Palcsu, L., Futo, I., & Szántó, Z. (2011). A 9-year record of stable isotope ratios of precipitation in Eastern Hungary: Implications on isotope hydrology and regional palaeoclimatology. *Journal of Hydrology*, *400*(1-2), 144-153.

Von Storch, H. (1999). Misuses of statistical analysis in climate research. In *Analysis of Climate Variability*, 11-26. Springer, Berlin, Heidelberg.

Vozinaki, A. E., Tapoglou, E., & Tsanis, I. K. (2018). Hydrometeorological impact of climate change in two Mediterranean basins. *International Journal of River Basin Management*, *16*(2), 245-257.

Vreča, P., Bronić, I. K., Horvatinčić, N., & Barešić, J. (2006). Isotopic characteristics of precipitation in Slovenia and Croatia: Comparison of continental and maritime stations. *Journal of Hydrology*, *330*(3-4), 457-469.

Vrochidou, A. E., Tsanis, I. K., Grillakis, M. G., & Koutroulis, A. G. (2013). The impact of climate change on hydrometeorological droughts at a basin scale. *Journal of Hydrology*, *476*, 290-301.

Vuai, S. A. H., & Tokuyama, A. (2011). Trend of trace metals in precipitation around Okinawa Island, Japan. *Atmospheric Research*, *99*(1), 80-84.

Vuille, M., Werner, M., Bradley, R. S., & Keimig, F. (2005). Stable isotopes in precipitation in the Asian monsoon region. *Journal of Geophysical Research: Atmospheres*, *110*(D23).

Vystavna, Y., Diadin, D., & Huneau, F. (2018). Defining a stable water isotope framework for isotope hydrology application in a large trans-boundary watershed (Russian Federation/Ukraine). *Isotopes in Environmental and Health Studies*, *54*(2), 147-167.

Walsh, K. J., McBride, J. L., Klotzbach, P. J., Balachandran, S., Camargo, S. J., Holland, G., ... & Sugi, M. (2016). Tropical cyclones and climate change. *Wiley Interdisciplinary Reviews: Climate Change*, *7*(1), 65-89.

Wang, B. (1994). Climatic regimes of tropical convection and rainfall. *Journal of Climate*, *7*(7), 1109-1118.

Wang, H., & Han, G. (2011). Chemical composition of rainwater and anthropogenic influences in Chengdu, Southwest China. *Atmospheric Research*, *99*(2), 190-196.

Wang, P., Yu, J., Zhang, Y., Fu, G., Min, L., & Ao, F. (2011). Impacts of environmental flow controls on the water table and groundwater chemistry in the Ejina Delta, northwestern China. *Environmental Earth Sciences*, *64*(1), 15-24.

Wang, R., Liu, Z., Jiang, L., Yao, Z., Wang, J., & Ju, J. (2016). Comparison of surface water chemistry and weathering effects of two lake basins in the Changtang Nature Reserve, China. *Journal of Environmental Sciences*, 41, 183-194.

Wang, S., Zhang, M., Hughes, C. E., Zhu, X., Dong, L., Ren, Z., & Chen, F. (2016). Factors controlling stable isotope composition of precipitation in arid conditions: an observation network in the Tianshan Mountains, central Asia. *Tellus B: Chemical and Physical Meteorology*, *68*(1), 26206.

Wang, W., Chen, Y., Becker, S., & Liu, B. (2015). Linear trend detection in serially dependent hydrometeorological data based on a variance correction Spearman rho method. *Water*, *7*(12), 7045-7065.

Wang, Y. Q., Zhang, X. Y., Arimoto, R., Cao, J. J., & Shen, Z. X. (2005). Characteristics of carbonate content and carbon and oxygen isotopic composition of northern China soil and dust aerosol and its application to tracing dust sources. *Atmospheric Environment*, *39*(14), 2631-2642.

Wang, Y., Wei, S., Wang, X., Lindsey, E. O., Tongkul, F., Tapponnier, P., ... & Sieh, K. (2017). The 2015 M w 6.0 Mt. Kinabalu earthquake: an infrequent fault rupture within the Crocker fault system of East Malaysia. *Geoscience Letters*, *4*(1), 6.

Warrier, C. U., Babu, M. P., Manjula, P., Velayudhan, K. T., Hameed, A. S., & Vasu, K. (2010). Isotopic characterization of dual monsoon precipitation-evidence from Kerala, India. *Current Science (00113891)*, *98*(11).

Wedepohl, K. H. (1995). The composition of the continental crust. *Geochimica et Cosmochimica Acta*, *59*(7), 1217-1232.

Wenguang, Z., Jingyi, M., Bo, L., Shichun, Z., Jing, Z., Ming, J., & Xianguo, L. (2017). Sources of monsoon precipitation and dew assessed in a semiarid area via stable isotopes. *Hydrological Processes*, *31*(11), 1990-1999.

Whitehead, P. G., Wilby, R. L., Battarbee, R. W., Kernan, M., & Wade, A. J. (2009). A review of the potential impacts of climate change on surface water quality. *Hydrological Sciences Journal*, *54*(1), 101-123.

WHO (2011). *Guidelines for drinking-water quality*. World Health Organization, 216, 303-4.

Wiedermann, W., & Hagmann, M. (2016). Asymmetric properties of the Pearson correlation coefficient: Correlation as the negative association between linear regression residuals. *Communications in Statistics-Theory and Methods*, *45*(21), 6263-6283.

Wigley, T. M. L., & Plummer, L. N. (1976). Mixing of carbonate waters. *Geochimica et Cosmochimica Acta*, *40*(9), 989-995.

Wilcox, L. V. (1955). *Classification and use of irrigation waters*. US Department of Agricultural Circular.

Wilks, D. S., & Haman, K. (1996a). Statistical methods in the atmospheric sciences. *Pure and Applied Geophysics*, *147*(3), 605-605.

Wilks, D. S., & Haman, K. (1996b). Climate time series analysis: Classical statistical and bootstrap methods. *Journal of Time Series Analysis*, *34*(2), 281-281.

Williams, P. R., & Harahap, B. H. (1987). Preliminary geochemical and age data from postsubduction intrusive rocks, northwest Borneo. *Australian Journal of Earth Sciences*, *34*(4), 405-415.

Williams, P. R., Johnston, C. R., Almond, R. A., & Simamora, W. H. (1988). Late Cretaceous to early Tertiary structural elements of West Kalimantan. *Tectonophysics*, *148*(3-4), 279-297.

Wilson, M. E., & Moss, S. J. (1999). Cenozoic palaeogeographic evolution of Sulawesi and Borneo. *Palaeogeography, Palaeoclimatology, Palaeoecology*, *145*(4), 303-337.

Winnick, M. J., Chamberlain, C. P., Caves, J. K., & Welker, J. M. (2014). Quantifying the isotopic 'continental effect'. *Earth and Planetary Science Letters*, *406*, 123-133.

Wirmvem, M. J., Ohba, T., Kamtchueng, B. T., Taylor, E. T., Fantong, W. Y., & Ako, A. A. (2017). Variation in stable isotope ratios of monthly rainfall in the Douala and Yaounde cities, Cameroon: Local meteoric lines and relationship to regional precipitation cycle. *Applied Water Science*, *7*(5), 2343-2356.

Wise, E. K., Woodhouse, C. A., McCabe, G. J., Pederson, G. T., & St-Jacques, J. M. (2018). Hydroclimatology of the Missouri river basin. *Journal of Hydrometeorology*, *19*(1), 161-182.

Wonnacott, T. H., & Wonnacott, R. J. (1990). *Introductory statistics* (Vol. 5). New York: Wiley.

Wooster, M. J., Perry, G. L. W., & Zoumas, A. (2012). Fire, drought and El Niño relationships on Borneo (Southeast Asia) in the pre-MODIS era (1980–2000). *Biogeosciences*, *9*(1), 317-340.

Wu, H., Chen, J., Qian, H., & Zhang, X. (2015). Chemical characteristics and quality assessment of groundwater of exploited aquifers in Beijiao water source of Yinchuan, China: a case study for drinking, irrigation, and industrial purposes. *Journal of Chemistry*, *2015*.

Wu, H., Myung, J. I., & Batchelder, W. H. (2010). Minimum description length model selection of multinomial processing tree models. *Psychonomic Bulletin & Review*, *17*(3), 275-286.

Wu, J., Ding, Y., Ye, B., Yang, Q., Zhang, X., & Wang, J. (2010). Spatio-temporal variation of stable isotopes in precipitation in the Heihe River Basin, Northwestern China. *Environmental Earth Sciences*, *61*(6), 1123-1134.

Wu, Z., Zhang, D., Cai, Y., Wang, X., Zhang, L., & Chen, Y. (2017). Water quality assessment based on the water quality index method in Lake Poyang: The largest freshwater lake in China. *Scientific Reports*, *7*(1), 17999.

Xia, Y., Fabian, P., Stohl, A., & Winterhalter, M. (1999). Forest climatology: estimation of missing values for Bavaria, Germany. *Agricultural and Forest Meteorology*, *96*(1-3), 131-144.

Xu, C. Y., Gong, L., Jiang, T., Chen, D., & Singh, V. P. (2006). Analysis of spatial distribution and temporal trend of reference evapotranspiration and pan evaporation in Changjiang (Yangtze River) catchment. *Journal of Hydrology*, *327*(1-2), 81-93.

Xu, Y., Yan, B., Luan, Z., Zhu, H., & Wang, L. (2013). Application of stable isotope tracing technologies in identification of transformation among waters in Sanjiang Plain, Northeast China. *Chinese Geographical Science*, *23*(4), 435-444.

Yang, P., Xia, J., Zhang, Y., & Hong, S. (2017). Temporal and spatial variations of precipitation in Northwest China during 1960–2013. *Atmospheric Research*, *183*, 283-295.

Yang, X., Xie, X., Liu, D. L., Ji, F., & Wang, L. (2015). Spatial interpolation of daily rainfall data for local climate impact assessment over greater Sydney region. *Advances in Meteorology*, *2015*.

Yang, X., & Yao, T. (2016). Different sub-monsoon signals in stable oxygen isotope in daily precipitation to the northeast of the Tibetan Plateau. *Tellus B: Chemical and Physical Meteorology*, *68*(1), 27922.

Yi, Z., & Small, M. (2006). Minimum description length criterion for modeling of chaotic attractors with multilayer perceptron networks. *IEEE Transactions on Circuits and Systems I: Regular Papers*, *53*(3), 722-732.

Yidana, S. M., Ophori, D., & Banoeng-Yakubo, B. (2008). A multivariate statistical analysis of surface water chemistry data—The Ankobra Basin, Ghana. *Journal of Environmental Management*, *86*(1), 80-87.

Yilmaz, A. G., & Perera, B. J. C. (2015). Spatiotemporal trend analysis of extreme rainfall events in Victoria, Australia. *Water Resources Management*, *29*(12), 4465-4480.

Yilmaz, A. G., Hossain, I., & Perera, B. J. C. (2014). Effect of climate change and variability on extreme rainfall intensity–frequency–duration relationships: a case study of Melbourne. *Hydrology and Earth System Sciences*, *18*(10), 4065-4076.

Young, K. C. (1992). A three-way model for interpolating for monthly precipitation values. *Monthly Weather Review*, *120*(11), 2561-2569.

Yu, S., Kuo, Y. M., Du, W., He, S., Sun, P. A., Yuan, Y., ... & Li, Y. (2015). The hydrochemistry properties of precipitation in karst tourism city (Guilin), Southwest China. *Environmental Earth Sciences*, *74*(2), 1061-1069.

Yu, X., Zhao, G., Zhao, W., Yan, T., & Yuan, X. (2017). Analysis of precipitation and drought data in Hexi Corridor, Northwest China. *Hydrology*, *4*(2), 29.

Yue, S., Pilon, P., & Cavadias, G. (2002). Power of the Mann–Kendall and Spearman's rho tests for detecting monotonic trends in hydrological series. *Journal of Hydrology*, *259*(1-4), 254-271.

Yue, S., Pilon, P., Phinney, B., & Cavadias, G. (2002). The influence of autocorrelation on the ability to detect trend in hydrological series. *Hydrological Processes*, *16*(9), 1807-1829.

Zadeh, F. K., Nossent, J., Sarrazin, F., Pianosi, F., van Griensven, A., Wagener, T., & Bauwens, W. (2017). Comparison of variance-based and moment-independent global sensitivity analysis approaches by application to the SWAT model. *Environmental Modelling & Software*, *91*, 210-222.

Zakhrouf, M., Bouchelkia, H., & Stamboul, M. (2016). Neuro-Wavelet (WNN) and Neuro-Fuzzy (ANFIS) systems for modeling hydrological time series in arid areas. A case study: the catchment of Aïn Hadjadj (Algeria). *Desalination and Water Treatment*, *57*(37), 17182-17194.

Zhang, C. (2005). Madden-Julian oscillation. *Reviews of Geophysics*, *43*(2).

Zhang, M., Wang, S., Wu, F., Yuan, X., & Zhang, Y. (2007). Chemical compositions of wet precipitation and anthropogenic influences at a developing urban site in southeastern China. *Atmospheric Research*, *84*(4), 311-322.

Zhang, S. R., Lu, X. X., Higgitt, D. L., Chen, C. T. A., Sun, H. G., & Han, J. T. (2007). Water chemistry of the Zhujiang (Pearl River): natural processes and anthropogenic influences. *Journal of Geophysical Research: Earth Surface*, *112*(F1).

Zhang, X., Jiang, H., Zhang, Q., & Zhang, X. (2012). Chemical characteristics of rainwater in northeast China, a case study of Dalian. *Atmospheric Research*, *116*, 151-160.

Zhang, X., Vincent, L. A., Hogg, W. D., & Niitsoo, A. (2000). Temperature and precipitation trends in Canada during the 20th century. *Atmosphere-ocean*, *38*(3), 395-429.

Zhao, P., Tan, L., Zhang, P., Wang, S., Cui, B., Li, D., ... & Cheng, X. (2018). Stable Isotopic Characteristics and Influencing Factors in Precipitation in the Monsoon Marginal Region of Northern China. *Atmosphere*, *9*(3), 97.

Zhao, W., Yu, X., Ma, H., Zhu, Q., Zhang, Y., Qin, W., ... & Wang, Y. (2015). Analysis of precipitation characteristics during 1957-2012 in the semi-arid Loess Plateau, China. *PloS one*, *10*(11), e0141662.

Zhao, X., Li, Z., & Zhu, Q. (2017). Change of precipitation characteristics in the water-wind erosion crisscross region on the Loess Plateau, China, from 1958 to 2015. *Scientific Reports*, *7*(1), 8048.

Zhou, X., Xu, Z., Liu, W., Wu, Y., Zhao, T., Jiang, H., ... & Wang, Y. (2019). Chemical composition of precipitation in Shenzhen, a coastal mega-city in South China: Influence of urbanization and anthropogenic activities on acidity and ionic composition. *Science of The Total Environment*, *662*, 218-226.

Zunckel, M., Saizar, C., & Zarauz, J. (2003). Rainwater composition in northeast Uruguay. *Atmospheric Environment*, *37*(12), 1601-1611.

Zurada, J. M. (1992). *Introduction to artificial neural systems* (Vol. 8). St. Paul: West publishing company.

Appendices

Appendix - 1: Physico-chemical parameters of RW-01 samples.

Sample ID.	pH	EC (µS/cm)	TDS (mg/L)	DO (mg/L)	Turbidity(NTU)	HCO_3 (mg/L)	Cl (mg/L)	Ca (mg/L)	Mg (mg/L)	Na (mg/L)	K (mg/L)	Co (mg/L)	Ni (mg/L)	Cd (mg/L)	Fe (mg/L)	Mn (mg/L)	Pb (mg/L)	Zn (mg/L)	Cu (mg/L)
RW-01 Oct 16	5.73	76.73	53.71	3.40	0.28	32.39	19.88	0.683	0.201	0.412	0.143	0.032	0.19	0.005	1.023	0.029	0.019	0.03	0.015
RW-01 Nov 16	7.14	58.17	40.72	9.19	2.01	18.30	17.73	1.254	0.760	2.470	0.21	0.04	0.119	0.008	1.609	0.034	0.115	0.025	0.013
RW-01 Dec 16	6.04	72.83	50.98	7.70	1.30	32.39	17.04	0.783	0.229	0.438	0.097	0.047	0.201	0.005	0.961	0.042	0.023	0.019	0.021
RW-01 Jan 17	5.93	71.40	49.98	7.80	1.61	32.39	15.62	0.699	0.296	0.833	0.136	0.021	0.212	0.006	1.013	0.032	0.058	0.024	0.022
RW-01 Feb 17	6.02	59.94	41.95	7.80	0.85	25.19	15.62	0.459	0.219	0.399	0.062	0.051	0.201	0.005	1.008	0.026	0.026	0.013	0.013
RW-01 Mar 17	5.33	77.96	54.57	7.60	0.06	35.99	17.04	0.618	0.244	0.589	0.085	0.022	0.21	0.006	0.986	0.023	0.029	0.022	0.026
RW-01 Apr 17	6.40	112.94	79.06	7.60	0.50	35.08	42.54	0.75	0.259	0.302	0.135	0.011	0.125	0.006	1.097	0.022	0.02	0.005	0.009
RW-01 May 17	6.42	97.79	68.45	7.60	1.11	35.08	31.91	0.684	0.250	0.368	0.169	0.028	0.107	0.006	1.158	0.029	0.032	0.007	0.016
RW-01 Jun 17	6.30	101.33	70.93	6.70	0.22	36.60	32.79	0.884	0.193	0.323	0.14	0.023	0.083	0.004	1.069	0.032	0.027	0.002	0.007
RW-01 Jul 17	5.53	105.79	74.05	6.60	1.13	36.60	35.45	0.738	0.269	0.482	0.515	0.008	0.105	0.006	1.064	0.03	0.012	0.011	0.01
RW-01 Aug 17	5.77	98.63	69.04	5.10	4.11	32.03	35.45	0.474	0.233	0.424	0.437	0.011	0.103	0.003	1.072	0.024	0.02	0.002	0.008
RW-01 Sep 17	6.21	117.16	82.01	6.00	2.56	41.18	39.00	0.875	0.303	0.414	0.251	0.01	0.101	0.010	1.051	0.041	0.035	0.007	0.016

Appendix - 2: Physico-chemical parameters of RW-02 samples.

Sample ID.	pH	EC (µS/cm)	TDS (mg/L)	DO (mg/L)	Turbidity(NTU)	HCO_3 (mg/L)	Cl (mg/L)	Ca (mg/L)	Mg (mg/L)	Na (mg/L)	K (mg/L)	Co (mg/L)	Ni (mg/L)	Cd (mg/L)	Fe (mg/L)	Mn (mg/L)	Pb (mg/L)	Zn (mg/L)	Cu (mg/L)
RW-02 Oct 16	7.22	59.07	41.35	8.71	0.87	24.40	13.29	0.897	0.620	1.870	0.269	0.025	0.124	0.008	1.621	0.026	0.109	0.028	0.014
RW-02 Nov 16	6.98	57.19	40.03	8.27	1.69	18.30	17.73	1.033	0.690	2.020	0.264	0.055	0.165	0.007	1.59	0.032	0.105	0.033	0.011
RW-02 Dec 16	5.75	70.65	49.45	7.60	0.88	32.39	15.62	0.59	0.208	0.512	0.129	0.016	0.18	0.004	1.004	0.042	0.033	0.022	0.014
RW-02 Jan 17	5.83	88.20	61.74	7.70	3.30	43.19	17.04	0.404	0.237	0.555	0.314	0.022	0.194	0.004	0.729	0.03	0.051	0.022	0.02
RW-02 Feb 17	5.68	67.09	46.96	7.70	1.52	28.79	17.04	0.413	0.182	0.412	0.12	0.023	0.191	0.004	0.752	0.025	0.007	0.022	0.01
RW-02 Mar 17	5.79	67.38	47.17	7.70	1.15	28.79	17.04	0.539	0.22	0.514	0.059	0.017	0.152	0.004	0.681	0.016	0.025	0.015	0.018
RW-02 Apr 17	6.00	97.97	68.58	4.70	1.08	33.55	33.68	0.689	0.216	0.340	0.105	0.045	0.103	0.005	1.07	0.024	0.029	0.013	0.01
RW-02 May 17	6.14	105.95	74.16	7.40	0.81	32.03	40.77	0.712	0.173	0.297	0.189	0.027	0.108	0.004	1.058	0.019	0.031	0.018	0.009
RW-02 Jun 17	5.93	107.42	75.20	7.30	0.58	38.13	35.45	0.803	0.174	0.474	0.17	0.018	0.112	0.003	0.995	0.031	0.021	0.006	0.012
RW-02 Jul 17	5.74	106.72	74.71	7.40	0.69	30.50	42.54	0.724	0.211	0.532	0.2	0.013	0.103	0.003	0.988	0.023	0.015	0.011	0.008
RW-02 Aug 17	5.98	100.12	70.08	4.60	0.42	35.08	33.68	0.726	0.129	0.339	0.137	0.011	0.114	0.003	1.045	0.03	0.017	0.009	0.01
RW-02 Sep 17	6.02	109.45	76.61	7.20	0.62	35.08	39.88	0.985	0.163	0.351	0.159	0.016	0.161	0.009	1.028	0.025	0.021	0.006	0.007

Appendix - 3: Physico-chemical parameters of RW-03 samples.

Sample ID.	pH	EC (µS/cm)	TDS (mg/L)	DO (mg/L)	Turbidity(NTU)	HCO_3 (mg/L)	Cl (mg/L)	Ca (mg/L)	Mg (mg/L)	Na (mg/L)	K (mg/L)	Co (mg/L)	Ni (mg/L)	Cd (mg/L)	Fe (mg/L)	Mn (mg/L)	Pb (mg/L)	Zn (mg/L)	Cu (mg/L)
RW-03 Oct 16	5.85	44.94	31.46	6.15	0.03	9.15	17.73	1.323	0.770	2.300	0.188	0.026	0.115	0.009	1.545	0.033	0.09	0.031	0.019
RW-03 Nov 16	6.25	47.95	33.57	8.07	0.09	12.20	17.73	0.922	0.650	1.910	0.159	0.056	0.118	0.007	1.643	0.036	0.108	0.029	0.015
RW-03 Dec 16	5.79	69.22	48.45	7.60	0.26	28.79	18.46	0.667	0.182	0.294	0.056	0.017	0.182	0.004	1.000	0.036	0.021	0.016	0.013
RW-03 Jan 17	5.48	73.23	51.26	7.60	0.13	35.99	14.20	0.281	0.208	0.392	0.188	0.023	0.207	0.003	0.933	0.036	0.054	0.014	0.017
RW-03 Feb 17	5.77	69.11	48.38	7.60	0.24	28.79	18.46	0.507	0.186	0.353	0.076	0.02	0.2	0.004	0.889	0.028	0.022	0.014	0.008
RW-03 Mar 17	5.90	69.05	48.34	7.70	1.02	28.79	18.46	0.414	0.186	0.395	0.086	0.017	0.174	0.003	0.834	0.024	0.025	0.022	0.02
RW-03 Apr 17	5.92	119.46	83.62	6.50	0.11	33.55	48.74	0.7	0.195	0.302	0.133	0.024	0.108	0.004	1.086	0.03	0.02	0.001	0.003
RW-03 May 17	6.23	97.24	68.07	7.10	0.16	30.50	36.34	0.621	0.168	0.298	0.145	0.02	0.143	0.004	1.11	0.017	0.021	0.023	0.009
RW-03 Jun 17	6.08	107.04	74.93	5.60	0.09	32.03	41.65	0.653	0.167	0.286	0.143	0.016	0.11	0.002	1.068	0.021	0.026	0.006	0.008
RW-03 Jul 17	6.04	120.93	84.65	7.30	0.09	41.18	42.54	0.406	0.149	0.215	0.166	0.005	0.063	0.004	1.082	0.024	0.012	0.011	0.009
RW-03 Aug 17	5.99	96.42	67.49	5.90	0.44	32.03	33.68	0.807	0.170	0.717	0.097	0.012	0.121	0.002	0.993	0.024	0.014	0.005	0.011
RW-03 Sep 17	6.86	148.94	104.26	7.40	0.17	50.33	35.45	17.16	0.324	0.593	0.409	0.026	0.119	0.006	0.971	0.016	0.03	0.005	0.008

Appendix - 4: Physico-chemical parameters of RW-04 samples.

Sample ID.	pH	EC (µS/cm)	TDS (mg/L)	DO (mg/L)	Turbidity(NTU)	HCO_3 (mg/L)	Cl (mg/L)	Ca (mg/L)	Mg (mg/L)	Na (mg/L)	K (mg/L)	Co (mg/L)	Ni (mg/L)	Cd (mg/L)	Fe (mg/L)	Mn (mg/L)	Pb (mg/L)	Zn (mg/L)	Cu (mg/L)
RW-04 Oct 16	5.70	52.13	36.49	7.56	0.10	15.25	17.73	1.132	0.730	1.520	0.137	0.037	0.124	0.008	1.583	0.034	0.097	0.026	0.011
RW-04 Nov 16	5.78	49.42	34.60	7.50	0.04	18.30	13.29	0.974	0.660	1.270	0.098	0.051	0.164	0.007	1.577	0.028	0.095	0.029	0.015
RW-04 Dec 16	5.82	67.74	47.42	7.40	0.36	28.79	17.04	0.723	0.232	0.458	0.171	0.054	0.202	0.005	1.024	0.043	0.031	0.016	0.015
RW-04 Jan 17	5.82	67.15	47.00	7.50	0.44	28.79	17.04	0.548	0.199	0.372	0.049	0.038	0.214	0.005	1.194	0.036	0.049	0.029	0.019
RW-04 Feb 17	5.72	77.68	54.37	7.60	0.28	35.99	17.04	0.474	0.197	0.405	0.265	0.021	0.219	0.004	0.941	0.034	0.025	0.018	0.014
RW-04 Mar 17	5.91	77.79	54.46	7.60	0.43	35.99	15.62	0.462	1.98	0.366	0.035	0.021	0.194	0.004	1.027	0.027	0.026	0.015	0.016
RW-04 Apr 17	6.24	103.57	72.50	7.00	0.19	32.03	37.22	0.886	0.268	1.914	0.183	0.03	0.112	0.004	1.09	0.038	0.018	0.003	0.011
RW-04 May 17	6.19	131.13	91.79	5.30	0.52	41.18	49.63	0.483	0.164	0.271	0.068	0.032	0.087	0.005	1.029	0.037	0.024	0.009	0.007
RW-04 Jun 17	6.05	103.71	72.60	7.20	0.39	30.50	40.77	0.698	0.172	0.319	0.139	0.017	0.112	0.003	0.942	0.022	0.026	0.007	0.008
RW-04 Jul 17	6.06	98.94	69.26	4.30	0.04	30.50	37.22	0.434	0.195	0.762	0.142	0.007	0.093	0.003	0.923	0.021	0.022	0.003	0.011
RW-04 Aug 17	5.96	113.33	79.33	3.70	0.68	38.13	39.88	0.851	0.141	0.255	0.081	0.011	0.082	0.005	0.903	0.045	0.019	0.005	0.01
RW-04 Sep 17	6.12	108.24	75.77	3.70	0.07	30.50	39.00	1.212	0.273	4.69	0.1	0.013	0.096	0.005	0.729	0.016	0.025	0.025	0.009

Appendix - 5: Physico-chemical parameters of RW-05 samples.

Sample ID.	pH	EC (µS/cm)	TDS (mg/L)	DO (mg/L)	Turbidity(NTU)	HCO_3 (mg/L)	Cl (mg/L)	Ca (mg/L)	Mg (mg/L)	Na (mg/L)	K (mg/L)	Co (mg/L)	Ni (mg/L)	Cd (mg/L)	Fe (mg/L)	Mn (mg/L)	Pb (mg/L)	Zn (mg/L)	Cu (mg/L)
RW-05 Oct 16	5.59	49.73	34.81	5.78	0.44	18.30	13.29	0.515	0.650	1.520	0.531	0.022	0.113	0.008	1.705	0.03	0.079	0.024	0.012
RW-05 Nov 16	5.25	51.67	36.17	7.46	2.65	15.25	17.73	0.746	0.660	1.530	0.255	0.048	0.087	0.007	1.424	0.022	0.078	0.025	0.014
RW-05 Dec 16	5.78	80.73	56.51	6.30	1.04	39.59	15.62	0.346	0.207	0.371	0.375	0.022	0.176	0.005	0.969	0.037	0.016	0.013	0.013
RW-05 Jan 17	5.54	86.04	60.23	7.50	1.38	43.19	15.62	0.516	0.205	0.528	0.169	0.013	0.199	0.004	1.006	0.037	0.056	0.02	0.018
RW-05 Feb 17	5.45	83.91	58.73	7.50	1.25	43.19	14.20	0.647	0.206	0.381	0.109	0.034	0.195	0.005	0.986	0.032	0.02	0.018	0.011
RW-05 Mar 17	5.64	66.15	46.31	7.60	0.31	32.39	12.78	0.46	0.218	0.376	0.08	0.014	0.18	0.004	0.989	0.037	0.023	0.014	0.019
RW-05 Apr 17	6.13	82.39	57.67	7.10	0.42	19.83	36.34	0.883	0.190	0.268	0.168	0.031	0.082	0.003	0.775	0.018	0.027	0.014	0.006
RW-05 May 17	5.85	95.16	66.61	6.00	0.36	30.50	34.56	0.777	0.195	0.322	0.253	0.03	0.093	0.004	0.736	0.031	0.016	0.011	0.008
RW-05 Jun 17	6.21	260.77	182.54	7.50	3.78	59.48	69.13	0.517	0.302	46.44	6.68	0.023	0.104	0.004	0.751	0.027	0.019	0.001	0.006
RW-05 Jul 17	5.83	163.91	114.74	7.30	1.94	35.08	54.06	0.457	0.345	20.55	4.25	0.007	0.09	0.004	0.732	0.023	0.021	0.004	0.009
RW-05 Aug 17	6.84	117.53	82.27	7.50	4.92	42.70	31.91	0.361	3.49	3.425	0.392	0.011	0.066	0.002	0.73	0.017	0.021	0.01	0.016
RW-05 Sep 17	7.23	110.80	77.56	4.40	0.65	38.13	37.22	1.484	0.199	0.373	0.155	0.014	0.091	0.011	0.625	0.023	0.034	0.01	0.008

Appendix - 6: Correlation analysis of physico-chemical parameters in RW-01 samples.

	pH	EC	TDS	DO	Turb	HCO_3	Cl	Ca	Mg	Na	K	Co	Ni	Cd	Fe	Mn	Pb	Zn	Cu
pH	1.00																		
EC	-0.10	1.00																	
TDS	-0.10	1.00	1.00																
DO	0.49	-0.34	-0.34	1.00															
Turb	0.14	0.15	0.15	-0.13	1.00														
HCO_3	-0.50	0.80	0.80	-0.42	-0.12	1.00													
Cl	0.09	0.95	0.95	-0.27	0.25	0.58	1.00												
Ca	0.72	-0.06	-0.06	0.38	-0.02	-0.29	0.01	1.00											
Mg	0.69	-0.37	-0.37	0.52	0.26	-0.68	-0.21	0.79	1.00										
Na	0.60	-0.54	-0.54	0.50	0.21	-0.76	-0.39	0.73	0.97	1.00									
K	-0.20	0.47	0.47	-0.32	0.59	0.18	0.53	-0.02	0.09	0.02	1.00								
Co	0.28	-0.83	-0.83	0.33	-0.26	-0.67	-0.77	0.08	0.20	0.29	-0.62	1.00							
Ni	-0.41	-0.70	-0.70	0.10	-0.35	-0.23	-0.82	-0.36	-0.18	-0.03	-0.59	0.53	1.00						
Cd	0.34	0.11	0.11	0.29	0.06	0.05	0.08	0.60	0.54	0.42	0.02	-0.14	-0.12	1.00					
Fe	0.79	-0.24	-0.24	0.43	0.22	-0.67	-0.04	0.76	0.94	0.89	0.13	0.16	-0.40	0.38	1.00				
Mn	0.30	-0.04	-0.04	0.09	0.20	0.07	-0.13	0.53	0.23	0.19	-0.03	0.24	-0.05	0.48	0.08	1.00			
Pb	0.70	-0.51	-0.51	0.56	0.21	-0.69	-0.39	0.73	0.93	0.95	-0.14	0.30	-0.02	0.47	0.85	0.26	1.00		
Zn	-0.10	-0.75	-0.75	0.04	-0.29	-0.44	-0.81	0.21	0.34	0.48	-0.36	0.48	0.73	0.21	0.15	0.15	0.42	1.00	
Cu	-0.32	-0.44	-0.44	0.24	-0.21	0.07	-0.64	-0.08	-0.02	0.07	-0.48	0.27	0.75	0.26	-0.26	0.22	0.14	0.63	1.00

Appendix - 7: Correlation analysis of physico-chemical parameters in RW-02 samples.

	pH	EC	TDS	DO	Turb	HCO_3	Cl	Ca	Mg	Na	K	Co	Ni	Cd	Fe	Mn	Pb	Zn	Cu
pH	1.00																		
EC	-0.46	1.00																	
TDS	-0.46	1.00	1.00																
DO	0.36	-0.53	-0.53	1.00															
Turb	-0.02	-0.33	-0.33	0.29	1.00														
HCO_3	-0.65	0.67	0.67	-0.40	0.19	1.00													
Cl	-0.30	0.93	0.93	-0.49	-0.53	0.34	1.00												
Ca	0.69	0.10	0.10	0.08	-0.48	-0.45	0.31	1.00											
Mg	0.91	-0.68	-0.68	0.52	0.20	-0.75	-0.52	0.52	1.00										
Na	0.91	-0.68	-0.68	0.54	0.16	-0.74	-0.52	0.54	0.99	1.00									
K	0.55	-0.11	-0.11	0.47	0.53	-0.04	-0.17	0.25	0.58	0.59	1.00								
Co	0.55	-0.36	-0.36	0.03	0.30	-0.52	-0.20	0.33	0.63	0.55	0.25	1.00							
Ni	-0.14	-0.54	-0.54	0.45	0.65	0.01	-0.68	-0.39	0.10	0.10	0.14	0.01	1.00						
Cd	0.68	-0.29	-0.29	0.40	-0.02	-0.43	-0.18	0.67	0.61	0.60	0.34	0.33	0.20	1.00					
Fe	0.93	-0.32	-0.32	0.21	-0.23	-0.65	-0.11	0.80	0.83	0.83	0.48	0.53	-0.28	0.61	1.00				
Mn	0.05	-0.19	-0.19	0.03	0.10	0.10	-0.31	0.07	0.15	0.19	0.24	0.02	0.36	0.00	0.23	1.00			
Pb	0.92	-0.61	-0.61	0.49	0.28	-0.58	-0.53	0.48	0.96	0.95	0.68	0.58	0.10	0.61	0.82	0.20	1.00		
Zn	0.60	-0.84	-0.84	0.57	0.51	-0.62	-0.76	-0.01	0.78	0.75	0.50	0.57	0.46	0.30	0.48	0.24	0.77	1.00	
Cu	-0.02	-0.47	-0.47	0.32	0.65	0.21	-0.71	-0.51	0.15	0.15	0.21	-0.07	0.45	-0.16	-0.26	0.12	0.28	0.36	1.00

Appendix - 8: Correlation analysis of physico-chemical parameters in RW-03 samples.

	pH	EC	TDS	DO	Turb	HCO_3	Cl	Ca	Mg	Na	K	Co	Ni	Cd	Fe	Mn	Pb	Zn	Cu
pH	1.00																		
EC	0.58	1.00																	
TDS	0.58	1.00	1.00																
DO	0.02	-0.24	-0.24	1.00															
Turb	-0.12	-0.15	-0.15	0.20	1.00														
HCO_3	0.34	0.87	0.87	0.05	0.06	1.00													
Cl	0.43	0.83	0.83	-0.52	-0.26	0.52	1.00												
Ca	0.80	0.58	0.58	0.12	-0.10	0.53	0.17	1.00											
Mg	0.15	-0.52	-0.52	0.02	-0.32	-0.72	-0.41	0.11	1.00										
Na	0.08	-0.58	-0.58	-0.06	-0.25	-0.78	-0.42	0.01	0.98	1.00									
K	0.71	0.53	0.53	0.05	-0.34	0.43	0.21	0.88	0.28	0.17	1.00								
Co	0.24	-0.42	-0.42	0.37	-0.25	-0.53	-0.37	0.13	0.70	0.66	0.22	1.00							
Ni	-0.51	-0.47	-0.47	0.45	0.36	-0.06	-0.71	-0.16	-0.21	-0.22	-0.32	0.04	1.00						
Cd	0.29	-0.31	-0.31	0.19	-0.38	-0.50	-0.31	0.32	0.90	0.83	0.44	0.59	-0.23	1.00					
Fe	0.15	-0.44	-0.44	-0.07	-0.50	-0.74	-0.14	-0.11	0.88	0.88	0.12	0.69	-0.44	0.76	1.00				
Mn	-0.66	-0.71	-0.71	0.28	-0.18	-0.58	-0.61	-0.47	0.41	0.41	-0.38	0.41	0.34	0.28	0.39	1.00			
Pb	-0.01	-0.64	-0.64	0.19	-0.31	-0.73	-0.54	-0.04	0.92	0.90	0.20	0.83	-0.03	0.74	0.84	0.56	1.00		
Zn	-0.15	-0.80	-0.80	0.37	0.07	-0.78	-0.68	-0.29	0.67	0.66	-0.16	0.48	0.19	0.59	0.60	0.36	0.70	1.00	
Cu	-0.35	-0.73	-0.73	0.28	0.41	-0.53	-0.81	-0.21	0.47	0.51	-0.12	0.22	0.36	0.29	0.24	0.43	0.56	0.73	1.00

Appendix - 9: Correlation analysis of physico-chemical parameters in RW-04 samples.

	pH	EC	TDS	DO	Turb	HCO_3	Cl	Ca	Mg	Na	K	Co	Ni	Cd	Fe	Mn	Pb	Zn	Cu
pH	1.00																		
EC	0.86	1.00																	
TDS	0.86	1.00	1.00																
DO	-0.55	-0.70	-0.70	1.00															
Turb	0.08	0.39	0.39	-0.07	1.00														
HCO_3	0.52	0.77	0.77	-0.40	0.67	1.00													
Cl	0.87	0.95	0.95	-0.72	0.23	0.54	1.00												
Ca	-0.03	-0.18	-0.18	-0.16	-0.42	-0.58	0.00	1.00											
Mg	-0.24	-0.37	-0.37	0.37	-0.03	-0.11	-0.48	-0.08	1.00										
Na	0.29	0.09	0.09	-0.37	-0.60	-0.27	0.17	0.74	-0.06	1.00									
K	-0.16	-0.11	-0.11	0.23	-0.34	-0.07	-0.10	0.00	-0.41	0.02	1.00								
Co	-0.44	-0.63	-0.63	0.64	-0.10	-0.51	-0.57	0.16	0.06	-0.15	0.01	1.00							
Ni	-0.70	-0.70	-0.70	0.74	0.05	-0.14	-0.86	-0.34	0.32	-0.32	0.17	0.50	1.00						
Cd	-0.51	-0.59	-0.59	0.23	-0.32	-0.74	-0.44	0.64	0.15	0.25	-0.16	0.62	0.07	1.00					
Fe	-0.54	-0.73	-0.73	0.58	-0.32	-0.78	-0.56	0.29	0.26	-0.14	-0.10	0.68	0.23	0.80	1.00				
Mn	-0.21	-0.06	-0.06	0.19	0.59	0.19	-0.13	-0.11	-0.19	-0.51	0.10	0.44	0.20	0.18	0.20	1.00			
Pb	-0.63	-0.77	-0.77	0.44	-0.44	-0.89	-0.58	0.46	0.22	0.07	-0.12	0.60	0.19	0.89	0.93	-0.01	1.00		
Zn	-0.65	-0.71	-0.71	0.37	-0.33	-0.61	-0.68	0.38	0.21	0.31	-0.18	0.52	0.52	0.71	0.53	-0.14	0.72	1.00	
Cu	-0.64	-0.74	-0.74	0.58	-0.01	-0.25	-0.86	-0.26	0.37	-0.27	-0.10	0.47	0.88	0.15	0.34	0.21	0.29	0.53	1.00

Appendix - 10: Correlation analysis of physico-chemical parameters in RW-05 samples.

	pH	EC	TDS	DO	Turb	HCO_3	Cl	Ca	Mg	Na	K	Co	Ni	Cd	Fe	Mn	Pb	Zn	Cu
pH	1.00																		
EC	0.38	1.00																	
TDS	0.38	1.00	1.00																
DO	-0.48	0.17	0.17	1.00															
Turb	0.28	0.54	0.54	0.47	1.00														
HCO_3	0.34	0.74	0.74	0.18	0.46	1.00													
Cl	0.48	0.91	0.91	0.02	0.42	0.45	1.00												
Ca	0.49	-0.09	-0.09	-0.67	-0.36	-0.20	0.13	1.00											
Mg	0.41	0.03	0.03	0.21	0.73	0.10	0.01	-0.31	1.00										
Na	0.13	0.94	0.94	0.28	0.52	0.59	0.83	-0.22	-0.06	1.00									
K	0.09	0.92	0.92	0.25	0.47	0.54	0.84	-0.24	-0.09	0.99	1.00								
Co	-0.47	-0.31	-0.31	0.11	-0.09	-0.45	-0.23	0.19	-0.24	-0.16	-0.22	1.00							
Ni	-0.51	-0.27	-0.27	0.24	-0.37	0.28	-0.57	-0.32	-0.42	-0.23	-0.24	-0.07	1.00						
Cd	0.20	-0.30	-0.30	-0.78	-0.38	-0.29	-0.22	0.70	-0.29	-0.27	-0.27	0.14	-0.07	1.00					
Fe	-0.64	-0.55	-0.55	0.04	-0.18	-0.57	-0.61	-0.26	-0.07	-0.27	-0.27	0.41	0.19	0.32	1.00				
Mn	-0.53	-0.22	-0.22	0.02	-0.47	0.22	-0.49	-0.33	-0.51	-0.15	-0.16	-0.10	0.88	0.00	0.25	1.00			
Pb	-0.37	-0.47	-0.47	-0.10	-0.08	-0.58	-0.43	0.09	-0.03	-0.25	-0.26	0.32	-0.05	0.49	0.84	-0.03	1.00		
Zn	-0.56	-0.85	-0.85	0.00	-0.33	-0.65	-0.85	0.01	-0.06	-0.69	-0.71	0.50	0.31	0.34	0.82	0.23	0.78	1.00	
Cu	-0.32	-0.49	-0.49	0.37	0.09	-0.05	-0.69	-0.48	0.32	-0.44	-0.46	-0.22	0.51	-0.14	0.37	0.43	0.29	0.48	1.00

Appendix – 11: Factor scores associated with monthly samples correspond to each sampling location RW – 01 and RW – 02 in LRB.

	RW - 01					**RW - 02**				
	Score					Score				
	1	2	3	4	5	1	2	3	4	5
Oct - 16	-0.79	-0.71	0.60	0.27	-0.16	1.82	0.70	-0.05	-0.29	0.80
Nov - 16	2.97	-0.88	-0.12	0.41	-0.01	2.06	0.98	0.14	0.31	-0.69
Dec - 16	-0.71	-1.11	-0.03	-0.31	1.85	-0.74	1.07	-0.50	2.11	0.29
Jan - 17	0.03	-0.55	1.27	0.10	0.02	-0.43	-0.34	3.04	0.43	0.25
Feb - 17	-0.59	-1.57	-0.85	-0.60	-0.39	-1.08	1.33	-0.17	-0.34	0.18
Mar - 17	-0.31	0.00	1.88	-0.86	-1.20	-1.10	1.34	-0.20	-1.69	0.38
Apr - 17	0.24	1.29	-0.66	-1.23	-1.05	-0.06	-0.43	-0.22	-0.36	-2.23
May - 17	0.05	0.41	-0.64	-0.66	0.07	0.12	-0.88	0.06	-1.19	-0.32
Jun - 17	-0.19	0.54	-1.47	-0.94	0.35	-0.19	-1.03	-0.18	0.62	0.19
Jul -17	-0.11	1.09	0.45	0.96	-0.54	-0.11	-0.96	-0.34	-0.64	0.28
Aug - 17	-0.71	-0.06	-1.07	2.35	-0.86	-0.49	-0.59	-0.78	0.91	-0.98
Sep - 17	0.13	1.56	0.65	0.51	1.92	0.20	-1.20	-0.80	0.12	1.85

Appendix – 12: Factor scores associated with monthly samples correspond to each sampling location RW – 03 and RW – 04 in LRB.

	RW - 03				**RW - 04**			
	Score				Score			
	1	2	3	4	1	2	3	4
Oct - 16	2.17	-0.40	-0.79	0.53	0.15	2.12	-0.26	-0.12
Nov - 16	2.07	-0.01	0.65	-0.53	0.70	1.66	-0.42	0.28
Dec - 16	-0.41	-0.79	0.99	-0.20	0.83	0.15	0.86	-0.95
Jan - 17	-0.36	-0.57	1.71	-0.59	1.04	0.11	0.65	0.70
Feb - 17	-0.54	-0.61	1.02	-0.28	1.30	-1.02	-0.03	-1.58
Mar - 17	-0.49	-0.11	0.49	2.59	1.16	-1.09	-0.15	2.26
Apr - 17	-0.51	-0.28	-0.70	-1.57	-0.61	-0.12	0.03	-1.05
May - 17	-0.23	0.21	-0.44	0.31	-1.47	-0.09	1.33	0.48
Jun - 17	-0.49	-0.26	-1.37	-0.30	-0.42	-0.64	-0.15	-0.38
Jul -17	-0.56	0.17	-0.88	-0.44	-0.29	-1.02	-0.96	-0.40
Aug - 17	-0.55	-0.37	-1.12	0.63	-1.27	-0.07	1.36	0.38
Sep - 17	-0.11	3.02	0.46	-0.15	-1.13	0.00	-2.24	0.37

Appendix – 13: Factor scores associated with monthly samples correspond to each sampling location RW – 05 in LRB.

RW - 05					
	Score				
	1	2	3	4	5
Oct - 16	-0.24	-0.67	2.07	-0.08	0.12
Nov - 16	-0.39	0.34	1.83	0.91	-1.25
Dec - 16	-0.39	0.15	-0.39	-1.06	0.38
Jan - 17	-0.31	0.50	0.50	-1.14	0.98
Feb - 17	-0.39	0.47	-0.32	-0.88	-0.50
Mar - 17	-0.74	0.63	-0.33	-1.11	0.55
Apr - 17	-0.56	-0.04	-1.03	0.81	-1.74
May - 17	-0.34	-0.32	-1.04	-0.13	-0.99
Jun - 17	2.82	0.33	0.05	-0.07	0.00
Jul -17	1.10	0.30	-0.44	0.19	-0.14
Aug - 17	-0.54	1.13	-0.47	2.21	1.73
Sep - 17	-0.02	-2.82	-0.43	0.37	0.87

Appendix - 14: Physical parameters of S1, S2 and S3 samples.

	pH			EC(µS/cm)			TDS(mg/L)			DO(mg/L)			Temperature (˚C)			Turbidity (NTU)		
Station ID	**S1**	**S2**	**S3**	**S1**	**S2**	**S3**	**S1**	**S2**	**S3**	**S1**	**S2**	**S3**	**S1**	**S2**	**S3**	**S1**	**S2**	**S3**
LRB SW-01	7.34	7.03	6.72	91.31	86.23	127.72	63.92	60.36	89.40	8.28	8.30	5.30	24.80	23.90	24.20	8.73	5.70	2.82
LRB SW-02	7.25	6.89	6.87	95.47	89.51	115.49	66.83	62.65	80.85	7.86	4.60	5.30	28.00	26.10	27.20	4.23	3.34	5.53
LRB SW-03	7.30	6.77	6.80	77.14	97.24	107.76	54.00	68.07	75.43	7.87	8.80	5.00	27.90	25.90	27.40	9.39	5.59	22.60
LRB SW-04	7.27	6.96	7.15	110.04	90.88	129.28	77.03	63.62	90.49	7.95	9.10	6.30	28.50	26.00	26.20	145.00	49.70	13.20
LRB SW-05	7.34	6.96	7.05	85.27	102.90	121.45	59.69	72.03	85.02	8.18	8.80	5.50	28.00	27.40	26.60	14.70	56.80	12.40
LRB SW-06	7.42	7.00	7.16	80.31	117.68	176.18	56.22	82.38	123.33	8.20	9.40	5.20	27.40	25.90	26.10	20.50	20.20	22.50
LRB SW-07	7.28	6.84	7.05	92.11	100.09	138.96	64.47	70.06	97.27	8.16	9.00	7.40	28.90	26.30	26.60	22.40	74.90	13.40
LRB SW-08	7.55	6.80	7.06	104.95	114.92	127.61	73.47	80.45	89.33	7.90	7.00	4.50	30.30	26.00	26.80	9.75	51.90	4.46
LRB SW-09	7.20	6.87	6.96	93.96	95.30	138.04	65.77	66.71	96.63	8.11	8.10	4.60	28.10	26.30	26.30	40.60	135.00	15.40
LRB SW-10	7.30	6.79	6.86	84.18	92.13	120.16	58.93	64.49	84.11	8.11	8.30	5.50	28.20	26.60	26.30	33.70	731AU	23.80
LRB SW-11	7.01	6.74	6.66	98.37	109.84	114.75	68.86	76.89	80.33	8.44	8.40	7.60	26.00	25.00	25.50	310.00	61.80	8.63
LRB SW-12	7.24	6.88	7.28	125.95	126.87	178.37	88.16	88.81	124.86	8.01	7.60	4.00	26.90	26.80	25.50	10.20	35.00	4.83
LRB SW-13	6.99	6.75	6.97	101.34	93.41	122.52	70.94	65.38	85.77	8.02	7.70	5.60	27.30	26.90	25.00	38.20	821AU	18.60
LRB SW-14	6.02	6.54	6.63	105.70	112.76	136.74	73.99	78.93	95.72	7.96	7.70	5.00	27.40	26.80	26.60	18.20	619AU	32.60
LRB SW-15	6.47	6.86	6.98	112.11	121.57	132.01	78.48	85.10	92.41	7.84	6.10	7.20	27.30	27.30	26.30	51.90	175.00	42.70
LRB SW-16	6.92	6.61	6.11	160.39	95.43	126.56	112.27	66.80	88.59	5.48	7.00	6.20	28.20	26.00	27.40	44.40	164.00	25.80
LRB SW-17	4.41	4.77	5.84	101.62	111.45	133.06	71.13	78.02	93.14	7.41	7.70	6.40	27.80	25.90	26.50	133.00	130.00	44.90
LRB SW-18	6.63	6.57	6.81	123.86	106.71	118.23	86.70	74.69	82.76	7.22	6.90	6.20	27.90	27.40	26.10	137.00	710AU	83.50
LRB SW-19	6.54	6.58	6.73	82.39	110.10	108.01	57.67	77.07	75.61	6.99	7.90	7.50	28.50	28.30	26.40	93.20	119.00	96.00
LRB SW-20	6.53	6.47	6.75	118.61	104.41	123.04	83.03	73.08	86.13	6.42	7.90	6.90	29.00	28.80	26.80	114.00	99.60	120.00
LRB SW-21	5.42	6.29	5.78	103.15	139.94	114.60	72.21	97.96	80.22	6.61	8.00	5.80	29.00	28.50	27.00	76.50	131.00	59.40
LRB SW-22	6.28	6.40	6.30	108.06	126.27	128.59	75.64	88.39	90.01	5.72	7.10	6.80	29.60	27.60	27.90	29.20	36.20	16.70
LRB SW-23	6.32	6.10	6.51	97.16	139.93	131.21	68.01	97.95	91.84	6.16	7.80	4.60	28.30	32.00	27.60	134.00	122.00	51.90
LRB SW-24	6.43	5.98	6.33	86.39	121.41	132.28	60.48	84.99	92.60	7.10	8.40	6.60	28.00	27.90	27.70	142.00	77.60	54.50

Appendix - 15: Chemical parameters of S1, S2 and S3 samples.

	Sulfate (mg/L)			Nitrate (mg/L)			Ammonia (mg/L)			Phosphate (mg/L)			Bicarbonate (mg/L)			Chloride(mg/L)		
Station ID	**S1**	**S2**	**S3**	**S1**	**S2**	**S3**	**S1**	**S2**	**S3**	**S1**	**S2**	**S3**	**S1**	**S2**	**S3**	**S1**	**S2**	**S3**
LRB SW-01	2.00	0.00	1.00	0.01	0.07	0.01	0.05	0.18	0.02	0.26	0.55	0.17	27.45	39.59	42.70	26.59	15.62	37.22
LRB SW-02	2.00	0.00	1.00	0.04	0.02	0.06	0.05	0.05	0.02	0.27	0.28	0.19	30.50	39.59	38.13	26.59	17.04	35.45
LRB SW-03	1.00	2.00	1.00	0.05	0.04	0.09	0.07	0.11	0.03	0.21	0.20	0.20	27.45	43.19	30.50	17.73	17.04	37.22
LRB SW-04	5.00	0.00	3.00	0.03	0.05	0.04	0.04	0.11	0.04	0.27	0.18	0.16	39.65	39.59	38.13	22.16	18.46	40.77
LRB SW-05	5.00	4.00	3.00	0.02	0.02	0.02	0.04	0.12	0.02	0.24	0.21	0.19	27.45	46.79	38.13	17.73	14.20	34.56
LRB SW-06	0.00	5.00	0.00	0.04	0.02	0.04	0.06	0.16	0.05	0.24	0.17	0.20	30.50	50.39	33.55	17.73	19.88	36.34
LRB SW-07	3.00	0.00	3.00	0.01	0.18	0.02	0.07	0.13	0.04	0.24	0.30	0.14	30.50	46.79	42.70	22.16	15.62	43.43
LRB SW-08	4.00	3.00	3.00	0.03	0.58	0.04	0.03	0.70	0.04	0.25	0.20	0.16	36.60	50.39	45.75	22.16	18.46	31.91
LRB SW-09	4.00	4.00	3.00	0.02	0.04	0.01	0.05	0.09	0.04	0.26	0.21	0.17	30.50	39.59	38.13	22.16	17.04	46.09
LRB SW-10	3.00	3.00	2.00	0.01	0.02	0.03	0.04	0.15	0.04	0.28	0.17	0.14	33.55	39.59	36.60	13.29	15.62	35.45
LRB SW-11	2.00	4.00	3.00	0.00	0.03	0.01	0.20	0.18	0.03	0.35	0.27	0.20	30.50	50.39	35.08	26.59	15.62	35.45
LRB SW-12	0.00	1.00	0.00	0.01	0.02	0.01	0.03	0.14	0.02	0.21	0.18	0.16	48.80	57.58	68.63	22.16	17.04	31.91
LRB SW-13	1.00	1.00	1.00	0.02	0.02	0.03	0.04	0.25	0.00	0.16	0.23	0.16	42.70	43.19	38.13	17.73	14.20	37.22
LRB SW-14	4.00	0.00	3.00	0.04	0.33	0.01	0.05	0.70	0.03	0.18	0.21	0.17	33.55	53.99	47.28	26.59	18.46	37.22
LRB SW-15	0.00	1.00	1.00	0.04	0.42	0.03	0.05	1.50	0.02	0.28	0.23	0.21	42.70	53.99	45.75	26.59	17.04	35.45
LRB SW-16	11.00	1.00	7.00	0.02	0.07	0.04	0.08	0.21	0.02	0.17	0.18	0.10	61.00	39.59	33.55	17.73	15.62	38.10
LRB SW-17	11.00	10.00	7.00	0.02	0.04	0.04	0.17	0.18	0.10	0.12	0.24	0.09	36.60	43.19	38.13	13.29	18.46	40.77
LRB SW-18	0.00	3.00	0.00	0.00	0.02	0.02	0.10	0.32	0.01	0.19	0.18	0.16	54.90	46.79	36.60	22.16	17.04	38.11
LRB SW-19	0.00	3.00	0.00	0.00	0.02	0.01	0.10	0.20	0.01	0.16	0.27	0.13	30.50	43.19	33.55	17.73	22.72	32.79
LRB SW-20	1.00	4.00	0.00	0.00	0.01	0.02	0.07	0.15	0.02	0.19	0.26	0.13	51.85	43.19	38.13	17.73	18.46	38.10
LRB SW-21	9.00	9.00	6.00	0.02	0.05	0.03	0.09	0.27	0.09	0.13	0.21	0.14	33.55	57.58	33.55	17.73	22.72	31.91
LRB SW-22	7.00	6.00	6.00	0.04	0.09	0.06	0.14	0.24	0.11	0.17	0.20	0.12	30.50	53.99	38.13	26.59	19.88	36.34
LRB SW-23	4.00	5.00	5.00	0.00	0.05	0.02	0.11	0.26	0.03	0.15	0.27	0.15	36.60	61.18	38.13	17.73	24.15	39.88
LRB SW-24	3.00	6.00	4.00	0.00	0.03	0.03	0.09	0.21	0.03	0.36	0.20	0.24	30.50	46.79	42.70	17.73	24.15	36.34

Appendix - 16: Chemical parameters of S1, S2 and S3 samples.

Station ID	Ca (mg/L)			Mg (mg/L)			Na (mg/L)			K (mg/L)		
	S1	S2	S3	S1	S2	S3	S1	S2	S3	S1	S2	S3
LRB SW-01	0.45	0.59	0.48	3.24	1.56	2.81	3.35	1.90	4.56	0.57	0.48	0.45
LRB SW-02	0.27	0.46	0.32	3.58	2.35	2.74	3.03	2.52	2.52	0.55	0.40	0.44
LRB SW-03	0.36	0.30	0.40	2.43	2.66	2.85	4.39	2.22	2.80	0.39	0.42	0.37
LRB SW-04	0.52	0.36	0.44	3.80	2.08	3.36	4.99	2.61	3.99	0.61	0.28	0.60
LRB SW-05	0.16	0.52	0.53	3.61	2.86	3.84	4.83	2.96	4.20	0.66	0.47	0.55
LRB SW-06	0.29	0.55	0.68	2.38	2.91	44.64	4.61	2.97	7.46	0.43	0.49	0.42
LRB SW-07	0.30	0.80	0.50	2.66	1.82	3.40	4.87	4.27	3.51	0.74	0.29	0.58
LRB SW-08	1.11	1.23	0.90	3.89	2.75	3.80	4.78	3.16	3.28	0.65	0.68	0.49
LRB SW-09	0.47	0.54	0.60	2.55	2.27	3.20	5.11	2.49	4.90	0.71	0.53	0.54
LRB SW-10	0.62	0.50	0.58	2.57	2.16	3.48	4.92	2.81	5.25	0.69	0.62	0.58
LRB SW-11	0.40	0.57	0.46	2.75	2.29	2.86	5.64	3.13	2.68	0.63	0.59	0.59
LRB SW-12	10.53	9.40	19.84	1.93	1.31	1.35	4.07	1.87	2.53	0.46	0.40	0.45
LRB SW-13	1.06	1.15	0.89	2.61	2.10	3.18	4.98	2.91	4.61	0.69	0.58	0.54
LRB SW-14	0.75	1.32	0.74	3.28	1.72	3.13	4.91	2.28	3.54	0.70	0.62	0.63
LRB SW-15	1.56	6.66	1.73	2.81	2.19	3.18	3.81	2.93	4.50	0.68	0.64	0.56
LRB SW-16	12.95	6.17	1.08	4.63	1.82	3.22	3.45	1.67	3.79	1.33	0.68	0.81
LRB SW-17	0.60	1.08	0.77	3.15	2.13	3.34	5.13	1.91	2.11	1.22	0.97	0.90
LRB SW-18	1.56	1.54	1.30	2.69	2.00	3.27	4.48	3.47	2.71	0.73	0.66	0.60
LRB SW-19	1.85	1.86	1.09	2.78	2.28	3.47	3.86	3.09	3.96	0.80	0.64	0.61
LRB SW-20	1.43	1.81	1.21	2.74	2.20	3.14	7.21	2.55	3.88	0.88	0.60	0.63
LRB SW-21	0.83	0.83	0.84	3.28	2.55	4.25	6.43	3.13	2.59	1.24	1.88	0.90
LRB SW-22	0.74	0.70	0.92	3.52	2.85	4.14	5.94	3.77	3.50	1.15	0.90	0.81
LRB SW-23	1.35	1.64	0.90	2.74	2.56	3.21	4.53	2.39	3.92	0.92	0.71	0.64
LRB SW-24	1.32	1.66	0.76	2.03	2.46	2.97	4.74	2.93	4.85	0.80	0.78	0.71

Appendix – 17: Chemical parameters of S1, S2 and S3 samples.

Station ID	Co (mg/L)			Ni (mg/L)			Cd (mg/L)			Fe (mg/L)		
	S1	S2	S3	S1	S2	S3	S1	S2	S3	S1	S2	S3
LRB SW-01	0.033	0.043	0.019	0.11	0.12	0.09	0.009	0.005	0.005	1.80	0.99	1.14
LRB SW-02	0.018	0.027	0.017	0.12	0.13	0.11	0.007	0.004	0.003	1.77	1.07	1.14
LRB SW-03	0.036	0.018	0.016	0.12	0.13	0.10	0.005	0.005	0.004	1.69	0.92	1.14
LRB SW-04	0.020	0.045	0.028	0.10	0.14	0.11	0.007	0.006	0.004	1.65	0.94	1.13
LRB SW-05	0.025	0.029	0.015	0.12	0.20	0.09	0.008	0.004	0.002	1.74	0.98	1.09
LRB SW-06	0.035	0.018	0.023	0.13	0.21	0.11	0.006	0.005	0.004	1.65	1.04	1.05
LRB SW-07	0.030	0.039	0.042	0.13	0.21	0.09	0.007	0.004	0.004	1.75	0.95	1.14
LRB SW-08	0.039	0.020	0.027	0.11	0.18	0.07	0.006	0.005	0.005	1.81	1.06	1.12
LRB SW-09	0.049	0.032	0.017	0.12	0.19	0.10	0.007	0.005	0.007	1.79	1.15	1.17
LRB SW-10	0.031	0.040	0.020	0.12	0.20	0.13	0.007	0.005	0.006	1.88	0.96	1.13
LRB SW-11	0.032	0.037	0.014	0.11	0.20	0.12	0.007	0.006	0.004	1.71	0.98	1.19
LRB SW-12	0.029	0.018	0.020	0.12	0.18	0.10	0.007	0.005	0.005	1.57	0.95	1.18
LRB SW-13	0.051	0.033	0.021	0.12	0.19	0.10	0.008	0.004	0.005	1.78	0.90	0.98
LRB SW-14	0.039	0.021	0.023	0.12	0.19	0.10	0.007	0.004	0.007	1.93	0.90	1.07
LRB SW-15	0.044	0.021	0.012	0.12	0.19	0.14	0.007	0.004	0.003	1.73	1.02	1.14
LRB SW-16	0.031	0.032	0.033	0.13	0.17	0.10	0.007	0.003	0.008	1.74	0.78	1.19
LRB SW-17	0.041	0.031	0.024	0.13	0.12	0.13	0.009	0.003	0.004	1.86	1.15	1.14
LRB SW-18	0.033	0.027	0.018	0.13	0.10	0.13	0.006	0.003	0.007	1.76	1.08	1.25
LRB SW-19	0.054	0.020	0.016	0.13	0.11	0.12	0.007	0.004	0.006	1.77	1.09	1.12
LRB SW-20	0.036	0.025	0.041	0.12	0.13	0.13	0.006	0.004	0.004	1.81	1.30	1.15
LRB SW-21	0.061	0.029	0.034	0.13	0.13	0.12	0.006	0.006	0.005	1.89	1.09	1.09
LRB SW-22	0.050	0.066	0.018	0.15	0.12	0.16	0.006	0.005	0.006	1.95	1.13	1.12
LRB SW-23	0.051	0.020	0.026	0.13	0.15	0.14	0.006	0.003	0.006	1.78	1.14	1.17
LRB SW-24	0.048	0.023	0.017	0.13	0.13	0.11	0.006	0.003	0.003	1.71	1.19	1.11

Appendix - 18: Chemical parameters of S1, S2 and S3 samples.

Station ID	Mn (mg/L)			Pb (mg/L)			Zn (mg/L)			Cu (mg/L)		
	S1	S2	S3	S1	S2	S3	S1	S2	S3	S1	S2	S3
LRB SW-01	0.030	0.031	0.025	0.097	0.031	0.023	0.022	0.012	0.005	0.017	0.023	0.011
LRB SW-02	0.027	0.033	0.037	0.102	0.026	0.017	0.021	0.01	0.007	0.014	0.023	0.012
LRB SW-03	0.031	0.036	0.064	0.101	0.023	0.021	0.019	0.01	0.007	0.011	0.022	0.008
LRB SW-04	0.031	0.036	0.032	0.08	0.027	0.019	0.030	0.009	0.003	0.016	0.023	0.006
LRB SW-05	0.022	0.035	0.028	0.098	0.03	0.024	0.027	0.010	0.006	0.018	0.025	0.008
LRB SW-06	0.019	0.034	0.016	0.101	0.034	0.024	0.029	0.014	0.011	0.025	0.021	0.009
LRB SW-07	0.025	0.033	0.031	0.091	0.040	0.025	0.025	0.019	0.014	0.021	0.021	0.010
LRB SW-08	0.030	0.034	0.024	0.095	0.046	0.026	0.025	0.019	0.012	0.017	0.031	0.010
LRB SW-09	0.028	0.041	0.035	0.102	0.042	0.026	0.025	0.014	0.012	0.022	0.014	0.007
LRB SW-10	0.025	0.038	0.019	0.111	0.047	0.021	0.027	0.013	0.016	0.018	0.025	0.009
LRB SW-11	0.035	0.042	0.032	0.079	0.048	0.029	0.020	0.024	0.027	0.011	0.021	0.017
LRB SW-12	0.024	0.041	0.035	0.100	0.041	0.021	0.094	0.010	0.012	0.024	0.025	0.012
LRB SW-13	0.026	0.037	0.035	0.103	0.044	0.022	0.092	0.012	0.016	0.017	0.014	0.010
LRB SW-14	0.031	0.033	0.032	0.094	0.031	0.019	0.033	0.016	0.016	0.021	0.016	0.009
LRB SW-15	0.039	0.046	0.022	0.108	0.045	0.027	0.091	0.011	0.022	0.017	0.016	0.012
LRB SW-16	0.032	0.046	0.048	0.109	0.049	0.020	0.026	0.013	0.022	0.018	0.019	0.003
LRB SW-17	0.140	0.127	0.112	0.122	0.056	0.022	0.426	0.017	0.024	0.026	0.025	0.006
LRB SW-18	0.020	0.060	0.027	0.117	0.035	0.027	0.056	0.012	0.032	0.024	0.018	0.012
LRB SW-19	0.034	0.058	0.031	0.131	0.044	0.015	0.160	0.025	0.021	0.022	0.042	0.004
LRB SW-20	0.024	0.071	0.018	0.095	0.037	0.017	0.047	0.011	0.029	0.028	0.019	0.009
LRB SW-21	0.102	0.111	0.121	0.084	0.041	0.013	0.043	0.024	0.025	0.040	0.023	0.008
LRB SW-22	0.050	0.071	0.028	0.089	0.050	0.021	0.026	0.024	0.031	0.028	0.025	0.008
LRB SW-23	0.044	0.057	0.019	0.086	0.042	0.022	0.035	0.030	0.028	0.017	0.030	0.009
LRB SW-24	0.029	0.066	0.038	0.081	0.044	0.030	0.027	0.014	0.023	0.018	0.027	0.010

Annexure -19: Minimum and maximum values of water quality indices calculated.

Water quality Indices		Fist season (S1)	Second Season (S2)	Third Season (S3)
Na%	Min	15.18	13.69	8.29
	Max	53.08	50.47	45.11
SAR	Min	0.21	0.15	0.15
	Max	0.81	0.60	0.57
RSC (meq/L)	Min	-0.03	0.19	-3.16
	Max	0.60	0.71	0.48
CR	Min	0.49	0.43	0.65
	Max	1.40	0.79	1.75
KR	Min	0.20	0.17	0.12
	Max	1.79	1.63	1.39
PI (%)	Min	97.69	159.98	26.45
	Max	231.45	369.48	256.42
LnR	Min	0.38	0.33	0.46
	Max	1.33	0.89	1.58
MR	Min	23.21	18.68	10.05
	Max	97.45	93.68	99.08
CAI	Min	0.32	0.56	0.67
	Max	0.81	0.82	0.90
	Min	0.15	0.31	0.69
	Max	1.20	0.64	1.76

Appendix - 20: Correlation analysis of physico-chemical parameters in S1 samples.

	pH	EC	TDS	DO	Temp	Turb	SO_4	NO_3	NH_4	PO_4	HCO_3	Cl	Ca	Mg	Na	K	Co	Ni	Cd	Fe	Mn	Pb	Zn	Cu
pH	1.00																							
EC	-0.14	1.00																						
TDS	-0.14	1.00	1.00																					
DO	0.45	*-0.51*	*-0.51*	1.00																				
Temp	-0.12	0.10	0.10	-0.47	1.00																			
Turb	-0.32	0.07	0.07	-0.11	-0.15	1.00																		
SO_4	*-0.53*	0.34	0.34	-0.48	0.32	0.05	1.00																	
NO_3	0.09	-0.08	-0.08	0.16	0.14	-0.54	0.11	1.00																
NH_4	-0.57	0.02	0.02	-0.35	-0.06	0.73	0.32	-0.29	1.00															
PO_4	0.55	-0.29	-0.29	0.53	-0.29	0.21	-0.38	-0.06	-0.13	1.00														
HCO_3	-0.09	0.89	0.89	-0.44	0.10	0.11	0.08	-0.23	-0.08	-0.31	1.00													
Cl	0.24	0.15	0.15	0.21	-0.27	-0.03	-0.26	0.27	-0.02	0.34	-0.12	1.00												
Ca	0.07	0.76	0.76	-0.39	-0.06	-0.13	0.21	-0.14	-0.11	-0.20	0.69	-0.09	1.00											
Mg	-0.04	0.45	0.45	-0.33	0.28	-0.14	0.64	0.31	-0.03	-0.21	0.18	0.17	0.19	1.00										
Na	-0.35	-0.03	-0.03	-0.21	0.39	0.35	0.21	-0.17	0.30	-0.17	0.00	-0.21	-0.32	-0.12	1.00									
K	*-0.71*	0.46	0.46	*-0.79*	0.39	0.2	0.81	-0.19	0.48	-0.54	0.31	-0.28	0.26	0.45	0.33	1.00								
Co	*-0.52*	-0.14	-0.14	-0.41	0.22	0.09	0.14	-0.13	0.27	-0.41	-0.12	-0.21	-0.14	-0.24	0.33	0.46	1.00							
Ni	-0.48	0.06	0.06	*-0.66*	0.40	-0.01	0.26	-0.14	0.45	-0.46	0.05	-0.23	0.05	-0.07	0.18	0.59	0.47	1.00						
Cd	-0.06	0.05	0.05	0.32	-0.48	-0.15	0.22	-0.06	-0.08	-0.08	-0.05	0.06	0.08	0.34	-0.39	0.04	-0.28	-0.20	1.00					
Fe	*-0.52*	-0.04	-0.04	-0.33	0.31	-0.11	0.45	0.08	0.22	-0.39	-0.17	0.01	-0.36	0.32	0.38	0.56	0.42	0.39	0.06	1.00				
Mn	*-0.86*	0.03	0.03	-0.27	0.12	0.22	0.68	0.05	0.53	-0.49	-0.08	-0.30	-0.10	0.16	0.28	0.65	0.40	0.27	0.19	0.42	1.00			
Pb	-0.15	0.06	0.06	-0.02	-0.04	-0.25	-0.10	-0.02	-0.04	-0.38	0.24	-0.32	0.18	-0.03	-0.40	0.07	0.04	0.23	0.37	0.07	0.12	1.00		
Zn	*-0.70*	0.03	0.03	-0.05	-0.05	0.18	0.30	-0.09	0.40	-0.45	0.10	-0.38	0.02	-0.06	0.01	0.35	0.20	0.23	0.44	0.14	0.74	0.57	1.00	
Cu	*-0.56*	0.18	0.18	-0.42	0.35	-0.09	0.33	-0.10	0.12	*-0.56*	0.16	-0.22	0.04	-0.03	0.54	0.54	0.47	0.48	-0.11	0.39	0.50	0.05	0.24	1.00

Appendix - 21: Correlation analysis of physico-chemical parameters in S2 samples.

	pH	EC	TDS	DO	Temp	Turb	SO_4	NO_3	NH_4	PO_4	HCO_3	Cl	Ca	Mg	Na	K	Co	Ni	Cd	Fe	Mn	Pb	Zn	Cu
pH	1.00																							
EC	-0.39	1.00																						
TDS	-0.39	1.00	1.00																					
DO	0.06	-0.04	-0.04	1.00																				
Temp	-0.31	0.64	0.64	-0.09	1.00																			
Turb	-0.01	-0.18	-0.18	-0.10	0.09	1.00																		
SO_4	*-0.72*	0.57	0.57	0.16	0.34	-0.16	1.00																	
NO_3	0.12	0.18	0.18	-0.28	-0.10	0.00	-0.23	1.00																
NH_4	0.05	0.31	0.31	-0.39	0.09	0.17	-0.16	0.80	1.00															
PO_4	0.09	-0.27	-0.27	-0.01	-0.25	-0.24	-0.23	-0.03	-0.07	1.00														
HCO_3	-0.14	0.91	0.91	-0.04	0.53	-0.09	0.29	0.30	0.40	-0.19	1.00													
Cl	-0.45	0.70	0.70	0.05	0.64	-0.26	0.52	-0.03	0.02	-0.12	0.45	1.00												
Ca	0.06	0.28	0.28	-0.33	0.09	-0.06	-0.24	0.17	0.39	-0.19	0.31	-0.08	1.00											
Mg	-0.07	0.29	0.29	0.10	0.29	-0.27	0.52	0.03	-0.02	-0.32	0.17	0.35	*-0.50*	1.00										
Na	0.17	0.18	0.18	0.10	0.16	0.09	0.10	0.17	0.10	-0.14	0.21	0.09	-0.36	0.39	1.00									
K	*-0.52*	0.60	0.60	-0.11	0.35	0.06	0.73	0.01	0.13	-0.13	0.40	0.50	-0.06	0.26	0.10	1.00								
Co	0.03	-0.26	-0.26	0.08	-0.26	0.01	0.02	-0.18	-0.26	0.20	-0.24	-0.25	-0.31	-0.02	0.30	0.04	1.00							
Ni	0.44	-0.05	-0.05	0.25	-0.18	0.16	-0.27	0.30	0.21	-0.24	0.17	-0.44	0.14	-0.02	0.17	-0.30	-0.09	1.00						
Cd	0.48	-0.04	-0.04	0.32	-0.38	-0.24	-0.05	0.03	-0.11	0.02	0.05	-0.13	-0.21	0.12	0.13	0.07	0.30	0.21	1.00					
Fe	-0.45	0.38	0.38	-0.11	0.47	-0.26	0.61	-0.12	-0.06	0.07	0.14	0.58	-0.24	0.37	0.19	0.32	-0.07	-0.44	-0.16	1.00				
Mn	*-0.85*	0.49	0.49	-0.07	0.34	-0.07	0.84	-0.21	-0.05	-0.10	0.21	0.48	-0.03	0.14	-0.02	0.78	0.06	*-0.52*	-0.20	0.55	1.00			
Pb	*-0.53*	0.36	0.36	-0.13	0.14	0.12	0.49	0.13	0.18	-0.16	0.19	0.14	0.27	-0.01	0.12	0.41	0.21	0.10	-0.20	0.18	0.49	1.00		
Zn	-0.36	0.61	0.61	0.06	0.47	-0.13	0.47	0.08	0.00	0.09	0.53	0.58	-0.21	0.30	0.35	0.49	0.12	-0.09	0.03	0.27	0.37	0.49	1.00	
Cu	-0.20	0.29	0.29	0.06	0.29	-0.36	0.24	-0.02	-0.18	0.09	0.11	0.54	-0.06	0.26	0.09	0.10	-0.12	-0.38	-0.03	0.25	0.17	0.16	0.49	1.00

Appendix - 22: Correlation analysis of physico-chemical parameters in S3 samples.

	pH	EC	TDS	DO	Temp	Turb	SO_4	NO_3	NH_4	PO_4	HCO_3	Cl	Ca	Mg	Na	K	Co	Ni	Cd	Fe	Mn	Pb	Zn	Cu
pH	1.00																							
EC	0.34	1.00																						
TDS	0.34	1.00	1.00																					
DO	-0.26	-0.38	-0.38	1.00																				
Temp	-0.41	-0.20	-0.20	0.08	1.00																			
Turb	-0.32	-0.28	-0.28	0.41	0.24	1.00																		
SO_4	*-0.76*	-0.13	-0.13	0.10	0.50	-0.14	1.00																	
NO_3	-0.14	-0.22	-0.22	-0.08	0.51	-0.21	0.16	1.00																
NH_4	*-0.57*	0.09	0.09	0.09	0.37	-0.09	0.66	0.32	1.00															
PO_4	0.43	0.09	0.09	-0.13	-0.10	-0.23	-0.44	0.04	-0.39	1.00														
HCO_3	0.36	0.62	0.62	-0.35	-0.27	-0.26	-0.21	-0.37	-0.15	0.11	1.00													
Cl	-0.01	0.06	0.06	0.09	0.04	-0.01	0.21	-0.06	0.06	-0.19	-0.23	1.00												
Ca	0.28	0.61	0.61	-0.36	-0.24	-0.14	-0.25	-0.23	-0.13	-0.03	0.83	-0.33	1.00											
Mg	0.21	0.55	0.55	-0.12	-0.07	-0.06	-0.22	0.12	0.14	0.21	-0.21	-0.04	-0.1	1.00										
Na	0.35	0.37	0.37	-0.08	-0.17	-0.05	-0.26	-0.13	-0.17	0.31	-0.17	0.14	-0.23	0.67	1.00									
K	*-0.86*	-0.22	-0.22	0.42	0.41	0.37	0.80	-0.05	0.61	*-0.58*	-0.23	0.09	-0.20	-0.24	-0.29	1.00								
Co	-0.19	0.10	0.10	0.11	0.19	0.24	0.27	-0.07	0.18	-0.54	-0.04	0.29	-0.06	0.03	-0.08	0.33	1.00							
Ni	-0.36	-0.13	-0.13	0.47	0.31	0.47	0.16	0.12	0.36	-0.22	-0.27	0.10	-0.13	0.02	0.01	0.45	-0.12	1.00						
Cd	-0.27	-0.05	-0.05	-0.16	0.13	0.18	0.25	-0.17	0.01	-0.52	-0.11	0.29	-0.02	-0.13	-0.06	0.30	0.23	0.12	1.00					
Fe	-0.08	-0.11	-0.11	0.11	0.10	0.15	0.05	-0.14	-0.08	-0.15	0.08	0.22	0.19	-0.35	-0.44	0.06	-0.03	0.17	0.27	1.00				
Mn	*-0.71*	-0.20	-0.20	0.03	0.18	0.09	0.54	0.26	0.57	-0.32	-0.20	-0.05	-0.03	-0.16	*-0.51*	0.58	0.18	0.03	-0.03	-0.05	1.00			
Pb	0.26	0.21	0.21	0.07	-0.16	-0.29	-0.04	-0.16	-0.16	0.52	0.16	0.22	-0.05	0.08	0.23	-0.23	-0.36	-0.11	-0.22	0.21	-0.35	1.00		
Zn	*-0.57*	-0.19	-0.19	0.47	0.32	0.64	0.31	-0.17	0.26	-0.33	-0.16	-0.01	-0.08	-0.14	-0.23	0.65	0.13	0.69	0.36	0.29	0.13	0.06	1.00	
Cu	0.32	0.09	0.09	0.01	-0.37	-0.23	-0.39	-0.2	-0.23	0.56	0.34	-0.24	0.20	-0.03	-0.15	-0.41	-0.3	-0.03	-0.36	0.17	-0.29	0.50	0.08	1.00

Appendix - 23: Log pCO_2 values corresponding to all sampling locations and sampling periods.

Sampling locations	Log pCO_2		
	S1	S2	S3
LRB SW-01	-2.89	-2.42	-2.08
LRB SW-02	-2.73	-2.27	-2.26
LRB SW-03	-2.83	-2.11	-2.29
LRB SW-04	-2.64	-2.34	-2.55
LRB SW-05	-2.87	-2.26	-2.45
LRB SW-06	-2.90	-2.28	-2.63
LRB SW-07	-2.76	-2.14	-2.40
LRB SW-08	-2.94	-2.08	-2.37
LRB SW-09	-2.68	-2.25	-2.36
LRB SW-10	-2.74	-2.17	-2.27
LRB SW-11	-2.50	-2.02	-2.10
LRB SW-12	-2.53	-2.10	-2.43
LRB SW-13	-2.33	-2.09	-2.37
LRB SW-14	-1.46	-1.78	-1.93
LRB SW-15	-1.81	-2.10	-2.30
LRB SW-16	-2.11	-1.99	-1.56
LRB SW-17	0.19	-0.11	-1.24
LRB SW-18	-1.86	-1.87	-2.23
LRB SW-19	-2.02	-1.91	-2.18
LRB SW-20	-1.78	-1.79	-2.14
LRB SW-21	-0.85	-1.49	-1.23
LRB SW-22	-1.75	-1.64	-1.69
LRB SW-23	-1.72	-1.25	-1.90
LRB SW-24	-1.91	-1.28	-1.67
Average	-2.18	-1.91	-2.11

Appendix - 24: Saturation index of carbonate minerals in S1 samples.

Sampling locations	Sampling period -1			
	Magnesite	Dolomite	Calcite	Aragonite
LRB SW-01	-2.27	-5.13	-2.89	-3.04
LRB SW-02	-2.20	-5.26	-3.11	-3.25
LRB SW-03	-2.35	-5.28	-2.97	-3.12
LRB SW-04	-2.03	-4.68	-2.69	-2.84
LRB SW-05	-2.15	-5.41	-3.31	-3.45
LRB SW-06	-2.21	-5.07	-2.91	-3.05
LRB SW-07	-2.27	-5.24	-3.02	-3.16
LRB SW-08	-1.74	-3.77	-2.10	-2.24
LRB SW-09	-2.39	-5.27	-2.92	-3.07
LRB SW-10	-2.24	-4.85	-2.66	-2.80
LRB SW-11	-2.60	-5.77	-3.21	-3.36
LRB SW-12	-2.31	-3.63	-1.36	-1.50
LRB SW-13	-2.46	-5.06	-2.64	-2.78
LRB SW-14	-3.44	-7.27	-3.87	-4.02
LRB SW-15	-2.95	-5.90	-3.00	-3.14
LRB SW-16	-2.15	-3.59	-1.50	-1.64
LRB SW-17	-5.03	-10.52	-5.54	-5.68
LRB SW-18	-2.69	-5.36	-2.72	-2.86
LRB SW-19	-3.00	-5.92	-2.97	-3.11
LRB SW-20	-2.78	-5.60	-2.87	-3.01
LRB SW-21	-4.01	-8.36	-4.41	-4.55
LRB SW-22	-3.15	-6.72	-3.63	-3.77
LRB SW-23	-3.16	-6.37	-3.26	-3.40
LRB SW-24	-3.26	-6.45	-3.24	-3.38
Average	-2.70	-5.69	-3.03	-3.18

Appendix - 25: Saturation index of carbonate minerals in S2 samples.

Sampling locations	Sampling period -2			
	Magnesite	Dolomite	Calcite	Aragonite
LRB SW-01	-2.75	-5.65	-2.93	-3.07
LRB SW-02	-2.66	-5.77	-3.15	-3.29
LRB SW-03	-2.70	-6.09	-3.43	-3.57
LRB SW-04	-2.65	-5.79	-3.18	-3.32
LRB SW-05	-2.41	-5.30	-2.94	-3.08
LRB SW-06	-2.37	-5.21	-2.87	-3.02
LRB SW-07	-2.75	-5.59	-2.89	-3.03
LRB SW-08	-2.59	-5.27	-2.72	-2.86
LRB SW-09	-2.70	-5.75	-3.10	-3.24
LRB SW-10	-2.79	-5.96	-3.21	-3.35
LRB SW-11	-2.75	-5.84	-3.12	-3.27
LRB SW-12	-2.77	-4.42	-1.69	-1.84
LRB SW-13	-2.80	-5.59	-2.84	-2.98
LRB SW-14	-3.00	-5.86	-2.90	-3.04
LRB SW-15	-2.58	-4.41	-1.88	-2.02
LRB SW-16	-3.06	-5.33	-2.31	-2.45
LRB SW-17	-4.81	-9.65	-4.88	-5.02
LRB SW-18	-2.96	-5.77	-2.86	-3.00
LRB SW-19	-2.91	-5.65	-2.79	-2.93
LRB SW-20	-3.02	-5.87	-2.91	-3.05
LRB SW-21	-3.03	-6.29	-3.31	-3.46
LRB SW-22	-2.92	-6.18	-3.31	-3.45
LRB SW-23	-3.11	-6.18	-3.13	-3.27
LRB SW-24	-3.45	-6.82	-3.42	-3.56
Average	-2.90	-5.84	-2.99	-3.13

Appendix - 26: Saturation index (SI) of carbonate minerals in S3 samples.

Sampling locations	Sampling period -3			
	Magnesite	Dolomite	Calcite	Aragonite
LRB SW-01	-2.78	-6.06	-3.31	-3.45
LRB SW-02	-2.62	-5.91	-3.34	-3.48
LRB SW-03	-2.76	-6.12	-3.41	-3.55
LRB SW-04	-2.28	-5.18	-2.94	-3.08
LRB SW-05	-2.31	-5.22	-2.95	-3.10
LRB SW-06	-1.27	-4.11	-2.87	-3.01
LRB SW-07	-2.32	-5.21	-2.93	-3.08
LRB SW-08	-2.22	-4.81	-2.63	-2.77
LRB SW-09	-2.49	-5.45	-3.00	-3.14
LRB SW-10	-2.57	-5.65	-3.12	-3.27
LRB SW-11	-2.88	-6.30	-3.45	-3.59
LRB SW-12	-2.33	-3.23	-0.94	-1.08
LRB SW-13	-2.51	-5.30	-2.83	-2.97
LRB SW-14	-2.73	-5.82	-3.14	-3.28
LRB SW-15	-2.39	-4.79	-2.43	-2.58
LRB SW-16	-3.37	-6.95	-3.63	-3.77
LRB SW-17	-3.59	-7.55	-4.01	-4.15
LRB SW-18	-2.64	-5.43	-2.82	-2.97
LRB SW-19	-2.73	-5.70	-3.01	-3.16
LRB SW-20	-2.69	-5.54	-2.89	-3.03
LRB SW-21	-3.58	-7.61	-4.07	-4.21
LRB SW-22	-3.00	-6.40	-3.45	-3.59
LRB SW-23	-2.91	-6.11	-3.25	-3.39
LRB SW-24	-3.07	-6.47	-3.45	-3.60
Average	-2.67	-5.71	-3.08	-3.22